Jinsong Wang

Editor

Proceedings of the First Symposium on Aviation Maintenance and Management-Volume II

Springer

Lecture Notes in Electrical Engineering

Volume 297

For further volumes:
http://www.springer.com/series/7818

About this Series

"Lecture Notes in Electrical Engineering (LNEE)" is a book series which reports the latest research and developments in Electrical Engineering, namely:

- Communication, Networks, and Information Theory
- Computer Engineering
- Signal, Image, Speech and Information Processing
- Circuits and Systems
- Bioengineering

LNEE publishes authored monographs and contributed volumes which present cutting edge research information as well as new perspectives on classical fields, while maintaining Springer's high standards of academic excellence. Also considered for publication are lecture materials, proceedings, and other related materials of exceptionally high quality and interest. The subject matter should be original and timely, reporting the latest research and developments in all areas of electrical engineering.

The audience for the books in LNEE consists of advanced level students, researchers, and industry professionals working at the forefront of their fields. Much like Springer's other Lecture Notes series, LNEE will be distributed through Springer's print and electronic publishing channels.

Jinsong Wang
Editor

Proceedings of the First Symposium on Aviation Maintenance and Management-Volume II

Springer

Editor
Jinsong Wang
Northwestern Polytechnical University
Xi'an
People's Republic of China

Printed on acid-free paper

Preface

Proceedings of the First Symposium on Aviation Maintenance and Management collects selected papers from the First Symposium on Aviation Maintenance and Management in China held in Xi'an on November 25–28, 2013. The book features state-of-the-art studies on aviation maintenance, test, fault diagnosis, and prognosis of aircraft electronic and electrical systems. The selected works can help promote development of maintenance and test technology toward important and complex aircraft systems. Researchers and engineers in the field of electrical engineering and aerospace engineering can benefit from the book.

We received 265 complete submissions, the largest number of submissions in the domain of aircraft maintenance. Thirty excellent papers were selected for oral presentation and 117 papers for poster presentation, resulting in acceptance rates of 11.3 % for oral, 44.2 % for poster, and 55.5 % in total.

The following is a brief description of the review process. After the submission deadline, each paper was assigned to one member of the Program Committee with the help of keyword searching system. Each member then made reviewer suggestions (an average of five per paper), which were load balanced and conflict resolved, giving two reviewers for each paper and a maximum of 10 papers per previewer. For the decision process, members of the Program Committee met in Northwestern Polytechnical University. They read the reviews and consolidation reports, jointly discussed all the submitted papers, and made acceptance\acceptance with revision\rejection decisions. They also recommended a small number of top-ranked papers for oral presentation, and made final oral and poster decisions.

We wish to thank everyone involved for their valuable time and dedication to making this conference possible, including authors who produced high-quality research, reviewers who gave professional comments, and committee members who made important decisions. The success of the conference entirely relied on their time and effort.

December 2013   Jinsong Wang

Committee

Editors

Jinsong Wang, Professor, Northwestern Polytechnical University, China
Jianping Yuan, Professor, Northwestern Polytechnical University, China

Program Committee Member

Weixin Wu, Professor, Beijing Aviation Technical Research Center, China
Feng Liu, Professor, Beijing Aviation Technical Research Center, China
Bifeng Song, Professor, Northwestern Polytechnical University, China
Guoqing Wang, Professor, Chinese Aeronautical Radio Electronics Research Institute, China
Mingyuan Jiang, Professor, Air Force Command College, China
Yujun Fu, Professor, Army Air Force College, China
Xueren Li, Professor, Air Force Engineering University, China
Changchun Deng, Professor, Aviation University of Air Force, China
Jianhua Zhang, Professor, First Aviation Academy of Chinese Air Force, China
Benwei Li, Professor, Naval Aviation Engineering Institute, China
Jun Diao, Professor, Naval Aviation Engineering Institute, China
Suguang Dong, Professor, China Southern Airlines, China
Yuliang Hu, Professor, Aircraft Maintenance and Engineering Corporation, China
Jie Bai, Professor, Civil Aviation University of China, China
Zuo Yang, Professor, Beijing Institute of Technology, China
Xicheng Chen, Professor, Shenyang Aircraft Design and Research Institute, China
Haifeng Wang, Professor, Chengdu Aircraft Design and Research Institute, China
Zhenguang Mou, Professor, AVIC Shenyang Aircraft Corporation, China
Wensheng Jiang, Professor, AVIC Chengdu Aircraft Corporation, China
Zheng Li, Professor, AVIC Chengdu Aero-Engine Corporation, China
Ge Gao, Professor, AVIC Liming Aero-Engine Corporation, China
Xiping Zhang, Professor, China Flight Test Establishment, China
Qiang Fu, Senior Engineer, AVIC Information Technology Co. Ltd, China

Ansheng Hou, Senior Engineer, AVIC Information Technology Co. Ltd, China
Cunbao Ma, Professor, Northwestern Polytechnical University, China
Haitao Wang, Associate Professor, Northwestern Polytechnical University, China
Zhenbao Liu, Associate Professor, Northwestern Polytechnical University, China
Hongkai Jiang, Associate Professor, Northwestern Polytechnical University, China
Shuhui Bu, Associate Professor, Northwestern Polytechnical University, China
Yong Zhou, Associate Professor, Northwestern Polytechnical University, China

Invited Keynote Speakers

Michael Pecht, Professor, University of Maryland, USA
Brian G. Falzon, Professor, Queen's University Belfast, UK
Guoqing Wang, Director, China Aeronautical Radio Electronics Research Institute, China
Andrei Zagrai, Associate Professor, New Mexico Institute of Mining and Technology, USA
Chuanjun Liu, Professor, Commercial Aircraft Corporation of China, China

Contents

Chapter 1
CoCluster: Efficient Mining Maximal Trend Biclusters Without Candidate Maintenance in Discrete Resource Effectiveness Matrix

Lihua Zhang, Miao Wang, Qingfan Gu, Zhengjun Zhai and Guoqing Wang

Abstract Studying the level of efficiency of resources is a footstone for building the prognostics and health management system. This paper proposed an efficient bicluster mining algorithm—*CoCluster*, which mines trend bicluster in discrete resource effectiveness matrices. To improve the mining efficiency, it mines maximal trend bicluster using sample-growth method and multiple pruning strategies without candidate maintenance. Meanwhile, *CoCluster* algorithm can not only mine resource patterns with effectiveness in the downtrend, but also mine those with effectiveness in the uptrend, thus providing further decision support for later decision support system. To improve the generality, *CoCluster* algorithm can also mine resource patterns without change in effectiveness. The experimental results show our algorithm is more efficient than traditional algorithm.

Keywords Bicluster · Trend · Candidate maintenance · Resource

1.1 Introduction

The level of efficiency of resources directly influences the effectiveness of the whole system. However, resource damage might cause some deficiencies in the system. Therefore, the level of efficiency of resources is very important for

L. Zhang · Z. Zhai · G. Wang
School of Computer Science and Engineering, Northwestern Polytechnical University, YouYiXiLu 127, Xi'an 710072, China

L. Zhang · M. Wang (✉) · G. Wang
Science and Technology on Avionics Integration Laboratory, Guiping Road 432, Shanghai 200233, China
e-mail: wang_miao@careri.com

M. Wang · Q. Gu · G. Wang
China National Aeronautical Radio Electronics Research Institute, Guiping Road 432, Shanghai 200233, China

building a footstone of prognostics and health management system [1]. It can be found which resources have a lower effective rate through real-time recording of the effectiveness of all resources in the system and frequent pattern mining for resource effectiveness matrix in a period of time or analysis on rules of resource relevancy, which helps to discover incorrect resources in advance and thus start using standby resources earlier. However, some resources are normal in a period of time, i.e., meet the threshold value of support degree or confidence degree, but might present a downtrend of effectiveness in a certain period. For example, when the system implements a certain function in a short period, the implementation of this function will make some resources present an unhealthy state. Earlier discovery of such fault helps to conduct health management over potential faults and thus reduce the risk of poor health of the system.

The feature of resource pattern with the effectiveness presenting some trend described above meets the feature of bicluster mining in data mining technology. Bicluster was first put forward by Cheng and Church [2] and used to find co-expression gene under specific experimental conditions in gene expression data. This algorithm uses a low square root residue to gradually delete redundant nodes. Many algorithms based on greedy strategy were proposed afterward [3–5]. Various algorithms above use the following two mining strategies—first, produce clustering globally according to the traditional clustering method and then optimize it gradually; second, mine biclusters respectively in two categories of data and then obtain the result through comparison and integration. However, neither strategy produces a high time efficiency of algorithm. First, bicluster is a NP-hard problem [6]; second, while processing original data, bicluster needs to solve the problem of sensitivity of original data to noise. Meanwhile, bicluster algorithm should allow the overlap among clusterings, which increases the computation complexity of bicluster algorithm; finally, as bicluster algorithm directly processes original data, it should have a very strong flexibility for different types of bicluster.

To improve the mining efficiency of bicluster algorithm, Wang et al. [6, 7] put forward the use of column extension to mine maximal bicluster in discrete data. However, the algorithm above can only mine biclusters meeting gene co-expression relation but cannot be used to mine trend bicluster. Based on the analysis above, this paper proposes an efficient bicluster mining algorithm: *CoCluster*, to mine trend bicluster in discrete resource effectiveness matrix. To improve the mining efficiency, *CoCluster* algorithm mines maximal trend bicluster using the sample-growth method and multiple pruning strategies without candidate maintenance. Meanwhile, *CoCluster* algorithm algorithm can not only mine resource patterns with effectiveness in the downtrend, but can also mine those with effectiveness in the uptrend, thus providing further decision support for later decision support system. To improve the generality, *CoCluster* algorithm can also mine resource patterns without change in effectiveness.

1.2 Problem Description

Resource effectiveness matrix is defined as a two-dimensional real matrix $D = R \times S$. Here, row collection R represents the resource name; column collection S refers to different sampling sites. Element D_{ij} of matrix D is a real number which refers to the effective value (BIT value) of resource i under sampling j. $|R|$ is the number of resources in data set D, and $|S|$ is the number of sampling sites in data set D. For the convenience of mining, the original effective value in resource effectiveness matrix can be discretized into 1, 2, 3,···, n values, where 1 represents the lowest health degree of resources and n represents very healthy resources. The number of discrete values is 4 in discrete resource effectiveness matrix shown in Table 1.1. Bicluster B means that resource in R meets some trend definition in the sampling site in S. Assuming that M is the collection of all biclusters in D, when and only when $N = K \times L(N \in M)$ and another bicluster $P = S \times T(P \in M)$ making $K \subseteq S$ and $L \subseteq T$ does not exist; N is called the maximal bicluster in M. A bicluster B can be defined as *Samples* (*Resources*), where *Resources* refer to the collection of resources in B. It can also be expressed as *B.Resources*; *Samples* refer to the collection of sampling sites where these resources meet the trend definition, which can also be expressed as *B.Samples*.

The form of mining result of *CoCluster* algorithm is the same variation trend of all resources within some consecutive sampling site, i.e., trend bicluster. The variation trend of resources that this paper pays attention to has three types: rising, decline, and invariance. *CoCluster* algorithm does not distinguish the degree of rising or decline. That is to say, variations in discrete value from 1 to 2 and from 1 to 3 are not distinguished. It is only necessary that both resources present a rising or decline state.

Definition 1 The relationship of two resources R_1 and R_2 in two consecutive samples S_1 and S_2 can be defined as follows: (1) If R_1 and R_2 both present uptrend or downtrend in S_1 and S_2, R_1 and R_2 are positively correlated and expressed as $R_1 R_2$; (2) For R_1 and R_2, if one of them presents uptrend and the other presents downtrend in S_1 and S_2, R_1 and R_2 are negatively correlated and expressed as $R_1 - R_2$; (3) If R_1 and R_2 both present invariance trend in S_1 and S_2, R_1 and R_2 are uniformly correlated and expressed as $R_1 \times R_2$; (4) For R_1 and R_2, if one of them presents uptrend or downtrend and the other presents invariance trend in S_1 and S_2, R_1 and R_2 are not correlated.

According to four relations defined above, there are two types of resource pattern in bicluster mined with *CoCluster* algorithm: first, positive correlation or negative correlation among resources; second, uniform correlation among resource. In conclusion, the mining with *CoCluster* algorithm aims at mining all maximal biclusters meeting conditions in definition 1 from discrete resource effectiveness matrix. To improve the mining efficiency of the algorithm, *CoCluster* algorithm will use sample-growth and multiple pruning strategies for mining without candidate maintenance. The specific mining process will be introduced in the next section.

Table 1.1 Discrete resource snapshot matrix

	S_1	S_2	S_3	S_4	S_5	S_6	S_7
R_1	1	2	3	4	2	1	3
R_2	2	3	4	3	2	1	2
R_3	4	3	2	1	3	1	2
R_4	4	4	4	4	4	4	4
R_5	1	1	3	4	3	3	3
R_6	1	1	3	4	3	3	3
R_7	4	4	2	1	4	4	4

1.3 CoCluster Algorithm

The mining process of *CoCluster* algorithm can be divided into two steps: first, construct a sample weight graph; second, mine all maximal trend biclusters with the method of sample-growth.

Different from the mining of bicluster with the traditional sample-growth method, the trend in trend bicluster is produced under consecutive time sample. Therefore, it is only necessary to build the weight on S_i and S_{i+1} edges when constructing the sample relational weighted graph. According to the analysis above, at most two groups of resource information exist simultaneously on the weight of each edge. In one of the group, resources have positive or negative correlation. In the other group, resources present invariance trend, i.e., uniform correlation. The sample weighted graph corresponding to Table 1.1 is shown in Fig. 1.1 where '0' refers to resource collection with positive or negative correlation among resources and '1' refers to resource collection with invariance trend among resources.

Then, *CoCluster* algorithm uses the method of sample-growth to mine maximal trend bicluster from the sample weighted graph made. As resources in bicluster mined with this algorithm has trend consistency, all resources in trend bicluster have a consistent relationship in all adjacent samples. That is to say, the variation trend of resources in bicluster is the same in all adjacent samples. Trend bicluster mined with *CoCluster* algorithm has the following three extension modes: (1) If it is positive correlation in initial two adjacent samples, it should be positive correlation or uniform correlation in all subsequent adjacent samples; (2) if it is negative correlation in initial two adjacent samples, it should be negative correlation or uniform correlation in all subsequent adjacent samples; (3) if it is uniform correlation in initial two adjacent samples, it should be uniform correlation or non-uniform correlation (positive or negative correlation) existed between two adjacent samples at first in all subsequent adjacent samples.

It will be illustrated below. Given a bicluster $S_1S_2S_3S_4(R_1R_2 - R_3)$, for $R_1R_2 - R_3$, if R_1 and R_2 are positively correlated, R_2 and R_3 are negatively correlated and R_1 and R_3 are negatively correlated in S_1 and S_2, R_1, R_2, and R_3 should also meet the relevancy above in S_3, S_3, and S_4, as shown in Table 1.2, or R_1, R_2, and R_3 meet uniform correlation in a certain group of adjacent samples, as shown in Table 1.3. At this time, all resources in S_3 and S_4 present invariance trend, i.e., uniform
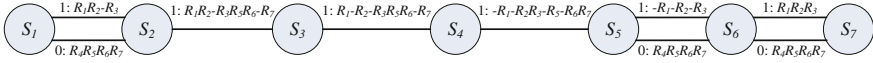
Fig. 1.1 Sample weight graph corresponding to Table 1.1

Table 1.2 Example matrix 1

	S_1	S_2	S_3	S_4
R_1	1	2	3	4
R_2	1	2	3	4
R_3	4	3	2	1

Table 1.3 Example matrix 2

	S_1	S_2	S_3	S_4
R_1	1	2	3	3
R_2	1	2	3	3
R_3	4	3	2	2

Table 1.4 Example matrix 3

	S_1	S_2	S_3	S_4
R_1	1	1	3	4
R_2	1	1	3	4
R_3	4	4	2	1

Table 1.5 Example matrix 4

	S_1	S_2	S_3	S_4
R_1	3	3	3	3
R_2	3	3	3	3
R_3	4	4	4	4

correlation. Table 1.4 shows the situation in (3) above, and resources have uniform correlation in S_1 and S_2. When there is $R_1R_2 - R_3$ correlation in S_2 and S_3, there should be the same in S_3 and S_4. Bicluster shown in Table 1.5 is a form of mining result, i.e., it is invariance trend, i.e., uniform correlation in all adjacent samples.

It can be seen from the analysis above that multiple groups of resource collection meeting the definition of resource trend will exist in a group of same sample collection. Therefore, multiple groups of resource collection meeting the definition will be produced in real time during sample-growth. Thus, multiple groups of trend bicluster can be mined with the method of sample-growth, thus improving the mining efficiency of the algorithm. To improve the mining efficiency, *CoCluster* algorithm mines maximal bicluster without candidate maintenance. Pruning strategies used by this algorithm are designed based on the method of prior candidate sample detection, i.e., if the weight of the current candidate sample is the subset of a prior candidate sample weight, trend bicluster obtained by the extension of weight of the current candidate sample can be obtained by the extension of weight of a

prior candidate sample. Therefore, the weight of the current candidate sample can be pruned. Based on the analysis above, Lemma 1 can ensure that *CoCluster* algorithm can prune candidate sample without candidate maintenance.

Lemma 1 *Assuming that P is the current bicluster to be extend, M is the candidate sample set of P and N is the prior candidate sample set of P, if a prior candidate sample $N_j(N_j \in N)$ making $PM_i.Resource$ a subset of $PN_j.Resource$ exists for candidate sample $M_i(M_i \in M)$, the bicluster obtained by extension of PM_i is a subset of that obtained by extension of PM_iN_j.*

Output strategy Assuming that *P* is the current bicluster to be extended and *M* is candidate sample set of *P*, if *P* has *n* weights and $P.Resource_m(m = 1, 2,...,n)$ does not have a candidate sample $M_i(M_i \in M)$ making $P.Resource_m$ a subset of $PM_i.Resource$(does not meet maximal definition), $P.Resource_m$ can be output.

Based on the analysis above, this algorithm can directly mine maximal trend bicluster with the method of column extension without storing the frequent pattern of candidate in internal memory. Figure 1.2 illustrates the mining process of *CoCluster* algorithm. Example data are shown in Table 1.1, and the threshold of minimum number of samples and resources is 2.

```
Algorithm: CoCluster algorithm
Input: threshold of number of samples or resources in
bicluster: r_min , resource effectiveness data: D
Output: all maximal trend biclusters meeting the thre-
shold
Initialization: sample weight graph: G =Null, current
bicluster to be extended Q =Null, S_i=Null and S_j=Null.
Algorithm description: CoCluster(r_min , D, Q, S_i, S_j)
 (1) If G is null, scan data set D and make its weight
graph. S_i is the first sample in the weight graph;
 (2) For each sample S_j connected with sample S_i,
 (3) If all resource linked lists in S_j meet pruning con-
ditions,
 (4)    Continue;
 (5) Else
 (6)    For resource linked lists not meeting pruning
conditions, Q.Sample= Q.Sample∪S_j ; Q. Resource=
Q.Resource∩S_iS_j.Resource;
 (7)        CoCluster (r_min , D, Q, S_i, S_j->next);
 (8)    Endfor
(9) Endif
 (10) If Q meets output conditions and threshold,
 (11)    Output Q;
 (12) Endif;
 (13) S_i = S_i->next;
 (14) Return
```
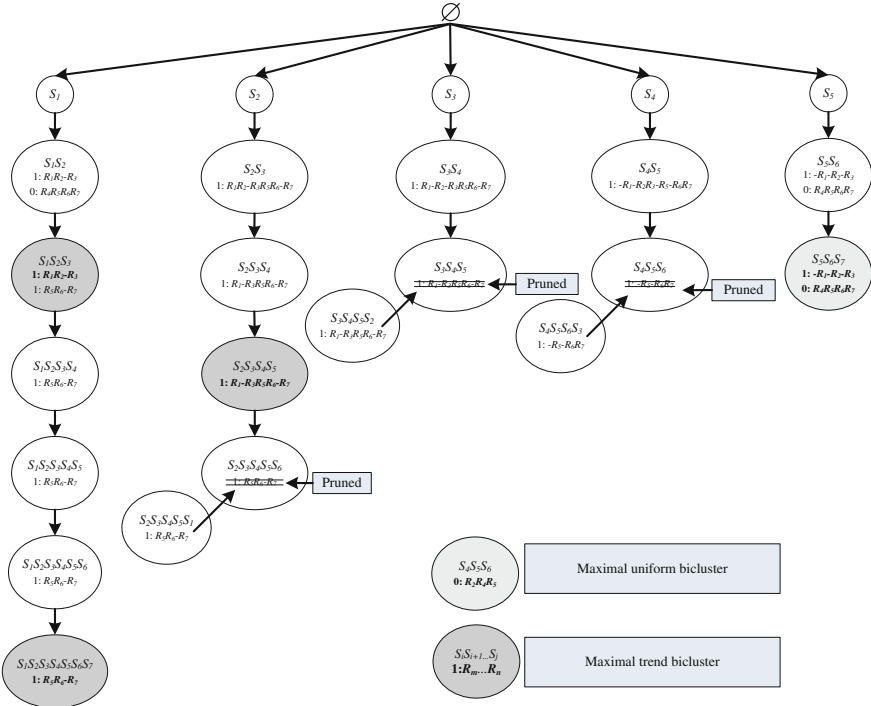
Fig. 1.2 Example mining process of *CoCluster* algorithm

1.4 Experimental Result and Analysis

In this section, we will make an experimental comparison on the mining efficiency and result of the algorithm above and existing algorithms. The hardware environment of the experiment is desktop computer: Intel(R) Core(TM)2 Duo 2.53 GHz CPU and 4G internal memory; the software environment is Microsoft Windows 7 SP1 operating system; the algorithm programming and operating environment is Microsoft Visual C++ 6.0 SP6. Experimental data used in this paper are simulation data. The method of data generation in block is used: Some region is set as uptrend (or downtrend or uniform trend), and all resources R in this region present uptrend (or downtrend or uniform trend). The data set contains 20 sampling sites and 800 resources. Table 1.6 describes the distribution of each sub-block in the data set, and the proportion of each sub-block is random.

CoCluster algorithm proposed in this paper is used to mine maximal trend bicluster in discrete resource effectiveness matrix. Therefore, we will discretize data with the method of k-means clustering put forward in *DiBiCLUS* algorithm and classify the expression value of each resource in all sampling sites into K. The initial central point in each classification is random. Discretization with k-means

Table 1.6 The distribution
of each sub-block

1-200	uptrend		random	
201-400	random		downtrend	
401-600	random	uniform trend		random
601-800	random			

has certain disadvantage, i.e., the result obtained by each discretization might be different. The reason is that the selection of initial central point might be different each time. Therefore, to avoid the influence of the selection of central point, we discretize each resource for 10 times and the result with minimum mean square error will be used as the final discretization result.

In this section, a comparison will be made on the operating efficiency of *Co-Cluster* algorithm and *TCBicluster* algorithm [8] (*TCB* for short) and *CoCluster* algorithm without using pruning strategies. Figure 1.3a–c provide the comparison of operating time of three algorithms above with values in discretization, respectively, 5, 10, and 20 and the number of resources, respectively, 100, 200, 300, 400, 500, and 600. It can be seen from these figures that the mining time of these three algorithms increases progressively with the increase in the number of resources in data set. Meanwhile, the mining efficiency of *CoCluster* algorithm is higher than that of the other two algorithms under each data size. In particular when the number of resources in data source is high, the mining efficiency of *CoCluster* algorithm is almost 1,000 times higher than that of *TCB* algorithm. The reason is that the pruning strategy used by *TCB* algorithm has a lower efficiency. With the increase in the number of resources in data set, this algorithm needs more pruning judgments to mine all biclusters meeting the threshold constraint. However, due to low success rate of pruning, the cost of pruning judgment is too high, thus influencing the mining efficiency of the algorithm. *CoCluster* algorithm uses high-efficiency pruning strategies for mining and will produce more maximal biclusters, especially when the number of resources in data set is high and data are dense. Thus, the pruning efficiency of *CoCluster* algorithm will be higher.

Fig. 1.3 Comparison of operating time under different number of resources in data sets with different discretization degree: **a** $K = 5$; **b** $K = 10$; **c** $K = 20$
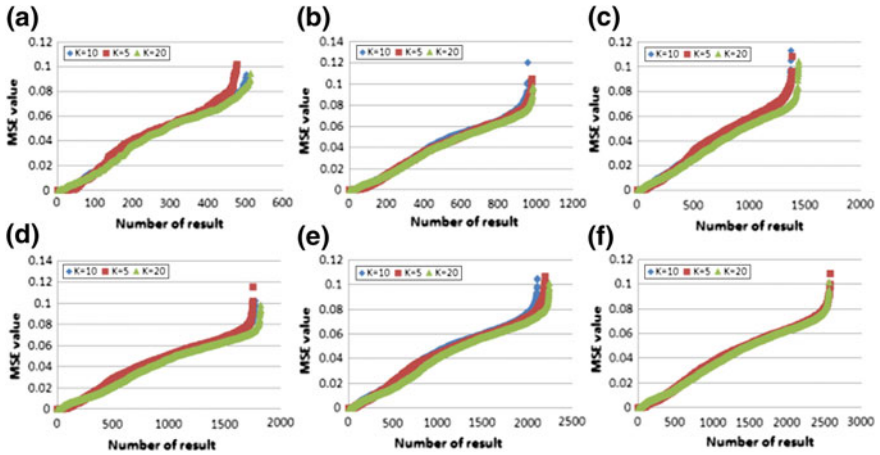
Fig. 1.4 Distribution of MSE value of mining result in data sets with different number of resources and degree: **a** 100 resources; **b** 200 resources; **c** 300 resources; **d** 400 resources; **e** 500 resources; **f** 600 resources

Then, we use mean square error (MSE) [2] to measure the difference degree of the model. Mean square error can be used to measure the relevancy of a group of resources in a group of sampling sites. Lower score of mean square error indicates lower difference degree and high relevancy of resources in a group of consecutive sampling sites. Assuming that I and J are respectively the collection of all sampling sites in a group of resources and data set and D_{ij} is the real value of resource i in sampling site j, the score of mean square error of this group of resources in all sampling sites can be calculated by the following formula.

$M(I,J) = \frac{1}{|I||J|} \sum_{i \in I, j \in J} \left(D_{ij} - D_{iJ} - D_{Ij} + D_{IJ}\right)^2$, where $D_{iJ} = \frac{1}{|J|} \sum_{j \in J} D_{ij}$ and $D_{Ij} = \frac{1}{|I|} \sum_{i \in I} D_{ij}$ are the mean value in row i and column j; $D_{IJ} = \frac{1}{|I||J|} \sum_{i \in I, j \in J} D_{ij}$ is the mean value of expression value of this group of genes under all experimental conditions.

Figure 1.4a–f provide the distribution of MSE value of mining result in data sets with different number of resources and degree. It can be seen from these figures that MSE value of almost all results is lower than 0.1, indicating that the mining result of *CoCluster* algorithm has certain correlation though it is mined from discrete data, thus showing that the effective value of resources in maximal trend bicluster mined with this algorithm has small variation. Thus, biclusters with weak trend can be mined from a lot of data so as to discover resources with fault trend in time in the earlier stage.

1.5 Conclusion

This paper proposed an efficient bicluster mining algorithm-*CoCluster* algorithm which mines trend bicluster in discrete resource effectiveness matrices. It mines maximal trend bicluster using sample-growth method and multiple pruning strategies without candidate maintenance. Meanwhile, *CoCluster* algorithm can not only mine resource patterns with effectiveness in the downtrend, but can also mine those with effectiveness in the uptrend, thus providing further decision support for later decision support system. To improve the generality, *CoCluster* algorithm can also mine resource patterns without change ineffectiveness. However, using discrete data may lose some original information. Next, we will use real-valued data set for mining trend bicluster.

References

1. Pecht M et al (2010) A prognostics and health management roadmap for information and electronics-rich systems. Microelectron Reliab 50(3):317–323
2. Cheng Y, Church GM (2000) Biclustering of expression data. In: Proceedings of 8th international conference intelligent systems for molecular biology (ISMB00), ACM Press, pp 93–103
3. Ben et al (2003) Discovering local structure in gene expression data: the order-preserving submatrix problem. J Comput Biol 10:373–384
4. Cheng KO et al (2007) Bivisu: software tool for bicluster detection and visualization. Bioinformatics 23:2342–2344

5. Zhao L, Zaki MJ (2005) MicroCluster: an efficient deterministic Biclustering algorithm for microarray data. IEEE intelligent systems 20(6):40–49. (Special issue on data mining for bioinformatics)
6. Wang M, Shang X, Zhang S, Li Z (2010) FDCluster: mining frequent closed discriminative Bicluster without candidate maintenance in multiple microarray datasets. In: ICDM 2010 workshop on biological data mining and its applications in healthcare, pp 779–786
7. Wang M, Shang X et al (2013) Efficient mining differential co-expression biclusters in microarray datasets. Gene 518:59–69
8. Yang M, Shang X et al (2013) Bicluster algorithm facing the time-series gene expression data. Appl Res Comput 30(8):2308–2314

Chapter 2
Trend Prognosis of Aero-Engine Abrupt Failure Based on Affinity Propagation Clustering

Limin Li, Zhongsheng Wang, Zhenbao Liu and Shuhui Bu

Abstract This paper presented a new method for trend prognosis of aero-engine abrupt failure which was based on clustering analysis. We used affinity propagation method to cluster vibration data from aero-engine rotating machinery to find the failure trend by means of features extracted from it. This system could remind rapidly which failure will happen next. It is possible to be applied to trend prognosis of aero-engine abrupt failure in airlines.

Keywords Trend prognosis · Aero-engine abrupt failure · Clustering analysis · Affinity propagation clustering

2.1 Introduction

In recent years, aero-engine catastrophic accidents happen occasionally and show an upward tendency [1–3]. Among these accidents, some were caused by abrupt failure. Because the occurrence time of aircraft abrupt failure is very short and highly random, it is very difficult to predict and prevent the accident. Although previous works [4–6] have focused on predicting gradual change failure of aero-engine, to our knowledge, there is little discussion about trend prognosis of abrupt failure. In order to enhance protection ability against abrupt failure, we attempt to address the important problem.

L. Li (✉) · Z. Wang · Z. Liu · S. Bu
School of Aeronautics, Northwestern Polytechnical University, Xi'an 710072, People's Republic of China
e-mail: liliminxiaomi@mail.nwpu.edu.cn

Methods of failure prognosis can be divided into two categories, model-based and data-driven methods [7]. Model-based methods require accurate process models. For data-driven approaches, only the availability of a large amount of process data is assumed. Because of the difficulty on modeling aero-engine system, in this paper we adopt data-driven method as our abrupt failure trend prognosis method. This can be achieved by intelligent data analysis based on features extracted from raw signals. Clustering data by identifying a subset of representative exemplars is important for handling sensory signals and detecting patterns in data. Generally, such 'exemplars' can be found by randomly choosing an initial subset of data points and then iteratively refining it. There are some methods which have been used in failure prognosis, such as k-means [8] and k-centers [9, 10]. Because these clustering methods are quite sensitive to initial selection of exemplars, it is usually rerun many times with different initialization in an attempt to find a good solution, whose cost is that it would take more time and obtain less accuracy rate. Another problem is that these algorithms have seldom been applied in abrupt failure trend prognosis. Affinity propagation [11] we adopted is an innovative clustering algorithm that identifies exemplars quickly and successfully. The speed of this method is fast and has smaller error rate; hence, it can satisfy the real-time requirement of abrupt failure trend prognosis.

The rest of this paper is organized as follows: in Sect. 2.2, we introduce our scheme of abrupt failure trend prognosis, as well as the principle of affinity propagation clustering. Then, in Sect. 2.3, we present the experiment results of our method. Finally, we conclude this paper in Sect. 2.4.

2.2 Trend Prognosis of Aero-Engine Abrupt Failure Based on Affinity Propagation Clustering

2.2.1 Trend Prognosis Module for Aero-Engine Abrupt Failure

We first collect vibration signals of abrupt failures generated from our test bench of aero-engine rotor and extract time-domain signals before failures to build a database of abrupt failure trend as shown in Fig. 2.1.

Then, we use affinity propagation algorithm to cluster these data in the database, find corresponding exemplars, and label them. When new data come, we cluster them and find their corresponding exemplar. After computing distance between new exemplar and old exemplars, choose the type which has the shortest distance to the result. Moreover, we set a threshold to decide whether the new data come from a new abrupt failure trend. If it is an unknown abrupt failure trend, we will use expert knowledge to analyze it and lastly enlarge the database of abrupt failure trend by increasing the number of classes of failures.
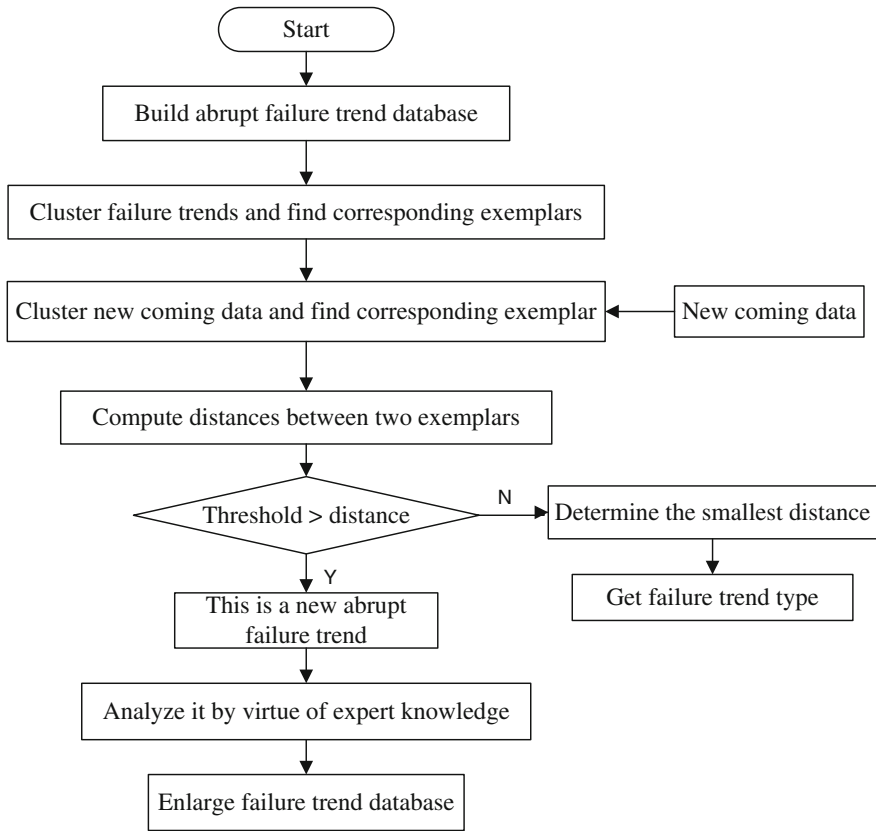
Fig. 2.1 Trend prognosis module for aero-engine abrupt failure

2.2.2 Feature Extraction

We adopted different feature extraction methods for failure signals. Fifteen basic features are extracted from raw signals, which include mean, median, variance, standard deviation, skewness, minimum value, maximum value, kurtosis, range, standard error, sum, maximum gradient, Hilbert-Huang Transform (HHT) spectrum, and first and second levels of energies in wavelet package decomposition. In order to choose discriminative features, reduce computational complexity, and add generalization performance, we use affinity propagation clustering to automatically select three features with high discrimination from these basic features. The resulting features are, respectively, kurtosis, HHT spectrum, and wavelet energy. Table 2.1 lists comparison between different failures in the feature space.

Table 2.1 Different failure features. (**a**) normal (**b**) abrupt failure of blade fracture (**c**) inner race failure of bearing (**d**) outer race failure of bearing
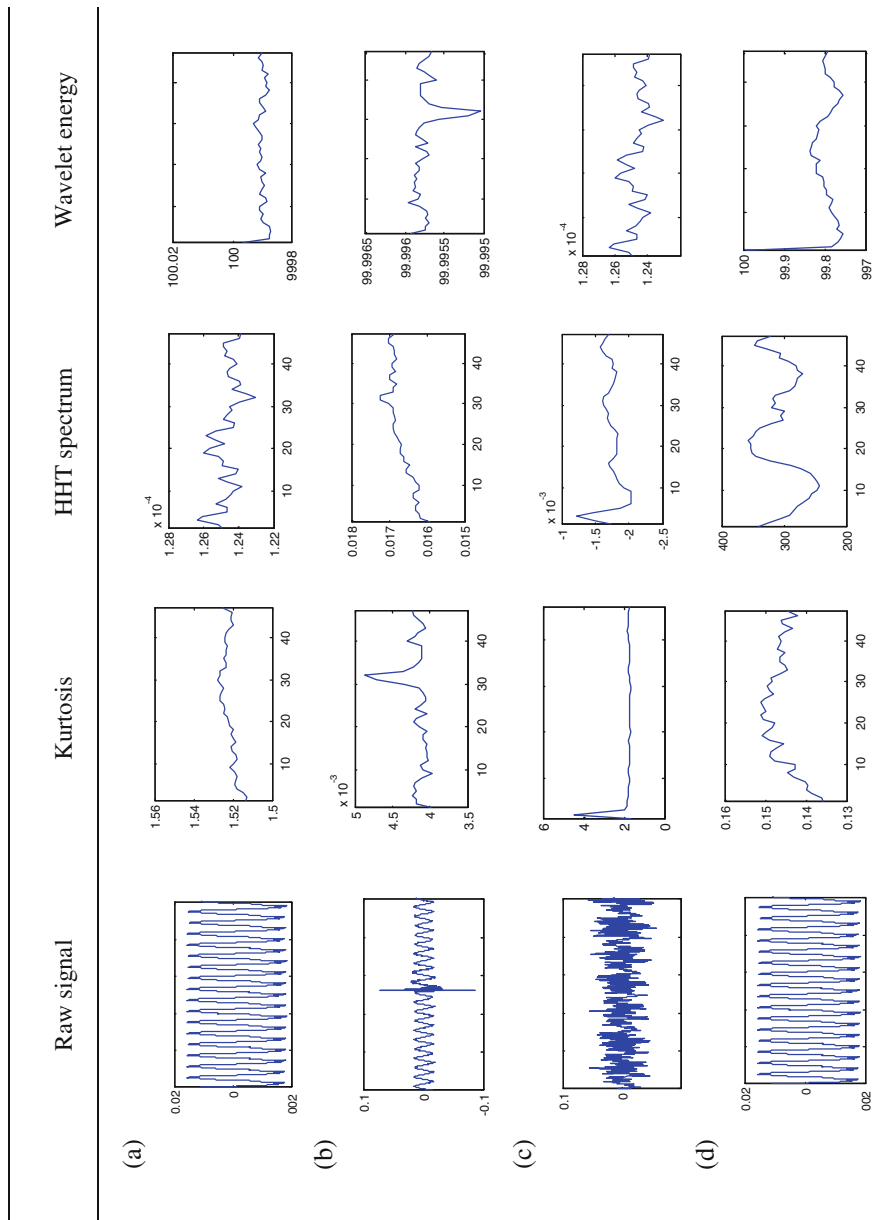
2.2.3 Affinity Propagation Clustering for Trend Features

The process of trend prognosis of aero-engine abrupt failure contains two steps, which contain finding exemplars of trend features in the database and prognosing failure trend by exemplars matching.

In the first step, according to the theory of affinity propagation, we need to determine the relationship between each pair of data points, through obtaining the index of each data point to determine which points are exemplars of failure trend database. A detailed process is as follows.

1. Calculate Euclidean distance d_{ij} between each pair of data points in X using Eq. 2.1.

$$d_{ij} = -\left\| x_i - x_j \right\|^2, \quad (1 \le i, j \le N) \tag{2.1}$$

2. Use binary variables $c_{ij}(1 \le i, j \le N)$ to represent the relationship of each pair of data points, such that $c_{ij} = 1$ if the exemplar for point i is point j; in this notion, $c_{jj} = 1$ indicates that j is an exemplar. c_{ij} is obtained by maximizing the sum of similarities between data points and their exemplars, which is shown in Eq. 2.2.

$$S(c_{ij}) = \sum_{i,j} s_{ij}(c_{ij}) + \sum_i I_i(c_{i1}, \ldots, c_{iN}) + \sum_j E_j(c_{1j}, \ldots, c_{Nj}). \tag{2.2}$$

In which

$$S_{ij}(c_{ij}) = \begin{cases} d_{ij} & \text{if } c_{ij} = 1, \\ 0 & \text{otherwise.} \end{cases} \tag{2.3}$$

$$I_i(c_{i1}, \ldots, c_{iN}) = \begin{cases} -\infty & \text{if } \sum_j c_{ij} \ne 1, \\ 0 & \text{otherwise.} \end{cases} \tag{2.4}$$

$$E_j(c_{1j}, \ldots, c_{Nj}) = \begin{cases} -\infty & \text{if } \sum c_{jj} = 0 \text{ and } \exists i \ne j \text{ s.t. } c_{ij} = 1, \\ 0 & \text{otherwise} \end{cases} \tag{2.5}$$

$S_{ij}(c_{ij})$ function nodes incorporate the input similarities d_{ij} between each data points and their potential exemplars. $\{I_i\}_{i=1}^N$ and $\{E_j\}_{j=1}^N$ are two constraint functions, function I_i operates on the ith row of c_{ij}, enforcing that x_i is assigned to only one cluster, the function E_j operates on the jth column of c_{ij}, ensuring that x_j chooses itself as an exemplar if another data point chooses x_j as its exemplar. We use graph theory to optimize the result of c_{ij}. We execute the max-sum algorithm

[12] on the graph; there are five message types passed between variable nodes and function nodes, update rules are Eqs. (2.6, 2.7).

$$\mu_{x \to f}(x) = \sum_{\{l | f_l \in ne(x) \setminus f\}} \mu_{f_l \to x}(x) \tag{2.6}$$

$$\mu_{f \to x}(x) = \max_{x_1, \ldots, x_M} \left[f(x, x_1, \ldots, x_m) + \sum_{\{m | x_m \in ne(f) \setminus x\}} \mu_{x_m \to f}(x_m) \right] \tag{2.7}$$

We use this algorithm to calculate the five messages, as shown in Eqs. (2.8–2.12).

$$s(i, j) = d_{ij} \tag{2.8}$$

$$\alpha_{ij} = \begin{cases} \sum_{k \neq j} \max[\rho_{kj}, 0], & i = j \\ \min\left[0, \rho_{jj} + \sum_{k \notin \{i, j\}} \max[\rho_{kj}, 0]\right], & i \neq j \end{cases} \tag{2.9}$$

$$\rho_{ij} = d_{ij} - \max_{k \neq j}(d_{ik} + \alpha_{ik}) \tag{2.10}$$

$$\beta_{ij} = d_{ij} + \alpha_{ij} \tag{2.11}$$

$$\eta_{ij} = -\max_{k \neq j} \beta_{ik} \tag{2.12}$$

Five messages are passed there iteratively, and the algorithm is said to converge once the message values no longer change. The final assignment of variable c_{ij} is based on the sum of all incoming messages to c_{ij}:

$$c_{ij}^* = \arg\max_{c_{ij}} \sum_{f_l \in ne(c_{ij})} \mu_{f_l \to c_{ij}}(c_{ij}) \tag{2.13}$$

where f_l represents S_{ij}, I_i, E_j. Till now, we get the result of c_{ij}, so we determine exemplars of failure trends in the database.

In the second step, we use the same algorithm to obtain the exemplar of new test data, and by matching the new exemplar with the exemplars in the first step by calculating Euclidean distances between them, as shown in Eq. 2.14.

$$D_i = \|X_i - X_n\| \tag{2.14}$$

where i is the index of exemplars in the database, and n represents the index of exemplar of new test data. If we set the threshold of distance as d, judge whether D_i are smaller than d; if it is so, choose the smallest value of D_i, the corresponding index is the failure trend class, inversely we can conclude that the new test data belongs to a new kind of failure trend.

2.3 Experiments

2.3.1 Physical Equipment Description

The data used in this paper is sampled from our test bench of aero-engine rotor as shown in Fig. 2.2, which is built for simulating failures including several types of abrupt failures of aero-engine.

As illustrated in Fig. 2.2, our rotor equipment contains blade, bearing, axle, motor, accelerometers, and eddy current sensors. Rated voltage of the motor is 220 V, rated current is 2 A, rated power is 300 W, and max rotation speed is 10,000 rpm. In this paper, we use two accelerometers to sample vibration signals, with a sampling frequency equal to 6 kHz, and set the motor speed to 1,200 rpm. After sampling data, we will test our method on these signals.

2.3.2 Trend Prognosis Results

In this paper, we simulated three kinds of failures in our experimental equipment. They contain blade fracture, inner race failure of bearing, and outer race failure of bearing. Features of failures are extracted, and a trend database is built for storing different types of failures. We sampled 47 feature points from each failure and clustered all the three kinds of points. Their exemplars are computed, and each point's class is determined. These points are labeled using different markers, and blank squares represent exemplars of failure trends in Fig. 2.3.

In order to test our prognosis scheme, we only extract exemplars of each type of failure trend, as shown in Fig. 2.3b. Point A is the exemplar of outer race failure trend, point B is the exemplar of abrupt blade fracture failure trend, and point C is the exemplar of inner race failure trend, respectively. The coordinates of three points A, B, and C are (1.5, 301.5, 99.9), (1.7, 214.7, 99.9), and (2.5, 104.6, 99.8), respectively. Then, we use another new sample of abrupt blade fracture failure as the test data, and Fig. 2.3c shows its exemplar. We first try to set the threshold to 1 according to the test data range. The coordinate of new test data exemplar N is (1.9, 127.7, 98.1); then, we calculate Euclidean distance between N and A, B, C. The distances d1, d2, and d3 are 0.41, 0.01, and 0.12, respectively. It is easy to see that d2 is smaller than two other values; moreover, it is smaller than the threshold value. Therefore, we can conclude that this new data belong to failure trend of abrupt blade fracture. Figure 2.3d shows that using our algorithm, the abrupt failure trend is able to be prognosed.
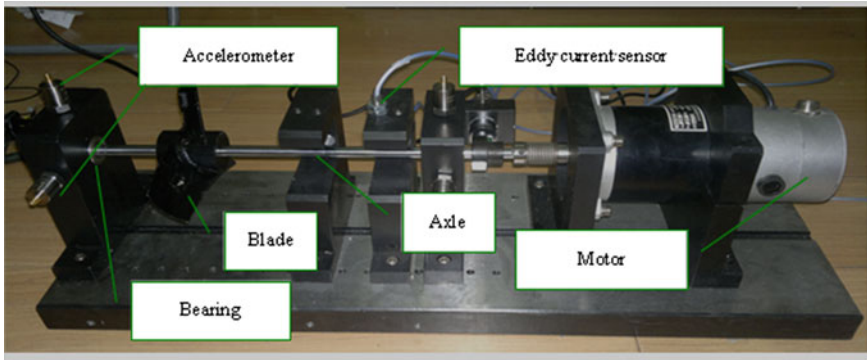
Fig. 2.2 Test bench of Aero-engine rotor
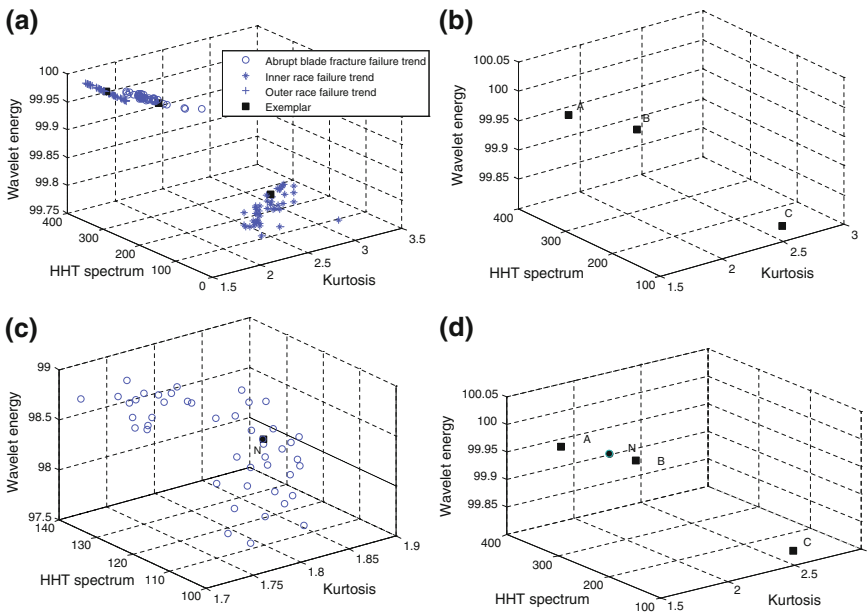
Fig. 2.3 Process of trend prognosis for aero-engine abrupt failure

2.3.3 Comparison with Other Methods

In order to check the performance of our scheme in aspects of time and accuracy, we compare clustering results on the same failure trend database to prognosis results on k-means [8] and k-centers [9, 10].

In order to reduce the random error, we run each program three times and got the average value of clustering time. From Table 2.2, we can see that while using

Table 2.2 Comparison of clustering time between methods based on affinity propagation, k-means, and k-centers

Time	Affinity propagation	k-means	k-centers
First	1.0168	3.0564	5.0513
Second	1.0021	3.0045	5.0141
Third	1.0007	3.0012	5.0002
Average	1.0215	3.0207	5.0219

Table 2.3 Comparison of error rate of failure trend prognosis between methods based on affinity propagation, k-means, and k-centers

	Affinity propagation	k-means	k-centers
Error (%)	0	16.31	46.09

affinity propagation to cluster failure trends, it took less time than k-means and k-centers methods.

The error of a clustering algorithm is the expected difference between its labels and the labels generated by the labeled point process Ξ, which was calculated by Eq. 2.15.

$$\varepsilon(S^{\Xi}, S^{\Phi}) = \frac{|\{x : I_{\Xi}(S; x) \neq I_{\Phi}(S; x)\}|}{|S|} \tag{2.15}$$

$I_{\Xi}(S; x)$ and $I_{\Phi}(S; x)$ denote the label of x for S^{Ξ} and S^{Φ} respectively, and $|\bullet|$ indicates the number of elements of a set. After running each algorithm for clustering failure trend one time, we obtained the error comparison results.

As shown in Table 2.3, while adopting affinity propagation algorithm to prognose failure trend, it produced less error than methods based on k-means and k-centers. The reason can be listed as follows:

1. Affinity propagation clustering determines relationship between points by adopting information exchange among all points, and this method belongs to global clustering partition. Moreover, it takes into account near regional relationship, which would produce less error, even no error at all.
2. K-means and k-centers clustering first divide data randomly into several parts and then adopt the iteration process to optimize some object functions.

However, the setting of iteration itself is a source of error.

2.4 Conclusion

This paper presented a new method for trend prognosis of aero-engine abrupt failure which was based on clustering analysis. We used affinity propagation method to cluster vibration data from aero-engine rotating machinery to find the

failure trend by means of features extracted from it. This system could remind rapidly which failure will happen next. It is possible to be applied to trend prognosis of aero-engine abrupt failure in airlines.

References

1. Silveira E, Atxaga Irisarri G (2010) Failure analysis of two sets of aircraft blades. Eng Fail Anal 17(3):641–647
2. Etemadi AR, Behjati P, Madaah Hosseini HR, Kokabi AH (2010) Failure analysis of brazed air passages of an aircraft fuel system. Eng Fail Anal 17(6):1495–1499
3. Ukil A, Zivanovic R (2007) The detection of abrupt changes using recursive identification for power system fault analysis. Electr Power Syst Res 77(3–4):259–265
4. Baker A, Rajic N, Davis C (2009) Towards a practical structural health monitoring technology for patched cracks in aircraft structure. Appl Sci Manuf 40(9):1340–1352
5. Sathiya Naarayan S, Pavan Kumar DVTG, Chandra S (2009) Implication of unequal rivet load distribution in the failure the and damage tolerant design of metal and composite civil aircraft riveted lap joints. Eng Fail Anal 16(7):2255–2273
6. Smith Cary, Akujuobi Cajetan M, Hamory Phil, Kloesel Kurt (2007) An approach to vibration analysis using wavelets in an application of aircraft health monitoring. Mech Syst Signal Process 21(3):1255–1272
7. Pecht M, Jaai R (2010) A prognostics and health management roadmap for information and electronics-rich systems. Microelectron Reliab 50(3):317–323
8. Yiakopoulos CT, Gryllias KC, Antoniadis IA (2011) Rolling element bearing fault detection in industrial environments based on a K-means clustering approach. Expert Syst with Appl 38(3):2888–2911
9. Ypma A, Pajunen P (1999) Rotating machine vibration analysis with second-order independent component analysis. In: Proceedings of the first international workshop on independent component analysis and signal separation, pp 37–42
10. Luo M (2006) Data-driven fault detection using trending analysis. PhD Dissertation, Louisiana State University
11. Frey BJ, Dueck D (2007) Clustering by passing messages between data points. Science 315(5814):972–976
12. Kschischang FR (2001) Factor graphs and the sum-product algorithm. IEEE Trans Inf Theory 47(2):498–519

Chapter 3
DOA Estimation of Coherent Resources Based on Matrix Reconstruction

Lu Tong

Abstract This study presents a direction-of-arrival (DOA) estimation method for coherent signals. DOA estimation is an important part in the target precision locating. But, when the signals are correlated, conventional algorithm will fail in DOA estimation such as MUSIC. A new de-correlation DOA estimation algorithm is proposed for this. It is based on the cross-correlation vector matrix reconstruction. For wide coherent signals, its performance is superior to ISM and CSM. Simulation results are presented to illustrate the efficiency and accuracy of this method.

Keywords Direction of arrival (DOA) · MUSIC algorithm · Conjugate data rearrangement · Matrix reconstruction · Coherent resources

3.1 Introduction

Signals are coherent at a high degree in the military environment, existing deception jamming or multi-path interference; this will lead to the loss of the rank of covariance matrix [1], and the conventional MUSIC [2] algorithm will fail in the direction-of-arrival (DOA) estimation. So, it is important to study an improved algorithm for mixed resources in the coherent environment.

Modified MUSIC (MMUSIC) algorithm based on the spatial smoothing is effective for the coherent resources, but its ability of de-correlation is obtained by sacrificing the effective number of arrays. There is a certain degree of loss of the array aperture, so a modified DOA estimation algorithm is proposed in this study. Because the actual observations matrix is a complex matrix, the proposed method

L. Tong (✉)
Department of Communication Engineering, The First Institute of Air Force,
Xinyang, 464000 Henan, China
e-mail: 1007913296@qq.com

makes the original data and its anti-conjugated matrix [3] together. This is equivalent to double the length of the data being used. It greatly improves the performance of the DOA estimation by taking full use of the self-correlation and cross-correlation information between the original data matrix and the conjugate matrix.

3.2 Signals Model

Consider a uniform linear array of N sensors receiving $K(K<N)$, and signals with same frequency are independent. The first sensor is reference sensor, the distance of sensors is d, and the incident angles are θ_k $(k = 1, \ldots, K)$, respectively, then the sensor output vector can be represented by

$$X(t) = A(t)S(t) + N(t) \tag{3.1}$$

where $X(t)$ is the $N \times 1$ array output vector, $N(t)$ is the $N \times 1$ sensor noise vector. So, we can get:

$$X(t) = [x_1(t), \ldots, x_N(t)]^T \tag{3.2}$$

$$N(t) = [n_1(t), \ldots, n_N(t)]^T \tag{3.3}$$

$S(t)$ is the $K \times 1$ signal vector

$$S(t) = [s_1(t), \ldots, s_k(t)]^T \tag{3.4}$$

$A(\theta)$ is the $N \times K$ response matrix of the uniform linear array. Suppose every sensor is consistent, then

$$A(\theta) = \left[1, e^{-j2\pi f d \sin \theta_i / c}, \ldots, e^{-j2\pi f d(M-1) \sin \theta_i / c} \right]^T. \tag{3.5}$$

Suppose the receiving noise vector is independent zero-mean vector with identical second-order moment. The noise vector and the signal vector are uncorrelated, then

$$E\left[n(t_1)n^H(t_2)\right] = \sigma^2 I \delta_{t_1 t_2} \tag{3.6}$$

$$E\left[n(t_1)n^H(t_1)\right] = 0 \tag{3.7}$$

The covariance matrix of the output vector can be represented by

$$R = \sum_{k=1}^{K} P_k A(\theta) A^H(\theta) + \sigma_n^2 I \tag{3.8}$$

where P_k is the output power of the output vector, $A(\theta)$ is the response matrix of the uniform linear array, and $\sigma^2_n I$ is the covariance matrix of the noise vector, in which I is the identity matrix.

3.3 Modified Algorithm

Suppose the snapshots matrix is $X(k)$, in the modified MUSIC algorithm [3, 4], $Y(k) = J_M X^*(k)$, where $X^*(k)$ is conjugate of $X(k)$. Suppose J is a $M \times M$ replaced matrix in which all elements are zeros except counter diagonal elements are ones. So, $J_M \cdot J_M = I_M$, in which I is the identity matrix. We can get the correlation matrix of $Y(k)$ as following: $R_{yy} = E[Y(k)Y^H(k)] = J_M R^*_{xx} J_M$.

Taking the average of covariance matrix R_{xx} and R_{yy}, we can obtain the matrix R, that is, $R = (R_{XX} + R_{YY})/2 = (R_{XX} + J_M R^*_{xx} J_M)/2$.

For coherent sources, the new matrix usually has full rank, solving the problem of matrix rank loss, so as to achieve the purpose of de-correlation. Therefore, MMUSIC algorithm is a special case of space-smoothing technology. It is equivalent that the space array is divided into two sub-arrays. The number of each sub-array is equal to the number of original array element. The number of array element is not lost, so the estimation performance for the relevant sources or irrelevant sources is better than original algorithm.

A modified algorithm is proposed which makes use of the matrix reconstruction based on the direct data snapshot matrix. The algorithm flow can be summarized as the following steps:

Step 1: Get the snapshots matrix by the antenna element $X(k)$, then calculate its correlation matrix R_{xx};
Step 2: Take the conjugate inversion matrix of $X(k)$, denote $Y(k)$, $Y(k) = J_M X^*(K)$, construct the new matrix $Z = [X(k)Y(k)]$;
Step 3: Calculate the correlation matrix of Z. Construct the covariance matrix $\hat{R} = [R_{xx}R_{zz}]$;
Step 4: Take the singular value decomposition of covariance matrix and isolate the signal subspace and the noise subspace;
Step 5: Complete the DOA estimation based on MUSIC algorithm.

3.4 Simulation for Narrowband Signals

Suppose that the array is an isotropy uniform linear array, wavelength $\lambda = 1$, array distance $D = 0.4\lambda$, snapshots $T = 1,024$, digital sensor channels $K = 8$. Receiving signals are long-range coherent narrowband signals, and noise is additive white Gauss noise (AWGN). The number of signals $M = 3$. Adopt MUSIC method,

Fig. 3.1 Estimation for far-angle interval at SNR = 20 dB
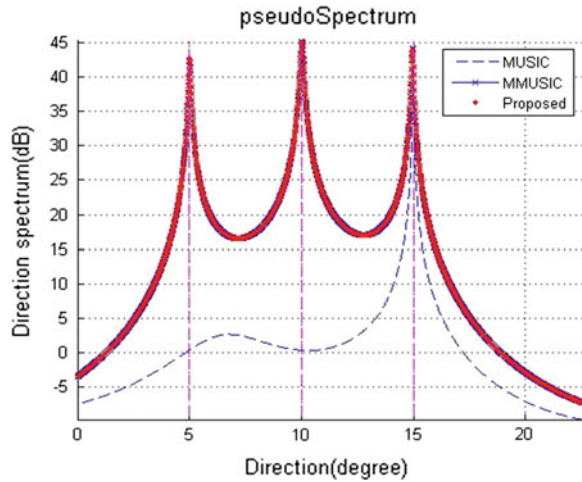
Fig. 3.2 Estimation for close-angle interval at SNR = 20 dB
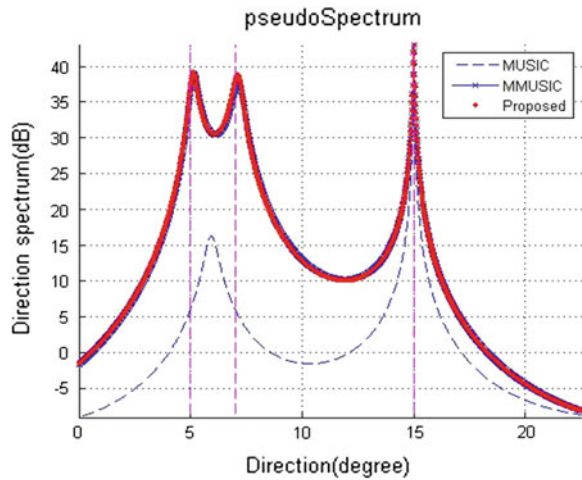
MMUSIC method, and method proposed in this article to estimate the DOA of the signals. The simulation results are as follows.

Experiment 1: The angles of incidence are 5°, 10°, and 15°, respectively. The first two sources are coherent and signal-to-noise ratio for each array element is 20 dB. The simulation result is shown in Fig. 3.1.

Experiment 2: Change the incident angles into 5°, 7°, and 15°, other parameters not changed. The simulation result is shown in Fig. 3.2.

Experiment 3: Reduce signal-to-noise ratio of each array element to 0 dB and keep other parameters not change. The simulation result is shown in Fig. 3.3.

From Figs. 3.1 and 3.2, it can be seen that MUSIC algorithm cannot correctly estimate the DOA for both far or close coherent sources. The modified MUSIC

Fig. 3.3 Estimation for close-angle interval at SNR = 0 dB
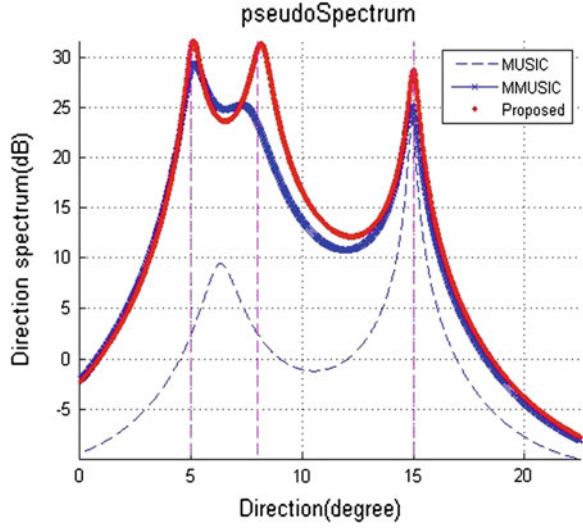
Table 3.1 Estimation mean and standard deviation (Std) of MMUSIC algorithm and this article algorithm

SNR (dB)	MMUSIC algorithm				Algorithm in the article			
	5°		15°		5°		15°	
	Mean	Std	Mean	Std	Mean	Std	Mean	Std
10	5.12	0.0182	15.16	0.0243	4.96	0.0175	15.08	0.0124
5	5.21	0.0843	15.25	0.0612	4.92	0.0723	15.14	0.0536
0	5.47	0.3046	15.47	0.3017	4.83	0.2634	15.23	0.2415
−5	5.81	0.7392	15.78	0.8192	4.64	0.6028	15.42	0.5897

algorithm and the algorithm of this article can estimate the DOA better under the condition of relatively high signal-to-noise ratio. When the signal-to-noise ratio turns worse, for the signal sources with relatively little angle interval, as shown in Fig. 3.3, MMUSIC algorithm is also powerless, and the algorithm in the article is still able to differentiate two close coherent signals sources.

Table 3.1 is the comparison result about the estimation mean and standard deviation of two algorithms [3]. From it, we can see that whether the coherent sources (5°) or non-coherent sources (15°), the DOA estimation performance of the algorithm is better than that of MMUSIC algorithm. Therefore, this algorithm has a good performance in the narrowband signal DOA estimation. In particular, when the signal-to-noise ratio changes worse, it can still identify very close coherent sources.

Fig. 3.4 DOA estimation of
ISM
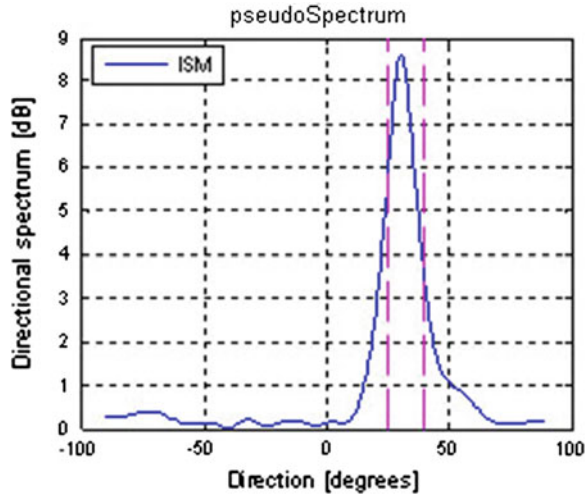
Fig. 3.5 DOA estimation of
CSM
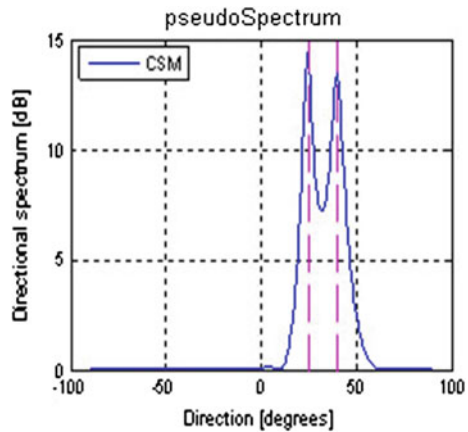
3.5 DOA Estimation for Wideband Signals

Adopting array is isotropy uniform linear array, wavelength $\lambda = 1$, array distance
$D = 0.4\lambda$, snapshots $T = 1,024$, digital sensor channels $K = 8$. Receiving signals
are long-range signals, and noise is normal random noise. The source signals are
coherent wideband signals, which have same carrierFreq $= 3e9$ Hz and
bandwidth $= 2e9$ Hz. The number of signals $M = 2$ and the angles of incidence
are $25°$ and $40°$, respectively, and the sensors SNR is 0 dB. Adopt ISM method,
CSM method, and modified ISM method to estimate the DOA of the signals. The
simulation results show as follows (Figs. 3.4, 3.5, 3.6, 3.7).

Simulation results show that both CSM and modified ISM can estimate the DOA
well except ISM when the signals are coherent wideband signals. The capability of

Fig. 3.6 DOA estimation of proposed ISM
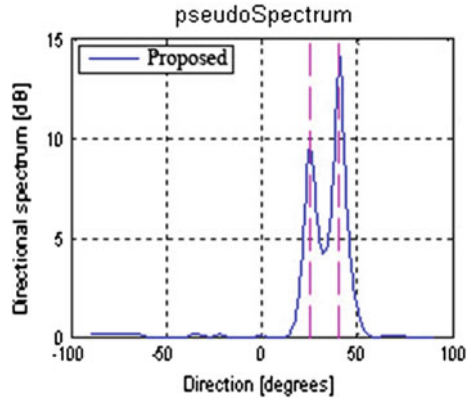
Fig. 3.7 Estimation results comparison between CSM and proposed ISM
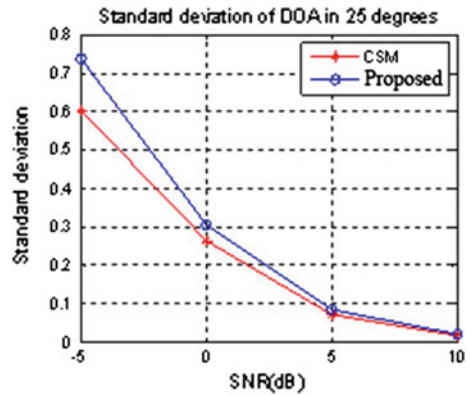
the CSM is better than the modified ISM, but it needs direction pre-estimation and consistent focusing matrix. And it is also easy affected by the signals and needs more computation, so the CSM cannot process the signals in real time. The algorithm proposed in this study does not need these steps and has less computation. The algorithm has the same capability as CSM when the SNR is high enough.

3.6 Conclusion

A de-correlation method is proposed in this study which is based on the snapshot matrix reconstruction. The accuracy is evaluated through simulation in comparison with some conventional methods, and we found that the proposed method is as accurate as the conventional methods and needs smaller computational cost. The simulation results prove that it can be used to complete the DOA estimation for narrowband and wideband coherent signals. For narrowband signals, the algorithm

is superior to the MMUSIC algorithm. And for wideband signals, the performance is below that of CSM algorithm, but because of its less computation, it is more practical to estimate the DOA of wideband coherent signals by the modified ISM in terms of real time. How to realize the algorithm by hardware should be improved as one of future studies.

References

1. Kim KK, Sarkar TK, Wang H et al (2004) Direction of arrival estimation based on temporal and spatial processing using direct data domain (D3) approach. IEEE Trans Antennas Propag 52(2):533–541
2. Salameh A, Tayem N (2006) Conjugate MUSIC for non-circular sources. Proc IEEE Int Conf Acoust Speech Signal Process 4:877–880
3. Cui D, Cong YL, Gu GH (2005) Channel prediction algorithm based on conjugate data rearrangement. J Jilin Univ (Inf Sci Ed) 23(6):574–577
4. Nikolakopoulos KV, Angnostou D, Christodoulou CG (2004) Estimation of direction of arrival for coherent signals in wireless communication systems. Antenna array processing signal. In: IEEE antennas and propagation society international symposium, Monterey, California, vol 1, no 6, pp 419–422

Chapter 4
Efficient Mining Frequent Closed Resource Patterns in Resource Effectiveness Data: The MFPattern Approach

Lihua Zhang, Miao Wang, Qingfan Gu, Zhengjun Zhai and Guoqing Wang

Abstract As the occurrence of failure of electronic resources is sudden, real-time record analysis on the effectiveness of all resources in the system can discover abnormal resources earlier and start using backup resources or restructure resources in time, thus managing abnormal situations and finally realizing health management of the system. This paper proposed an algorithm for mining frequent closed resource patterns from data effectiveness matrix with the method of column extension: *MFPattern*, which uses effective pruning strategies to guarantee the mining of all frequent closed patterns without producing candidate item-sets. Different from the traditional frequent closed pattern, *MFPattern* algorithm can mine resource combination patterns with all resources very effective during work, those with simultaneous failure of resources and combination patterns in which some resources are very effective while some other resources have failure. The experimental result shows that this algorithm has a higher mining efficiency than existing mining methods of frequent closed pattern.

Keywords Frequent pattern · Closed · Resource

L. Zhang · Z. Zhai · G. Wang
School of Computer Science and Engineering, Northwestern Polytechnical University, YouYiXiLu 127, Xi'an 710072, China

L. Zhang · M. Wang (✉) · G. Wang
Science and Technology on Avionics Integration Laboratory, Guiping Road 432, Shanghai 200233, China
e-mail: wang_miao@careri.com

M. Wang · Q. Gu · G. Wang
China National Aeronautical Radio Electronics Research Institute, Guiping Road 432, Shanghai 200233, China

4.1 Introduction

Resources are the physical support of system. The effectiveness of resources will directly influence the effectiveness of the system. Due to the influence of environmental factors and performance degradation of materials, electronic resources in the system will inevitably experience a process of capability loss. The influence of external stress in the process of system operation might cause acceleration of the degradation process of electronic resources and even damage and failure in extreme situations. Due to the aggravation of degradation, if not found in time, resource damage might finally cause system failure. Therefore, research on resource effectiveness is the footstone of prognostics and health management [1] of the system. As the occurrence of failure of electronic resources is sudden, real-time record analysis on the effectiveness of all resources in the system can discover abnormal resources earlier and start using backup resources or restructure resources in time, thus managing abnormal situations and finally realizing health management of the system.

Due to the great number of resources in system and the huge size of effectiveness value matrix of resources sampled in a period of time, how to mine the required resource pattern from these data efficiently is vital for health management of the system. Data mining technology widely used currently can mine various required knowledge from a lot of complex data. Frequent pattern mining [2, 3] is an important branch of data mining technology. This method can mine patterns meeting some rule and occurring frequently from huge data. However, this method has a disadvantage, i.e., existence of excessive redundancy modes. References [4, 5] reduce redundancy modes with the method of mining with frequent closed pattern. An important feature of frequent closed pattern algorithm is reserving and detecting strategies with candidate item. However, when there is a great number of item-sets in data set, it will produce a lot of candidate item-sets and thus cause the breakdown of internal memory. Therefore, *BIDE* [6] algorithm put forward by Han et al. uses precursor detection method to avoid frequent item reservation, thus improving the mining efficiency. However, when the data set is sparse, the method of precursor detection has a low pruning efficiency, thus increasing the complexity of the algorithm. *WIBE* [7] algorithm put forward by Wang et al. judges frequent closed pattern based on item-set weight information detection. If all items in the current candidate item-set have the same weight, this pattern is the subset of a frequent closed gene pattern that has been output and can be pruned. However, if the data set is large or sparse, this algorithm needs to store a lot of weight information in the internal memory, thus influencing its efficiency and causing the breakdown of internal memory. Cong et al. [8] and Pan et al. [9] put forward a sample enumeration method of exploring enumeration space through recursive establishment and transposition of project database. Due to the lack of effective pruning strategy, the mining efficiency of this algorithm will be influenced when there is a great number of samples.

To discover abnormality or failure in time, there should not be excessive sampling sites when the effectiveness value of resources is collected. There are two reasons as follows: (1) excessive sampling sites will influence the mining efficiency of the algorithm, thus causing the failure to report abnormal situations of resources in time; (2) excessive sampling sites will influence the real-time property of the system, thus causing the failure to ensure normal operation of the system and finally influencing the health of the whole system. Based on the analysis above, this paper proposes an algorithm: *MFPattern*, for mining frequent closed resource pattern from resource effectiveness matrix with the method of column extension. To improve the mining efficiency, this algorithm uses effective pruning strategies to ensure the mining of all frequent closed patterns without producing candidate item-set. *MFPattern* algorithm can mine the following three patterns: (1) resource combination pattern with very effective resources during system operation; (2) resource combination pattern with simultaneous failure of resources during system operation; and (3) resource combination pattern in which some other resources will inevitably have failure during efficient operation of some resources.

4.2 Problem Description

Resource effectiveness matrix is defined as a two-dimensional real matrix $D = R \times S$. Here, row collection R represents the resource name; column collection S refers to different sampling sites. Element D_{ij} of matrix D is a real number which refers to the effective value (e.g., BIT value) of resource i under sampling j. $|R|$ is the number of resources in data set D, and $|S|$ is the number of sampling sites in data set D. For the convenience of mining, the original effective value in resource effectiveness matrix is generally discretized into 1, -1 and 0, where 1 represents resource health, 0 represents sub-health and -1 represents resource failure, as shown in Table 4.1. The relationship between two resources R_1 and R_2 can be defined as follows:

1. If R_1 and R_2 are both very effective (value $= 1$), they have effective positive correlation, expressed as R_1R_2. The support degree is $\sup(R_1R_2) = \frac{|R_1R_2|}{|S|}$, where $|R_1R_2|$ is the number of sampling sites when R_1 and R_2 are both very effective (the same below);
2. If R_1 and R_2 both have failure (value $= -1$), they have failure positive correlation, expressed as $-R_1-R_2$. The support degree is $\sup(-R_1 - R_2) = \frac{|-R_1-R_2|}{|S|}$.
3. If R_1 is very effective while R_2 has failure, they have effective negative correlation, expressed as $R_1 - R_2$; if R_2 is very effective while R_1 has failure, they also have effective negative correlation, expressed as $-R_1-R_2$; when R_1 and R_2 have effective negative correlation, the support degree is $\sup(R_1 - R_2) = \frac{|R_1-R_2|}{|S|} + \frac{|-R_1R_2|}{|S|}$.

Table 4.1 Discrete resource effectiveness matrix

	S_0	S_1	S_2	S_3	S_4
R_1	1	−1	1	−1	1
R_2	1	−1	1	−1	−1
R_3	0	1	−1	1	1
R_4	1	1	0	1	1
R_5	−1	−1	0	−1	1

Among three relationships above, the first one mines resource combination patterns in which resources are all very effective, i.e., there is a high efficiency when these resources work together; the second one mines resource combination patterns in which resources have failure together; in such patterns, potential reasons of failure can be found and decisions can be made for the use of backup resources; the third one mines resource patterns when some resources are very effective while some other resources have failure, in which potential unstable resources can be found and replaced earlier.

The mining purpose of *MFPattern* algorithm is to mine all frequent closed resource patterns from resource effectiveness data set, i.e., mine resource patterns without superset and with the same support degree which meet the threshold of support degree. To improve the mining efficiency of the algorithm, *MFPattern* algorithm mines frequent closed patterns with column extension without storing candidate set. The mining process of this algorithm will be introduced in detail in the next section.

4.3 MFPattern Algorithm

Most traditional mining methods of frequent closed pattern are based on row extension. However, there are some disadvantages of using row extension as follows: (1) resources might have three relations simultaneously. If the method of row extension is used for mining, the number of resource patterns produced will present 3^n increase in extreme situations, thus increasing the complexity of mining; (2) if there are many resources and a few sampling sites, the use of row extension will increase the number of iterations of the algorithm, thus influencing the time efficiency and space efficiency of the algorithm; (3) as resource sampling is dynamic, with the use of row extension, the support degree of resources will change when the column of original data increases, thus making the design of incremental frequent closed pattern mining algorithm relatively complex. Therefore, *MFPattern* algorithm uses the method of column extension for mining.

As resources in the system are effective in most cases, health management will be conducted in the case of failure. Therefore, the resource effectiveness matrix used in this paper is dense. *MFPattern* will mine frequent closed resource patterns with the method of column extension and precursor detection. The mining process of this algorithm can be divided into two steps: first, make a sample weight graph;

second, mine all frequent closed resource patterns with the method of sample extension.

The method of mining patterns with sample weighted graph was first used in the mining of bicluster in *MicroCluster* algorithm [10]. Then, Wang et al. [11, 12] used sample weight graph to mine bicluster and fault-tolerant bicluster. *MFPattern* algorithm put forward in this paper will use undirected sample relation weight graph (sample weighted graph for short, the same below) to mine frequent closed resource patterns.

Definition 1 Sample weighted graph can be expressed with set $G = \{E, V, W\}$. Each vertex in vertex set V in the weighted graph represents a sampling site; if an edge exists between a pair of vertexes, it means that there are resources with effectiveness relationship under two sampling sites represented by this pair of vertexes. The collection of edge is expressed with E; the weight on each edge is resource collection with effectiveness relationship under two sampling sites connected with this edge. The weight set is expressed with W.

Figure 4.1 shows the sample weighted graph corresponding to Table 4.1. Weight on each edge is expressed as the collection of effective resources under two sampling sites connected with this edge. The effectiveness relationship among resources is obtained through the third relationship among resources defined in Sect. 4.2 of this paper.

Next, we will introduce how *MFPattern* algorithm mine frequent closed resource patterns from sample weight graph in detail. For the convenience of designing effective pruning strategies, *MFPattern* algorithm conducts extension according to the depth-first principle. It is assumed that frequent closed resource patterns are mined from the sample weight graph in Fig. 4.1. First, extend the edge connected with S_0 node, i.e., $S_0 \rightarrow S_0S_1 \rightarrow S_0S_1S_2$; then extend S_1 after the extension of S_0 branch. The support degree of resource pattern under sample $S_0S_1S_2S_3S_4$ is 1; that under samples $S_0S_1S_2S_3$, $S_0S_1S_2S_4$, $S_0S_2S_3S_4$ and $S_1S_2S_3S_4$ is 0.8; that under samples $S_0S_1S_2$, $S_0S_1S_3$,…, and $S_2S_3S_4$ is 0.6. It can be seen from the extension method above that the method based on sample extension has a different process from the mining of frequent closed patterns with resource extension. Mining with resource extension first produces the support degree of two item-sets and then extends to three and four item-sets etc. According to a priori principle, the support degree decreases with the increase in the number of resources in item-set. The size of frequent patterns (the number of resources in the pattern) mined under the same sample branch with the method of sample extension arranges from large to small, and the support degree of pattern increases progressively. As there are only two samples during the extension, with the increase in the number of samples, the number of resources meeting the definition together under the sample must decrease. However, the support degree of resource pattern increases (because the number of samples increases). Therefore, when frequent closed resource patterns are mined based on resource extension, extension can stop as long as the support degree of resource does not meet the threshold value. However, when patterns are mined based on sample extension, it is necessary to continue the extension of

Fig. 4.1 Undirected sample
relational weighted graph
corresponding to Table 4.1
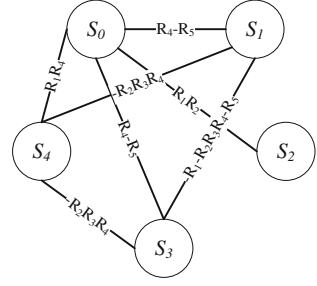
sample set as long as the weight under the sample set extended is not null or not
more than the minimum number of resources defined by users.

Definition 2 P is the current extended resource pattern. If all samples in S_i and
P have a link in the sample weight graph and the number of intersections
(expressed as $S_i.Resources$) of weights of all join edges meets the number defined
by users, S_i is the candidate sample of P.

Definition 3 P is the current extended resource pattern. If S_i and S_j are candidate
samples of P, but S_i has been extended by P and S_j has not been extended by P yet,
for S_j, S_i is precursor candidate sample of P.

It can be known from descriptions of the definition above that, a candidate
sample becomes precursor candidate sample if it has been extended. According to
the principle of mining frequent closed patterns with precursor detection, if the
resource under the current extended sample set is the subset of resources under a
precursor candidate sample or candidate sample, the resource pattern under the
current extended sample must not be frequent closed resource pattern. For
example, assuming that the order of sample extension is from S_0 to S_4, based on the
name. For the current extended sample set S_0S_1, S_3 and S_4 are its candidate samples
and S_2 is its precursor candidate sample (i.e., mining of $S_0S_1S_2$ branch has been
completed). If the current sample to be extended is S_3, for $S_0S_1S_3$, S_2 is its pre-
cursor candidate sample. That is to say, $S_0S_1S_2S_3$ must have been extended before
$S_0S_1S_3$ is extended. If the resource pattern under $S_0S_1S_3$ is a subset of that under
$S_0S_1S_2$, the resource pattern that can be obtained by extension of $S_0S_1S_3$ can
definitely be obtained by extension of $S_0S_1S_2$ as well as $S_0S_1S_2S_3$ (because the
resource pattern under $S_0S_1S_2S_3$ is the same as that under $S_0S_1S_3$ at this time); as
the support degree of $S_0S_1S_2S_3$ is higher than that of $S_0S_1S_3$, $S_0S_1S_3$ can be pruned
according to the definition of frequent closed pattern.

Lemma 1 *Assume that P is the current extended resource pattern, M is the
candidate sample set of P and N is the precursor candidate sample set of P, if a
precursor candidate sample $N_j(N_j \in N)$ making $PM_i.Resource$ a subset of
$PN_j.Resource$ exists for candidate sample $M_i(M_i \in M)$, PM_i. Resource should be
pruned.*

Candidate samples meeting Theorem 1 should be directly pruned and those not meeting pruning conditions should continue extension. However, whether the current extended pattern is output should be judged according to the following output strategy (which actually meets the definition of frequent closed pattern):

Output strategy. Assuming that P is the current bicluster to be extended, M is candidate sample set of P and N is precursor candidate sample set of P; if there is no candidate sample M_i making *P.Resource* a subset of *PM_i.Resource* for all candidate samples $M_i(M_i \in M)$ of P (subset means equivalence), *P.Resource* can be output.

Based on the analysis above, *MFPattern* algorithm can directly mine frequent closed resource pattern with the method of column extension without storing candidate frequent pattern in internal memory. Figure 4.2 illustrates the mining process of *MFPattern* algorithm. Example data are shown in Table 4.1, the threshold of support degree is 0.4 and the minimum number of resources in pattern is 2.

```
Algorithm 1: MFPattern algorithm
Input: threshold of support degree: r_min; resource effec-
tiveness data: D
Output: all frequent closed resource patterns meeting the
threshold value
Initial value: sample weight graph: G = Null; current bi-
cluster to be extended Q = Null, S_i = Null, S_j = Null
Algorithm description: MFPattern (r_min, D, Q, S_i, S_j)
```

(1) If G is null, scan data set D and make its weight graph. S_i is the first sample in the weight graph;
(2) For each sample S_j connected with sample S_i,
(3) If all resource linked lists in S_j meet pruning conditions,
(4) Continue;
(5) Else
(6) For resource linked lists not meeting pruning conditions, $Q.Sample = Q.Sample \cup S_j; Q.Resource = Q.Resource \cap S_iS_j.Resource$;
(7) MFPattern (r_{min}, D, Q, S_i, $S_j \rightarrow$next);
(8) endif
(9) endfor
(10) if Q meets output conditions, then
(11) Output Q;
(12) endif;
(13) $S_i = S_i \rightarrow$next;
(14) return
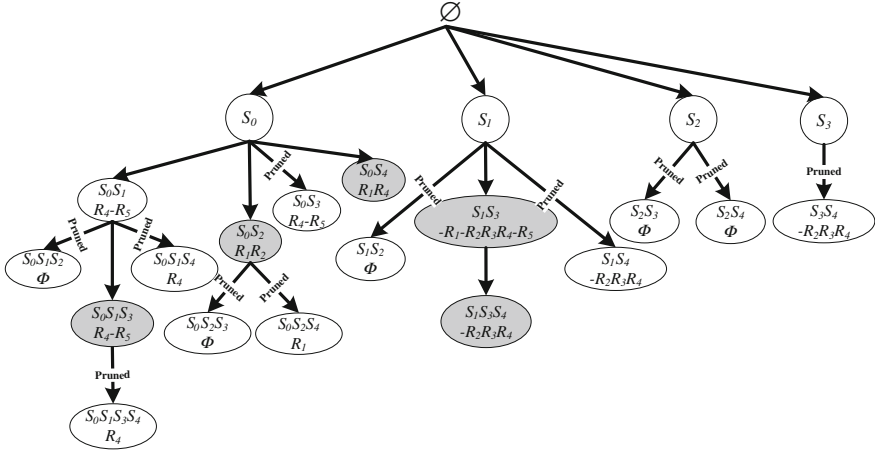
Fig. 4.2 Example mining process of MFPattern algorithm

4.4 Experimental Result and Analysis

In this section, we will make an experimental comparison on the mining efficiency and result of the algorithm above and existing algorithms. The hardware environment of the experiment is desktop computer: Intel(R) Core(TM)2 Duo 2.53 GHz CPU and 4G internal memory; the software environment is Microsoft Windows 7 SP1 operating system; the algorithm programming and operating environment is Microsoft Visual C++ 6.0 SP6. Experimental data used in this paper are simulation data. To fully test the performance of the algorithm, we generate six data sets randomly. Each data set contains 35 sampling sites and 800 resources. Table 4.2 describes the proportion of 1, 0 and −1 in each row in each data set.

In this section, *MFPattern* algorithm will be compared with *MFPattern* algorithm without pruning (expressed as *MFPattern_nonpruning*), *Backward Checking* algorithm, *WIBE* algorithm and *WIBE2* algorithm. *MFPattern_nonpruning* algorithm uses the same mining method as *MFPattern* algorithm, i.e., mine frequent closed patterns with the method of column extension. Different from *MFPattern* algorithm, *MFPattern_nonpruning* algorithm does not use pruning strategies described in Theorem 1, but mines with the method of full extension. *Backward Checking* algorithm uses precursor detection method described in Ref. [6] and mines frequent closed patterns without storing frequent item-sets. *WIBE* algorithm uses pruning strategies described in Ref. [7] and can mine frequent closed patterns without storing candidate set. *WIBE2* algorithm uses the same pruning strategies as *WIBE* algorithm to mine frequent closed patterns. Different from *WIBE* algorithm, *WIBE2* algorithm uses coexpression support degree for mining.

The mining efficiency of five algorithms above will be compared. To fully compare the extendibility of algorithms, we produce multiple groups of data sets

Table 4.2 Distribution of numerical value proportion in six data sets

	1	0	−1
D_1	0.4	0.2	0.4
D_2	0.4	0.3	0.3
D_3	0.5	0.2	0.3
D_4	0.4	0.4	0.2
D_5	0.5	0.3	0.2
D_6	0.5	0.25	0.25
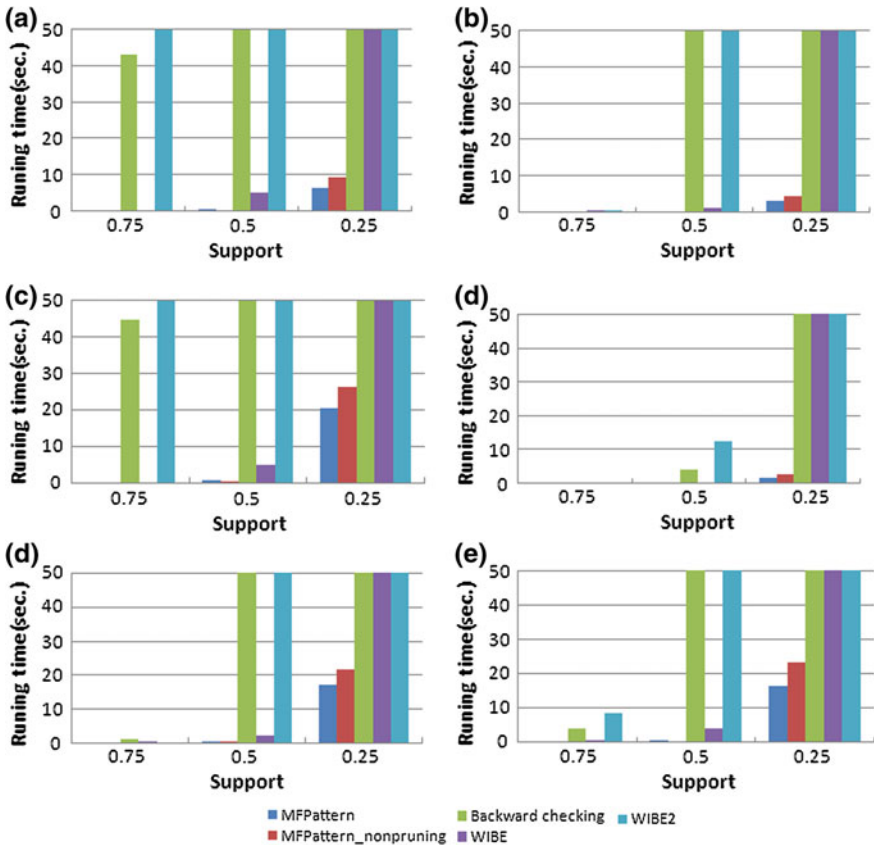
Fig. 4.3 Comparison of operating time of five algorithms under different data sets with 200 resources and 20 sampling sites: **a** D_1, **b** D_2, **c** D_3, **d** D_4, **e** D_5, **f** D_6

with different numbers of resources and sampling sites in allusion to six data sets in Table 4.2. Resources and sampling sites are selected according to the order of resources and sampling sites in data sets. Figure 4.3a–f provides the comparison of operating time of five algorithms above under different data sets with 200 resources and 20 sampling sites. It can be seen from these figures that *MFPattern*

and *MFPattern_nonpruning* algorithms can complete the mining process within 1 s and have higher mining efficiency than other algorithms when the support degree is 0.75 and 0.5 under each data set. As *Backward Checking* algorithm judges frequent closed patterns with the method of precursor detection, when the data set is dense (the proportion of 0 is low), it is necessary to frequently use precursor detection strategy. Thus, the mining efficiency is low. Therefore, even when the support degree is 0.75, *Backward Checking* algorithm cannot complete the mining process in limited memory space under dense D_1 and D_3 data sets. When the support degree is 0.5, *Backward Checking* algorithm can only complete the mining process under data set D_4 with the lowest density of data. When the support degree is 0.25, only *MFPattern* and *MFPattern_nonpruning* algorithms can complete the mining process and other three algorithms cannot complete mining in limited memory space. As more frequent closed patterns can be produced when the support degree is low, pruning strategies used in *MFPattern* algorithm can reduce the mining space of the algorithm. Thus, it has a higher mining efficiency than *MFPattern_nonpruning* algorithm. It is thus clear that the mining of frequent closed patterns with column extension is highly efficient, and meanwhile pruning strategies used in *MFPattern* algorithm can improve the mining efficiency of the algorithm.

4.5 Conclusion

This paper proposed an algorithm mining frequent closed resource patterns from data effectiveness matrix with the method of column extension: *MFPattern*, which uses effective pruning strategies to guarantee the mining of all frequent closed patterns without producing candidate item-sets. Different from the traditional frequent closed pattern, *MFPattern* algorithm can mine resource combination patterns with all resources very effective during work, those with simultaneous failure of resources and combination patterns in which some resources are very effective while some other resources have failure. The experimental result shows that this algorithm has a higher mining efficiency than existing mining methods of frequent closed pattern. However, mining on discrete data will cause the loss of original data information. Our next research direction is to mine frequent closed patterns related to resource health from true resource effectiveness data.

References

1. Pecht M et al (2010) A prognostics and health management roadmap for information and electronics-rich systems. Microelectron Reliab 50:317–323
2. Han J, Pei j, Mortazavi-Asl B, Chen Q, Dayal U, Hsu M-C (2000) FreeSpan: frequent pattern-projected sequential pattern mining. In: Proceeding of 2000 ACM SIGKDD international conference knowledge discovery in databases (KDD'00), pp 355–359
3. Pei J, Han J (2004) Mining sequential patterns by pattern-growth: the prefixspan approach. IEEE Trans Knowl Data Eng 6(10):1–17
4. Pasquier N, Bastide Y, Taouil R, Lakhal L (1999) Discovering frequent closed itemsets for association rules. In: Beeri C et al (eds) Proceedings of the 7th international conference on database theory. Springer, Jerusalem, p 398–416
5. Pei J, Han J, Mao R (2000) CLOSET: an efficient algorithm for mining frequent closed itemsets. In: Gunopulos D et al (eds) Proceedings of the 2000 ACM SIGMOD international workshop on data mining and knowledge discovery. ACM Press, Dallas, p 21–30
6. Wang, J, Han, J (2004) BIDE: efficient mining of frequent closed sequences. In: Proceedings of data engineering, 2004, p 79–90
7. Wang M, Shang X, Diao J, Li Z (2010) WIBE: mining frequent closed patterns without candidate maintenance in microarray dataset. In: DMIN, pp 200–205
8. Cong G, Tan K, Tung A et al (2004) Mining frequent closed patterns in microarray data. In: ICDM'04. IEEE press, p 363–366
9. Pan F, Cong G, Tung K, Yang J, Zaki M (2003) Carpenter: finding closed patterns in long biological datasets. In: Proceedings of the ACM SIGKDD international conference on knowledge discovery and data mining (KDD), pp 637–642
10. Zhao L, Zaki MJ (2005) MicroCluster: an efficient deterministic biclustering algorithm for microarray data. IEEE Intell Syst 20(6):40–49 (special issue on Data Mining for Bioinformatics)
11. Wang M, Shang X, Miao M, Li Z, Liu W (2011) FTCluster: efficient mining fault-tolerant biclusters in microarray dataset. In: Proceedings of ICDM 2011 workshop on biological data mining and its applications in healthcare, p 1075–1082
12. Wang M, Shang X, Zhang S, Li Z (2010) FDCluster: mining frequent closed discriminative bicluster without candidate maintenance in multiple microarray datasets. In: ICDM 2010 workshop on biological data mining and its applications in healthcare, p 779–786

Chapter 5
Efficient Mining Maximal Trend Biclusters in Real-Valued Resource Effectiveness Matrix: The CeCluster Algorithm

Lihua Zhang, Miao Wang, Qingfan Gu, Zhengjun Zhai and Guoqing Wang

Abstract The efficiency of resources is the footstone for building prognostics and health management system or safety system. In this study, we proposed an efficient bicluster mining algorithm: *CeCluster* algorithm, which mines trend bicluster in real-valued resource effectiveness matrices. To improve the mining efficiency, *CeCluster* algorithm mines maximal trend bicluster using the method of column extension and multiple pruning strategies without candidate maintenance. *CeCluster* algorithm can not only mine resource patterns with effectiveness in the downtrend, but also mine those with effectiveness in the uptrend. *CeCluster* algorithm can also mine resource patterns without change of effectiveness. The experimental result shows our algorithm is efficient than traditional algorithm.

Keywords Trend bicluster · Real-valued · Resource

5.1 Introduction

The level of efficiency of resources directly influences the effectiveness of the whole system. However, resource damage might cause some deficiencies of the system. Therefore, studying the level of efficiency of resources is the footstone for

L. Zhang · Z. Zhai · G. Wang
School of Computer Science and Engineering, Northwestern Polytechnical University, YouYiXiLu 127, Xi'an 710072, China

L. Zhang · M. Wang (✉) · G. Wang
Science and Technology on Avionics Integration Laboratory, Guiping Road 432, Shanghai 200233, China
e-mail: wang_miao@careri.com

M. Wang · Q. Gu · G. Wang
China National Aeronautical Radio Electronics Research Institute, Guiping Road 432, Shanghai 200233, China

building prognostics and health management system [1]. It can be found which resources have a lower effective rate through real-time recording of the effectiveness of all resources in the system and frequent pattern mining for resource effectiveness matrix in a period of time or analysis on rules of resource relevancy, which helps to discover incorrect resources in advance and thus start using standby resources earlier. However, some resources are normal in a period of time, i.e., meet the threshold value of support degree or confidence degree, but might present a downtrend of effectiveness in a certain period. For example, when the system implements a certain function in a short period, the implementation of this function will make some resources present an unhealthy state. Earlier discovery of such fault helps to conduct health management over potential faults and thus reduce the risk of poor health of the system.

The feature of resource pattern with the effectiveness presenting some trend described above meets the feature of bicluster mining in data mining technology. Bicluster was first put forward by Cheng and Church [2] and used to find co-expression gene under specific experimental conditions in gene expression data. This algorithm uses a low square-root residue to gradually delete redundant nodes. Many algorithms based on greedy strategy were proposed afterward [3–5]. Various algorithms above use the following two mining strategies—first, produce clustering globally according to the traditional clustering method and then optimize it gradually; second, mine biclusters, respectively, in two categories of data and then obtain the result through comparison and integration. However, neither strategy produces a high time efficiency of algorithm. First, bicluster is an NP-hard problem [6]; second, while processing original data, bicluster needs to solve the problem of sensitivity of original data to noise. Meanwhile, bicluster algorithm should allow the overlap among clusterings, which increases the computation complexity of bicluster algorithm; finally, as bicluster algorithm directly processes original data, it should have a very strong flexibility for different types of bicluster.

To improve the mining efficiency of bicluster algorithm, Wang et al. [6, 7] mine maximal bicluster using sample-growth method in discrete data. However, the algorithm above can only mine biclusters meeting gene co-expression relation but cannot be used to mine trend bicluster. Based on the analysis above, this study proposes an effective bicluster mining algorithm: *CeCluster* algorithm to mine trend bicluster in real-valued resource effectiveness matrix. To improve the mining efficiency, both algorithms mine maximal trend bicluster using the method of column extension and multiple pruning strategies without candidate maintenance. Meanwhile, *CeCluster* algorithm can not only mine resource patterns with effectiveness in the downtrend, but also mine those with effectiveness in the uptrend, thus providing further decision support for later decision support system. *CeCluster* algorithms can also mine resource patterns without change of effectiveness. Meanwhile, it can mine multiple biclusters: (1) basic trend bicluster with uptrend or downtrend considered; (2) traditional constant row bicluster, i.e., without variation trend; (3) bicluster with ratio relationship among columns; (4) bicluster with certain difference relationship among columns.

5.2 Problem Description

Resource effectiveness matrix shown in Table 5.1 is defined as a two-dimensional real matrix $D = R \times S$. Here, row collection R represents the resource name; column collection S refers to different sampling sites. Element D_{ij} of matrix D is a real number which refers to the effective value (BIT value) of resource i under sampling j. $|R|$ is the number of resources in data set D, and $|S|$ is the number of sampling sites in data set D. Bicluster B means that resource in R meets some trend definition in the sampling site in S. Assuming that M is the collection of all biclusters in D, when and only when $N = K \times L(N \in M)$ and another bicluster $P = S \times T(P \in M)$ making $K \subseteq S$ and $L \subseteq T$ does not exist, N is called as the maximal bicluster in M. A bicluster B can be defined as *Samples(Resources)*, where *Resources* refer to the collection of resources in B. It can also be expressed as *B.Resources*; *Samples* refer to the collection of sampling sites, where these resources meet the trend definition, which can also be expressed as *B.Samples*.

The form of mining result of *CeCluster* algorithm is the same variation trend of all resources within some consecutive sampling site, i.e., trend bicluster. As long as the variation in resource effectiveness exceeds certain threshold, it is considered as uptrend or downtrend as long as both resources present uptrend or downtrend. Similarly, if the variation in resource effectiveness is within the constraining range of certain threshold, it is considered as invariance trend. In conclusion, Definition 1 provides how to define the trend of resources in actual resource effectiveness matrix.

Definition 1 Assuming that values of resource R_1 in two consecutive samples S_1 and S_2 are expressed as V_1 and V_2, the trend of resource R_1 in S_1 and S_2 can be defined as:

1. If $\frac{V_2 - V_1}{\min\{V_2, V_1\}} \geq \alpha$, resource R_1 present uptrend between S_1 and S_2;
2. If $\frac{V_2 - V_1}{\min\{V_2, V_1\}} \leq -\alpha$, resource R_1 present downtrend between S_1 and S_2;
3. If $-\beta \leq \frac{V_2 - V_1}{\min\{V_2, V_1\}} \leq \beta$, resource R_1 present invariance trend between S_1 and S_2.

According to four relations defined above, there are two types of resource pattern in bicluster mined with *CeCluster* algorithm: first, positive correlation or negative correlation among resources; second, uniform correlation among resource. In conclusion, the mining with *CeCluster* algorithm aims at mining all maximal biclusters meeting conditions in Definition 1 in real-valued resource effectiveness matrix. To improve the mining efficiency of the algorithm, *CeCluster* algorithm will use sample growth and multiple pruning strategies for mining without candidate maintenance. The specific mining process will be introduced in the next section.

Table 5.1 Real-valued resource snapshot matrix

	S_1	S_2	S_3	S_4	S_5	S_6
R_1	0.73	0.81	0.9	1	0.89	0.77
R_2	0.62	0.71	0.83	0.69	0.68	0.71
R_3	0.2	0.3	0.38	0.45	0.38	0.2
R_4	0.62	0.54	0.3	0.39	0.4	0.41
R_5	0.8	0.9	0.6	0.68	0.69	0.72
R_6	0.98	0.87	0.79	0.68	0.75	0.84

5.3 CeCluster Algorithm

As there are two types of resource pattern in bicluster mined with *CeCluster* algorithm—positive or negative correlation among resources and uniform correlation among resources, if the method of resource extension is used for mining, it is necessary to first calculate the sample set of each resource meeting the requirement of trend definition under all samples and then calculate the intersection of the same sample sets for resource extension, which will increase the complexity of the algorithm. Meanwhile, high number of resources will also influence the mining efficiency of the algorithm. Moreover, excessive resource trend sample information produced in step 1 will also cause a low mining efficiency during the calculation of intersection for resource extension. Therefore, *CeCluster* algorithm mines trend bicluster from resource effectiveness matrix with the method of sample growth. In addition, the method of sample growth can also be specific to certain function or subsystem implementation period, i.e., mine resource collections with the same trend within a certain consecutive sample interval for the convenience of analysis on resource effectiveness by decision supporting system. The mining process of *Ce-Cluster* algorithm can be divided into two steps: first, construct a sample-weighted graph; second, mine all maximal trend biclusters with sample-growth method.

The trend of all resources between some pair of adjacent samples can be obtained from Definition 1. Then, the trend relationship between two or among more resources can be obtained according to Definition 1. Thus, the relationship between resources in real-resource effectiveness matrix can be obtained. After making clear the relationship of resources between samples, *CeCluster* algorithm makes a sample weight graph. Different from the mining of bicluster with the traditional sample-growth method, the trend in trend bicluster is produced under consecutive time sample. Therefore, it is only necessary to build the weight on S_i and S_{i+1} edges when constructing the sample relational weighted graph. According to the analysis above, at most two groups of resource information exist simultaneously on the weight of each edge. In one of the group, resources have positive or negative correlation. In the other group, resources present invariance trend, i.e., uniform correlation. The sample-weighted graph corresponding to Table 5.1 is shown in Fig. 5.1 where '0' refers to resource collection with positive or negative correlation among resources and '1' refers to resource collection with invariance trend among resources.
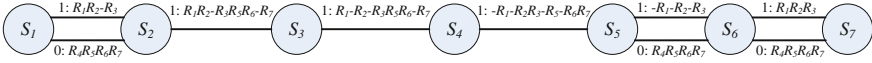
Fig. 5.1 Sample weight graph corresponding to Table 5.1

Then, *CeCluster* algorithm uses the method of sample growth to mine maximal trend bicluster from the sample-weighted graph made. As resources in bicluster mined with this algorithm have trend consistency, all resources in trend bicluster have a consistent relationship in all adjacent samples. That is to say, the variation trend of resources in bicluster is the same in all adjacent samples. Trend bicluster mined with *CeCluster* algorithm has the following three extension modes: (1) If it is positive correlation in initial two adjacent samples, it should be positive correlation or uniform correlation in all subsequent adjacent samples; (2) if it is negative correlation in initial two adjacent samples, it should be negative correlation or uniform correlation in all subsequent adjacent samples; (3) if it is uniform correlation in initial two adjacent samples, it should be uniform correlation or non-uniform correlation (positive or negative correlation) existed between two adjacent samples at first in all subsequent adjacent samples.

It can be seen from the analysis above that multiple groups of resource collection meeting the definition of resource trend will exist in a group of same sample collection. Therefore, multiple groups of resource collection meeting the definition will be produced in real time during sample growth. Thus, multiple groups of trend bicluster can be mined with the method of sample growth, thus improving the mining efficiency of the algorithm. To improve the mining efficiency, *CeCluster* algorithm mines maximal bicluster without candidate maintenance. Pruning strategies used by this algorithm are designed based on the method of prior candidate sample detection, i.e., if the weight of the current candidate sample is the subset of a prior candidate sample weight, trend bicluster obtained by the extension of weight of the current candidate sample can be obtained by the extension of weight of a prior candidate sample. Therefore, the weight of the current candidate sample can be pruned. Based on the analysis above, Lemma 1 can ensure that *CeCluster* algorithm can prune candidate sample without candidate maintenance.

Lemma 1 *Assuming that P is the current bicluster to be extend, M is the candidate sample set of P and N is the prior candidate sample set of P, if a prior candidate sample $N_j(N_j \in N)$ making $PM_i.Resource$ a subset of $PN_j.Resource$ exists for candidate sample $M_i(M_i \in M)$, the bicluster obtained by extension of PM_i is a subset of that obtained by extension of PM_iN_j.*

However, candidate sample might have multiple weights. Only when all weights in the candidate sample are pruned, this candidate sample can be pruned. Based on the lemma above, *CeCluster* algorithm uses the following two pruning strategies for pruning of candidate sample, thus improving the mining efficiency of the algorithm.

Pruning 1 Assuming that *P* is the current bicluster to be extended, *M* is candidate sample set of *P* and *N* is prior candidate sample set of *P*, if a prior candidate
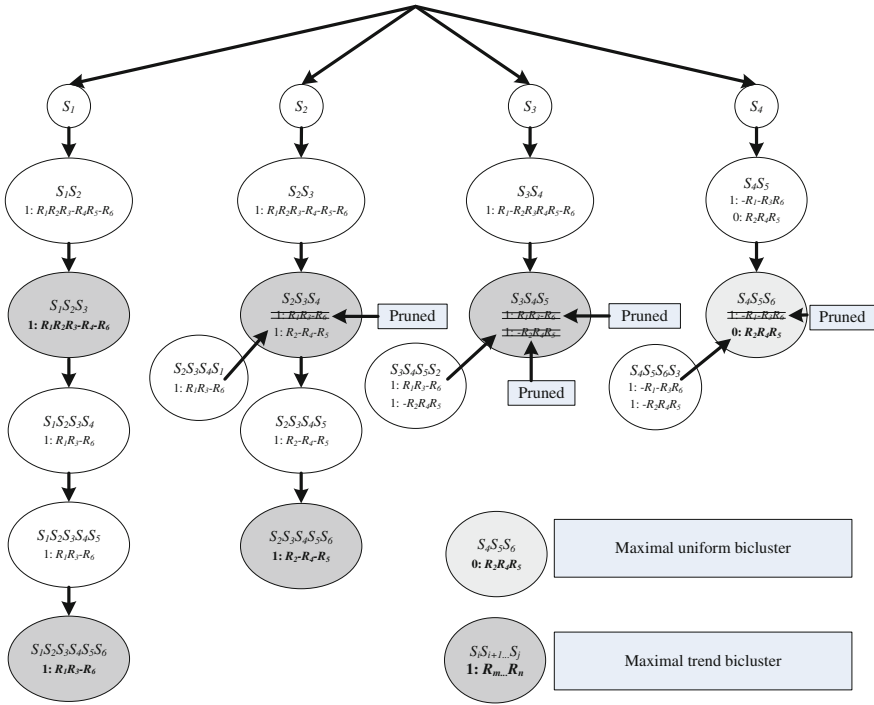
Fig. 5.2 Example mining process of *CeCluster* algorithm

sample $N_j(N_j \in N)$ making $PM_i.Resource$ a subset of $PN_j.Resource$ exists for candidate sample $M_i(M_i \in M)$, $PM_i.Resource$ should be pruned.

Pruning 2 Assuming that P is the current bicluster to be extended, M is candidate sample set of P and N is prior candidate sample set of P, if a prior candidate sample $N_j(N_j \in N)$ making $PM_i.Resource_m$ a subset of $PN_j.Resource$ exists in all $PM_i.Resource_m$ ($m = 1, 2, \ldots, n$) for candidate sample $M_i(M_i \in M)$, PM_i should be pruned.

Those meeting pruning conditions should be directly pruned and those not meeting pruning conditions should continue extension. However, whether the current extension mode is output should be judged according to the following output strategy (which actually meets the definition of maximal bicluster):

Output strategy. Assuming that P is the current bicluster to be extended and M is candidate sample set of P, if P has n weights and $P.Resource_m$ ($m = 1, 2, \ldots, n$) does not have a candidate sample $M_i(M_i \in M)$, making $P.Resource_m$ a subset of $PM_i.Resource$ (does not meet maximal definition), $P.Resource_m$ can be output.

Based on the analysis above, this algorithm can directly mine maximal trend bicluster with the method of column extension without storing the frequent pattern of candidate in internal memory. Figure 5.2 illustrates the mining process of *CeCluster* algorithm. Example data are shown in Table 5.1.

```
Algorithm: CeCluster algorithm
Input: threshold of trend: α, threshold of uniform: β,
resource effectiveness data: D
Output: all maximal trend biclusters meeting the
threshold
Initialization: sample weight graph: G =Null, current
bicluster to be extended Q =Null, Sᵢ=Null and Sⱼ=Null.
Algorithm description: CeCluster(α, β, D, Q, Sᵢ, Sⱼ)
  (1) If G is null, scan data set D and make its weight
graph. Sᵢ is the first sample in the weight graph;
  (2) For each sample Sⱼ connected with sample Sᵢ,
  (3) If all resource linked lists in Sⱼ meet pruning
conditions,
  (4)    Continue;
  (5) Else
  (6)    For resource linked lists not meeting pruning
conditions, Q.Sample= Q.Sample∪Sⱼ; Q. Resource=
Q.Resource∩SᵢSⱼ.Resource;
  (7)       CeCluster(α, β, D, Q, Sᵢ, Sⱼ);
  (8)    Endfor
(9) Endif
  (10) If Q meets output conditions and threshold,
  (11)   Output Q;
  (12) Endif;
  (13) Sᵢ = Sᵢ->next;
  (14) Return
```

5.4 Experimental Results

In this section, we will make an experimental comparison on the mining efficiency and result of the algorithm above and existing algorithms. The hardware environment of the experiment is desktop computer: Intel(R) Core(TM)2 Duo 2.53 GHz CPU and 4G internal memory; the software environment is Microsoft Windows 7 SP1 operating system; the algorithm programming and operating environment is Microsoft Visual C++ 6.0 SP6. Experimental data used in this study are simulation data. The method of data generation in block is used: Some region is set as uptrend (or downtrend or uniform trend) and all resources R in this region present uptrend (or downtrend or uniform trend). The data set contains 20 sampling sites and 800 resources. Table 5.2 describes the distribution of each sub-block in the data set, and the proportion of each sub-block is random.

In this section, a comparison will be made on the operating efficiency of *Ce-Cluster* algorithm and *TCBicluster* algorithm [8] (*TCB* for short) and *CeCluster* algorithm without using pruning strategies. Figure 5.3a–d provides the comparison of operating time of three algorithms above with different parameters and the

Table 5.2 The distribution
of each sub-block

1-200	uptrend	random
201-400	random	downtrend
401-600	random / uniform trend / random	
601-800	random	

number of resources, respectively, 200, 400, 600, 800, and 1,000. It can be seen
from these figures that the mining time of these three algorithms increases pro-
gressively with the increase in the number of resources in data set. Meanwhile, the
mining efficiency of *CeCluster* algorithm is higher than that of the other two
algorithms under each data size. In particular, when the number of resources in
data source is high, the mining efficiency of *CeCluster* algorithm is almost 1,000
times higher than that of *TCB* algorithm. The reason is that the pruning strategy
used by *TCB* algorithm has a lower efficiency. With the increase in the number of
resources in data set, this algorithm needs more pruning judgments to mine all
biclusters meeting the threshold constraint. However, due to low success rate of
pruning, the cost of pruning judgment is too high, thus influencing the mining
efficiency of the algorithm. *CeCluster* algorithm uses high-efficiency pruning
strategies for mining and will produce more maximal biclusters, especially, when
the number of resources in data set is high and data are dense. Thus, the pruning
efficiency of *CeCluster* algorithm will be higher.

Then, we use mean square error (MSE) [2] to measure the difference degree of
the model. Mean square error can be used to measure the relevancy of a group of
resources in a group of sampling sites. Lower score of mean square error indicates
lower difference degree and high relevancy of resources in a group of consecutive
sampling sites. Assuming that I and J are, respectively, the collection of all
sampling sites in a group of resources and data set, and D_{ij} is the real value of
resource i in sampling site j. The score of mean square error of this group of
resources in all sampling sites can be calculated by the following formula.
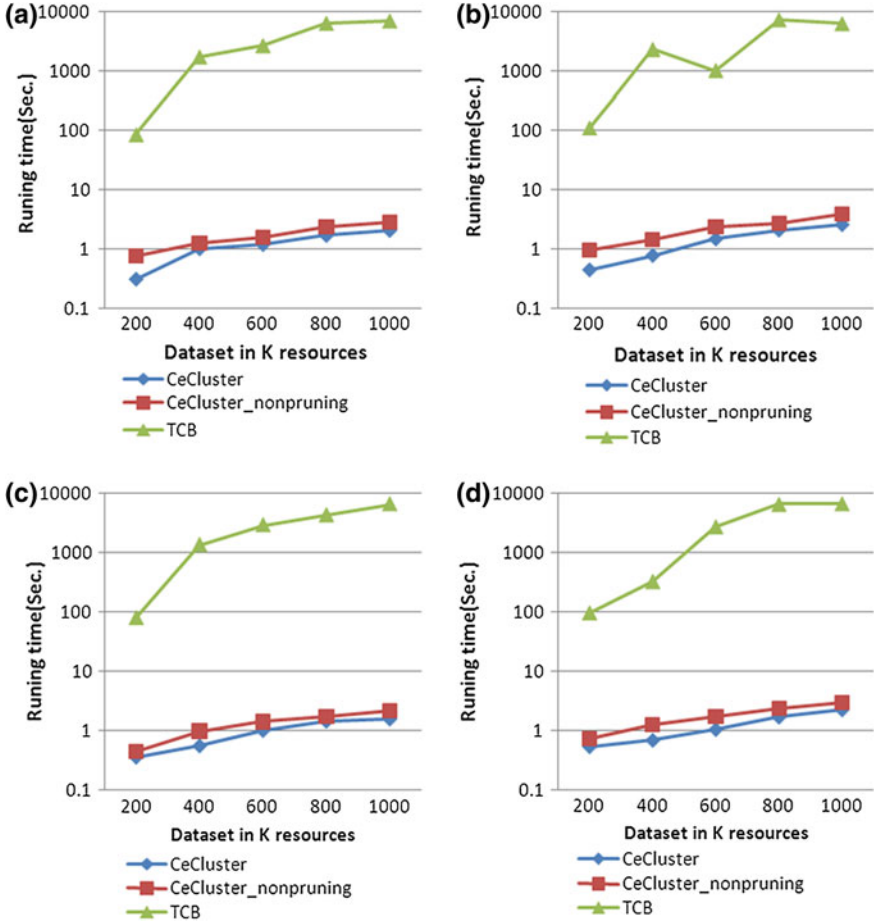
Fig. 5.3 Comparison of operating time of three algorithms under different parameters: **a** α = 0.2, β = 0.03; **b** α = 0.2, β = 0.06; **c** α = 0.3, β = 0.03; **d** α = 0.3, β = 0.06

$$M(I, J) = \frac{1}{|I||J|} \sum_{i \in I, j \in J} \left(D_{ij} - D_{iJ} - D_{Ij} + D_{IJ} \right)^2,$$

where $D_{iJ} = \frac{1}{|J|} \sum_{j \in J} D_{ij}$ and $D_{Ij} = \frac{1}{|I|} \sum_{i \in I} D_{ij}$ are the mean value in row i and column j; $D_{IJ} = \frac{1}{|I||J|} \sum_{i \in I, j \in J} D_{ij}$ is the mean value of expression value of this group of genes under all experimental conditions.

Figure 5.4a–f provides the distribution of MSE value of mining result in data sets of *CeCluster* algorithm with different mining parameters when the number of resources is 1,000. It can be seen from these figures that MSE value of almost all results is lower than 0.1, indicating that the mining result of *CeCluster* algorithm has certain correlation, thus showing that the effective value of resources in
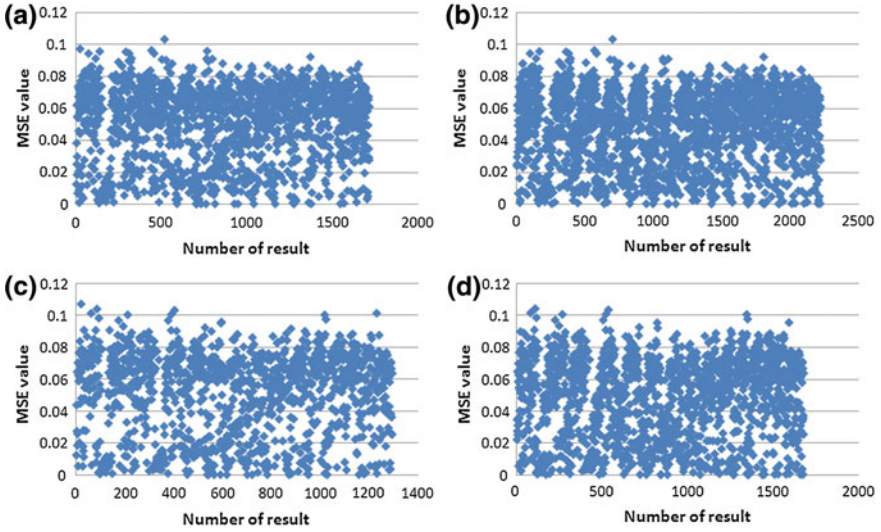
Fig. 5.4 Distribution of MSE value of mining result of CeCluster algorithm under different parameters when the number of resources is 600: **a** $\alpha = 0.2$, $\beta = 0.03$; **b** $\alpha = 0.2$, $\beta = 0.06$; **c** $\alpha = 0.3$, $\beta = 0.03$; **d** $\alpha = 0.3$, $\beta = 0.06$

maximal trend bicluster mined with this algorithm has small variation. Thus, biclusters with weak trend can be mined from a lot of data so as to discover resources with fault trend in time in the earlier stage.

5.5 Conclusion

In this study, we proposed an efficient bicluster mining algorithms: *CeCluster* algorithm, which mines trend bicluster in real-valued resource effectiveness matrices. To improve the mining efficiency, *CeCluster* algorithm mines maximal trend bicluster using the method of column extension and multiple pruning strategies without candidate maintenance. *CeCluster* algorithm can not only mine resource patterns with effectiveness in the downtrend, but also mine those with effectiveness in the uptrend. *CeCluster* algorithm can also mine resource patterns without change of effectiveness. However, due to the lack of real test data, all experimental results of the algorithm in this study are mined based on artificially generated data. Our next research direction is mining trend biclusters from resource effectiveness matrix measured in real environment.

References

1. Pecht M et al (2010) A prognostics and health management roadmap for information and electronics-rich systems. Microelectron Reliab 50:317–323
2. Cheng Y, Church GM (2000) Biclustering of expression data. In: Proceedings of the 8th international conference intelligent systems for molecular biology (ISMB00). ACM Press, pp 93–103
3. Ben A et al (2003) Discovering local structure in gene expression data: the order-preserving submatrix problem. J Comput Biol 10:373–384
4. Cheng KO et al (2007) Bivisu: software tool for bicluster detection and visualization. Bioinformatics 23:2342–2344
5. Zhao L, Zaki MJ (2005) MicroCluster: an efficient deterministic biclustering algorithm for microarray data. IEEE Intell Syst 20(6):40–49 (special issue on Data Mining for Bioinformatics)
6. Wang M, Shang X, Zhang S, Li Z (2010) FDCluster: mining frequent closed discriminative bicluster without candidate maintenance in multiple microarray datasets. In: ICDM 2010 workshop on biological data mining and its applications in healthcare, p 779–786
7. Wang M, Shang X et al (2013) Efficient mining differential co-expression biclusters in microarray datasets. Gene 518:59–69
8. Yang M, Shang X et al (2013) Bicluster algorithm facing the time-series gene expression data. Appl Res Comput 30(8):2308–2314

Chapter 6
Research About Algorithm and Application of Tunable Activation Function Neural Network

Zhengwu Wang and Hang Cui

Abstract The paper improved the traditional transferring pattern and function about the BP neural network, it replaced the fixed transfer function with the mutative activation function to construct the tunable activation function neural network; it also gave the improved network algorithm and the conclusion. The actual diagnosis was imitated on the engine lubricating oil fault; the simulation indicated the method had the characters that the convergence speed was quick; the precision was high, and the generalization capability was best.

Keywords Tunable activation function · Neural network · Algorithm · Diagnosis

6.1 Introduction

Many experts and academicians research the aviation engine lubricating oil fault currently, they attach importance to find the reasons about the fault quickly and exactly. In order to take actions to maintain the aviation engine and enhance its properties, some surface men put their attention to the study work especially. The conventional method is that the technicians take advantage of the instrument to observe and inspect the correlative signals, then analyze and judge the failure reasons and the appearing place correspondingly with experiences. Along with the aviation engine lubricating oil system changing more complex continuously, the faults' inspection and diagnosis change more difficult gradually. Neural network has many functions, such as nonlinear approach, self-memory, self-study, and

Z. Wang (✉)
The First Aeronautic Institute of the Air Force, Xinyang, Henan, China
e-mail: wangzhengwu000@sina.com

H. Cui
Zhengzhou University, Zhengzhou, Henan, China

strong simulation; it is used in engine lubricating oil system widely. However, with the self-defects of the gradient algorithm, the network can fall into the local optimal minimum during the convergence process easily. It had insurmountable bottlenecks, the Refs. [1, 2] discussed it specially. How to break the bottlenecks? This paper constructed the tunable activation function neural network to solve the problem. It replaced the fixed transferring function with the mutative activation function and put the method into the aviation engine lubricating oil fault diagnosis. The experiments indicated the method could conquer the problem and enhance the generalization capability, the precision, and application results were best.

6.2 The Tunable Activation Function Neural Network

6.2.1 The Network Constitution

The activation function of the tunable activation function neural network was not fixed; it could adjust with the neural network changing appropriately, to increase its mapping capacities. Its structure and the nerve cell are just like in Figs. 6.1 and 6.2.

In Fig. 6.1, x_i $(i = 1, \ldots, n)$ denoted the known parameters and represented the input signal values, y_j $(j = 1, \ldots, r)$ represented the middle-layer output values, o_s $(s = 1, \ldots, m)$ represented the output-layer values, $(\omega_{ij})_{n \times r}$ represented the connection weights values from the input layer to the middle layer, $(c_{js})_{r \times m}$ and represented the connection weights values from the middle layer to the output layer. In Fig. 6.2, the nerve cell activation function was composed by a series of base functions $\phi_0(x_i), \ldots, \phi_h(x_i)$, here:

$$\phi_0(x) = \frac{e^x - e^{-x}}{e^x + e^{-x}}, \ldots, \phi_h(x) = \phi_0^{(h)}(x), \quad y_j = f(\phi_i(x_i)),$$

just like a series of base function operated on the input signals and executed nonlinear changing; the transmission function were $y_j = f(\phi_i(x_i))$, we used the tan-sigmoid function replace the sigmoid function as the initial base function to enlarge the mapping value region from (0, 1) to (−1, 1), just like Fig. 6.3.

6.2.2 The Forward Transfer Process of the Network

According to the Figs. 6.1 and 6.2, denoted

$$\overline{O}_s = \sum_{j=1}^{r} c_{js} \cdot y_j - \theta_{2s}, \quad \overline{X}_j = \sum_{i=1}^{n} \omega_{ij} \cdot x_i - \theta_{1j},$$

Fig. 6.1 The network
structure
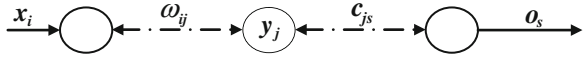
Fig. 6.2 The nerve cell
structure
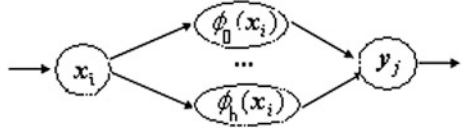
Fig. 6.3 The tan-sigmoid
function graph
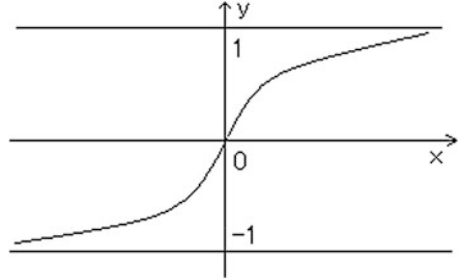
then $y_j = \sum_{i=0}^{h} a_i \cdot \phi_i(\overline{X}_j)$, $o_s = \sum_{i=0}^{h} b_i \cdot \phi_i(\overline{O}_s)$, so we got a series of data stream from the front to back correspondingly. The θ_{1j}, θ_{2s} were the middle layer and output layer's threshold values, and a_i, b_i were coefficients of the base function.

6.2.3 The Parameter Decision During the Backwards Feedback Process

6.2.3.1 The Basic Thought of the Decision

Suppose there were training samples $\left\{ \overset{\leftrightarrow}{o}_s^{(\alpha)}, o_s^{(\alpha)} \right\}$, $(s = 1 \sim m, \alpha = 1 \sim p)$, here, $\overset{\leftrightarrow}{o}_s^{(\alpha)}$ denoted the ideal outputs, $o_s^{(\alpha,k)}$ denoted the network outputs, the superscript α denoted the sample sequence number, k was the study time, we calculated the optimal solutions about the equation

$$\min_{\omega_{ij}, C_{js}} E^{(k)} = \frac{1}{2} \sum_{\alpha=1}^{p} \sum_{s=1}^{m} \left(o_s^{(\alpha,k)} - \overset{\leftrightarrow}{o}_s^{(\alpha)} \right)^2$$

to decide the network parameters' values.

6.2.3.2 The Determination Process About the Parameters' Values

Here, we adopted the fast-speed descend method to find the optimal solution, let
the weights change along the function error negative gradient direction, ensure the
error convergence to the smallest value.

$$\Delta\omega_{ij}^{(k+1)} \propto -\frac{\partial E^{(k)}}{\partial \omega_{ij}^{(k)}}, \quad \Delta C_{js}^{(k+1)} \propto -\frac{\partial E^{(k)}}{\partial C_{js}^{(k)}},$$

Let the coefficients be -1, the study process as follows:

$$\frac{\partial E^{(k)}}{\partial C_{js}^{(k)}} = \sum_{s=1}^{m} \frac{\partial E^{(k)}}{\partial o_s^{(k)}} \cdot \frac{\partial o_s^{(k)}}{\partial C_{js}^{(k)}}, \quad \frac{\partial E^{(k)}}{\partial o_s^{(k)}} = 2 \cdot \sum_{\alpha=1}^{p} \left(o_s^{(k,\alpha)} - \overleftrightarrow{o}_s \right),$$

in order to quicken the changing speed and avoid the positive values and negative
values counteracted each other during the adding process, we took

$$\frac{\partial E^{(k)}}{\partial o_s^{(k)}} = 2 \cdot \sum_{\alpha=1}^{p} \left| \left(o_s^{(k,\alpha)} - \overleftrightarrow{o}_s \right) \right|,$$

$$\frac{\partial o_s^{(k)}}{\partial C_{js}^{(k)}} = y_j \cdot \sum_{t=0}^{h} b_t \cdot \frac{d\phi_t\left(\overline{O}_s^{(k)} \right)}{d\left(\overline{O}_s^{(k)} \right)} = 2 \cdot \sum_{s=1}^{m} \sum_{\alpha=1}^{p} \left| \left(o_s^{(k,\alpha)} - \overleftrightarrow{o}_s \right) \right| \cdot y_j \cdot \sum_{t=0}^{h} b_t \cdot \phi_t'\left(\overline{O}_s^{(k)} \right),$$

$$\frac{\partial o_s^{(k)}}{\partial y_j^{(k)}} = \frac{\partial o_s^{(k)}}{\partial \overline{O}_s^{(k)}} \cdot \frac{\partial \overline{O}_s^{(k)}}{\partial y_j^{(k)}} = c_{js} \cdot \sum_{t=0}^{h} b_t \cdot \phi_t'\left(\overline{O}_s^{(k)} \right),$$

$$\frac{\partial E^{(k)}}{\partial \omega_{ij}^{(k)}} = \left(\sum_{s=1}^{m} \frac{\partial E^{(k)}}{\partial o_s^{(k)}} \cdot \frac{\partial o_s^{(k)}}{\partial y_j^{(k)}} \right) \cdot \frac{\partial y_j^{(k)}}{\partial \omega_{ij}^{(k)}},$$

$$\frac{\partial E^{(k)}}{\partial \omega_{ij}^{(k)}} = \sum_{s=1}^{m} \left(2 \cdot \sum_{\alpha=1}^{p} \left| \left(o_s^{(k,\alpha)} - \overleftrightarrow{o}_s \right) \right| \cdot c_{js} \cdot \sum_{t=0}^{h} b_t \cdot \phi_t'\left(\overline{O}_s^{(k)} \right) \right) \cdot x_i \cdot \sum_{t=0}^{h} a_t \cdot \phi_t'\left(\overline{X}_j^{(k)} \right).$$

6.2.4 The Feedback Process

Adopted the BP algorithm including momentum factors δ_1 and δ_2, modified the
convergence speed step by step properly.

$$\omega_{ij}^{(k+1)} = \omega_{ij}^{(k)} + \Delta\omega_{ij}^{(k)} + \delta_1 \cdot \left(\omega_{ij}^{(k)} - \omega_{ij}^{(k-1)} \right),$$

$$c_{jr}^{(k+1)} = c_{jr}^{(k)} + \Delta c_{jr}^{(k)} + \delta_2 \cdot \left(c_{ij}^{(k)} - c_{ij}^{(k-1)} \right).$$

6.3 The Application Simulation

6.3.1 The Case Analysis

One type of engine lubricating oil system was complex, the oil amount consumed was large, and many reasons could cause this situation. How to select symptom parameters and dispose them originally was important during inspecting process. We combined experiences and inspecting means, analyzed, and disposed some cases from the factory and the outfield, used the primary component analytical method, selected the typical failure symptom parameters. (1) There were 9 groups of typical symptoms: x_1, during plane parking, the grease-box lubricating oil auto kinetic decreased; x_2, during flying, the number was larger than usual about oil consumed; x_9, the turbine shell had oil mark. These properties' values could reflect working status characters. (2) The 9 groups of possible reasons: y_1, the entering circle oil pump was not sealed; y_2, the turbine start machine was not sealed; y_9, the axes brass bushes break off. According to the numerical values between the symptoms and the failures, we neatened 10 groups of typical samples; Table 6.1 gave some among them. The simulation process and purpose as follows: (1) used 7 groups to train the network, watch its convergence speed; (2) used another 3 groups to inspect the network, observe its precision, and analyze its generalization capability.

6.3.2 The Simulation Results

We constructed 9 inputs, 3 middle layer nodes, and 9 outputs neural network, inputs represented the symptoms, outputs represented the reasons, the number of the base function was 3, the base functions were

$$\phi_0(x) = \frac{e^x - e^{-x}}{e^x + e^{-x}}, \quad \phi_1(x) = \frac{4}{(e^x + e^{-x})^2}, \quad \phi_2(x) = \frac{-8(e^x - e^{-x})}{(e^x + e^{-x})^3}$$

just like Fig. 6.4. Let the beginning weight values, the coefficients a_i, b_i ($i = 0, 1, 2$) values be 0.5, the momentum factor values be 0.01, the base function coefficients and the momentum factor values increased according to the step $\Delta h = 0.01$, we used one-dimensional search method to find the optimal solution one by one to get the optimal values. The results are as follows: (1) Fig. 6.5 gave the contrast results among the usual algorithm BP network, the improved BP network including momentum factors and the tunable function neural network, the error units were $10^{-1}, 10^{-2}, 10^{-3}, 10^{-4}, 10^{-5}$ from the upper to lower in turn, the study step unit was 10^3. The results told us that the tunable activation function neural network convergence speed was quickest, and the application effect was perfect. (2) Table 6.2 gave the outputs about the 7 groups training samples and 3 inspecting samples, we found the results were all right, and the generalization capability was best.

Table 6.1 The typical training samples

The failure samples	The typical symptoms								
	x_1	x_2	x_3	x_4	x_5	x_6	x_7	x_8	x_9
y_1	0.234	0.102	0.278	0.256	0	0	0.100	0	0.211
y_2	…	…	…	…	…	…	…	…	…
y_3	…	…	…	…	…	…	…	…	…

Fig. 6.4 The base function images
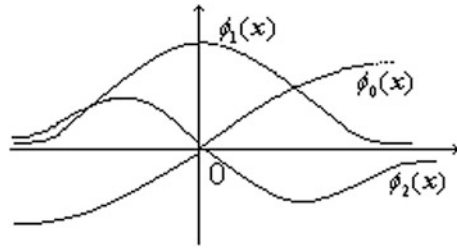
Fig. 6.5 The contrast among three results
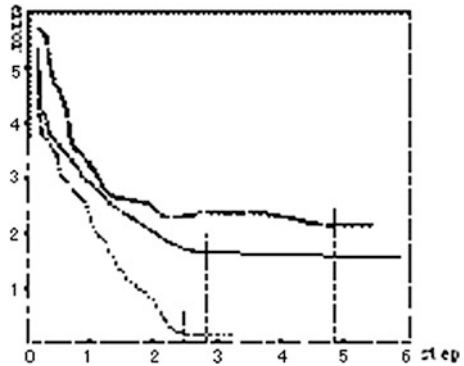
Table 6.2 The properties' test results

The contrast between the training samples								The contrast between the testing samples	
Network results	y_1	y_2	y_3	y_4y_5	y_1y_7	y_6	y_7	y_8	y_1y_4
Actual results	y_1	y_2	y_3	y_4y_5	y_1y_7	y_6	y_7	y_8	y_1y_4

6.4 Conclusion

Using the changeable function replacing conventional fixed function to construct the tunable activation function neural network, it could enlarge the network capability, quicken the convergence speed, and enlarge its precision; it had

important significance in practice. However, how to decide the concrete form and the number about the base function had no theoretic interpretation, it needs simulation and summarization from many cases.

References

1. Wu Y, Zhao M (2001) Adjusting study and application about tunable activation function neural network model. Sci China E 31(3):263–272 (in Chinese)
2. Shen Y, Wang B (2003) One fast algorithm about tunable activation function neural network. Sci China E 33(8):733–739 (in Chinese)

Chapter 7
LowCluster: Efficient Mining Maximal Constant-Row Bicluster with Low Usage Rate in Function–Resource Matrix

Miao Wang, Lihua Zhang, Qingfan Gu and Guoqing Wang

Abstract This paper proposed an efficient bicluster mining algorithm: *LowCluster*, to effectively mine all the maximal constant-row biclusters with low usage rate in real-valued function–resource matrix. First, a sample weighted graph is constructed; it includes all resource collections between both samples that meet the definition of low usage rate; then, all the maximal constant-row biclusters with low usage rate are mined using sample-growth and depth-first method in the sample weighted graph. In order to improve the mining efficiency, *LowCluster* algorithm uses pruning strategy to ensure the mining of maximal bicluster without candidate maintenance. The experimental results show that *LowCluster* algorithm is more efficient than traditional constant-row biclusters mining algorithm.

7.1 Introduction

Although studying the effectiveness degree of resources is the base to construct a prognostics and health management system [1], the health degree of resources directly influences functional health. Therefore, analysis of the relation among

M. Wang (✉) · L. Zhang · G. Wang
Science and Technology on Avionics Integration Laboratory, Guiping Road 432,
Shanghai 200233, China
e-mail: wang_miao@careri.com

L. Zhang · G. Wang
School of Computer Science and Engineering, Northwestern Polytechnical University,
YouYiXiLu 127, Xi'an 710072, China

M. Wang · Q. Gu · G. Wang
China National Aeronautical Radio Electronics Research Institute, Guiping Road 432,
Shanghai 200233, China

functions and resources can mine the health relations so as to complete the functions through using healthy resources and improve the health degree of functions. The call relation of functions and resources can be denoted as a matrix, in which each row means a resource and each column means a function; the value in the matrix is the usage degree of a function to a resource. This value is defined during functional design, i.e., resource dependence degree of this function in aircraft system in order to complete a function. Through function–resource matrix mining, in order to achieve a group of functions, the resources which can meet all functional demands simultaneously and the resources which can satisfy all functional demands through multiple accesses can be mined. Therefore, using data mining technology, we can construct the call relation between function and resource, so as to construct the model which can compute the health degree of functions using the health degree of resources.

The above mining concept complies with the mining concept of bicluster in data mining field. Biclustering [2] is a methodology allowing for condition set and item set points clustering simultaneously. It finds clusters of items possessing similar characteristics together with conditions creating these similarities. The main advantage of biclustering is the simultaneous mining module on items and conditions; another advantage is its applicability on original data instead of discretized data. However, mining biclustering approach presents the following four challenges [3]. First, the computing of biclustering method is NP-hard [2]. Second, biclustering method deals with original data; it should adapt to the noise-sensitive character of microarray data set. Third, the biclustering method should allow overlapping biclusters which share some genes or conditions, which would increase the complex of biclustering algorithm. Finally, the biclustering method should be flexible enough to handle different types of biclusters. Madeira and Oliveira [4] classified biclusters into four categories.

Currently, large quantities of algorithms based on greedy strategy or exploratory strategy are applied in mining bicluster. Cheng and Church [2] proposed an algorithm based on greedy strategy. This algorithm adopts a low square root residue to delete redundant nodes step by step. After that, many algorithms based on greedy strategy were raised [5–9]. All the above algorithms' efficiency is not high. Thus, to design a high-efficiency bicluster mining algorithm is current research hotspot. So, Wang et al. came up with the mining algorithm to mine the maximal bicluster from discretized data [5]. However, this algorithm cannot effectively mine bicluster with low usage rate meeting difference restraint from function–resource matrix.

Based on above analysis, in this paper, we proposed a new bicluster mining algorithm: *LowCluster* algorithm to mine all maximal low-usage rate constant-row biclusters without candidate maintenance in real-valued function–resource matrix. Since the number of functions is far lower than that of resources in function–resource matrix, our algorithm uses sample-growth method for mining. First, a sample weighted graph is constructed, which includes all the pairs of resources between both samples that meet the definition of low usage rate; then, all maximal biclusters with low usage rate definition and constant row definition are mined

using sample-growth and depth-first method in the constructed weighted graph. In order to improve the mining efficiency of the algorithm, *LowCluster* algorithm uses multiple pruning strategies to ensure the mining of maximal bicluster without candidate maintenance.

7.2 Problem Definition

Function–resource matrix is defined as a two-dimensional real matrix $D = R \times F$. Row set R represents the set of resources, and column set F refers to the set of functions. Element D_{ij} of matrix D is a real number which represents the ability validity or usage rate of resource i supporting function j. $|R|$ is the number of resources in data set D, and $|F|$ is the number of functions in data set D. For the convenience of mining, the domain of definition of the original effective value in resource effectiveness matrix is [0,1], where '0' means that this resource is not required during the implementation of some function and '1' means that this resource must be used during the implementation of some function, as shown in Table 7.1.

The significance of bicluster to be mined from function–resource matrix as shown in Table 7.1 is to mine a group of functions executed; under this group of functions, the usage rate of the resource is higher, i.e., which resources can reach the highest usage rate when used together. In other words, the resources have the highest effectives when all functions are executed. For example, for a group of functions F_1F_2 ($F_1 ==> R_1R_2R_3$, $F_2 ==> R_2R_4$), these three functions may be called simultaneously. For resource R_2, there are three situations for supporting F_1 and F_2. For both F_1 and F_2, the usage rate of R_2 is low, as shown in Table 7.2, the health degree is higher. Since the resource R_2 can serve F_1 and F_2 at the same time, our proposed algorithm *LowCluster* aims to mine all the maximal low-usage rate constant-row biclusters in real-valued function–resource matrix. We will give definitions of low usage rate of resources in real data below:

Definition 1 D is a function–resource usage rate matrix; α is a user-defined parameter used for measuring the degree of association of functions in resources; β is a parameter restricting low usage rate of resources; r is any resource in function–resource usage rate matrix D; F_1 and F_2 are any two functions in D; r should meet the following conditions for relevance in F_1 and F_2 $[\forall r \in R|$ $\left(\max\limits_{f \in \{F_1,F_2\}} D_{r,f} - \min\limits_{f \in \{F_1,F_2\}} D_{r,f} \right) \leq \alpha \left(\min\limits_{f \in \{F_1,F_2\}} |D_{r,f}| \right)$ and $\max\limits_{f \in \{F_1,F_2\}} D_{r,f} \leq \beta]$. If all resources and functions meet the conditions above in a bicluster, this bicluster is one with low usage rate of resources.

It can be obtained from the description in definition 1 that α and β are used to restrict resources with a low usage rate producing each function, e.g., bicluster $F_2F_3F_4$ (R_1R_3) in Table 7.1.

Table 7.1 An example of function–resource matrix

	F_1	F_2	F_3	F_4	F_5
R_1	0.8	0.1	0.12	0.09	0.9
R_2	0.2	0.9	0.19	0.21	1
R_3	0.9	0.3	0.29	0.28	0.55
R_4	0.58	1	0.2	0.21	0.9

Table 7.2 An example of low usage rate

	F_1	F_2
R_1	0.8	0
R_2	0.2	0.1
R_3	0.5	0
R_4	0	0.1

Therefore, each resource in bicluster mined by *LowCluster* algorithm satisfies the Definition 1. To improve the mining efficiency of the algorithm, *LowCluster* algorithm mines all the maximal low-usage rate constant-row biclusters without candidate maintenance using sample-growth method in real-valued function–resource matrix. The mining process of this algorithm will be introduced in detail in the next section.

7.3 The LowCluster Algorithm

The mining process of *LowCluster* algorithm can be divided into two steps: firstly, scan original function–resource matrix; according to the definition of biclusters with low usage rate and constant row definition, the sample weighted graph is produced; then, all the maximal constant-row biclusters with low usage rate are generated using sample-growth method.

7.3.1 Construct the Sample Weighted Graph

The method of mining modes with sample relational weighted graph was used in *MicroCluster* algorithm [8] to mine bicluster at the earliest. Then, Wang et al. [10, 11] also used sample relational weighted graph to mine bicluster and fault-tolerant bicluster. *LowCluster* algorithm in this paper will adopt undirected sample relational weighted graph (hereinafter referred to as sample weighted graph) to mine maximal constant-row biclusters with low usage rate.

Fig. 7.1 The sample weighted graph constructed from Table 7.1
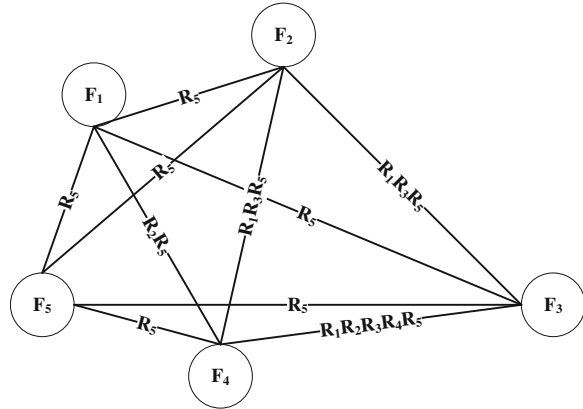
Definition 2 Sample weighted graph can be denoted as the set $G = \{E, V, W\}$. Each node in the node set V in the weighted graph represents a function. If an edge exists between a pair of nodes, this means the resource with variant usage rate or low usage rate exists below two functions represented by this pair of nodes. The set of the edges is expressed as E. The weights of each edge are the resource set meeting the definition of variant usage rate or the definition of low usage rate under the two functions connected with this edge. The set of the weights is expressed as W.

According to the description in Definition 1, when the resources among functions satisfy the definition of low usage rate, the weight between two functions meets commutativity. For instance, the weight under F_3F_4 is $R_1R_2R_3R_4R_5$, while the weight under F_3F_4 is $R_1R_2R_3R_4R_5$. Figure 7.1 shows sample weighted graph corresponding to Table 7.1.

7.3.2 Mining Maximal Constant-Row Biclusters with Low Usage Rate

After the sample relational weighted graph is constructed, this section will introduce how *LowCluster* algorithm mines all the maximal constant-row biclusters with low usage rate in the sample weighted graph without candidate maintenance in detail. According to the description in Definition 1 and Theorem 1, biclusters with low usage rate extended meet anti-monotonicity, i.e., if the bicluster obtained by extension of $F_1F_2...F_n$ does not meet constraint conditions, neither does any superset $F_1F_2...F_nF_m$. Therefore, biclusters with a greater scale can be obtained by extension of the weight on each edge in the weight graph in terms of intersection. According to descriptions in Definition 1, when a new function is introduced in bicluster, it is necessary to calculate the intersection of all

edges of the function newly introduced and the resource collection of bicluster extended, thus ensuring that the resource collection under the function newly introduced and that under existing functions meet constraint conditions in Definition 1.

Theorem 1 *The sample range support measure is anti-monotonic*

Theorem 1 states that our low usage rate satisfies the anti-monotonic property, which guarantees that we can use *Apriori*-like efficient pattern mining framework to discover biclusters. Therefore, our *LowCluster* algorithm adopts *Aprioir*-like procedure to produce constant-row bicluster with low usage rate using sample-growth in sample weighted graph. The following lemma can guarantee that *LowCluster* algorithm mines all the maximal low-usage rate constant-row biclusters without candidate maintenance.

Lemma 1 *Given P be the current extending constant row bicluster with low usage rate, M is the candidate sample set of P and N is the priori candidate sample set of P. Supposed the current candidate sample is M_i, $M_i \in M$, and N_j is a priori candidate sample where $N_j \in N$. If it is satisfied the following criteria: (1) $PN_jM_i.Resources$ is the same as $PM_i.Resources$; (2) For each other candidate sample M_p in M, $PN_jM_i.Resources$ is the subset of $PN_jM_p.Resources$, all the constant row bicluster with low usage rate generated by PM_i can also be produced by extending PN_j.*

Lemma 1 states how to escape of producing non-maximal low-usage rate constant-row biclusters without candidate maintenance. According to above lemma, *LowCluster* algorithm exploits the following pruning technique to achieve mining maximal low-usage rate constant-row biclusters without candidate maintenance in real-valued function–resource matrix.

Pruning 1 Given *P* be the current extending constant-row bicluster with low usage rate, *M* is the candidate sample set of *P* and *N* is the priori candidate sample set of *P*. Suppose the current candidate sample is M_i, $M_i \in M$, and N_j is a priori candidate sample where $N_j \in N$. If it satisfies the following criteria: (1) $PN_jM_i.Resources$ is the same as $PM_i.Resources$ and (2) for each other candidate sample M_p in *M*, $PN_jM_i.Resources$ is the subset of $PN_jM_p.Resources$, M_i should be pruned.

We will explain the algorithm mining process through an example. The data in the example are function–resource use relationship matrix shown in Table 7.1. Firstly, construct the sample weighted graph among functions, as shown in Fig. 7.1. The mining process of *LowCluster* for mining Table 7.1 expressed matrix is shown in Fig. 7.2. The specific description of *LowCluster* algorithm is as follows:
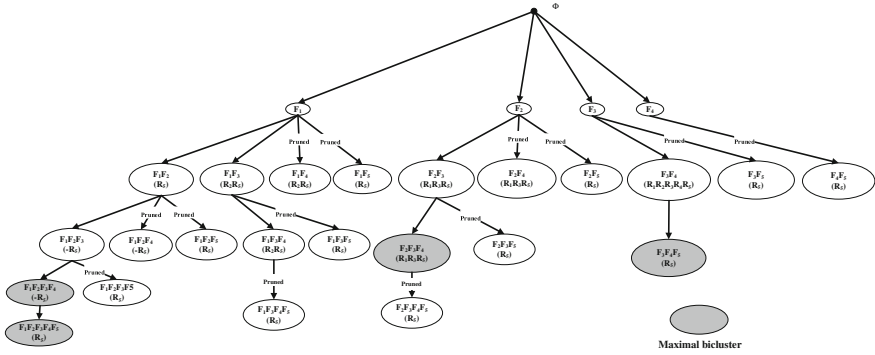
Fig. 7.2 The example mining procedure of *LowCluster* algorithm

```
Algorithm 1: LowCluster algorithm
Input: number threshold: n, coherent threshold: α, low
usage rate threshold: β, function-resource matrix: D
Output: all the maximal constant row biclusters with
low usage rate meeting the threshold
Initial value: sample weight graph: G =Null, current
bicluster to be extended Q =Null, S_i=Null and S_j=Null.
Algorithm description: LowCluster(n, α, β, D, Q, S_i, S_j)
 (1) If G is null, scan data set D and make its weight
graph. S_i is the first sample in the weight graph;
 (2) For each sample S_j connected with sample S_i
 (3)     If all resource linked lists in S_j meet pruning
technique, then
 (4)          Continue;
 (5)      Else
 (6)         For resource linked lists not meeting prun-
ing conditions, Q.Sample= Q.Sample∪S_j; Q. Resource=
Q.Resource∩S_iS_j.Resource;
 (7)          LowCluster(n, α, β, D, Q, S_i, S_j);
 (8)     Endif
 (9) Endfor
(10) If Q meets output conditions, then
(11)   Output Q
(12) Endif;
(13) S_i = S_i->next;
(14) Return
```

7.4 Experimental Results

In this section, we will make an experimental comparison on the mining efficiency and result of the algorithm above and existing algorithms. The hardware environment of the experiment is Intel(R) Core(TM)2 Duo 2.53 GHz CPU and 4G internal memory; the software environment is Microsoft Windows 7 SP1 operating

Table 7.3 The proportion of each value in three data set

	0	0.1	0.2	0.8
D_1	0.2	0.2	0.2	0.4
D_2	0.2	0.3	0.3	0.2
D_3	0.4	0.2	0.2	0.2
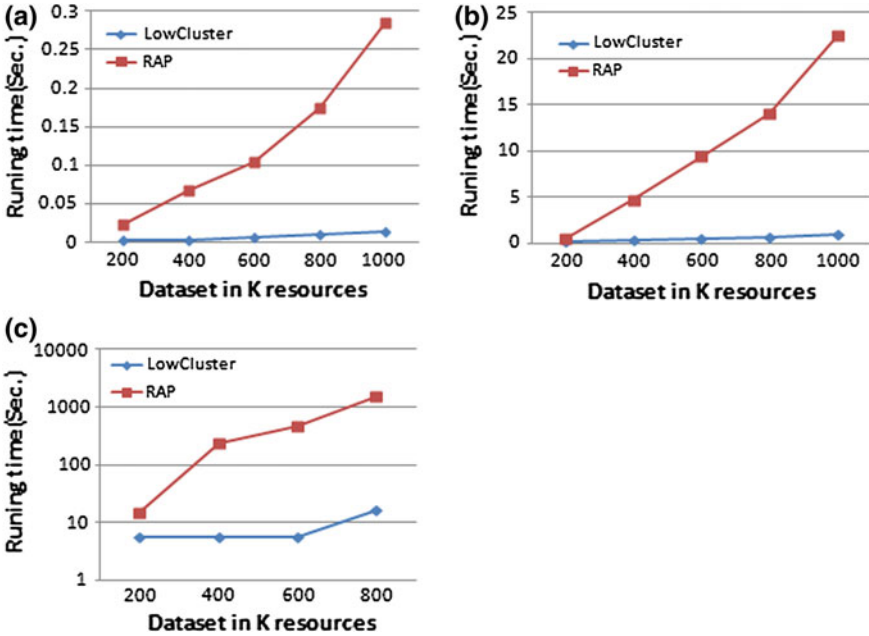
Fig. 7.3 The running time comparison between two algorithms under different number of resources and functions in D_1 when $\alpha = 1$: **a** 10 functions; **b** 20 functions

system; the algorithm programming and operating environment is Microsoft Visual C++ 6.0 SP6. Experimental data used in this paper are simulation data. To fully test the performance of the algorithm, we produce three data sets randomly, each of which contains 20 sampling sites and 1,000 resources. Table 7.3 describes proportions of 0, 0.1, 0.2, and 0.8 in each row in each data set.

In this section, we will compare the mining efficiency between *LowCluster* algorithm and RAP algorithm [5]. In order to fully compare the extendibility of algorithms, we produce multiple groups of data sets with different numbers of resources and functions in allusion to three data sets in Table 7.2. The selection of resources and functions are based on the order of resources and functions in data set. The parameter of low usage rate is 0.5. Figure 7.3a, b provides the comparison of performance period when the number of functions of two algorithms above is 10, 20, and 30, respectively, and the number of resources is 200, 400, 600, 800,
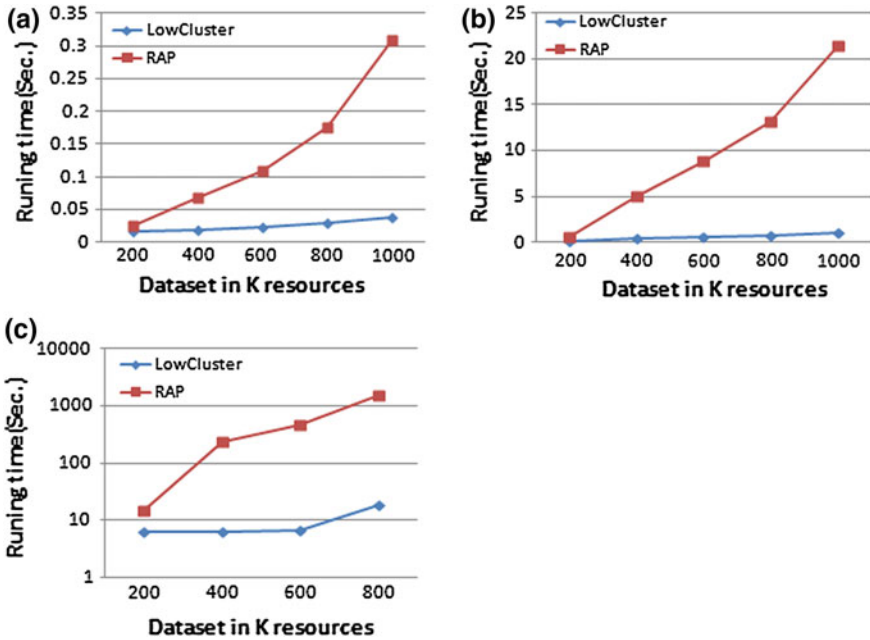
Fig. 7.4 The running time comparison between two algorithms under different number of resources and functions in D_1 when $\alpha = 2$: **a** 10 functions; **b** 20 functions

and 1,000, respectively, and the parameter of relevancy under data set D_1 is 1. It can be seen from these figures that the mining time of both algorithms increases progressively with the increase in number of resources in data set. Meanwhile, the mining efficiency of *LowCluster* algorithm is higher than that of RAP algorithm under each data size. In particular, when the number of resources in data set is high, the mining efficiency of *LowCluster* algorithm is nearly 20 times higher than that of RAP algorithm. Meanwhile, according to the increase in the total of functions, *LowCluster* algorithm is nearly 100 times higher than that of RAP algorithm. The reason is that RAP algorithm mines bicluster with the method of resource extension. With the increase in number of resources in data set, this algorithm needs more iterations to mine all biclusters meeting threshold conditions. However, *LowCluster* algorithm uses high-efficiency pruning strategies for mining and will produce more maximal biclusters, especially when the number of resources in data set is high and data are dense. Therefore, *LowCluster* algorithm has a higher pruning efficiency. Figure 7.4a, b provides the comparison of performance period under data sets with different resources of functions and resources when the parameter of relevancy of three algorithms above is two in data set D_1. Similar to the description in Fig. 7.3a–c, the mining efficiency of *LowCluster* algorithm is higher than that of RAP algorithm under each data size.
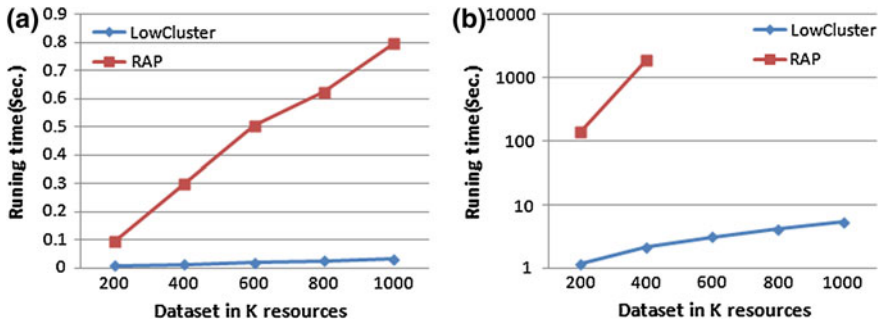
Fig. 7.5 The running time comparison between two algorithms under different number of resources and functions in D_2 when $\alpha = 1$: **a** 10 functions; **b** 20 functions
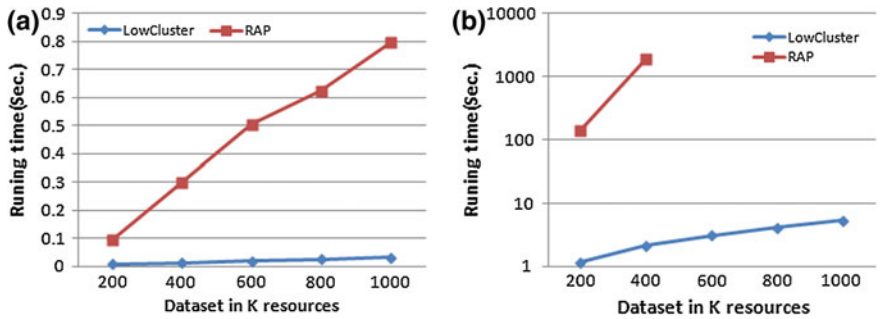
Fig. 7.6 The running time comparison between two algorithms under different number of resources and functions in D_2 when $\alpha = 2$: **a** 10 functions; **b** 20 functions

Figures 7.5a, b and 7.6a, b, respectively, provide the comparison of performance period of both algorithms above under data sets with different numbers of sampling sites and resources when their parameters of relevancy under data set D_2 are, respectively, 1 and 2. It can be seen that, as proportions of 0.1 and 0.2 in data set D_2 increase compared to those in data set D_1, according to descriptions of the definition of variant usage rate and low usage rate, mining data set D_2 will produce more biclusters than mining data set D_1 under the same parameter. Therefore, when the number of functions is 20, RAP algorithm cannot mine data sets with the number of resources higher than 400 in limited memory space, but *LowCluster* algorithm can complete all mining processes within 10 s. Figures 7.7a, b and 7.8a, b, respectively, provide the comparison of performance period of both algorithms above under data sets with different numbers of sampling sites and resources when their parameters of relevancy under data set D_3 are, respectively, 1 and 2.
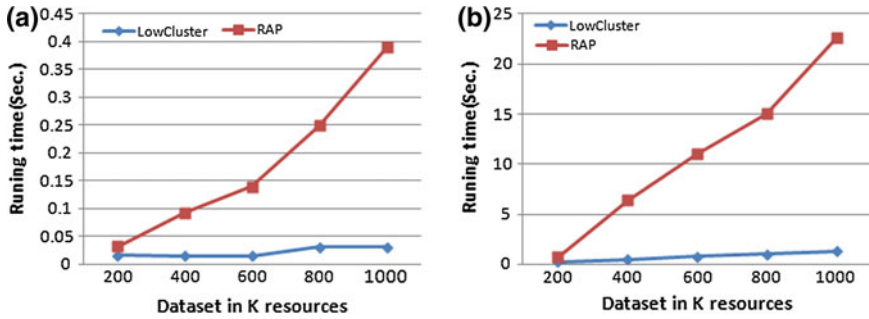
Fig. 7.7 The running time comparison between two algorithms under different number of resources and functions in D_3 when $\alpha = 1$: **a** 10 functions; **b** 20 functions
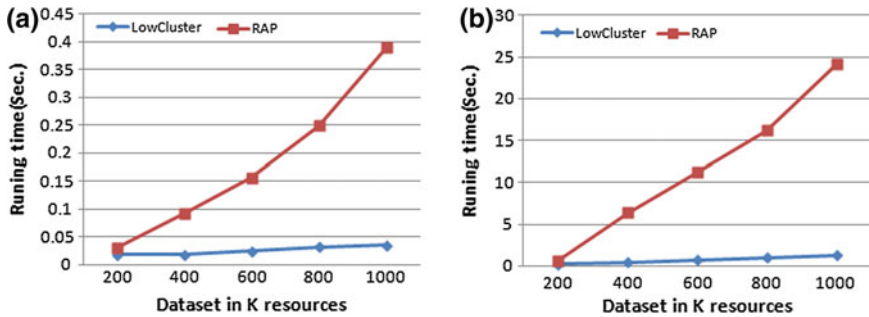
Fig. 7.8 The running time comparison between two algorithms under different number of resources and functions in D_3 when $\alpha = 2$: **a** 10 functions; **b** 20 functions

7.5 Conclusion

In order to mine the relation between function and resource for improving the health of functions, this paper proposed an efficient bicluster mining algorithm: *LowCluster* algorithm, to effectively mine all the maximal constant-row biclusters with low usage rate in real-valued function–resource matrix. First, a sample weighted graph is constructed; it includes all resource collections between both samples that meet the definition of low usage rate; then, all the maximal constant-row biclusters with low usage rate are mined using sample-growth and depth-first method in the sample weighted graph. In order to improve the mining efficiency of the algorithm, *LowCluster* algorithm uses pruning strategy to ensure the mining of maximal bicluster without candidate maintenance. However, due to the lack of true test data, all experimental results of the algorithm in this paper are evaluated based on artificially generated data. Our next research direction is mining constant-row biclusters with low usage rate in real-valued function–resource matrix.

References

1. Pecht M et al (2010) A prognostics and health management roadmap for information and electronics-rich systems. Microelectronics Reliability 50(3):317–323
2. Cheng Y, Church GM (2000) Biclustering of expression data. In: Proceedings of the 8th international conference on intelligent systems for molecular biology (ISMB00), ACM Press, New York, pp 93–103
3. Becquet C, Blachon S, Jeudy B, Boulicaut JF, Gandrillon O (2003) Strong-association-rule mining for large-scale gene-expression data analysis: a case study o human SAGE data. Genome Biol 12:1–16
4. Madeira SC, Oliveira AL (2004) Biclustering algorithms for biological data analysis: a survey. IEEE/ACM TCBB 1(1):24–45
5. Pandey G, Atluri G, Steinbach M, Myers CL, Kumar V (2009) An association analysis approach to biclusting. In: Proceedings of the ACM conference on knowledge discovery and data mining, pp 677–686
6. Ben et al (2003) Discovering local structure in gene expression data: the order-preserving submatrix problem. J Comput Biol 10:373–384
7. Cheng et al (2007) Bivisu: software tool for bicluster detection and visualization. Bioinformatics 23:2342–2344
8. Zhao L, Zaki MJ (2005) MicroCluster: an efficient deterministic biclustering algorithm for microarray data. IEEE Intell Syst Spec Issue Data Min Bioinf 20(6):40–49
9. Torgeir RH, Astrid L, Jan K (2003) Learning rule-based models of biological process from gene expression time profiles using gene ontology. Bioinformatics 19:1116–1123
10. Wang M, Shang X, Zhang S, Li Z (2010) FDCluster: mining frequent closed discriminative bicluster without candidate maintenance in multiple microarray datasets. In: ICDM 2010 workshop on biological data mining and its applications in healthcare, pp 779–786
11. Wang M, Shang X, Miao M, Li Z, Liu W (2011) FTCluster: efficient mining fault-tolerant biclusters in microarray dataset. In: Proceedings of ICDM 2011 workshop on biological data mining and its applications in healthcare, pp 1075–1082

Chapter 8
Optimal Quasi-Periodic Preventive Maintenance Policies for a Two-unit Series System with Dynamic Maintenance Plan

Wenke Gao, Zhisheng Zhang, Zhiqiang Zhang and Yifan Zhou

Abstract Most research on preventive maintenance (PM) assumed that a PM interval is a fixed value. However, practical PM actions usually are affected by some internal and external random factors, which make the PM interval become a limited random value rather then a fixed value. Few of the existing research consider this situation for two-unit system in their models. In this paper, a quasi-periodic PM policy for one type of two-unit series system with a dynamic maintenance plan is proposed, in which PM for U_1 is perfect whereas for U_2 is imperfect, and the dynamic PM plan is executed in each implemented period, and PM activities are performed through competing results of the dynamic PM plan and a catastrophic failure of U_2. The optimal implemented period of PM and PM number is obtained which minimizes the excepted cost per unit time of the system in long run. Finally, a numerical example is given to illustrate the proposed model.

Keywords Quasi-periodic preventive maintenance policy · Implemented period · Two-unit series system · Dynamic preventive maintenance plan

8.1 Introduction

Most practical engineering assets are multi-unit systems, i.e., they have more than one unit. During optimizing the maintenance of these multi-unit systems, one needs to consider three interactions among components: economic dependence, stochastic dependence, and structural dependence. Economic dependence means

W. Gao · Z. Zhang (✉) · Y. Zhou
School of Mechanical Engineering, Southeast University, Nanjing 211189, China
e-mail: oldbc@seu.edu.cn

Z. Zhang
Locomotive Depot of Urumqi Railway Bureau, Korla 841000, China

that the cost of grouping maintenance is different from the sum of individual maintenance costs. Stochastic dependence implies that degradation processes of different components influent each other. Structural dependence means that a certain group of components are connected together and should be replaced together. The three interactions make the maintenance strategy optimization of a multi-unit system much more complex than that of a mono-unit system.

Two-unit system is the simplest system among multi-unit system, on which various approaches have been developed to optimize the maintenance strategy [1]. Some of them were based on the lifetime distribution of system components [2–5], among which the maintenance optimization for a system with a redundant unit is considered. Other of them discussed the maintenance optimization for two-unit systems in the context of condition-based maintenance [6–9]. For preventive maintenance (PM) policy, most of the existing research regarded that the maintenance period is a fixed time, while it should be a time period in some practical cases because of influence of some random factors which make the maintenance actions unable to be performed as soon as a planned maintenance period reaches. A typical example is that PM interval on some Japanese planes is 12–18 months [12] and it is 2,300–2600 km on some Chinese diesel locomotives [10, 11]. Only few of them discussed the maintenance optimization for a mono-unit system with a time delay on implementing PM actions considering a job cycle or a failure occurrence [13–16]. Tahara and Nishida [13] introduced a maintenance policy that a unit is replaced when the first failure after t_0 hours of operation or when the total operating time reached $T(0 < t_0 < T)$, whichever occurs first. Sheu et al. [14] examined a generalized age replacement policy, in which the system is subject to a perfect repair with $p(y)$, or undergoes a minimal repair with probability $q(y) = 1 - p(y)$ if a unit fails at age $y < t$. Otherwise, the unit is replaced when the first failure after t occurs or the total operating time reaches age $T(0 < t < T)$, whichever occurs first. Castro and Sanjuan [15] analyzed a maintenance policy for a repairable system with delay repairs. In that paper, if the system fails in [0, T^*], then it is repaired, whereas if it fails in (T^*, T] the repair is not performed, and the system is replaced when the non-repairable failures reached N over (T^*, T]. Chen [16] considered an age replacement policy for a system, which continuously works for multiple jobs with random working times and can undergo minimal repairs upon failures. The planned replacement is postponed at the first completion of the working time or when a job incurs some damage to the system over a planned time T. Gao et al. [17] modeled a replacement policy that a replacement action is randomly performed over an implemented period under a consideration of a catastrophic failure and a dynamic replacement schedule. Most of these papers are focused on mono-unit system, while two-unit system is widely used in practice, and thus, as a beginning, the PM optimization for a two-unit series system considering the influence of some random factors is considered.

In practice, one type of two-unit series system, in which the lifetime of unit 1 (U_1) is always stochastically much smaller than unit 2 (U_2), is widely existent, e.g,. piston matching parts for diesel engine, the lifetime of a piston ring is stochastically much smaller than a cylinder liner, and PM for piston ring is nearly perfect while for

a cylinder liner is imperfect, and the planned PM interval may be modified for some influence, such as production task, transport cycle of an aircraft. Therefore, a periodic imperfect PM policy for a two-unit series system with dynamic PM plan is proposed in this paper, which is different with the general periodic PM policy because the determination of the PM policy simultaneously considers some external and internal random factors, and the actual PM period is a limited random value rather than a fixed value. Herein, it is termed as a quasi-periodic PM policy. In this policy, the first $(N - 1)$ PM intervals are divided into a planned PM period and an implemented period. The length of the planned PM period is made by a scheduled PM plan and it is a fixed value, while the length of the implemented period is given by engineers' experience in which a dynamic PM plan is randomly performed. Assume that a failure of U_2 either is a minor or a catastrophic one with stochastic probability, and failures of U_1 are minor failure. The scheduled PM plan would be changed by some random factors, and thus, actual PM activities are randomly performed considering the dynamic PM plan and the occurrence of the catastrophic failure of U_2. The main characteristic of this model is that catastrophic failures of U_2 and dynamic PM plan are competing to cause a PM action with different PM cost. The object of this paper is to optimize the proposed maintenance policy for a two-unit series system which minimizes the excepted cost per unit time in long run. Finally, a numerical example is given to illustrate the proposed model.

8.2 Notation and Model Assumptions

For ease of reference, some notations are stated as follows:

a_i	adjustment factor in hazard rate function after the $(i - 1)$th PM $(1 = a_1 \leq a_2 \leq ,...., \leq a_N)$
$A_i(t)$	total minimal repair cost occurred over $(0, t]$ in the ith PM interval
C	mean cost rate of the system
C_e	extra cost caused by a catastrophic failure
$C_{p,i}$	cost of the ith PM
C_r	cost of a replacement
$C_m^{(i)}(t)$	minimal repair cost of U_i $(i = 1, 2)$
$F^{(i)}(t)$	cdf of $U_i(i = 1, 2)$ failures
$F^{(i)}(t)$	pdf of $U_i(i = 1, 2)$ failures
$F_{p,i}^{(2)}(t)$	cdf of minor failures of U_2 occurred in the ith PM interval
$F_{q,i}^{(2)}(t)$	cdf of catastrophic failures of U_2 occurred in the ith PM interval
$h_i^{(j)}(t)$	hazard rate function at time t of $U_j(j = 1, 2)$ subject to $(i - 1)$ PM, $i = 1, 2,...,N$
N	threshold of PM number
p_i	the probability of a failure of U_2 is a minor failure when the system fails in the ith PM interval

q_i	the probability of a failure of U_2 is a catastrophic failure when the system fails in the ith PM interval
R	total maintenance cost over a renewal cycle
T	length of the planned periodic PM interval
W	length of the impended period of PM activities
Y	renewal cycle
$Y_{s,i}$	occurring time of a catastrophic failure of U_2 occurred in the ith PM
Y_{sc}	dynamic PM schedule over $[T\ T + W]$
Z	random variable.

$$H_m = \frac{C_m^{(1)}}{C_m^{(2)}}$$

In the system, lifetime of U_1 is always stochastic much less than U_2. Failures of U_1 are minimal failure which can be removed by minor repair, and a failure of U_2 is either a minor one with probability p_i or a catastrophic one with probability $q_i = 1 - p_i$, where $0 \le q_i \le 1$ and q_i is non-decrease in i. Minor failures of U_2 can be rectified by minimal repair, and catastrophic failures can be removed by an unplanned PM with an extra cost. A PM is performed to the system either at the scheduled PM plan in the implemented period, or when a catastrophic failure of U_2 arrives, whichever comes first. PM to U_1 is perfect, while to U_2 is imperfect. A replacement of the system is performed either when the operational time of the system reaches T, or when a catastrophic failure of U_2 comes in the last maintenance period, whichever comes first. When the operational time of the system reaches time $T + W$ after a PM, the system will arrange to be preventively maintained and thus assume that the dynamic PM plan follows the uniform distribution. A replacement cycle is defined as the time interval between the installation of the system and the first replacement or between two consecutive replacements. In this framework, replacement cycles constitute a regenerative process.

Finally, five model assumptions are given following the above maintenance process:

1. Failures of U_1 and U_2 are independent and can be instantly detected and repaired.
2. The hazard rate function of U_1 and U_2 is continuous, positive, and non-decrease in t. If the hazard rate function of new U_2 is $h(t)$, it becomes $h_i^{(2)}(t) = a_i h^{(2)}(t)$ in the ith PM interval; here, $1 = a_1 \le a_2 \le \ldots \le a_N$. After a replacement, the system can be restored to "as good as new" state.
3. The mean cost of the minor repair $C_m^{(1)}$ and $C_m^{(2)}$ for U_1 and U_2 is unrelated to the occurred failures and the total severed times of the system. The PM cost $C_{p,i}$ (i denotes the ith PM, $i = 1, 2,\ldots, N - 1$) is relevant to the number of PM and it is a constant sequence increasing in i. A catastrophic failure causes an additional cost C_e. The cost of replacement is a constant C_r ($C_e + C_{p,i} < C_r$, $C_m^{(1)} < C_m^{(2)} < C_r$).

4. The system can be arranged to be completely preventively maintained in each implemented period.
5. All minimal repair, PM, and replacement time are negligible.

8.3 The Cost Model

In terms of the model assumptions given in Sect. 8.2, if no PM or replacement action is performed, the cumulative distribution function of minor failures of U_1 between the $(i - 1)$th and ith ($i = 1, 2,...,N$) PM can be written as

$$F^{(1)}(t) = 1 - \exp\left(-\int_0^t h^{(1)}(y)dy\right)$$

For U_2, the cumulative probability distribution of minor failure between the $(i - 1)$th and ith ($i = 1, 2,...,N$) PM is, respectively, stated as follows:

$$F_{p,i}^{(2)}(t) = 1 - \exp\left(-\int_0^t p_i h_i^{(2)}(y)dy\right)$$

8.3.1 The Excepted Renewal Cycle Cost

A renewal cycle is defined as the time interval between the installation of the system and the first replacement or between two consecutive replacements. It consists of N PM intervals, in which minor repair and PM and replacement are jointly considered. Minor failure of the system is removed by minimal repair; the expected total minimal repair cost of the system over $(0, t)$ can be denoted as follows:

$$A_i(t) = C_m^{(2)} \int_0^t \left(p_i h_i^{(2)}(u) + H_m h^{(1)}(u)\right)du \tag{8.1}$$

For each PM activity, which may be an unplanned one caused by a catastrophic failure or may be a scheduled one triggered by a provisional plan in the implemented period. According to this situation, there are four different scenarios for the occurrence of PM activity.
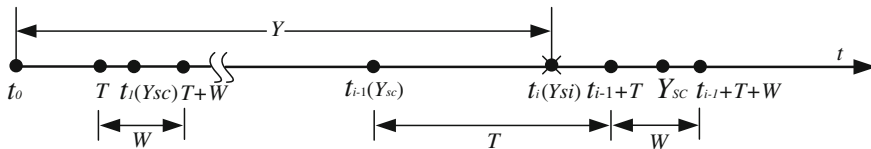
Fig. 8.1 PM is caused by a catastrophic failure in (0, T)

1. $P(Y_{s,i} < T)$

In this scenario, the ith PM, which is caused by a catastrophic failure of U_2, is performed at t_i, and $Y_{s,i} < T$. The expected maintenance cost is given by (Fig. 8.1)

$$R_{1,i} = I_{Y_{(s_i)} < T}\left(A_i(Y_{s_i}) + C_{p,i} + C_e\right)$$

$$E[R_{1,i}] = \int_0^T \left[A_i(y) + C_{p,i} + C_e\right]f_{q,i}^{(2)}(y)\mathrm{d}y$$

where $I_B(Z)$ is an indicator function of the set B, i.e.,

$$I_B(Z) = \begin{cases} 1, & \text{if } Z \in B \\ 0, & \text{otherwise} \end{cases}$$

2. $P\left[(T < Y_{s,i}) \cap (Y_{s,i} < T + Y_{sc})\right]$

The second case corresponds to the scenario where the ith PM is caused by a catastrophic failure of U_2, and $T < Y_{s,i} < T + Y_{sc}$. The catastrophic failure of U_2 is ahead of a planned PM in the implemented period. The expected maintenance cost is given by (Fig. 8.2)

$$R_{2,i} = I_{T < Y_{(s_i)} < T + Y_{(sc)} < T + W}\left[A_i(Y_{s_i}) + C_{p,i} + C_e\right]$$

$$E[R_{2,i}] = \frac{1}{W}\int_0^W \int_T^{T+u} \left[A_i(y) + C_{p,i} + C_e\right]f_{q,i}^{(2)}(y)\mathrm{d}y\,\mathrm{d}u$$

3. $P\left[(T + Y_{(sc)} < Y_{(s_i)}) \cap (Y_{(s_i)} < T + W)\right]$

The third case corresponds to the scenario where the ith PM is caused by a scheduled plan occurred at $T + Y_{sc}$, and $T + Y_{sc} < Y_{s,i} < T + W$. The scheduled plan is ahead of a catastrophic failure of U_2 in the implemented period. The expected maintenance cost is given by (Fig. 8.3)
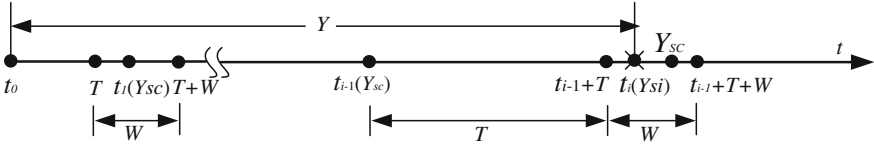
Fig. 8.2 PM is caused by a catastrophic failure in (T, Y_{sc})
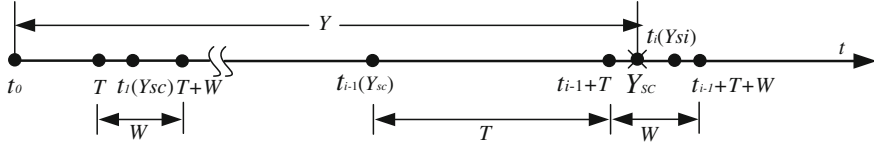
Fig. 8.3 PM is caused by a scheduled plan in (T, Y_{si})

$$R_{3,i} = I_{T+Y_{(sc)} < Y_{(s_i)} < T+W} \left[A_i(T + Y_{sc}) + C_{p,i} \right]$$

$$E\left[R_{3,i}\right] = \frac{1}{W} \int_0^W \int_{T+u}^{T+W} \left[A_i(T + u) + C_{p,i} \right] f_{q,i}^{(2)}(y) \mathrm{d}y\, \mathrm{d}u$$

4. $P\left[\left(T + Y_{(sc)} < T + W \right) \cap \left(T + W < Y_{(s_i)} \right) \right]$

The forth case corresponds to the scenario where the ith PM is caused by a scheduled plan occurred at $T + Y_{sc}$, and $T + Y_{sc} < T + W < Y_{s,i}$. The scheduled plan is also ahead of a catastrophic failure of U_2 in the implemented period. The expected maintenance cost is given by (Fig. 8.4)

$$R_{4,i} = I_{T+Y_{(sc)} < T+W < Y_{(s_i)}} \left[A_i(T + Y_{sc}) + C_{p,i} \right]$$

$$E\left[R_{4,i}\right] = \frac{1}{W} \int_0^W \int_{T+W}^{+\infty} \left[A_i(T + u) + C_{p,i} \right] f_{q,i}^{(2)}(y) \mathrm{d}y\, \mathrm{d}u$$

In the Nth PM interval, a replacement is performed for an occurrence of a catastrophic of U_2 or the operating time is reached T, whichever comes first. Thus, there are two scenarios for the occurrence of replacement activity.

1. $P\left(Y_{(s_N)} < T\right)$

The first case corresponds to the scenario where the replacement is caused by a catastrophic failure of U_2 occurred at $Y_{s,N}$, and $Y_{s,N} < T$. The catastrophic failure of U_2 is ahead of scheduled time T in the last PM interval. The expected maintenance cost is given by (Fig. 8.5)
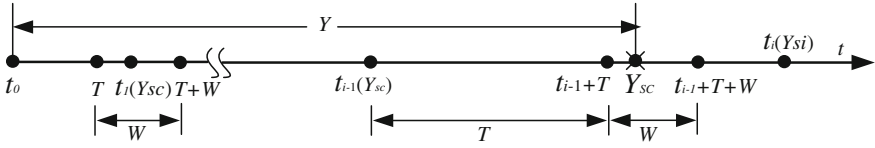
Fig. 8.4 PM is caused by a scheduled plan in $(T, T+W)$
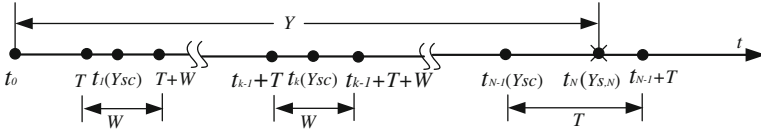
Fig. 8.5 The replacement is caused by a catastrophic failure of U_2

$$R_{5,i} = I_{Y_{(s_N)} < T}[A_N(Y_{s_N}) + C_e + C_R]$$

$$E[R_{5,i}] = \int_0^T (A_N(y) + C_e + C_R)f_{q,N}^{(2)}(y)\mathrm{d}y$$

2. $P(T < Y_{(s_N)})$

The last case corresponds to the scenario where the replacement is performed for the operating time is reached the planned time T, and the scheduled time T is ahead of a catastrophic failure of $U_2(T < Y_{s,N})$. The expected maintenance cost is given by (Fig. 8.6)

$$R_{6,N} = I_{T < Y_{(s_N)}}[A_N(T) + C_R]$$

$$E[R_{6,i}] = (A_N(T) + C_R)\bar{F}_{q,N}^{(2)}(T)$$

The total expected maintenance cost can be given by

$$R = \sum_{j=1}^{4}\sum_{i=1}^{N-1} R_{j,i} + R_{5,N} + R_{6,N} \tag{8.2}$$

$$E[R] = \frac{1}{W}\sum_{j=1}^{4}\sum_{i=1}^{N-1} E[R_{j,i}] + E[R_{5,N}] + E[R_{6,N}]. \tag{8.3}$$
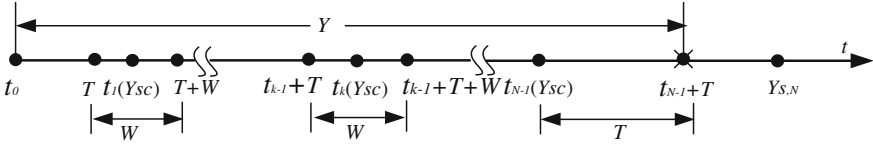
Fig. 8.6 The replacement is performed at T

8.3.2 The Excepted Renewal Cycle Length

According to the introduction of maintenance process and model assumptions, there are also four cases of the length of a PM interval, and two case of the length of the last PM interval, and thus, the renewal cycle Y of the system can be denoted as follows, where Ys_i, Y_{sc} are presented in notations.

$$Y = \sum_{i=1}^{N-1} \left\{ \begin{aligned} &I_{Y_{(s_i)} < T}(Y_{s_i}) \\ &+ I_{T < Y_{(s_i)} < T + Y_{(sc)} < T + W}(Y_{s_i}) \\ &+ I_{T + Y_{(sc)} < Y_{(s_i)} < T + W}(T + Y_{sc}) \\ &+ I_{T + Y_{(sc)} < T + W < Y_{(s_i)}}(T + Y_{sc}) \end{aligned} \right\} + I_{Y_{(s_N)} \in (0,T)}(Y_{s_N}) + I_{Y_{(s_N)} > T}(T) \quad (8.4)$$

Then, the *s*-excepted total cost of the renewal cycle can be stated as below:

$$E[Y] = \frac{1}{W} \sum_{i=1}^{N-1} \left\{ \int_0^W \int_0^{T+u} \bar{F}_{q,i}^{(2)}(y)\mathrm{d}y\,\mathrm{d}u \right\} + \int_0^T \bar{F}_{q,N}^{(2)}(y)\mathrm{d}y. \quad (8.5)$$

8.3.3 The Excepted Cost Per Unit Time

Based on the expected cycle cost and length, the *s*-expected cost per unite time is stated as follows using the renewal reward theorem:

$$g = \lim_{t \to +\infty} C(t)/t = E[R]/E[Y] \quad (8.6)$$

where $E[R]$ and $E[Y]$ are, respectively, given as notions.

Let $M(T, N)$ denote the items that are relative to the minor repair cost, and $J(T, N)$ denote the items that are relative to the extra cost. They can be, respectively, interpreted as below:

$$M(T,N) = \frac{1}{W}\sum_{i=1}^{N-1}\left\{\int_T^{T+W}\int_0^u \left(p_i h_i^{(2)}(y) + H_m h^{(1)}(y)\right)\bar{F}_{q,i}^{(2)}(y)\mathrm{d}y\,\mathrm{d}u\right\}$$

$$+ \int_0^T \left(p_N h_N^{(2)}(y) + H_m h^{(1)}(y)\right)\bar{F}_{q,N}^{(2)}(y)\mathrm{d}y$$

$$J(T,N) = \frac{1}{W}\sum_{i=1}^{N-1}\int_T^{T+W} F_{q,i}^{(2)}(y)\mathrm{d}y + F_{q,N}^{(2)}(T)$$

Further, the *s*-excepted total cost is rewritten as:

$$E[R] = \sum_{i=1}^{N-1} C_{p,i} + C_R + C_m^{(2)}M(T,N) + C_e J(T,N) \tag{8.7}$$

Then, the *s*-expected cost per unite time can be given by Eq. (8.8).

$$C(T,N) = \frac{E[R]}{E[Y]} = \frac{\sum_{i=1}^{N-1} C_{p,i} + C_m^{(2)}M(T,N) + C_e J(T,N)}{\frac{1}{W}\sum_{i=1}^{N-1}\left\{\int_0^W\int_0^{T+u} \bar{F}_{q,i}(y)\mathrm{d}y\,\mathrm{d}u\right\} + \int_0^T \bar{F}_{q,N}(y)\mathrm{d}y} \tag{8.8}$$

The object of the model is to find an optimal N^* and optimal T^* which together minimize $C(T, N)$ in the infinite-horizon case.

8.4 Numerical Example

Assume that the lifetime distribution of the two units follows the Weibull distribution. Its hazard rate function and the probability density function for the two units are given as below:

$$h^{(i)}(t) = \frac{\beta_i}{\eta_i}\left(\frac{t}{\eta_i}\right)^{\beta_i-1} \quad \text{and} \quad f^{(i)}(t) = \frac{\beta_i}{\eta_i}\left(\frac{t}{\eta_i}\right)^{\beta_i-1}\exp\left(-\left(\frac{t}{\eta_i}\right)^{\beta_i}\right) \quad (i = 1,\,2).$$

The implemented period $W = 0.5$, and it is assumed that a_i and p_i are discrete functions of i, as stated below:

$$p_i = \gamma^{\theta^i} - \gamma^{(i+1)^\theta} + \gamma, \quad \text{and } a_i = \frac{6i}{5i+1} (= 1,2,\ldots,N).$$

Set $\gamma = 0.85$, $\theta = 0.75$, and $q_i = 1 - p_i$. Let $\beta_1 = 1.5$, $\eta_1 = 0.5$, $\beta_2 = 1.2$, $\eta_2 = 2$, $C_m^{(2)} = 2$, $C_{p,i} = 2.5 + 0.05i$, $H_m = 0.25$, $C_r = 4$, $C_e = 2.5$.

Fig. 8.7 Mean cost rate versus $(T; N)$
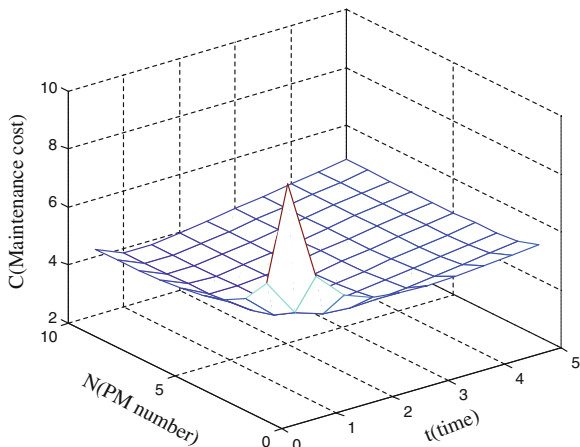
Then, according to Eq. (8.8), the optimal $N^* = 6$, $T^* = 1.88$, and min $C(T^*, N^*) = 4.565$ are obtained under the MATLAB 2010. That is to say, PM plans are randomly executed at each implemented interval [1.88, 2.38], and at the end of the sixth PM interval, a replacement is performed.

Figure 8.7 shows the plot of the mean cost rate versus (T, N) with above parameters. As can be observed, a smaller N or T may cause a greater mean cost rate C. However, the mean cost rate changes slowly and only slightly as N or T increases.

8.5 Results

In this paper, we proposed a quasi-periodic imperfect PM policy with dynamic PM plans and established to determine the optimal implemented period and PM number for a two-unit series system. The proposed model aimed at one type of two-unit series system that the lifetime of U_1 is always stochastically much smaller than U_2, and PM for U_1 is perfect and for U_2 is imperfect, and the dynamic PM plans are randomly modified considering needs of practice in the implemented period, and unplanned PM activities also take into account for an occurrence of a catastrophic failure of U_2. Based on the characters of the model, the PM period becomes a limited random value rather than a fixed value. Through analysis, we have modeled the expected system cost per unit of time, which is also the objective to be minimized for determining the optimal implemented period of PM activities and PM number. Numerical example was provided for verification of the proposed model. The obtained results can be extended to further studies on modeling and optimizing the sequential PM for a two-unit series or parallel system with stochastic maintenance interval. We are currently working on some of these topics.

References

1. Nicolai RP, Dekker R (2008) Optimal maintenance of multi-component systems: a review, complex system maintenance handbook. Springer, London, pp 263–286
2. Sandve K, Aven T (1999) Cost optimal replacement of monotone, repairable systems. Eur J Oper Res 116(2):235–248
3. Pham H, Wang H (2000) Optimal (τ, T) opportunistic maintenance of a k-out-of-n: G system with imperfect PM and partial failure. Naval Res Logistics 47(3):223–239
4. Taghipour S, Banjevic D, Jardine AKS (2010) Periodic inspection optimization model for a complex repairable system. Reliab Eng Syst Saf 95(9):944–952
5. Laggoune R, Chateauneuf A, Aissani D (2010) Impact of few failure data on the opportunistic replacement policy for multi-component systems. Reliab Eng Syst Saf 95(2):108–119
6. Zhang Z, Wu S, Li B (2011) A condition-based and opportunistic maintenance model for a two-unit deteriorating system. In: International conference on quality, reliability, risk, maintenance, and safety engineering. Chengdu, China, pp 590–595
7. Castanier B, Grall A, Bérenguer C (2005) A condition-based maintenance policy with non-periodic inspections for a two-unit series system. Reliab Eng Syst Saf 87(1):109–120
8. Naini SGJ et al (2009) Condition based maintenance for two-component systems with reliability and cost considerations. Int J Ind Eng Prod Res 20(3):107–116
9. Zhang Z et al (2012) Condition-based maintenance optimization without a predetermined strategy structure for a two-component series system. Eksploatacja i Niezawodnosc–Maintenance Reliab 14(2):120–129
10. Gao W et al (2013) Optimal combinatorial replacement policy under a given maintenance interval for the combined governor in diesel locomotives. Eksploatacja i niezawodnosc-Maintenance Reliab 15(2):89–98
11. Zhang Z et al (2012) Reliability modeling and maintenance optimization of the diesel system in locomotives. Eksploatacja i niezawodnosc–Maintenance Reliab 14(4):302–311
12. Kodo I, Toshio N (2012) Optimal operation censoring policy of aircraft, 2012. Asia-Pacific international symposium on advanced reliability and maintenance modeling. Nanjing, China, pp 184–191
13. Tahara A, Nishida T (1975) Optimal replacement policy for minimal repair model. J Oper Res Soc Jpn 18:113–124
14. Sheu SH, Kou C, Nagagawa T (1993) Extended optimal age replacement policy with minimal repair. RAIRO: Recherche Operationnelle 27(3):337–351
15. Castro IT, Sanjuan EL (2008) An optimal maintenance policy for repairable systems with delayed repairs. Oper Res Lett 36(5):561–564
16. Chen M (2013) Optimal random replacement models with continuously processing jobs. Appl Stoch Models Bus Ind 29:118–126
17. Gao W et al (2013) Maintenance optimization for a system with an implemented interval of replacement activities. In Proceedings 2013 international conference on quality, reliability, risk, maintenance, and safety engineering, pp 664–669

Chapter 9
Bayesian Network Technology to Analyze Fault Trees

Yao Wang and Qin Sun

Abstract Analyzing a fault tree using Bayesian network (BN) technology has gotten lots of attention, in which a fault tree is mapped into an equivalent BN. Combining three kinds of problems in BNs, a systematic BN method used to analyze fault tree is raised and the corresponding algorithm flowchart is designed. With the new method, a fault tree for the main landing gear of a certain aircraft is analyzed and the result shows that more useful and accurate information can be achieved through this new method.

Keywords Fault tree · FTA · Bayesian network · Inference

9.1 Introduction

Bayesian networks (BNs) developed in recent years have much similarity with fault trees from the aspect of inference and the way they describe the failure of a system. However, BN has an ability of describing systems, in which events/components have multiply failure modes and dependable [1, 2]. Thus, BN is a suitable model for system evaluation and fault diagnosis [3, 4].

Using BN methods instead of fault tree analysis (FTA) to analyze the fault tree is one research direction in the field of BN application. It mainly involves two aspects: the method for solving minimal cut/path set, structure importance degree, probability importance degree and critical importance degree [1], and the method

Y. Wang (✉) · Q. Sun
Aeronautics Building A517, School of Aeronautics, Northwestern Polytechnical University, Laodong Road, Xi'an, 710072 Shaanxi, China
e-mail: wangyaorose@126.com

Q. Sun
e-mail: sunqin@nwpu.edu.cn

for bidirectional reasoning in an equivalent BN [2]. The results gotten from the former one are the traditional measures which also can be computed by FTA. In contrast, the results gotten from the latter method are the ones that cannot be computed by traditional FTA. However, both methods can provide useful information to evaluate systems.

Based on the research above, three kinds of problems in BNs are discussed first. Then, a systematic approach for applying BN technology to analyze fault tree which should be mapped into its equivalent BN first, as well as a corresponding algorithm flowchart is proposed. Finally, the method raised above is further discussed through a fault tree example.

9.2 Bayesian Network Technologies

9.2.1 Three Kinds of Problems in BNs

Inference is a process of answer problems/queries by calculation. Three groups of problems are included in BN inference theory: posterior probability (Pr), maximum a posterior hypothesis (MAP) and most probable explanation (MPE) [3].

In a BN, all the variables which is represented with set N can be divided into three subsets: E, M and S. E stands for the set of evidence variables that have been known and $E = e$ holds; S stands for the variables whose values should be summed out that people do not care about; M stands for the variables that people are interested in.

Pr problem. Pr is the probability over M given $E = e$ and is defined as

$$\Pr(M|E = e) = \frac{\Pr(M, E = e)}{\Pr(E = e)}. \tag{9.1}$$

MAP problem. The MAP probability over variables M given evidence e is defined as

$$\Pr(M = m^*|E = e) = \max_m \Pr(M = m|E = e) \tag{9.2}$$

In Eq. (9.2), m represents an instantiation of M and when M takes the instantiation m^*, the posterior probability $\Pr(M = m|E = e)$ has the maximum value.

MPE problem. The MAP probability is just the MPE probability when set S is empty, which means that in a MPE problem, all the variables except E are the ones people care about.

9.2.2 A Systematic Bayesian Network Approach for Analyzing Fault Trees

The first step is to map a fault tree to its equivalent BN [1]. In the following, lowercase stands for events of a fault tree, and their corresponding uppercase stands for nodes of the fault tree's equivalent BN. Specifically, in a fault tree, x_i represents a bottom event, a_i represents an intermediate event and t represents top event. X_i, A_i and T represent nodes in the equivalent BN. Besides, q_i is the failure probability of x_i. In addition, 1 stands for the failure state and 0 stands for the normal or workable state, separately.

The steps for mapping a fault tree into its equivalent BN are given in the below. The topological structure of the BN can be finished by the former two steps. Each node in the BN has a conditional probability distribution (CPD) which parameterizes the BN. The latter two steps are intended to assign the right CPDs to each node in the BN.

1. For each event in the fault tree, map only one node in the BN even if such a node in the fault tree belongs to several logic gates. The new node in the BN also has two states: 0 and 1.
2. According to the cause–effect relationship (such a relationship is represented with different kinds of logic gates) in the fault tree, link the nodes that built in Step 1.
3. The root nodes in the BN correspond to the bottom event which has a failure probability. X_i stands one of the root nodes and the node's CPD is $\Pr(X_i = 1) = q_i$ and $\Pr(X_i = 0) = 1 - q_i$.
4. The rest nodes in the BN correspond to top or intermediate events. Such nodes' CPDs are determinate by the concrete logic gates that the top/intermediate events correspond to [1, 2]. For example, event t is caused by two bottom events (denoted by x_1 and x_1) and any one bottom event happens, the top event t happens. Thus, event t corresponds to "or" logic gate and the CPD of node T is determined by such a logic: $\Pr(T = 0|\ X_1 = 0,\ X_2 = 0) = 1$, $\Pr(T = 0|\ X_1 = 1,\ X_2 = 0) = 0$, $\Pr(T = 0|\ X_1 = 0,\ X_2 = 1) = 0$, $\Pr(T = 0|\ X_1 = 1,\ X_2 = 1) = 0$.

In traditional FTA, three measures are calculated quantitatively: reliability, probability importance degree and critical importance degree [5]. In essence, these three quantities are Pr problems. However, BN involves MAP and MPE problems, which cannot be solved by FTA. Table 9.1 shows both FTA and BN method for analyzing a fault tree.

Table 9.1 Two methods for analyzing a fault tree

Measures	FTA	Bayesian network technology
Reliability	$1 - g(q)$	$1 - \Pr(T = 1)$
Probability importance degree	$I_g(i) = \dfrac{\partial g(q)}{\partial q_i}$	$I_g(i) = \Pr(T = 1 \mid X_i = 1)$ $- \Pr(T = 1 \mid X_i = 0)$
Critical importance degree	$I_c(i) = I_g(i) \dfrac{q_i}{g(q)}$	$I_c(i) = \dfrac{q_i}{\Pr(T = 1)} \cdot I_g(i)$
MAP	Unsolvable	$\Pr(M = m^* \mid T = 1)$ $M \subset (A_i \cup X_i)$
MPE	Unsolvable	$\Pr(A_i \cup X_i \mid T = 1)$

9.3 Algorithm Design

Variable elimination algorithm [6] and jointree algorithm [7, 8] are two main-stream methods used to inference in a BN exactly. The former algorithm can only deal with Pr problems one by one, while the latter one can deal with several Pr problems through two times calculation (inward and outward calculation) [3]. In a fault tree, each event's importance degree needs calculation, which means many Pr problems are involved. Hence, jointree algorithm is more suitable than variable elimination algorithm for calculating importance degree measures of all the bottom events.

Pr problem is NP-hard [9] and can be solved effectively through the two classic algorithms stated above. Nevertheless, MAP problem is NP^{PP}-hard [10, 11] which cannot be solved effectively using traditional algorithms. Recently, a systematic search method raised by Park and Darwiche [4] represents the new state of the art in the field of solving MAP and it works effective. Hence, such a systematic search algorithm is chosen to solve MAP.

MPE problem is NP-hard as well as Pr problem [9]. The difference lies in that Pr contains multiplication and summation, two kinds of operations, while MPE contains multiplication and maximization, two kinds of operations [4]. MPE problem can be solved by changing summation operation in traditional algorithm into maximization.

Figure 9.1 is the algorithm flowchart that describes the procedure for analyzing a fault tree using BN technology systematically.

9.4 Case Studies

Figure 9.2a is a fault tree for the main landing gear of a certain aircraft [5], and Fig. 9.2b is its equivalent BN. Here, the new BN approach for analyzing fault tree stated above will be discussed in depth; the concrete physical meaning is omitted here and failure probability of each event is listed on Table 9.2.
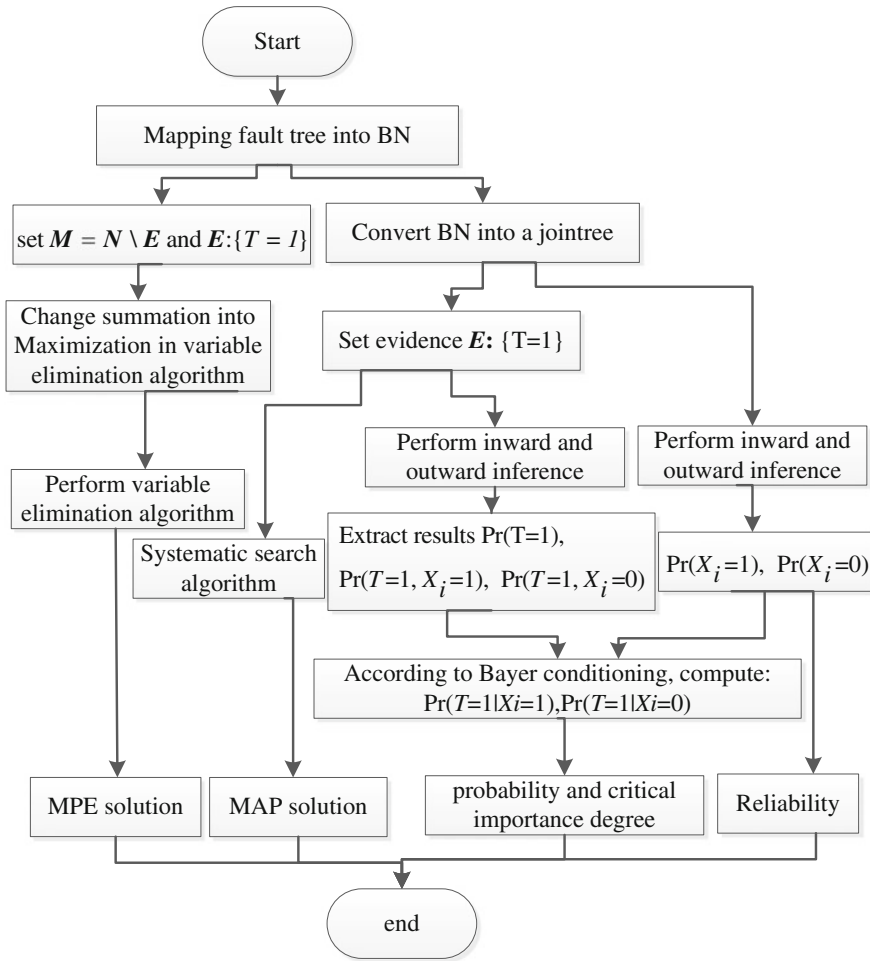
Fig. 9.1 Algorithm flowchart for analyzing fault tree using BN technology

Applying the new BN method illustrated in Fig. 9.1, the calculation results are given as below.

1. Solution to traditional measures

Reliability: $\Pr(T = 0) = 1 - \Pr(T = 1) = 0.99998750$

The reliability is consistent with the original literature. If one wants to compute probability and critical importance degree exactly in a fault tree through FTA, disjoint of Boolean function is the first step. It is such a big workload that barely can be realized. In view of the difficulty in precise calculation, original literature just provides the probability importance degree sequence and critical importance degree separately, rather than the exact probabilities. In contrast, the BN method

Fig. 9.2 a Fault tree for a
main landing gear.
b Equivalent BN

(a)

(b)
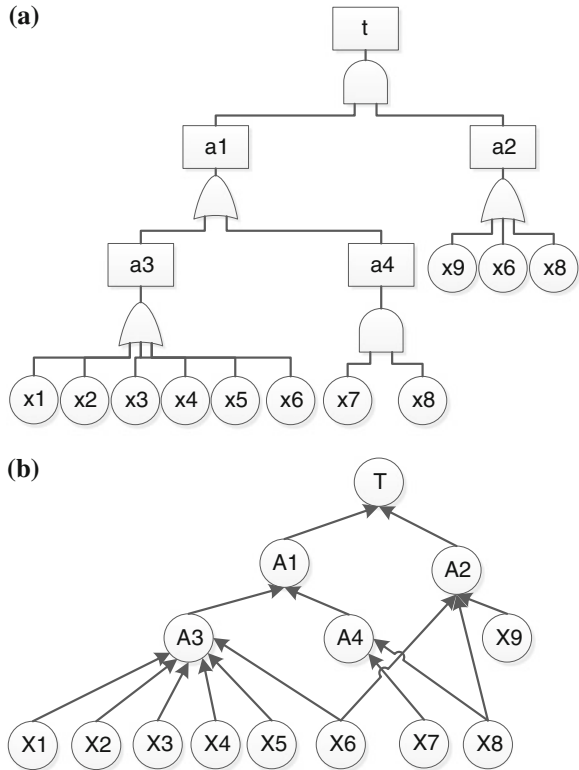
Table 9.2 Failure probability of each bottom event

Bottom event	Failure probability	Bottom event	Failure probability
x1	2.5000e−5	x6	1.2500e−5
x2	1.2500e−5	x7	2.0000e−8
x3	1.0000e−13	x8	1.5000e−5
x4	7.1500e−5	x9	3.5700e−5
x5	2.0000e−13		

stated can arrive at the exact solutions, through which disjoint calculation is
avoided. The two sequences agree with the results in Table 9.3.

2. Solution to MAP

   In fact, MAP is used to identify the most probable state/instantiation of set
M when top event happens and M consists of several events. Nevertheless, through
FTA, one can merely work out the probability of one event, not several events
(Table 9.4).

Table 9.3 Results for probability and critical importance degree

Bottom event	Probability importance degree	Critical importance degree
x1	6.31973e−5	1.26347e−5
x2	6.31980e−5	6.31741e−5
x3	6.31988e−5	5.05399e−13
x4	6.31943e−5	3.61335e−4
x5	6.31988e−5	1.01080e−12
x6	0.99999	0.99961
x7	2.75037e−5	4.39893e−8
x8	1.21504e−4	1.45761e−4
x9	1.21491e−4	3.46848e−4

Table 9.4 Solutions to MAP

Evidence variables	MAP variables	Solutions to MAP
$T = 1$	$M = \{x3, x4\}$	x3 = 0, x4 = 0 0.999639
$T = 1$	$M = \{x1, x7\}$	x1 = 0, x7 = 0 0.999975
$T = 1$	$M = \{x6, x8\}$	x6 = 1, x8 = 0 0.999543

3. Solution to MPE

MPE is used to identify the most probable state/instantiation of all the intermediate and bottom events when top event happens. MPE solution gives the most probable explanation of system's failure. When $T = 1$ holds, the rest events' state/instantiation and the corresponding probability are as follows:

$$m^* = \left\{ \begin{array}{l} A1 = 1, \ A2 = 1, \ A3 = 1, \ A4 = 0, \ x1 = 0, \ x2 = 0, \\ x3 = 0, \ x4 = 0, \ x5 = 0, \ x6 = 1, \ x7 = 0, \ x8 = 0, \ x9 = 0 \end{array} \right\};$$

$$\Pr(m^*|T = 1) = 0.999462$$

These three results show that x6 is the most probable event responsible for system's failure, and for the designers, it is the weakest link and it is necessary to decrease x6's failure rate. Such a consistent conclusion cannot be arrived at through FTA because of its insufficient calculation ability.

These three results above explain the system's failure in different ways. Combining all the results, a comprehensive evaluation about the system can be formed, which not only help people identify the cause for system's failure but also help the designer looking for system's weak line.

9.5 Summary

Combining with BN technology, a systematic method for analyzing fault trees is proposed. Moreover, a fault tree example is discussed to exemplify the method and the conclusions are as follows:

1. The method not only has the ability of avoiding disjoint of Boolean function but also can calculate reliability, probability importance degree and critical importance degree exactly. So, BN technology makes calculating traditional measures in a precise way possible.
2. Through BN technology, solutions to MAP and MPE can be worked out, which cannot be calculated through FTA. Thus, systems can be evaluated comprehensively by synthesizing all these results.

References

1. Portinale L, Bobbio A (1999) Bayesian networks for dependability analysis: an application to digital control reliability. In: Proceedings of the 15th conference on uncertainty in artificial intelligence. Morgan Kaufmann Publishers Inc., San Francisco, pp 551–558
2. Bobbio A, Portinale L, Minichino M et al (2001) Improving the analysis of dependable systems by mapping fault trees into Bayesian networks. J Reliab Eng Syst Safe 71:249–260
3. Zhang LW, Guo HP (2006) An introduction to Bayesian network. Science Press, Beijing (in Chinese)
4. Darwiche A (2009) Modeling and reasoning with Bayesian networks. Cambridge University Press, New York
5. Deng Q (2009) Safety system engineering. Northwest Industrial University Press, Xi'an (in Chinese)
6. Zhang NL (1998) Computational properties of two exact algorithms for Bayesian networks. J Appl Intell 9:173–183
7. Pearl J (1986) Fusion, propagation, and structuring in belief networks. J Appl Intell 29:241–288
8. Shenoy PP (1997) Binary join trees for computing marginals in the Shenoy-Shafer architecture. J Int J Approx Reason 17:239–263
9. Cooper GF (1990) The computational complexity of probabilistic inference using Bayesian belief networks. J Appl Intell 42:393–405
10. Shimony SE (1994) Finding MAPs for belief networks is NP-hard. J Appl Intell 68:399–410
11. Abdelbar AM, Hedetniemi SM (1998) Approximating MAPs for belief networks is NP-hard and other theorems. J Appl Intell 102:21–38

Chapter 10
Research on Data Mining Technology in IMA Safety Analysis

Miao Wang, Lihua Zhang, Qingfan Gu and Guoqing Wang

Abstract This study aims at the following problems brought by avionics system integration: failure spread caused by resource integration, failure implication and chaos resulted from function information fusion, and the difficulty in diagnosing the failure and expansion of failure damages triggered by mission synthesis. In this paper, we analyze the key problems of IMA system safety and take resource integration safety, function information fusion, and mission synthesis as the major objects of study to construct resource integration safety model, function information fusion safety model, and mission synthesis safety model and adopt data mining technology to set up knowledge transmission relationship among layers so as to reach safety management for top-layer mission execution in accordance with resource-layer safety data support.

Keywords Safety · IMA · Data mining

10.1 Introduction

As functional requirements of avionics system increase, system performance requirements improve, system resource ability requirements boost by a large margin, system complexity rises substantially, and huge pressures emerge to the

M. Wang (✉) · L. Zhang · G. Wang
Science and Technology on Avionics Integration Laboratory, Guiping Road 432,
Shanghai 200233, China
e-mail: wang_miao@careri.com

L. Zhang · G. Wang
School of Computer Science and Engineering, Northwestern Polytechnical University,
YouYiXiLu 127, Xi'an 710072, China

M. Wang · Q. Gu · G. Wang
China National Aeronautical Radio Electronics Research Institute, Guiping Road 432,
Shanghai 200233, China

constitution of avionics system. Integrated modular avionics (IMA) synthesize the information, resource, ability, and process of avionics system to form unified information collection, united resource allocation, unified capacity organization, unified process synergy, unified function integration, and unified system management through sharing, integration, synergy, and fusion so as to achieve the goal of low cost, high efficiency, high efficacy, high performance, and high reliability. Integration is currently the most important development direction of avionics system. Both Airbus A380 and Boeing 787 regard system integration as the core technology and capacity for development of avionics system. IMA adopts system integration method to improve resource ability and usage efficiency, adopts information fusion method to improve function capacity and processing quality, and adopts mission synthesis method to improve mission capacity and application efficacy. But, safety issue is caused in system integration process: (1) resource integration gives rise to failure spread, forming system capability operation safety problem; (2) function information fusion causes failure implication and chaos, forming system information processing safety problem; (3) mission synthesis leads to the difficulty in diagnosing the failure and expansion of failure damages, forming system result application safety problem. Thus, it is necessary to study the safety of IMA system.

Currently, China's IMA study is still in the initial stage. There are no special materials about IMA system safety in domestic public literatures and topics. So, it is badly necessary to establish basic theory on IMA system safety, safety guarantee, measurement, and evaluation system for IMA system to lay the foundation for studying new generation of IMA system. In order to effectively analyze safety of airplane operation state, large quantities of state monitoring and data processing modules are used in the airplane. According to incomplete statistics, condition monitoring sensors installed in A380 exceed 15,000, and these sensors are collecting data all the time when the airplane is flying. Due to numerous sensors, a large quantity of information based on time series will be produced. Effective analysis of these data is the foundation for constructing IMA safety model. These are exactly the research contents of data mining technology [1].

Based on the above analysis, this paper aiming at IMA system safety plans to take resource integration safety, function information fusion safety, and mission synthesis safety as the main objects of study to construct resource-layer safety model, function-layer safety model, and mission-layer safety model, respectively, and to use data mining technology to construct knowledge transmission model among the layers so as to achieve safety prognostics and management of top-layer mission execution according to resource-layer safety data support. The organizational structure in IMA system safety is shown in Fig. 10.1. IMA system safety analysis model based on data mining technology can be established through using data mining technology and combining IMA system safety structure. Figure 10.2 describes IMA system safety monitoring process based on data mining technology. In the following part, this paper will introduce each part in the structure diagram in detail.

Fig. 10.1 Organizational structure in IMA system safety
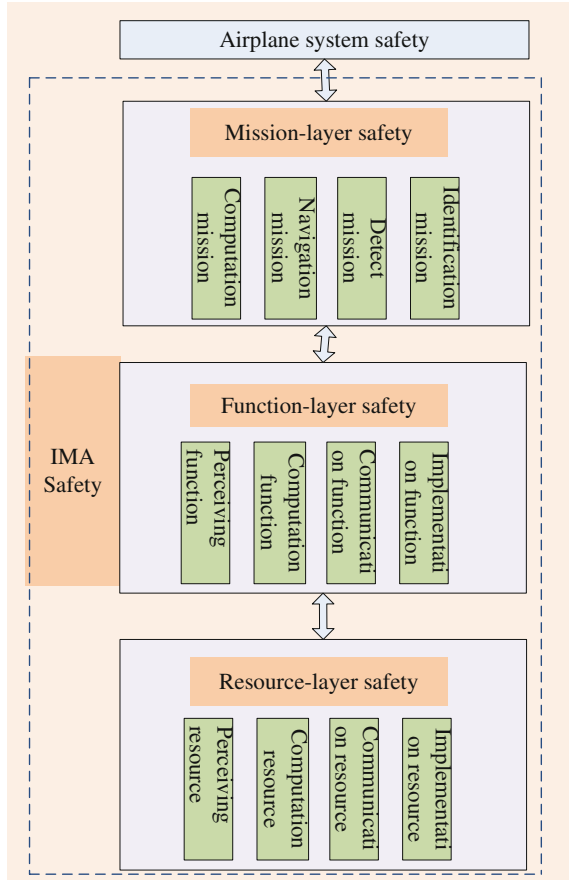
10.2 Study of Resource-Layer Safety Problem Based on Data Mining Technology

10.2.1 Safety Problem of IMA-Based Resource Sharing Integration

From the perspective of system design, every resource can be regarded as a subsystem with specific ability. On the one hand, physical integration boosts resource utilization rate through resource capacity sharing; on the other hand, it improves resource capacity efficiency through resource capacity organization and allocation. The above two aspects can reduce system resource allocation and decrease complexity influences. But resource integration makes the resource produce capacity relevance at the operation layer and organization layer. Thus,
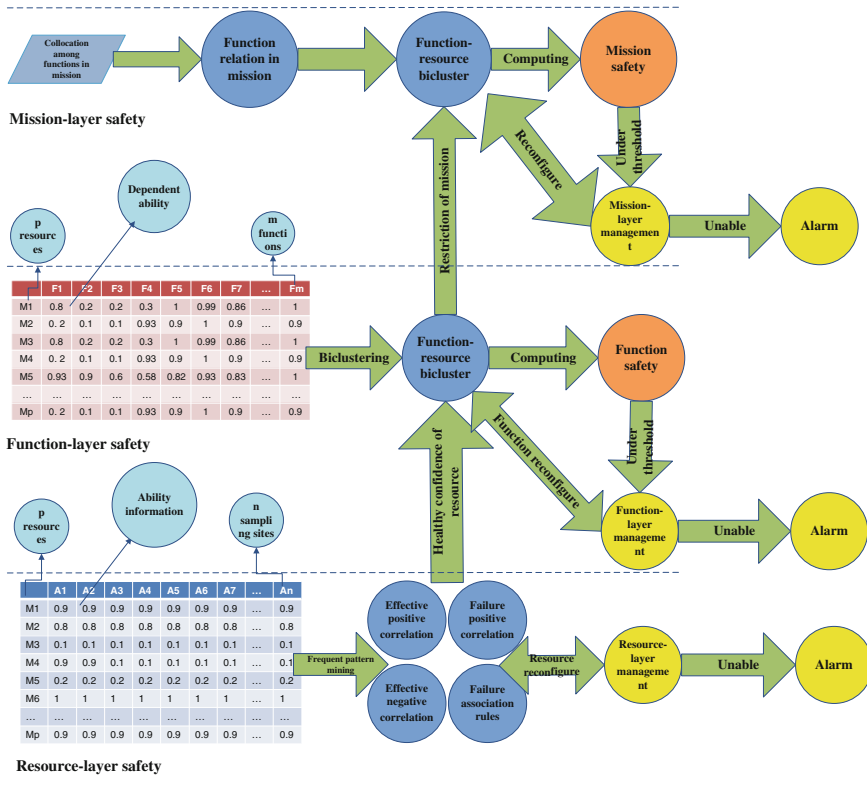
Fig. 10.2 IMA system safety monitoring process based on data mining technology

shared resource fault gives rise to failure spread and leads to mutual infection of different function errors, finally triggering greater safety problem. Aiming at the safety problem caused by failure speared resulted from IMA resource dynamic sharing, through studying the elements influencing resource integration, mutual relations among elements and resource capacity model, defining relevant rules, and limiting or reducing unpredictable behaviors, resource uncertainty is transformed to system behavior determinacy so as to achieve resource dynamic sharing and reconfiguration based on safety level. To realize the above functions, resource-layer safety management is divided into three parts logically: safety information collection, safety information analysis, and safety information modeling. The logic structure is shown in Fig. 10.3.

Safety information collection unit is responsible for collecting all input information related to resource integration, mainly involving resource capacity information, environmental state information, resource state information, and resource interaction information. Resource capacity information is the capacity set (resource space) which can be supplied by resource cooperation behaviors.
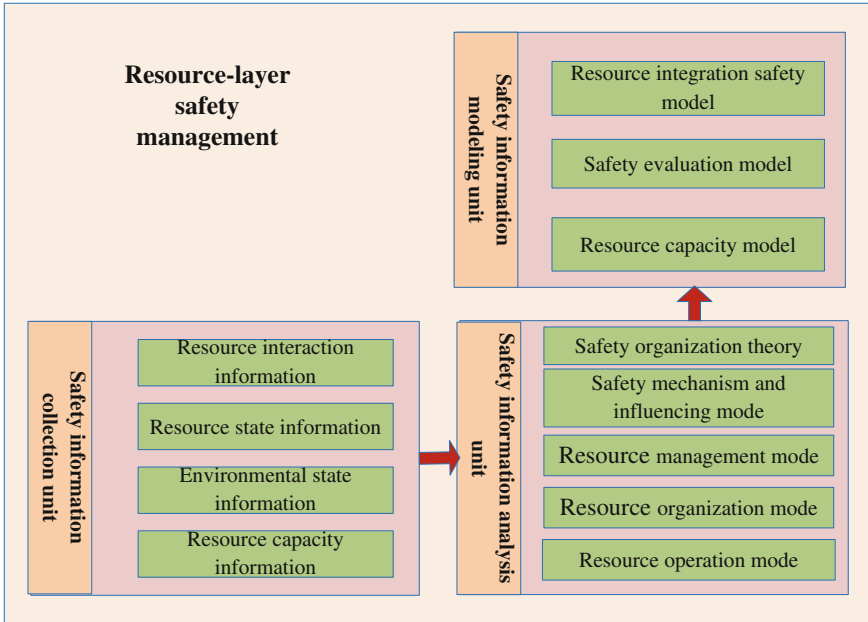
Fig. 10.3 Structure chart of resource-layer safety

Environmental state information includes ambient temperature, vibration, and other information. Resource state information contains validity, fault, sharing, conflict, activation, idleness, current value, voltage value, performance parameter, and resource redundancy. Resource interaction information involves the communication between processing resource and communication resource or the communication between processing resource and I/O resource.

Safety information analysis unit takes charge of analyzing and studying the information collected, mainly including resource operation mode, organization mode, management mode, system safety mechanism, and influencing mode. On this basis, resource safety organization theory is formed. Resource organization mode refers to different resource allocations according to resource requirements. Different resource organizations have diverse capacity integration ways, while the influences of capacity relevance caused by different capacity integration ways on system safety and results are also different. Resource operation mode means due to different resource types, resource operation modes and results are different. Thus, heritage relevance safety mechanism and influencing modes are different. Resource management mode refers to resource allocation management based on resource demands. Through resource capacity organization and allocation, resource sharing based on time sharing and changes of system state can be realized. Since resource capacities are different, the changes of system state are also diverse. Thus, safety influences caused by state relevance are different, too. From

the above, it is necessary to analyze and study safety mechanism and influencing mode and form integrated safety organization theory.

Safety information modeling unit contains modeling for resource capacity model, safety evaluation model, and resource integration safety model. Resource capacity model is a process of mapping resource space, system state, and demand space to resource capacity space. The following three aspects are mainly considered: (1) resource operation behavior (resource space); (2) organization behaviors among resources (demand space); and (3) resource allocation management (system stage space). In resource space, the operation attribute of resource capacity model is formed through analysis of resource operation mode. In demand space, sharing attribute of resource capacity model is formed through analysis of resource organization mode. In system state space, management attribute of resource capacity model is formed through analysis of resource management mode. Safety evaluation model means to study the technique to assess the influence of resource integration on system safety to achieve safety evaluation of resource integration, aiming at safety requirement of integrated system resource capacity sharing. Resource integration safety model considers inter-behaviors of components, constructs the relationship between safety elements influencing system safety behaviors and safety elements, forms resource equivalence class, and adopts formalization method to set up system safety model based on event relevance and behavior restriction on the basis of analyzing system safety mechanism caused by resource capacity sharing, operation result sharing, and resource management mode sharing.

10.2.2 Application of Data Mining in Analysis of Resource-Layer Safety

From the above analysis, it can be seen resource capacity model is the foundation to construct physical integration safety model. Safety analysis of the influence of resource integration on system state can be gained only through analysis of resource ability safety and safety among resource organizations. Thus, resource-layer safety evaluation and modeling can be realized. So, collection and analysis of real-time resource capacity information are the basis to construct resource-layer safety model. During real-time operation, resource capacity information during some period when the airplane flies can be collected, such as BIT value and sensor state parameters. Thus, the capacity matrix of M resources under N sampling sites can be set up. How to efficiently mine necessary resource modes from these data is very important for resource safety. At present, widely applied data mining technology can mine necessary knowledge from large quantities of complex data, where frequent pattern mining [2, 3] is a significant branch of data mining technology. This method can mine the modes meeting some rule and occurring frequently from vast data. These modes contain the following: (1) effective resource

combinations with high work efficiency; use of these modules together can provide high safety; (2) resources which go wrong simultaneously; find out the potential faults causes and provide decision support for using standby resources; (3) some resources present effective state and other resources go wrong; find out potential unstable resources to replace them early. Through the above mining process, resource capacity space can be measured to construct safety analysis model for resource operation behaviors. Meanwhile, frequent pattern mining algorithm can also measure with resource set capacity so as to set up safety analysis model for organizational behaviors among resources. Resource system space can be estimated through resource capacity measurement and measurement of behavior capacity among resources.

Association rule mining [4, 5] is a significant branch of data mining technology. This method can mine the resource pattern with some derivation relation from large quantities of data. The form of association rules is $X \Rightarrow Y$, where X and Y represent the data item of data concentration. The occurrence of X leads to the occurrence of Y. In resource validity matrix analysis, the form of association rules is $R_1 \Rightarrow R_2$ (support 80 %, confidence 100 %), where R_1 and R_2 are two different resources or a group of resources. The meaning of this rule is that when R_1 is very healthy, R_2 is 100 % healthy. Besides, in the whole resource validly matrix, the proportion of R_1R_2 health meanwhile is 80 %. According to the results of association rules, the resources which go wrong and need replacement can be gained. Assume an association rule $-R_3 \Rightarrow -R_4$ (support 80 %, confidence 100 %) exists, where "$-$" means fault. It can be seen from the above association rule after R_3 goes wrong, the probability of R_4 fault is 100 %. R_4 fault may be caused by R_3 cascading. Only from the perspective of frequent pattern mining, resource R_4 may be regarded as fault resource. But from the perspective of association rules, R_4 may be normal after R_3 is replaced. So, the association rules to mine resource fault can carry out prognostic and management of resource cascading fault and establish resource fault spread model so as to confirm the changes in system state caused by resource fault and ensure system safety.

Although the resources with low efficiency can be found through frequent pattern mining or resource association rule analysis for resource effectiveness matrix in a period to discover error resources in advance and start to use standby resources early, some resources show normal in a period (i.e., meeting support threshold or confidence threshold) and show validity downtrend in another period. For instance, in a short period, the system executes a function. The execution of such function will make some resources show low safety state. The characteristics of resource mode that the validity presents some trend described above comply with the features of bicluster mining in data mining technology. Resource failure can be found early through mining trend resource mode, which contributes to safety management of potential faults and improving system safety.

10.3 Study on Function-Layer Safety Problem Based on Data Mining Technology

10.3.1 Safety Problem of IMA-Based Function Information Fusion

Function information fusion means to establish function specialty, process reuse, and input difference processing modes and form system function information fusion capability according to function structure organization. Function information fusion optimizes system function organization, boosts the quality of mission system function capability, and specifies system validity capability. However, although information quality improves, sensor input, processing process reuse, and processing capability fusion arouse failure fuzziness, implication, and chaos, which gives rise to difficulties for failure diagnosis and prognostic, thus leading to safety problems.

Aiming at safety problems that resulted from function information fusion, this paper studies the influence mechanism and influencing mode of function information fusion on safety from three attributes (professional complementation of capability model, process reuse, and input difference) through setting up function capability model; analyzes dependency relationship of each function in the system, failure spread mode, sequential relationship of function invalidation, as well as time-dependent dynamics and random characteristics of system state in the failure state; and finally achieves function reconfiguration based on safety level. In a bid to realize the above functions, function-layer safety management is similar to resource-layer safety management and is also divided into three parts logically. The logic structure is shown in Fig. 10.4.

Safety information collection unit is responsible for collecting function capability information, environmental state information, function state information, and function interaction information. Function capability information is the capability set which is supplied by the function itself (individual space). Environmental state information includes ambient temperature, vibration, and other information. Analysis of environmental state information aims the effects of environmental changes on function performance. Function status information contains basic ability and track information of the function, interior structure and top-grade configuration information of the function, as well as function state parameter information. Function interaction information involves topological relation and cross-linking relation information among functions.

Safety information analysis unit takes charge of analyzing and studying the information collected, mainly including analysis and research of professional fusion mode, processing fusion mode, performance fusion mode, system safety mechanism, and influencing mode. Safety organization theory is formed in this basis. Function specialty refers to the classification of function execution results based on system resource capacity type. Professional fusion mode means to study
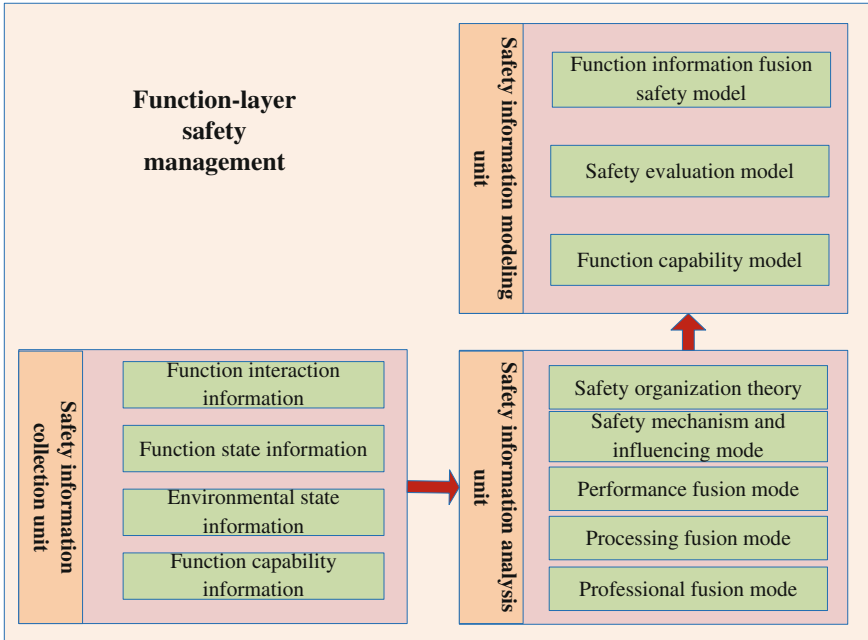
Fig. 10.4   Structure chart of function-layer safety

the influencing mode of function fusion on safety from the perspective of professional complementation. Processing fusion mode means to study the influencing mode of function fusion on safety from the perspective of input difference. Since safety-influencing factors related to function capability caused by function specialty fusion, safety-influencing factors related to function quality caused by function processing fusion, and safety-influencing factors related to sensors caused by function performance fusion are different, it is necessary to analyze capability integration mode of each function. In addition, it is required to analyze corresponding safety mechanisms and finally form safety organization theory of function information fusion.

Safety information modeling unit contains modeling for function capability model, safety evaluation model, and function information fusion safety model. Function capability model describes function capability from three aspects: result capability, processing capability, and input capability. Since function specialties are different, the processing process is different, too. Thus, the influences on result quality are diverse. Therefore, professional capability attribute of capability model is formed through analysis of professional capability fusion. As the function environments are diverse, the influences of processing process on result ability are different. Thus, processing capacity attribute of capability mode is formed through analysis of processing fusion mode. As the input of function information processing, the usability, integrity, and reliability of resources directly influence

system information processing quality. So, input capacity attribute of function capability model is formed through analysis of sensor information fusion of function performance. Safety evaluation model means aiming at safety demand of integrated system information processing to study the technique to assess the influences of function information fusion on system safety and achieve evaluation of the safety of function information fusion. The operation of integrated avionics system is based on information processing, so the precondition of achieving system safety operation is to study system function fusion safety model and explore safety-influencing factors in operation. Function fusion safety model establishes information processing logic equivalence model, analyzes interaction process of function logic, defines system safety state, studies the causes, and finally forms system function fusion safety model based on research and analysis of function capability model.

10.3.2 Application of Data Mining Technology in Analysis of Function-Layer Safety

It can be seen from the above analysis that function capability model is the foundation to construct function information fusion safety model. Function-layer safety can be evaluated and modeled only through analysis of function capability safety and the safety of three fusion models. So, analysis of organizing ability triggered by real-time function capacity and function fusion is the foundation to construct function-layer safety model. From the perspective of system health management, function error is the deviation of relative functional specification of operation process and results. The errors caused by some functions are resulted from resource fault. So, the essence of function error reconfiguration is to reconfigure resource fault supporting this function. Thus, it is necessary to analyze the call relationship between multiple functions and multiple resources through analyzing function–resource call relationship and construct function capability model and function organization model according to resource capacity model so as to set up function-layer safety evaluation model and function information fusion safety model.

Function–resource call relationship can be abstracted as a matrix. In other words, each row means a resource and each column means a function; the value in the matrix is resource usage degree of a function. Through mining the above function–resource matrix, the usage relation between a group of functions and a group of resources can be gained. For instance, for a group of functions $F_1F_2F_3$, the resource relations called by each function are as follows: $F_1 ==> R_1R_2R_3$, $F_2 ==> R_2R_4R_5$, and $F_3 ==> R_6R_7$. Assuming $F_1F_2F_3$ need to cooperate to complete a mission T, these three functions may be called at the same time. For resource R_2, it supports F_1 and F_2 simultaneously. If (1) R_2 has high validity for F_1 and has low validity for F_2 and (2) R_2 has high validity for both F_1 and F_2, safety degree of the former condition is higher than that of the latter. This is because in the former condition, R_2 can serve F_1 and F_2 at the same time, while in the former

condition, R_2 needs to serve the two resources respectively. From the perspective of function health, if R_2 goes wrong, the influence degree on the former condition is lower than that on the latter condition.

Bicluster mining algorithm [6–8] in data mining can mine function–resource relation from the above function–resource usage matrix to describe the safety of a function or multiple functions with module safety so as to establish function capacity operation attribute and construct function safety model. In the meantime, the relations between multiple functions and multiple resources are included in bicluster, so organizational behavior safety analysis model among functions can be constructed; the connection model of resource safety model and function safety model can be established to complete evaluation of function-layer safety.

10.4 Study on Mission-Layer Safety Problem

In application space, the integration of new generation of avionics system is reflected in mission organization synthesis. Mission synthesis involves the significance of two layers: on the one hand, in line with total user demands, combine avionics system resource and function capability to disintegrate demands to the resources and functions with corresponding capability (the capability to meet demands), i.e., generation process of mission execution plan; on the other hand, based on mission plan and current resource and function capacities as well as system state, select suitable path to execute the mission, i.e., execution process. Essentially, mission synthesis is process integration. Mission synthesis achieves system mission organization optimization and improves mission system application efficiency. Although it can improve mission efficiency, it meanwhile causes such problems that it is hard to confirm failure state and diagnose failure constitution. Aiming at the difficulty of failure diagnosis caused by mission synthesis, this paper starts from the three aspects (environmental conditions, mission object, and mission process) influencing mission completion and focuses on mission organization decision process and improving mission execution management ability to reveal the relationship among the elements influencing system safety at the organization layer of system mission, establishes system application safety evaluation system, and provides theoretical support for analysis and evaluation of application safety of IMA system.

To achieve the above functions, mission-layer safety management is also classified into three parts logically. The logic structure is shown in Fig. 10.5. Safety information collection unit includes environmental condition information, mission objective information, mission priority information, mission combination information, and mission operation information. Similar to function capability information and resource capacity information, mission demand information is the demand set of mission operation behaviors transforming to system space; mission objective information is the specific description information of mission purpose; mission priority information refers to the priority relation of a series of missions;

**Mission-layer
safety management**

Safety information modeling unit

Mission synthesis safety model

Safety evaluation model

Safety information collection unit

Mission demand information

Mission combination information

Mission priority information

Mission objective information

Environmental condition information

Safety information analysis unit

Safety organization theory

Safety mechanism and influencing mode

Management synthesis mode

Organization decision model

Situation synthesis mode

Fig. 10.5 Structure chart of mission-layer safety

mission combination information is the organization relationship among missions, i.e., which missions can be executed simultaneously, which missions are of mutual exclusion during execution; mutual exclusion ability condition information covers multi-source sensor information, navigation information, and corresponding 3D terrain data.

Information analysis unit is in charge of analyzing situation synthesis mode, organization decision model, and management synthesis mode, analyzing the influencing modes on safety and exploring safety mechanism on this basis and finally forming safety organization theory of mission synthesis. Situation synthesis aims at environmental condition elements of the mission to provide perceiving ability for the mission. It is the base to boost mission synthesis validity. Situation synthesis can be deemed as longitudinal capability synthesis of system application mission. The synthesis result corresponds to a snapshot in time series of application mission execution. Organization decision aims at mission environment ability to provide decision reference for mission synthesis and finally provides safety design and verification of avionics system. Mission organization synthesis is lateral organization synthesis of system application mission. In essence, the process is the generation process of a mission plan. Management synthesis refers to element management in the process of mission execution. Under the conditions where the resource has fault, the function goes wrong or the mission breaks down;

the effects on system safety can be eliminated or reduced through effective state organization and management.

Information modeling unit contains the modeling for safety evaluation and mission synthesis safety. Mission synthesis safety model studies the elements influencing mission objective, environmental conditions, and mission process and their relations from application perspective and guides mission execution plan and generation process of mission execution. Safety evaluation model aiming at integrated system application safety requirements researches the technique to assess the influences of mission synthesis on system safety and achieves evaluation of mission synthesis safety. Evaluation of mission-layer safety can be finished through function usage allocation relation of one or multiple missions and combining function safety model and resource safety model. System safety monitoring process based on flight mission is displayed in Fig. 10.2.

10.5 Conclusion

Aiming at the problems brought by avionics system integration, this paper starts from the key problems of IMA system safety and takes resource integration safety, function information fusion, and mission synthesis as the major objects of study to construct resource integration safety model, function information fusion safety model, and mission synthesis safety model and adopt data mining technology to set up knowledge transmission relationship among layers so as to reach safety management for top-layer mission execution in accordance with resource-layer safety data support.

References

1. Han J, Kamber M, Pei J (2012) Data mining concepts and techniques (trans: Fan M, Meng X). China Machine Press, China
2. Pei J, Han J (2004) Mining sequential patterns by pattern-growth: the prefixspan approach. IEEE Trans Knowl Data Eng 6(10):1–17
3. Zaki M (2001) SPADE: an efficient algorithm for mining frequent sequences. Mach Learn 40:31–60
4. Cong G, Tung A, Xu X et al (2004) FARMER: finding interesting rule groups in microarray datasets. In: Proceedings of ACM SIGMOD international conference on management of data. pp 143–154
5. Wang M, Shang X et al (2009) Strong association rules mining without using frequent items for microarray analysis. In: Proceedings of the 3rd international conference on bioinformatics and biomedical engineering , ICBBE 2009

6. Cheng Y, Church GM (2000) Biclustering of expression data. In: Proceedings of 8th international conference on intelligent systems for molecular biology (ISMB00). ACM Press, pp 93–103
7. Wang M, Shang X et al (2010) FDCluster: mining frequent closed discriminative bicluster without candidate maintenance in multiple microarray datasets. In: ICDM 2010 workshop on biological data mining and its applications in healthcare, p 779–786
8. Wang M, Shang X et al (2013) Efficient mining differential co-expression biclusters in microarray datasets. Gene 518:59–69

Chapter 11
Research on Maintenance Safety Evaluation of the Aging Aircraft

Tao An, Yuting He and Chao Gao

Abstract In this paper, the maintenance safety evaluation of the aging aircraft was studied. Firstly, the safety evaluation index system was built based on human factors, structure factors, and management factors. And nine indexes were included in these factors. Secondly, the weight of each index was calculated with rough set and information entropy. And then the safety evaluation model was built. Finally, taking an aircraft as example, the evaluation result could reflect the actual condition of the aircraft. The method was of great help to the maintenance of aging aircrafts and the development of new aircrafts.

Keywords Aging aircraft · Safety evaluation · Maintenance

11.1 Introduction

Generally, the aircraft which has served for 14 years or more is defined as aging aircraft in the world [1]. In China, more and more civil aircrafts and military aircrafts are entering the aging stage [2]. By the end of 2011, the average age of the transport aircrafts was 8.7 years. Figure 11.1 shows the proportion of the aircrafts which belonged to three different age groups in the fleet. The aircrafts under 10 years accounted for 75 % of the total quantity, the ones used for 10–20 years accounted for 23.5 %, and the aircrafts used for over 20 years were up to 1.5 % of the whole fleet [3].

T. An (✉) · Y. He · C. Gao
Aeronautics and Astronautics Engineering College, Air Force Engineering University,
Xi'an 710038, China
e-mail: rainman767@163.com

Fig. 11.1 The proportion of
the aircrafts in three different
age groups
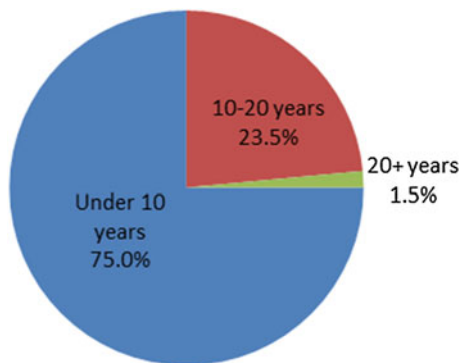
After servicing for so many years, the safety of the aging aircraft is bound to decline. In recent years, many accidents happened on aging aircrafts all over the world. The best-known one is the Aloha event [4] which happened in 1988. The Boeing 737–200 aircraft lost one piece of the ceiling at 7,300 m, and a stewardess was sucked out of the aircraft. Although the aircraft was broken very hard, other persons were lucky to survive. The picture is shown in Fig. 11.2. After investigation, it was found that the accident was caused by the failure of the aluminum rivets because of metal fatigue. But the fundamental reason was the aircraft had served for 19 years. The service life was 14,000 life cycles more than the design life. There are a lot of other accidents caused by kinds of factors, such as maintenance management and human factor. So it is important to insure the maintenance security of the aging aircrafts. In this paper, we discussed the method to evaluate the safety of the aging aircraft maintenance based on the rough set. The rough set is a mathematic tool to analyze indeterminate and imprecise data.

11.2 Basic Concepts of the Rough Set Theory

11.2.1 Information System

Formally, an information system [5–7], *IS* or an approximation space, can be seen as a system $IS = < U, A, V, f >$, where U is the universe (a finite set of objects, $U = \{x_1, x_2, \ldots, x_m\}$). In this paper, it represents different kinds of aging aircrafts. A is the set of attributes (features, variables). $A = C \cup D$, C is the condition attribute set, and D is the decision attribute set. Each attribute $a \in A$ (attribute a belonging to the considered set of attributes A) defines an information function $f : U \times A \rightarrow V$, where V is the set of values of a, called the domain of attribute a.

Fig. 11.2 The successful ditching of the Aloha flight No. 243, with only one loss of life among the 65 people on board, was an extraordinary feat in the aviation history

11.2.2 Indiscernibility Relation

For every set of attributes $B \subset A$, an indiscernibility relation Ind(B) is defined in the following way: x_i and x_j are indiscernible by the set of attributes B in A, if $b(x_i) = b(x_j)$, for every $b \in B$.

The equivalence class of Ind(B) is called elementary set in B because it represents the smallest discernible groups of objects. For any element x_i of U, the equivalence class of x in relation Ind(B) is represented as [x_i] Ind(B). The construction of elementary sets is the first step in classification with rough set.

11.2.3 Lower and Upper Approximations

The rough sets approach to data analysis hinges on two basic concepts, namely the lower approximations and the upper approximations of a set (Fig. 11.3).

The lower approximations of a set denote the elements that doubtlessly belong to the set. Let X denote the subset of elements of the universe $U(X \subset U)$. The lower approximation of X in B, denoted as BX, is defined as the union of all these elementary sets which are contained in X. More formally $\underline{BX} = \left\{ x_i \in U \middle| [x_i]_{\mathrm{ind}(B)} \subset X \right\}$.

The upper approximations of a set denote the elements that possibly belong to the set. Denoted as BX, the upper approximation of X in B is the union of these elementary sets, which have a non-empty intersection with X: $BX = \left\{ x_i \in U \middle| [x_i]_{\mathrm{ind}(B)} \cap X \neq \phi \right\}$.

Fig. 11.3 Schematic
demonstration of the *upper*
and *lower approximations* of
set *X*. The *lower
approximations* denote the
elements that doubtlessly
belong to the set. The *upper
approximations* denote the
elements that possibly belong
to the set
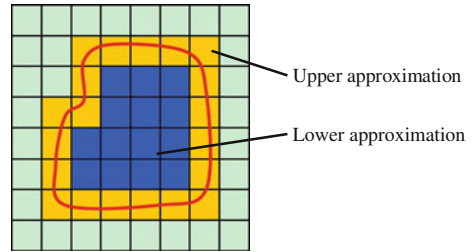
11.2.4 Independence of Attributes

In order to check whether the set of attributes is independent or not, one checks for
every attribute whether its removal increases the number of elementary sets in the
IS or not.

Let $a_i \in A$, if $\text{Ind}(A) = \text{Ind}(A - a_i)$, then the attribute a_i is called superfluous.
Otherwise, the attribute a_i is indispensable in *A*.

11.2.5 Core and Reduct of Attributes

Reduct of attributes: *A* subset $B \subseteq A$ is called a reduct of *IS* if and only if
$\text{Ind}(B) = \text{Ind}(A)$ and *B* is independent. The set of all reducts in *IS* is denoted by
Red(*IS*) or Red(*A*).

Core: The core of *A* is a set of all indispensable attributes of *A*, denoted by
$\text{Core}(A) = \cap \text{Red}(A)$.

11.3 The Algorithm of the Maintenance Safety Evaluation

11.3.1 Maintenance Safety Evaluation Indexes

The factors which could lead to the aircraft maintenance accidents were found out.
It mainly includes three aspects: human factors, structure factors, and management
factors.

Human Factors The statistics show that the human factors are the main reason
that leads to flight accidents and signs of the accidents. The maintenance errors
account for 85 % of the aviation accidents in the world. In addition, 20–30 % of the
engine off in flights, 80 % of the crashes, 80 % of veering off a runway, 50 % of the
flight delays, and 80 % of the flight cancellations are all related to maintenance
errors. And the human errors account for 80 % of the maintenance errors [8].

So the influence of human on maintenance cannot be underestimated. The evaluation indexes of the human factors mainly include the following:

1. Body and Mind (C1): Due to physical and psychological dysfunction, the maintenance engineer's judgment ability will be reduced, which is likely to make mistakes.
2. Responsibility (C2): If the engineer takes bad attitude, careless work, little responsibility, and violation of operations and regulations, the probability of making mistakes would substantially grow up.
3. Professional Ability (C3): Professional ability includes many kinds of capabilities. If the engineer lacks the necessary professional knowledge, skills, and trainings, they will make mistakes sooner or later.

Structure Factors After years of using, a number of problems will emerge in aircraft structures. The performance of the aircraft' systems and parts will decline obviously [9]. We summarized these phenomenons into three classical indicators:

1. Fatigue (C4): Fatigue failure is the main failure form in aircraft structures. Many flaws could be found in the skins and frames during overhaul. If these flaws cannot be found and fixed in time, they will cause the sudden breakage of the structures.
2. Corrosion (C5): Corrosion is a kind of recessive damage for the aging aircrafts. It would lead to pitting and peeling off, but usually difficult to be detected. The beam, kitchen, washroom, and oil tank are easier to be corroded.
3. Aging (C6): The phenomenon of aging often occurs in rubber, organic glass, and other nonmetallic materials. Aging of the electrical wiring would lead to short-circuit and fire. The sealing of the rubber grommets after several years would be bad.

Management Factors High-quality and efficient maintenance management is of great significance to reduce human errors and ensure flight safety [10]. The maintenance management includes a lot of concerns. We summarized them into three aspects:

1. People Oriented (C7): People are the basic of management. The potential and motivation could be stimulated by handling the relationships correctly, allocating and utilizing human resource reasonably, and effective incentive. The manager also should provide a broad space and plenty of opportunities for subordinates.
2. Rules and Regulations (C8): The safety of maintenance must base on the regulatory and institutional management strictly. Various rules and regulations should be comprehensive, meticulous and matching. They also should be combined into a strict management system.
3. Communication (C9): Many departments and links related to the aging aircraft maintenance management. The company must strengthen the communication with manufactures and get full technological support. Meanwhile, they also should strengthen exchanges, learn from each other, and share technology.

11.3.2 Maintenance Safety Evaluation Based on Rough Set

We chose several aging aircrafts' attribute data as training set and calculated the weight of each evaluation index with rough set and information entropy. The maintenance safety coefficient of a given aircraft could be calculated based on these weights. The algorithm is shown below:

Step 1: Four classic aircrafts from different airports were selected, which were maintained by different engineers. According to the specific condition of each aircraft, the exports score for every index. The scores were divided into five levels as 1, 2, 3, 4, 5 from bad to good.

Step 2: The decision table for Rough Set was built with data from step 1. The table was shown in Table 11.1.

Step 3: The weight of each evaluation indicator was calculated based on Rough Set and information entropy.

Let U be a domain, p is a indiscernibility relation family of U, $U/\text{ind}(p) = \{X_1, X_2, \ldots, X_n\}$. Then, the distribution probability of p is shown as follows:

$$[X; p] = \left\{ \begin{matrix} X_1, X_2, \ldots, X_n \\ p(x_1), p(x_2), \ldots, p(x_n) \end{matrix} \right\}. \tag{11.1}$$

Based on this distribution probability and information theory, the information entropy of p is

$$H(P) = -\sum_{i=1}^{n} p(x_i) \log p(x_i). \tag{11.2}$$

Then, we can calculate the degree of each indicator with $H(P)$:

$$S_c(c_i) = |H(P) - H(P - \{X_i\})|. \tag{11.3}$$

Finally, the weight of each indicator can be calculated with the following equation:

$$\omega_i = \frac{S_c(c_i)}{\sum_{i=1}^{j} S_c(c_i)}, \quad (i = 1, 2, \ldots, 9). \tag{11.4}$$

After normalizing, the weights are 0.12, 0.13, 0.16, 0.11, 0.10, 0.07, 0.12, 0.10, and 0.09.

Step 4: After an aircraft's indicators were given, the evaluation result could be calculated based on the following equation:

$$S = \sum_{i=1}^{9} (\omega_i \cdot x_i) \tag{11.5}$$

Table 11.1 The decision table

Aircrafts	Aircraft 1	Aircraft 2	Aircraft 3	Aircraft 4
C1	3	4	3	5
C2	4	1	5	3
C3	3	4	2	3
C4	2	3	1	4
C5	5	1	3	2
C6	3	4	5	1
C7	4	5	1	3
C8	4	3	3	5
C9	1	5	3	4

Take an aircraft as example, if the indicator set is $C = \{4, 2, 5, 4, 3, 4, 3, 5, 1\}$, the evaluation result will be $S = 3.51$ (the full mark is 5.00). This means the maintenance safety of the aircraft is good.

11.4 Conclusion

Using of the aging of aircrafts is becoming an urgent problem all over the world. The maintenance quality is very important to ensure the normal flight. The method proposed in this paper provided some new ideas to evaluate the aircraft maintenance safety. Nine indexes were summarized through analyzing human factors, structure factors, and management factors in the process of maintenance. These indicators could represent the basic safety level of an aging aircraft. Then, the weights of indexes were calculated based on rough set and information entropy. Finally, the maintenance safety of aging aircraft could be calculated with these weights. The method was helpful for the maintenance of the aging aircraft. The research also could be used in the development and maintenance of new aircrafts.

References

1. Li L (2005) Reliability and safety administration on the aging airplane (in Chinese). Aviat Maintenance Eng 2:73–75
2. Wang M, Gao X, Cai F (2001) Overview of research on military aircraft combat effectiveness analysis (in Chinese). Flight Dyn 4:233–238
3. Yu D (2012) Research on policy of aging aircraft maintenance management (in Chinese). Aviat Maintenance Eng 2:81–83
4. Jia B, Du Y, Xie B (2010) The institute, promulgation and implementation of aging aircraft damage tolerance airworthiness regulation (in Chinese). Aviat Maintenance Eng 1:32–35
5. Pawlak Z (1991) Rough sets: theoretical aspects of reasoning about data. Kluwer Academic Publish

6. Wu SZ, Gou PZ (2011) Attribute reduction algorithm on rough set and information entropy and its application (in Chinese). Comput Eng 37(7):231–232
7. Ahn BS, Chao SS, Kim CY (2000) The integrated methodology of rough set theory and artificial neural network for business failure prediction. Expert Syst Appl 18(7):65–74
8. Cao Y (2010) The influence of human factors to the safety of aircraft in maintenance process (in Chinese). Value Eng 3:204
9. Zeng T, Zhang B (2005) Challenges and prospects of military aircraft maintenance (in Chinese). Aviat Maintenance Eng 1:28–31
10. Lujian Xv (1996) The effect of human factors on maintenance quality of aircraft (in Chinese). Int Aviat 2:5–6

Chapter 12
Research on System-Level Maintenance Operation Sample Allocation Method Validation

Anwei Shen, Jilian Guo and Jianwei Li

Abstract Combined with military aircraft maintenance identification of the actual test in the flight test stage, the method of GJB2072 sample allocation is improved in this paper based on in-depth analysis of the characteristics of maintainability data. A maintenance operation sample allocation methods based on the LRU is proposed, thus improving the operability of maintenance operation sample allocation. Finally, the validity of the method is confirmed by assigning testing samples of 30 within the improved method.

Keywords Maintainability · LRU · Sample allocation · Test flight stage

12.1 Introduction

Maintainability is an important design feature of modern combat aircraft and is also an important factor affecting their combatant effectiveness. With the development of science and technology, many new technologies and new equipment are widely used in the development of military aircraft. With the development in the direction of electronic, digital, and intelligent, the technical complexity and the more stringent requirements for maintenance are increasing inevitably. In order to

A. Shen (✉) · J. Guo
Air Force Engineering University, Xi'an 710038, China
e-mail: zjsaw@foxmail.com

J. Guo
e-mail: guojilian@aliyun.com

J. Li
Military Representative Office of the Army Aviation, Jingdezhen 333002, China
e-mail: lijianwei403@163.com

confirm whether the aircraft maintenance work meets the design requirements, we must assess it in the flight test aircraft under field environment.

For the method of system-level verification, whether it is a classic or a small sample authenticate method, the selection and assignment of the sample should be carried out. Only the sample assigned to each component reasonably can we elect maintenance operation samples representatives to the entire system and thus ensure the accuracy of the maintenance verification results in the system level [1]. Maintenance operation sample selection and allocation is a better way to solve the problem [2].

Currently, the military standard GJB2072 "Maintenance Test and Evaluation" [3] stipulates that in equipment maintenance verification requirements, the operation samples of natural failure when equipment qualification test under specified conditions are preferred. When the maintenance operations number of natural failure is not enough to guarantee the required sample size of verification method, the simulation failure is used.

The method is to put maintenance operation in a close repair time (a difference of not more than 25 %) into a group after estimating the repair time for each maintenance operation. But sometimes this method is inconvenient in operation. So, Ref. [4] proposed improvements for the proportional assignment of repair operation samples' failure rate. The method fully mobilizes the limited maintenance resources in maintainability trials. Aimed at the proportion assignment method for the failure rate of maintenance sample in "Maintenance Test and Evaluation," the improvement opinion is proposed in Ref. [5]. The repeated maintenance is avoided, and the maneuverability of the assignment for maintenance sample is increased.

In order to improve the operability of maintenance sample allocation, sample allocation method for maintenance operation has been improved in this paper combined with the actual of military aircraft maintenance test identified. Then, the maintenance operation sample allocation method based on the line replaceable unit (LRU), which makes the maintenance operations personnel convenient to operate is proposed.

12.2 Characteristics of the Maintainability Data

The maintenance operation sample allocation is very important to make the result of statistical inference accurate and reliable. In order to ensure the representativeness of the samples, the characteristics of maintainability data should be fully understand. The maintainability data have the following characteristics:

1. The collectivity of maintenance tasks is highly uneven and highly layered, but each individual in each layer is even. A maintenance task may be frequently occurred during the use of equipment and will provide greater data layer with unique average.

2. For the actual maintenance time of the equipment during the use phase experienced, only a test trial sample may cause large engender illusions. To avoid this situation, repeated sampling should be taken to repair verification.
3. For each specific type of maintenance tasks, its maintenance time depends not only on the distribution of the mean maintenance time of various subsystems, but also be affected by the following factors:

   (a) The number of units contained in each subsystem.
   (b) Each unit's position in the system. Position has an impact on the time required to achieve. So even identical unit is located in different positions, the time required to achieve is different.
   (c) To make the necessary maintenance activities become frequency. Because of the frequency is connected with a particular unit in each of their particular position possibilities (for example due to vibration, temperature, humidity, and pressure).

12.3 Maintenance Work Samples Allocation Method

12.3.1 The Allocate Method in GJB2072

The sample allocation of maintenance operations should be based on the complexity of the system and the analysis of reliability. Currently, samples allocation usually adopts proportional stratified sampling method in GJB2072 in engineering practice of maintenance operations. Specifically allocated as follows:

1. List the equipment component units.
2. Subdivide the units down to the product level which need maintenance.
3. List the maintenance operations of product level which need maintenance, for example debugging, removement, replacement, repairmen, and other work.
4. According to engineering analysis, maintainability prediction or experience data to estimate maintenance time $\overline{M}_{cti}$ for each maintenance job.
5. List the failure rate λ_i of each product which needs maintenance. Only the corresponding troubleshooting failure rate needs to be listed for different maintenance levels.
6. List the product number Q_i and the weighting factor T_i of work hours of each product which need maintenance. The T_i of products which work all the time equal to one and the T_i of products which work not all the time equal to the ratio of their working hours to working time throughout.
7. Group maintenance operation samples. Put the similar maintenance activities and repair time close (a difference of not more than 25 %) of the maintenance operations sample into a group within the same unit.
8. Calculate the failure rate $Q_i\lambda_iT_i$ and their relative occurrence frequency C_{pi} of each group:

$$C_{pi} = Q_i \lambda_i T_i \Big/ \sum_{i=1}^{m} Q_i \lambda_i T_i. \tag{12.1}$$

where m is the number of groups.

9. Calculate validation sample size n_i:

$$n_i = nC_{pi}. \tag{12.2}$$

From the specific calculation process, we can see that the method itself does not solve the problems caused by too much maintenance operation but with small total sample relatively. For example, there is aviation equipment with 200 organizational-level maintenance operations. Obviously, their frequency is 1/200. If the sample size is 50, it is clear that without regard to maintenance operation time grouping problems, we could not get a sample size of maintenance operation on a specific number of allocations using proportional stratified sampling method. When considering the grouping problems of maintenance operation time, it may produce two special cases within 25 % of the maintenance time. The one is unable to determine the number of samples after grouping due to much difference of maintenance time. The other is the maintenance close time; thus, one group may share a lot of similar samples after grouping. It is very difficult in defining the samples to a specific maintenance operation. Otherwise, the above method is also difficult to operate because a system often includes many organizational-level maintenance operations.

12.3.2 The Improvement of Maintenance Operation Sample Allocation Methods

Considering the previous analysis of the factors, this paper proposes an improved sample allocation method. The main principle and standard are basically the same. The improved method can only be partially improved operability. The principle of sample allocation is based on LRU rather than each maintenance operation. After allocating, the sample size is selected randomly from all maintenance operations of each LRU, so that the improved method can not only makes it operational, but also ensure the samples taken sufficiently representative.

The allocation method based on LRU should first remove the LRU of the sample. Then, the remaining LRU is grouped. The principle of grouping is in accordance with time in the order from large to small order. And then the sort order for summation of each LRU C_{pi} is followed. When the product of n with the summation of C_{pi} is greater than one, allocate them to one group. The specific method is as follows:

1. List the equipment component units.
2. Subdivide the units down to the product level which need maintenance.
3. Estimate maintenance time $\overline{M}_{cti}$ for each maintenance job according to engineering analysis, maintainability prediction, or experience data.

4. List the failure rate λ_i of each product which needs maintenance. Only the corresponding troubleshooting failure rate needs to be listed for different maintenance levels.
5. List the LRU number Q_i and the weighting factor T_i of work hours of each product which need maintenance. The T_i of products which work all the time equal to 1 and the T_i of products which work not all the time equal to the ratio of their working hours and working time throughout.
6. Calculate the failure rate $Q_i\lambda_iT_i$ and their relative frequency C_{pi} of occurrence of each group: $C_{pi} = Q_i\lambda_iT_i / \sum\limits_{i=1}^{m} Q_i\lambda_iT_i$, where m is the number of LRU.
7. Calculate the validation sample size n_i of every LRU that need to be allocated: $n_i = nC_{pi}$, where n_i is the sample size of ith LRU. If $n_i \geq 1$, round the number as the sample size of the component should be assigned. If the $\sum_{i=1}^{m} n_i = n$, then end the extraction.
8. When the $\sum_{i=1}^{m} n_i < n$, first remove all LRU of $n_i \geq 1$, then in accordance with $\overline{M}_{cti}$ descending order all remaining LRU. If the $\overline{M}_{cti}$ is the same, in accordance with C_{pi} Descending order. Grouping the LRU, calculate $\sum\limits_{i=1}^{l} C_{pi}$ from the first term of the max $\overline{M}_{cti}$. Let $n_i = n \times \sum\limits_{i=1}^{l} C_{pi}$, where n_i is the sample size should be allocated in this group, l is the number of LRU in this group. The value of l is calculated by $n\sum\limits_{i=1}^{l} C_{pi} \geq 1$ and $n\sum\limits_{i=1}^{l-1} C_{pi} < 1$. When $n_i \geq 1$ round numbers according to the principle of rounding. Now $n_i = 1$ or $n_i = 2$ the allocation in the group according to the principle of the maximum C_{pi}. If $n_i = 1$, allocate the max LRU to C_{pi}. If $n_i = 2$, allocate the two of the maximum LRU to C_{pi}. If the C_{pi} is the same in group, then can allocate randomly.
9. Repeat step (8) until all maintenance operations are grouped and then end the extraction. In the last group, if $n_i < 1$, round the number.
10. Put in order the allocated sample size. In the above (7)–(9) steps, the sample numbers should be rounded. If the sample size of the final allocation is less than the amount of validation requirements, then all remaining LRU be resorted in descending order. The allocation from the LRU that has the max C_{pi} starts one by one until validation sample size requirements have been met, and then ends the allocation. If the sample size of the final allocation is more than the amount of validation requirements, then all selected LRU be resorted in descending order. To make the allocate sample size equal to the required sample size; remove the least one or several sample.

The selection method of total sample size mentioned above is generally according to the selected test method. When using the military standard method to validate, sample size generally should not too small (no less than 30). If the sample size is too small, the risk of developing side or the military may increase.

Table 12.1 The first sample allocation

Units	LRU	λ_i	T_i	Q_i	$\lambda_i \times T_i \times Q_i$	C_{pi}	$\overline{M}_{cti}$	n_i
Unit 1	LRU1	0.075	1	1	0.075	0.1390	50	4
Unit 2	LRU2	0.05	1	1	0.05	0.0927	60	3
	LRU3	0.03	1	1	0.03	0.0556	65	2
	LRU4	0.027	0.6	1	0.0162	0.0300	75	1
Unit 3	LRU5	0.0003	1	1	0.0003	0.0006	150	0
	LRU6	0.005	1	1	0.005	0.0093	200	0
	LRU7	0.0264	1	1	0.0264	0.0489	90	1
	LRU8	0.006	0.7	1	0.0042	0.0078	80	0
Unit 4	LRU9	0.0004	1	1	0.0004	0.0007	90	0
Unit 5	LRU10	0.07	1	1	0.07	0.1297	65	4
Unit 6	LRU11	0.0002	1	1	0.0002	0.0004	90	0
	LRU12	0.06	0.2	1	0.012	0.0222	115	1
Unit 7	LRU13	0.003	1	1	0.003	0.0056	175	0
Unit 8	LRU14	0.002	1	1	0.002	0.0037	85	0
Unit 9	LRU15	0.04	1	1	0.04	0.0741	95	2
	LRU16	0.025	1	1	0.025	0.0463	105	1
	LRU17	0.0125	1	1	0.0125	0.0232	123	1
Unit 10	LRU18	0.005	1	2	0.01	0.0185	110	1
	LRU19	0.0125	0.8	2	0.02	0.0371	105	1
Unit 11	LRU20	0.02	1	3	0.06	0.1112	90	3
Unit 12	LRU21	0.0045	1	1	0.0045	0.0083	85	0
	LRU22	0.003	0.8	1	0.0024	0.0044	80	0
Unit 13	LRU23	0.018	1	2	0.036	0.0667	75	2
	LRU24	0.003	1	1	0.003	0.0056	60	0
	LRU25	0.0024	0.8	1	0.00192	0.0036	100	0
Unit 14	LRU26	0.005	1	1	0.005	0.0093	90	0
	LRU27	0.0045	1	1	0.0045	0.0083	180	0
Unit 15	LRU28	0.02	1	1	0.02	0.0371	98	1
Total						1		28

12.4 Example Calculation and Analysis

Assume that the total amount of the validation sample size is 30. Constituent elements of a system and the number of LRU, the failure rate of each of the LRU λ_i, weighting factor of work hours T_i, estimated maintenance time $\overline{M}_{cti}$ are known (estimate according to engineering analysis, maintainability prediction, or experience data). In such cases, it is difficult in sample allocating with the method of military standard. Now using the improved method of sample allocation. The results of the first sample allocation are shown in Table 12.1.

Allocated from the first sample, the total sample size is less than the required sample size. So we need for a second sample allocation for the remaining two

Table 12.2 The final sample allocation results

Units	LRU	λ_i	T_i	Q_i	$\lambda_i \times T_i \times Q_i$	C_{pi}	$\overline{M}_{cti}$	n_i
Unit 1	LRU1	0.075	1	1	0.075	0.1390	50	4
Unit 2	LRU2	0.05	1	1	0.05	0.0927	60	3
	LRU3	0.03	1	1	0.03	0.0556	65	2
	LRU4	0.027	0.6	1	0.0162	0.0300	75	1
Unit 3	LRU6	0.005	1	1	0.005	0.0093	200	1
	LRU7	0.0264	1	1	0.0264	0.0489	90	1
Unit 5	LRU10	0.07	1	1	0.07	0.1297	65	4
Unit 6	LRU12	0.06	0.2	1	0.012	0.0222	115	1
Unit 9	LRU15	0.04	1	1	0.04	0.0741	95	2
	LRU16	0.025	1	1	0.025	0.0463	105	1
	LRU17	0.0125	1	1	0.0125	0.0232	123	1
Unit 10	LRU18	0.005	1	2	0.01	0.0185	110	1
	LRU19	0.0125	0.8	2	0.02	0.0371	105	1
Unit 11	LRU20	0.02	1	3	0.06	0.1112	90	3
Unit 12	LRU21	0.0045	1	1	0.0045	0.0083	85	1
Unit 13	LRU23	0.018	1	2	0.036	0.0667	75	2
Unit 15	LRU28	0.02	1	1	0.02	0.0371	98	1
Total						1		30

samples. The LRU allocation with the result of 0 is put out and arranged the estimated mean maintenance time to by descending order. The grouping principle is calculating the sum of LRU according to the arranged order. When the product of n with the summation of C_{pi} is greater than 1, allocate them to one group. The allocation in group can be in order from large to small.

Through a second sample allocation, all the samples have been allocated. The final results are shown in Table 12.2.

12.5 Conclusions

Whether it is a good representative sample or not is necessary to ensure the trustiness of maintenance validation work. How to ensure the credible verification results in the case, making the choice of most scientific sample size, is a system-level verification work urgently needed to solve. In this paper, GJB sample allocation method has been developed to an improved sample allocation method. The method is not according to the sample allocation of maintenance work, but according to LRU. The method allocated the total sample to each LRU based on

the complexity of the system and the analysis of reliability. The method can solve sample allocate problem of identification in the flight test stage of military aircraft maintenance better, with engineering practice guidance to a certain extent.

References

1. Li J (2010) Test phase system-level mean time to repair verification method. Air Force Engineering University, Xi'an (in Chinese)
2. Xu H (2009) System maintainability validation studies. Ship Electron Eng 29:149–152 (in Chinese)
3. National Defense Military Standardization Center (1994) GJB2072-94 Maintainability test and evaluation. National Defense Military Standard Publishing Department, Beijing (in Chinese)
4. Li X, Yu L (2009) Sample allocation methods to improve maintenance operations research. Tactical Missile Technol 87–89 (in Chinese)
5. Yu L, Han B (2012) Anti-ship missile maintenance operations improved sample allocation method. Tactical Missile Technol 58–61 (in Chinese)

Chapter 13
Research on HAZOP-Based Safety Methods of Equipment Usage

Kui Huang and Jing Sun

Abstract This paper presents HAZOP-based (hazard and operability) safety methods of equipment usage. It provides scientific, reasonable, and feasible safety measures by analyzing and assessing the inherent and potential risks while using equipment. It lays the technical foundation for the safety usage of equipment.

Keywords HAZOP · Safety usage of equipments · Risk

13.1 Introduction

Personal safety is the top priority in the process of studying, using, and maintaining equipment. In terms of equipment system, safety is the most important factor as well as the prerequisite and basis to ensure the battle effectiveness.

In order to enhance the safety of equipment system, researchers usually do the fault hazard analysis (FHA), fault model and effect analysis (FMEA), and fault tree analysis (FTA) when designing the system. It helps to identify potential risks and measure the levels of damages which impose to individuals and equipment. Based on the results, researchers can take appropriate measures to improve the system. These methods provide ways to eliminate or control hazard in a system and thus greatly improve the inherent safety of the system. According to statistics, with the development of technology, the number of incidents which is triggered by equipment deficiency is decreasing year by year, while most of the incidents were caused by incorrect manual operations. But in the phase of equipment operation, there are few methods of safety analysis. The safety usage of equipment is the greatest concern of every maintenance and support personnel. This article presents

K. Huang (✉) · J. Sun
Qingdao Branch Naval Aeronautical and Astronautical University Qingdao, Qingdao, China
e-mail: 520079453@qq.com

J. Sun
e-mail: sj_sunny@hotmail.com

HAZOP-based (hazard and operability) safety methods of equipment usage [1–3]. It starts from equipment's manual operations and combines the equipment structure and working principles to identify the inherent and potential risks in using process. It also analyzes the causes and consequences which are triggered by system malfunction. It proposes scientific, reasonable, and feasible safety measures for references of the safety usage of equipment.

13.2 HAZOP-Based Equipment Safety Usage

HAZOP is proposed by ICI in 1970s. It is mainly for petroleum industry and chemical industry to analyze and assess potential safety risks in craft processes and system operations.

The guidance theory of HAZOP is that any phenomenon which deviates from presented operational condition value could cause hazards and finally lead to incidents and losses.

In order to guarantee the proper functioning of equipment, the equipment must be operated within an expected or given range. But in practical work, some dangerous events may occur and cause accidents or unexpected losses if some key performance indicators (KPIs) beyond design range because of equipment malfunction, incorrect manual operations, environment, etc. Typically, this condition is defined as deviation of equipment usage.

The principle of HAZOP-based safety equipment usage is to locate any deviation which may occur in operating equipment and provide technical support measures based on analysis results on the root cause of deviation and its consequences. Please refer to Fig. 13.1 for detailed procedures.

13.2.1 HAZOP Node

In traditional ways, HAZOP nodes are categorized by flowchart or operation process. In petroleum and chemical industry, HAZOP node usually refers to an equipment unit that is involved in the reaction process such as gasifies, reaction tower, etc. When performing equipment safety usage analysis, it mainly focuses on any potential hazard during equipment usage. Thus, the analysis is based on the equipment operation procedures. It combs the process of operation and maintenance. Every step within the process of operation and maintenance is defined as a HAZOP node.

According to different results from each operating step, the operating steps can be mainly divided into two types: The first one is to locate a unit by changing its location or state, such as valve-opening, button-pushing, and air-break-switching. This kind of nodes is defined as execution nodes. For the second type, it measures certain physical quantity to keep the value within the standard range, such as temperature: 15–60 °C and pressure: 8 ± 0.5. These kinds of nodes are defined as checking nodes.

Fig. 13.1 The analysis process
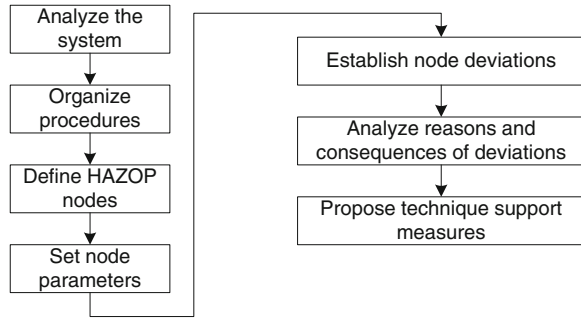
13.2.2 Select Node Parameters and Define Node Deviations

Node parameters refer to the attributes related to operating procedures. It is a factor that impacts the operating procedures. Based on above two attributes, the node parameters can be divided into two types: suite and physical quantity. The parameters of execution nodes are related suite for the step. After performing one step, if the suite status is inconsistent with standard value, deviations should be taking place. The parameters of checking nodes are the physical quantities observed during performing operating procedures, such as liquid level, temperature, and pressure. The corresponding deviations reflect status such as high liquid level and low temperature.

13.2.3 Root Cause and Consequence Analysis

Using equipment can be seen as a course of man–machine interaction, so any incorrect manual operation or equipment malfunction may introduce deviations. The causes of deviation can be divided into two types: The first one is related to human factor, such as missing or incorrect operating step. The second one is caused by equipment itself, such as low temperature due to heater malfunction or circuit break due to relay malfunction.

13.2.4 Technical Support Measures

The purpose of hazard analysis is to reduce or eliminate hazard by formulating safety measures. In order to reduce man-made fault rate, proper operating procedures are listed to avoid deviations that are caused by incorrect manual operations. A checklist for equipment safety usage will be generated in the form of chart based on above procedures. It will be used as guidance for specific operations to improve operating accuracy. Meanwhile, according to deviations triggered by

Table 13.1 The safety check table

No.	Check item	Yes	No	People on duty
1	The amount of oil tank should meet a criterion (2/3–3/4)			
2	The temperature of oil should be 15–60 °C			
3	1# and 2# signal ball valves are fully open			
4	Accumulator stop valve is fully open			
5	Accumulator safety valve is off			
6	The inflation pressure of the accumulator is between 5.5 and 6.5 MPa			

Table 13.2 The failure table

No.	Phenomenon	Reason
1	Low pressure of the hydraulic system	① the pressure of the accumulator is low
		② accumulator safety valve is on
		③ the status of oil is too low
2	Low work speed of the hydraulic cylinder	Accumulator stop valve is not fully open

equipment itself, a malfunction report will be generated against the ones introduced by deviations and their possible root causes. This report will be used as guidance for maintenance and debugging of equipment malfunction.

13.3 Application

The preoperation procedure of the hydraulic system of equipment is as follows:

1. Make sure that the amount of oil tank meets a criterion (2/3−3/4 of the liquid meter);
2. Make sure that the temperature of oil is 15–60 °C (when the temperature is below 15 °C, oil should be heated to allowed range);
3. Check whether both 1# and 2# signal ball valves are fully open;
4. Make sure that accumulator stop valve is fully open (up is on, down is off);
5. Make sure that accumulator safety valve is off;
6. Make sure that the inflation pressure of the accumulator is 5.5–6.5 MPa.

So 6 HAZOP nodes should be defined before analysis of preoperation safety check to corresponding to (1)–(6), (3)–(5) are performance nodes and (1), (2) and (6) are checking nodes. Deviations of each node should be defined. And then, the preoperation HAZOP table (see Table 13.3) of this hydraulic system could be generated by analyzing reasons and consequences of deviations according to the architecture and theory of the equipment. Based on analysis of HAZOP, the safety check table (see Table 13.1) and the failure table (see Table 13.2) could be obtained.

Table 13.3 The preoperation HAZOP table

Operation	Parameter	Deviation	Reason	Consequence	Suggestion	Font size and style
Check the amount of oil tank	Liquid meter	<2/3	Disoperation	Low hydraulic pressure, easily damaged, and suction of hydraulic pump	Draw up safety check table and strictly carry out operation procedures	14 point, bold
		>3/4	Disoperation	Oil may overflow when the hydraulic system works	Draw up safety check table and strictly carry out operation procedures	12 point, bold
Check the temperature of oil	The temperature of oil	<15 °C	Failures of electric-controlled system QF3 or electric heater	Suction and cavitation caused by over-sized oil particles when starting the hydraulic pump	Change QF3; change electric heater	10 point, bold
		>60 °C	Oil flows back to the tank through safety valve due to low setting pressure	The seal ring is damaged by oxidative deterioration of oil	Set the pressure of safety valve correctly	10 point, bold
Check whether both 1# and 2# signal ball valves are fully open	1# and 2# signal ball valves	Not open	Distraction of operators	Motor does not start	Draw up safety check table and strictly carry out operation procedures	10 point, italic
Make sure that the accumulator stop valve is fully open	Accumulator stop valve	Not open	Distraction of operators	Overtime operation	Draw up safety check table and strictly carry out operation procedures	

Table 13.3 (continued)

Operation	Parameter	Deviation	Reason	Consequence	Suggestion	Font size and style
Make sure that the accumulator safety valve is closed	Accumulator safety valve	Not close	Distraction of operators	The equipment does not work; no pressure of the system	Draw up safety check table and strictly carry out operation procedures	
Make sure that the inflation pressure of the accumulator is 5.5–6.5 MPa	The inflation pressure of the accumulator	<5.5 MPa	Damage of accumulator seal ring	High pressure pulsation occurs when starting the hydraulic pump; insufficient holdup time	Change seal ring	
		>6.5 MPa	Distraction of operators	Low work speed of the hydraulic cylinder; low oil reserve capacity	Draw up safety check table and strictly carry out operation procedures	

References

1. Fan J-H, Dai X-J (2006) Introduction of HAZOP analysis and applying in mineral. Sci Technol Ind 6(2):34–36 (in Chinese)
2. Jiao J, Wang W (2009) HAZOP study for weapon system operational safety. Ordnance Ind Autom 28(9):58–61 (in Chinese)
3. Crawley F (2000) HAZOP: guide to best practice: guidelines to best practice for the process and chemical industries

Chapter 14
Design and Realization of Aero-Engine Status Monitor System Platform Based on Various Information

Hongwei Li, Kai Zhang, Shufeng Li and Yan Feng

Abstract After collection and classification of aero-engine information, the paper used such technologies as trend analysis and reliability assessment to assess the working status of aero-engines. On this basis, the aero-engine status monitor system platform was designed and applied into reality.

Keywords Aero-engine · Status monitor · System

14.1 Introduction

The engine status monitor is to judge engine's safety, reliability, reasons for abnormity, or failures and to predict the influence on the future to realize the engine status monitor, failure diagnosis, life assessment, aero-engine fleet management, etc., by synthesizing the human factors and various testing equipment, relying on various information and technologies, and analyzing the engine status variables in flight, on ground, in the past, and at present [1–4]. One of the key points to design the status monitor system is the information collection, and the other is the information analysis and treatment. On the basis of the classification and collection of the aero-engine information, the paper designed an engine status monitor system platform by adopting trend analysis and then used software to develop and realize it.

H. Li (✉) · K. Zhang · S. Li · Y. Feng
Naval Aeronautical Engineering Institute Qingdao School, Qingdao 266041, China
e-mail: Llihongwei_zhang@tom.com

14.2 Design of the Status Monitor System

Corresponding to the functions and definition of the aero-engine status monitor system, this paper designed three layers for the system: supporting layer, running layer, and executing layer, as shown in Fig. 14.1.

1. Supporting layer

Supporting layer is the basis of the status monitor system and is made up of hardware support, software support, information support, personnel support, etc. The hardware support includes computer system, network system, lubricant testing devices, ground trial-run testing devices, and nondestructive testing devices. The software support includes aero-engine parameter information treatment software, critical part life assessment software, vibration signal analysis software, failure diagnosis software, lubricant spectroscopic analysis software, and monitor system software platform. The information support includes various aircraft parameter information, repair information, routine maintenance information, routine testing information, and ground trial-run information. Responsible for providing technological and running support, the personnel support includes people in engine monitor room, ground crew, repairmen in factory, and experts in factories, institutes, and academies.

2. Running layer

Running layer is the core of the status monitor system. Through the technological means provided by the supporting layer, it analyzes and treats information and realizes data interaction between clients and the system to reach the specific realization of the designed functions, including realization of critical part life assessment, aero-engine failure diagnosis and prediction, vibration signal analysis, lubricant analysis, nondestructive testing picture analysis, a great deal of trial-run and aircraft parameter data analysis, and the all-status monitor.

By means of the fast Fourier transform, wavelet analysis, smoothing filter, and other related statistical methods to treat a great deal of information, and by using comprehensively various intelligent and model-based failure diagnostic technologies and critical part life assessment technology based on the flight conversion, the layer diagnoses critical parts and subsystems, isolates failures if possible, predicts engine's healthy status, depicts engine's performance trend, and estimates residual life of the aero-engine fleet.

3. Executing layer

Facing ground maintenance and management personnel, executing layer, by means of man–machine interactive interface and on the basis of the analysis, results the running layer proposed, proposes such maintenance measures as replacement, repair, routine maintenance schedule, special check schedule, and proposes the possible spare parts need to the aviation material management department and provide grounds of the flight decision for the upper executive departments.
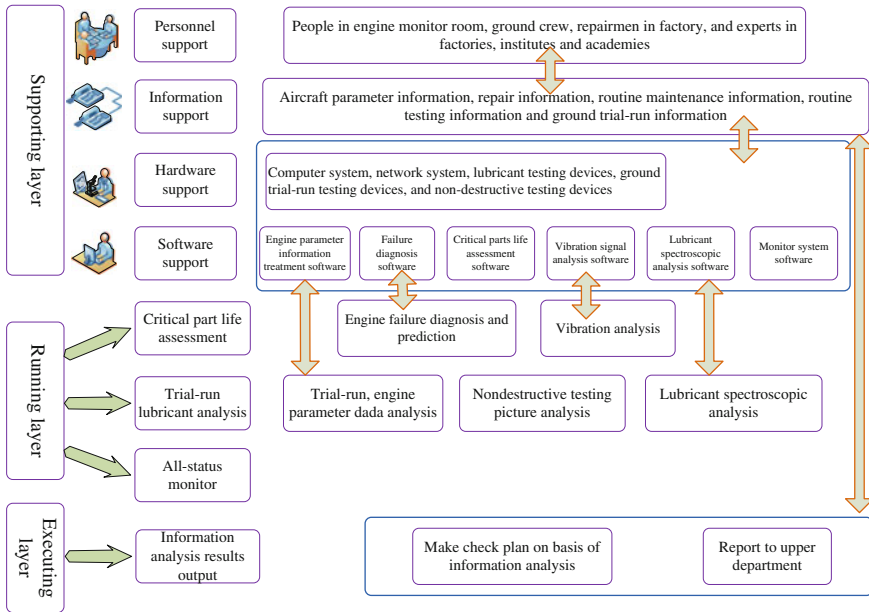
Fig. 14.1 Design diagram of the aero-engine status monitor system platform

14.3 Realization of the Status Monitor System Platform

According to the monitor system designed by the upper departments, by means of Borland Delphi7 software as the platform, the paper used such application software as Borland C++, Microsoft Office Access, Wise Installation System, and Microsoft Office Word to develop the system platform, realized the information management, analysis, maintenance, and the report formation of the aero-engines, and also realized the engine status assessment by such background technological means as trend analysis, reliability assessment, and failure diagnosis. The system diagram is shown in Fig. 14.2.

Considering data management and the customer's security needs, the system adopted C/S structure. The data server and the client software were installed on the same computer. In order to facilitate the use, the system adopted access database and can be used immediately after the installation, thus saving the complicated operation of configuring the data server.

Fig. 14.2 System diagram
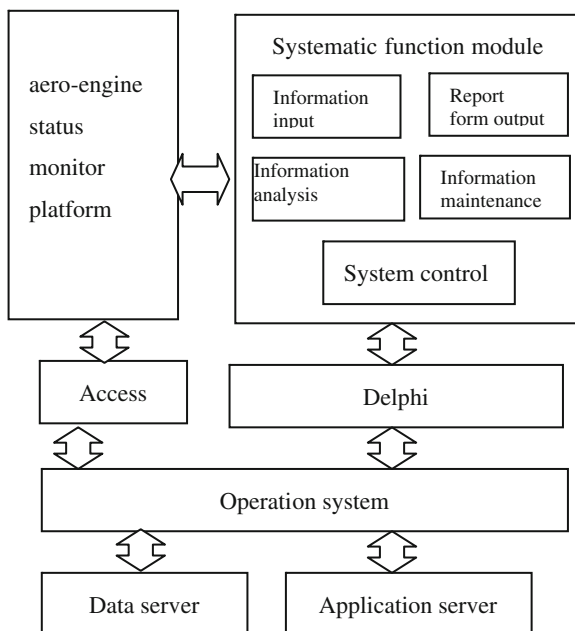
14.3.1 Information Input and Maintenance

Through surveys in various military and civil airports, the information that can be collected currently and used into the aero-engine status monitor includes: (1) basic information of the aero-engines, including engine number, installation position, aircraft number, engine status, manufacturer, production date, and installation date; (2) performance information, including total life span, service time, exhaust temperature-limited value, and maximum vibration value; (3) airborne information. Different aircrafts are equipped with different aircraft parameter systems, so the parameters the engine can collect are different, but most can collect flight time, flight speed, flight height, flight Mach number, air temperature, exhaust temperature, high- and low-pressure RPM, etc.; (4) ground routine information, including trial-run data, outlet pressure value of the high-pressure lubricant filter, average lubricant consumption, and vibration value measurement; (5) ground testing and maintenance information, including blade borescope check and ground routine or regular check information; (6) ground trial-run information, including starting status information, idling information, and also maximum status information and boost status information as for the military aircrafts [5, 6].

The data input function has the following features:

1. Out-of-limit Data Alarming function: During engine trial run, some higher or lower data may appear than the standard ones. When such data are input, the system can compare automatically correlative standards at background. The

figure automatically turned into red when out-of-limit data appeared. In storage, according to the system cues, the clients can select automatically whether the out-of-limit data should be input into database. When the data are checked, the out-of-limit data would turn red all along.

2. Self-definition function of the data standard value: As for different aircraft types or the same type of aircraft but in different airports and meteorological surroundings, the standard value of the trial-run and other data may be different. This system allows clients to define the standard value of the data alarming (as to standard value setting, please refer to "data maintenance" module), to make the system adapt to the requirements of different surroundings.

3. The engine fault attributes are full, complete, standard, and accurate. The low-pressure rotor RPM differences are input in the form of results from automatic computing, excluding wrong data caused by human error.

14.3.2 Information Analysis

Accurate analysis is the basis of the engine status assessment and also the key to the status monitor. The system basically adopts universal trend graph analysis. On the one hand, the system analyzes and judges the data deflecting obviously from the standard data by observing and recording trial-run data on the spot. On the other hand, by long-term record and observation, the system can forecast the failures, diagnose short-term failures, and determine the performance deterioration because of wear and tear.

Data trend analysis includes engine trial-run data analysis, the statistical data analysis of the average lubricant consumption, engine vibration measurement data analysis, and aircraft parameter data analysis. High-pressure rotating speed of some aero-engine was taken as example with lubricant light off when trial-run started. Figure 14.3 depicts its trend curve.

According to the curve diagram formed by the data of different parts of engine, the clients can check the curve of some datum or the curve drawn according to the time points and can zoom in or out or turn the curves to check multi-angularly. At the time of checking, the client can change the engine or aircraft number.

14.3.3 Reliability Assessment

The engine reliability assessment includes fault information input and the reliability assessment of the whole engine and engine at different life stages. The reliability assessment of the whole engine mainly assesses and compares the reliability index of the new engines and the overhauled engines. Considering engine of different working time differing in reliability indexes, there are four fault

Fig. 14.3 High-pressure
RPM with the lubricant light
off during engine trial run
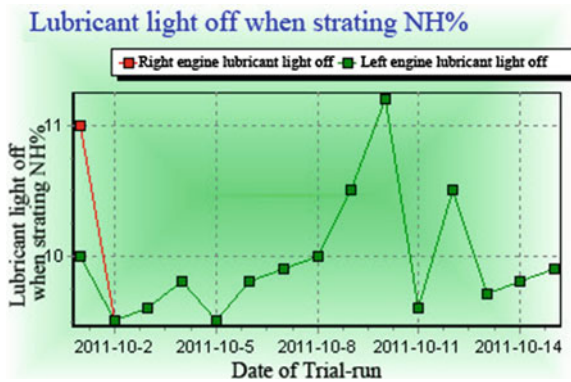
Table 14.1 Computing results of engine reliability assessment parameters

Life zone	Total working time of the fleet	Failure number of the fleet	MT_{BF}	Removal number of the fleet	r_{UER}	In-flight shut-down number of the fleet	r_{IFS}
0–100	130.44	6	21.74	0	0	0	0
100–200	289.61	2	144.8	0	0	0	0
200–300	211.58	1	211.58	0	0	0	0
300–400	0	0	0	0	0	0	0
400–500	470.15	1	470.15	1	2.12	0	0
500–600	2326.26	4	581.56	2	0.85	0	0

selection principles: fault year, the user, the engine type, and the prescribed life of engines (repaired initially or overhauled).

1. Selection of reliability parameters

   The frequently used parameters of aero-engines are mean time between failures T_{BF}, mean time to repair $\bar{M}_{CT}$, in-flight shut-down rate r_{IFS}, unscheduled engine removal rate r_{UER}, mean time between maintenance T_{BM}, shop visit rate r_{SV}, direct man-hour per flight hour L_{DMF}, etc. The paper selects T_{BF}, r_{IFS}, and r_{UER} as the engine reliability assessment parameters.

2. Assessment Realization

   The results of the reliability assessment are displayed in both ways of data table and data curve. The data table includes the mean time information for computing reliability indexes, and such three indexes are as follows: the mean time between failures, the unscheduled engine removal rate, and the in-flight shut-down rate. Table 14.1 shows the computing results of some engine reliability assessment parameters in the form of data table, and Fig. 14.4 shows MTBF curve of some engine in the form of data curve.
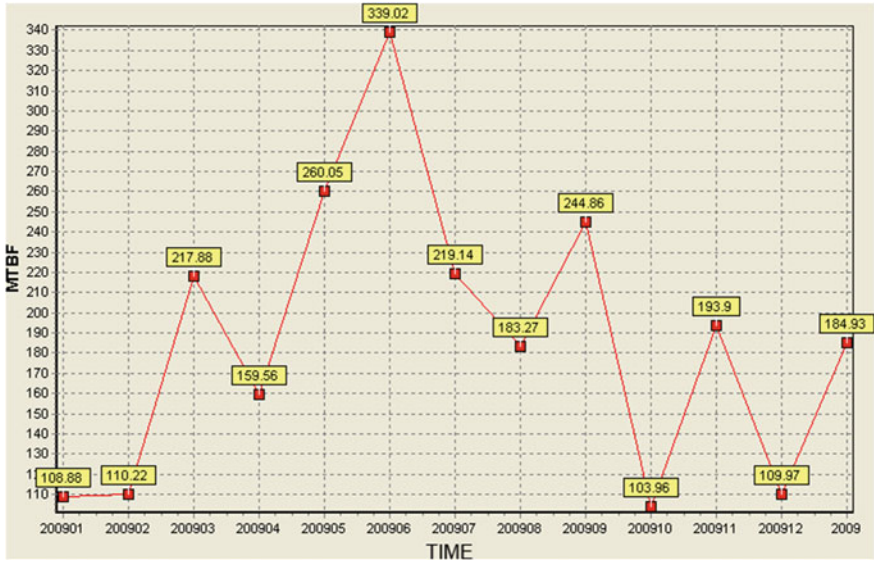
Fig. 14.4 MT_{BF} *curve*

14.3.4 Report Formation

The output of the engine data report includes engine's basic information, maintenance log, repairing record of the basic data, great event, trial-run data, and the output of failure information data. All the management modules of the engine data include report form of output function. The output report form, in the form of Word and Excel, can be printed into paper document and can be saved in the form of electrical document or electrical table.

14.4 Conclusion

The engine status monitor system designed in the paper is constructed on the basis of the performance information, which can be collected in the outfield, and has been put into use in monitoring some type of aero-engine in the outfield. It needs to be noted that the platform design is open, so other things the engine monitors, such as life assessment of the critical parts and failure diagnosis, can be further developed and realized.

References

1. Kejun X, Xinnong Y (2006) Study on assessment method of comprehensive flight conversion ratio for aeroengine. J Propul Technol 17(1):24–29 (in Chinese)
2. Yong Z, Duokui Y (2004) Constitution of multi-parameter loading spectrum of turbojets and turbofans. Aeroengine 30(1):6–13 (in Chinese)
3. Yirui X, Yongqi W, Kejun X (2010) Establishment of turbine components load spectrum for a high-pressure motor based fly parameters. Sci Technol Eng 17(2):1623–1627 (in Chinese)
4. Song Y, Gao D (2002) The principal component analysis method for engine flight mission profiles categorization. J Aerosp Power 17(2):196–200 (in Chinese)
5. Sun B, Xu L, Pei X et al (2003) Model-based knowledge representation in case-based reasoning systems. Expert Syst 20(2):92–99
6. Jie H, Dajun Z, Jibin H (2000) Design of life usage monitoring system of aeroengine critical part 26(1):45–48 (in Chinese)

Chapter 15
The Optimal Design for Offset Slider-Crank Mechanism in Aviation Machinery

Rengang Tang and Zhaoming Meng

Abstract For an offset slider-crank mechanism, the larger its imbalance angle is, the faster its return stroke is, and the higher its work efficiency is in a single-track. Moreover, the larger its transmission angle is, the better its motion performance is. This paper aims to deduce the maximum imbalance angle φ_{0max} available in the mechanism and the function expressions of the optimal crank, coupler link, and offset distance according to the permissible transmission angle, and then, the simple and practical corresponding diagram is drawn so as to obtain the best design results quickly and accurately.

15.1 Introduction

Offset slider-crank mechanism is often used for the design of hydraulic driving device in Aviation Machinery. For an offset slider-crank mechanism, the larger its imbalance angle is, the faster its return stroke is, and the higher its work efficiency is in a single-track. Meanwhile, the larger its transmission angle is, the better its motion performance is. On designing a slider-crank mechanism, the imbalance angle φ_0 is often blindly set firstly, and then the crank, coupler link and offset distance are defined according to the stroke H, finally the minimum transmission

R. Tang (✉)
Aviation Mechanical Engineering Department, Qingdao Branch, Navy Aeronautical Engineering Academy, Qingdao 266041, China
e-mail: trg-2008@163.com

Z. Meng
College of Mechanical and Electrical Engineering, Qingdao University of Science and Technology, Qingdao 266061, China
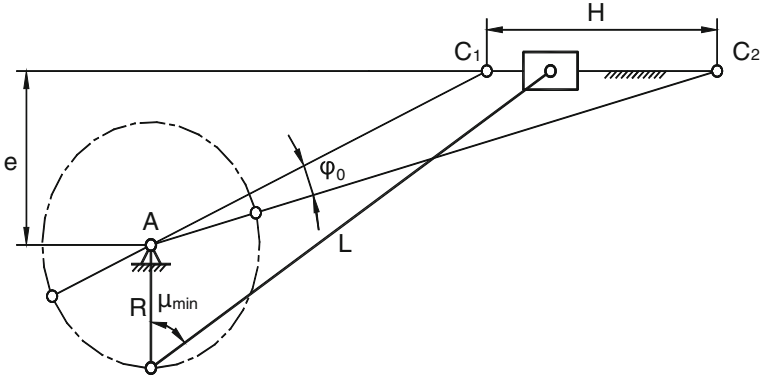
Fig. 15.1 Geometric relationship of offset slider-crank mechanism

angle μ_{min} will be checked. If it doesn't meet the condition $\mu_{min} \geq [\mu]$, the design will fail and start all over again. It is mostly due to the lack of a rational imbalance angle to maximize the work efficiency. This paper aims to deduce the maximum imbalance angle φ_{0max} available in the mechanism and the function expression of the optimal crank, coupler link, and offset distance according to the permissible transmission angle, and then, the simple and practical corresponding diagram is drawn so as to obtain the best design results quickly and accurately.

15.2 Geometric Relationship of Offset Slider-Crank Mechanism

The relationship of the stroke H, crank R, coupler link L, offset distance e, and imbalance angle φ_0 of the offset slider-crank mechanism is shown in Fig. 15.1.

In $\triangle AC_1C_2$,

$$H^2 = (L+R)^2 + (L-R)^2 - 2(L+R)(L-R)\cos\phi_0$$

or

$$L^2 = \frac{H^2 - 2R^2(1 + \cos\phi_0)}{2(1 - \cos\phi_0)} \tag{15.1}$$

$$\frac{H}{\sin\phi_0} = \frac{L+R}{\sin\angle AC_1C_2} = \frac{L+R}{e/(L-R)} = \frac{L^2 - R^2}{e}$$

or

$$L^2 = \frac{H \cdot e}{\sin\phi_0} + R^2 \tag{15.2}$$

The minimum transmission angle of the mechanism [1]:

$$\cos \mu_{\min} = \frac{e + R}{L}$$

or

$$L = \frac{e + R}{\cos \mu_{\min}} \tag{15.3}$$

15.3 Definition of the Maximum Imbalance Angle $\varphi_{0\max}$ of the Mechanism

Equation (15.1) plus Eq. (15.2) gives

$$e = \frac{\sin \phi_0}{2H(1 - \cos \phi_0)}(H^2 - 4R^2) = \frac{H^2 - 4R^2}{2H \cdot \tan \frac{\phi_0}{2}}. \tag{15.4}$$

Equation (15.2) plus Eq. (15.3) gives

$$(e + R)^2 = \cos^2 \mu_{\min}\left(\frac{H \cdot e}{\sin \phi_0} + R^2\right). \tag{15.5}$$

Equation (15.4) plus Eq. (15.5) gives

$$\left(H^2 - 4R^2 + 2HR \cdot \tan \frac{\phi_0}{2}\right)^2 = H^2 \cdot \cos^2 \mu_{\min}\left[H^2\left(\tan^2 \frac{\phi_0}{2} + 1\right) - 4R^2\right]. \tag{15.6}$$

Setting $x = \frac{R}{H}$, $y = \tan \frac{\phi_0}{2}$, from Eq. (15.6) we have

$$(1 - 4x^2 + 2xy)^2 = \cos^2 \mu_{\min} \cdot (y^2 - 4x^2 + 1) \tag{15.7}$$

Taking derivative on both sides of Eq. (15.7) and setting $\frac{dy}{dx} = 0$, we have

$$(1 - 4x^2 + 2xy)(y - 4x) + 2x \cos^2 \mu_{\min} = 0 \tag{15.8}$$

Eliminating $\cos^2 \mu_{\min}$ from Eqs. (15.7) and (15.8), we have

$$y^3 - 4xy^2 + y - 2x + 8x^3 = 0$$

or

$$(2x - y)(4x^2 + 2xy - y^2 - 1) = 0 \tag{15.9}$$

From Eq. (15.9), we have the following solution:

$$
\begin{cases}
x_1 = \frac{-y-\sqrt{5y^2+4}}{4} \\
x_2 = \frac{y}{2} \\
x_3 = \frac{-y+\sqrt{5y^2+4}}{4}
\end{cases}
\tag{15.10}
$$

Equation (15.10) is discussed:

1. If $x = \frac{-y-\sqrt{5y^2+4}}{4}$

$$
\phi_0 > 0 \quad y > 0 \quad x < 0
$$

It does not accord with $x = \frac{R}{H} > 0$, so this solution can be removed.
2. If $x = \frac{y}{2}$, rewriting Eq. (15.7), we have

$$
\cos \mu_{\min} = 1, \ \mu_{\min} = 0°
$$

The mechanism is in a state of self-lock, so this solution can be removed too.

3. If $x = \frac{1}{4}(\sqrt{5y^2+4} - y)$, rewriting Eq. (15.7), we have

$$
\cos^2 \mu_{\min} = \frac{2y(2y - \sqrt{5y^2+4})^2}{\sqrt{5y^2+4} - y}
\tag{15.11}
$$

If setting $\mu_{\min} = [\mu]$ and seeking the optimal values with the Fibonacci method, we have

$$
\min f(y) = \left| \frac{2y(2y - \sqrt{5y^2+4})^2}{\sqrt{5y^2+4} - y} - \cos^2[\mu] \right|_{y \in (0,1)}
\tag{15.12}
$$

The parameter y^* can be worked out, and thus, the maximum imbalance angle in accordance with the permissible transmission angle is

$$
\Phi_{0\max} = 2\arctan y^*
$$

15.4 Definitions of Other Optimal Design Parameters and Their Function Diagrams

From Eq. (15.10),

$$x^* = \frac{1}{4}\left(\sqrt{5y^{*2} + 4} - y^*\right)$$

So, the optimal crank $R^* = H \cdot x^*$.

From Eq. (15.1), the optimal coupler link $L^* = H\sqrt{\frac{1-2X^{*2}(1+\cos \phi_0)}{2(1-\cos \phi_0)}}$.

From Eq. (15.3), the optimal offset distance

$$e^* = H\left(\sqrt{\frac{1 - 2x^{*2}(1 + \cos \phi_0)}{2(1 - \cos \phi_0)}} \cdot \cos \mu_{\min} - x^*\right).$$

Diagrams of optimal design parameters are shown in Fig. 15.2.

The optimal design parameters with different permissible transmission angles are shown in Table 15.1.

15.5 Comparison of Design Results

1. From Ref. [1] page 38, $\varphi_0 = 20°$ and $H = 100$ mm, the contrast of new and old design results is shown in Table 15.2.

From Table 15.2, we know: the design in Ref. [1] is fussy and has large calculation error. If adopting its result and rewriting Eq. (15.1), we can obtain

$$\phi_0 = \cos^{-1} \frac{2(L^2 + R^2) - H^2}{2(L^2 - R^2)} = 19.62545^\circ \neq 20^\circ.$$

2. From Ref. [2] page 158, $H = 200$ mm and $[\mu] = 50°$, the contrast of new and old design results is shown in Table 15.3.

From Table 15.3, we can conclude that with the same minimum transmission angle obtained, the efficiency of new design is higher (The imbalance angle φ_0 is larger).
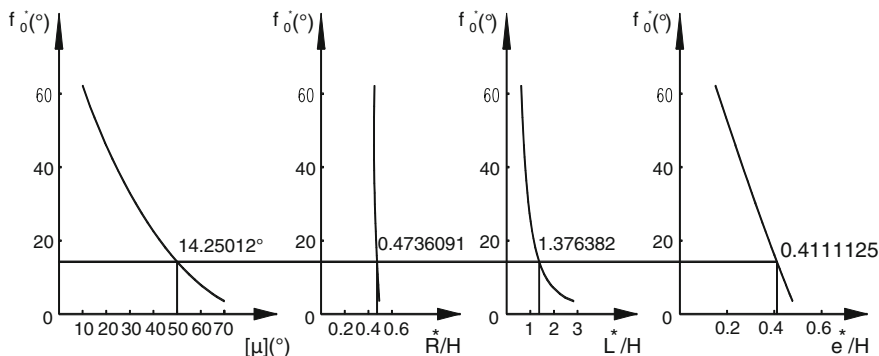
Fig. 15.2 Diagrams of optimal design parameters

Table 15.1 Optimal design parameters with different permissible transmission angles

$[\mu](°)$	$\varphi_0{}^*(°)$	$K = \frac{180° + \phi_0}{180° - \phi_0}$	R^*/H	L^*/H	e^*/H
10	62.2285	2.056767	0.4523018	0.6121143	0.1505131
15	53.52726	1.846463	0.4479247	0.6663861	0.1957548
20	45.89813	1.684526	0.4473415	0.7268015	0.2356286
25	39.08841	1.554793	0.4491937	0.7954184	0.2717002
30	32.9697	1.448475	0.4526744	0.8745534	0.3047112
35	27.46745	1.360152	0.4572304	0.9671733	0.3350317
40	22.53389	1.286206	0.4624476	1.077334	0.362838
45	18.13615	1.224091	0.4679973	1.210841	0.3881967
50	14.25012	1.171947	0.4736091	1.376382	0.4111125
55	10.85776	1.128386	0.4790555	1.58757	0.4315372
60	7.944112	1.092343	0.4841453	1.867145	0.4494272
65	5.497554	1.063008	0.4887169	2.256	0.46471
70	3.508413	1.039757	0.4926365	2.835993	0.4773303

Table 15.2 Comparison of new and old design results

	Φ_0 (°)	R	L	e	μ_{min} (°)
Old design	20	46.6	116.1	38	43.2
New design	20	46.88239	114.9193	37.75669	42.80781

Table 15.3 Comparison of new and old design results

	Φ_0 (°)	R	L	e	μ_{min} (°)
Old design	12.55814	90.0135	408.333	172.458	50
New design	14.25012	94.72182	275.2764	82.2225	50

References

1. Jensen PW (1991) Classical and modern mechanisms for engineers and inventors. [M] Marcel Dekker, Inc., New York, p 38
2. Danian H (1995) Design for linkage mechanism. [M] Shanghai Science and Technology Press, Shanghai, p 158 (in Chinese)

Chapter 16
The Analysis of Aircraft A320S Inert Gas Generation System Fault Message "ASM Performance Degraded"

Yusheng Weng

Abstract According to the troubleshooting manual (TSM) program and trouble-shooting experience, this thesis analyzes the inert gas generation system and the fault message "ASM Performance Degraded" and summarizes troubleshooting solutions. Based on actual atmospheric pollution condition and aircraft mainte-nance cost controlling consideration, the thesis also lists maintenance suggestions.

Keywords ASM · Troubleshooting · Cost controlling · Maintenance suggestion

16.1 Introduction

Inert gas generation system (IGGS) uses air separation module (ASM) to generate nitrogen-enriched air (NEA) which is continuously supplied to the aircraft fuel oil-free space, to ensure that the oxygen content in the tank is in a safe value, so as to reduce the possibility of tank explosion. There are one air-flow-steadying valve and one oxygen content-monitoring sensor in the system. This paper is to study the fault related to IGGS monitoring system which monitors ASM work performance.

Generally, troubleshooting manual (TSM) program firstly distinguishes the true or false fault and then further troubleshoots. However, according to the fault message "ASM Performance Degraded" troubleshooting program, we inspect sealing of system and ASM directly; there is no mention of monitoring system troubleshooting. In view of this doubt, a series of studies are conducted.

Y. Weng (✉)
Line Maintenance Division 2#, Aircraft Maintenance Base, CSN Shenzhen Branch,
Shenzhen Baoan International Airport, Shenzhen, People's Republic of China
e-mail: weng040141425@126.com

Moreover, it cannot be ignored that air quality has a serious effect on the ASM performance. Granular pollutants monitoring is aimed at particulate whose size is about 0.001–100 μm, "China atmospheric environment quality standard" called it "total suspended particulate." The particle, whose size is larger than 10 μm and can quickly fall into the ground because of gravity, is called "fall dust." The particle, whose size is less than 10 μm and can float in the air for a long time, is called "floating dust." The chemical composition of particulate pollutants is more complex, such as water-soluble inorganic salts, water-insoluble metal compounds, inorganic nonmetal compounds and organic compounds.

In 2012, cities in which annual average concentration of inhalable particles reached or exceed level-II standard accounted for 92 %, and cities which are worse than level-III standard accounted for 1.5 %. Annual average concentration of inhalable particles ranges from 0.021 to 0.262 mg/m^3 and is mainly from 0.060 to 0.100 mg/m^3 [1]. A series of data show poor air quality in most area of China, which has a great influence on the ASM performance. So it needs proper maintenance program to relieve the impact of air pollution on the ASM performance.

16.2 System Introduction

16.2.1 System Composition [2]

The main components of IGGS: IGGS control unit (ICU), D-ULPA air filter, ASM, dual-flapper check valve, isolation valve, temperature sensor, pressure sensor, oxygen sensor, and dual-flow shut-off valve (DFSOV).

The isolation valve has a pneumatic piston actuator, spring loaded to the closed position. The isolation valve closes if

- The air stream pressure is less than 15 psi (1.0342 bar) and/or
- The air stream temperature is hotter than 85 °C (185.00 °F).

The D-ULPA filter cartridge cleans the air stream to make sure that only clean air goes into the ASM. The filter has a thermal insulation, to make sure that the temperature of the air stream that goes into the ASM is over 54 °C (129.20 °F) (low temperature will affect the ASM separation of oxygen effect).

The housing of the dual-flapper check valve has a dual-flapper check valve cartridge. This cartridge has two spring-loaded check valves that prevent fuel ingress from the fuel tank back to the IGGS. The valves open when the pressure in the NEA line is 0.29 psi (0.0200 bars).

The temperature sensor gives over-temperature protection. The temperature sensor gives temperature data to the ICU, to optimize ASM inlet temperature control, independently of IGGS over-temperature stop control function.

The pressure sensor gives over-pressure or under-pressure protection.
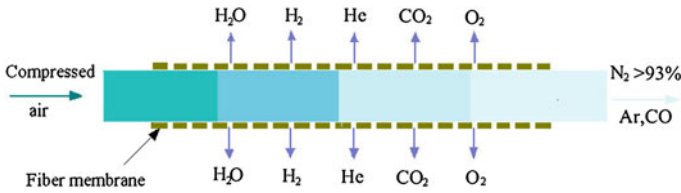
Fig. 16.1   Hollow fiber air separation schedule

The oxygen sensor measures the oxygen concentration of NEA flow and gives the data to the ICU to monitor the ASM performance one time for each flight during the cruise flight phase. The oxygen sensor also gives a pressure signal of the NEA that helps to know incorrect conditions.

The DFSOV is normally closed and isolates the IGGS from the fuel tank. The DFSOV closes if

- The pressure of the NEA flow is less than 15 psi (1.0342 bar) and/or
- The NEA flow temperature is hotter than 85 °C (185.00 °F).

With two solenoids, the ICU controls the DFSOV to the open position, and the NEA has three different flows of low/mid/high.

As shown in Fig. 16.1, ASM is permeable membrane ASM. Because oxygen and nitrogen have different permeation rate in membrane, oxygen can be separated from the air. ASM is an aluminum housing that contains several hundred thousands of very small-diameter hollow fibers. The gas whose permeation rate is faster seeps out from the hollow fiber when air flows through it. A lot of nitrogen is left, the purity is affected by air flow velocity and temperature, and there is also a small amount of other gas left.

16.2.2 Monitoring Principle

As shown in Fig. 16.2, the ICU monitors ASM downstream oxygen concentration once for each flight during the cruise flight phase. If it is higher than the reference value, the ICU will provide a fault message "ASM Performance Degraded." Oxygen sensor detects oxygen concentration of ASM downstream pipe and generates a 4–20 mA current signal, and then sends it to ICU according to different concentration. ICU determines whether the ASM downstream oxygen concentration meets the requirement with reference to different cruise altitude.
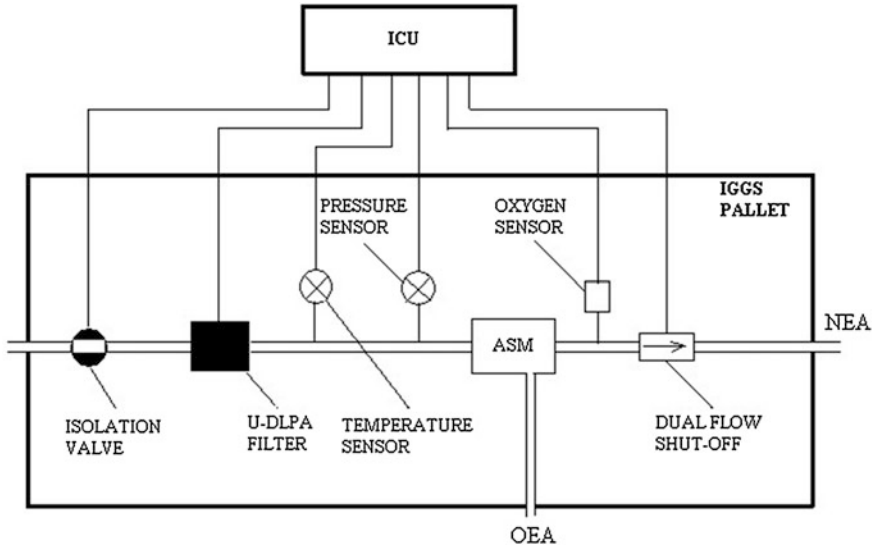
Fig. 16.2 System schedule

16.3 Fault Mode Analysis

16.3.1 Real Fault

Real fault means under the good condition of monitoring system, the oxygen concentration of ASM downstream exceeds the general standard, which is detected by the oxygen concentration sensor. Fault is caused by ASM downstream pipe leakage or ASM performance degradation.

There are two reasons that lead to ASM downstream pipe leakage:

- The sealing connecting pipeline and ASM are damaged.
- The pipeline itself is damaged.

The leakage points caused by reasons above would be found by the ground operation test.

There are two main reasons referring to ASM performance degradation:

- The damage of ASM internal structure mainly arises from the internal hollow fiber aging; it should be determined to change a new one for obvious structural damage.
- ASM hollow fiber polluted by dust particles suspended in the air affects gas permeability and air separation. It could be judged whether fault message comes from ASM performance degradation by swapping ASM with other aircraft. It can be obviously seen that the polluted ASM is covered with dust all over in the

Fig. 16.3 Polluted ASM

Fig. 16.4 Cleaning ASM
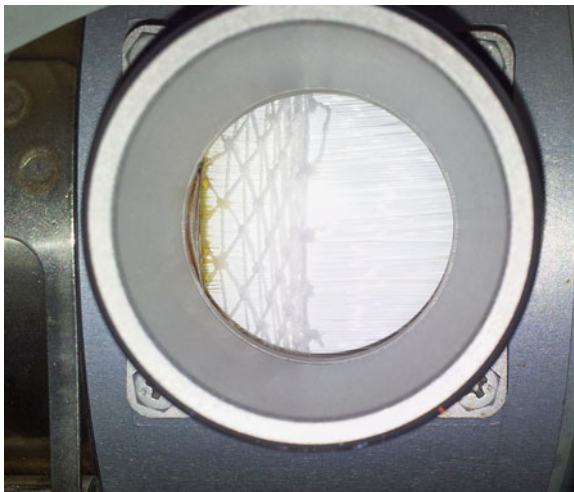
Fig. 16.3, but the one in the Fig. 16.4 is as clean as new. Figure 16.5 shows that many fiber pipes of ASM-contaminated area are blocked by yellow object.

In addition, there are few troubleshooting experience related to aircraft A320 series IGGS, so we also obtain reference from 737NG aircraft troubleshooting records. According to the Southern Airlines reliable data, it shows that troubleshooting cases as 737NG aircraft IGGS fault by replacing the damaged or polluted ASM are common. Thus, the reliability of ASM is relatively low.

Fig. 16.5 The contaminated
area enlargement
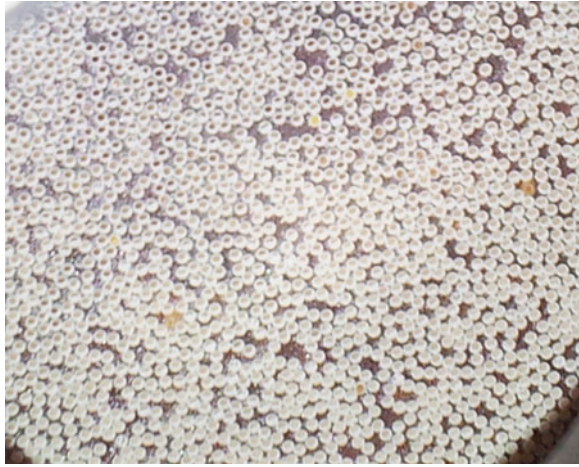
16.3.2 False Fault

Because fault of oxygen sensor, wiring and control unit in monitoring system gives
misleading message, and the false fault appears. False fault can be judged by
swapping component with other aircraft. The oxygen sensor and control unit can
be swapped with two other aircrafts. If the fault is removed to other aircraft, the
fault component should be found. If there is only one aircraft for swapping, we
should replace oxygen sensor and swap control unit with other aircraft, or replace
control unit and swap oxygen sensor with other aircraft. It can be determined that
the wiring is fault or not by comparing it with other aircraft.

16.4 Troubleshooting

We can consider the troubleshooting program according to the following aspects:
Since there is no fault isolation suggestion of monitoring system given by TSM,
we should swap component with other aircraft for troubleshooting. ASM is a high-
cost material, which cannot be hastily replaced. As the environmental pollution is
very serious, we should check the condition of air filter and ASM pollution.
Operation schedule should be implemented efficiently and completely. In my
opinion, the troubleshooting programs are as follows.

1. Test IGGS on ground to check whether ASM downstream pipe is leaking. If
   there is leakage, replace the pipe or sealing. Otherwise, go to the next step.
2. Remove the ASM; inspect whether ASM has serious pollution or obvious
   damage. If there are any, replace ASM and D-ULPA gas filter and clean the
   pipe between the two. Otherwise, go to the next step.

3. Swap ASM with other aircraft. If fault is removed to other aircraft, replace the fault ASM. Otherwise, go to the next step.
4. If condition permits, the oxygen sensor and control unit can be swapped with two other aircrafts. If there is only one aircraft for swapping component, we should replace oxygen sensor and then swap control unit with other aircraft, or replace control unit and swap oxygen sensor with other aircraft. If fault is removed to other aircraft, replace the fault component. Otherwise, go to the next step.
5. Check whether the wiring of ICU and oxygen sensor is damaged, and measure the circuit resistance. It can be concluded whether the wiring is default or not by comparing it with other aircraft. Replace the wiring if it is damaged or the resistance is inconsistent with other aircraft.

16.5 Maintenance Suggestions

Equipped with IGGS, the relevant airworthiness requirement has officially joined into the FAA regulations and stipulates time limit for completion, and verification of the airworthiness by the Civil Aviation Administration of China (CAAC) is in progress now. If all the aircrafts are equipped with IGGS, the cost of ASM material will become a huge expenditure, so it is imperative that we should develop a reasonable maintenance plan to reduce the cost.

1. As the air pollution becomes increasingly serious, the impurities from air filter will increase, and the speed of filter being blocked is obviously accelerated. The D-ULPA air filter ensures high-quality air in ASM. If the air quality is higher, the level of ASM pollution is lower, and the service life of ASM will be longer. ASM cost is ten times more than D-ULPA air filter. Under this situation, it is necessary to regularly check and replace air filter, maintain D-ULPA air filter technical performance, and prolong ASM service life, so as to reach the purpose of cost controlling. When we replace ASM, check whether the D-ULPA air filter and pipe are polluted and replace air filter and clean the pipe if they are polluted.
2. It is known that hollow fiber ultrafiltration membrane in ASM has been widely used in petroleum, chemical industry, environmental protection, energy, power, food, pharmaceutical, bioengineering, and other fields, which has achieved remarkable economic, social, and ecological benefits. At the same time, the membrane pollution problem has been one of the biggest challenges that engineering researchers confront. Membrane pollution can lead to serious decline in permeation and separation performance. Membrane cleaning is an important method to recover membrane performance. Cleaning method includes physical cleaning, chemical cleaning, and both of them. Physical cleaning method of hollow fiber ultrafiltration membrane uses mechanical power to remove surface contaminants. The whole cleaning process is without any chemical reaction. Chemical cleaning means chemical reaction or

dissolution between chemical and pollutants to reach the purpose of cleaning [3, 4]. From a long-term point of view, if we can find suitable cleaning method for ASM hollow fiber, then reuse the contaminated ASM; it would save a lot of material expenses. So we should actively seek manufacturers and related domestic repair company to provide technical support as soon as possible.

References

1. Zhou S (2013) Atmospheric environment. China Environ State Bull 2012:22–24 (in Chinese)
2. Airbus (2013) Description and operation of inert gas generation system. Airbus A319/A320/A321 Aircraft Maintenance Manual
3. Ya J, Qiu T (2003) Research progress of ultrasonically enhanced membrane separation process. Chin Acad J 22:45–48 (in Chinese)
4. Ma X, Song Y, Li X, He T (2013) Chemical cleaning of polyether sulphone hollow fiber ultrafiltration membrane. Nanjing Univ Technol J 35:85–90 (in Chinese)

Chapter 17
The Research on the Reliability of Helicopter Life Based on Analysis of the Data of Flight Data Recorder

Xu Dong Li and Xiao Hua Yang

Abstract If aviation maintenance wants to change from the current reactive, fault-based maintenance to state-based maintenance program transformation, we need to reduce or even abolish schedule maintenance tasks based on the fatigue life assumptions or standardized timing overhaul. First of all, in this paper, the loading spectrums of center of helicopter gravity were obtained by analysis of the data of flight data recorder. Then, the nominal stress method based on the data of flight data recorder was developed and the opposite fatigue damage of every helicopter in some air fleet was computed. The results accorded well with fact. Lastly, the reliability of the life by computing opposite fatigue damage was analyzed. Analysis results showed that the management of helicopter structure life was a dynamic process and the main idea of conversion from time maintenance to state maintenance was rational and feasible.

Keywords Time maintenance · State maintenance · Fatigue damage · Flight data recorder

17.1 Introduction

If aviation Maintenance wants to change from the current reactive, fault-based maintenance to state-based maintenance programe transformation, we need to reduce or even abolish schedule maintenance tasks based on the fatigue life assumptions or standardized timing overhaul [1]. From the point of view of strength, aircraft design evolved from static strength, static and dynamic strength, fatigue strength, damage tolerance, and reliability of the five stages of design.

X. D. Li (✉) · X. H. Yang
Naval Aeronautical Engineering Academy Qingdao Branch, Siliu Road,
Qingdao 266041, People's Republic of China
e-mail: xdli236415064@163.com

From the design principle point of view, damage tolerance and reliability of the design are more in line with the idea of condition-based maintenance. But for the present time, the airframe structure life is still based on fatigue strength design principle for helicopters imported or homemade by our nation [2, 3]. When the maintenance mode changed, it became key problem to determine the helicopter airframe structural reliability and renovation of the time of current status. Based on research of overload flight data normal to the helicopter gravity center, the present thesis tries to provide theoretical basis of state-based maintenance for the helicopter airframe [4–7].

17.2 Overload Spectrum Normal to the Center of Gravity Based on Flight Data

Flight data of helicoper generally contain more than 20 switch parameters such as normal overload and remaining fuel. Based on the fatigue damage feature, the thesis considers only the normal overload.

17.2.1 Acquisition of Flight Data

The flight data are analog signal instead of digital signal for helicopters imported from abroad, as well as homemade Thus, the selected flight data measured values can be transcribed into engineering data according to the parameter calibration table of each aircraft, and a common software module can be developed to save the original machine code as standard ASCII code files directly, depending on the sample rate set (typically 8 times/s).

17.2.2 Establishment of Normal Overload Spectrum of Helicopter

Figure 17.1 shows a typical fragment of overload spectrum obtained from flight data. Statistical counting process must be conducted first for the spectrum for calculation and experimentation for convenience. Rain flow counting method is thought to reflect the material stress–strain response under repeated loads, which is widely used for fatigue analysis and is adopted in the present thesis. Following Amendments are made when adopting rain flow method considering the mechanical characteristics of helicopter airframe structure.

Fig. 17.1 Original overload
spectrum normal to gravity
center
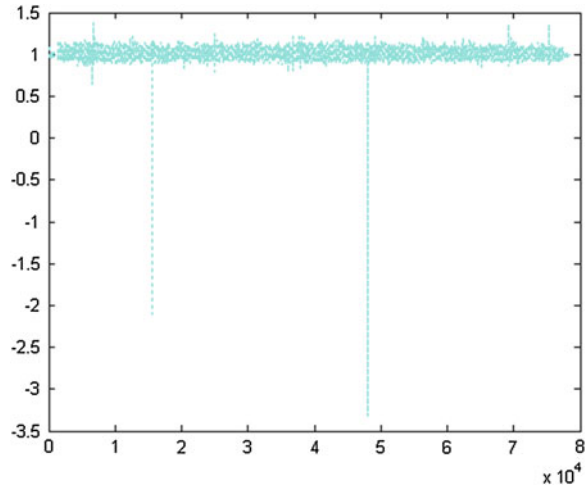
1. Filtering to remove small jitter. When counting, just take the maximum or minimum value by removing intermediate points and if an overload spectrum emerges by consecutive increasing or decreasing data points.
2. Filtering to remove severe noise. A large number of flight data showed that helicopter flight overload is within the range of 0.1–0.25, with some exception of 0.5. And overload data points from flight data far beyond that range are invalid data and must be removed.
3. Overall deviation correction. Some individual overload spectrum as a whole deviates significantly from overload as a horizontal line, some all in 1.1 above, which probably results from inaccurate adjustment of overload sensor, with which the calculated damage is obviously larger than the actual flighting damage. The overload spectrum must be corrected to be around 1.
4. Filtered to remove a small value cycle. It was generally believed that the helicopter airframe fatigue is high cycle fatigue, numerous low-value loops in load spectrum will cause little damage on structure, which can be removed in engineering calculations. And a certain number of high-value loops (overload cumulative appears less than 105 times for every 1,000 flight hours) are retained, as well as the loops whose mean value deviates from that of whole overload spectrum.
5. Convergent, divergent wave treatment. According to rain flow method, the overload loop of spectrum after filter when counting for the first time will exhibit convergent, divergent wave. The wave is separated into two fragment from the point with maximum amplitude. Then swap the two fragment to form a new convergent-divergent wave. Both ends of such a waveform are naturally closed, which can be counted for the second time. Figure 17.2 is a fragment spectrum obtained according to the above-mentioned amendation.

Fig. 17.2 Fragment of
spectrum after amendation
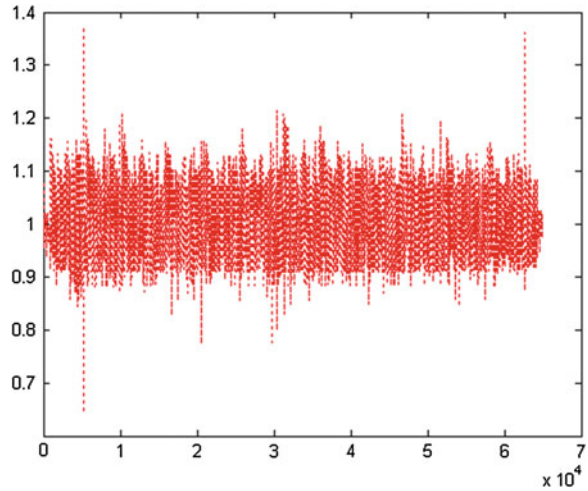
17.3 Calculation of Fatigue Damage

The airframe of helicopter is mainly subjected to low cycle fatigue loads from change of flight state and ground–air–ground loop. But the stress level of helicopter is relatively low compared to fixed-wing aircraft. Fatigue life can be directly identified with reasonable calculation method, without full-size structural fatigue test. In order to calculate fatigue damage with overload spectrum of gravity center, the present thesis proposed a flight data-based nominal stress method for damage calculation.

Nominal stress method is among the earliest method formed for anti-fatigue design, which is used for fatigue strength check or fatigue life calculation based on S–N curve of materials, combined with stress concentration factor and nominal stress of dangerous part of specimen or structure and fatigue damage accumulation theory. The nominal stress method regards that any structure made of the same material shares the same fatigue life if their stress intensity factor and load spectrum are the same. The control parameters are nominal stress and stress intensity factors in this theory. And the steps when applied this method for fatigue life calculation are as follows:

1. Indentify the dangerous location of structure when subjected to fatigue load.
2. Calculate the nominal stress and stress intensity factor KT of the dangerous location.
3. Calculate the nominal stress spectrum of the dangerous location based on load spectrum.
4. Calculate the S–N curve subjected to present stress intensity factor and stress level with interpolation method.
5. Calculation of fatigue life for the dangerous location applying fatigue damage accumulation theory.
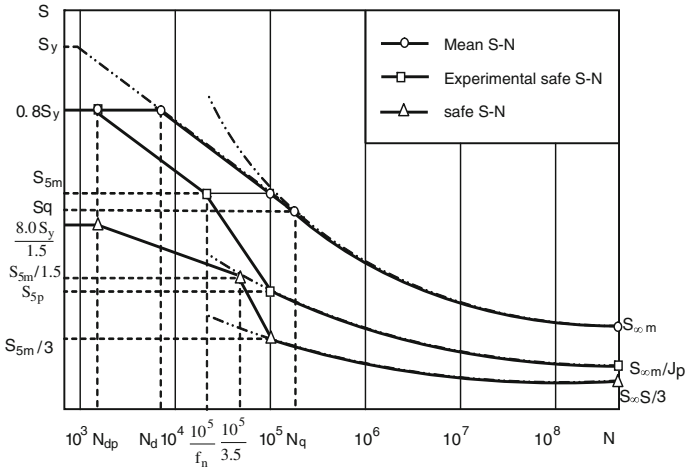
Fig. 17.3 Full-range *S–N* curve of materials

S–N curve of materials is the elementary data, which can be found in numerous material handbooks [8, 9]. According to helicopter structural fatigue design engineering features and for convenience, the literature collated *S–N* curve of commonly used materials' experimental data and gave the full-range *S–N* curve of material, which is shown in Fig. 17.3.

Helicopter structural fatigue design is accustomed to be represented by *S–N* curve formula and parameter.

S–N curve of high cycle fatigue is

$$\frac{S_a}{S_\infty} = 1 + \frac{A}{N^\alpha} \tag{17.1}$$

where stress ratio is −1, and *A* and *α* are material-dependent constants. For LY12CZ, *A* is 0.4828 and *α* is 0.5. Low cycle fatigue *S–N* curve is obtained by connecting the point of material yield strength and the point of high cycle fatigue *S–N* curve when *N* equals to 10^5 [7].

Use Goodman mean stress correction

$$S_{a1} = \frac{S_b - S_{m1}}{S_b - S_{m2}} S_{a2} \tag{17.2}$$

S_{a1} is fatigue strength or alternating load after correction (including average load S_{m1}). S_{m1} is average load after correction. S_{a2} is fatigue strength or alternating load before correction (including average load S_{m2}). S_{m2} is average load before correction. S_b is structural strength limit load.

In order to turn the overload spectrum into nominal stress spectrum, it is reasonable to assume plastic deformation will not occur for airframe structural materials in all cases of helicopter imported from abroad without the original

design information and data. So stress corresponds to equivalent overload cycle g_{dl} of the spectrum in the S–N curve

$$\frac{S_{10^n}}{g_T} = \frac{S_i}{g_{dl}}$$

(17.3)

where S_{10^n} is the stress value of S–N curve corresponding to N equal to 10^n. When $n = \infty$, S_{10^n} is the fatigue limit. g_T is the threshold value of overload cycle. g_{dl} is the equivalent overload cycle which is defined as follows:

$$g_{dl} = \frac{g_b - g_{m0}}{g_b - g_m} g_a$$

(17.4)

where g_b is the maximum overload, which is 2 in this thesis. g_{m0} is the average value of the whole overload spectrum, which is 1. g_{mi} is average value of overload cycle. g_{ai} is amplitude of overload cycle. Fatigue life N_i can be found from full-range S–N curve of aluminum alloy corresponding to S_i. Fatigue damage of structure D_i can be calculated as $1/N_i$. So damage of the whole overload spectrum is

$$D = \sum D_i.$$

(17.5)

17.4 Relative Damage-Controlled Life of Helicopter

Relative damage of eight helicopters after 1,000 flying hours (FH) is calculated following the above-mentioned method. Results indicate No. 3 helicopter suffers the most serious damage. If the relative damage of No. 3 helicopter is regulated as 1, the damage value of the other seven helicopters is listed in Table 17.1. No. 1 and No. 3 helicopters are mostly damaged. Flight log analysis indicates that two helicopters are often used aerobatic with more extraordinary maneuvers, so the damage is more serious. This reflects the above-mentioned method is reasonable. Relative damage of No. 6 is unusual slight, and flight data inspection suggests the data are far from complete, which indicates the flight data recorder needs to be re-adjusted.

17.5 Reliability Analysis of Fleet Life

Unlike the former life analysis, the data in Table 17.1 are the helicopter time between failures; even with the relative serious damage, No. 3 helicopter can actually still fly. It can be assumed that the helicopter airframe fatigue life follows a lognormal distribution, that is

Table 17.1 Relative damage calculated by nominal stress method based on flight data

	No. 1	No. 2	No. 3	No. 4	No. 5	No. 6	No. 7	No. 8
Relative damage	0.8583	0.6643	1	0.4279	0.6655	0.1260	0.6378	0.7323
Fight hours needed for the plane to reach the very same damage as No. 3 helicopter	1,165	1,505	1,000	2,337	1,502	7,930	1,568	1,365

For helicopter imported, if the manufacturer suggests the first renovation takes place after 1,000 flying hours, helicopters except No. 3 can be extensively used.

$$F(t) = \frac{1}{\sqrt{2\pi}\sigma} \int_0^t \frac{1}{x} e^{-\frac{1}{2}\left(\frac{\log x - \mu}{\sigma}\right)^2} = \phi\left(\frac{\log t - \mu}{\sigma}\right) \tag{17.6}$$

where μ and σ are logarithmic mean and standard deviation. In the $(1 - \alpha)$ confidence level, the reliability $R(t)$ optimal one-sided confidence limit is

$$R_l(t) = \begin{cases} \phi(\mu(\sigma_1)) & \text{when } t \geq t_n \\ \phi(\mu(\sigma_2)) & \text{when } t \leq t_0 \\ \phi(\mu(\sigma_1)) & \text{when } t_0 < t < t_n, \text{ and } \sigma_1 > \sigma_0 \\ \phi(\mu(\sigma_2)) & \text{when } t_0 < t < t_n, \text{ and } \sigma_2 > \sigma_0 \\ \phi(\mu_0) & \text{when } t_0 < t < t_n, \text{ and } \sigma_1 < \sigma_0 < \sigma_2 \end{cases} \tag{17.7}$$

where $t_n = \max(t_1, t_2, \ldots, t_n)$, (μ_0, σ_0) is the solution of following equations.

$$\sum_{i=1}^n \frac{\phi'\left(u + \frac{1}{\sigma}\log(t/t_i)\right)}{\phi\left(u + \frac{1}{\sigma}\log(t/t_i)\right)}(\log(t/t_i) = 0 \tag{17.8}$$

$$\prod_{i=1}^n u + \frac{1}{\sigma}\log(t/t_i) = \alpha \tag{17.9}$$

$u(\sigma)$ is calculated from Eq. (17.8). Let $\sigma = \sigma_1$, $u = u(\sigma_1)$; Let $\sigma = \sigma_2$, $u = u(\sigma_2)$. In engineering application, logarithmic standard deviation of fatigue test data covers a large range, which ranges from 0.01 to 0.2. If we suggest $\sigma_1 = 0.01$ and $\sigma_2 = 0.1$, one-sided confidence limit of reliability of first renovation after 1,200 FH is 96.1 % in the 95 % confidence level.

17.6 Conclusion

1. The proposed method of life calculation is carried out without the original design data, which gives the relative damage and relative life expectancy. The method provide a theoretical basis for reasonable echelon overhaul arrangements for aircraft.

2. Life management is a dynamic process.
3. Through the analysis of center of gravity overload spectrum from helicopter flight data, transit from regular maintenance to condition-based maintenance can be achieved using helicopter flight data.

References

1. Tao C (1997) Modern airframe design. Northwestern Polytechnical University Press, Xian (in Chinese)
2. Wang Y (1981) Aviation metal fatigue performance handbook. Beijing Institute of Aeronautical Materials, Beijing (in Chinese)
3. Yao W (2003) Structural fatigue life analysis. National Defense Industry Press, Beijing (in Chinese)
4. Li X-D, Wang X-S, Ren H-H, Chen Y-L, Mu Z-T (2012) Effect of prior corrosion state on the fatigue small cracking behaviour of 6151-T6 aluminum alloy. Corros Sci 55(2):26–33
5. Wang X-S, Li X-D, Ren H-H, Zhao H-Y, Murai R (2011) SEM in situ study on high cyclic fatigue of SnPb-solder joint in the electronic packaging. Microelectron Reliab 51:1377–1384
6. Cai Z, Li X, Jia M (2014) SEM in situ study on fatigue crack growth of LC9 aluminum alloy subjected to elevated temperature. Adv Mater Res 834–836:356–359
7. Li X, Mu Z, Sun W (2014) Fatigue crack prediction of LC9 with corrosion damage considering effect of load frequency. Adv Mater Res 842:356–359
8. He G (1995) Reliability of the data collection and analysis. National Defense Industry Press, Beijing (in Chinese)
9. Li X, Mu Z, Liu Z (2013) SEM in situ study on pre-corrosion and fatigue cracking behavior of LY12CZ aluminum alloy. Key Eng Mater 525–526:81–84

Chapter 18
Turbofan Engine Overhaul Quality Evaluation Based on Cloud Theory

Yanxiao Huang and Wenli Lv

Abstract The paper was aimed to construct the engine overhaul quality cloud model on the basis of the randomness and fuzziness of overhaul test data. The engine overhaul quality evaluation system was established by nine parameters of engine performances at the condition of the engine taking-off test under engine stable thrust and engine pressure ratio (EPR). In the meantime, the test quantitative data recording five times of engine overhaul parameters were transformed to the qualitative data in the cloud model. The weight values of the calculated parameters were given by method of the information entropy theory. The cloud gravity center weighted deviation degree was accordingly given as an evaluation criterion of the engine overhaul quality. The overhaul test data concerning turbofan engine TRENT 700 were chosen in order to validate the model. The results of the paper show that the calculated performance deviation degree was separately 0.5188, 0.4851, and 0.5288. The first and third values were nearly equivalent, while the second one was lower in comparisons with the other two values. As for the two former, the two engines were equipped on the same airplane. Therefore, the cloud model proposed in the paper can be applied to accurately make assessments of the engine performances. The accuracy of the aero-engine quality evaluation is further improved. The results can provide the references for the engine fleet management.

Y. Huang (✉)
Vocational Technical College, Civil Aviation University of China, Tianjin 300300, China
e-mail: oldsea0592@163.com

W. Lv
Aeronautical Engineering College, Civil Aviation University of China, Tianjin 300300, China

18.1 Introduction

Engine overhaul quality decides directly engine reliability based on engine fleet management. Overhaul quality using engine test data are usually evaluated: abroad Pratt & Whitney company developed module analysis program network (MAP-NET) test data processing system, which can correct and analyze the gas performance test data with the specific baselines [1]; however, in the domestic, Beijing Aircraft Maintenance and Engineering Corporation (AMECO) deals with engine test original performance data and data of MAPNET report to analyze engine performance trends [2]. However, randomness and fuzziness of engine test data can affect directly accuracy of engine overhaul quality evaluation and reduce engine fleet management level.

So the paper constructs turbofan overhaul quality evaluation model by the cloud theory [3], which can characterize randomness and fuzziness precisely to solve the characteristic of test data and improve accuracy of turbofan engine overhaul quality evaluation.

18.2 The Cloud Theory Research and Constructing Qualitative Review Series

The cloud theory [3] mainly applies to larger fuzzy concept in nature. The cloud eigenvalue is expectation Ex, entropy En, and hyper-entropy He, which can integrate randomness and fuzziness to mapping from quantitative to qualitative. Figure 18.1 shows normal cloud distribution figure of "around 0.28."

18.2.1 The Cloud Eigenvalue Approach

1. Calculating sample mean and variance of the reverse normal cloud generator from quantitative to qualitative by swatch x_i

$$\text{Sample mean} \quad \bar{x} = \frac{1}{n}\sum_{i=1}^{n} x_i$$

$$\text{Sample variance} \quad S^2 = \frac{1}{n-1}\sum_{i=1}^{n} (x_i - \bar{x})^2 \tag{18.1}$$

Fig. 18.1 Normal cloud distribution figure of "around 0.28"
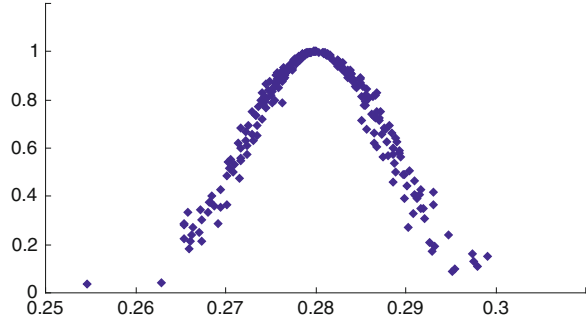
2. Calculating eigenvalue of reverse normal cloud generator

$$Ex = \bar{x}; \ En = \sqrt{\frac{\pi}{2}} \times \frac{1}{n}\sum_{i=1}^{n}|x_i - \bar{x}|; \ He = \sqrt{S^2 - En^2} \qquad (18.2)$$

3. Calculating cloud generator eigenvalue of overarching goal by multi-parameters fusion

$$Ex = \frac{Ex_1En_1 + Ex_2En_2 + \cdots + Ex_lEn_l}{En_1 + En_2 + \cdots + En_l}; \ En = \frac{En_1 + En_2 + \cdots + En_l}{l} \qquad (18.3)$$

18.2.2 The Cloud Representation of Qualitative Review Series

All qualitative review series are represented by forms of qualitative approach and the cloud figure. Each range of qualitative review series is (0, 1), and middle section's review of bilateral constraints, for example (d_{min}, d_{max}), can be represented by symmetry the cloud model; however, reviews on both sides represent expectation value with exact value of both sides and entropy value with half of entropy of corresponding symmetric cloud model. The eigenvalues are calculated by approximate formula because the reviews are constructed by left and right value.

Assuming the review series include ten sections, the range of which is in (0, 1), then corresponding range of every review is shown in Table 18.1.

Table 18.1 The section's review corresponding indicators

	First	Second	Third	…	Eighth	Ninth	Tenth
Range	$(0, d_1)$	(d_1, d_2)	(d_2, d_3)	…	(d_7, d_8)	(d_8, d_9)	$(d_9, 1)$

The eigenvalue calculation approach about middle section review of dual constraints:

$$\text{Ex} = \frac{d_{\max} + d_{\min}}{2}; \quad \text{En} = \frac{d_{\max} - d_{\min}}{6}. \tag{18.4}$$

The eigenvalue calculation approach about reviews on both sides:

$$\text{Ex} = (\text{exact value of constraint}); \quad \text{En} = \frac{d_{\max} - d_{\min}}{12}. \tag{18.5}$$

Hyper-entropy is approximated value 0.02 because there is not special significance in the review series. So Fig. 18.2 shows cloud model of review series constructing by cloud eigenvalue.

18.3 Constructing Engine Overhaul Quality Evaluation Model by the Cloud Theory

18.3.1 Constructing Engine Overhaul Quality Evaluation System

The engine test data are chosen to evaluation engine overhaul quality through the idle condition, the maximum continuous condition, the taking-off condition, and the cruise condition after the engine overhaul. The paper uses test data of the cruise condition as raw data to evaluate engine overhaul quality because engine performance parameters changes small in the cruise condition. Table 18.2 shows that all parameters are classified on the basis of test list.

Figure 18.3 shows the overhaul evaluation system in the cruise condition.

18.3.2 The Weights Algorithm of Characterizing Engine Overhaul Quality

The engine overhaul quality is fully characterized by single parameter as complex system, so using multi-parameters improves the accuracy; however, the problem is proposed to calculate weights of all parameters accurately. The method is given to calculate weights by information entropy theory [4].
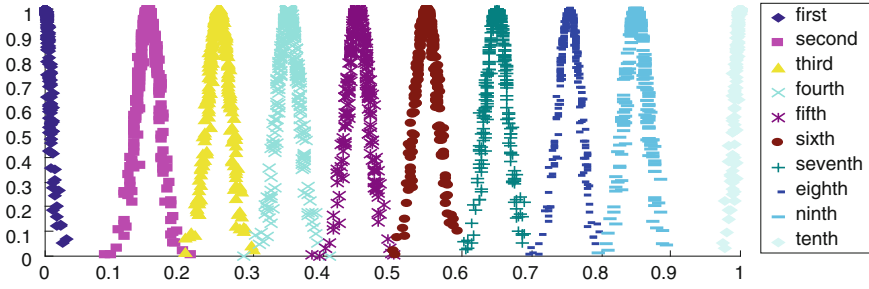
Fig. 18.2 Review series of qualitative cloud

Table 18.2 Engine test parameters and types in the cruise condition

Types	Test parameters
Economy	N1vib, N2vib, N3vib, oilcons, EGT, SFC
Efficiency	EPR, F, N1, N2, N3
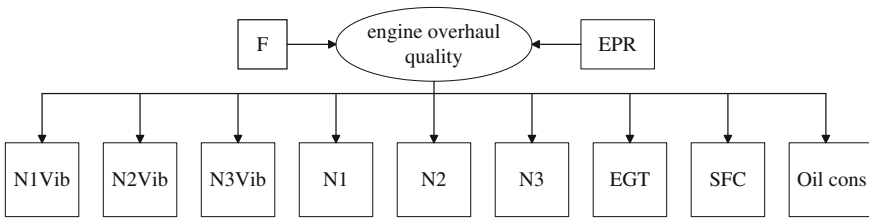
Fig. 18.3 Engine overhaul quality evaluation system

1. Calculating information entropy of all parameters.

$$P_{ij} = \frac{x_{ij}}{\sum_{i=1}^{m} x_{ij}} \qquad (18.6)$$

2. Calculating entropy value of all parameters.

$$e_j = -k \sum_{i=1}^{m} p_{ij} \cdot \log p_{ij} \qquad (18.7)$$

3. Calculating the weights of all parameters.

$$w_j = \left(1 - e_j\right) \bigg/ \sum_{j=1}^{n} \left(1 - e_j\right) \tag{18.8}$$

where w_j is the weights of jth parameters.

18.3.3 Constructing the Cloud Gravity Center Weighted Deviation Model of the Engine Overhaul Quality

1. Standardization approach of engine overhaul quality parameters.

The engine overhaul quality parameters are standardized according to the formula approach [5, 6]

$$\text{economy:} x(ij) = \frac{x_{\min}(ij) - x(ij)^*}{x_{\max}(ij) - x_{\min}(ij)} \tag{18.9}$$

$$\text{efficiency: } x(ij) = \frac{x(ij)^* - x_{\min}(ij)}{x_{\max}(ij) - x_{\min}(ij)} \tag{18.10}$$

2. The cloud model of engine overhaul quality parameters.

The paper takes quantitative data in five times of engine overhaul parameters to transform qualitative data of cloud model according to formula (18.1–18.2).

3. Overarching the engine overhaul quality cloud.

The paper proposes fusing n-dimensional parameters into overarching cloud because the difference of engine overhaul quality represents the difference of engine overhaul performance parameters. So take gravity center O of n-dimensional parameters' overarching cloud with T-dimensional vector:

$$\begin{cases} O = (O_1, O_2, \ldots O_n) = L \times H \\ O_i = L_i \times H_i, \quad i = 1, 2, 3, \ldots, n \end{cases} \tag{18.11}$$

Among gravity center can be divided into position and height, such as L_i and H_i:

$$L_i = (\text{Ex}_1, \text{Ex}_1, \ldots, \text{Ex}_l); H_i = (h_1, h_2, \ldots, h_l) \tag{18.12}$$

4. Evaluating overhaul quality by cloud gravity center weighted deviation degree criterion.

The paper chooses the best and worst value from test data on the basis of TOPSIS in the engine fleet and constructs the stable best vector of engine parameters. Setting overarching cloud gravity center vector in the best condition:

$$O^0 = L \times H^T = \left(G_1^0, G_2^0, \ldots, G_n^0\right);$$
$$L = \left(Ex_1^0, Ex_2^0, \ldots, Ex_n^0\right); \quad H = \left(h_1^0, h_2^0, \ldots, h_n^0,\right) \tag{18.13}$$

Then standardizes cloud gravity center vector O of engine overall performance:

$$O_i^T = \frac{O_i}{O_i^0}, \quad i = 1, 2, \ldots, n \tag{18.14}$$

Standardizing overarching cloud gravity center vector O of the overall performance parameters: $O^0 = (1, 1, \ldots, 1)$.

At last calculate cloud gravity center weighted deviation degree of engine by which it can be ranked to engine overhaul quality.

$$\lambda = \sum_{j=1}^n \left(h_j \times O_i^T\right), \quad \lambda \in (0, 1) \tag{18.15}$$

18.4 The Examples Verification of Turbofan Overhaul Quality Evaluation

1. Constructing engine overhaul quality evaluation system by Trent 700 (Fig. 18.1).
2. With five times of three engine overhaul parameters as case, such as the 41413, 41390 and 41492 engine.
3. Calculate three eigenvalues to represent five times of each engine overhaul test data by cloud theory and eigenvalues of overarching cloud of engine overhaul quality by formula (18.3). The results are shown in Table 18.3.

Then input the overarching clouds of three engines overhaul quality into the qualitative review series. The results is shown by Fig. 18.4.

4. Calculating the performance parameters weight by information entropy, such as Table 18.4.
5. Calculating the gravity center vector of three engines overhaul quality.

Firstly, calculate the best gravity center vector of taking-off condition by formula (18.10):

Table 18.3 The test parameters cloud eigenvalue of Trent 700 engine through the cruise condition

S/N		N1vib	N2vib	N3vib	N1	N2	N3	EGT	SFC	Oilcons	Overall
41413	Ex	0.5154	0.4634	0.4325	0.5008	0.5020	0.4990	0.4995	0.4981	0.5358	0.4792
	En	0.1797	0.1467	0.2543	0.0229	0.0108	0.0141	0.0053	0.0134	0.1112	0.0838
41390	Ex	0.5113	0.5217	0.5142	0.4997	0.5008	0.5023	0.5000	0.4993	0.5108	0.5156
	En	0.0895	0.2180	0.1274	0.0051	0.0055	0.0076	0.0021	0.0032	0.0849	0.0604
41492	Ex	0.3950	0.5185	0.5263	0.5005	0.4947	0.4995	0.4996	0.4921	0.5107	0.4890
	En	0.2191	0.2228	0.3166	0.0142	0.0137	0.0161	0.0040	0.0193	0.0786	0.1005
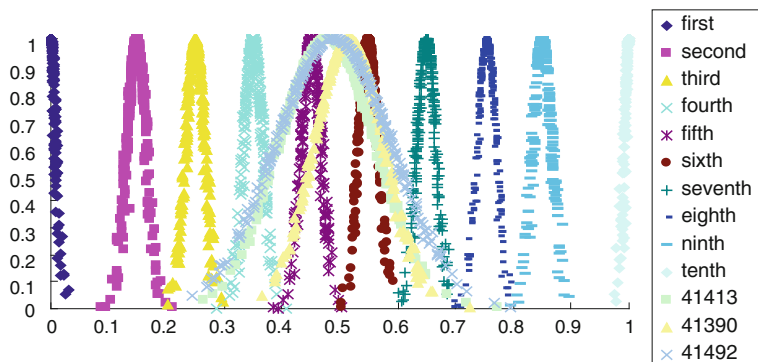
Fig. 18.4 Overall cloud figure of engine overhaul quality

Table 18.4 The parameters' weight values of Trent 700 engine

Parameters	N1vib	N2vib	N3vib	N1	N2	N3	EGT	SFC	Oilcons
Weight values	0.3674	0.2875	0.2504	0.0005	0.0014	0.0008	0.0030	0.0048	0.0840

$$
\begin{aligned}
O^0 = \left(O_1^0, O_2^0, \ldots, O_9^0\right) &= L \times H^T \\
&= (0.3674, 0.2875, 0.2504, 0.0005, 0.0014, 0.0008, 0.0030, 0.0048, 0.0084) \\
&\quad \times (1.0, 1.0, 1.0, 1.0, 1.0, 1.0, 1.0, 1.0, 1.0) \\
&= (0.3674, 0.2875, 0.2504, 0.0005, 0.0014, 0.0008, 0.0030, 0.0048, 0.0084)
\end{aligned}
$$

Then calculate the engine gravity center vectors of the cruise condition by formula (18.10):

$$O_{41413} = (O_1, O_2, \cdots O_9) = L \times H^T$$
$$= (0.1894, 0.1332, 0.1083, 0.0002, 0.0007, 0.0004, 0.0015, 0.0024, 0.0450)$$
$$O_{41390} = (O_1, O_2, \cdots O_9) = L \times H^T$$
$$= (0.1879, 0.1500, 0.1288, 0.0002, 0.0007, 0.0004, 0.0015, 0.0024, 0.0429)$$
$$O_{41492} = (O_1, O_2, \cdots O_9) = L \times H^T$$
$$= (0.1451, 0.1491, 0.1318, 0.0002, 0.0007, 0.0004, 0.0015, 0.0024, 0.0429)$$

6. The gravity center vectors of three engines overhaul quality are normalized by formula (18.13):

$$O^T_{41413} = (0.4846, 0.5366, 0.5675, 0.4992, 0.498, 0.501, 0.5005, 0.5019, 0.4642)$$
$$O^T_{41390} = (0.4887, 0.4783, 0.4858, 0.5003, 0.4992, 0.4977, 0.5, 0.5007, 0.4892)$$
$$O^T_{41492} = (0.605, 0.4815, 0.4737, 0.4995, 0.5053, 0.5005, 0.5004, 0.5079, 0.4893)$$

7. Calculating the weighted deviation degrees of three engines overhaul quality by formula (18.15):

$$\lambda_{41413} = 0.5188; \quad \lambda_{41390} = 0.4851; \quad \lambda_{41492} = 0.5258$$

The results are shown that the weighted deviation degree of engine overarching cloud in cruise conditions is difference with weighted deviation degree in the best conditions. The best overhaul quality is the 41492, and the worst is the 41390; however, the 41413 is within them. At the same time, the difference of 41492 and 41413 weighted deviation degree is 0.0070, which represents two engine overhaul quality is close, but the 41390 is very worst in three engines. So the 41492 and the 41413 engines are used preferentially and can be assembled in the same aircraft simultaneously.

18.5 Conclusion

1. The paper indicated the greater impact to engine performance when performance parameters change greater based on engine performance degradation.
2. Then proposed method to calculate quantitatively weights of all parameters by information entropy theory on the basis of the characteristics that entropy was able to measure the amount of information based on the model in probability and statistics.

3. Construct evaluation system based on nine parameters of engine test data to evaluate overhaul quality of Trent 700 engines through established cloud gravity center model.
4. The results show that the 41390 engine performances is the worst one of three engines, in the meantime, the 41492 engine and the 41413 engines were nearly equal. So they could be assembled on the same airplane.
5. So the result is accurate by comparing the calculated performance results of the engine fleet. It can be concluded that cloud model improves the accuracy deeply.

References

1. He JL, Hong J, Li QH (1996) Research on aero-engine real life monitor and data processing method. J Aerosp Power 11(4):345–348 (in Chinese)
2. Liu B (2004) Research on engine module health model and assessment criterion. Civ Aviation Univ China, Tianjin (in Chinese)
3. Li DY et al (2005) Uncertainty artificial intelligence. National Defense Industry Press, Beijing (in Chinese)
4. Guo QJ, Sai YX (2007) The project plan evaluation based on entropy weight decision. Stat Decis 8:50–51 (in Chinese)
5. Dai CH, Zhu YF (2007) Adaptive genetic of the normal cloud model. Control Theor Appl 24(4):646–648
6. Liu SY (2005) Some statistical analysis of the normal cloud model. Inf Control 4(2):236–239

Chapter 19
Research on Condition-Based Maintenance for Airborne Equipments

Bin Luo, Ting Tang, Zhi Qiu and Wenling Zhong

Abstract This paper analyzes the present situation and advantages of the foreign airborne equipments, demonstrates the feasibility of maintenance for airborne equipments in the army, expounds the monitoring parameters as the technical features of the maintenance, and formulates the surge protector as the implementation of maintenance scheme.

The condition-based maintenance (CBM) is proposed against the regular maintenance, which is an advanced maintenance mode. The research and implementation of CBM has a very important practical significance for our military maintenance mode reformation. According to the fundamental principle of maintenance theory, the CBM is a predictive and preventable maintenance method based on the aircraft's specific system, equipment, parts to repair, and to replace. The characteristics of this maintenance method are as follows: It is premise on an accurate master of the "practical technology" (advanced technology, accurate instrument, correct method), and it aims to extend the parts' working life to the largest and increase the economic benefits (time-saving, effort-saving, people-saving, material-saving, good quality, high efficiency). We can tell from its characteristics: The CBM depends on the superior performance of the aircraft, advanced technology of the testing equipment and method. Therefore, the CBM is the inevitable result of the high-speed development of aerotechnics. It is the inexorable law for the CBM to replace the regular maintenance.

Due to the development of CBM, which is followed with the aircrafts' continuous technological progress, the foreign countries had begun to use it in the early 1970s, also had obtained good military and maintenance efficiency.

B. Luo (✉) · T. Tang · Z. Qiu · W. Zhong
Department of Instrument and Electrical Engineering, Naval Aeronautical Engineering
Institute Qingdao Branch, Qingdao 266041, China
e-mail: luobin234@163.com

Methods	Periodical maintenance (%)	Condition-based maintenance (%)
Series		
Boeing 707	40	60
Boeing 727	40	60
Boeing 737	29	71
Boeing 747	0.30	99.7
DC-10	2	98

Table 19.1 Comparison table for periodical maintenance and condition-based maintenance

Table 19.1 is the comparison between the regular maintenance and CBM of the series of Boeing machines of USA in the early 1990s.

From Table 19.1, we can see that the more advanced the aircraft is, the more project on CBM will be. The CBM has been applied to Boeing 747 for all.

The CBM has brought great benefits on military and civil aviation industry. For example, with regular maintenance, 1,200 appendixes in hydraulic system need to be removed to repair in nine Boeings 727 of American airlines each year, but the number of the cases fell to 33 after 1993 when using the CBM. It can save millions of dollars on the repair and changing. It had reduced 1,000 working hours for each machine. Meanwhile, it improved the good rates of the aircraft.

Foreign countries can use CBM. Then, how about us? Can we use the CBM? The answer is definitely yes! In fact, many navy and air force have canceled the regular maintenance for 50 and 100 h. Because recently the types of aircraft are updated largely, also the electronic equipments increase heavily. They are incomparable to the 1960s and 1970s. We should say that CBM can be carried out in most of our navy and air force planes, or at least in some parts, such as the power system in electric profession. At present, the manufacturing technology of generator has reached the international level, the lifetime for generator ZF-18 has amounted to 1,000 h. The voltage regulator has been electronized, and many electronic devices have been able to calculate and test out the average time of trouble-free time and working lifetime precisely, so it has possessed the conditions to use CBM. Therefore, our implement of CBM is not only necessary but also feasible.

So far, there are two kinds of CBM used internationally, one is monitoring the level of reliability, and the other one is monitoring parameters.

One: Monitoring the level of reliability
It means to collect, process, and analyze the reliability of the overall parts on the same type and its effective and validated data. It has to make a decision on the necessary preventive work for overall or certain parts of the whole machine.

This kind of CBM have to solve the organization and technical issues as follows: (1) often collect and process the reliability of the data uninterruptedly to determine the actual reliability level of all parts, (2) analyze the comparison between the actual level of the reliability and the reliability with the allowable standard, (3) calculate and test part reliability and lifetime, and (4) make decision.

Its characteristic are: need a lot of statistics, analysis, data processing, and calculation. Systematic high difficulty, has certain limitations, only applies to the

developed countries and the aircraft with highly advanced technology, and all kinds of data especially the reliability data.

Two: Monitoring parameters

Monitoring parameters of CBM needs to test the equipment system and the parts' technical state continuously and regularly. When the testing parameter is close to the critical value, then it will decide whether to replace or repair the system or parts.

This kind of CBM has to solve the technical issues as follows: (1) analyze, calculate, and research all the critical values on the parts' reliable work and do the test; (2) have the advanced testing instrument in situ, especially electric testing record analysis instrument in situ and machinery nondestructive testing instrument; and (3) set parameters monitoring period and testing methods.

Monitoring parameters of CBM is a way of active preventive maintenance. It needs to monitor the objects' (system or individual parts) technical status, based on its maintenance content, cycle, and way of monitoring, so as to find out the fault warning in time according to the critical value.

The first characteristic is: Objects have no repair life, only have lifetime prescribed by the manufacturer. To determine which kind of maintenance should be used should follow the comparison between the parameters of the specified value and critical value on the installed system or mechanism. Sometimes, we can use the specific local maintenance, minimize the repair operations, and maximum its work time. In some cases, parts have reached their lifetime regulated by the factory, but the monitoring parameters' conclusion is still available, so you can prolong its working lifetime. The feasibility of this approach has been proved through the case that has solved the problem of some old aircraft in prolonging its life by the method of fatigue analysis.

The second is: require the maintenance objects to have good testing parameters of technology for assessing and predicting state, that is, "adapt to check," so that we can make testing instrument according to their needs, to test and evaluate based on the parameters. Otherwise, you would not achieve the monitoring parameters in CBM.

The third is: the maintenance object is required to be able to draw the parameters that is detected and draw the changes of the function and the image of the function, so that various problems can be found timely when calibration or input computer processing is done in each test.

The monitor parameter is more widely used between the two CBM, especially when testing a single system, an individual parts in the aircraft. So, it is a suitable CBM for our navy and air force planes to research and test.

Then, how to use CBM for a model, a system or even a part? Generally speaking, we should formulate corresponding technical plan firstly and then officially carry it out after trial and modification. The following case of maintenance on the surge protector briefly explains the specific steps: the first step, the feasibility analysis of maintenance on the parts. Mainly to analyze surge protector testability parameters of each link and the relationship between its performances item by item; the second step is to calculate the average surge protector trouble-free working time as the basis of reference data to determine the longest maintenance overhaul time.

Because the surge protector is mainly composed of electronic device, the device of the basic failure rate can be calculated.

According to the formulas, the basic failure rate is:

$$\lambda = \sum_{i=1}^{t4} N_i \lambda G_i = 125 \times 10^{-5} \tag{19.1}$$

The average time of trouble-free is :

$$\text{MTBF} = 1/\lambda = 800\,\text{h} \tag{19.2}$$

It is clear that as long as the important monitoring parameters meet the requirements, it does not need complete repair within 800 h. If the parameters are right after 800 h, we could extend its work time. The third step is to determine the static and dynamic testing parameters and the critical value.

1. Static parameters: (1) The external inspection should conform to the existing regulations and (2) the static resistance between inspection parameters and the critical value of sprig.
2. Dynamic parameters A (driving): (1) The generator speed $n = 4{,}500 \sim 7{,}000$ r/min, voltage $= (28.5 + 1.5)$ V; (2) to adjust resistance of generator voltage regulator hole to limit, the voltage is $26.5 \sim 29.5$ V. (3) generator speed 9,000 r/min, add, and subtract 100 A load, the voltage oscillation time changed not more than 0.5 s; (4) add and subtract the load, the voltage should be pulsed.
3. Dynamic parameter B (simulated): (1) The voltage is lower than 14 V, or higher than 32 V, trouble light should be lighted; (2) input examines the dynamic parameters, inspect the analog signal; (3) input analog signal to check voltage regulator waveform and the standard waveform, the change is less than 5 %.

The fourth step, the design and development of in situ testing instrument and expert system for CBM. It should be automatic and intelligentized, high-speed, large-capacity requirements.

Fifth, make detailed rules for CBM of voltage regulation protector. The main content is: (1) according to regulations to do external examination before and after every flight. (2) Inspect data in the control panel in each drive. (3) Check dynamic parameters for every 5 day (can drive, also can be simulated). (4) Check resistance parameters every 10 day. Above all, every data should be recorded. (5) Input data to computer on maintenance expert system every 10 day for statistics, to carry on the analysis and calculation, to get the reliability conclusions on the machine parts, and to make decisions. For instance, adjustments in aircraft and maintenance out of the aircraft, if pass muster, will continue to use, until to the critical value; (6) do not remove the maintenance within 800 h in principle, if the performance is good, also can prolong lifetime. This case shows that the parameter of CBM for airborne equipments has strong practicability, relatively easy to organize and carry out.

Research on CBM is not only the reformation of the maintenance modes, but also the reformation of the maintenance system and techniques. It is a system engineering, involving many problems and aspects, thus it will have a bigger cost at the early stage, but the military and economic benefits will be very remarkable. It is estimated that the maintenance personnel can be reduced by about 60 %, the workload 50 %, aeronautical material, and other cost more than 40 %.

Meanwhile, the CBM has new requirement on the maintenance personnel and system:

Firstly, the maintenance personnel should be proficient in both profession and maintenance theory. At the same time, they must be very skillful when using all kinds of advanced equipment and operating the computer to monitor data analysis; Secondly, we should be equipped with high technological test and experiment facility. Thirdly, we must build a high-speed, large-capacity maintenance information system. Fourthly, the reformation on the maintenance management system should move forward faster to adjust itself to the new maintenance methods.

In order to adapt to circumstance mentioned above, we should strengthen the learning on the maintenance theory, especially on the advanced CBM theory and its experience from home and abroad, and combine the theory with practice to vigorously promote the research and practice on CBM. We must make great efforts to reform and consolidate the naval maintenance modes.

It is clear that as long as the important parameters to monitor meet the requirements, it cannot repair completely at least within 800 h. If the parameters are right after 800 h, we could extend its work time. The third step is to determine the static and dynamic testing parameters and the critical value.

1. Static parameters: (1) to conform to the external inspection, all according to the existing regulations; (2) the static resistance between inspection parameters and the critical value of sprig.
2. Dynamic parameters A (driving): (1) The generator speed $n = 4,500 \sim 7,000$ r/min, voltage $= (28.5 + 1.5)$ V; (2) to adjust resistance of generator voltage regulator hole to limit, the voltage is $26.5 \sim 29.5$ V. (3) Generator speed 9,000 r/min, add and subtract 100 A load, the voltage oscillation time changed not more than 0.5 s; (4) add and subtract the load, the voltage should be pulsed.
3. Dynamic parameter B (simulated): (1) The voltage is lower than 14 V, or higher than 32 V, trouble light should be lighted; (2) input examines the dynamic parameters, inspect the analog signal; (3) input analog signal to check voltage regulator waveform and the standard waveform, the change is less than 5 %.

The fourth step is the design and development of in situ testing instrument and expert system for CBM. It should be automatic and intelligentized, high-speed, large-capacity requirements.

Fifth, make detailed rules for CBM of voltage regulation protector. The main capacity is: (1) according to regulations to do external examination before and after every flight. (2) Inspect data in the control panel each drive. (3) Check

dynamic parameters for every 5 check day (can drive, also can be simulated).
(4) Check resistance parameters every 10 check day. Above all, every data should
be recorded. (5) Input data to computer maintenance expert system every 10 check
day for statistics, to carry on the analysis and calculation, get the machine parts
reliability conclusions, and make decisions. For instance, adjustments in aircraft
and maintenance out of aircraft, if pass muster, will continue to use, until to critical
value; (6) do not remove the maintenance within 800 h in principle, the perfor-
mance good, also can prolong lifetime. This case shows that the parameter of CBM
for airborne equipments has strong practicability, relatively easy to organize and
carry out.

Research on CBM is not only the reformation of the maintenance modes, but
also the reformation of the maintenance system and techniques. It is a system
engineering, involving many problems and aspects, thus it will have a bigger cost
at the early stage, but the military and economic benefits will be very remarkable.
It is estimated that the maintenance personnel can be reduced by about 60 %, the
workload 50 %, aeronautical material, and other cost more than 40 %.

Meanwhile, the CBM has new requirement on the maintenance personnel and
system: Firstly, the maintenance personnel should be proficient in both profession
and maintenance theory. At the same time, they must be very skillful when using all
kinds of advanced equipment and operating the computer to monitor data analysis;
Secondly, we should be equipped with high technological test and experiment
facility. Thirdly, we must build a high-speed, large-capacity maintenance infor-
mation system. Fourthly, the reformation on the maintenance management system
should move forward faster to adjust itself to the new maintenance methods.

In order to adapt to circumstance mentioned above, we should strengthen the
learning on the maintenance theory, especially on the advanced CBM theory and
its experience from home and abroad, and combine the theory with practice to
vigorously promote the research and practice on CBM. We must make great efforts
to reform and consolidate the naval maintenance modes.

References

1. Tsang AHC, Yeung WK, Jardine AKS, et al (2006) Data management for CBM optimization.
   J Qual Maintenance Eng 12(1):37–51
2. Garg A, Deshmukh SG (2006) Maintenance management: literature review and directions.
   J Qual Maintenance Eng 12(3):205–238
3. Jardine AKS, Lin D, Banjevic D (2006) A review on machinery diagnostics and prognostics
   implementing condition-based maintenance. Mech Syst Signal Process Press 20(7):1483–1510
4. Jaw LC (2005) Recent advancements in aircraft engine health management (EHM)
   technologies and recommendations for the next step. In: Proceeding of 50th ASME
   international gas turbine & aeroengine technical congress. [S.l.]. ASME Press, pp 1–13
5. Wei X, Lu C, Wang C et al (2004) Applications of support vector machines to aeroengine fault
   diagnosis. J Aerospace Power 19(6):844–848 (in Chinese)

Chapter 20
Research on Mathematical Model of Mission Effectiveness for Tanker Aircraft

Zhe Li, Yuanda Wang and Qian Zhang

Abstract Using probability method, mathematical model of mission effectiveness for tanker aircraft is established based on operation service condition. It is a feasible model to demonstrate indicators for tanker aircraft reliability, maintainability and supportability (RM&S). Quantitative evaluation for RM&S factors effect on tanker aircraft in combat can be calculated and analyzed. A concrete example is given to show the model is valuable. Tanker aircraft RM&S demonstration process is greatly simplified, and the demonstration effectiveness is vastly advanced.

Keywords Mathematical model · Mission effectiveness · Tanker aircraft

20.1 Introduction

Tanker aircraft is a kind of combat support aircraft specially used for supplying fuel for aircrafts and helicopters in the air. It is usually refitted by transport aircrafts or bombers. Tanker aircraft is an indispensable strategic weapon and changes the traditional operational concept. The effect on aviation is as follows: increase the voyage and operational radius for aircrafts, to enhance long-rang combat capacity for aviation; aggrandize bomb load and cargo load, to enhance combat power; prolong loiter time, to enhance sustained operation capacity; reduce aircrafts' dependence on ground support, to enhance the flexibility capacity and quick response capacity.

Like other aircrafts, to demonstrate the indicator RM&S, experiment on prototype or analog simulation is required. While lots of manpower and material

Z. Li (✉) · Y. Wang · Q. Zhang
Department of Aircraft and Propulsion System, Aviation University of Air Force, Nanhu Road 2222, Changchun 130022, China
e-mail: li_1989_zhe@163.com

resources are indispensable. Moreover, experiment period is rather long. Establishing the mathematical model of mission effectiveness for tanker aircraft, the demonstration process for RM&S is much more simplified; the demonstration cost is compared quite less; the demonstration period is much shorter. Relative indicators' identification can rely on the model.

20.2 Effectiveness, System Effectiveness and Mission Effectiveness

There are several different definitions for effectiveness. Generally, effectiveness is the indicator for the system completing given mission in given time. Based on specific mission, effectiveness includes three concrete coordinate concepts: quota effectiveness, system effectiveness and combat effectiveness. System effectiveness is compared more used to evaluate the weapon and equipment.

There is no common concept for system effectiveness at present. According to GJB451-91 Reliability and Maintainability Term, as in [1], the system effectiveness definition for weapon and equipment is "in certain conditions, the capacity of completing given quantitative characteristic and service requirement." It is a comprehensive measure of system availability, dependability and inherent capacity.

In general, the preferable definition for the system effectiveness is given by the U.S. WSEIAC. System effectiveness is the degree metrics for system completing series of given missions and the function of system availability, dependability and capability. The model is

$$E = A \cdot D \cdot C$$

where E is for system effectiveness; A is for availability vector; D is for dependability matrix; C is for capacity matrix (vector).

In the system effectiveness model above, A and D are the measure for equipment reliability and maintainability and C is the capacity measure for equipment completing mission during combat. If only consider the effect of weapon system RM&S during combat, while neglect the system capacity, WSEIAC model can be simplified. Reduce the matrix C, we can get mission effectiveness for weapon system. It is the indispensable top indicator for analysis and evaluation weapon system RM&S.

Mission effectiveness of weapon system is the probability of system initiating and completing the mission. It is the measure of the availability when the mission begins and the dependability during the mission. According to the American Air Force Instruction Document, mission effectiveness is

$$E = A \cdot D \tag{20.1}$$

Based on (20.1), a mathematical model of mission effectiveness for tanker aircraft is established to provide reference for tanker aircraft indicators' demonstration about RM&S.

20.3 Basic Combat Assumption

When researching on weapon system effectiveness model or mission effectiveness model, generally, the operational background is the average conditions of weapon system completing a single mission. Using this kind of background assumption, application details and the reliably continuous operation capacity in actual combat are neglected. In order to establish a mission effectiveness model for tanker aircraft more exactly and closely to actual combat, here are several basic combat assumptions:

1. A basic tanker aircraft unit (or a flight squadron) refuels the receivers in given aerial refueling area.
2. Every refueling mission for tanker aircraft includes three phrases: phrase of preparation on ground, taking off and arriving at the given aerial refueling area; phrase of refueling in the given area (including rendezvous, docking, fueling and separate phase); phrase of return.
3. During tanker aircraft completing the mission, all kinds of failures may happen to the aircraft and stop refueling. All failures can not be repaired in the air. When critical failures happen to the aircraft that it can not go on completing the mission, tanker aircraft must return immediately and can be back to the base safely.
4. According to troop practice, all tanker aircrafts in the unit should take turns to complete refueling mission.
5. Neglect aircraft scheduled maintenance and weather influence.

20.4 Operational Availability Model

Operational availability is the weapon system probability of enabling to work and implementing mission at any time as in [2]. For combat aircraft under demonstration, in general, the availability evaluation indicator is

$$A_0 = \frac{MTBF + RT}{MTBF + MTTR + MPT + MLDT + RT} \tag{20.2}$$

where, MTBF is for mean time between failures; MTTR is for mean time to repair; MPT is for mean prevention time; MLDT is for mean logistics delay time; RT is for reaction time.

In order to obtain data and calculate conveniently, convert (20.2) to (20.3) as in [3]:

$$A_0 = 1 - \frac{\text{MTTR} + K_p T_{\text{pm}} \text{MTBF} + K_d \text{MLDT}(1 + K_p \text{MTBF})}{\text{MTBF} \cdot K} \qquad (20.3)$$

where K is operational coefficient, namely the rate between system all calendar time and all working time; K_p is prevention maintenance frequency, namely the rate between prevention maintenance time and operational time; K_d is maintenance delay coefficient, namely the rate between delay times and all maintenance times; T_{pm} is mean prevention time coefficient.

If the operational availability A_0 for single tanker aircraft is known, assuming that a basic combat unit contains n tanker aircrafts and there are m tanker aircrafts ready for a single mission, the operational availability A for the basic combat unit is

$$\begin{aligned} A &= 1 - (1 - A_0)^m \\ &= 1 - \left(\frac{\text{MTTR} + K_p T_{\text{pm}} \text{MTBF} + K_d \text{MLDT}(1 + K_p \text{MTBF})}{\text{MTBF} \cdot K}\right)^m \end{aligned} \qquad (20.4)$$

20.5 Operational Dependability Model

Operational dependability is the weapon system probability of enabling to work and completing series of missions at any given time in the mission, as in [4]. Generally, operational dependability can be expressed by

$$D = R_{\text{M}} + (1 - R_{\text{M}}) \cdot M_{\text{m}}$$

where R_{M} is mission reliability, M_{m} is mission maintainability.

Normally, tanker aircraft can not be repaired during the mission. So the common indicator to evaluate the dependability is mission dependability. But for longtime or long-distance combat aircrafts, as in [4], using R_{M} is too simple and inaccurate to evaluate the dependability. Define an indicator "mission flight reliability coefficient r_{m}" to evaluate the operational dependability for tanker aircraft.

According to basic combat assumption, assume that the whole mission flight time is T, taking off and arriving at refueling area time is t_1 and that the time return to base is same to the time arriving at the area. When critical failure happens, tanker aircraft must return immediately. Taking off time is related to the distance to refueling area, aircraft rising ability, refuelling speed and altitude and so on. The parameters can be calculated according to the concrete mission.

Assume the tanker aircraft critical failure probability accords with Poisson distribution and the tanker aircraft mean time between critical failures is MTBCF, the probability of critical failure happening at time t during the mission time is

$$P(t) = 1 - e^{-\frac{t}{\text{MTBCF}}}$$

$$\frac{\text{d}P}{\text{d}t} = \frac{1}{\text{MTBCF}} e^{-\frac{t}{\text{MTBCF}}}$$

Critical failure may happen during the phrase of departing, refueling or returning. When critical failure happens, tanker aircraft must return immediately and the all fight time is mission flight time.

Firstly, critical failure happens during the departing phrase. Tanker aircraft does not fly to the refueling area and returns immediately. The practical mission flight time is $2t$.

Secondly, critical failure happens during the refueling phrase. Tanker aircraft stops refueling and go back immediately. The practical mission time is $t + t_1$.

Thirdly, critical failure happens during the returning phrase. Tanker aircraft can be back to base safely. The practical flight time is still T.

Mission flight reliability coefficient is

$$r_{\text{m}} = \frac{\bar{t}_p}{T} \tag{20.5}$$

where T is the whole mission flight time, $\bar{t}_p$ is the average mission flight time of critical failure happening in the three cases above. Each case above may happen, and the mission flight time t_p for each case is $2t$, $t + t_1$ and T. Given tanker aircraft mean time between critical failures, the mission flight time t_p for each case can be integrated, respectively. Mean mission flight time is the average of mission time for the three cases. So mean mission flight time is

$$\bar{t}_p = \int_0^1 t_p \text{d}P = \int_0^{+\infty} t_p \frac{\text{d}P}{\text{d}t} \text{d}t$$

Notion: when the failure probability is 1, the corresponding time is infinite. So the time integral upper limit should be infinite. Based on the equation above, mean mission flight time $\bar{t}_p$ is

$$\bar{t}_p = \int_0^{t_1} 2t \frac{e^{-\frac{t}{\text{MTBCF}}}}{\text{MTBCF}} \text{d}t + \int_{t_1}^{T-t_1} (t + t_1) \frac{e^{-\frac{t}{\text{MTBCF}}}}{\text{MTBCF}} \text{d}t + \int_{T-t_1}^{\infty} T \frac{e^{-\frac{t}{\text{MTBCF}}}}{\text{MTBCF}} \text{d}t$$

$$= (\text{MTBCF})[2 - e^{-\frac{t_1}{\text{MTBCF}}} - e^{-\frac{T-t_1}{\text{MTBCF}}}]$$

Put it in (20.5), the mission flight reliability coefficient r_{m} is

$$r_{\text{m}} = \frac{(\text{MTBCF})[2 - e^{-\frac{t_1}{\text{MTBCF}}} - e^{-\frac{t_3-t_1}{\text{MTBCF}}}]}{T} \tag{20.6}$$

20.6 Reference System Effectiveness Model

Replace operational dependability D with mission flight reliability coefficient r_{m} (20.5) and put (20.4) into (20.1). So, for continuous combat, the mission effectiveness formula for tanker aircraft unit is

$$E = \left[1 - \left(\frac{\mathrm{MTTR} + K_p T_{\mathrm{pm}}\mathrm{MTBF} + K_d\mathrm{MLDT}(1 + K_p\mathrm{MTBF})}{\mathrm{MTBF} \cdot K}\right)^m\right]$$
$$\left(\frac{(\mathrm{MTBCF})[2 - \mathrm{e}^{-\frac{t_1}{\mathrm{MTBCF}}} - \mathrm{e}^{-\frac{T-t_1}{\mathrm{MTBCF}}}]}{T}\right) \tag{20.7}$$

20.7 Example

Assume RT, MPT and MLDT are zero; the MTBF of the tanker aircraft is 7 h, and the MTTR is 1 h. By Eq. (20.2), we can get

$$A_0 = \frac{\mathrm{MTBF}}{\mathrm{MTBF} + \mathrm{MTTR}} \approx 0.875$$

$$r_{\mathrm{m}} = \frac{\mathrm{MTBCF}\left(2 - \mathrm{e}^{-\frac{t_1}{\mathrm{MTBCF}}} - \mathrm{e}^{-\frac{T-t_1}{\mathrm{MTBCF}}}\right)}{T} \approx 0.814$$

Assume MTBCF is 5 h; refueling time is 0.25 h; the time for arriving the designated aerial is 2 h. Then

$$E = A_0 r_{\mathrm{m}} \approx 0.712$$

In addition, we can estimate the number of tanker aircrafts required in order to reach the certain effectiveness.

Using (20.7), the effectiveness of m tanker aircrafts ready for a single mission can be estimated.

20.8 Conclusions

The mathematical model established for tanker aircraft contains basic parameters of RM&S, and main time parameter in missions. Main tanker aircraft indicators about RM&S can be demonstrated and balanced synthetically by using analytical method. Based on the mission effectiveness model, demonstration process can be greatly

simplified and demonstration cost can be reduced. Experiment on prototype or analog simulation can be avoided. The demonstration requirement for technology and instrument can be vastly reduced. Demonstration period is compared shorter.

References

1. Pei Y, Wang B (2008) Analysis of the fighter airplane system's combat efficiency. Fire Control Command Control 33:126–129
2. Zhu BL (1993) The grid: operational aircraft effectiveness assessment. Aviation Industry Press, Beijing (in Chinese)
3. Song BW, Ru SX, Mao ZY (2012) Analysis of evaluation model for torpedo weapon system. Fire Control Command Control 37:1–7
4. Sun YF, Wang Y (2006) Analysis of evaluation model for torpedo weapon system. Acta Aeronaut Astronaut Sinica 27:893–896

Chapter 21
Prediction of Air Materiel in Small Samples' Fault

Zuogang Zhang and Guowei Cui

Abstract In small samples' fault data information of air materiel, Kolmogorov–Smirnov (K–S) test method, using fault distribution on materiel fitting, finally selected two kinds of distribution, fitting high for prediction. Through the use of matlab inverse cumulative number of commands, for fault prediction, the results accord with the actual situation.

Keywords Small sample · Nonparametric · Failure prediction

21.1 Introduction

In general, aircraft materiels are very reliable, and breakdowns are rare when they are used. Its fault and consumption information is very little, which makes it difficult to predict fault. The data information of aircraft materiels is usually less than 20, which is called small sample. Therefore, the problem of how to solve the small sample of aircraft materiels is worth studying to predict fault effectively.

21.2 Small Sample Prediction Analysis

Since the data information of aircraft-materiel fault is mostly small sample, in addition, some aircraft materiels lack fault information recording, which brings great difficulty to predict fault frequency. Besides, all we know about the information collected is that the overall distribution is continuous or discrete, and we do

Z. Zhang · G. Cui (✉)
Qingdao Branch, Naval Aeronautical and Aeronautical University,
Qingdao 266041, China
e-mail: cuiguowei2013@163.com

not know the detailed format of its distribution, and therefore, we need to use the method that does not depend on the specific format of the overall distribution. This method is called nonparametric. Compared with parametric tests [1], nonparametric tests have the characteristics as follows [2]:

1. Nonparametric tests especially fit for ordinal data.
2. Nonparametric tests generally do not require strict assumptions.
3. Nonparametric tests are applicable to small sample, and the calculation is simple.
4. In nonparametric test method, the biggest shortcoming is not able to take full advantage of all the data information.
5. Nonparametric test method is not used to handle the interaction between factors.

For all these characteristics, we can use it to solve the problem of small sample. After determining the distribution of aircraft materiel faults by nonparametric method, we can predict the faults based on the format of distribution.

21.3 Analysis of Nonparametric Tests

For the problem of the samples number is less than 20, we can use nonparametric test, K–S (Kolmogorov–Smirnov) test, method for goodness of fit test solution [3, 4]. The method is to study whether the distribution of sample observation is consistent with the designed theoretical distribution and to confirm whether there is reason to think the sample observation results from designed theoretical distribution by analyzing the difference between the two distributions. The K–S test step is as follows:

1. The hypothesis: H_0:$F(x) = F_0(x)$, H_1:$F(x) \neq F_0(x)$

   $F(x)$ is empirical distribution function, also a random sample observations cumulative probability distribution function for n times.
   $F_0(x)$ is theoretical distribution function, also a specific cumulative probability distribution function.

2. Calculation of the various D, find statistics $D_{\max}$

   D is the absolute value of empirical distribution $F(x)$ function and theoretical distribution function $F_0(x)$, it can be expressed as a formula.

3. Find Threshold: according to the given significance level α and sample data number n, check the "single-sample K–S test statistic scale," threshold can be obtained.
4. Make a judgment: If $D_{\max} > D_{\alpha}$, in the level α, reject H_0; if $D_{\max} < D_{\alpha}$, cannot refuse H_0.

As used herein, an important formula to the following expression:
Sample mean:

$$\bar{X} = \frac{1}{n} \sum_{i=1}^{n} X_i. \tag{21.1}$$

Sample variance:

$$S^2 = \frac{1}{n-1} \sum_{i=1}^{n} (X_i - \bar{X})^2. \tag{21.2}$$

Sample standard deviation:

$$S = \sqrt{S^2}. \tag{21.3}$$

21.4 Nonparametric Test Solution and the Predicted Number of Failures

In order to predict of the air materiel's number of failures, first need to know the laws of the failure, so need to fit out the laws and then to predict. Now, let the air materiel's number of failures be: 1, 4, 2, 1, 3, 1, 5, 1, 4, 1, 3.

21.4.1 Using the K–S Test to Determine Distribution Form

To calculate the convenience of data processing by means of SPSS19 and MATLAB2010, two softwares for data analysis and calculations were used in this article. The common types of air-materiel fault distribution are: normal distribution, Poisson distribution, uniform distribution, exponential distribution, lognormal distribution, and Weibull distribution. SPSS19 software provides a normal distribution, Poisson distribution, uniform distribution, and exponential distribution test methods, in addition to the lognormal distribution of test data that can be logarithmic; the SPSS19 reuses the test for normal distribution; Weibull distribution can be fitted with MATLAB2010 software to analyze. SPSS19 was used to obtain the distribution of the four test results as shown in Tables 21.1, 21.2, 21.3, 21.4.

From the test results, the mean number of aviation materiel failure is 2.36, and the standard deviation is 1.502. Uniform distribution progressive testing significantly is 0.021, less than 0.05, so the number of failure does not confirm uniform distribution. From the significant point of view, progressively acceptable forms are normal distribution, Poisson distribution, and exponential distribution.

Next, respectively, lognormal distribution and Weibull fit testing, the test process of lognormal is: data X: 1, 4, 2, 1, 3, 1, 5, 1, 4, 1, 3, set $Y = \ln X$, to verify

Table 21.1 Test results of uniform distribution

One-sample Kolmogorov–Smirnov test		
		y
N		11
Uniform parameter[a,b]	Minimum	1
	Maximum	5
Most extreme differences	Absolute	0.455
	Positive	0.455
	Negative	−0.091
Kolmogorov–Smirnov Z		1.508
Asymp.sig.(2-tailed)		0.021

[a] Test distribution is Uniform
[b] Calculated according to the data

Table 21.2 Test results of normal distribution

One-sample Kolmogorov–Smirnov test		
		y
N		11
Normal parameter[a,b]	Mean	2.36
	Std. Deviation	1.502
Most extreme differences	Absolute	0.273
	Positive	0.273
	Negative	−0.182
Kolmogorov–Smirnov Z		0.904
Asymp.sig.(2-tailed)		0.387

[a] Test distribution is Normal
[b] Calculated according to the data

Table 21.3 Test results of exponential distribution

One-sample Kolmogorov–Smirnov test		
		y
N		11
Exponential parameter[a,b]	Mean	2.36
Most extreme differences	Absolute	0.345
	Positive	0.121
	Negative	−0.345
Kolmogorov–Smirnov Z		1.144
Asymp.sig.(2-tailed)		0.146

[a] Test distribution is Exponential
[b] Calculated according to the data

whether the data X lognormal distribution problems can be equivalently transformed to Y following a normal distribution. Logarithmic data were: 0, 1.3863, 0.693, 0, 1.0986, 0, 1.6094, 0, 1.3863, 0, 1.0986. Test results are shown in Table 21.5.

Table 21.4 Test results of Poisson distribution

One-sample Kolmogorov–Smirnov test		
		y
N		11
Poisson parameter[a,b]	Mean	2.36
Most extreme differences	Absolute	0.138
	Positive	0.138
	Negative	−0.094
Kolmogorov–Smirnov Z		0.458
Asymp.sig.(2-tailed)		0.985

[a] Test distribution is Poisson
[b] Calculated according to the data

Table 21.5 The test result after data conversion

One-sample Kolmogorov–Smirnov test		
		y
N		11
Normal parameter[a,b]	Mean	0.661118
	Std. deviation	0.6723247
Most extreme differences	Absolute	0.292
	Positive	0.292
	Negative	−0.197
Kolmogorov–Smirnov Z		0.968
Asymp.sig.(2-tailed)		0.306

[a] Test distribution is Normal
[b] Calculated according to the data

Significant progressive is much larger than 0.05, to accept the normal distribution, that data can be accepted lognormal distribution, progressive significance for the 0.306. The inspection process of Weibull distribution uses MATLAB2010 software to verify Weibull distribution, the test results are as follows.

[H, p, ksstat, cv] = kstest(x, [x, weibcdf(x, 2.36, 1.502)], 0.05) H = 1, reject the null hypothesis is Weibull distribution.

In summary, comparing several distributed computing results, materiel failure can be accepted in the form of normal distribution, lognormal distribution, exponential distribution, and Poisson distribution, wherein Poisson distribution is the highest progressive significant to 0.985, followed by 0.387.

21.4.2 Air-Materiel Failure Prediction

After determining the distribution of air-materiel faults' form, it can, according to their distribution form, reverse to seek their confidence level in a certain number of
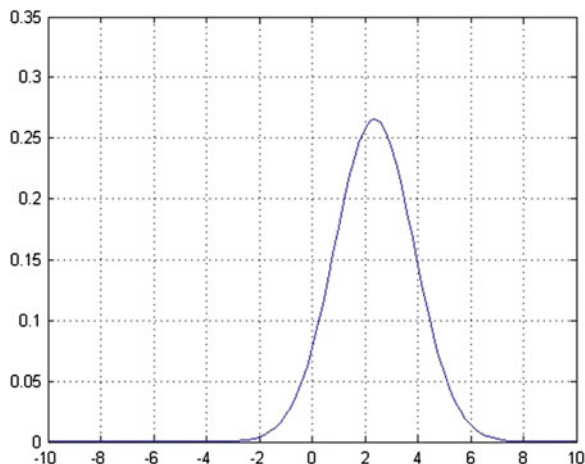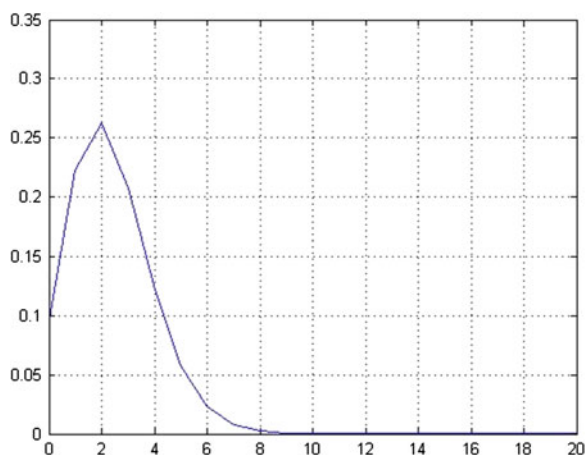
failures, the study selected in the $\alpha = 0.05$ level, the highest progressive signifi-
cance air materiel with two distributions to predict failure times. Air-materiel
failure distribution in the normal and Poisson is shown in expressions of the form
(21.1), (21.2), the graphic shown in Figs. 21.1 and 21.2.

Air-materiel failure prediction problem can be equivalently transformed: Let
the expected number of aircraft materiels' failure is a and the actual number of
faults is b, (when $b > a$, time must not exceed 5 % probability of occurrence of
known actual failure occurrence obey a certain distribution); with the mean value
of 2.36 and the standard deviation of 1.5022, find $p \{b < a\} = 0.95$, the value of
a.

$$f(x) = \frac{1}{\sqrt{2\pi}1.502} e^{-\frac{1}{2}\left(\frac{x-2.36}{1.502}\right)^2}. \tag{21.4}$$

$$p(x) = \frac{2.36^x}{x!} e^{-2.36}. \qquad (21.5)$$

Using matlab inverse cumulative distribution function, run the commands and results are as follows

Norminv(0.95, 2.36, 1.502) 4.8306
Normal distribution of the calculated result is 4.8306
Poissinv(0.95, 2.36) 5
Poisson distribution of the calculated result is 5.

The results from the calculation when $b > a$ is the probability of not more than 5 %, normal distribution of the results obtained under the situation is slightly less than the results obtained under Poisson distribution. In practice, usually has a fractional part of results rounded up, so that the two distributions result would be the same. Predicted results of 5, actually mean to 2.36, the result is greater than the mean prediction, than the mean in the case of materiels to meet shipping, usually during failure prediction, and then, the actual value is compared to the consumption of which is greater than most values, the number of failures to meet the forecast well.

21.5 Conclusion

Through analyzing of small sample failure data information about air materiel, using K–S test methods, effective solution was formed to the failure in a distributed fashion, by fitting a different form of distribution, with high levels of selected significant forms of distribution, and to determine air-materiel failure distribution form. In the air-materiel fault prediction, the predicted number of faults into equivalence problem solved the problem; after transforming the problem, it became simple, clear, and easy to solve.

References

1. Wu X, Li YL, Hu QJ (2010) Mathematical statistics. National Defense University Press, Beijing, pp 102–121
2. Xie LH, Shang T (2012) SPSS statistical analysis and data mining. Electronics Industry Publishing House, Beijing, pp 148–149
3. Zhao JC, Zhu HY, Wang WX (2010) Aviation equipment and technical support logistics analysis. National Defense Industry Press, Beijing, pp 34–35
4. Dong ZJ (2008) Fault-based distribution strategy study IBA inventory of spare parts. Thesis, Dalian Maritime University

Chapter 22
An Approach for Determining Activity Implementation Time in Multitask Flow Network Plan

Xiaowei Guo, Baogang Li, Xiaoyan Qu and Dengwu Ma

Abstract Determining the specific construction time forms the important content of construction in multitask flow network plan. A general calculating approach of time parameters is proposed in the process of dealing with such problems by flow network planning, and their features are collected preparedly. Main critical impact parameters are picked up, and procedure waiting float and global critical activity are defined as well. Determination approaches of activity construction time with various project duration desires are proposed when work intensity is considered, and application of flow network planning is extended. Finally, an example is given to analyze and demonstrate that the approach is available.

Keywords Multitask · Flow network planning · Global critical activity · Planned project duration (PPD) · Work intensity

22.1 Introduction

As the modern method of scientific management, network planning technique is applied more and more widely while the engineering technique becomes more complicated, with which practical application results have been achieved in many

X. Guo (✉) · B. Li · X. Qu · D. Ma
Naval Aeronautical and Astronautical University, Yantai 264001, China
e-mail: hailangxianshen@163.com

B. Li
e-mail: lbgbcg@163.com

X. Qu
e-mail: quxiaoyan_sxq@sina.com

D. Ma
e-mail: mdw0020201@163.com

aspects such as construction engineering, product development, military support, and so on. Application areas of it constantly expands, especially when which syncretizes such disciplines as graph theory, topology, operations research, systems engineering, and computer science [1, 2]. Flow network planning is proposed by science and technology workers of our country as an extension of network planning, which combines the advantages of flow construction basic principle and network planning to use network chart of flow construction project correctly [3–5].

Project plan is subdivided into multiple stages in a flow network plan without strict logical relations of activities, as long as time distance relation is satisfied. Determination of activity implementation time is made according to the earliest start time, when only time factor is considered. However, engineering tasks tend to be more to arrive [6, 7] in the actual operation, whose activities have strict logical relations and request for the continue construction. Such network planning of multitask process comply with the definition of flow network planning, under the same process, activity durations of different tasks have obvious differences, and so it is different from the general flow network planning. Other factors should be considered except project duration during execution process of high strength task. Therefore, in this paper, a general calculating method of time parameters of flow network planning for multitask process, and considering the work intensity, we get the determination methods of activity implementation time under the different planned project durations to ensure the practical application.

22.2 Analysis of the Multitasking Process

22.2.1 The General Flow Network Planning

Flow network planning combines flowing theory and network planning, whose main characteristic is that the whole project plan is broken down into multiple construction stages to complete the continuous compact engineering task.

Relations of time distance during activities of flow network planning are shown in Fig. 22.1, and an activity is not required to start after complete of its preceding activities, but only needs an interval of start time distance.

Flow relations are formed as if the equation of time distance is satisfied, which is defined as:

$$K_{i,i+1} + t_{i+1} = J_{i,i+1} + t_i. \tag{22.1}$$

where $K_{i,i+1}$ represents start time distance ($K_{i,i+1} > 0$), $J_{i,i+1}$ represents finish time distance ($J_{i,i+1} > 0$), and t_i represents duration of activity $i(t_i > 0, i \geq 0)$.

Fig. 22.1 Relations of start time distance and finish time distance during activities
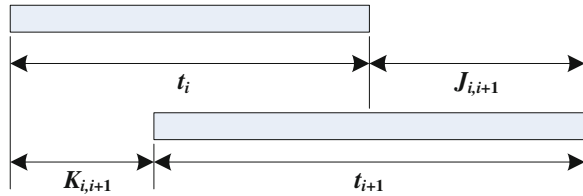
22.2.2 Features of the Multitasking Process

1. The whole plan consists of multiple same task processes, and each task process has the same network chart of logical order. Those task processes are carried out in order according to the constraint conditions until the whole plan ends with the complete of the last task process.
2. Each activity is implemented by its respective personnel and resources, and different tasks are shown as different durations of the activity, which do not need the adjustment of logical relation of activities.
3. The calculation of network time parameters in each task process is not only impacted by the preceding (following) activities, but also restrained by the time parameters of the same activity of the preceding task process. An activity could start only after the complete of its preceding activities, and that is to say that time distance equation of general flow network planning is added a condition $K_{i,i+1} \geq t_i$, which is depicted in Fig. 22.2.
4. Activities of a logical relation make up of a task process, which is the object to study. This is different from flow construction of one activity in the general flow network planning.
5. Most of activities could not construct continuously because of increase in constraint conditions, and float time exists as mentioned in the network planning. So detailed calculation of time parameters in the flow network planning is very necessary and offers some data to optimize construction control measures.
6. Task risk is needed to consider and effect of activity is analyzed, and critical activities are got to reduce task risk.

Multitask process is considered as a whole task, and activities of each process are refined into construction segments of flow network planning. Under the condition of reliable work, general flow network planning is improved to be suitable for the task analysis and process control with the above characteristics.

22.3 Calculation of Time Parameters

There is no actual application value if only calculation of time distance parameters is carried out, so we take the time parameters of network planning as the research object. Activity-on-arrow network is taken in this paper. Suppose that the plan is
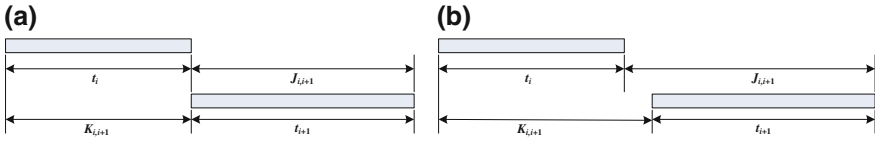
Fig. 22.2 Time distance relations of activities in multitask process. **a** $K_{i,i+1} = t_i$, **b** $K_{i,i+1} > t_i$

made up of Q task processes, and there are n nodes in the network chart. Time parameters of activity $i - j$ in the qth task process are denoted, respectively, as: activity duration D_{i-j}^q, earliest start time ES_{i-j}^q, earliest finish time EF_{i-j}^q, PPD T_p^q, latest finish time LF_{i-j}^q, latest start time LS_{i-j}^q, and total float TF_{i-j}^q. General calculating equations of time parameters in the flow network planning need revised, because the constraint conditions have changed. On the basis of these parameters, start implementation time CS_{i-j}^q and finish implementation time CF_{i-j}^q of activity $i - j$ are determined according to different targets.

22.3.1 The Basic Time Parameters

In the deterministic network, durations of one activity in each task process may vary, which are connected with task objects. And in the indeterministic network, the mean and the variance of activity duration could be determined with three estimate approaches; at this basis activity duration is generated randomly.

22.3.1.1 Earliest Start(Finish) Time of Activities

Earliest start time of activity in the single process is that the activity is likely to start at the earliest time when all preceding activities have finished. However, in the multitask process, one activity is carried out by the same personal and resource, so its earliest start time must be late after the finish time of the same activity in the preceding process. Calculation steps are as follows:

1. Starting activities

$$\mathrm{ES}_{1-j}^q = \begin{cases} 0, & q = 1 \\ \mathrm{EF}_{1-j}^{q-1}, & q > 1 \end{cases}.$$ (22.2)

2. Other activities

$$\mathrm{ES}_{i-j}^q = \begin{cases} \max\{\mathrm{ES}_{h-i}^q + D_{h-i}^q\}, & q = 1 \\ \max\{\max\{\mathrm{ES}_{h-i}^q + D_{h-i}^q\}\mathrm{EF}_{i-j}^{q-1}\}, & q > 1 \end{cases}.$$ (22.3)

where ES^q_{h-i} represents the earliest start time of each preceding activity $h - i$ of the activity $i - j$, D^q_{h-i} represents the duration of preceding activity $h - i$, and EF^{q-1}_{i-j} represents the earliest finish time of the activity $i - j$ in the preceding process.

Calculation starts at the starting node of network, and the calculation of each task process is carried out in turn along the direction of the arrow.

The calculation method of earliest finish time in multitask process is the same as in the single process with the equation below.

$$EF^q_{i-j} = ES^q_{i-j} + D^q_{i-j}. \tag{22.4}$$

22.3.1.2 Project Time of Flow Network Plan

Project time is the finish time of the last activity in the last process, and we represent calculating duration of the whole project with T_c, calculating duration of the qth task process with T^q_c, so $T_c = T^Q_c$ obviously. There is no practical significance if required project duration of each process, which can be get with the equation:

$$T^q_c = \max\{EF^q_{i-n}\}. \tag{22.5}$$

where EF^q_{i-n} represents the earliest finish time of activity $i - n$ taking the final node as the finish node in the qth task process.

If the required duration of the whole project is specified, the PPD $T_p \leq T_r$; if not, $T_p = T_c$. So PPD of each process is the finish time that does not delay the next process to finish, and they are calculated as follows:

$$T^q_p = \begin{cases} \min\{T_p, T_c\}, & q = Q \\ \min\{T^{q+1}_p - \max\{D^{q+1}_{i-n}\}, T^q_c\}, & q < Q \end{cases}. \tag{22.6}$$

22.3.1.3 Latest Finish (Start) Time of Activities

Latest finish time of activity is defined as the finish time of the activity that does not delay the required duration of the whole project, but in the multitask network planning, this parameter is calculated considering other processes inevitably. Calculation order is just opposite the earliest start time, which starts with the last node of network in turn reversing the direct of the arrow, and calculation steps are as follows:

1. Activities with the final node

$$LF^q_{i-n} = T^q_p. \tag{22.7}$$

2. Other activities

$$\mathrm{LF}^q_{i-j} = \begin{cases} \min\left\{\mathrm{LF}^q_{j-k} - D^q_{j-k}\right\}, & q = Q \\ \min\left\{\min\left\{\mathrm{LF}^q_{j-k} - D^q_{j-k}\right\}, \mathrm{LS}^{q+1}_{i-j}\right\}, & q < Q \end{cases}. \tag{22.8}$$

where LF^q_{j-k} represents the latest finish time of each following activity $j - k$ of the activity $i - j$ in the process, D^q_{j-k} represents the duration of the following activity $j - k$, LS^{q+1}_{i-j} represents the latest start time of the activity $i - j$ in the next process.

The calculation method of latest start time in multitask process is the same as in the single process with the equation below.

$$\mathrm{LS}^q_{i-j} = \mathrm{LF}^q_{i-j} - D^q_{i-j}. \tag{22.9}$$

22.3.1.4 Floats of Activities

1. Total float

Total float of the activity represents the spare time, which can be used, and we also take the equation of the single process as follows:

$$\mathrm{TF}^q_{i-j} = \mathrm{LS}^q_{i-j} - \mathrm{ES}^q_{i-j}. \tag{22.10}$$

To be sure that total float of activity in the multitask affects not only all preceding (following) activities in this process, but also available time of activities in other process.

2. Waiting float

There is an obvious time parameter in the multitask process, and it is the difference of the same activity between neighboring processes. We call it waiting float defining the difference time of start time in the process and finish time in the preceding process, and waiting float of activity in the first process is regulated 0. They are calculated as follows:

$$\mathrm{WF}^q_{i-j} = \begin{cases} 0, & q = 1 \\ \mathrm{CS}^q_{i-j} - \mathrm{CF}^{q-1}_{i-j}, & q > 1 \end{cases}. \tag{22.11}$$

3. Others

Free float, dependent float, and independent float represent transferring and utilizing relations of activity floats, but they do not have the original meaning. So, we need not discuss temporarily.

22.3.2 Determination of the Critical Path

In the single process network, the activities whose total float is 0 are critical activity when the PPD is equal to the calculating duration, and the activities with the minimum total float are the critical activity when the PPD is not equal to the calculating duration. All the activities make up the path with the longest duration, i.e., the critical path. Critical path represents the critical path of each process in the multitask process network. However, the total float of critical activity is not necessarily 0 because of time constraint of processes, even if the PPD is equal to the calculating duration. According to the principle that duration of the path made up of critical activities is the longest one, we define the method to determine the critical activities of each process: find the activities with the minimum total float from the last node in turn reversing the direct of the arrow.

Calculating equation of critical activities taking the final node as the finish node is as follows:

$$(c' - n)^q = \arg \min_{(i-j) \in U(i-n)} \left\{ \mathrm{TF}_{i-j}^q \right\}. \tag{22.12}$$

where $U(i - n)$ represents the activity set taking the final node as the finish node.

Other activities:

$$(c'' - j)^q = \arg \min_{(i-j) \in U(j-c')} \left\{ \mathrm{TF}_{i-j}^q \right\}. \tag{22.13}$$

where $U(j - c')$ represents preceding activity set of critical activity calculated in the previous step.

Critical activities calculated in turn make up the critical path of each process, obviously total float of critical activities only in the first process is 0, and critical path is not necessarily the same in each process even if activity durations remain unchanged.

22.3.3 Global Critical Activity

Activities whose waiting float is 0 in Sect. 22.3.1.4 represents that the activity in the previous process constraints directly the same activity in this process. Waiting floats of the activity in each process are not at all 0, so we define that the activity whose sum of waiting float in every process is less than a small value ε is the global critical activity, which can be calculated as follows:

$$\mathrm{GCA}_{i-j} = \arg_{i-j} \left\{ \sum_{q=1}^{Q} \mathrm{WF}_{i-j}^q < \varepsilon \right\}. \tag{22.14}$$

Waiting floats of activities beginning with the start node are all 0, because they are constrained only by the same activity in the previous process, and obviously they are global critical activities. Global critical activities directly reflect the restrict relationship between processes, and one activity has played a role in the preceding activity for the activity in the next process.

22.4 Calculation of Activity Implementation Time

Determination of activity implementation time in each process is the ultimate objective and detailed planning of the network planning. What the earliest and latest start time of activity in each process provides is the scope of implementation time in the previous section, not the final implementation plan. Activity implementation time is constrained by not only network planning relationship, but also by the work intensity of activity construction team. Determination of activity implementation time is discussed in three different cases, according to the size relationship between the PPD and calculating duration.

We define work intensity of activity $i - j$ construction team as the ratio of sum of the activity durations in all processes to period between the beginning and the end of activity construction, which is

$$\mathrm{LW}_{i-j} = \sum_{q=1}^{Q} D_{i-j}^{q} / \left(\mathrm{CF}_{i-j}^{Q} - \mathrm{CS}_{i-j}^{1} \right). \tag{22.15}$$

22.4.1 No PPD

If there is no PPD in the multitask process, i.e., the PPD is equal to the calculating duration, activities of each process are in turn to carry out, and activity durations remain unadjusted. From the parameters calculated in Sect. 22.3.1, we can see that activity waiting float calculated by the latest start(finish) time is significantly longer than by the earliest start(finish) time, and it is to say that work intensity calculated by the former is smaller for actual execution.

So, in this case, we take the latest start(finish) time as the implementation time, i.e., $\mathrm{CS}_{i-j}^{q} = \mathrm{LS}_{i-j}^{q}$ and $\mathrm{CF}_{i-j}^{q} = \mathrm{LF}_{i-j}^{q}$.

22.4.2 The PPD is Shorter

When the PPD is shorter than the calculating duration of network planning, project schedule optimization is needed to achieve purpose, so resources and cast means are taken to compress the duration of the critical activities to shorten the
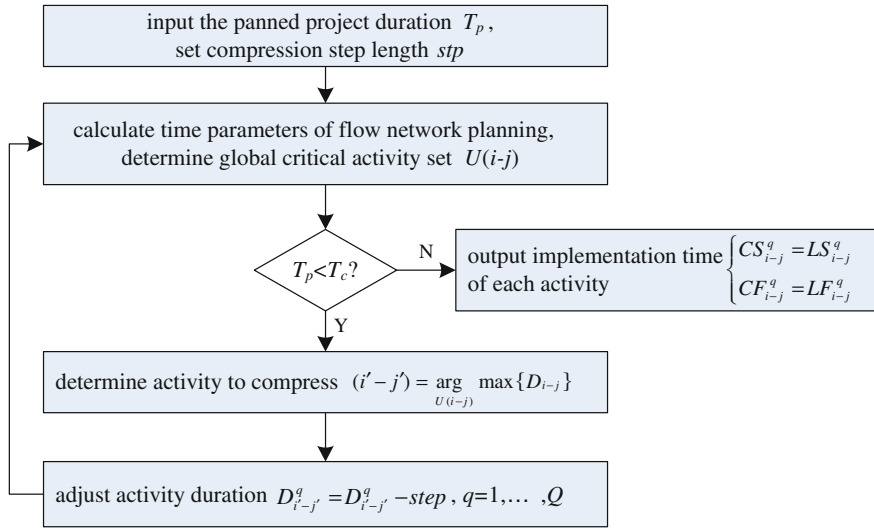
Fig. 22.3 Iterative process of project duration compression

calculating duration. Calculating duration of multitask flow network planning is mainly affected by global critical activities, so project schedule optimization is carried out by compressing duration of global critical activities, selecting the global critical activities to compress, and determining amount of compressing becomes the research focus.

Compression amount of an activity in different processes is supposed to be the same, and duration of activity $(k - l)$ is compressed gradually to reach the goal setting with the iterative algorithm. Every time the amount of compression is expressed as the step length stp, and activity duration is adjusted to $D_{k-l}^q = D_{k-l}^q - step(q = 1, \ldots, Q)$.

The selecting principles of activities compressed to: (1) get all global critical activities by the latest start(finish) time in Sect. 22.3.1.4; (2) set the global critical activity with the longest duration compression target, and judge the activity by the sum of its durations if they are different in all processes.

Termination conditions of iterative algorithm: PPD T_p is not less than the calculating duration T_c of flow network planning at this time, or the next iterative compression is operated. Iterative operation process of project duration compression is shown in Fig. 22.3.

22.4.3 The PPD is Longer

In some cases, multiple tasks are required to finish successively in flow network planning, or the whole project is not allowed to complete in a certain time period

to prevent the accumulation of tasks, the situation that PPD is longer than the calculating duration appears. In this case, we can consider to lengthen duration of some activities, or to lengthen the waiting float of the activity to reduce the work intensity. The former could be carried out with the method in contrast to Sect. 22.4.2, and we discuss the calculation method of the later.

Work intensity of the global critical activity is highest by its definition in Sect. 22.3.3, and they are the targets to compress the waiting float. Elongation amount of global critical activity in each process is supposed to be the same, and it is also controlled by the step length *stp* every time. Iterative operation is performed until the project duration meets the requirement, and obviously relevant time parameters of other activities will change therewith.

For ease of calculation, elongation amount of the waiting float is merged into the activity duration to form the new activity duration $\tilde{D}_{i-j}^{q}$ used to calculate. Work intensity calculated by the latest start(finish) time is taken as the judgment standard, activity $(k-l)$ is selected to execute $\tilde{D}_{k-l}^{q} = \tilde{D}_{k-l}^{q} + stp(q = 1,\ldots,Q)$ gradually.

If work intensity of global critical activities is equal, activity with longer duration is selected to lengthen. And at this time, work intensity of activity construction team is represented as

$$\text{LW}_{i-j} = \sum_{q=1}^{Q} D_{i-j}^{q} / \left(\text{CF}_{i-j}^{Q} - \text{CS}_{i-j}^{1} \right) = \sum_{q=1}^{Q} D_{i-j}^{q} / \left(\widetilde{\text{LF}}_{i-j}^{Q} - \widetilde{\text{LS}}_{i-j}^{1} \right). \quad (22.16)$$

Termination condition of iterative algorithm is that, the difference T_d between PPD T_p and the calculating duration T_c of flow network planning at that time is less than value $Q \cdot stp$, i.e., elongation allowance of the calculating duration is not enough to complete an iteration. Specific operation is shown in Fig. 22.4.

22.5 An Example

To show the specific implementation time of activities of multitask process in flow network planning in different cases, we take activity-on-arrow network plan graph in [8] as the relationship of single task network planning (see Fig. 22.5). Number of tasks is set to $Q = 6$, the step length of iterative algorithm is set to $stp = 1$. Activity durations are shown in Table 22.1, and all time parameters have the same unit.

Activities implementation time is shown in Fig. 22.6 when there is no PPD, where the progress bars with light and deep color represent, respectively, implementation of activities according to the latest and earliest start time. The numerals in the middle of the figure represent serial number of tasks (the same below). Obviously, waiting float of most activities is longer according to the former, i.e., work intensity is smaller.
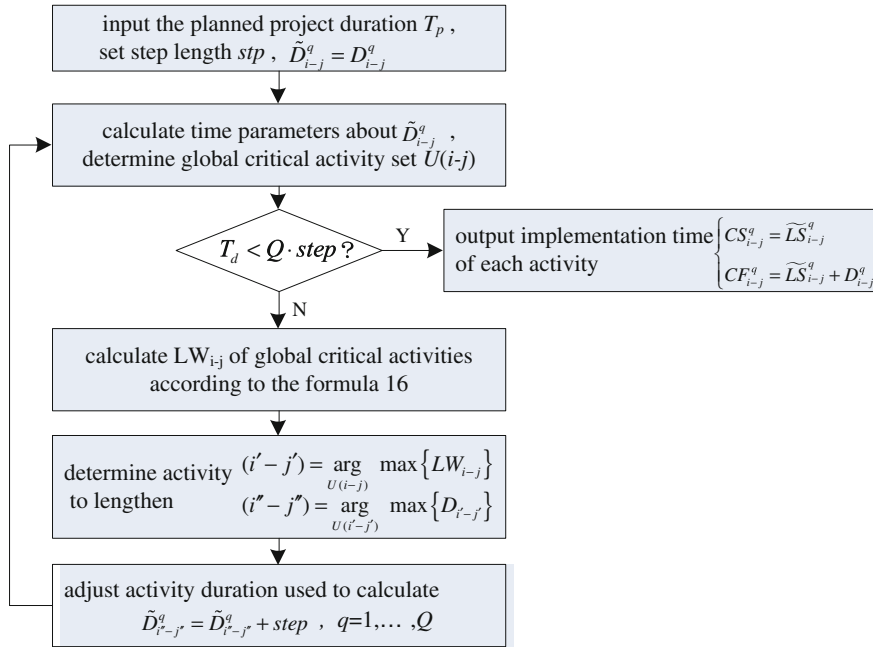
Fig. 22.4 Iterative process of lengthening waiting float

Fig. 22.5 Network plan graph of single task
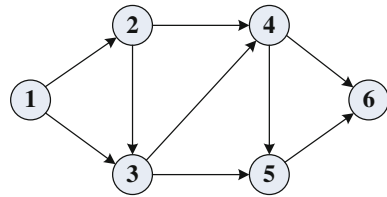
Activities implementation time is shown in Fig. 22.7 represented by bars with deep color, when the planned project is set to $T_p = 50$, which is shorter than the calculating duration. For comparison, the progress bars with light color represent implementation of activities according to the latest start time before the adjustment of activities durations.

Activities implementation time is shown in Fig. 22.8 represented by bars with deep color, when the planned project is set to $T_p = 90$, which is longer than the calculating duration. Work intensity of activities become smaller significantly after adjustment, and it is proportionate.

Specific data of activities are shown in Table 22.1 in three different cases.

Table 22.1 Related parameter summary of activities (ACTs) in different cases

No.	ACT	D	No PPD $T_p = T_c$		PPD is shorter $T_p = 50$			PPD is longer $T_p = 90$	
			Waiting float	Work intensity	D after adjustment	Waiting float	Work intensity	Waiting float	Work intensity
1	1–2	2	6–6–6–6–6	0.2857	2	4–4–3–3–3	0.4138	10–10–10–10–10	0.1935
2	1–3	5	3–3–3–3–3	0.6667	5	1–1–0–0–0	0.9375	7–7–7–7–7	0.4615
3	2–3	4	4–4–4–4–4	0.5455	4	2–2–1–1–1	0.7742	8–8–8–8–8	0.3750
4	2–4	7	0–0–0–0–0	1.0000	5	1–1–0–0–0	0.9375	3–3–3–3–3	0.7000
5	3–4	8	0–0–0–0–0	1.0000	5	1–1–0–0–0	0.9375	4–4–4–4–4	0.6667
6	3–5	5	0–0–0–0–0	1.0000	5	0–0–0–0–0	1.0000	2–2–2–2–2	0.7143
7	4–5	4	1–1–1–1–1	0.8276	4	1–1–1–1–1	0.8276	3–3–3–3–3	0.6154
8	4–6	7	0–0–0–0–0	1.0000	6	0–0–0–0–0	1.0000	3–3–3–3–3	0.7000
9	5–6	5	0–0–0–0–0	1.0000	5	0–0–0–0–0	1.0000	2–2–2–2–2	0.7143
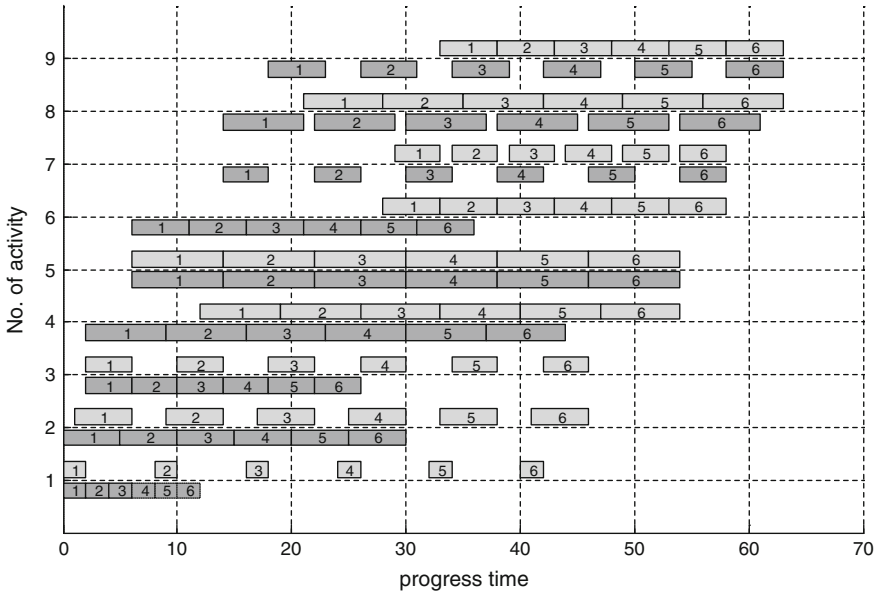
Fig. 22.6 Implementation Gantt chart of activities when there is no PPD
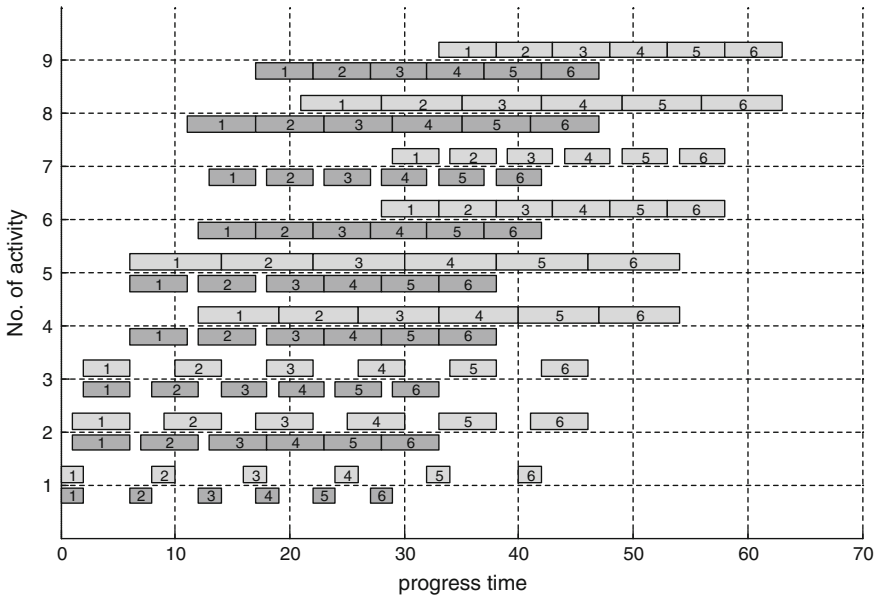
Fig. 22.7 Implementation Gantt chart of activities when the PPD is shorter
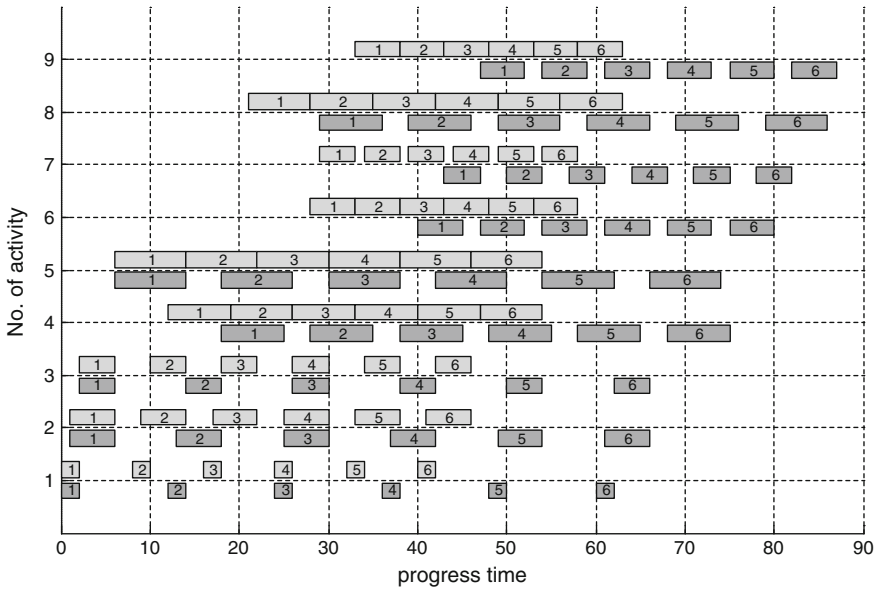
Fig. 22.8 Implementation Gantt chart of activities when the PPD is longer

22.6 Conclusion

Application of the general flow network planning is improved and revised in this paper, and approach of analyzing and calculating time parameters of flow network planning in multitask process is presented. Calculating methods of specific implementation time are given according to the relationship between the PPD and calculating duration based on the work intensity, and the superiority of methods can be reflected with strong practical application if there are more activities. Each process has the same task object, but the later work could focus on parameter analyzing of different task objects with uncertain activity durations on this basis. In addition, the influence factors such as resources and costs are considered according to the practical application besides the work intensity, and determination of activity implementation time are optimized comprehensively.

References

1. Wang Z, Ding J, Liu Y et al (2012) Analysis of critical path and most critical activity in PERT networks based on Monte Carlo method. Syst Eng Electron 34(8):1646–1651 (in Chinese)
2. Cho JG, Yum BJ (2004) Functional estimation of activity criticality indices and sensitivity analysis of expected project completion time. J Oper Res Soc 55(8):850–859

3. Yang B (2002) Unifying calculating models for the network planning. Syst Eng Theor Pract 3:51–55 (in Chinese)
4. Li W, Meng W (2009) Engineering network planning technique. Science Press, pp 95–113(in Chinese)
5. Song X, He Y (2002) Comparative study between flow process plan and network plan. J Huazhong Univ Sci Tech (Urban Science Edition) 19(2):75–78(in Chinese)
6. Ma D, Guo X, Deng L (2012) Ammunition scheduling of carrier-based aircraft based on modified ant colony algorithm. J Syst Simul 24(6):1207–1211 (in Chinese)
7. Wu W, Qu J, Hu X (2010) Optimization analysis of technical preparation procedure for missile based on PERT simulation. Ordnance Ind Autom 29(8):1–3 (in Chinese)
8. Liu Y, Wang Z, Zhang Y (2007) Time-resources tradeoffs of PERT construction schedule under resource constraint. Adv Sci Technol Water Res 27(1):27–30 (in Chinese)

Chapter 23
One Research on Fault Diagnosis Method of Aircraft Inertial Navigation System

Ji-en Yang, Ming-qiu Zhou and Fei Meng

Abstract This paper analyses the fault diagnosis of hardware and software of some aircraft inertial navigation system, designs relevant diagnosis project of hardware and software fault, especially studies and deduces diagnosis formula and method when one of four level gates of inertial navigation main and standby platform system appears slow excursion. The experiment proves the following: This method can achieve fast fault orientation, its process of analysis and deduction is in accordance with reality of some aircraft inertial navigation manufactures, and it has very important reference value to inertial navigation fault diagnosis.

Keywords Inertial navigation system · Fault diagnosis · Hardware fault · Software fault

23.1 Introduction

Fault diagnosis is the key to ensure system work normally. Only effective fault diagnosis and troubleshooting can ensure the normal operation and improve the reliability of the system [1]. Inertia navigation system is an autonomous reckoning navigation system [2]. As long as the initial conditions of navigation are given, according to the angular rate measured by system gyro and the specific force measured by accelerometer, the system can determine parameters of the carrier such as the orientation, position and speed according to the Newton's Law of Inertia.

J. Yang · M. Zhou · F. Meng (✉)
The First Aeronautic Institute of Air Force, Xinyang, Henan, China
e-mail: mengfei1979@yeak.net

23.2 System Configuration

The main and standby inertial navigation platform subassemblies of the fault diagnosis system are made up of the tetracyclic triaxial inertial navigation platform, the platform servo circuit, temperature and power input circuits, calibration circuit and monitoring circuit, etc. The tetracyclic triaxial inertial platform consists of two flexible gyro and three accelerometers. The main and standby subassemblies sent three acceleration information (three components of the platform coordinate system) and three angle information (roll angle, pitch angle and gyro azimuth) to the detection and diagnosis part simultaneously. At the same time, the main platform subassembly also sends acceleration information to the controlled crosslinking subassembly. The crosslinking subassembly then quantifies the information from the detection and diagnosis part and outputs the digital information of γ, θ and φg. The crosslinking subassembly also quantifies the information from the main subassembly and outputs the digital speed information of Vx, Vy, Vz [3]. With other heading information, the crosslinking subassembly can also complete the processing and calculations of the true heading and output digital and analog true heading information φ.

The primary scheme relation of main and standby inertial navigation system is shown in Fig. 23.1

23.3 Monitoring of Main and Standby Inertial Navigation Platform Subassemblies' Hardware Fault

The main and standby inertial navigation platform subassemblies are composed of the same internal hardware; thus, fault monitoring process is identical. Each circuit has a special fault sensor, namely the threshold measuring device [4]. When a fault signal is detected, in addition to turn some certain normal signal lights off, the sensors will send fault signal to the fault signal recorder which is a relay controlled circuit. In addition to rapidly disconnecting the faulted circuit to protect the subassembly from damage, it can record the corresponding circuit fault permanently even if the power is off. The basic principle is as follows: an exiting winding in the electromagnetic system receives the fault signal and forms a magnetic pull to change the fault display window from white to black. Only when the other exciting coil is energized, will the window change back to white. It will maintain black even if the system power is on and thus protects the whole system. The fault control relation of internal inertial navigation platform subassembly is shown in Fig. 23.2.

Thermostat circuit: Measures system overheat and disconnects the 115 V, 400 Hz heating power.

Power circuit: Outputs fault signal when anyone of the secondary power supply (+5 V, +15 V, −15 V, +27 V) is missing.
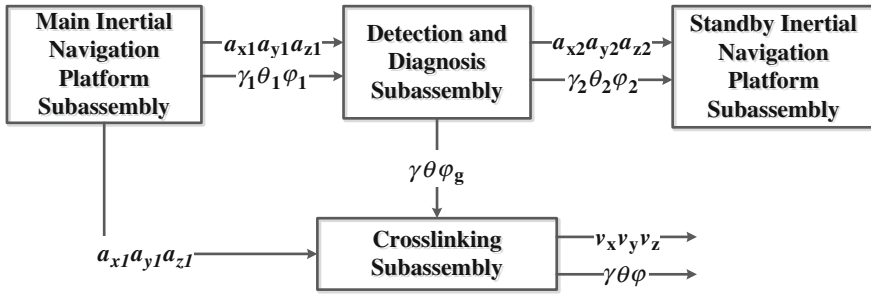
Fig. 23.1 Primary scheme relation of main and standby inertial navigation system
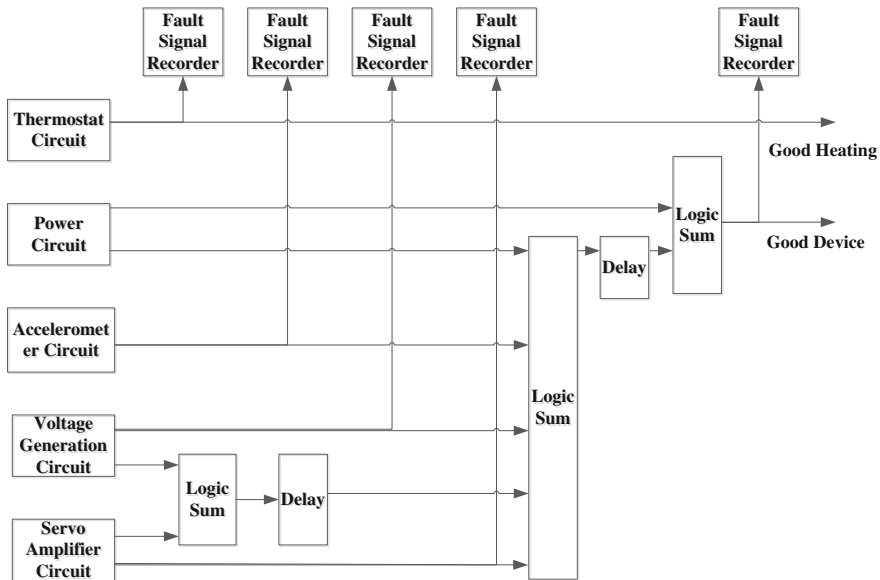
Fig. 23.2 Fault control relation of internal inertial navigation platform subassembly

Accelerometer circuit: Measures the outputs of 2 horizontal amplifiers, 3 voltage frequency converters and 3 torque amplifiers.

Voltage generation circuit: Outputs fault signal when the motor power lacks phase or acts abnormally.

Servo amplifier circuit: Detects the existence of pulse-modulated signal in 4 amplification circuit.

Tests on a series of hardware circuits within the controlled crosslinking assembly will also be done, as well as the formation of 3 monitoring signals of "controlled crosslinking subassembly well", "heading well" and "horizontal channel digital integral well".

23.4 Monitoring of Inertial Navigation System's "Message Good"

The "device good" signal of hardware monitoring can not guarantee that the inertial navigation system outputs correct parameters and performs well enough. A series of other monitoring information required is as follows: Fast analog leveling is completed within 20 s, after which the corresponding main and standby monitoring lamps light up. Fast alignment is completed within 3 min, after which the corresponding main and standby monitoring lamps light up. Normal preparation is completed within 7 min, after which the corresponding main and standby monitoring lamps light up. "Message good" is formed on the basis of "device good", through detecting 6 output angle of the rotary transformer and the output of 3 integrator. The forming process is shown in Fig. 23.3.

Obviously, the requirement of "message good" is higher than "device good". Not only the hardware circuit should work properly, the exported angle parameters and the acceleration parameters should also be limited in a certain range.

23.5 Monitoring of Inertial Navigation Platform's Software Fault

In order to monitor slow shift of the gyro platform, diagnostic monitor is specifically set up in the system. It can accurately locate the software fault of poor performance among four channels of the main and standby platforms. The basic principle is creating an orientation deflection angle between main and standby platforms by torqueing the directional gyro of the standby platform on the ground. Thus, the measurements of the same input acceleration on 4 axes have a certain relative relationship. If one of the axis deviates from the horizontal plane, it will detects the component of gravitational acceleration, and the acceleration measured on 4 axes will change.

As shown in Fig. 23.4, the standby platform makes a counterclockwise rotation of 45° relative to the main platform (at first they share the same axial direction). Given the same acceleration a, the relationship of horizontal acceleration components between main platform (a_{x1}, a_{y1}) and standby platform after the rotation (a_{x2}, a_{y2}) is as follow:

Given (a_{x2}, a_{y2}) and find out (a_{x1}, a_{y1}):

$$\begin{bmatrix} a_{x1} \\ a_{y1} \end{bmatrix} = \begin{bmatrix} \cos 45° & -\sin 45° \\ \sin 45° & \cos 45° \end{bmatrix} \begin{bmatrix} a_{x2} \\ a_{y2} \end{bmatrix} \tag{23.1}$$
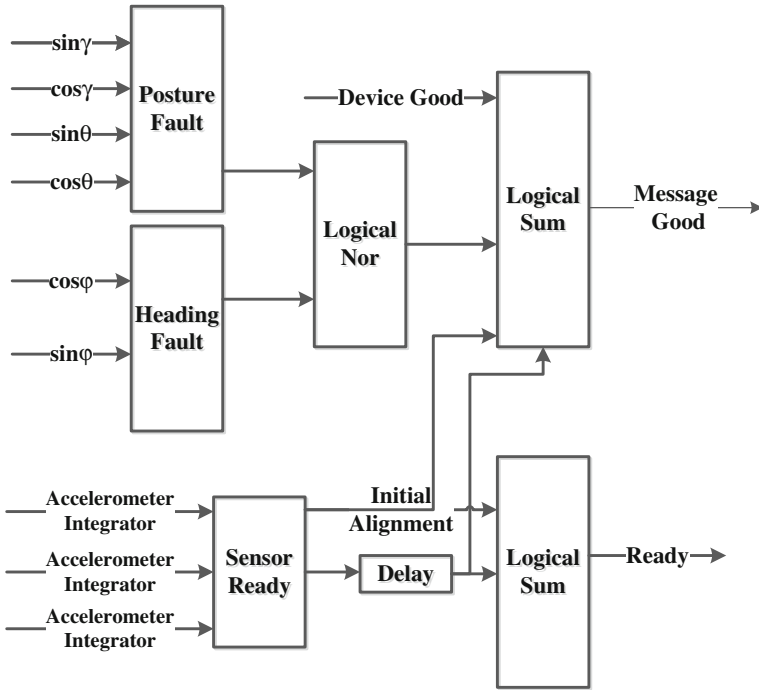
Fig. 23.3 Forming process of "message good"

Fig. 23.4 Orientation deflection angles of main and standby platforms
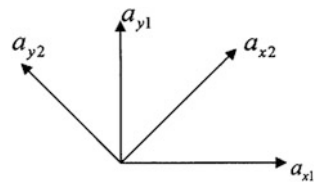
So

$$\begin{cases} a_{x1} = \frac{\sqrt{2}}{2}a_{x2} - \frac{\sqrt{2}}{2}a_{y2} \\ a_{y1} = \frac{\sqrt{2}}{2}a_{x2} + \frac{\sqrt{2}}{2}a_{y2} \end{cases} \tag{23.2}$$

Approximated by:

$$\begin{cases} a_{x1} - 0.7a_{x2} + 0.7a_{y2} = 0 \\ a_{y1} - 0.7a_{x2} - 0.7a_{y2} = 0 \end{cases} \tag{23.3}$$
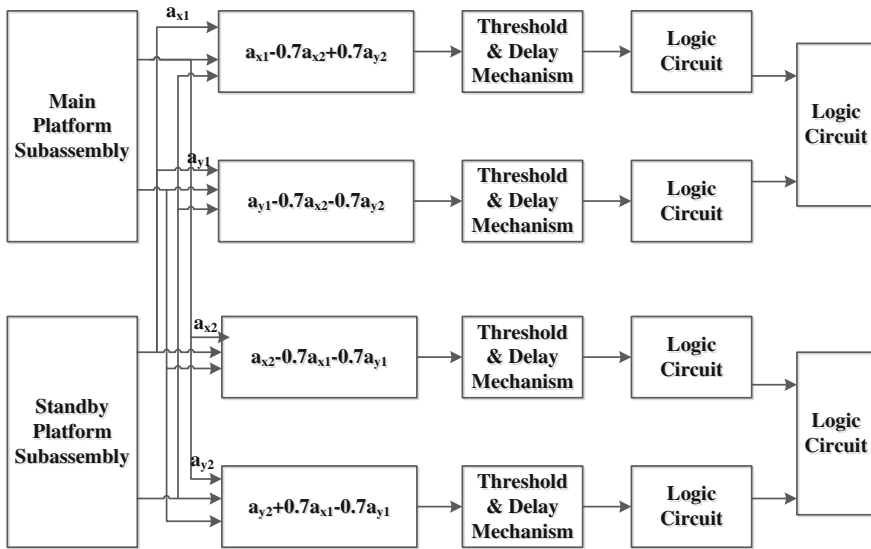
Fig. 23.5 Block diagram of diagnosis and check

Given (a_{x1}, a_{y1}) and find out (a_{x2}, a_{y2}):

$$\begin{bmatrix} a_{x2} \\ a_{y2} \end{bmatrix} = \begin{bmatrix} \cos 45° & \sin 45° \\ -\sin 45° & \cos 45° \end{bmatrix} \begin{bmatrix} a_{x2} \\ a_{y2} \end{bmatrix} \tag{23.4}$$

So

$$\begin{cases} a_{x2} = \frac{\sqrt{2}}{2} a_{x1} - \frac{\sqrt{2}}{2} a_{y1} \\ a_{y2} = -\frac{\sqrt{2}}{2} a_{x1} + \frac{\sqrt{2}}{2} a_{y1} \end{cases} \tag{23.5}$$

Approximated by:

$$\begin{cases} a_{x2} - 0.7 a_{x1} - 0.7 a_{y1} = 0 \\ a_{y2} + 0.7 a_{x1} - 0.7 a_{y1} = 0 \end{cases} \tag{23.6}$$

Obviously, the equations above hold up under normal circumstances. If one platform axis deviates from the horizontal plane due to gyro drift, it will no longer hold up. Only Eq. (23.3), which has nothing to do with $ax1$, still holds up. This can be used to determine which horizontal channel is faulty. The block diagram of diagnosis and check is shown in Fig. 23.5.

If only one of the four equations holds up while the value of the other 3 equations exceed a certain threshold (240 ± 50 mv), a control signal will be sent to cut off the "message good" signal of the main and standby platforms after a 1 s delay, which is used to make sure the result is reliable.

In order to rotate the standby platform in orientation, a switch is set to control related relay circuit, send special sine and cosine transformer signals to the standby platform, create platform position control signal and make the standby platform rotate 45° counterclockwise.

23.6 Summary

A series of analysis and experiment prove that the method above is correct and feasible. Fault diagnosis and troubleshooting procedures prove that the criteria for software and hardware fault diagnosis are very practical, which improves system reliability effectively and has considerable application value.

References

1. Zhang L-X (2004) One research on fault check and diagnosis of navigation system and related theoretical issues, Northwestern Polytechnical University, Xian
2. Zhang Z-L (2002) Inertial navigation and integrated navigation, Aviation Industry Press, Beijing
3. Zhou D-H, Ye Y-Z (2006) Modern fault diagnosis and fault-tolerant control, Tsinghua University Press, Beijing
4. Wang D-P, Zhang Y-Z (2009) Theory and methods of intelligent fault diagnosis system, Metallurgical Industry Press, Beijing

Chapter 24
The Discussion of Crucial Technology on Remote Detection of Composite Material Damage in Aerial Honeycomb Cellular Structure

Hongyan Sun, Haibing Zhang and Xiaoli Li

Abstract The paper describes the remote detection system of composite material damage in aerial honeycomb cellular structure combining fault diagnosis technology with modern communication and computer network technology and studies the crucial technologies of data and image transmission, image processing, injury characteristics extraction, etc. The remote detection system puts forward the design plan of sense organ, which offers technical support for construction of remote detection system.

Keywords Honeycomb cellular structure · Composite material · Remote detection · Injury characteristics

24.1 Introduction

Honeycomb composite material mainly consists of skin, honeycomb core, and adhesive composition; its high specific strength, high specific stiffness, and thermal insulation performance are outstanding; and light-weight properties have achieved a lot in aerospace applications. Due to the coexistence of progressiveness and quality discrete nature and high cost of composite materials, in practical application, even if it is reasonable to process through research and experimental development, structures' defect also could be produced in the process of manufacturing, causing quality problems, lead to write-off of the whole structure if question is serious. At present, the cellular structure nondestructive testing of

H. Sun
Aerotrechnics Ensure Branch of Navy Equipment Department, Beijing 100071, China

H. Zhang (✉) · X. Li
Qingdao Branch of Navy Aviation Engineering Institute, Qingdao, 266041 Shandong, China
e-mail: ndt_zhb@126.com

composite materials in the field of aviation repair work has been carried out [1]. Due to the damage form is complexity and defect feature is not obvious, these serious problems plaguing the gleam of nondestructive testing personnel. Remote detection system is defined by means of information method, realize remote detection mode by network [2], the system stores in the precondition of not changing the field work mode, the picture and testing information are transferred to the backstage expert diagnosis through the Internet and other means of information, especially for emergency, more remote detection system support, is the future direction of development.

24.2 The Key Technology of Remote Damage Detection

24.2.1 Achievement of Damage Information

At present, the application of new technologies in the cellular structure more nondestructive testing of composite materials, the majority of equipment with the data and image storage, processing and transmission function [3]. According to the study on damage detection of composite material the author for many years, the force of air honeycomb structure of composite materials, application of ultrasonic testing, laser speckle detection, and digital X-ray detection method can detect all kinds of damage [4]. The damage image honeycomb composite typical is shown in Figs. 24.1, 24.2, and 24.3.

24.2.2 Data and Image Transmission

Damage image information of honeycomb composites is acquired by testing equipment, which is transmitted to the receiver through the wireless communication, and the video information is transmitted to the working computer by image acquisition card, then processing the real-time display image information in computer.

PC video capture system usually adopts PCI 32-bit bus interface, which realizes communication and data transmission with PC machine by plug-in card, but the mouth of PCI image acquisition card can only be used for a desktop computer or computer and cannot be used in notebook computer [5]. The use of USB image acquisition card is convenient for many.

MV-U2000 external image acquisition card is portable USB color/monochrome image acquisition card, this card can connect through USB3.0 bus and the host, with portable or desktop computer, the formation of various types of mobile image processing workstation, especially suitable for outdoor, activities, and work environment narrow occasions.

Fig. 24.1 Laser detection image of honeycomb structure debonding
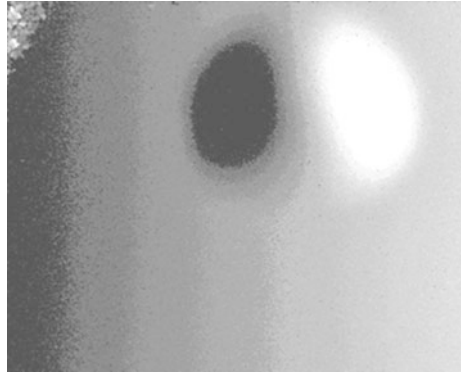
Fig. 24.2 Radiographic detection image of core crushing
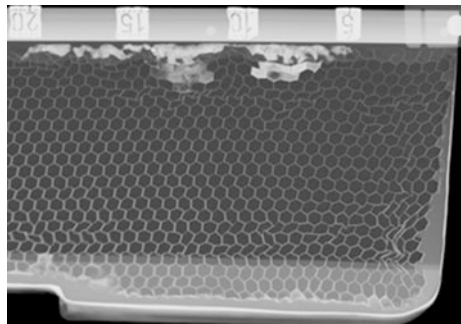
Fig. 24.3 Inlet radiographic detection image of cellular structure
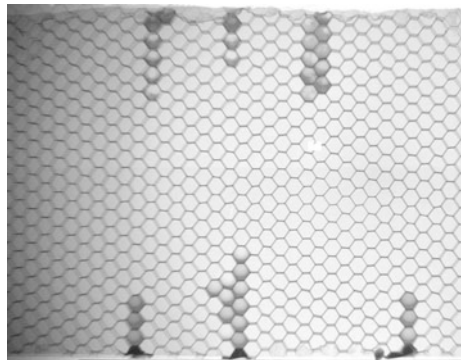
The workflow diagram of MV-U2000 external image acquisition card: collecting analog image data from the camera, processing by the video encoding chip, converted into digital image, to the programmable logic device FPGA; the FPGA receives the digital image data, sends RAM cache, and then removes the data from RAM, to the USB 3 control chip, and the chip using USB 3 interface data eventually passed to the computer real-time display and storage. The overall structure and the information processing procedure are shown in Figs. 24.4, 24.5, and in 24.6.

Fig. 24.4 The workflow
diagram of image acquisition
card

Beiginning

Parameter settings

The image acquisition into memory

Image processing

Beiginning
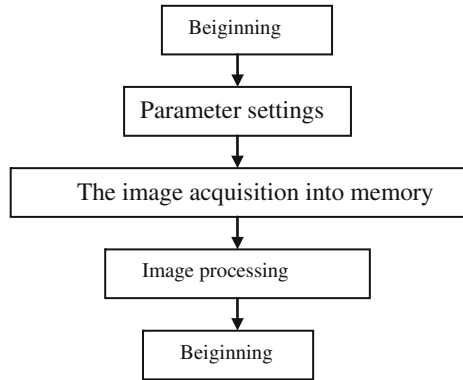
Fig. 24.5 Information
processing platform
architecture based on PC

Camera

Wireless video transmitter

Wireless video receiver

Image acquisition card

Image processing
Feature extraction
Determination and classification
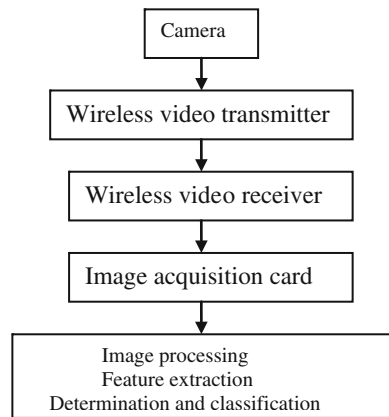
24.2.3 Image Processing

We need to process the image before image feature extraction. The common image
processing methods include image smoothing, threshold transform, morphological
filtering, etc. For the composite image detection, in addition to ultrasonic detection
by waveform to judge damage, detection of laser speckle image detection and ray
are required to handle, convenient for later damage evaluation.

Image Smoothing. Because of electromagnetic interference and other causes,
when carry out image acquisition CCD will produce noise in the image, image
display effect, in order to reduce and suppress image noise of image smoothing [6].
Image smoothing methods include mean filter, Gauss filter, median filter, etc.

The median filter method is a nonlinear smoothing technique, and its gray value
of each pixel is set for all pixel gray values in the window. Is actually a containing
an odd number of pixels in the sliding window, with window median each point
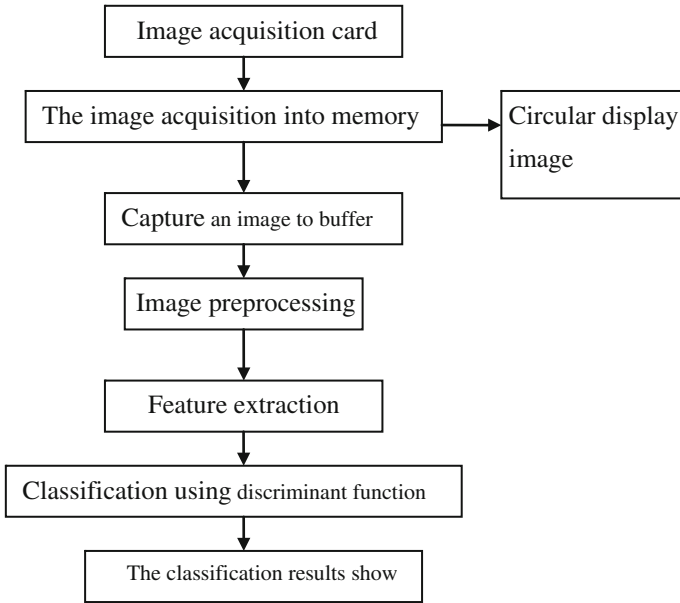
Fig. 24.6 The workflow diagram of image processing on PC

instead of the gray-level window is the midpoint value. A mathematical formula can be expressed as:

$$X_i = Med\{f_{i-v} \ldots f_i \ldots f_{i+v}\}, i \in Z, v = \frac{m-1}{2} \tag{24.1}$$

Threshold Transform. Threshold transformation can be a gray image is converted to black-and-white two-value image. The user specifies a boundary effect to gray value, if the intensity of a pixel in the image is less than the gray value, then the pixel gray value is set to 0, otherwise, it is set to 255. The function expression threshold transform as follows:

$$f(x) = \begin{cases} 0 & x < T \\ 255 & x \geq T \end{cases} \tag{24.2}$$

Threshold transform method transforms a gray image into two-value image that divides the image directly into two parts: we care about and do not care, resulting in complex background to extract the target of interest.

Morphological Processing. Corrosion and expansion are the two basic morphological operations. Corrosion is the role of the image thinning, so it can be used for image filtering, proper structure element's size and shape and can filter out noise points all not contain structural elements. Effect and corrosion expansion instead, expansion can make the object boundary expansion. The expansion is used to image was apart of the same object bridging, after the image of two value,

it makes a Unicom object that breaks into two parts easily, then you can use the expansion gap bridging. Opening operation refers to the treatment process to the corrosion expansion. Means it can filter out noise information independent, have obvious features of images.

24.2.4 Damage Features Extraction

The difference between one object and other objects is their characteristics. According to their own features of the images, partitioning method can be divided to two categories: texture description and shape description. For the damage of composite materials, texture feature is the most common used.

Texture feature is calculated by smoothing filtering gray image method. Gray-level co-occurrence matrix is a typical representation of object texture information. Assuming the image's gray level is L, the image's gray-level co-occurrence matrix P_δ is L × L matrix.

where $P_\delta(i,j)$ denotes the spatial relationship of $\delta = (D_x, D_y)$ and gray level are, respectively, i and j on the number of pixels. Pixel of space position relation consists of 0°, 45°, 90°, 135° four directions, corresponding $\delta = (\pm 1, 0)$, $\delta = (1, -1)$ or $\delta = (-1, 1)$, $\delta = (0, \pm 1)$, $\delta = (-1, -1)$, or $\delta = (1, 1)$

Characteristic quantity that stands for texture can be extracted from gray-level co-occurrence matrix:

1. Angle of two-order moment (ASM)

$$g_2 = -\sum_{i=1}^{n}\sum_{j=1}^{n} p(i,j)^2 \tag{24.3}$$

ASM is the gray-level co-occurrence square and matrix element values, which reflect the image gray distribution uniformity and texture coarseness. When the co-occurrence matrix elements are concentrated in the main diagonal, the gray distribution of image is relatively uniform, the macrotexture rough comparison, the ASN value. Whereas ASM is small, image texture distribution uneven or the texture is fine.

2. The main diagonal moment of inertia (CON)

$$g_2 = -\sum_{i=1}^{n}\sum_{j=1}^{n} (i-j)^2 p(i,j) \tag{24.4}$$

CON reflects the definition of image and texture groove depth degree. Texture grooves deeper, the moment of inertia is greater, the visual effect more clear; and moment of inertia is small, shallow grooves, fuzzy.

3. The entropy (ENT)

$$g_2 = -\sum_{i=1}^{n}\sum_{j=1}^{n} p(i,j)\log[p(i,j)] \tag{24.5}$$

ENT said the non-uniformity of image texture or complexity. If the texture is not obvious or no texture, the ENT is smaller; conversely, the ENT is large.

I need that when the image gray-level co-occurrence matrix is large, the amount of data will be very great, is not conducive to the subsequent parameter calculation. This can reduce the gray series, the gray level is reduced to 32 or 64. The calculated gray-level co-occurrence matrix is the need for gray-level co-occurrence matrix normalized after gray matrix parameters.

24.3 Sensor System

24.3.1 Function Design of Sensor System

The sensor system is the most basic unit of the structure damage wireless detection system. To acquire the damage information, it must rely on the laying of various sensor system in the cellular structure parts, timely and accurate collection of displacement, acceleration, vibration frequency, amplitude, temperature, humidity, and timely transmission of information to calculate the related equipment. The sensor system should also have the function of calculation, in order to complete the digital to analog conversion, the encapsulated data frames, and other functions [7]. As the design of sensor detection system in the practical, it should have corresponding data transmission function. At the same time, the sensor system also should have the ability in some cases, to accept some from the local processor command, for example, somewhere there is sign of damage occurs, the local processor will continue to send information to a number of sensor unit of the specific position in order to get more data. Of course, the best sensor system and energy self-sufficiency function, in order to reduce dependence on external energy detection, enhance its usability.

24.3.2 Design of Sensor System

Sensor Materials. At present, the sensor materials often used mainly the piezoelectric material, shape memory alloy material, and optical fiber materials. Among them, because the optical fiber has fine, flexible, small volume, light weight, high sensitivity, immunity to electromagnetic interference, low energy consumption, low cost, easy to realize distributed and quasi-distributed detection, information transmission and sensing in one, broadband and high data rate and high-temperature

resistance, corrosion resistance, and other excellent properties; therefore, in aviation composite, remote damage detection using optical fiber sensor is ideal. At present, in the optical fiber sensor and fiber Bragg grating (FBG) sensor is one of the most important. The grating uses photosensitive fiber materials, including external incident photon which interacted with the core and cause permanent changes in the refractive index, directly go into the space phase grating and form the fiber's UV laser of single-mode. Compared with the traditional electric sensor, fiber grating sensor has very obvious advantages in sensor network applications. The production of UV in the photosensitive fiber core grating has the following these characteristics: low loss optical fiber connection, good spectrum characteristic, high reliability, strong ability of anti electromagnetic interference, small size (standard bare fiber is 125 μm), suitable for a variety of applications, particularly suitable for embedded material called intelligent materials or the structure of light weight, good temperature resistance (upper limit working temperature can reach 400–600 °C), multiplexing capability, long transmission distance (sensor to control end up to several kilometers), corrosion resistance, high sensitivity, passive devices, etc. But as the sensing element, it is one of the most prominent advantages, namely the sensing information in a wavelength encoding, wavelength of the absolute parameters will not be affected by the light source power fluctuation and influence or coupling loss connection. The special thing is also very easy in one fiber continuously making multiple gratings, the grating array of light and soft, combined with time division multiplexing and wavelength division multiplexing technology, suitable for distributed sensing elements embedded in the internal structure of materials, or sticking on the surface of it, their temperature, pressure, strain to realize multi-point detection, sensitivity, and range of measurement and high.

The Sensor System Structure. With the rapid development of electronic technology and communication technology, it has been able to realize the data acquisition, data transmission, energy supply in a sensor, and all functions.

Traditional monitoring system based on wired network has obvious shortcomings: (1) Complex wiring, the enormous costs; (2) a disaster occurs, the cable itself more likely impaired, effective operation will affect the whole monitoring system. With the rapid development of key technologies of sensor, microprocessor, wireless communication, and reduce the cost, the sensor instead of traditional wireless network technology based on the sensor cable technology based on possible. The distributed sensor system a large number of such small size, light weight, low energy consumption, low price of wireless networks in various parts of the plane composed of distributed sensor system, we can build a strong function, high efficiency, low cost.

1. The calculation module is the core of the sensor unit. It is mainly responsible for data collection force sensing converter from the accelerometer, empty the sensor unit memory, and processes the original data. Calculation module can choose various programmable gate array calculation module (FPGA) or digital signal processing (DSP) chip. The final choice will depend on the comprehensive consideration on energy utilization and performance.

2. The communication module to the wireless monitoring system should meet the communication requirements of high reliability and low power consumption. In order to meet the requirements of different kinds of sensors, wireless communication module is designed into a unified form and compatible for any type of sensors, different sensors system and wireless communication module make up sensor system through their specific interface.

3. The sensor type of wireless monitoring system mainly includes stress gauge, accelerometer, accelerometer, and displacement meter. Corresponding to the damage detection method is different, need to choose different types of sensors. In the detection method based on modal analysis, structure dynamic parameter identification using the acceleration, displacement, and other information, so as long as the general mechanical sensor can. But all the detection methods which are based on strain modal analysis use the strain sensor. As a result of the difference between various sensors and the collected data in the format, such as the sampling frequency, we need to design a special sensor interface module. In other words, a variety of sensors are available through a sensor interface module integration into the sensor system.

24.4 Conclusion

With the rapid development of aviation industry, safety and reliability of honeycomb composite material is pay more attention, the key technologies involved in honeycomb composite remote detection is proposed in this paper, the fault diagnosis and modern communication and computer network technology, solve the problem of detecting cellular structure field. Based on the cellular remote structural damage detection system as the research object, the remote detection of data transmission, image processing, feature extraction, and damage key technology studies and puts forward the design scheme, which provides technical support for remote detection system.

References

1. Zhengxian M, Xiong J (1999) Application of OTDR in optical fiber measurement. J Laser 20:1–7 (in Chinese)
2. Wang J (2004) Using light sensors in structural health monitoring of civil Engineering structures. J Guizhou Univ Technol (Nat Sci Ed) 33:35–37 (in Chinese)
3. Straser E, Kiremidjian A (1998) A modular wireless damage monitoring system for structures. Technical report, Stanford University, Stanford
4. Xie X (1999) Computer networks. Electronic Industry Press, Beijing, pp 82–85 (in Chinese)
5. Wang W, Duan B, Liu H (1999) Remote detection and fault diagnosis of machinery equipment based on web. J Manuf Autom 21:103–105 (in Chinese)

6. Hongsheng L, Lingsong H, Tielin S, Shuzi Y (2000) Remote fault diagnosis system architecture based on internet. J Huazhong Univ Technol 28:45–47 (in Chinese)
7. Wu G, Jie H, Hu J, Yinglong G (2001) Research and practice of remote diagnosis system of equipment failure. J Wuhan Univ 34:68–70 (in Chinese)

Chapter 25
A New Method to Determine Equipment Testing Period Based on Mission Reliability

Kuan Hu, Lin Zhang, Zhaoxia Wang and Pengya Fang

Abstract To avoid the problem caused by classical strategy of fixed testing period, in which equipment failure may happen before testing, a new method to determine testing period was put forward. In this method, mission reliability of interval between arbitrarily neighboring twice testing was regarded as constant or transformed into specified area; according to this principle, an optimal model to calculate equipment testing period was established; in this model, optimal variables included parameters of testing times, mission reliability time offset, and testing interval. A more reasonable and scientific equipment testing period can be received by solving the model. Finally, an example was given to demonstrate how to apply the method, and the results show that mission reliability of interval gradually descends by using fixed testing period, and rational testing period should be variational.

Keywords Mission reliability · Testing period · Optimization

25.1 Introduction

Equipment reliability gradually descends and failure probability ascends during storage and use; accordingly, it is necessary to designedly check equipment and repair failure components discovered by testing. Apparently, if interval between

K. Hu (⊠) · P. Fang
Xi'an Hi-tech Institute, Xi'an, China
e-mail: huk1976@sina.com

L. Zhang
Xi'an Aerospace Composites Research Institute, Xi'an, China

Z. Wang
Northern Nondestructive Test Center of China, National Erzhong Group Co, Beijing, China

testing were overlong, failure components should not be found in good time by testing, which affect equipment readiness or cause severe accident. By contraries, maintenance resources waste and needless equipment damage may happen by reason of overshort interval.

So, how to determine equipment optimal testing period is very important, and it has been discussed in references [1–11]. However, no matter what method has been adopted, it always gives a fixed testing period, which is simple and easy to operate. In fact, for many equipments that have been tested and repaired, their performance closes with the state when failure happened just now and it is very difficult to make its performance revert to initial status. Because of gradually descending reliability of equipment during storage and use, if fixed testing period adopted, equipment failure probability will increase continuously in each neighboring testing interval with testing times. In this way, failure may be happen before next testing. Accordingly, the strategy of using fixed testing period has potential limitation to find failure in good time.

To solve the problem, the rule that mission reliability is regarded as constant in each neighboring testing interval can be used to determine equipment testing period. Mission reliability is the ability that equipment achieves specified functions during specified mission time and under specified maintenance conditions; here, mission time is equal to testing period. Because mission reliability is constant in each neighboring testing interval, testing period during storage and use will vary, foremost it eliminates the likelihood that failure happens before testing. Based on the idea, a new method to determine testing period will be put forward in this paper.

25.2 Mission Reliability

Mission reliability means the ability that equipment achieves prescribed functions in mission section. Mission reliability evolved from operation reliability, it can be measured by the probability of equipment following a burn-in period T or after a warranty period T, noted by $R(T + \Delta T)$. According to condition probability formula, following expression can be obtained.

$$R_M(T + \Delta T) = P[t > T + \Delta T | t > T] = R(T + \Delta T | T) = \frac{R(T + \Delta T)}{R(T)}$$

(25.1)

where $R(T)$, $R(T + \Delta T)$ is, respectively, reliability of T and $(T + \Delta T)$.

25.3 Optimal Model to Determine Testing Period Based on Mission Reliability

For most equipments with aging characteristic, when life distribution cannot be confirmed by the reason of inadequate statistical data, from approximation of view, bi-parameter Weibull distribution is always adopted [12], and then, the life reliability is formulated as follow.

$$R(t) = \exp\left\{ -\left(\frac{t}{\eta}\right)^m \right\} \tag{25.2}$$

where m, η is, respectively, shape and dimension parameter of bi-parameter Weibull distribution.

Furthermore, assuming that equipment reliability does not improve after testing and repairing, it approximates reliability when failure happened just now.

If fixed testing strategy is adopted, and testing period is one year, through formula (25.1) and (25.2), it can be easily seen that equipment task reliability is as follows by i-th testing and repairing.

$$R'_i = \frac{R(i)}{R(i-1)} = \exp\left\{ \left(\frac{i-1}{\eta}\right)^m - \left(\frac{i}{\eta}\right)^m \right\} \quad i = 1, 2, 3\ldots$$

Obviously, equipment mission reliability decreases gradually with checking times by annually fixed testing, that is, equipment failure probability will increase gradually with checking times, and the result is possible that equipment will be failure before some testing.

To avoid the problem, mission reliability in each neighboring testing interval will be regarded as constant, namely.

$$R\left(\left(\sum_{j=1}^i T'_j + T'_{i+1}\right) \middle| \sum_{j=1}^i T'_j\right) = \frac{R(\sum_{j=1}^i T'_j + T'_{i+1})}{R(\sum_{j=1}^i T'_j)} = R(T'_1) = \text{const.} \tag{25.3}$$

where T'_i is ith testing interval, and it satisfies the following requirement.

$$\sum T'_i < T^{\text{opt.}} \tag{25.4}$$

where $T^{\text{opt.}}$ is preventive maintenance period of equipment.

However, if given mission reliability is very high, there will be overshort testing period calculated by formula (25.3), it means testing times is numerous, but it is unnecessary and harmful to practice frequent testing for equipment. Therefore, a compromise scenario will be accepted, that is, mission reliability is permitted to decrease with testing times, but it must be greater than an accepted lower limit R_{low}. Here, assuming mission reliability can be expressed by $R(T'_0 + i\Delta T')$, $\Delta T'$

means mission reliability time offset. Obviously, it decreases gradually with testing times, and reduced amplitude is related with $\Delta T'$. So, testing period can be calculated by the following formula.

$$\frac{R\left(\sum_{j=1}^{i} T'_j + T'_{i+1}\right)}{R\left(\sum_{j=1}^{i} T'_j\right)} = R(T'_0 + i\Delta T') \geq R_{\text{low}} \quad (i = 1, 2 \ldots) \tag{25.5}$$

In formula (25.5), selected value of $\Delta T'$ is closely connected with R_{low} and i. When R_{low} is given, if $\Delta T'$ is less, testing period is longer and testing times is more or vice versa. In general, if only $R(T'_0 + i\Delta T') \geq R_{\text{low}}$, selected $\Delta T'$ should make testing period longer as soon as possible. Therefore, the problem how to determine testing period can be transferred to following optimization model.

$$\max \quad \min\left(T'_j, j = 1, 2, \ldots, i\right)$$

$$s.t.$$

$$\left.\begin{array}{l} \dfrac{R\left(\sum_{j=1}^{i} T'_j + T'_{i+1}\right)}{R\left(\sum_{j=1}^{i} T'_j\right)} = R(T'_0 + i\Delta T') \geq R_{\text{low}} \\[2mm] \sum T'_i \leq T^{\text{opt.}} \\[1mm] i = 1, 2, 3, \ldots \geq 0 \\[1mm] 0 \leq i\Delta T' \leq T^{\text{opt.}} \end{array}\right\} \tag{25.6}$$

In the model, i, $\Delta T'$ and $T'_j (j = 1, 2, \ldots, i)$ are optimal variables and the number of variables is $(i + 2)$. Generic optimal algorithm can be used to solve the model.

25.4 Numerical Example

Assuming equipment life can be expressed by Weibull distribution; in Weibull distribution, $m = 2.86$ and $\eta = 18$. Equipment preventive maintenance period and the first testing interval are, respectively, 9.8a and 1a; the given mission reliability lower limit is 0.97. Equipment testing period should be calculated.

To solve testing period optimal model expressed by formula (25.6), the optimal value of $\Delta T'(\Delta T'_{\text{opt}})$ is 0.2269a, in preventive maintenance period, 19 times of testing will be operated. The relation among testing period, mission reliability, and testing times can be, respectively, figured by Fig. 25.1a and b.

It can be seen from Fig. 25.1a, when mission reliability changes little, testing period decreases earlier and increases later, average testing period is 0.48a, not 1a.
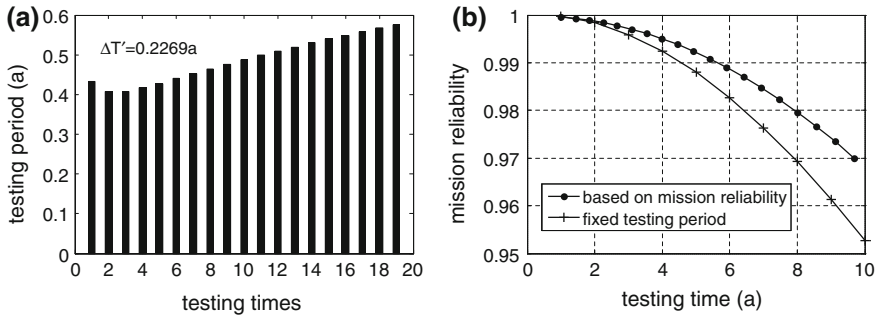
Fig. 25.1 Test period and mission reliability at $\Delta T' = 0.2269a$. **a** The relation between number and period of test. **b** Mission reliability's change with test number
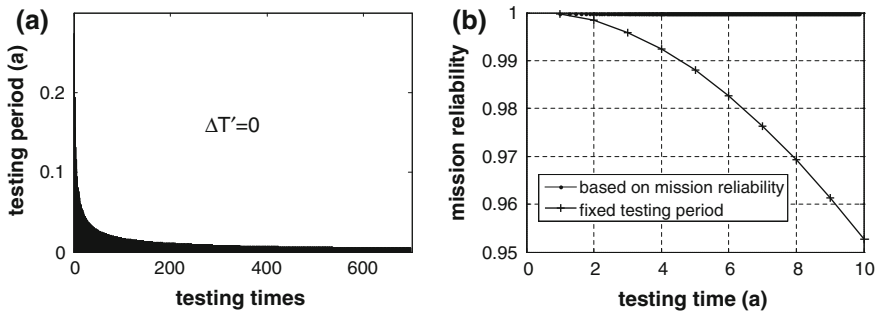
Fig. 25.2 Test period and mission reliability at $\Delta T' = 0$. **a** The relation between number and period of test **b** Mission reliability's change with test number

Also, from Fig. 25.1b, we can see mission reliability at time of eighth testing is less than 0.97 by fixed annual testing. So, it is difficult to satisfy given mission reliability by using fixed annual testing strategy.

If $\Delta T'$ is equal to 0, the relation among testing period, mission reliability, and testing times can be, respectively, figured by Fig. 25.2. In this instance, mission reliability is constant, but 700 times of testing will be operated in preventive maintenance period; average testing period is only 4.5d. It can be seen from above that if only $\Delta T'$ is selected with reason, testing times in preventive maintenance period can be remarkably reduced when given mission reliability lower limit.

25.5 Results

1. Strategy of fixed testing period can bring the problem that equipment will be failure before next testing, using the method in this paper to determine testing period can avoid the problem.

2. The optimal model constructed in this paper provides an effective technical approach to determine equipment testing period; under the condition of guaranteeing mission reliability steadiness, equipment testing period should vary.
3. In testing period optimal model, if only mission reliability time offset is selected correctly, it can satisfy mission reliability requirement, but also effectively reduce testing times in preventive maintenance period.

References

1. Ruflin SJ (1998) Optimum preventive maintenance policies for the AMRAAM missile. Master thesis, Engineering Air Force of Technology Air University
2. Reinertsen R (1996) Residual life of technical systems: diagnosis, prediction and life extension. Technical report, reliability engineering and system safety
3. Dinesh Kumar U (1999) Evolutionary maintenance for aircraft engine. In: Proceedings annual reliability and maintainability symposium. Technical report
4. Lian-yan S, Riu Zhang, Wen-yuan Song (2004) Method of determining check period during storage of missile weapon system (in Chinese). J Tactical Missile Technol 3:22–25
5. Zheng L, Bao-wei S, Jun L et al. (2004) Testing period optimal model about storage reliability of equipment (in Chinese). J Mach Des Manuf 5:1–2
6. Zheng L, Sheng-li L, Lei-jiang Y et al (2007) To determine Weibull system optimal testing period based on performance aging (in Chinese). Technical report, The 2007 Annual Academica Session of China Aviation Association
7. Yong W (2006) Research of check period way during storage based on torpedo weapon (in Chinese). J Ship Electron Eng 26:177–180
8. Zheng L, Bao-wei S, Qing-wei L et al (2004) A method of ensuring material testing period based on fuzzy reliability (in Chinese). J Mach Des Manuf 3:1–2
9. Xiao-song Y (2005) Large slew bearing condition based maintenance and emulation research about best testing periodic time (in Chinese). Ph.D. dissertation, Wu Han University of Technology
10. Jun-wei F, Hong-wei D, Wei Z (2010) Torpedo inspection period forecast based on storage time (in Chinese). J Ship Sci Technol 32:95–98
11. Hua-yuan F, Chang-hua HU, Qing–liang MA (2009) Determination of optimal inspection period for degradation system operating in dynamic environment (in Chinese). J Syst Eng Electron 31:100–103
12. Charles EE (2008) An introduction to reliability and maintainability engineering. Tsinghua University Press, Beijing

Chapter 26
The Hybrid Probabilistic and Non-Probabilistic Model of Structural Reliability Analysis

Pengya Fang, Xinlong Chang, Kuan Hu, Zhaoxia Wang and Bing Long

Abstract The original hybrid probabilistic and non-probabilistic reliability model is only suitable for simple reliability analysis problem. To extend its usability, the model was improved, in which the reliability is measured with the bound of the random reliability and some interval variables are transformed into random variables based on the maximum entropy principle to improve the computational efficiency. Moreover, considering the influence of the fuzzy uncertainty in the reliability analysis, the hybrid probabilistic, fuzzy, and non-probabilistic model was presented, in which the fuzzy variables are transformed into equivalent random variables and the fuzzy limit state is dealt with the modified Monte Carlo method. The model is an effective way to analyze the reliability in the situation that random variables, fuzzy variables, and interval variables coexist in a problem.

Keywords Structural reliability · Fuzzy variable · Interval variable

26.1 Introduction

In the structural reliability analysis, a great deal of uncertain factors need to be dealt with reasonably. Research [1, 2] shows that the uncertainty of the variables can be divided into two forms to describe. One is the probabilistic form, which uses the probability distribution function or membership functions to describe the uncertainty. The other is the non-probabilistic form, which uses convex set or interval to describe the uncertainty. Commonly, it is recognized that the

P. Fang (✉) · X. Chang · K. Hu · B. Long
Xi'an Hi-tech Institute, Xi'an, China,
e-mail: littlefun123@126.com

Z. Wang
Northern Nondestructive Test Center of China, National Erzhong Group Co., Beijing, China,

probabilistic form is more accurate and convenient in describing the variables with abundant experimental data, and the non-probabilistic form is more accurate and objective in describing the variables with a few of experimental data [3]. Corresponding to these two conditions, two reliability analysis methods, namely the probabilistic reliability method and the non-probabilistic reliability method, were presented by the researchers. The probabilistic reliability method can get more accurate results when the experimental data of variables are sufficient, while the non-probabilistic method can get more reliable results when the experimental data of variables are in lack [4, 5]. However, in an engineering condition, some variables may have sufficient data and the other may have a few of data. It is impossible to apply only one method, probabilistic method or non-probabilistic method, to solve this problem. Therefore, the research of the hybrid probabilistic and non-probabilistic model is very important.

The paper [6] established the hybrid probabilistic and non-probabilistic model of structural reliability analysis, in which the reliability is calculated by establishing two-level limit state equations. However, the model cannot solve complicated nonlinear limit state problem, and neglect the influence of the fuzzy variables, which may also exist in some engineering. Aiming to these problems, the original hybrid probabilistic and non-probabilistic model was improved and the hybrid probabilistic, fuzzy, and non-probabilistic model was presented in this paper.

26.2 The Improved Probabilistic and Non-Probabilistic Reliability Model

26.2.1 The Strategy

According to the definition of interval model, interval variable can be assigned any value within the interval bound. When the interval variable is assigned one fixed value within the defined bound, the hybrid probabilistic and non-probabilistic model degenerates into the probabilistic model. Supposing that we assign each value in the bound to the interval variable and calculate the corresponding random reliability, respectively, the bound of the reliability can be easily confirmed. To accomplish the object, the optimization method and enumeration method can be applied to solve the problem. However, these methods are computationally expensive. When the number of variables is large and the interval variables take the majority, or the problem analysis, such as finite element analysis, is complicated, the calculation cost will become higher.

As we know, in the reliability analysis, the random reliability method is more mature and the treatment of random variables is easier than that of interval variables. Therefore, if the interval variables can be replaced with the random variables, the calculation cost will be reduced and the calculation process will become easy.

Then, the key to improve computational efficiency is determining one method to transform interval variables into random variables. Here, interval variables are transformed into random variables based on the maximum entropy principle [7].

26.2.2 The Maximum Entropy Principle

According to the information theory, the entropy is used to measure the uncertainty of the phenomenon. When the interval bound of the variable is known, the uniform distribution has the maximum entropy [8]. That is to say the uniform distribution represents that the probability distribution within the interval bound is completely unknown and the degree of uncertainty is the largest at the moment.

In the engineering practice, quite a number of uncertain parameters are geometric parameters and material parameters. To improve the reliability, the designers and producers will try their best to make the geometric dimension and material property as accurate as possible. Based on the fact, the paper [9] points out it is credible that the distribution of uncertainty under this condition is between the normal distribution and uniform distribution. According to the maximum entropy principle, it is recognized conservatively that these parameters, whose tolerance can be controlled through the technology or human factors, obey the uniform distribution in the defined intervals.

26.2.3 The Procedure

The procedure of the improved probabilistic and non-probabilistic reliability model is as follows:

Step 1. Divide the variables into interval variables and random variables. And transform those interval variables, whose tolerance range can be controlled in the engineering project, into random variables under uniform distribution in the defined interval.

Step 2. Apply the optimization method [10] or enumeration method to calculate the reliability bound. Here only introduce the enumeration method as follows. Firstly, divide each interval variable into n subintervals and get $n + 1$ endpoint values. Secondly, combine the endpoint values of these interval variables and calculate the corresponding reliability of each combination with the random reliability method. At last, choose the maximum and minimum of the results as the upper and lower limits of the reliability.

It is noted that the calculation precision of the enumeration method will be improved with the increment of the value of n, but the calculation burden will be also increased with it. Therefore, both the calculation precision and the calculation

cost should be given consideration in determining the value of n. If the number of interval variables is m, there will be $(n + 1)^m$ combinations of the endpoint values and $(n + 1)^m$ reliability values correspondingly.

26.3 The Hybrid Probabilistic, Fuzzy, and Non-Probabilistic Model

In the above section, the hybrid probabilistic and non-probabilistic model was discussed. However, this model has two limitations. (1) In addition to random variables and interval variables, there are still fuzzy variables existing in some engineering practice. So it is necessary to consider the influence of the fuzzy variables in the hybrid reliability model. (2) The handling method to distinguish failure and safety based on the limit state function is rough, because the transformation from the safety to the failure is usually a gradual process and there is a fuzzy domain in the transition process [11]. In this section, such a new reliability model was established that is suitable for the situation in which random variables, fuzzy variables, and interval variables coexist.

26.3.1 Fuzziness and the Handling Method of Fuzzy Variables

Because the concept does not have the clear extension, fuzziness is such a kind of uncertainty that can not give the clear definition and evaluation standard to certain things. The most common method to study fuzzy reliability theory is to describe the fuzzy random phenomena with the fuzzy random variables and transform the fuzzy reliability problem into the conventional random reliability problem.

At present, there are usually two methods to transform fuzzy variables into random variables [12]. (1) λ-cut set method. Its computation is complicated and there is not a fixed standard to choose the probability distribution in the cut sets, which will influence the failure probability greatly. (2) The transformation of fuzzy variables to equivalent random variables based on entropy equality [13]. Its computational cost is small, and the influence brought by the probability distribution form is avoided. Its detailed content is as follows:

The entropy of variables is a measure of the uncertainty. As two different kinds of uncertainty, randomness and fuzziness can be measured with the entropy, respectively. The measure of the randomness is called probabilistic entropy, and the measure of the fuzziness is called fuzzy entropy.

According to the definition of probabilistic entropy given by Shannon, the probabilistic entropy is expressed as:

$$H_x = -\int_R f(x) \ln f(x) \mathrm{d}x \qquad (26.1)$$

where $f(x)$ is the probability density function of the random variable x.

According to the definition of the non-probabilistic entropy given by DeLuca and Termini, the fuzzy entropy is expressed as:

$$G'_x = -\int_R f'(x) \ln f'(x) \mathrm{d}x \qquad (26.2)$$

and

$$f'(x) = \frac{\mu(x)}{\int_R \mu(x) \mathrm{d}x} \qquad (26.3)$$

where $\mu(x)$ is the membership function of the fuzzy variable.

From the basic concept of entropy, it is known that the fuzzy uncertainty can be transformed into random uncertainties, and the transformation must be on the basis of the invariance of the measures, namely that the premise of the transformation is entropy equality. Therefore, according to the formulas (26.1) and (26.2), the transformation equation from the fuzzy entropy to the equivalent random entropy is established as:

$$H_x = G'_x. \qquad (26.4)$$

When

$$f(x) = f'(x) = \frac{\mu(x)}{\int_R \mu(x) \mathrm{d}x} \qquad (26.5)$$

$$H_x = G'_x. \qquad (26.6)$$

Therefore, $f(x)$ is called the probability density function of the equivalent random variable, which is the transformation of the fuzzy variable.

26.3.2 The Procedure

It is assumed that uncertain factors influencing the reliability are random variable x with the probability density function $f_x(x)$, fuzzy variable y with the membership function $\mu(y)$, and interval variable z with the upper limit z^u and the lower limit z^l. Also, assume that the variables are independent, the limit state function is $M = g(x, y, z)$, and the fuzziness of the failure state is expressed by the

membership $\mu_{\tilde{\Omega}_f}(M)$ of the state variable M attributed to fuzzy failure domain $\tilde{\Omega}_f$. Then, the reliability can be calculated as follows:

Step 1. Transform fuzzy variables into equivalent random variables and derive the probability density functions of the equivalent random variables as follows:

$$f_y(y) = \frac{\mu(y)}{\int_R \mu(y)\mathrm{d}y}. \qquad (26.7)$$

Step 2. Regard the interval variables as certainty and calculate the probability density function $f(M)$ of the state variable M according to $f_x(x)$ and $f_y(y)$.

Step 3. According to the calculation steps of the improved probabilistic and non-probabilistic model, consider the uncertainty of interval variables and calculate the failure probability based on the formula (26.8). Through comparing different values of the failure probability, which are, respectively, corresponding to different valuations of the interval variable, the bound of the failure probability can be derived.

$$P_f = \int\limits_{-\infty}^{+\infty} f(M)\mu_{\tilde{\Omega}_f}(M)dM \qquad (26.8)$$

However, when the forms of $\mu_{\tilde{\Omega}_f}(M)$ and $f(M)$ are complicated, it is difficult and even impossible to apply the analytical method to calculate the failure probability. The numerical simulation method, such as Monte Carlo method, will be a better choice.

In the two-state model, the Monte Carlo method compares the state variable with 0 and records one realization of the limit state function when the state variable is less than 0. However, in the fuzzy-state model, it is not suitable to compare the state variable with 0 and the Monte Carlo method needs some revisions. In order to facilitate the presentation, assume that the membership of the state variable attributed to fuzzy failure domain is minor type trapezium distribution, as shown in Fig. 26.1, and its specific expression is:

$$\mu_{\tilde{\Omega}_f}(M) = \begin{cases} 1 & M < a_1 \\ \frac{a_2 - M}{a_2 - a_1} & a_1 \leq M \leq a_2 \\ 0 & M > a_2 \end{cases} \qquad (26.9)$$

The Monte Carlo method is revised as follows:

Step 1. Like the traditional Monte Carlo method, produce the corresponding pseudo-random numbers according to the probability distribution function of variables.

Fig. 26.1 Minor type
trapezium distribution
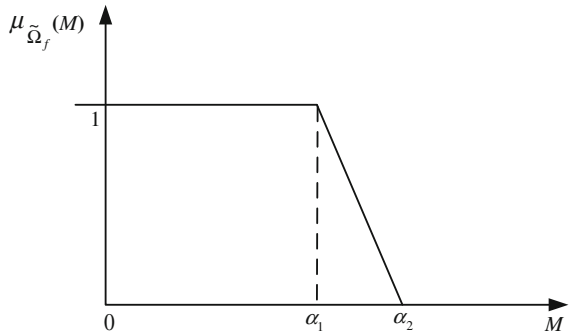
Step 2. Substitute these pseudo-random numbers into the state variable and derive its value M_i. Then use the variable m to record the times of the realization of the limit state function and give it an initial value of 0. If $M_i < a_1$, add 1 to m. If $M_i > a_2$, remain the value of m. If $a_1 \leq M_i \leq a_2$, add $\frac{a_2 - M_i}{a_2 - a_1}$ to m.

Step 3. Repeat steps 1 and 2 until completing the predetermined number of cycles K and finally derive the failure probability $P_f = m/K$.

26.4 Conclusion

The hybrid probabilistic and non-probabilistic reliability model was improved to solve the reliability problem with any complicated limit state function. And based on the improved model, the hybrid probabilistic, fuzzy, and non-probabilistic model was established, which not only considers the effect of the fuzzy variables but also the effect of the fuzzy failure state. Therefore, the model can effectively solve the reliability analysis problem that random variables, fuzzy variables, and interval variables coexist. However, usually it is difficult to apply analytical method to calculate the integral function of the reliability. To solve the problem, Monte Carlo method was modified and applied, which can reduce the analytical complexity greatly.

References

1. Elishakoff I (1995) Essay on uncertainties in elastic and viscoelastic structures: from AM Freudenthal's criticisms to modern convex modeling. J Comput Struct 56(6):871–895
2. Guangyuan Wang (1992) Theory of soft design in engineering. Science Press, Beijing (in Chinese)
3. Guo S (2002) Non-Stochastic reliability and optimization of uncertain structural systems (in Chinese). Ph.D. dissertation, Northwestern Polytechnic University
4. Ben-Haim Y (1994) A non-probabilistic concept of reliability. J Struct Saf 14(4):227–245

5. Elishakoff I (1995) Discussion on: a non-probabilistic concept of reliability. J Struct Saf 17(3):195–199
6. Shuxiang Guo (2002) LV Zhenzhou : hybrid probabilistic and non- probabilistic model of structural reliability. J Mech Strength 24(4):524–526 (in Chinese)
7. Ping Yi (2006) Discussions on reliability measure for problems with bounded-but-unknown uncertainties. Chin J Comput Mech 23(2):152–156 (in Chinese)
8. Li X (1997) Probability theory basis. High Education Press, Beijing (in Chinese)
9. Zhaotong Wu, Zhaotong Wu (1999) Computer aided tolerance optional design. Zhejiang University Press, Hangzhou (in Chinese)
10. Du X (2012) Reliability-based design optimization with dependent interval variables. J Int Numer Meth Eng 91:218–228
11. Li Y (2005) Robust reliability theory and optimization methods (in Chinese). Ph.D. dissertation, Dalian University of Technology
12. Zhao Y, Zhang X, Shi H (2008) Computation of structural system reliability with hybrid uncertainty of fuzzy variables and random variables. J. Mech Strength 30(1):72–77 (in Chinese)
13. Liu C, Chen Q (2003) Analysis of structural general reliability of the loading and strength based on information entropy. J Mech Sci Technol 22(3):444–446 (in Chinese)

Chapter 27
Research on Proactive Maintenance Strategy Based on CBM for the Aviation Ground Support Facility

Hongjun Fan, Youlong Chen and Xunzhang Li

Abstract With the increasing of the amount of the aircraft flight mission and the raising of electronic and digital level of the aviation ground support facility, CBM becomes the inevitable trend of the maintenance management. This paper introduces the defining, range of application, composing and implementing steps of the CBM. Combination with the specialty of the ground support facility, the proactive maintenance strategy based on CBM is dealt with. The proactive maintenance strategy will greatly promote the maintenance management reform and the popularization of CBM for the aviation ground support facility.

Keywords The aviation ground support facility · CBM · Condition inspecting · Judging and predicting · Proactive maintenance strategy

27.1 Introduction

The aviation ground support facility offers the required power supply, gas source and hydraulic production. For a long time, planned maintenance has been the major way of maintenance management. As a large number of advanced technology and electronic components are adopted, the degree of complexity and automation of the facility is increasing. Disadvantages of planned maintenance are becoming more and more highlighted, "Excess repair" or "insufficient maintenance" for the facility leads to frequent breakdowns, which seriously affect the security and the service life of the facility. And the extended downtime caused by maintenance seriously restricts the support capability of the ground support troops.

H. Fan (✉) · Y. Chen · X. Li
The Sixth Department of Naval Aeronautical Engineering Institute, Qingdao Branch, No.2 of Siliu Middle Road, Qingdao 266041, China
e-mail: fhj421@163.com

With the application of condition monitoring technology, computer technology and analysis technology, CBM that has great superiority has been achieved rapidly. CBM aiming at improving the facility intact rate is truly the maintenance indeed. In accordance with the specialty of the aviation ground support facility, the paper researches on the implementation of proactive maintenance strategy based on CBM. And the specific method and thought based on proactive management is put forward, which has a realistic significance to promote reform for the maintenance management for the ground support facility.

27.2 Theory of CBM

27.2.1 Meaning of CBM

CBM is a maintenance when the performance of the facility degrades significantly by monitoring the condition and parameters [1]. Clearly, CBM is a needed maintenance. By capturing the current condition of the equipment, analyzing the occurrence of defects or potential faults, CBM can predict the remaining life and the function failure probability of the equipment. Then, the needed repair time is given.

Usually, the equipment has a gradual degradation process. Figure 27.1 illustrates the fault phase which is P–F curve, which shows how to start the faults and degrade to "P" point. If the "P" point was not detected, the equipment will quickly degrade to the functional failure point "F".

The interval of potential fault detect point to function point of failure is further, the possibility of equipment failure is smaller and the maintenance cost is less. Conversely, the possibility of equipment failure is greater and the maintenance cost is larger. The purpose of proactive maintenance is to find and correct any operation or performing resulting in failure. It should be pointed out that CBM does not reduce maintenance and cancel the planed maintenance. Furthermore, it integrates the planed maintenance, beforehand maintenance, after repair and reliability-centered maintenance as a whole [2]. However, considering of reducing the maintenance cost, it is not realistic to put all of the equipment into CBM practice. CBM should be applied to the component or part which is the key to run security and reliability for the equipment which has greater influence on the maintenance economy.

27.2.2 Basic Constitute of CBM

CBM includes three parts: the condition monitoring, the fault diagnosis and prediction, as well as the maintenance decision. What is more, the implementation of condition maintenance must have a high level of information management system as a basic support [3].

Fig. 27.1 P—F interval
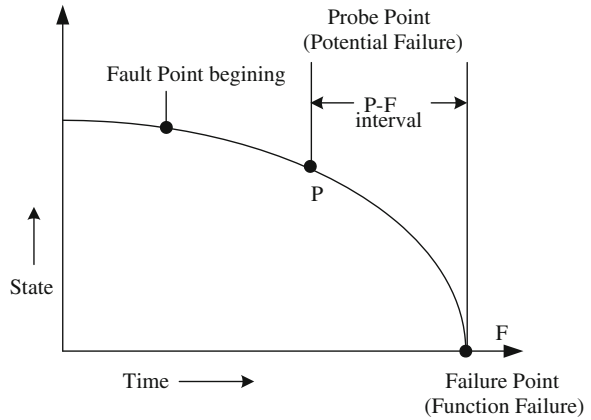
(1) *Condition Monitoring*

Presently, the most direct and effective way of condition monitoring is to pick up status signals in the process of running through the sensor and its related auxiliary test instrument. The general steps of the condition monitoring include monitoring objects choosing, the choosing of method for condition monitoring, the monitoring plan and procedures determining and the allowed limit value determining, etc.

(2) *Fault Diagnosis and Prediction*

The main purpose of the fault diagnosis and prediction is to find out the hidden dangers and the early abnormal. So that the fault source can be identified and located and the remaining life of the device can be predicted. Combining with the history parameters, the impact of the fault diagnosis and prediction can estimate whether the equipment is in a normal, abnormal or fault condition by analyzing the running operation parameters. And the fault diagnosis and prediction can identify the character, category and reasons of the failure occurred or occurring. What is more, it can find out the occurrence and development trend of the fault which is the basis of putting forward the countermeasures to eliminate the emergent fault occurring.

(3) *Maintenance Decision*

After determining the equipment status and fault analysis, the maintenance decision deals with a series of problems which includes determining whether the equipment needing to be repaired, and when to repair according to the results of the analysis of equipment status.

```
┌─────────────────────────┐
│  Information System of   │
│     the Equipment        │
└─────────────────────────┘
             │
             ▼
┌─────────────────────────┐
│          FMEA            │
└─────────────────────────┘
             │
             ▼
        ╱─────────╲          N    ┌──────────────────────────┐
       ╱ Suitable for╲─────────────│  Other maintenance way   │
       ╲   CBM ?    ╱              └──────────────────────────┘
        ╲─────────╱
             │ Y
             ▼
┌─────────────────────────┐
│ Choice of State parameter and │
│  condition monitoring method  │
└─────────────────────────┘
             │
             ▼
┌─────────────────────────┐
│   Condition Monitoring,  │
│ Fault diagnosis and prediction │
└─────────────────────────┘
             │
             ▼
┌─────────────────────────┐
│      Maintenance         │
│       decision           │
└─────────────────────────┘
```

27.3 Proactive Maintenance Procedures

Before carrying out CBM, we should comprehensively acquaint the possible
trouble and analyze all kinds of failure modes. By obtaining the condition infor-
mation of the equipment with the monitoring and diagnosis technology, we can
precisely diagnose the current health of the equipment and determine whether the
equipment or system has met causes speeding up the progress of the failure. And
then, we can make maintenance strategy timely ahead of the system performance
degradation. The general procedure of implementation of proactive maintenance is
shown in Fig. 27.2.

27.3.1 Basic Information of the Equipment Collection

The information management system can dispose analysis and research with a
large amount of data quickly and accurately. And it can provide the necessary
mathematical model and algorithm of science for analysis and evaluation to
equipment status. Before implementing CBM, basic information of the equipment

should be collected and stored which includes the performance information, the changed information, the operation information, the defect and fault information and the maintenance information, etc.

27.3.2 Important Functional Items Determination

The important functional item is the one affecting system safety significantly and having a significantly economic consequence to the system. Combining the FMEA based on the information, reliability and security of the equipment, the important functional items of the system, subsystem or component are determined. Then, the suitable system or components for condition-based maintenance can be chosen.

27.3.3 Status Parameter and Monitoring Means Selection

Once the important functional items are identified, the appropriate status parameters must be chosen. The state parameters are typical parameters which change with degradation or failure trend of the equipment. And the transformation of these parameters must be more clearly than others. The typical state parameters in running process of the equipment include the vibration data, the acoustic data, the oil analysis data, and as well as the temperature, pressure, humidity data. After choosing the condition monitoring parameters, appropriate monitoring technique should be chosen to collect data. According to the signs of detection or the potential failure effect, status monitoring technology includes the dynamic effect, the particle effect, the chemical effect, the physical effect, the temperature effect and the electric effect, etc.

27.3.4 Condition Monitoring, Fault Diagnosis and Prediction

Once the status parameters and the monitoring method are determined, the condition monitoring of the system should be done by sensors and online or offline detector. Usually, the signal obtained by condition monitoring contains noise which should be eliminated maximally. Combining the signal preprocessed with the reliability data, life prediction data, maintenance history data and design parameters, we can diagnose the equipment whether in a current failure or a possible failure. And then, the cause, site and severity of the failure can be estimated, which provides the basic information to the maintenance decision.

27.3.5 Maintenance Decision

The ultimate goal of condition monitoring, fault diagnosis and forecast is to make decision and implement maintenance scientifically. There are two important contents should be done during the maintenance decision: the optimization cycle of maintenance and the scheme of maintenance [4]. The optimal maintenance cycle is determined by a certain goal (mission reliability, availability, maintenance cost, etc.), and the optimal maintenance scheme can be chosen on the basis of the results of the status analysis and evaluation. For various equipments or components, the establishment of the target function should be done according to the reliability or failure probability, mission availability, maintenance cost, etc. Then, the optimal maintenance cycle for different decision target is obtained. And the equipment optimization maintenance decision for different constraint conditions is done.

27.4 Proactive Maintenance Based on CBM for the Ground Support Facility

27.4.1 Characteristics of the Aviation Ground Support Facility

The aviation ground support facility is one which produces and supplies electricity, hydraulic oil and oxygen (nitrogen). The characteristics of the aviation ground support facility are as follows:

(1) *With Great Varieties and Large Quantities*

The facility involves not only various mobile vehicles directly docking to the aircraft outfield but also fixed fixture producing infield.

(2) *With High Complex Level and Failure Rate*

With the wide application of a large number of the electronic components, the structure of the facility becomes more and more complex. The facility usually has dozens of functional systems. And the systems can be divided into subsystem or sub-subsystem.

With the raising of electronic and digital level, the variety of failure modes for the ground support facility is becoming more and more widely [5]. Because of the unusually severe environment, the rate of facility failure is becoming higher and higher. For the above reasons, the scheduled maintenance mode is restricting the support ability of the facility badly. To promote the availability and support capability of the aviation ground support facility, it is necessary to transform from passive maintenance to the proactive maintenance which is more scientific and reasonable.

27.4.2 *Implementation Process of Proactive Maintenance Strategy*

The proactive maintenance based on CBM for the ground support facility is a maintenance mode combining the planed maintenance with CBM. But in the process of maintenance implementation, the proportion of CBM should be increased consciously. Figure 27.3 shows the implementation process for the aviation ground support facility based on proactive maintenance strategy. The steps of the proactive maintenance for the ground support facility are as follows: integrated information system establishing, establishment of the facility tree, failure mode and effect analysis (FMEA), important degree evaluation, condition evaluation and fault diagnosis, as well as maintenance decision.

(1) *Integrated Information System Establishing*

The integrated information system stores a large amount of data which is the foundation of the proactive maintenance. Once status of the facility is evaluated, real-time data and information from the integrated information system are called. At the same time, the judging data of the facility state and the evaluation result are stored into the system. And when fault diagnosis and remaining life prediction is done, the needed historical data and information from the system are chosen. The result of fault diagnosis and condition prediction is stored into the integrated information, too. During maintenance decision, the data of the information system are called. After the maintenance decision result is stored into the integrated system, maintenance implementation can be done.

(2) *Establishment of the Facility Tree*

For the variety and complexity of the aviation support facility, the analysis process must be simplified. According to a certain rule, the facility can be divided into system, subsystem or sub-subsystem. Then, a hierarchy tree of the facility is formed.

(3) *Failure Mode and Effect Analysis*

Calling the data of the integrated information system, FMEA is done for each system, subsystem or sub-subsystem. Then, the main failure modes and causes of the failure are obtained, which are stored into the integrated information database at the same time.

(4) *Important Degree Evaluation*

Using the results of FMEA and the expert knowledge, the important items are found and the important index is gotten. Then, various maintenance modes are determined: Once the facility is in a normal state, routine maintenance is adopted. When the facility is in the stage of potential failure, the monitoring should be strengthen to avoid the occurrence of the emergent failure; corrective maintenance should be adopted when the value of state parameter transcends the potential
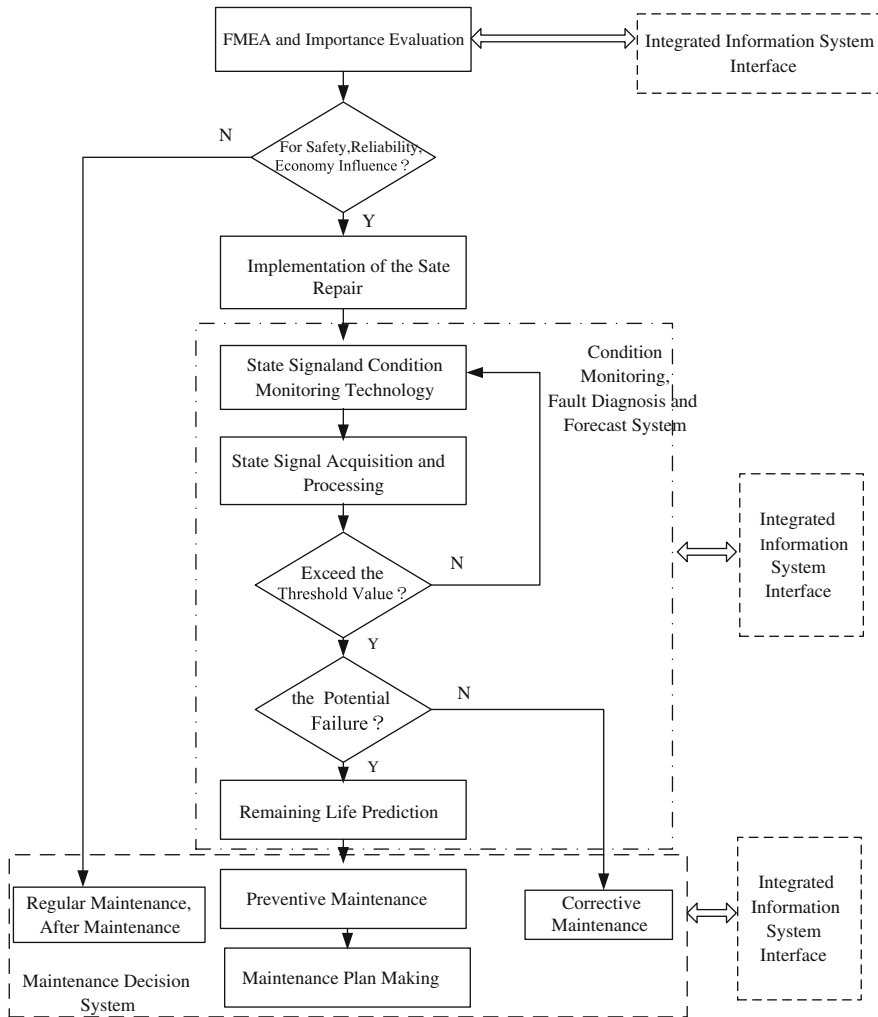
Fig. 27.3 Proactive maintenance strategy implementation process for the ground support facility

failure stage which can lead to suddenly shut down for the facility. At the same time, the maintenance modes are determined and the reasonable maintenance cycles are chosen. The evaluation results and maintenance decision results are also stored in the integrated information system.

(5) *Condition Evaluation and Fault Diagnosis*

The state parameters and condition monitoring technology must be chosen for the important item. Then online or offline status evaluation and prediction is done. If the state is normal, the facility can continue to run. If the state value exceeds a predetermined threshold, the fault diagnosis will be done. Then, the preventive

maintenance is determined according to the diagnosis result and the task of the facility.

(6) *Maintenance Decision*

For the maintenance indeed, the practical and effective maintenance scheme must be drawn up. The establishment of maintenance scheme bases on the facility condition evaluation and prediction, the facility operation as well as maintenance experience. The formulated maintenance scheme should be submitted to the maintenance support staff for comprehensive evaluation. The optimum facility maintenance scheme is one ensuring the flight maximum benefits, fitting the practice of troops and facility operating conditions.

27.5 Conclusion

The complex degree of the equipment is higher; the running condition monitoring and fault prevention is more necessary to be reinforced [6]. It is shown that once the implementation of the proactive maintenance is adopted, failures of the equipment reduce by about 75 % and maintenance costs reduce by 25 % to 50 %. That is to say, in the maintenance management, the ideas of proactive maintenance based on CBM must be introduced, and the proportion of proactive maintenance should be added gradually.

References

1. Gu Y (2009) Power generation equipment state maintenance theory. China Electric Power Press, Beijing (in Chinese)
2. Yang YO, He X (2007) Weapons and equipment state overhaul decision. J Equip Command Inst Technol 10:111–114 (in Chinese)
3. Chen D, Zhao J (2011) Aircraft maintenance decision-making system based on real-time condition monitoring information. Aviat Maintenance Eng 6:40–42 (in Chinese)
4. Wang S, Jia Y (2011) Decision analysis system development based on the condition-based maintenance. Comput Eng Des 32:366–369
5. Hu J, Ge X (2011) Aviation equipment integrated condition-based maintenance framework. J Air Force Eng Univ (Natural Science Edition) 12:1–6 (in Chinese)
6. Willetts R, Jardine A (2011) Optimizing complex CBM decisions using hybrid fusion methods. In: Proceedings of 14th international congress on conditions monitoring and diagnostic engineering management, pp 909–918

Chapter 28
A Simulation Method of Reconfigurable Airborne Display and Control System

Zhile Wang, Hui Yu and Xiuzhi Zhou

Abstract Display and control system is used as the display and operation of modern aircraft comprehensive avionics system and has extremely high information and the integration, Display and control system simulation in the development process of the simulator is one of the major problems. Combined with the development needs of the simulator, proposed the simulation method based on instructions to realize drawing and real-time control on the graphics elements for the display and control system. Used GL Studio to create the system's foreground basic graphics elements, display characters and interactive interface, used the object-oriented technology realize the code design on reusable class. Used the object-oriented technology to achieve the background logic, graphics display, data disposal on the code design of the reusable class. Airborne display and control simulation system could reconfigurable by modifying the foreground graphics elements and the background logic, realized resource shared, to supported the development of a variety of simulator on the display and control system.

Keywords Display and control system · GL studio · Instruction · Object-oriented technology · Reconfigurable

28.1 Introduction

Display and control system as a core part of modern aircraft avionics integrated system will be responsible for the management of aviation electronic system work mode and status, and various operations on the cockpit for processing [1], integrated processing, and display various data from other systems, through the display device to show the output information to the pilot [2].

Z. Wang (✉) · H. Yu · X. Zhou
Naval Aeronautical Engineering Institute, Qingdao Branch, Qingdao 266041, China
e-mail: wgzhile@163.com

The simulation of the display and control system is an important part of the simulator [3, 4]. The traditional simulation method of the display and control system is based on the display scene, organize the display scene, then develop the display scene one by one, finally, finish the inter logic between the display scene, the data process of the crosslinking system is concentrated in the development of the display screen. Such as Chen Xi, Li Guo-qing, "a type of military multifunction display system simulation". This method will increase the complexity of the logic programming, easy to cause the screen overlap, a plurality of display terminal data will delay real-time capability, and the system have poor flexibility and versatility. When develop the same type of another function simulator or apply in the virtual environment will can not adapt, but the development cost of simulator is expensive, so the new test based on improved simulator is very important. NASA LaSRS++ project oriented object technology to design the simulator framework was improved continuous years, project code reuse rate of 96 %. In this paper, the front display is designed separately and the background of control software, combined with software reconfigurable characteristics, design patterns, and code reusability, put forward a kind of simulation method for control and display system based on the instruction control. When developing the background graphics elements control and data processssing software don't need to consider how many the display screen and the switches relationship between the display screen. Which greatly improves the efficiency and reliability of the display and control system, improves simulator developed reconfiguration.

28.2 Simulation Software Design

The display and control system structure of the software division includes the following: comprehensive task processor software and graphic elements display software.

1. Comprehensive task processor software as the background control software (paper referred to as processor software), mainly to complete avionics display software logic processing and drawing scene.
2. Graphic display software as the front display software, mainly to accept scene information from processor software.

Since the display and control system needs to display more content, the large amount of graphic and image needs to be calculated; the logic and data processing has large quantity, but also as the system requirements are high real time, also has a certain degree of reconfigurability and maintainability. So the design of the simulation software is the key.

28.2.1 Software Simulation Environment

Processor simulation software uses Visual C++.Net, using the object-oriented development technology; the processor simulation software of each function are encapsulated into classes; graphic display software uses professional instrument simulation software GL Studio.

28.2.2 Instruction Model Structure

Instruction is a user-defined graphics draw and control interface. The instruction contains the instruction code and character. After an instruction is called, each graphic elements instruction code and features are stored in the unsigned short array as 16 hexadecimal data, forming the instruction frame. The network module through UDP sends instruction to the graphic display software.

Processor software draws the screen on graphic elements display software, completed by the call instruction. Processor software will put the instruction frame stored in the array _BUFFA2048]; information field in instruction frame is shown in the following Table 28.1.

According to the display symbols feature can put graphic elements instructions divided into general instructions and special instructions.

28.2.3 General Instructions

General instructions are used for drawing rectangular, arc, straight line, character, etc.

Multifunctional display instrument (MFD) are measured as the pixels, from top to bottom for 0–1023 and from left to right for 0–767, and the upper left corner of monitor is (0, 0). Using the instruction description graphic elements coordinates (x, y), through the pixel point, coding mode for binary coding letters, numbers, Chinese characters, and punctuation number using inside code is achieved. The lower 8 bits of letter and number code are the same as the ASCII code values, high 8 bits equal 0, for example, round (arc) instruction and character display instruction. See Tables 28.2 and 28.3.

Character format: 0xXXXX(hex).

$$\underbrace{\text{X}}_{\text{font}}\ \underbrace{\text{X}}_{\text{flash}}\ \underbrace{\text{X}\ \text{X}}_{\text{color}}$$
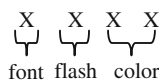
Table 28.1 The information field in instruction frame

Number	Content	Explanation
1	Information segment	M
2	Instruction 1	The meaning and
3	Instruction 1—data 1	characteristic of each
	Instruction 1—data N1	instruction data elements
M	Instruction N	

Table 28.2 The round(arc) instruction

Data word 1: Instruction code	A020H
Data word 2	Arc radius r
Data word 3	Arc center coordinates x
Data word 4	Arc center coordinates y
Data word 5	Arc start angle θ
Data word 6	Arc end angle φ
Data word 7	Character word

Table 28.3 The character display instruction

Data word 1: Instruction code	A040H
Data word 2	Coordinate X
Data word 3	Coordinate Y
Data word 4	Character number
Data word 5	Character word

Font size: 0, No. 16 font; 1, No. 10 font.
Flash: 0, said no flicker; 1, said flicker.
Color: according to the need of user.

28.2.4 Special Instructions

The special graphic element instruction draws a special graphic element. Every special graphic element needs definition instruction code and character word. For example, flight attitude is shown in Fig. 28.1, and instruction description is shown in Table 28.4.

Data word 2: roll angle, in degrees, encoding for the binary code; the lowest was 0.1. The data word 3: pitch angle, in degrees, encoding for the binary code; the lowest was 0.1.
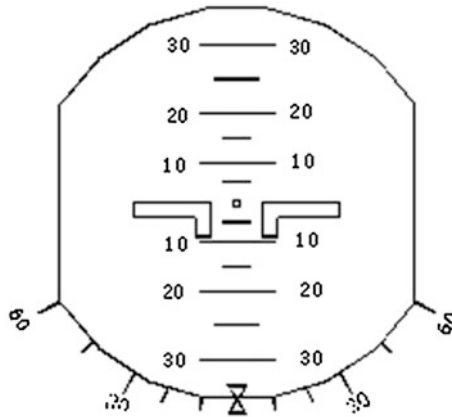
Fig. 28.1 Flight attitude graphic element

Table 28.4 Flight attitude display instruction	Data word 1: Instruction code B010H

Data word 1: Instruction code	B010H
Data word 2	Roll angle
Data word 3	Pitch angle

28.2.5 Graphic Element Display Software Structure

Graphic display software using GL Studio development, through receive the display instruction set from the processor software, completed the real-time drawing and refresh for every graphic element. Specific process is shown in Fig. 28.2.

28.2.6 Graphic Element Process

The general graphic elements are dynamic founded through the GL Studio interface; specific graphic elements are loading the textures and then drive by call the GL Studio interface.

The general instructions are stored by defining a respective container; the advantages can be dynamic storage indefinite quantity graphic element data; the container is versatile, capable of operating a variety of data structures and algorithms for template class and function library, and is very convenient to deal with the data.

It first defines the data structure according to instructions and then defines the data container, the same graphic elements data stored in containers (such as strings, waypoints, and routes). The paper designed character and round (arc) graphic elements.
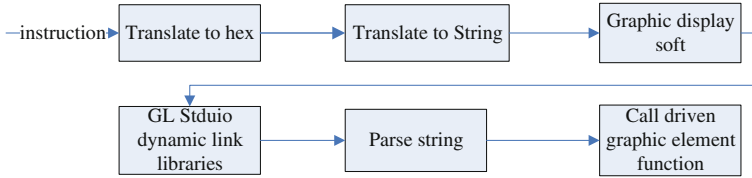
Fig. 28.2 Graphic element development process. For graphic element display software, graphic processing function all is completed in GL Studio dynamic library, mainly including instruction parsing, general graphic elements processing algorithm, and special graphic elements processing algorithm

```
// declare the character structure displayed in MFD
struct  MFD_DISP_ CHAR_TYPE   {
        char Disp_Ch;      //display character
        float Disp_Pos_X; //location in GL
        float Disp_Pos_Y; //location in GL
        unsigned short Disp_Trait; //character word
};
// define the character graphic element data container
std::vector<MFD_DISP_CHAR_TYPE>  _ENWordsPosition_ ;
//character data stored in container
 MFD_DISP_ENWORD_TYPE  tempENWord;
 _ENWordsPosition_.push_back(tempENWord);
// round ( ARC ) structure
struct  MFD_DISP_CIRCLE_TYPE   {
        unsigned short R;        //radius
        unsigned short X;        //circle center X
        unsigned short Y;        //circle center Y
        unsigned short Q;        //start angle
        unsigned short P;        //end angle
        unsigned short T;        //character word
};
// definition the circle ( arc ) data container
std::vector<MFD_DISP_CIRCLE_TYPE> _CirclesPosition_ ;
// round ( arc ) data stored in a container
MFD_DISP_CIRCLE_TYPE tempCircle;
_CirclesPosition_.push_back(tempCircle);
```

It has the same special graphic elements in scene; therefore, it also needs to define containers stored objects, here defined character objects container, and is used for storing the circle (arc) container object.

```
std::vector<GlsTextGrid *> _ENWordsGroup_;
std::vector<GLPolygon *> _CirclesGroup_;
```

Then, according to the graphic element data in container call interface of GL Studio to dynamic draw graphic element, it drives graphic element display or movement. Dynamic draw graphic element is very important in the development of GL Studio.
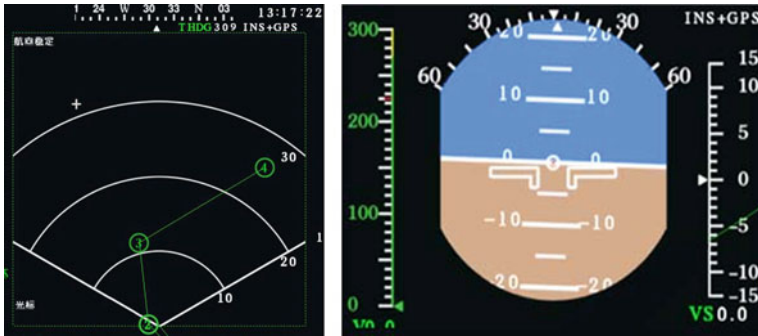
Fig. 28.3 The significant part of the simulator control running effect diagram

Table 28.5 Simulation time of instruction store and graphics driver

MFD scene	Instruction	Send time less (ms)	Update time (ms)
Flight	742	3	21
Navigation	1,210	4.5	24
Communicate	1,224	4.5	24.3
Attack	1,328	5	24.8

28.3 Simulation Application

This method has been successfully applied to a certain type of aircraft simulator. Processor software runs on Intel (R) Core(TM)2 CPU 4300 @1.80 GHz, 1 G memory, and graphics NVIDIA GeForce 9300 of hardware conditions; graphic display software runs on a single machine. Figure 28.3 is a significant part of the simulator control running effect diagram. Define instruction frame unsigned short _BUFF[2048], through analysis of instruction frame of each scene, found that 2048 was enough space to display and control system of graphic element data storage, in the process of testing with the simulator of flight and weapon control function; graphics element driving for real time completely achieves the flight training needs. In graphic element, more complex pages do analysis, see Table 28.5.

Display control system real-time operation response will seriously affect the simulator performance, thereby affecting the fidelity and the effect of pilot training. The main factors affecting the real-time software are processor software that accepts the user operation signal, the logic operation, and display time. The display control system scene is complex and changeable, so the logic relation of the solution is extremely complex, the traditional simulation method is based on every scene simulation, logic judgment is deeply nested, sometimes a menu or a symbol change must act as a scene, the menu or symbol or scene easily appear overlapped, or after many times, operation showed error. Tables 28.6 and 28.7 show the efficiency of logic 2 design solution.

Table 28.6 Logic processing time based on instruction

Type system	Instruction size	Calculate time (less) (ms)	Operate respond time (ms)
Navigation	<1,210	8	0–31
Communicate	<1,224	6	0–34
Sensor	<1,328	8.3	0–34
Radar	<1,328	8	0–37

Table 28.7 Logic processing time based on scene

Type system	Scene amount (more)	Calculate time (less) (ms)	Operate respond time (ms)
Navigation	30	11	0–45
Communicate	35	12.4	0–51
Sensor	40	12.7	0–55
Radar	55	14	0–72

Fig. 28.4 The graphic display software overlay radar simulation video realizes the software reconfigurable
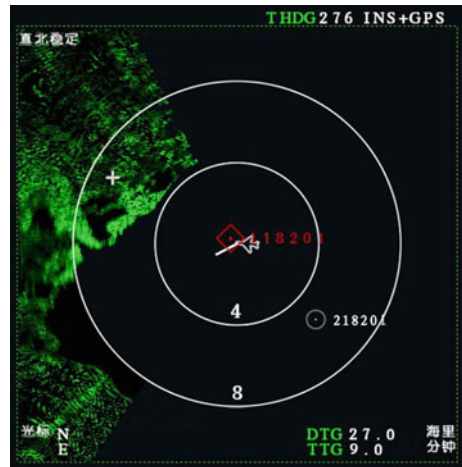
This type of display and control software is also applied to simulator of the helicopter radar and without changing the instruction and processor software, directly in the graphic display software overlay radar simulation video, realizes the software reconfigurable, see Fig. 28.4. Also the display and control simulation software used in other flight simulators, general instructions, and special instruction for graphic element display software does not need to be changed, need to only modify the processor software, by calling the instruction to organize new scene.

28.4 Conclusion

The display and control system development based on instruction can be adapted to different simulator, along with the change of research objective needs the new development demand, and can effectively deal with system changes. By comparing the development of traditional control system, the method effectively simplifies the process of display scene development for display and control system, convenient for system change and maintenance, and increased system stability and real time.

References

1. Fan T (2008) Airborne integrated display system (in Chinese).M. Beijing, National Defence Industry Press
2. Wu H, Kang F, Huang W, Lu Y (2012) Software simulation of display and control simulation system for aircraft based on virtual reality. J Syst Simul 24(6):1232–1235 (in Chinese)
3. Luo C, Shen W, Song Z (2004) Research and implementation of simulation system for flight multi-function display. J Comput Simul 21(12):249–251 (in Chinese)
4. Zhang F, Chu W, Fan X, Wan M (2009) Research on architecture of integrated modular avionics. J Electron Opt Control 16(9):47–51 (in Chinese)

Chapter 29
Application of Plasma Electrolytic Oxidation to the Novel Aircraft Aluminum Alloy for Enhancing Corrosion Resistance

Zuoyan Ye, Daoxin Liu, Chongyang Li, Xiaoming Zhang, Zhi Yang and Mingxia Lei

Abstract Plasma electrolytic oxidation (PEO) has been considered as a novel technique to form ceramic coatings on aluminum alloys for corrosion protection. The effect of PEO on the intergranular corrosion (IGC) behavior of the novel high-strength aluminum alloy 7A85 was investigated. Electrochemical polarization technology was used to study the influence of PEO on the electrochemical corrosion behavior of AA 7A85. The IGC mechanisms of PEO and PEO combined with sealing-treated AA 7A85 were studied by metallographic analysis, XRD analysis, and scanning electron microscopy. The results show that AA 7A85-T7452 is very sensitive to IGC. PEO would reduce the largest corrosion depth by 41.6 %. PEO without sealing did not eliminate the IGC for the micropores and microcracks in the oxide coating. However, PEO combined the SiO_2 sol gel sealing treatment could effectively protect the AA 7A85-T7452 from IGC for the good corrosion resistance and barrier function of the sealed coating.

Keywords 7A85 aluminum alloy · Plasma electrolytic oxidation · Intergranular corrosion

29.1 Introduction

Aluminum alloy 7085 which has been developed in 2003 by Alcoa as the next generation of high-strength, high-toughness, and low-quenching sensitivity alloy supplied an urgent need of thick aluminum forgings for the next generation

Z. Ye · D. Liu (✉) · C. Li
Corrosion and Protection Research Laboratory, Northwestern Polytechnical University, Xi'an 710072, China
e-mail: liudaox@nwpu.edu.cn

X. Zhang · Z. Yang · M. Lei
AVIC the First Aircraft Institute, Xi'an 710089, China

aircraft. It has been successfully applied to large aircraft such as the Boeing 787 for main bearing components [1]. Drawing on the advanced characteristics of this material, China developed 7A85 aluminum alloy, performance of which can be comparable with 7085 and laid a good material foundation for the development of new advanced aircraft. Comparing with other's 7xxx aluminum alloy, AA7085 has a high fracture toughness and low quench sensitivity for the higher zinc along with the lower copper content. Generally, the combination of high strength and good corrosion resistance was contradictory. For example, higher Zn content increased the strength while decreased the corrosion resistance. T6 peak-age temper provided high strength but low corrosion resistance. T7x over-aged temper increased the corrosion resistance but reduced some strength. In order to achieve both high strength and good corrosion resistance, lots of effort has been carried out on developing new heat-treatment process. Such as retrogression and reaging (RRA) temper which increased the corrosion resistance while kept the strength levels similar to T6 temper [2]; two-step aging temper by which the stress corrosion cracking resistance and strength were both higher than that of T6 temper [3]. However, the effects of temper on strength and corrosion resistance of aluminum with different composition differed greatly [4]. So it is difficult to achieve a good combination performance of new aluminum by current heat-treatment process.

Surface treatments could obtain the desired surface performance without changing the overall property of materials. Numerous surface treatment technologies have been applied to aluminum alloy, such as anodic oxidation, plasma electrolytic oxidation (PEO), shot peening, nitriding, electroplating, and vacuum coating, in which anodic oxidation is widely used in the aerospace industry for enhancing corrosion and wear performance. As developed from anodic oxidation, PEO technology could produce ceramic coatings on aluminum alloy surface in situ. The thickness, hardness, and density are significantly improved than that of conventional anodic oxide film. In recent years, much attention has been attracted to PEO technology for its good prospects in aviation industry. PEO treatment on uniform corrosion of aluminum alloy has been widely investigated [5], but the intergranular corrosion (IGC) of new high-strength aluminum alloy applied in the aircraft structure in acid rain environment is less reported. As mentioned earlier, the effect of PEO treatment on the corrosion behavior of new high-strength aluminum alloy 7A85 in acid IGC solution was studied. The purpose of the article is to provide a reference for the using of PEO on the novel aluminum alloy 7A85 in improving corrosion performance.

29.2 Experimental

29.2.1 Materials and Specimens

The present investigation was carried out on the 220-mm-thick 7A85 aluminum alloy plate with chemical composition of Al–7.76Zn–1.69Mg–1.75Cu–0.026Fe–0.013Si–0.017Zr–0.0022Ti (wt%). The plates were solution-treated at 470 °C for

1 h, quenched in room temperature water, compressed to generate a 1–5 % constant deformation, and then aging at 110 °C for 6 h and 160 °C for 10 h. All the specimens were sampled at the surface of the forging by machinery cutting. Samples for IGC tests and electrochemical tests were flat rectangular specimens with dimensions, respectively, $40 \times 25 \times 5$ and $15 \times 15 \times 5$ mm. The through-thickness direction of samples was the same as that of the forging.

29.2.2 Surface Treatments

Specimens were firstly polished to 1200# emery paper and then cleaned in anhydrous alcohol and distilled water. Test specimens were prepared with three different surface finishes: polishing, PEO, and PEO combined with sealing (PEO + S). PEO treatment was performed in an alkaline silicate solution (NaOH 1 g/L, Na_2SiO_3 15 g/L) with additions of $(NaPO_3)_6$ 10 g/L and $NaAlO_2$ 1 g/L. A pulsed bipolar current supply was used with frequency set at 1 kHz and current ≈ 6 A/dm^2. The temperature of the electrolyte was maintained at 20 ± 2 °C using a heat exchanger throughout the coating process. Samples were treated 1 h then took out of the electrolyte, thoroughly washed in cold running water, and ultrasonically cleaned in the anhydrous alcohol and dried. The average thickness of the PEO coating was 35 μm.

The sol used for sealing consisted of TEOS, ethanol, and distilled water (the volume ratio is 2:4:1) with adjusting the pH to 3–4 by dilute hydrochloric acid. In sealing process, PEO-treated samples were immersed in the sol after cleaning and treated with ultrasonic vibration for 1 min to exhaust the air in the film defects, forming negative pressure and inhaling the sol particles into the defects. Then, removed the sample from the sol vertically, the sample surface would be covered with a sol layer, after solidifying at room temperature for 24 h and baking at 120 °C for 1 h, a SiO_2 gel layer formed on the surface of PEO coating.

29.2.3 Corrosion Test

The corrosion resistance of specimens was examined by IGC solution immersion test. A liter IGC solution contained 30 g NaCl and 10 mL HCl (36 wt%). The ratio of specimen area to solution volume is less than 2 dm^2/L. IGC immersion tests were carried out at 35 °C for 24 h. After the IGC test, samples were immersed in dilute nitric acid to remove the corrosion products and then rinsed thoroughly with running water and dried in air. The surface corrosion morphology was recorded by photographing. A 5-mm-long part was cut out from the bottom of the sample and mounted with bakelite. The mounted samples were polished to measure the corrosion depth by optical microscopy.

29.2.4 Characterization

The surface morphology after corrosion was recorded by a camera. The composition and morphology of PEO coating were analyzed by using a JEOL JSM-6360LV SEM with EDS. Coating phase analysis were investigated using a Siemens D5000 X-ray diffractometer in a standard $\theta - 2\theta$ arrangement between $10°$ and $90°$. The coating thickness and the corrosion depth measurements were performed by optical microscopy equipped with a digital camera. Electrochemical studies were conducted in IGC solution using a PARSTAT-2273 electrochemical workstation. A standard three-electrode system with the sample as the working electrode, a saturated calomel electrode (SCE) as the reference electrode, and a platinum sheet as the counter electrode was used in the tests. Measurements were carried out in IGC solution and the exposed area was 1 cm^2.

29.3 Results

29.3.1 Characterization of PEO and PEO + S Coating

The SEM surface morphology of PEO coating was shown in Fig. 29.1a. From the SEM image, it can be seen that many micropores and microcracks exist on the coating surface. Micropores were formed by gas bubbles thrown out of microarc discharge channels. Microcracks were induced from thermal stress due to rapid solidification of molten oxide in the cool electrolyte. The existence of pores and cracks decreased the corrosion resistance of the oxide coating. SiO$_2$ sol gel treatment was employed to seal the PEO coating. Figure 29.1b shows the SEM surface morphology of sealed coating. After the sealing treatment, micropores and cracks were filled, and the coating surface was seen smoothly.

Figure 29.2 shows the SEM image of cross-sectional view of PEO coating (unsealed). The oxide coating was closely combined with the aluminum alloy substrate. Micropores and microcracks also can be seen in the cross-sectional view of the coating, and microcracks were mainly distributed in the outer layer of the coating.

Energy-dispersive spectrometer (EDS) and X-ray diffraction (XRD) were used to analyze the chemical composition and phase of PEO coating; the results were shown in Fig. 29.2. As can be seen, qualitatively, the chemical composition of the coating is mainly aluminum, oxygen, and silica. This indicated that the coating was mainly composed of aluminum oxide. The XRD spectra indicated that the oxide coating was mainly composed of $\alpha - Al_2O_3$ and $\gamma - Al_2O_3$, and the Al phase was from substrate. The oxide coating can be divided into two parts: a porous outer layer and a more compact inner layer. The inside layer mainly composed of $\alpha - Al_2O_3$, and the outside layer mainly composed of $\gamma - Al_2O_3$. The silicon existed in the silica and Al_2SiO_5 phase of oxide coating [6].
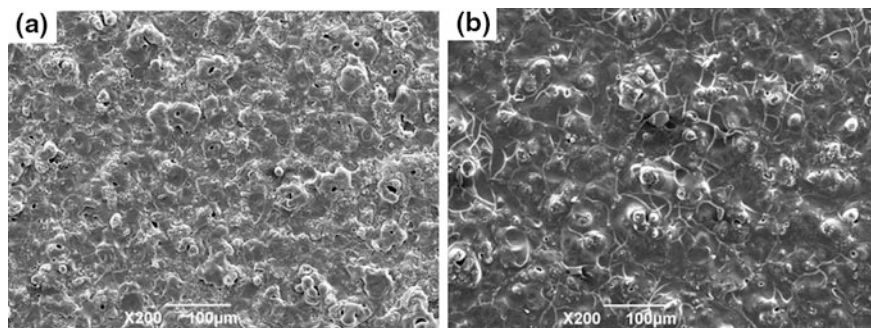
Fig. 29.1 SEM surface morphology of coatings. **a** PEO. **b** PEO + S
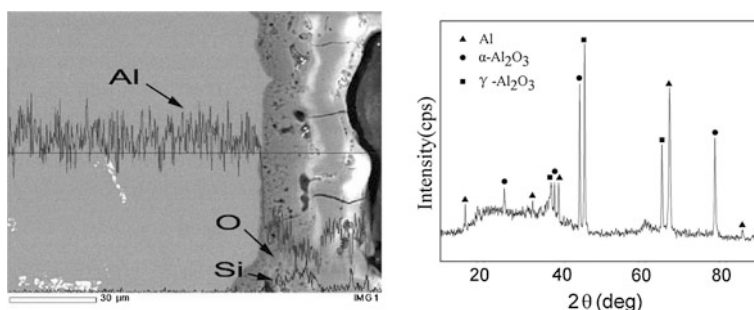
Fig. 29.2 Sectional element distribution and surface XRD patterns of PEO coating

29.3.2 Electrochemical Behavior of PEO and PEO + S Coating

The polarization curves of PEO and PEO + S coatings are shown in Fig. 29.3. Corrosion potential (E_{corr}), corrosion current density (I_{corr}), and polarization resistance (R_p) values are presented in Table 29.1. As can be seen, sealing treatment had no significant effect on the E_{corr} of coating but decreased the I_{corr} by three orders of magnitude.

29.3.3 Effect of PEO and PEO + S on IGC Performance of 7A85

When immersed in IGC solution, the polished samples reacted quickly with the solution, and a large number of bubbles were produced on the surface of samples. No corrosion reaction was observed on the surface of PEO and PEO + S samples

Fig. 29.3 Tafel polarization
plots for coatings immersed
in IGC solution at 35 °C for
30 min. **a** PEO. **b** PEO + S
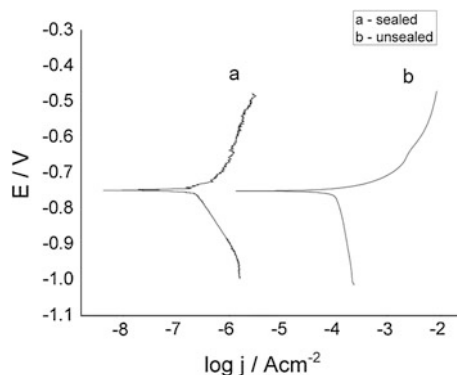
Table 29.1 Calculated Tafel parameters from PEO to PEO + S coating specimens

	E_{corr} (V)	I_{corr} (A $\times$ cm^{-2})	R_p ($\Omega \times$ cm^{-2})
PEO	−0.749	1.22E−4	1.32E+5
PEO + S	−0.740	2.28E−7	8.09E+7

at the beginning of immersion. After immersed for 1 h, the polished 7A85 base
material samples had lost metallic luster and the number of bubbles decreased. A
few bubbles began to form on the PEO coating surface, with extension of the
immersion time, the number of pores giving off gas is increasing. Then, the coating
surface began to blister, at last the PEO coating flaked off with the bursting of
blisters. No corrosion was observed on the PEO + S treated samples after
immersed for 24 h. Even extending the immersion time to 100 h, the composite-
treated samples were also not corroded. Figure 29.4 shows the surface morphology
of samples immersed in the IGC solution for 24 h. As can be seen, the surface
roughness of polished samples was significantly increased for appearance of ridges
along the rolling direction. Almost all of the coating of PEO samples was flaked
off in the corrosion test, and the corrosion morphology of the exposed base
material is the same with that of the polished samples. The immersion only
induced light discoloration on the PEO + S samples, and the coating remained
intact after corrosion test. Evaluating the severity of corrosion from surface
characteristics, corrosion sensitivity arranged from low to high, respectively, are
PEO + S samples (Fig. 29.4c), PEO samples (Fig. 29.4b), and polished samples
(Fig. 29.4a).

Figure 29.5 shows the section morphology of samples with different surface
finishes after corrosion tests. It can be seen that the corrosion of polished samples
is serious, grain boundaries network can be seen clearly, and corrosion affected a
deep zone. Figure 29.5b shows the section morphology of PEO sample with
residual coating, the corrosive solution had penetrated the PEO coating and
induced serious IGC. There is no corrosion on the PEO + S samples for the good
corrosion resistance of sealed coating.
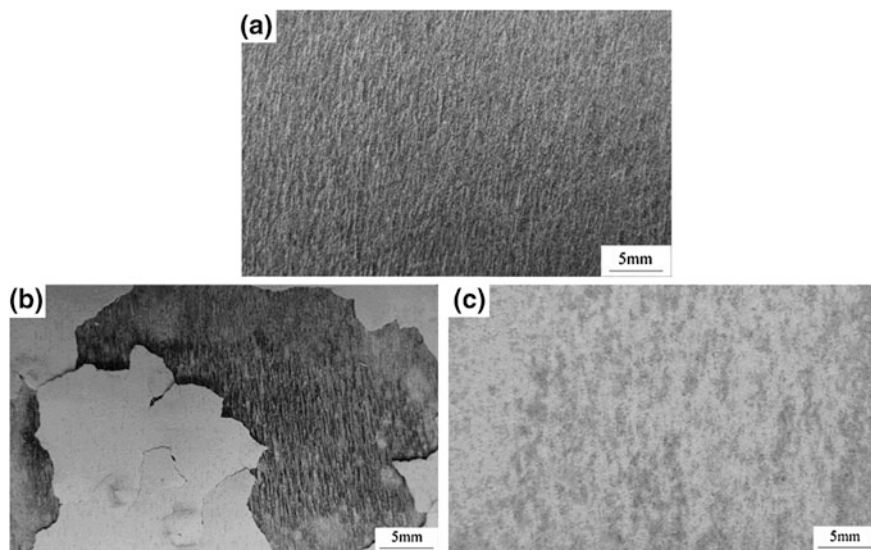
Fig. 29.4 Corrosion morphologies of samples after 24-h immersion. **a** Polished. **b** PEO. **c** PEO + S

The corrosion depth is shown in Table 29.2. The 7A85 aluminum alloy base material samples suffered serious IGC, the most corrosion depth reaches 200 μm. The PEO coating delayed the contacting of IGC solution and the base material, so decreased the corrosion sensitivity to a certain extent. The barrier layer formed by PEO and sealing composite treatment isolated the corrosion environment and the base material, so the base material was protected against corrosion. Corrosion sensitivity evaluated by corrosion depth arranged from low to high, respectively, are PEO + S samples, PEO samples, and BM samples. This is consistent with which evaluated by surface characteristics as shown in Fig. 29.3.

29.4 Discussion

29.4.1 IGC Performance of 7A85 Al Alloy

The mechanical property and corrosion performance of high-strength aluminum alloy mostly depend on the microstructure such as matrix precipitates (MPt), grain boundary precipitates (GBP), and precipitation free zone (PFZ), in which GBP and PFZ play an important role in the IGC behavior of aluminum alloy. Although the effect mechanism of GBP and PFZ is not fully understood, it has been widely accepted that the decreasing in copper content or increasing in zinc content in the GBP result in corrosion sensitivity of aluminum [7]. IGC initials at the alloy surface and extends to inner material along the grain boundaries; GBP generally
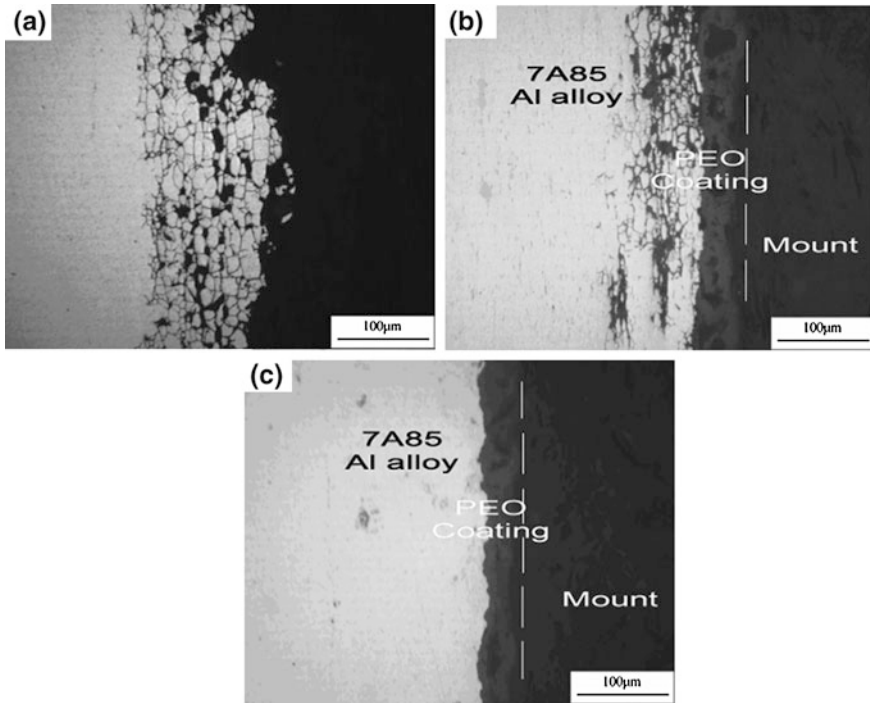
Fig. 29.5 Section morphology of the sample after IGC test. **a** polished. **b** PEO. **c** PEO + S (The *dotted lines* indicate the boundary of PEO coating and mount)

Table 29.2 The IGC depth of 7A85 Al alloy with different surface treatment

Surface treatment	Average depth/μm	Great depth/μm
Polished	176.4	200.2
PEO	108.7	116.9
PEO + S	0	0

corroded firstly as the anode. If GBP distribute continuously, the dissolution of GBP forms corrosion tunnel. The corrosion products have a larger volume than the original material and the expansion causes stresses that lift the grains, so the corrosion continually extends to the inner base material [8].

29.4.2 Effects of PEO and PEO + S on the Corrosion Behavior of AA 7A85

As shown in Table 29.1, sealing treatment had no significant effect on the E_{corr} of coating but increased the R_p by almost three orders of magnitude and decreased the I_{corr} by three orders of magnitude. This is because there are many micropores and

microcracks in the unsealed coating, so the corrosive ions reached the base material through these defects and reacted with the aluminum alloy. Corrosion current is formed by exchanging electronic between aluminum alloy and corrosive solution. The PEO coating became integrated and compact after sealing treatment and effectively protected the aluminum alloy from corrosion, so the corrosion current was remarkably decreased.

As shown in Figs. 29.1 and 29.2, many micropores and microcracks existed in the PEO coating. Micropores were formed by residual gas evolution channels during microarc process, and microcracks were resulted from thermal stress due to rapid solidification of molten oxide in the cool electrolyte. So the PEO coating have a lot of defects, when the coating is in a corrosive environment, corrosive medium will reach the aluminum alloy substrate along these defects, resulting in corrosion of the substrate. When reached the substrate, corrosive ions penetrated to the inner aluminum alloy along the grain boundaries and caused IGC of the substrate. Meanwhile, corrosive ions penetrated into the interface of PEO coating and aluminum alloy substrate, corroded the interface, and formed crevice corrosion environment. PEO coating ruptured then flaked off in the effect of bubbles produced by corrosion. PEO coating lost its protection function and aluminum substrate exposed to the corrosive solution. However, PEO coating can delay the corrosive ions reaching the substrate. Within 1-h immersion, no corrosion was observed on PEO samples, with immersion time increasing, corrosive ions reached the substrate through the defects of coating and reacted with aluminum alloy. Bubbles began to emerge from some pores on the coating surface; the number of pores producing bubbles increased with extension of immersion time. PEO coating without sealing treatment can not effectively protect the aluminum alloy substrate from IGC but lightened the corrosion by delaying the contact of corrosive medium and aluminum alloy substrate.

After the SiO_2 sol gel sealing treatment, most of the micropores disappeared and microcracks also were closed (Fig. 29.1b). SiO_2 gel layer itself has strong corrosion resistance, so the SiO_2 sol gel sealed PEO coating can effectively protect the aluminum alloy substrate from IGC by insulating corrosive medium.

29.5 Conclusions

1. 7A85-T7452 aluminum alloy is sensitive to the IGC. Severe IGC occurred with immersing in IGC solution for 24 h.
2. PEO could not effectively protect the aluminum alloy substrate for the micropores and microcracks in the coating.
3. SiO_2 sol gel sealing treatment can fill the micropores and microcracks of PEO coating and form a SiO_2 gel layer on the coating surface. The sealed PEO coating can eliminate IGC of 7A85-T7452 aluminum alloy attribute to insulating corrosive medium from substrate.

References

1. Chakrabarti DJ, Liu J, Sawtell RR et al (2004) New generation high strength high damage tolerance 7085 thick alloy product with low quench sensitivity. Mater Forum 74:969–974
2. Baruch MC, Ramat G (1974) US Patent 3,856,584
3. Wang D, Ni DR, Ma ZY (2008) Effect of pre-strain and two-step aging on microstructure and stress corrosion cracking of 7050 alloy. Mater Sci Eng 494:360–366
4. Chen S, Chen K, Peng G et al (2012) Effect of heat treatment on strength, exfoliation corrosion and electrochemical behavior of 7085 aluminum alloy. Mater Des 35:93–98
5. Asquith DT, Yerokhin AL, Yates JR et al (2006) Effect of combined shot-peening and PEO treatment on fatigue life of 2024Al alloy. Thin Solid Films 515:1187–1191
6. Curtis S, de Los Rios ER, Rodopoulos CA et al (2003) Analysis of the effects of controlled shot peening on fatigue damage of high strength aluminium alloys. Int J Fatigue 25:59–66
7. Wloka J, Hack T, Virtanen S (2007) Influence of temper and surface condition on the exfoliation behaviour of high strength Al–Zn–Mg–Cu alloys. Corros Sci 49:1437–1449
8. Mcnaughtan D, Worsfold M, Robinson MJ (2003) Corrosion product force measurements in the study of exfoliation and stress corrosion cracking in high strength aluminium alloys. Corros Sci 45:2377–2389

Chapter 30
Defects Analysis and Strategy Seeking of Automatic Test and Diagnosis System (ATDS) for Airborne Equipment

Xiaojun Chu, Shengli Luan and Qian Wen

Abstract First of all the paper describes the typical hardware structure and software platform of automatic test and diagnosis system (ATDS) for airborne equipment, analyzes main defects of ATDS which includes concentrated 19-inch rack plus single operation site not convenience to maintenance, momentary test not help to monitor the whole operating status, the confidence of test data, the problem of microwave parameters test, the choice of test path either through the unit connector or the test point on PCB, the progress of chip and data bus confuse the ATDS, and then describes the strategy and progress tendency of the future ATDS such as multi-data buses fusion ATDS, distributional ATDS and network ATDS, major synthetic ATDS, and portable ATDS.

Keywords Automatic test and diagnosis system (ATDS) · Strategy seeking · Airborne equipment · Developing tendency

30.1 ATDS Situation of Domestic Airborne Equipment

Nowadays, most of the large ATDS is based on VXI + GPIB hybrid data buses structure as shown in Fig. 30.1; meanwhile, small ATDS seems like PXI, PCI + GPIB hybrid data buses structure. The low transport speed and less amount

X. Chu (✉)
Naval Aeronautical Engineering Academy Qingdao Branch, Qingdao 266041, China
e-mail: 519464203@qq.com

S. Luan
Naval Equipment Department, Beijing 100841, China
e-mail: luanjunyue0411@gmail.com

Q. Wen
School of Information Engineering,
Nanchang Hong Kong University, Nanchang 330063, China
e-mail: wenqian511@126.com

Fig. 30.1 ATDS hardware
platform based on
VXI + GPIB hybrid data bus
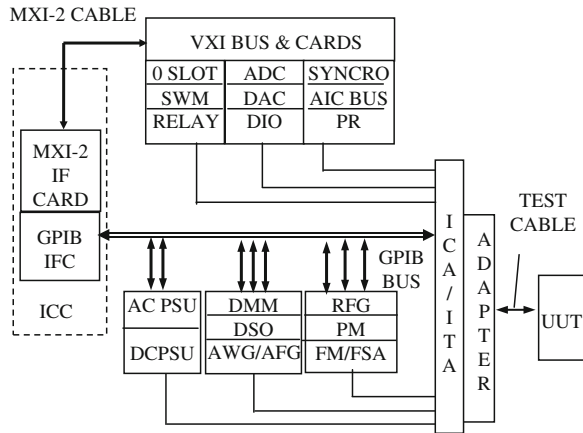
of connecting instruments cannot cover its many perfects, and cannot be replaced by VXI/PXI/PCI card instruments completely, especially for reliability and electromagnetic compatibility of GPIB microwave instruments.

In Fig. 30.1, the industrial control computer (ICC) is the ATDS manager, duty on the system configuration, instruments initiating, data process, interactive talk and the reading, processing, storing, displaying of test data. The avionic adapter provide the signal process, interface between ICA/ITA and unit under testing (UUT), in order to make different avionic devices testing under the same hardware platform. Under the control of testing software, some sources provide different signals, some instruments works on measuring state, to finish the testing procedure passing through the matrix switch, adapter and linking with UUT.

The general VXI cards include VXI-PCI-8015 "0" slot controller, E1466A matrix switch module (SWM), E1458A digital IO(DIO), E8311A pulse generator (PSG), VM7004 programmable resistor, JV53113 analog–digital convertor (ADC), JV53204 digital–analog convertor (DAC), 5310 programmable syncro, and CONDOR AIC data bus card.

The common GPIB apparatus consists of power supply (C801R AC power supply and N67000 DC power supply modules), general instruments (Agilent 33401A DMM, 54642A DSO, 33250A AWG), microwave test set (8257D RF generator, Agilent 8652 power meter, and 2393A frequency spectrum analyzer), etc.

Figure 30.2 shows the ATDS software consists of three parts: performance test platform, fault diagnosis platform, and system management platform. Test program developing environment has the following two kinds:

1. Test language based on instruments, which includes graphic programmable language such as Labview and HPVEE, text programmable language such as VC++, VB, LabWindows/CVI. Those program languages depend on the interface functions provided by instrument manufacturer and make the test procedure to face the instrument function directly, and more high requirements
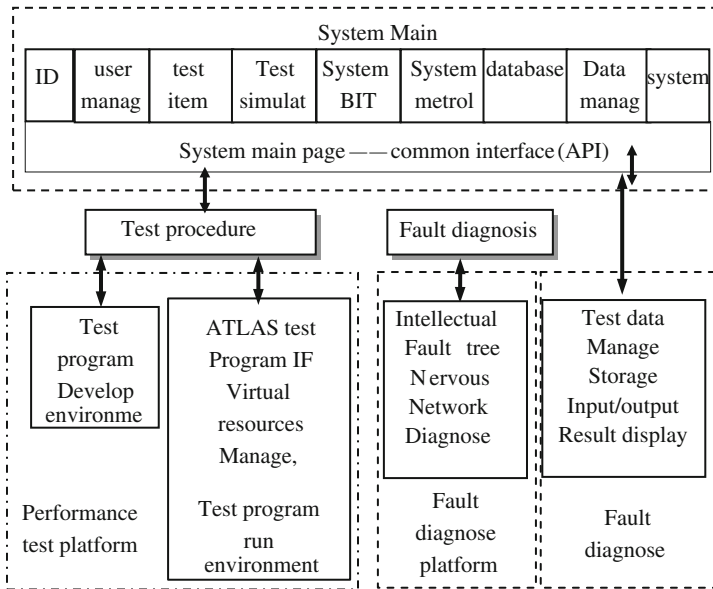
Fig. 30.2 ATDS software platform

to test procedure developer are deep understanding feature, function of those instruments [1].

2. Test language based on signal. Now, the current ATDS software platforms such as the PAWS of TYX company Usa, SMART of aerospace company France, and GPTS of EastBecon company China, all apply ATLAS program language with very highly efficient development of TPS. The most benefit is the test procedure developer need not to deep understand the inner structure of ATDS hardware platform and software platform, they only need to know the actual definition of ICA/ITA, decrease the difficult of programming, due to the test procedure face the under test signal depending on the interface function provided by software platform.

INCON is a famous intellectual fault diagnosis platform in China, which effectively combines the expert diagnosis system, ambiguous logic, and nervous network technology together. The INCON executes a fault diagnosis as follows: first, run the fault diagnosis procedure; second, get the test data from the ACCESS database; third, start the back reasoning servicer; forth, diagnose the fault by intellectual fault diagnosis platform; and finally, feedback the result to display and store.

30.2 Defects Analysis of Current ATDS

Although the ATDS has developed three generation, from special equipment ATDS to Bricks, from GPIB bus to VXI/PXI, final to LXI, many good properties are well known, but some defects also present step by step.

30.2.1 Concentrated 19-inch Rack Plus Single Operation Site Not Convenience to Maintenance

The ATDS manufactured before 2005 usually had applied three or four concentrated 19-inch racks with 2 m high plus single operation site. It is very difficult to move those racks from one airport to another aerobase; at least 3 days or 1 week has to be spent to separate and assemble. Although the ATDS beyond 2005 normally has overcome the transport maneuver problem by applied portable apparatus box, it still had no way to handle single operation site problem. When one ATDS covers all subsystems or major such as airborne communication, airborne navigation, airborne radar, ECM/ECCM, airborne power supply, EFIS and so forth, the test procedure has only been operated with serial operation mode, one by one, just because single operation site. If one ATDS takes care of several aircrafts, it seems no problem, but if there are 24 or 36 aircrafts in one airport, the conflict among different departments due to single operation site and serial test mode in very short test period is very conspicuous.

30.2.2 Momentary Test Not Help to Monitor the Whole Operating Course and Status

Nowadays, most ATDS uses momentary test method; first, the industry control computer executes test procedure, and ATDS provides various power supplies, controlling signals, input signals to airborne radar LRU passing through matrix switch, ICA/ITA, radar adapter; makes the radar LRU to work in a special mode; connects the apparatus with UUT passing through matrix switch, ICA/ITA, radar adapter; and after reading out one or some parameters, finally removes the input and controlling signals, the power supplies, disconnects the link between apparatus and radar LRU, and completes the test procedure. Such test work is single and momentary test. The airborne radar just like other avionic devices may occur fault after a operating time period due to the changing of environment reasons such as temperature, pressure, moisture, for example, RT-1401B receiver–transmitter, the SCR modulating switch breakdown after 50-min working because of the bad switch property, the transmitter cease-fire. We cannot find such fault with ATDS several times as the momentary test mode [2].

30.2.3 The Confidence Problem of Test Data

The user of ATDS usually writes the test report, fills in the equipment experience book, and diagnoses fault of the equipment depending on the test data of ATDS. The confidence of test data is concerned with the test apparatus, test environment, test method, test time, etc. and also depends on the UUT manufacturer, the product part number, the service period of UUT. If the test data conflict with the standard data provided by manufacturer, how to handle? The different test environment between the user and the manufacturer may cause the difference of test data; the different measure method between the user and the manufacturer may cause the difference of test data. For example, the telephonics company confirms that the operating frequency of RT-1401B receiver–transmitter is $9{,}375 \pm 5$ MHz, but I test one RT-1401B five times on ATDS, all test data show 9,360 MHz, is the LRU fault? Or test data fault? No problem, the LRU is new one, I can confirm the ATDS working normally by testing other LRU, the frequency deviates due to the magnetron special oscillating module. If you take the standard data $9{,}375 \pm 5$ MHz as fault judgment, there is no doubt that the RT-1401B LRU is fault [3].

30.2.4 The Test Problem of Microwave Parameters

For most engineer, microwave parameters test is troublesome, and microwave parameter for avionic devices includes average or peak transmitting power, operating frequency, spectrum of transmitting signal, phase noise or scatter clutter of local oscillator, VSWR, receiver sensitivity. In order to measure such parameters, some microwave instruments such as microwave signal generator, microwave power meter, microwave counter, frequency spectrum analyzer, and microwave network analyzer, should be used. In ATDS, microwave parameters are measured by two means: passing through ICA/ITA and passing through microwave controller.

Before 2005, most ATDS in China had measured the microwave parameters passing through ICA/ITA, which cause too much attenuating of microwave signal as shown in Fig. 30.3. RF generator, for example, the RF signal path as follows: microwave signal generator → RF cable → ICA/ITA → program control microwave switch → RF cable → ICA/ITA → RF cable → adapter → RF cable → - UUT; such RF path causes too much transmitting loss and non-enduring electromagnetic interference because the ICA/ITA is not special designing for microwave band, not designing for high power, plus too many times connection of microwave signal.

Since 2005, for most ATDS in China, microwave parameters have measured passing through microwave controller, which cause less attenuation of microwave signal as shown in Fig. 30.4. RF generator for example, the RF signal path as follow: microwave signal generator → RF cable → microwave controller (some

Fig. 30.3 Early microwave
test in ATDS passing through
adapter and ICA/ITA
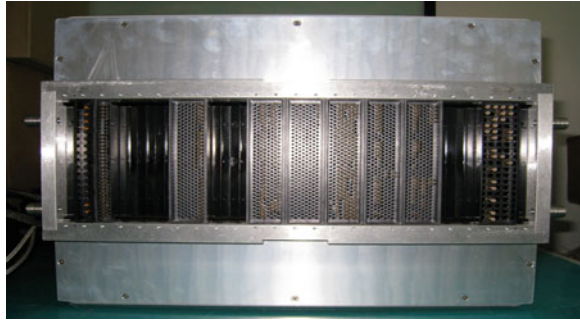
programmable microwave switches, attenuators, and dummy load inside) → RF
cable → UUT. The advantage of microwave controller is overcoming the defect
of ICA/ITA in microwave band, enhancing the performance of electromagnetic
compatibility, decreasing the loss of transmission. Due to the microwave, con-
troller is common part for communication, navigation, radar, ECM/ECCM, power
supply control, EFIS, etc., and the problems such as the connection times and the
short life of microwave switch still presents.

30.2.5 Enough for Performance Test, Less Satisfaction of Fault Diagnosis

The common feature of ATDS is enough for performance test, less satisfaction of
fault diagnosis. Two main missions of ATDS of airborne equipment are perfor-
mance test and fault diagnosis. The ATDS has enough capability to finish per-
formance testing to meet the need of 600- or 1,200-h period test work of avionic
devices of aircraft, but the fault diagnosis capability of ATDS deep depends on
that the software developer of ATDS, the familiarity of UUT, the master of fault
phenomenon, the fault law of UUT, and so forth [4].

30.2.6 Difficult Choice Between Connector Test and Open-Case Test (Board Test)

The test procedure of most ATDS for airborne equipment depends on those signals
provided by the connector of LRU, although the ATDS developer may have the
capability of ATDS to execute the open-case test, but it does not open to the user
or does not get the authorization of senior department, considering the user's
actual maintenance capability or other reasons.

Fig. 30.4 Latest microwave test in ATDS passing through microwave controller

Tell you the truth, the connector of each LRU which has serviced many years cannot provide enough information to make more effective performance test and fault diagnosis, except the new type of airborne equipment must have ATE connectors. The connector's information of old airborne equipment or inport airborne equipment cannot support effective fault diagnosis; meanwhile, open-case test or board-grade test deep depends on the user's actual maintenance capability and technical maintenance manual of avionic equipment. The advantage of ATDS is high efficient and automatic, open-case test or board-grade test must be executed by maintenance technician step by step, contrary to the advantage of ATDS [5].

30.2.7 *Chip and Bus Updating Bring New Confusion to ATDS*

With the progress of embedded computer technology and chip technology, FPGA, CPLD, ARM come to world one by one, since 1995, the synthetic processor unit of airborne radar has been designed by supper speed parallel DSP array with 64 pieces SHARC21060 or TMS320C80, each DSP has 240 pins, dual buffer memory, high-speed internal bus, plus software and hardware safety control, software rebuilding technique, etc. The updating of chip and data bus just likes the firewall between avionic equipment producer and ATDS developer. If the airborne radar designer does not open the software core of synthetic processor, what research work can the ATDS developer do is just low-level automatic test, but not high-level automatic fault diagnosis. More or less, there are something concerning to intellectual property protection.

30.3 Strategy Seeking or Progress Tendency of Future ATDS

In order to settle defects of ATDS described above, there are some strategy or progress tendency discussed as follows:
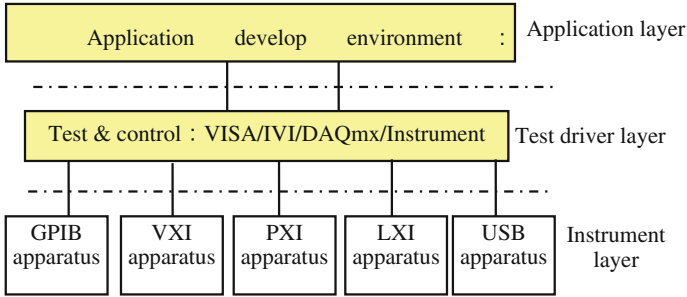
Fig. 30.5 Multi-bus fusion ATS

30.3.1 Multi-bus Fusion ATDS

Today, the ATDS based on VXI + GPIB or PXI + GPIB hybrid bus; such system structure not only applies effectively the high speed of VXI/PXI data bus, the fine integratility of VXI/PXI card instrument, but also utilizes many good test functions of GPIB apparatus.

To step toward future, Fig. 30.5 shows the multi-bus fusion ATDS, just means integrating many different data buses such as GPIB, VXI, PXI, LAN, LXI, and USB in one ATDS. If ATDS developer constructs the automatic test platform with module, opening configuration, meanwhile unites the test procedure structure, the multi-bus fusion ATDS will meet the need of the future test requirements, utilizing the advantage of different automatic test platforms based on various data bus.

30.3.2 Distributional ATDS or Network ATDS

The main difference between distributional ATDS and network ATDS is the form of network. The distributional ATDS is constructed with the independent local network, but the network ATDS is built with Internet. The network ATDS sometimes is called remote ATDS, which seems like the hospital remote diagnosis system to some extent. In recent years, several distributional ATDS or remote network ATDS has been developed in China.

Figure 30.6 gives us the distributional ATDS illustration. The distributional ATDS consists of three parts: the public apparatus and main control and management computer, various test terminals, and local network. The amount of test terminal is determined by the amount of subsystem of an aircraft, or by the amount of maintenances department in one airport.

The first advantage of the distributional ATDS is overcoming the defect of single operation site and serial test mode and increasing the efficiency of test work due to the parallel test mode. The second advantage of distributional ATDS is
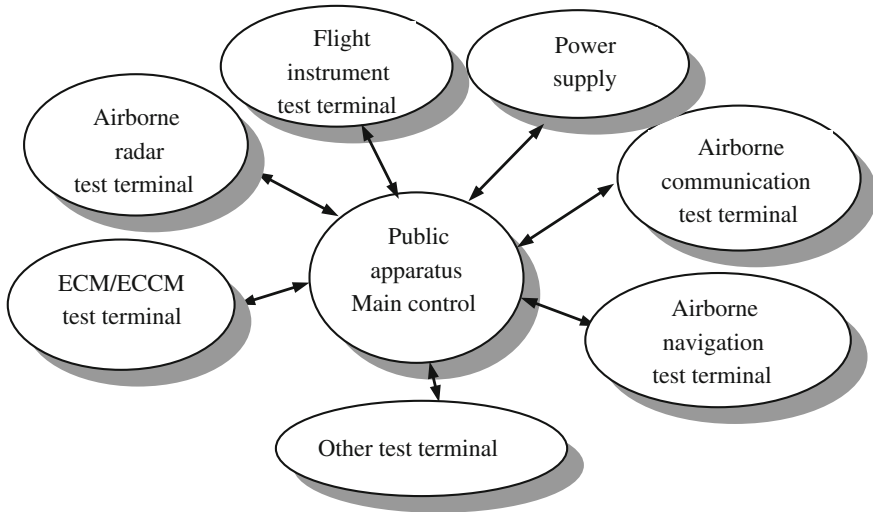
Fig. 30.6 Distributional ATDS illustration

controlling the operation mode: some test terminals working or the whole ATDS working, according to the actual situation. The third advantage of distributional ATDS is designating the apparatus location according to the test function, most of the instruments such as Agilent 33401A digital multimeter, DSO6052A digital storage oscilloscope, E8311A dual channels function generator belong to the public apparatus, special instrument like radio synthetic test set only belong to the airborne communication test terminal [6].

About the distributional ATDS and network ATDS, there are many new problems need us to pay more attention as follows:

1. the main control and management computer how to deal with the parallel test to each test terminal?
2. the public apparatus how to cease the conflict between two test terminals?
3. how to ensure the local network operating reliable? How to ensure the test procedure and proceed safety on Internet.

30.3.3 Major Synthetic ATDS

As you know, the ATDS user really do not like the concentrated 19-inch rack ATDS for the whole aircraft airborne equipment, although the least ATDS has been divided into two sets, avionic ATDS and flight control ATDS, and also applied portable apparatus box, try to overcome the defect of single operation site and serial test mode, but such a design does not fit for the actual situation in domestic.

Fig. 30.7 Portable ATDS

Fig. 30.8 Portable ATDS
software structure
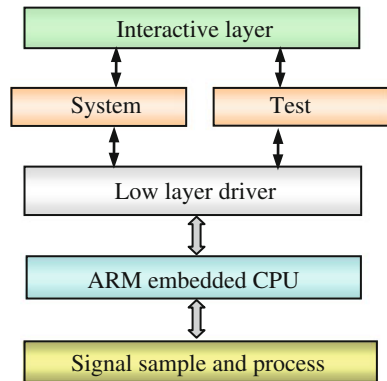
Various major synthetic ATDS, but not aircraft ATDS, should be developed because the domestic maintenance department is divided according to major, not type of aircraft. Go to a airport, you will find airborne radio rig, airborne radar rig, airborne navigation rig, airborne ECM/ECCM rig, and so on. If there are three kinds of aircrafts in one airbase, for example, transport aircraft with airborne weather radar, maritime portal aircraft with airborne pulse doppler radar, fight aircraft with airborne active phase control radar, which kind of ATDS the maintenance technician would like? The airborne radar synthetic ATDS is the best answer that has the capability to test and diagnose three kinds radar described above.

30.3.4 Portable ATDS

With the quick progress of electronic and computer technology, especially for embedded technology, the ATDS has been promoted to the evolution of minimization. Figure 30.7 shows us the portable ATDS; Fig. 30.8 demonstrates the software module layer structure. It is possible to concentrate the DMM, DSO, AFW/AWG, and FSA into one single instrument, depending on the embedded processor, plus Windows CE.net operating system, and various test cards based on USB2.0 or supper USB communication [7].

30.4 Conclusion

The defects of the current ATDS to seek the actual strategy or the tendency of the future ATDS are analyzed correctly. The tendency of ATDS is to develop the portable and major synthetic ATDS to meet the need of the field maintenance requirements and to research the multi-bus fusion ATDS, distributional ATDS or network ATDS to meet the need of the base maintenance requirements.

References

1. Chu XJ, Qu ZHB (2013) Analysis of the developing tendency of ATDS for avionic equipment. National Defense Industry Press, Beijing, pp 497–502 (in Chinese)
2. Wang Y, Shao XF, Ye LW (2011) The design and realization of airborne equipment ATS based on PXI. In: International conference on computer science and service system, 2011.06
3. Wang Y, Li SH, Shao XF (2011) The study on radar synthesis measurement technology (in Chinese). In: The 2nd international conference on mechanic automation and control, 2011.07
4. Jia ZhJ, Yan GQ, Wu GQ (2003) The developing tendency of ATE/ATDS of foreign army. Comput Autom Meas Control 11(1):1–4 (in Chinese)
5. Hu P, Li Q, Gao A, Qi SH (2002) The remote fault diagnosis system of INS based on PXI data bus. Electron Eng 67(3):31–34 (in Chinese)
6. Li BA, Li XSH (2003) The developing and key technology of automatic test system. Meas Control Tech 22(1):1–4 (in Chinese)
7. Du X, Tang DQ, Yang LCH (2003) The developing of key technology of ATDS for airborne equipment. Comput Autom Meas Control 11(1):5–8 (in Chinese)

Author Biography

Xiaojun Chu born in China Shandong Wendeng, he is a professor of Naval Aeronautical Engineering Academy Qingdao Branch and engaged in teaching and research about processing of information and simulation of radar and ATE.

Chapter 31
Strategies of Testing and Repairing Carrier-Based Aircraft Accessories

Li Ling, Wei Huakai, Zhao Xiaofang, Li Xudong and Wang Chaoyong

Abstract Carrier-based aircrafts operate on the sea all the year round, and lots of aircrafts take off from and land on the carrier. Overloaded aircrafts result in great load fluctuation of various mechanical system accessories. In addition, the phenomenon of severe corrosion exists in the atmospheric environment. The probability of accessory failures on carrier-based aircrafts is much higher than that on land-based airplanes. Since the space on the carrier is limited, it is impossible and unnecessary to move the accessory repair shop onto the carrier. With carrier-based aircrafts in service, developing a rapid accessory test and repair shelter for the carrier special use according to the characteristics of carrier-based aircrafts and providing the shelter with such functions as scientific management, software consultation, and maintenance and arbitrary combination of hardware module boxes can satisfy not only the requirement of daily carrier-based aircraft accessory test and repair but urgent need in wartime.

Keywords Carrier-based aircraft accessories · Test and repair shelter · Module box

31.1 Introduction

Carrier-based aircrafts operate on the sea all the year round, and lots of aircrafts take off from and land on the carrier. Carrier-based aircrafts employ the accurate glide landing, and they descend about 215 times as fast as land-based airplanes; therefore, their landing gears absorb more than 6 times as much vertical kinetic energy as those of land-based airplanes, and their instantaneous velocity of landing comes up to 6 m per second (as for land-based airplanes, the velocity is only

L. Ling (✉) · W. Huakai · Z. Xiaofang · L. Xudong · W. Chaoyong
Faculty of Aviation Machinery Repairing, Qingdao Branch, Naval Aeronautical Engineering
Institute, Qingdao 266041, China

3.6 m per second) [1]. The overload results in great load fluctuation of various mechanical system accessories. In addition, atmospheric environment is rather harsh, which leads to severe corrosion and threatens the proper operation of mechanical systems and their accessories. The probability of such failures as excessive pressure and oil leak of various pumps, control valves, high-pressure gas containers, oil filters, and tube joints on carrier-based aircrafts is much higher than that on land-based airplanes. Data show that one of big failures of the carrier-based aircraft, J-15, is the hydraulic system's leak and decompression during landing, which lead to the aircraft's failure to land normally. Owing to limited space, it is impossible and unnecessary to move the accessory repair shop onto carrier. Therefore, with carrier-based aircrafts in service, drawing up plans for testing and repairing aircraft accessories according to the characteristics of carrier-based aircrafts and developing a rapid accessory test and repair shelter suitable for the carrier can not only meet everyday demands for testing and repairing different aircraft accessories but also satisfy urgent need in wartime.

Statistics show that the utilization percent of aircraft equipment recovery and reuse in western countries is beyond 95 %. At present, the carrier-based aircrafts of the People's Liberation Army Navy include carrier-borne aircrafts and all kinds of helicopters. Although the aircrafts that are to land on the carrier must go through preflight inspection before and after takeoff, such failures as decompression and leak with various accessories are unavoidable. Repairing and recovering faulty accessories within shortest time and guaranteeing that operations and drills go on normally are of far-reaching significance to increasing the ratio of aircraft equipment in serviceable condition and maintaining troops' combat effectiveness [2].

31.2 Plan for Testing and Repairing Carrier-Based Aircraft Accessories

Generally speaking, carrier-based aircraft maintenance is also divided into three levels: in situ, intermediate, and depot. In situ maintenance directly performed on board is usually daily maintenance, check, minor repair, etc. The flight squadron and the aircraft maintenance squadron take charge of in situ maintenance. Intermediate maintenance is maintenance that is performed in the simply equipped repair shop on the carrier. Depot maintenance is overhaul performed in the base or the plant. The first two levels of maintenance are carried out on the carrier, and therefore, whether the maintenance capacity is a perfect match for the quantity of carrier-based aircrafts should be considered.

31.2.1 Requirements of Testing and Repairing Carrier-Based Aircraft Accessories

Testing and repairing aircraft accessories are inspecting and correcting faulty accessories as well as periodically checking accessories and testing their performance, mainly including disassembling, cleaning, testing and repairing, and assembling and adjusting accessories [3]. All these are performed by the intermediate maintenance station on the carrier.

The carrier has just seen service, and the carrier-based aircraft maintenance is basically of the plant's follow-up service. It is imperative that the department in charge of the carrier-based aircraft maintenance draws up plans for rapid aircraft accessory test and repair and build the corresponding system.

31.2.2 Conception of Rapid Carrier-Based Aircraft Accessory Test and Repair Shelter

Carrier-based aircraft maintenance involves airframes, accessories, engines, electronic equipment, weapons, etc., and corresponding repair shops need to be set up according to division of labor. For carrier-based aircrafts, accessories include relevant accessories in the following mechanical systems: hydraulic (pneumatic), control, tank-off and landing, fuel, etc. It is necessary to build the system of rapid aircraft accessory maintenance in accordance with the characteristics of these mechanical systems, which can not only meet the requirement of in situ maintenance but also save the space intermediate maintenance occupies on the carrier.

Based on the tentative idea of rapid maintenance and saving precious space on the carrier, we research into the rapid test and repair shelter for maintaining mechanical system accessories of carrier-based aircrafts (for short, rapid carrier-based aircraft accessory test and repair shelter) [4]. The shelter combines test with repair: The repair submodule box in the shelter can be separately brought on the aircraft to carry out in situ maintenance, and the test and repair of mechanical system accessories can also be accomplished in the repair shop on the carrier.

31.3 Function of Rapid Carrier-Based Aircraft Accessory Test and Repair Shelter

Using common failures of various accessories on land-based military aircrafts and considering characteristics of carrier-based aircraft takeoff and landing and severe sea erosion, we define the rapid accessory test and repair shelter should have the following functions.

31.3.1 Function of Scientific and Effective Management

The whole management course employs the 6S methodology, which refers to sorting, setting in order, systematic cleaning, standardizing, self-discipline, and security.

Sorting
Go through all tools, materials, and so forth in the work area. Distinguish between necessary items and unnecessary items. Keep only essential items and eliminate what is not required.

Setting in order
Arrange essential items and keep them in easily accessible places.

Systematic cleaning
Clean the work area and keep it clean, tidy, and organized.

Standardizing
Keep the state of the work area after the above three phases. Standardize the procedures and improve continuously.

Self-discipline
Ensure disciplined adherence to rules and procedures.

Security
To prevent accidents, attach importance to safety education and create a safe production environment.

31.3.2 Software Consultation and Maintenance

The procedures and regulations for testing and repairing different kinds of typical accessories need to be developed, which mainly include the computer expert consultation management system, the maintenance regulations for accessories of different specific aircraft types, and techniques of repairing accessories and repairing technique cards (ready) [5]. In the computer expert consultation management system, aiming at the problems and failures of accessories, the corresponding software inquiry mechanism is built, which includes cases and reference schemes of correcting previous failures and the external expert advisory system The accessory maintenance regulations include requirements for in situ and dislocated accessory test and repair. The content of the software can rely on the support offered by the plant and the repair experiences provided by land-based troops, and it further needs accumulating and expanding in the course of carrier-based aircraft accessory maintenance.

31.3.3 Combination of Hardware Module Boxes

1. Develop a small synthetical hydraulic accessory test stand for carrier-based aircrafts special use, which is mainly used to check hydraulic (cool air) accessories after testing, repairing and assembling, and test the performance of accessories.
2. Develop a portable accessory grinding and repairing box for carrier-based aircrafts special use. In the box, there are accessory repairing and grinding tools, plane grinding tables, grinding paste, and grinding fluid.
3. Allocate a portable hydraulic repair emergency box. The box contains seal rings commonly used in hydraulic systems, tubes, flat nozzles, sleeve nuts, and so on. The emergency box can also be used in the in situ maintenance.
4. An equipment box for nondestructive inspection. The box mainly contains handheld eddy current flaw detectors, magnetic powder flaw detectors, etc.
5. Rapid oil contamination detection and analysis instrument. Allocate necessary oil detection and analysis equipment which can determine the oil contamination level through real-time oil monitoring and predict failures of hydraulic system accessories.
6. Allocate a general toolbox. The toolbox contains worktables, vices, bench drills, leveling blocks, multi-meters, etc.
7. Allocate a specialized toolbox according to the aircraft type. The toolbox contains spanners, pliers, screwdrivers, hammers, files, all kinds of fuses, etc.
8. A common accessory spare part case. In the case, there are carrier-based aircraft accessories that may be used to replace faulty parts on the carrier, such as oil filters, valves, switches, safety valves, etc.
9. A corrosion repair toolbox. Since carrier-based aircraft accessories are in harsh environment, corrosion resulting from sea and air is a problem of particular concern in accessory maintenance.

   (1) Corrosion inspection tools

Portable endoscopic testers; triple prisms or crazing testers; stub brushes; industrial alcohol; silk cloth; reflectors; diode flashlights; others.

(2) Corrosion repair tools

Nonmetallic scrapers (made of wood chips, bamboo chips, bakelite or plastic boards); metallic scrapers; hard metal (like steel sheets) and soft metal (aluminum sheets); sand paper (cloth) of various precision numbers, sand paper (cloth) of different abrasives; abrasive paste, leather, flannelette, cotton cloth; chromium oxide polishing paste, cloth wheels, a polishing machine; quartz sand, corundum sand, a sand-blasting chamber, an air compressor; glass beads, steel shots.

31.4 Conclusion

Aiming at the daily carrier-based aircraft flight drill and the urgent need in wartime, referring to the practical experience of the Naval Air Force repair shops and airfields and the carrier-based aircraft maintenance ideas of western developed countries, developing a modern shelter, which employs scientific management, complete software, and comprehensive hardware, and can rapidly test and repair accessories of carrier-based aircraft mechanical systems adapts to the urgent development of the Navy carrier-based aircrafts. Developing the shelter will have far-reaching and great significance to building and improving the two-level carrier-based aircraft maintenance system and the rapid and effective accessory maintenance.

References

1. Wang W, Chen M (2012) Thought on establishment and characteriscs of deck-landing aircraft support system. Trainer AVIC 22(1):60–63 (in Chinese)
2. Feng Q, Ceng S, Kang R (2010) Multiagent-based modeling for integrated logistic support of the carrier aircraft. Syst Eng Electron 57(1):212–215 (in Chinese)
3. Li L, Zhao H, Wang G (2013) Frequently problem and replace about typical attachment seal ring of a certain of aircraft. Hydraulics Pneumatics Sesls 23(6):78–80 (in Chinese)
4. Xu T, Zhenyu S, Peng X, Chen F (2012) Analysis of carrier-based helicopter's flight material maintenance model. Value Eng 33(2):113–114 (in Chinese)
5. Zhang H (2010) Review of research on ship integrated logistics support. Ship Sci Technol 46(2):128–132 (in Chinese)

Chapter 32
Moisture Absorption and Desorption Behavior of Composites in Cyclic Hygrothermal Environment

De Wang, Ping Jin and Xiaoming Tan

Abstract The moisture absorption and desorption behavior of CCF300/BA9916 composites in cyclic hygrothermal environment was investigated. The experiment was performed for 70 °C/100 % RH, to find out moisture absorption as a function of time. The results show that the moisture absorption and desorption behavior of CCF300/BA9916 composites basically conforms the Fickian's second law. After 36 days of moisture absorption, the composites reach the effective moisture equilibrium level, and the effective moisture equilibrium content is about 0.849 %. Hygrothermal environment destroys the interface of fiber and matrix; moisture absorption has reversible and irreversible destructive effect on CCF300/BA9916 composites. Reversible damage on fiber/matrix interface can be eliminated after desorption processing, while the irreversible damage still exists.

32.1 Introduction

Carbon fiber-reinforced polymer composites (CFRP) have been increasingly used in aviation components during the past decades due to their attractive properties. In particular, the low density, high strength, high stiffness-to-weight ratio, excellent durability, and design flexibility of fiber-reinforced polymers are the primary reasons for their use in many structural components in the aircrafts [1]. The composite materials applied in aviation components not only suffered the effect of complicated fatigue loading, but also are affected by the interaction of temperature and humidity. The mechanical properties of CFRP composites may deteriorate

D. Wang (✉) · P. Jin · X. Tan
Siliu Middle Road No. 2, Qingdao 266041, China
e-mail: wd_chzh@163.com

when exposed to moisture environment for a long period [2]. The presence of moisture within a polymer composite can lead to significant changes in the physical and chemical characteristics of the polymeric matrix. Deformation in laminated composites can occur because of changes in temperature and the absorption of moisture. This is known as the hygrothermal effect [3–5]. Moisture absorption in the polymer matrix of a composite material can sometimes exert a greater influence on composite mechanical properties. The main mechanism of moisture behavior in CFRP composite materials is water diffusion, which is dependent on environment temperature and relative humidity [6–9].

Feng [10] has investigated the cyclic moisture absorption and desorption behavior of CCF300 carbon fiber/5405 bismaleimid composites immersed in 71 °C distilled water. The results show that the moisture absorption behavior of CCF300/5405 composites basically conform the Fickian's second law. After 14 days of moisture absorption, the composites reach the saturated moisture level, and saturated moisture uptake is about 0.66 %. Additionally, after cycles of moisture absorption process, the interface between fiber and matrix is damaged by moisture, which leads to a large number of voids and cracks. As a result, water diffusion coefficient increases significantly and saturated moisture uptake rises slightly. Furthermore, the damage is irreversible even after the moisture desorption.

Jiang et al. [11] studied the moisture diffusion process of pultruded FRP composites. By gravimetric experiments, the moisture absorption was obtained as the function of exposure time under four aging conditions. Based on the one-dimensional moisture diffusion theory, the moisture diffusion coefficients of FRP composites under different aging conditions were identified by the best least-square curve fitting to the experimental data. The obtained results indicated that high temperature can speed up the moisture diffusion rate, and the moisture equilibrium contents were mainly governed by the humidity of aging environment. The moisture desorption tests of FRP composites were conducted to investigate the contribution of polymer relaxation and mass loss phenomenon.

In this paper, the moisture absorption and desorption behavior of CCF300/BA9916 materials in cyclic hygrothermal environment was investigated. According to ASTM D5229 [12], the experiments were performed for 70 °C/100 % RH, to find out moisture absorption as a function of time. The effect of moisture absorption and desorption behavior on CCF300/BA9916 materials was studied for the development and maintenance of aircraft structures.

32.2 Experiment

32.2.1 Materials

CCF300/BA9916 composite laminates were prepared for moisture absorption experiments; all specimens were cut in the dimensions of $60 \times 60 \times 2$ mm.

32.2.2 Moisture Absorption

The moisture absorption of CFRP materials was measured according to ASTM D 5229 (2004). Specimens were dried in a vacuum oven at 80 °C until a constant weight was achieved. Then, they were immersed in distilled water at 70 °C. During the wet time, specimens were periodically taken out of the chamber, wiped dry with tissue paper, and weighed using an analytical balance having a precision of ±0.1 mg. The weights of the specimens were measured as a function of time. Specimens were allowed to cool down for a short period of time before weighing. The effect of removing the specimens from the chamber for a short period of time on the measurement of weight gains was seen to be negligible. This procedure was repeated day by day until the limit of saturation (constant weight) was reached.

The percent moisture content M_t is defined as

$$M_t = \frac{W_t - W_i}{W_i} \times 100 \ \%$$

(32.1)

where W_t is the weight of moist material and W_i is the weight of dry material.

Specimens were dried in a vacuum oven at 80 °C until a constant weight was achieved. During the wet time, specimens were periodically taken out of the chamber and weighed using an analytical balance. The same processing is performed for the next cyclic moisture absorption and desorption.

32.3 Results and Discussion

32.3.1 The Long-Term Absorption

Most of the studies on moisture diffusion in FRP composites rely on one-dimensional Fickian process, whose equation is expressed as

$$\frac{\partial c}{\partial t} = D \frac{\partial^2 c}{\partial^2 x}$$

(32.2)

where c represents the moisture concentration; x is the space coordinate measured parallel to the diffusion; and D is the moisture diffusion coefficient in the x direction.

According to Shen [13], the percent moisture content M_t

$$M_t = M_m\{1 - \exp[-7.3(Dt/b^2)^{0.75}]\}$$

(32.3)

where M_m is effective moisture content and b is the plate thickness.

Fig. 32.1 The dimension of
CCF300/BA9916 composite
specimens
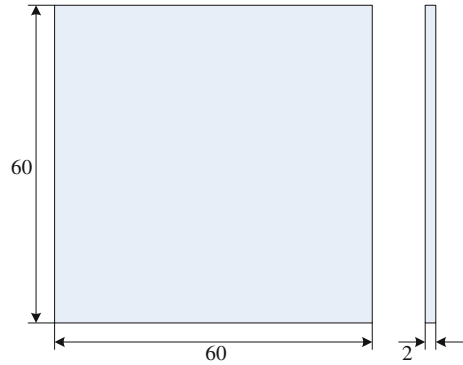
Diffusivity values for all specimens were calculated, using the equation

$$D = \pi \left(\frac{b}{4M_m} \right)^2 \left(\frac{M_2 - M_1}{\sqrt{t_2} - \sqrt{t_1}} \right)^2 \tag{32.4}$$

where M_1 and M_2 are moisture contents at times t_1 and t_2.

Figure 32.1 shows plots of % moisture absorption versus square root of time in hours for test specimens of CCF300/BA9916 composite laminates conditioned at 70 °C/100 % RH. After 36 days of moisture absorption, the composites reach the effective moisture equilibrium level, and the effective moisture equilibrium content is about 0.849 %. The nature of the curves indicates a Fickian diffusion pattern for the initial portion and thereafter remains concave to the time axis until maximum moisture content is reached. Generally, Fickian diffusion takes place at low temperatures and for materials exposed to humid air. Deviation from Fickian behavior occurs at elevated temperature and for materials immersed in liquid. Hence, Fickian diffusion is a reasonable approximation in this case, which is evident from the figure.

In Fig. 32.2, we can see that CCF300/BA9916 composite materials attended to its effective moisture equilibrium state after 36 days; hence, the following experiments were all immerged in 36 days for moisture absorption.

32.3.2 Cyclic Moisture Absorption

Figure 32.3 shows that the cyclic moisture absorption experiments data and the fitted curves. It is found that the material still obeyed Fickian's second law after cyclic moisture absorption, while the initial linear slope of the curves rises a little, which means that the velocity of water diffused in composite materials ascends too. In Table 32.1, the diffusion coefficients and effective moisture content were gained.

Fig. 32.2 The long-term moisture absorption curve of CCF300/BA9916 composites
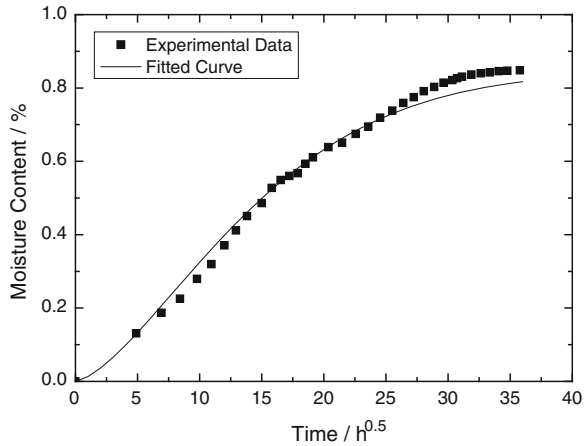
Fig. 32.3 Moisture absorption curves of CCF300/BA9916 composites with different times of cycles
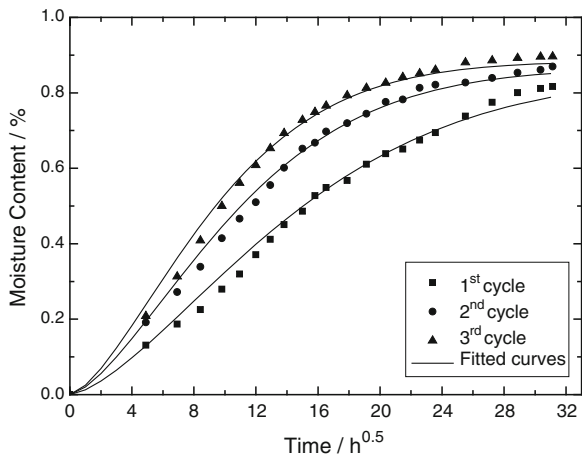
Hygrothermal environment destroys the interface of fiber and matrix; moisture absorption has reversible and irreversible destructive effect on CCF300/BA9916 composites. Reversible damage on fiber/matrix interface can be eliminated after desorption processing, while the irreversible damage still exists.

32.3.3 Cyclic Moisture Desorption

In desorption process, the initial moisture content is M_m and the final content is almost zero.

$$M_t = M_m \exp[-7.3(Dt/b^2)^{0.75}] \tag{32.5}$$

Table 32.1 Saturated moisture uptake and moisture diffusion coefficient during cyclic hygrothermal aging of CCF300/BA9916 composites

Times of cycles	Saturated moisture uptake/(%)	Diffusion coefficient/(mm^2/h)
1st	0.849	0.0011
2nd	0.871	0.0019
3rd	0.884	0.0025

Fig. 32.4 Moisture desorption curves of CCF300/BA9916 composites with different times of cycles
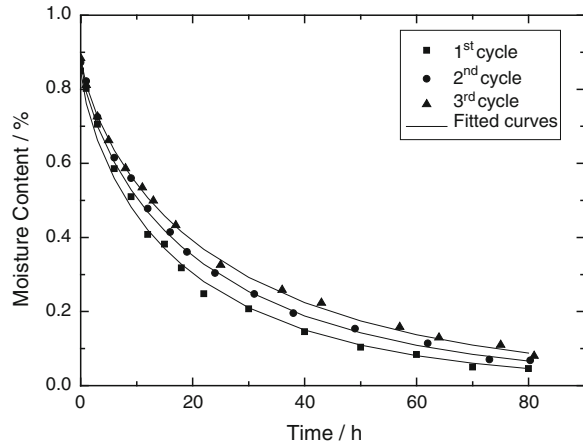
The cyclic moisture desorption experiment data and the fitted curves are shown in Fig. 32.4. Desorption coefficients are nearly same, which means that destruction of composite material interface has maxim after the first moisture absorption and desorption process.

32.4 Summary

1. Moisture experiments were performed in at 70 °C/100 % RH. After 36 days of moisture absorption, the composites reach the effective moisture equilibrium level, and the effective moisture equilibrium content is about 0.849 %.
2. The moisture absorption and desorption behavior of CCF300/BA9916 composites basically conforms the Fick's second law.
3. Hygrothermal environment destroys the interface of fiber and matrix; moisture absorption has reversible and irreversible destructive effect on CCF300/BA9916 composites. Reversible damage on fiber/matrix interface can be eliminated after desorption processing, while the irreversible damage still exists.

References

1. Du S (2007) Advanced composite materials and aerospace engineering. Acta Materiae Compositae Sinica 24(1):1–12 (in Chinese)
2. Xuemei H, Xiaojie W, Lihong Y (2006) Study on hygrothermal properties of ce/ep/cf composites. Eng Plast Appl 34(5):49–51 (in Chinese)
3. Imaz JJ, Rodriguez JL, Rubio A (1991) Hydrothermal environment influence on water diffusion and mechanical behavior of carbon fibre/epoxy laminates. J Mater Sci Lett 10(11):662–665
4. Guo M, Yan Z, Ling X (2002) Study on hygrothermal ageing mechanisms of aerospace structural composites. Aerosp Mater Technol 32(4):51–54 (in Chinese)
5. Zheng L, Chang XL, Zhao F (2007) Research on moisture absorption of composites in the hydrothermal environment. J Mol Biol 24(2):37–39 (in Chinese)
6. Li J (2010) Moisture absorption and soaking deformation of fiber reinforced resin composites. Spacecr Recovery Remote Sens 4:69–71 (in Chinese)
7. Zhang AY, Zhang D, Li D et al (2011) Advances of hydrothermal property study of carbon fiber reinforced epoxy laminates. China Mech Eng 22(4):494–498 (in Chinese)
8. Sun L, Huang Y, Wan Y et al (2007) Finite element analysis of moisture distribution within carbon fiber reinforced epoxy composite. Ordnance Mater Sci Eng 30(4):5–8 (in Chinese)
9. Zhang L, Zhao Y, Luo Y, Duan Y (2012) On the interfacial properties of ccf300/qy8911 composite with cyclical hygrothermal treatments. J Mater Eng 2:25–29 (in Chinese)
10. Feng T, Zhao Y, Luo Y et al (2010) Effect of cyclic hygrothermal environment on interfacial property of ccf300/bmi composites. J Beijing Univ Aeronaut Astronaut 36(12):1427–1431 (in Chinese)
11. Jiang X, Kolstein H, Bijlaard FSK (2012) Moisture diffusion and hygrothermal aging in pultruded fibre reinforced polymer composites of bridge decks. Mater Des 37:304–312
12. American Society for Testing and Materials (2004) ASTM D5229, PA: ASTM International
13. Shen CH, Springer GS (1976) Moisture absorption and desorption of composite materials. J Compos Mater 10(1):2–10

Chapter 33
Study on Aviation Objective Examination System Development and Construction

Shouquan Wang, Shuhua Li, Dong Xia and Jian Ren

Abstract Aviation objective examination system is based on objective data recorded, which provide technical support for people to discover and correct the practice of aviation science biases and guide weapons and equipment scientific use and maintenance. Development of this system improves the air force's capability to combat and support, but there are still problems of independent data recording methods, low accidental survival rate, and bad data integration applicating effect, and therefore, various flight data collection, transmission, and application need to be considered to build a comprehensive aviation objective examination system and promote the scientific development of aviation flight training.

Keywords Objective examination system · Integrated collection · Real-time transmitting back · Data applications

33.1 Introduction

Over the past decade, with the rapid development of airborne aero parameters, video-recording, and other means of objective data collection, people increase their capacity of interpretation and application of various types of flight data gradually, which played an important role in the safe flight guarantee, faults diagnosis, and postmortem analysis and improved the air force's capability to combat and support greatly. But parameters of collected data were not all side, recording means were independent, the accidental survival rate was low, judgment

S. Wang
College of Automation Engineering of NUAA, Nanjing, China

S. Wang · S. Li · D. Xia (✉) · J. Ren
Qingdao Branch of NAAU, Qingdao 266041, China
e-mail: sheldondonne@gmail.com

reaction time was poor, and application software was outdated, which make objective recorded data cannot play its role adequately, and some analysis of difficult problems cannot achieve the accurate and objective conclusions. Some "deviations" exposure repeatedly, limiting the improvement of equipment quality and enhance of the combat effectiveness. So people require breaking the traditional concept, building a comprehensive aviation objective examination system, taping the record data performance fully, and discovering and correcting deviations in time.

33.2 System Definition

Aviation objective examination system is total name of equipments that can complete the flight information objective recording, faithful playback, effective assessment, and long-term monitoring, which include the airborne equipment and (ship) ground equipment [1]. The system, based on record objective fact, using performance indicators and technical requirements as the criterion, and using the information interpretation, statistics, and the depth excavation as means, provides technical support for people to discover and correct the practice of aviation science and guide the development of weaponry, scientific use, and maintenance. Objective examination system has the features of opening concept, systems compatibility, and scalability. The structure is shown in Fig. 33.1, in which the task data collection and recording system such as traditional flying parameters, audio and video, as well as possible future similar data collection tools, together with equipment and software of supporting information delivery, processing, analysis and management, all belong to the category of objective examination system.

33.3 Development History

Human aviation history is a developing history of correction process of aviation science and practice activities. With the advancement of science and technology and frequent human aviation activities, objective examination system, flying parameters as the representative, appeared to correct deviation of the aircraft accurately and timely in the phase of design, manufacture, repair, maintenance, and use [2]. Since more than half a century, as new technologies, new materials, and new techniques have been applied, objectively, record information has been increased, while timeliness of data applications is enhanced. Flying parameters and other objective examination system has experienced the development from simple to complex, from artificial to intelligence, from discrete to integrated, and from without to higher anti-damage ability, providing strong support to corrective work in aviation science and practice activities.
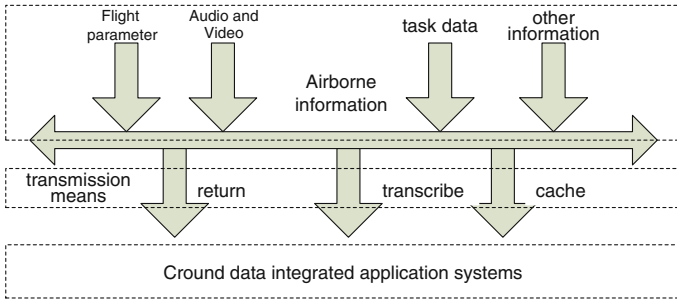
Fig. 33.1 Constitution of aviation objective inspection system

33.3.1 Collecting and Recording Equipment's Developing Process: From the Simple to the Complex, and from Discrete to Integrated

Flight accident investigation is the extreme behavior in correcting deviations of aviation science practice. Flying parameters system abroad was developed in the 1940s to make identification of causes of accidents easier and more accurate and to prevent similar problems from happening again. At present, the parameters recorded by the system have been grown to thousands from the initial five, while the recording medium from the foil, tape to solid state and its enhanced type, and the protection of recorder against crash performance develop from the initial unprotected capacity to strong protection capability (meet TSO-C124b crash test standards, strong anti-impact ability no less than 5,100 g/5 ms); sources of signal collection shift from shared sensors, independent sensors, to the bus mode; redundant design is strong and extends from device level to the extension level.

To check the effect of combat training, in the 1950s, the airborne gun camera began to appear in the United States and the Soviet Union, recording the shooting effect of aviation weapon by film. Traditional gun camera is restricted by interpretation environment, with existing problems such as low accuracy and poor reliability. With the development of the civil camera and video-recording technology and the constantly improving image information real-time acquisition and real-time compression processing algorithm, video-recording system gradually replaced the airborne gun camera; it is from analog to digital, and its record information is also increasing. At present, it can complete the recording of outside sight in front of plane nose, multi-channel videos such as the head-up display and the below display in cockpit and audio information in the plane at the same time, and plays a very important role in judgment and analysis of combat training effectiveness; it is extremely beneficial for improving the quality and technical level of pilot training and has become an important information-recording device of modern aircraft.

In order to meet the requirement of research and testing fault location of avionics, the discrete data-recording device that is installed in various electronic devices emerged in the 1960s, with the avionics bus technology; these recording devices have been used to record the work of the entire avionics system from discrete devices to integrated. Since the recording substantial have increased greatly and all kinds of information closely related, these bring great convenience to the research and testing and troubleshooting and use judgment of airborne electronic equipment and gradually used to monitor the performance of these devices, such as the objective examination system of Russian Su-30 aircraft, which can achieve comprehensive record of information such as a fire control, weapon control, electronic warfare, communication navigation, flight control, and recording parameters are more than 7000.

33.3.2 Information Transfer Means Changing from Artificial to Intelligent, Afterward to Real-Time

Artificial to intelligent refers to the change from artificial data download and transfer to with network automatic control; the shift afterward to real-time refers to the change from downloading and transferring flight data to delivering and receiving flight data while flying at the end of the flight or at the moment of the accident.

The effectiveness of the flight data from collecting and recording layer to data application layer is the precondition of the flight data role. Taking the flight parameter system for example, first you need to open the protection recorder to unload the data, so flight parameters can be took down only after the accident while flying, which was used in correcting deviation through the accident investigation. In the late 1990s, there was a field detection equipment; it could download the flight parameters onboard, but due to the slow download speed, it could only be downloaded every once in a while. At the beginning of the twenty-first century, there were a handheld unloader and a cache recorder, which greatly improve the speed of data uninstalling and could realize the downloading data of every flight, because it can be used for checking problems and correcting deviation after every flight; flight parameters have become an important basis about whether the plane can fly or not. With the wide application of the wireless data transmission means, flight data real-time transmission is realized, which makes people have the conditions for real time correcting deviation of flight.

Western developed countries pay much attention to real-time flight data transmission and application. The US military used the then relatively mature shortwave, FM digital communication technology to carry out real-time transmission of objective record data in the early 1970s, which was initially used for air traffic control and was later gradually improved. With the advances in satellite, radio communication, network technology [3], the US military has formed an objective record data transmission system that is based on satellite

communications mainly, and broadband digital communications supplemented after 40 years of development. In the 1990s, ICAO started using UAT aeronautical mobile satellite communication data link in air traffic control and monitoring information over the transocean, polar, and desert. In order to ensure real-time monitoring and security tips of flight status, France air aircraft mandatorily install satellite communication systems on international routes and real return flight data currently.

33.3.3 Data Management and Application Developing from Separated to Integrated, the Single to the Comprehensive

In order to realize data processing and reappearance, the purpose of recording flight data is to provide the basis of analysis and research for people, so that it can make the correct conclusion for various judgments. Therefore, at the beginning of the design of recording system of flight parameter, video, and mission data, the corresponding data analysis software has been manufactured simultaneously. With the improvement of the aviation objective examination system, the type and amount of recording data has increased dramatically, people gradually realize that it contains useful connection among the data information, and demand for integrated application of various data increases while depth expands. The requirement of software turns higher and higher, and more attention has been paid to the construction of bundled software, data management develops from separated to integrated, the application of data changes from single to comprehensive, and integrated application of ground data system arises at the historic moment. Western developed countries use data mining and data fusion technology to deal with and analyze these huge amounts of data on the basis of achieving comprehensive analysis of the objective recording data, to build technical files of controllers, pilots, and aircraft and engine through the complete data statistics methods, which provide data support for flight training, equipment maintenance, service equipment improvement and new equipment development.

33.4 Construction Direction

33.4.1 Flight Data Management Recorder System

Currently, there has been flight data management recorder system (referred as FDMRS) in the Western developed countries, and it was applied to the fourth-generation fighter. The system is a synthesis of all the work-related data records in existing aircraft avionics to achieve a comprehensive acquisition, storage,

transmission, processing of all flight data, and management and utilization of information. The specific composition shown in Fig. 33.2, where the data analysis control unit includes a data management computer (DMC), flight data acquisition processing unit (FDAU), engine parameters acquisition processor (EDAU), real-time communication transmission system (CTS Interface), airborne data transmission systems (DTS Interface), the aircraft intercom system interfaces, airplanes, ground communication interface, BIT information display unit, and the auxiliary data acquisition unit (ADAU). Flight data recorder management system has improved aircraft faults' location function and real-time analysis of aircraft flight status based on collected data. If faults appear, it will alarm, show the fault level, and provide countermeasures [4]. Grasping quiver and overrun can be detected through engine monitoring and processing in order to find early faults [5]. The damage of aircraft and engine may be found through surveillance to the health status of the aircraft. In this technology field, the United States, Britain, France, and Russia all use the relevant flight data multi-information management recording technology in their development of advanced new-generation military and civil aircraft and pay much attention to its use and technological development.

33.4.2 Construction Plan

Based on learning design concept of Western countries, and adopting mature domestic technology with flying parameters system construction achievement, aviation objective examination system construction constitute construction plans from five aspects "build, training, use, management, and protection," in order to improve the flight data survival rate and the quality of record data, carry out an integrated application of all kinds of flight data acquisition, promote the construction of flight data real-time return as the main means, satisfy flight data using needs of air and ground, play the correcting role of flight data fully, deepen the design of research aircraft health management system through flight data real-time applications, and ultimately achieve an integrated application of objective record data on the machine. To achieve the above goal, there are three stages to carry out:

Stage one: New flying parameter protection recorder must be added to active aircrafts and aircrafts in making, in order to improve data survival probability in an accident as well as follow the new national military standard requirements timely.

Stage two: Flight parameter system of active aircraft needs to be renovated, technical specifications and standards would be published, and competition mechanism needs to be introduced. All kinds of flight data should be recorded with a universal means of a more comprehensive and accurate device, in order to achieve comprehensive realization of machine information collection of the third-generation machines. According to different flight subjects and different evaluation purposes, combinations of data of different configurations should be returned with low dependence on wideband wireless communication for the real-time flight data transmission applications. Automatic multi-level group net technology is adopted
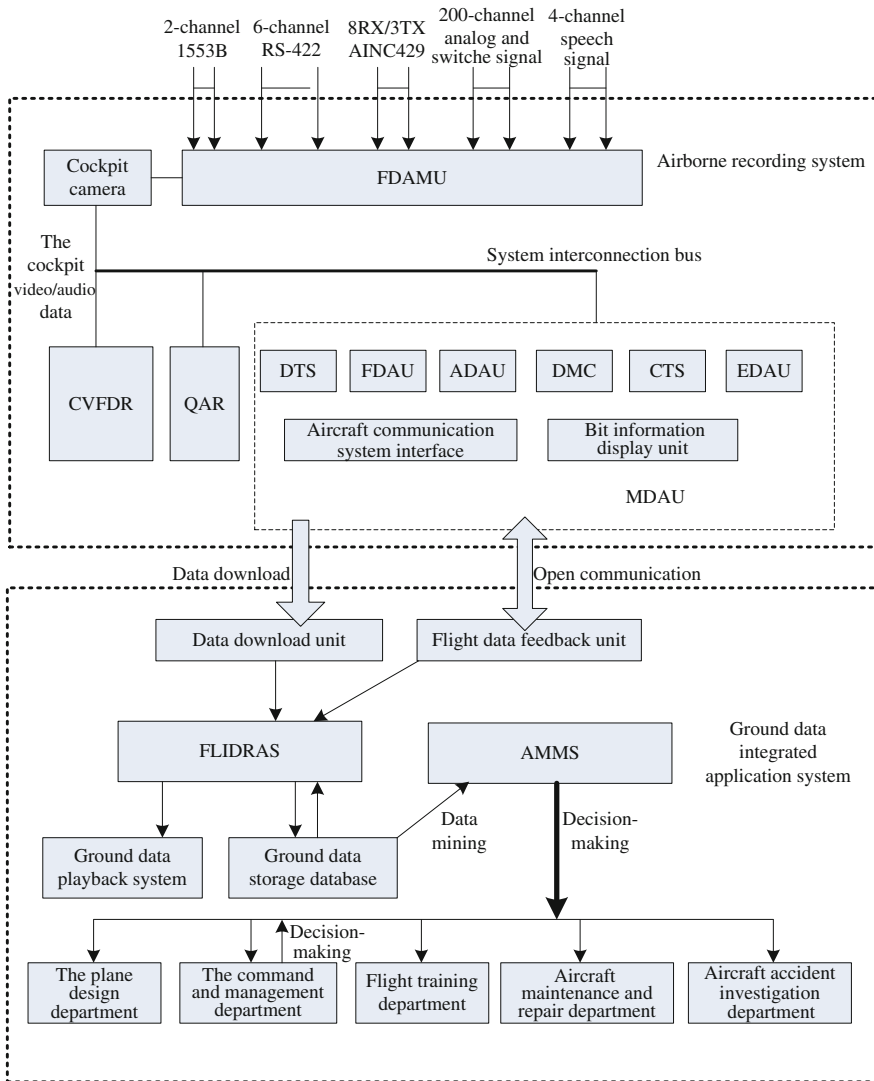
Fig. 33.2 Structure of flight data management recording system

to achieve real-time flight data remote transmission and meet the usual tactics and combat training assessment and correction. Software functional requirements and technical specifications should be constructed with data record separated from data applications design, providing software secondary development interface, as well as realizing software functions plug oriented, in order to complete a shift from a single software development model to a diversified software development paradigm. A set of network servers with centralized management of flight data providing different data services to various departments eventually become digital

important part of the airport. Flying parameter department's duty would become flight data centralized management, flight preliminary analysis, and provide data services to other organizations from current task of flying data download and interpretation. A mode that individual officers using flight data would extend to full depth applications of the required flight data using.

Stage three: Based on flying perfect real-time transfer of parameters data, real-time analysis on the plane would be achieved, mastering pilot action and judging security on the basis improved foundation real-time applications of flight data, achieving implementation working status determination and trend analysis of aircraft and equipment, providing recommendations for the pilots and realizing all kinds of flight data, the transition from the passive role to the active role.

33.5 Conclusion

In summary, accident prevention can bring enormous military and economic benefits, so people promote the development of objective inspection system. The system to experience a development process from nothing to something, from simple to complex, from discrete to integrated. With the increasing awareness level and advancements in aviation technological, the system will continue to expand and improve and play a greater role in research, testing, using, and security of the aircraft and make a greater contribution for the timely detection and correction of aviation science exist in practice deviations to ensure that "fly boldly, scientifically, and safely."

References

1. Tongjiang S (2003) Research on the application of flight data. Nanjing University of Aeronautics and Astronautics, Nanjing (in Chinese)
2. Hill A (2004) The flying object: a flight data management concept
3. Laneman JN, Tse DN, Wornell GW (2004) Cooperative diversity in wireless networks efficient protocols and outage behavior. IEEE Trans Inf Theory 50:3062–3080
4. Yiyan X (2006) Fault diagnosis design of aeroengine. Northwestern Polytechnical University, Xi'an (in Chinese)
5. Hong X, Qian X, Xiaochun L (2005) Fault diagnosis for aeroengine without components' performance. J Aerosp Power 20:746–751 (in Chinese)

Chapter 34
Research on Standardization of Ground Process Software for Flight Data

Dong Xia, Zhigang Peng, Yan Tang and Lei Yang

Abstract As important flight information including airplane kinematic parameters, equipment status, operations, etc., was recorded in flight data, the abilities of supporting aircraft, fly training, and fighting way study could be enhanced through process to flight data by ground process software. However, domestic ground process software is various in kinds but not compatible with each other, and flight data are managed separately which could not be utilized synthetically. The way by standardized design to solve problem of ground process software's no compatibility and separated data management was put forward. Requirements were raised from aspects of software functions standardized, data format standardized, interface standardized, performance standardized, documents standardized, etc., in the developing process of software, which ensured standard design of ground process software. Standard design in flight data ground process software could increase the use efficiency of flight data, and make full use of latent value of flight data.

Keywords Flight data · Process on ground · Standard design of software · Functions' standardization

34.1 Introduction

Flight data, namely data recorded in airplane's flying process, such as aircraft kinematic parameters, airborne equipments' working status, and pilots' operations, include flight parameters data, audio and video data, and various task data [1]. Flight data ground process software could be used to complete flight data's process and objective analysis, which serve to supporting aircraft, fly training, and fighting

D. Xia (✉) · Z. Peng · Y. Tang · L. Yang
Qingdao Branch of NAAU, Qingdao 266041, China
e-mail: sheldondonne@gmail.com

way study [2]. Flight data ground process software makes great sense in the following aspects:

1. Service ability of aircraft crew is enhanced. Airborne equipment's status and performance can be watched over though flight data analysis and process by ground process software, and faults and underlying threaten can be discovered on time, which assures aircrafts flying safely.
2. Pilots' training effect is improved. Pilots' operation and control to aircraft as well as airborne equipment use process in flying can be displayed through ground process software, which can be used to evaluate flying and fighting abilities and modify wrong action.
3. Effective method is introduced for evaluating fighting way's effect. Fighting effects can be analyzed in microcosmic view including time and parameters varying by ground process software, which is much persuasive.

Flight data ground process software plays an important role in fields of supporting aircraft and fighting and training. However, problems of various kinds, without compatibility, separated data management, unfriendly interface, etc., still exist in domestic ground process software. In order to improve ground process software's quality and to make full use of flight data, ground process software's standardization was studied in this article.

34.2 Status in Quo of Domestic Ground Process Software

Nowadays, many problems exist in domestic ground software for flight data process, which are shown in Fig. 34.1 and explained as follows.

1. Ground process software is various in kinds but without uniform standards or criterions, and bad in compatibility. A ubiquitous phenomenon that different companies develop different data process software to their products universally existing in the field of domestic flight data ground process software, which leads to that different ground process software, is adopted in different types of aircraft, and even interior the same aircraft type, different software was used because of different airborne record devices. Different process software cannot interact with each other, and data recorded by different device are separated from each other, which result in impossibility of integrated use and analysis [3].
2. Data management is rough and tumble. The airborne record device's kinds are various, and their management and maintenance belonging to different department on duty, which leads to different flight data's management, are separated and go against data reserving and integrated use.
3. The abilities of file management and information statistic are poor. When history data needed, operators could only seek the required data by hand in folders with low efficiency. Meantime, as important information in each flight
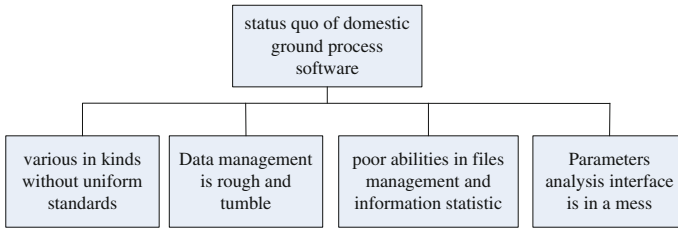
Fig. 34.1 Structure of flight data ground process software standardization

data files has not been extracted, the effect on long-time accumulation of flight data would not emerge.

4. Parameters' analysis interface is in a mess, which make it difficult to observe parameters' curves. Parameters' curve varying with time is an important way in analyzing flight data. However, the function has not been realized commendably in domestic ground process software; the limitation existing in that the curve menu is in a mess; curves cross each other and curves' colors contrast badly, which lead to poor observing.

34.3 Realization of Ground Process Software Standardization

In order to solve problems that ground software's types are various, the compatibility is poor, data management is separated, etc., the standardization of flight data ground process software needs to be studied, and standards/criteria would be constructed to guide the development of ground process, which would realize the full use of flight data and reduce the using difficulty of operators. In the first place, software reliability must be ensured, and self-contained functions, standard interface [4], straightforward operations, extensibility, compatibility, safety, etc., also to be satisfied [5]. Client/Server model is introduced in architecture, which ensures safety and clarity in data management. The standard design of ground process software is constitutive of functions standardization, data standardization, interface standardization, performance standardization, and other standardization requirements, as shown in Fig. 34.2.

34.3.1 Software Functions Standardization

In order to make full use of flight data, sufficient functions must be realized in standard ground process software [6], as shown in Fig. 34.3.
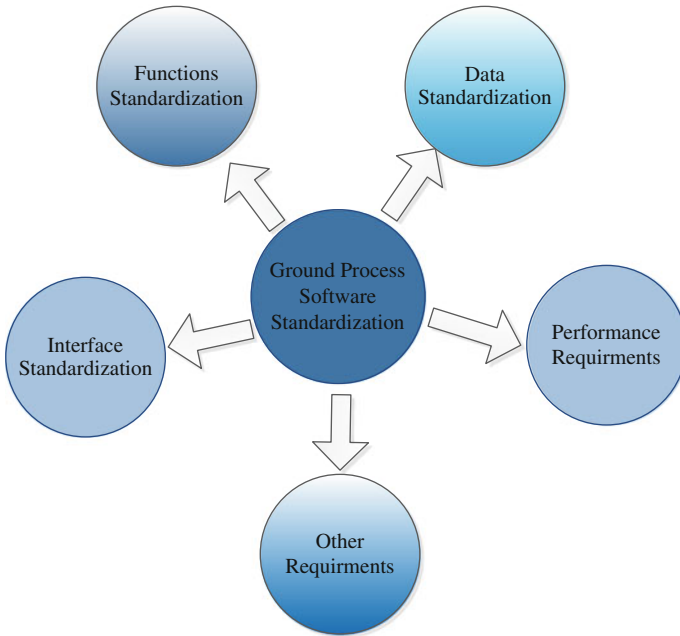
Fig. 34.2 Structure of flight data ground process software standardization

Fig. 34.3 Standard
requirements of ground
process software
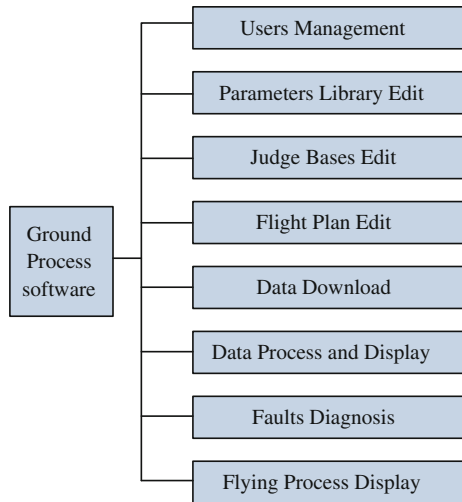
The functions realized by each blocks are described as follows.

1. User management carries out tasks in managing software users, including user additions, omits, entering, setting of users' operation puissance, etc.
2. Operations on different parameters recorded would be realized by parameters' library edit. Those operations include record device type editing, parameters' decoding way editing, parameters' display method editing, parameters' adjusting, etc.
3. Judge bases edit fulfill experts' judge basis edit to flight data, including addition, omit, and modification of expert judge basis, which is used in fast judge of flight data.
4. Flying information management of different flights is realized by flight plan edit, including edit of airplane's number, pilots' information, flying time, and corresponding data files in each flight.
5. By data download function block, flight data in airborne record devices are downloaded to ground computer and stored following standard format.
6. Data process and display fulfill tasks of process and display to raw data based on parameters' library and fast judge to flight data according to expert basis.
7. Based on faults' tree or corresponding algorithm, faults' diagnosis can find out the fault causation through processing flight data.
8. Airplane's flying process can be reappeared through flying process display according to flight data, which can be used to evaluate pilots' technology.

34.3.2 Non-Functional Standard Requirements

Except functional standard, there are some non-functional standard requirements need to be satisfied in flight data ground data process software, mainly including data standardization, interface standardization, and performance standardization.

1. Data standardization requires ground process software to store flight data in standard form into ground computer, in order to be compatible with other types of record devices in decoding.
2. Interface standardization requires ground process software to adopt standard men–machine interactive interface and universal response behavior to external actions, which avoid repeated training to operators of different types of airplane.
3. Performance standardization require download time, process time, and user operation respond time of flight data that must meet the requirements of standardization, in order to ensure the software's high reliability and efficiency.
4. Software architecture standardization means that Client/Server model is adopted in architecture of ground process software, and the flight data are managed in integrity, which ensure the safety of flight data.

5. Documents' standardization requires that there are detailed description on software operations and management, especially unambiguous description on parameters' format of different types of recording device.
6. Other standardization requirements include restrictions in operating environment and platform, such as temperature, humidity, OS, and developing language.

34.4 Summary

In domestic flight data ground process software, problems such as various types, messy data management, unkind interface exist in nowadays, and those problems can be solved by standard software design. In order to realize ground software design standardized, standard requirements need to be followed in software function, data downloads and storage, interface, etc. Standard design in ground process software can increase flight data's using efficiency and make full use of flight data's latent value.

References

1. Hill A (2004) Flight data management concept. Aerosp Electron Syst Mag
2. Tongjiang S (2003) Research on the application of flight data. Nanjing University of Aeronautics and Astronautics, Nanjing (in Chinese)
3. Brooks FP (2002) The mythical man-month. Addison Wesley Longman, New York
4. Bhaskar NU, Naidu PP, Babu SR et al (2011) General principles of user interface design and websites. Int J Softw Eng:45–60
5. Sommerville I (2009) Software engineering. Pearson Education, New York
6. Pressman RS (2010) Software engineering: a practitioner's approach. McGraw-Hill, New York

Chapter 35
The New Estimated Method for Refrigerating Capacity Produced by an Inward Turbine in the Aero-oxygen Plant

Lijun Xie, Dexin Wang, Feng Lu and Feng Yan

Abstract The loss of reheating shortage and Joule–Thomson effect are considered in the conventional estimated method for refrigerating capacity produced by an inward turbine in the aero-oxygen plant process. The deficiency of the method is analyzed in this article. The new estimated method is shown, that is using process calculation software. A calculation example is given also.

Lijun Xie, associate professor, engaged in teaching and research about the technical support and equipments for aviation depot. Dexin Wang, associate professor, engaged in teaching management and research about the aviation technical support and equipments. Feng Lu, Feng Yan, instructor, engaged in teaching management and research about the aviation technical support and equipments.

L. Xie (✉) · D. Wang · F. Lu · F. Yan
Qingdao Branch, Naval Academy of Aeronautical Engineering, Qingdao 266041, China
e-mail: Xie.Lijun@Springer.com; lijunxieqd@sina.com

D. Wang
e-mail: Wang.Dexin@Springer.com

F. Lu
e-mail: Lu.Feng@Springer.com

F. Yan
e-mail: Yan.Feng@Springer.com

35.1 Introduction

The conventional estimated method is consumption time and hard sledding that runs through considering the loss of reheating shortage and Joule–Thomson effect, but hardly carrying out computer program. The computer simulation software of modern air separation process is introduced to estimate refrigerating capacity produced by an inward turbine in the aero-oxygen plant process in this article.

35.2 Analyzing the Conventional Estimated Method

The heat equilibrium figure of steady-state system is shown in Fig. 35.1, the following heat equilibrium equations may be got

$$\sum_{J=1}^{M} H_{\text{flow}-\text{unit}}^{\text{inJ}} + Q_{\text{loss}} + Q_{\text{refrigerating capacity}} = \sum_{I=1}^{N} H_{\text{flow}-\text{unit}}^{\text{outI}} \tag{35.1}$$

$$Q_{\text{refrigerating capacity}} = \sum_{I=1}^{N} H_{\text{flow}-\text{unit}}^{\text{outI}} - \sum_{J=1}^{M} H_{\text{flow}-\text{unit}}^{\text{inJ}} - Q_{\text{loss}} \tag{35.2}$$

where H is enthalpy of flow-unite.

Before the enthalpy of flow-unite was calculated, difficulty for different pressure, temperature, and component, therefore, the front two terms' difference of right equal sign in Eq. (35.2) was calculated approximately. Now, T–S chart (shown Fig. 35.2) was analyzed in order to make out the conventional estimated method.

The enthalpy potential coming into and out the system was changed to calculate approximately in the conventional estimated method.

$$\sum_{J=1}^{M} H_{\text{flow}-\text{unit}}^{\text{inJ}} - \sum_{I=1}^{N} H_{\text{flow}-\text{unit}}^{\text{outI}} \approx \sum_{I=1}^{N1} G_{\text{flow}-\text{unit}}^{\text{outI}} \times \Delta T_I$$
$$\times \text{CP}_I + \sum_{I=1}^{N2} G_{\text{flow}-\text{unit}}^{\text{outI}} \tag{35.3}$$
$$\times \text{CP}_I - \sum_{I=1}^{N} G_{\text{flow}-\text{unit}}^{\text{outI}} \times \Delta h_I$$

Suppose $N1$ unit gas flows out the system, and $N2$ unit liquid flows out the system $N = N1 + N2$. The CP_I value of $N2$ unit liquid can be obtained with cryogenics manual. Δh_I is the enthalpy potential of Joule–Thomson effect, which can be got by checking Δh–T chart. For according practice of checking parameter form, $\Delta h_I > 0$ [1]. The front two terms' summation of right equal sign in Eq. (35.3) is the loss of reheating shortage, and Joule–Thomson effect is the rear one term connected by subtraction sign.
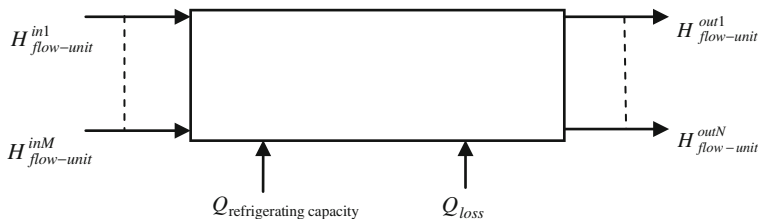
Fig. 35.1 The heat equilibrium figure of steady-state system

Fig. 35.2 The T–S chart of gas
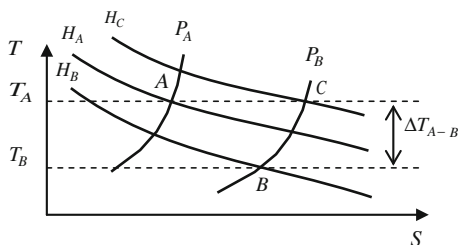
35.3 Improvement of a Conventional Estimated Method

The Q_{loss} includes the adiabatic refrigerating capacity loss of system and the refrigerating capacity loss of liquid pump in Eq. (35.2). The adiabatic refrigerating capacity loss of system divides into two parts that are the adiabatic refrigerating capacity loss of primary air separation and the refrigerating capacity loss of the argon system.

The adiabatic refrigerating capacity loss of primary air separation, the refrigerating capacity loss of the argon system, and the refrigerating capacity loss of liquid pump are

$$0.8 \times 21.5 \times G_{in}^{0.671} \quad (\text{kcal/h}) \tag{35.4}$$

$$0.2 \times 21.5 \times G_{in}^{0.671} \quad (\text{kcal/h}) \tag{35.5}$$

$$23.4 \times \frac{V_Z \times \gamma_Z \times \Delta P}{\eta_P \times \gamma_{LZ}} + V_Z^{0.77} \quad (\text{kcal/h}) \tag{35.6}$$

where G_{in} is operating air quantity. V_Z is flux at standard state. γ_Z is specific gravity at standard state. γ_{LZ} is liquid specific gravity. ΔP is pressure potential of liquid pump. η_P is prescription efficiency of liquid pump. Z is component.

If known pressure, temperature, and component about flow-unite coming into and out the system, the enthalpy is computed using the computer simulation software of modern air separation process. The $Q_{refrigerating\ capacity}$ is got easy that is in Eq. (35.2).

35.4 Example Computed

The air separation process with argon system is shown Fig. 35.3. The parameters of the aero-oxygen plant process are as follows.

Operating air quantity is 51,500 m^3/h, pressure is 598.2 kPa, temperature is 295 K; gas-nitrogen production is 10,000 m^3/h, pressure is 120.8 kPa, temperature is 299.3 K; gas-oxygen production is 9,700 m^3/h, pressure is 127.8 kPa, temperature is 299.3 K; liquid-oxygen production is 300 m^3/h, pressure is 146.8 kPa; Liquid-argon production is 308.7 m^3/h, pressure is 140.0 kPa; residual-gas is 6.3 m^3/h, pressure is 132.5 kPa; residual-gas includes 75 % N$_2$ and 25 % Ar, gas-nitrogen is 500 m^3/h, pressure is 559.2 kPa, temperature is 299.3 K, waste-nitrogen pressure is 122.8 kPa, temperature is 292.0 K.

Let whole devices be a system that are a compressor, an inward turbine, a gas-pressured cooler, a chief heat exchange, an up column, a down column, and an argon system [1]. The adiabatic refrigerating capacity loss of system and the refrigerating capacity loss of liquid-argon pump are

$$0.8 \times 21.5 \times 51,500_{\text{in}}^{0.671} + 0.2 \times 21.5 \times 51,500_{\text{in}}^{0.671} = 31,193.28 \ (\text{kcal/h})$$

$$23.4 \times \frac{12,033 \times 1.7252 \times 4.5}{0.4 \times 1,391.78} + 12,033^{0.77} = 5,312.94 \ (\text{kcal/h})$$

So, the refrigerating capacity loss of system is

$$Q_{\text{loss}} = 31,193.28 + 5,312.94 = 36,506.22 \ (\text{kcal/h})$$

The "separator" computing module is contained in the computer simulation software of modern air separation process. Now, the refrigerating capacity of system is not the refrigerating capacity of an inward turbine. One part of the work by inward turbo-expander done is given to the compressor, using to gas pressure. This part work is put up in the system entrails, being independent of the refrigerating capacity given by the exterior system, so the refrigerating capacity of the system is built with the two parts that are the bearing consumed power LOSTW and the cold capacity Q_{COD} of a gas-pressured cooler [2, 3]. So

$$Q_{\text{refrigeratingcapacity}} = \text{LOST} + Q_{\text{COL1}} \tag{35.7}$$

Let the adiabatic refrigerating capacity loss of system is the SYSH, and the refrigerating capacity loss of a liquid pump is the HLARP. The SYSH includes the adiabatic refrigerating capacity loss of primary air separation system and the refrigerating capacity loss of argon system. Paying attention to

$$\text{QDIF} = \sum_{J=1}^{M} H_{\text{flow-unit}}^{\text{inJ}} - \sum_{I=1}^{N} H_{\text{flow-unit}}^{\text{outI}}$$
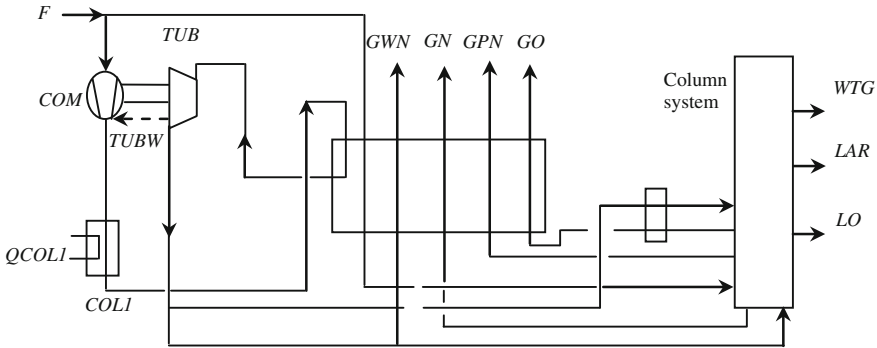
Fig. 35.3 The air simple separation process with argon system

Thus, Eq. (35.2) is changed as follows.

$$Q_{\text{refrigerating capacity}} = -\text{QDIF} - Q_{\text{LOSS}} = -\text{QDIF} - (\text{SYSH} + \text{HLARP}) \quad (35.8)$$

For finding the expanding air capacity and the expanding refrigerating capacity, we let the adiabatic efficiency of inward turbine $\eta_{\text{TUB}} = 83.5\,\%$, the conversion efficiency of compressor $\eta_{\text{COM}} = 65.5\,\%$, the machine efficiency of inward turbine $\eta_{\text{MACH}} = 90.0\,\%$, the cold temperature of gas-pressured cooler $T_{\text{COD}} = 31$ K, the import temperature of inward turbine $T_{\text{in}} = 160$ K, the export pressure of inward turbine $P_{\text{out}} = 1{,}463$ kPa. And let 100 m^3 air come into the system. Hence,

$$Q_{\text{refrigerating capacity}}^{100} = \text{LOST}^{100} + Q_{\text{COL1}}^{100}$$

The expanding air capacity and the expanding refrigerating capacity are

$$G_{\text{TUB}} = \frac{Q_{\text{refrigerating capacity}}}{Q_{\text{refrigerating capacity}}^{100}} \times 100.0 \quad (35.9)$$

$$\text{TUB}_{\text{refrigerating capacity}} = \frac{\text{TUBW}^{100}}{\eta_{\text{MACH}} \times 100.0} \times G_{\text{TUB}} \quad (35.10)$$

where TUBW^{100} is the conversion work that is given from inward turbine to compressor when the import air of inward turbine is 100 m^3. In the example, $\text{QDIF} = 61{,}075.62$ kcal/h

$$Q_{\text{refrigerating capacity}} = -61{,}075.62 - 36{,}506.22 = -97{,}581.84 \ (\text{kcal/h})$$

$$Q_{\text{refrigerating capacity}}^{100} = -(154.90 + 907.33) = -1{,}062.23 \ (\text{kcal/h})$$

So, we have

$$G_{\text{TUB}} = 9{,}186.49 \quad (\text{m}^3)$$

$$G_{\text{TUB}} = 9,186.49 \ (\text{m}^3)$$

$$\text{TUB}_{\text{refrigerating capacity}} = \frac{-1.6213 \times 859.85}{0.9 \times 100.0} \times 9,186.49 = -142,296.16 \ (\text{kcal/h})$$

It must be indicate the relation closely between the import temperature of the inward turbine and the least temperature potential of primary heat exchanger.

References

1. Hangzhou S (2011) Oxygen plant manufactory: the practice information about 10000 m³/h oxygen plant in Linde Corporation. Hangzhou Oxygen Plant Factory, pp 2–5, 11–17
2. Min YI (2004) The process of imported 10000 m³/h air separation plant and installation characteristics, pp 25–28
3. Agahi RR, Allen MT (1997) Geothermal energy recovery using turbines. Geothermal Power in Asia "97", pp 321–326

Chapter 36
The Design of CFM56-5B Engine Inlet Cowl Repair Platform

Feng Lu, Xiang Li, Wenting Zhang and Tao Jiang

Abstract In the reference of the repair platform of RSE1116 recommended by CMM, and according to the actual work requirements, the necessity of designing a more efficient engine inlet cowl repair platform exists, with which the disassembly, install, transport, storage, and repair of CFM56-5B engine would be much more convenient. This article gives the methods that abolish the original method of displaying CMM and that design a saddle bracket car and a maintenance shelf. These two methods cover all the need of engine inlet cowl disassemble, install, transport, storage, and overhaul.

Keywords Inlet cowl · Repair platform · Repair · Disassembly/assembly · RSE1116

36.1 Introduction

The design of the repair platform refers to the use and storage methods recommended by current CMM. From the CMM, firstly loosen the fasteners, then use cranes and spreader to lift the engine inlet cowl stably, disassemble or install the engine inlet cowl, and finally lift it on the stock shelf. See Figs. 36.1 and 36.2.

This platform design concerns two aspects: (1) Abolish the original method of disassembly/install with lift from CMM and design a saddle bracket car to support engine inlet cowl (the saddle can go up and down, and be adjust to different height). (2) Abolish the original method of displaying CMM and design a maintenance shelf, which is available in 360° in horizontal direction and 0–90° vertical rotation angles (equipment 1 and 2 can operate independently or assemble together

F. Lu · X. Li (✉) · W. Zhang · T. Jiang
BM Department, CES E&T Xi'an Maintenance Base, Konggang East 2 Road, Xi'an Xianyang International Airport, Weicheng, 712035 Shaanxi, China
e-mail: xiangleenwpu@hotmail.com

321

SLING - AIR INTAKE COWL

PART NUMBER: RSE1112

Description.......... This tool is used to lift an engine inlet cowl and hold
                     it during installation/removal so that the bolts can be
                     inserted or removed.

Weight............... 5 kg (11 lb)

Dimensions........... 381 x 381 x 101 mm (15n x 15 x 4 in)
                     (Including packing)

NOTE: This tool is used for CFM56-5 engines.
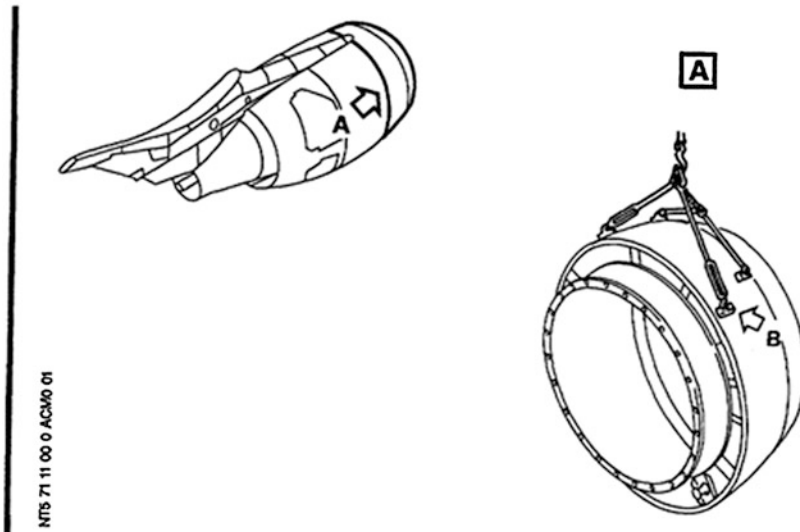
Fig. 36.1 Lift the engine inlet cowl

to form a repair platform). These two methods cover all the need of engine inlet cowl disassemble, install, transport, storage, and overhaul.

36.2 Integrated Design of CFM56 Engine Inlet Cowl Mechanical Structure of Disassembly/Install

36.2.1 The Composition of Repair Platform

The repair platform consists of following parts: Disassembling bracket consists of a fixed saddle and lifting machine, hydraulic systems, chassis, and so on.

PART NUMBER: RSE1116

Description........... This tool is used to transport, store and serve as a work
                      stand for the inlet cowl.

Weight............... 635 kg (1400 lb)

Dimensions........... 1765 x 2692 x 1803 mm (69.5 x 106 x 71 in)

NOTE: This tool is used for CFM56-5 engines.
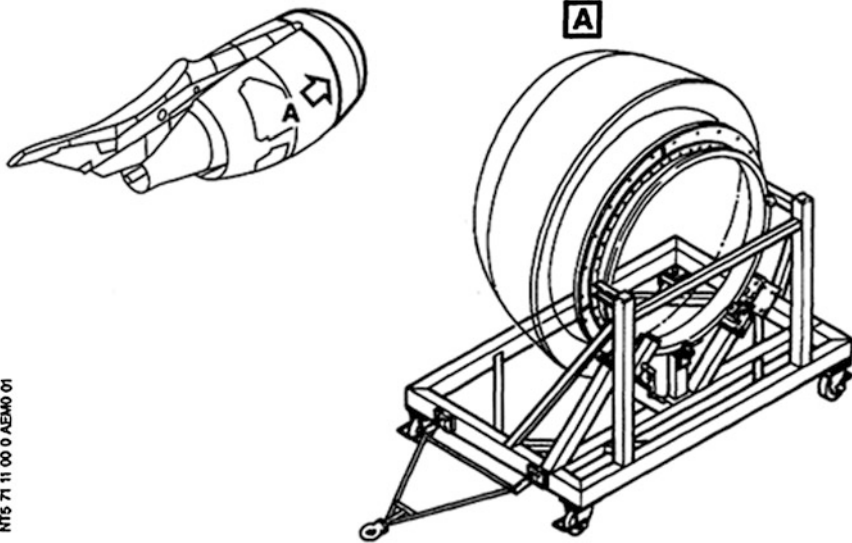
Fig. 36.2 Transport, store, and serve as a work stand for inlet cowl

36.2.2 Technical Parameters

Extension of lifting platform: 0–1000 mm.
Power of lift: 600–800 kg.
Most parts of the repair platform are made of steel, and its weight is 550 kg.
Maximum working pressure of hydraulic is 14 MP.
Surface is painted with orange color.

36.2.3 Integrated Design of CFM56 Engine Inlet Cowl Mechanical Structure of Disassembly/Install (Fig. 36.3)

Fixed saddle for disassembly/install is composed by the former and latter two saddles, front stopper, and fixing equipment. Former and latter saddles have the function of supporting and restricting from the four directions. Using straps and tie to fix the inlet cowl, two fasteners are installed on the front and rear saddle to fix the inlet cowl. Figure 36.4 illustrates in order to fix the saddle in position, screws and the lift bracket are connected, and all the surface that face the inlet cowl are covered with soft rubber. In this design, the saddles can be removed and replaced, which is used to adjust different engine inlet cowls.

36.2.3.1 Material Structure

The saddle is made from multiple high-quality laminates and is according to the curvature of the inlet cowl. In order to prevent damage to the inlet cowl saddle, the saddle arc is with wool felt and rubber on top. And around the saddle, steel is used to protect the frames, and equipment is mounted on the bottom of the bracket, which is connected with the lift. See Fig. 36.4.

36.2.3.2 Former Stopper

It contains two stoppers which can be flipped to the left and right and is installed in front of the former saddle, screw driven by a hand wheel to adjust the fixed distance between the stopper and the inlet cowl. See Fig. 36.5.

36.2.3.3 Lift System

The lift bracket takes the way of scissors fork and contains the upper frame, scissors forks, hydraulic cylinders, hydraulic pumps, tank valves, and other components. When disassembling the inlet cowl, turn the hand pump to drive the hydraulic system to push hydraulic cylinders, then drive the scissor fork to make the platform go up, then lift the saddle inlet cowl for disassembly work. When needing to put the platform down, just release the switch of the hydraulic cylinders. See Fig. 36.6.
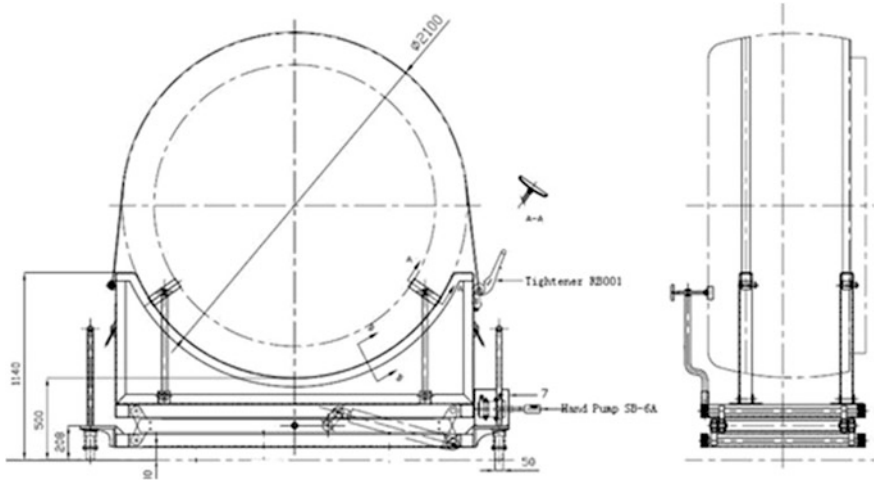
Fig. 36.3 CFM56 engine inlet cowl
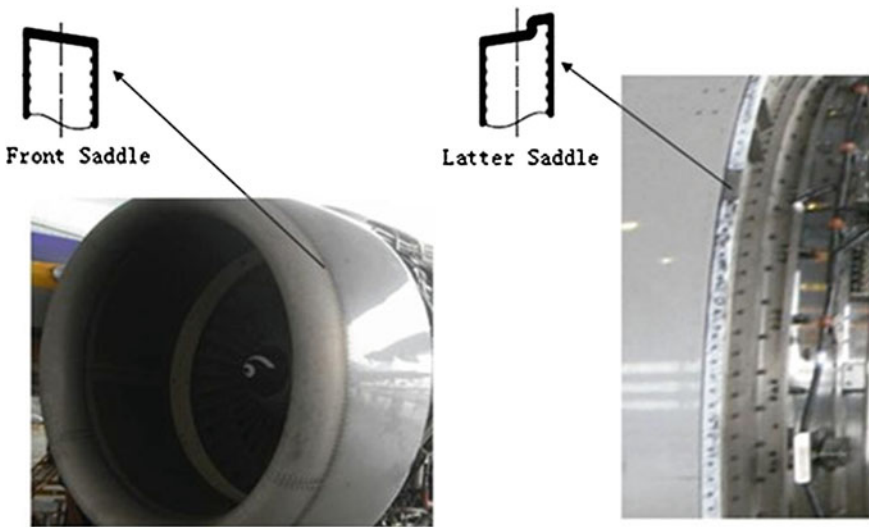
Fig. 36.4 Inlet cowl saddle

36.2.3.4 Bracket

Bracket is welded by channel frame; on the bottom, it is fitted with two all directional wheels and two specifically directional wheels, and all the four wheels are equipped with brake and shock absorption. The all directional wheels are side with self-locking function screw, which is to fix with the ground. See Fig. 36.7.
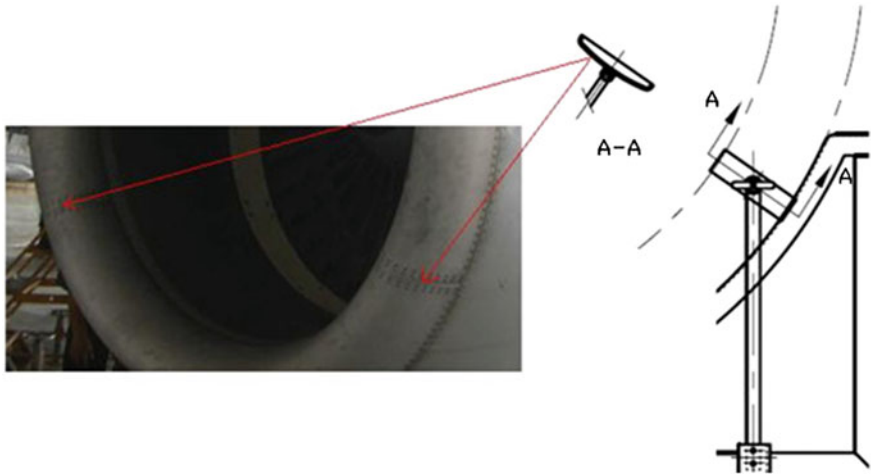
Fig. 36.5 Former stopper
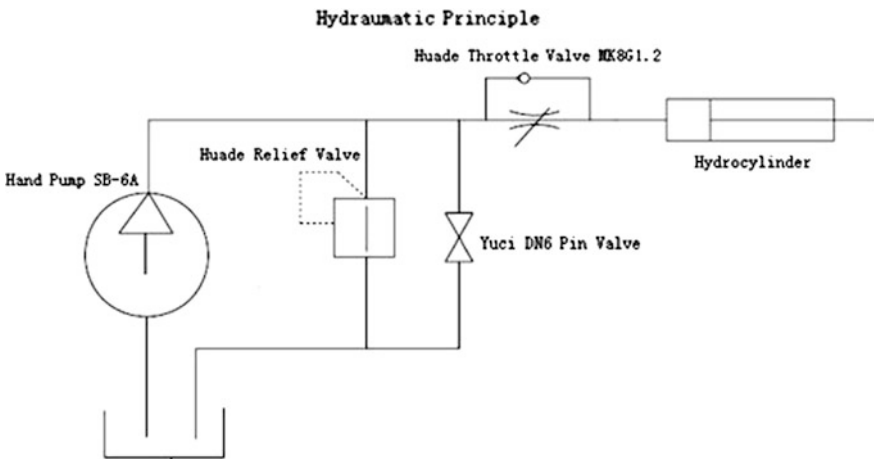
Fig. 36.6 Lift system

As the overall bracket is too long, for the convenience of peering position, the design does not contain drawbar, instead it contains sliding armrest with soft foam. See Fig. 36.8.
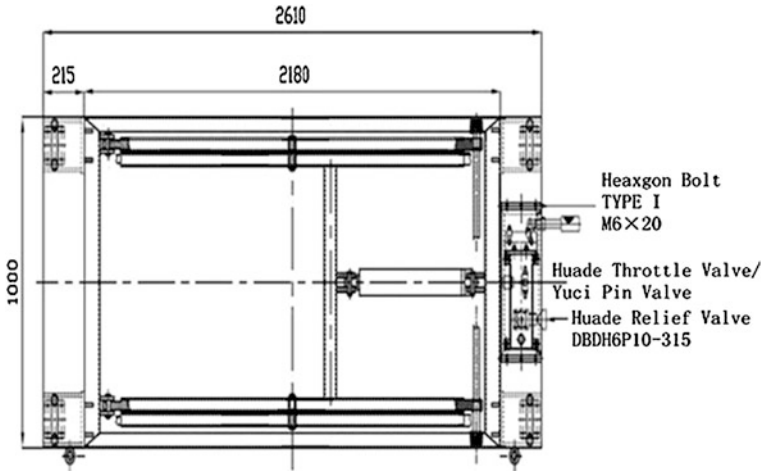
Fig. 36.7 Structure of bracket

Fig. 36.8 Sliding armrest with soft foam
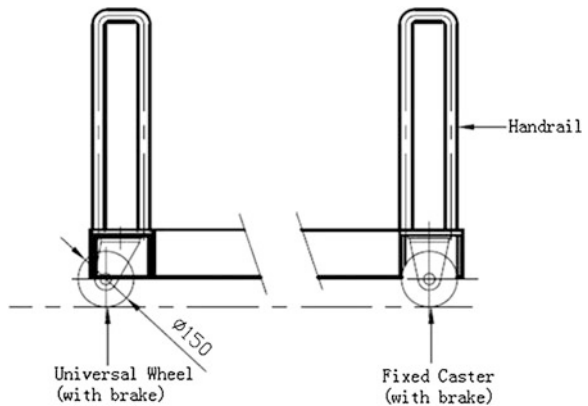
36.3 Integrated Design of CFM56 Engine Inlet Cowl Mechanical Structure of Repair

36.3.1 Component of Repair Platform

The repair bracket is together with the inlet cowl disassemble bracket to fix the inlet cowl; the bracket consists of inlet cowl holder, holder lifting turning systems, holder horizontal rotation, positioning systems, hydraulic systems, chassis, and other components.

Fig. 36.9 RSE1116 bracket
(*side view*)

36.3.2 References

The bracket refers to the Part Number recommended by Airbus: RSE1116, for details see Figs. 36.9 and 36.10. The bracket takes some function and fixing method of RSE1116.

36.3.3 Technical Parameters

Rotation angle of the rotating platform: 360° in horizontal rotation, vertical 0–90°.
Capacity: 400–600 kg.
Most repairs overall structure is a steel platform. Repair platform weight: 650 kg.
Maximum working pressure of hydraulic: 14 MP.
Surface painted with orange painting.
The disassembly/assembly and repair of the inlet cowl can be together.

36.3.4 The Structure of Inlet Cowl Holding Bracket

When doing maintenance work to inlet cowl, hydraulic mechanism is driven through the hand pump to stand up and then align the inlet cowl connection via screws. The holding bracket is of square outer and circle inner structure;

Fig. 36.10 RSE1116 bracket (*front view*)

box-shaped outer bracket mainly supports the fixed bracket, the inner ring for fixing the inlet cowl; there are screw holes on the outer ring to match the screws of inlet cowl, the use of screws and retaining ring to fix the inlet cowl. The fixing ring is suspended with four wheels to support the inlet cowl so as to facilitate the rotating of inlet cowl in horizontal level when repairing. See Fig. 36.11.

The flip structure of inlet cowl bracket: The flip of the bracket is driven by hydraulic; the angle can be at random within 0–90; the bracket has two working condition; when receiving and completed inlet cowl maintenance, it is driven by a hydraulic mechanism; and it is in the upright position, as shown in Fig. 36.12. When under maintenance, the bracket stays in horizontal level. The bracket using the yaw drive to accomplish mounting bracket flip, and the power source is hydraulic system, which consists of hydraulic cylinders and hydraulic pumps, hydraulic source tank valve, and other components, see Fig. 36.6.

The horizontal rotation of Inlet cowl: The rotatable bracket flange has rotating track on the outer side, the rolling of outer bracket rollers can achieve any angle 0–360° rotation. Use eccentric friction plate to achieve fastening and limiting function.
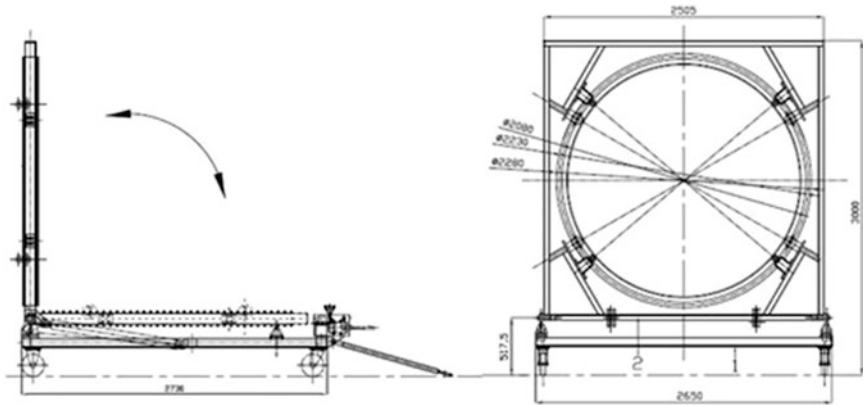
Fig. 36.11 Rotating of inlet cowl

Fig. 36.12 Upright position
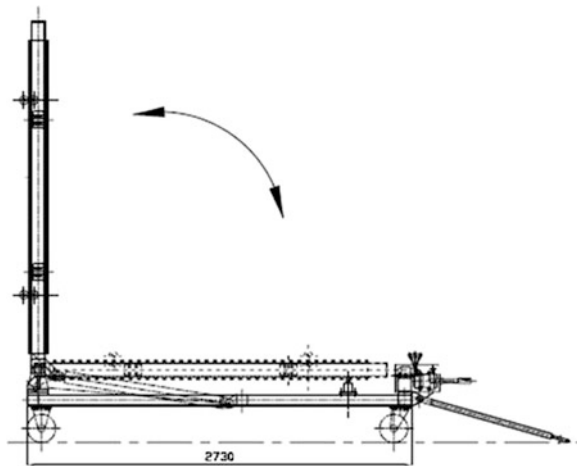
36.3.5 Connect with the Repair Bracket

When the inlet cowl removed for repair, put the flange bracket of repair bracket and the bracket side by side, connect the flanges with screws, release the retaining strap and oil return valve so that the saddle comes down; then the inlet cowl is on the bracket. See Fig. 36.13.
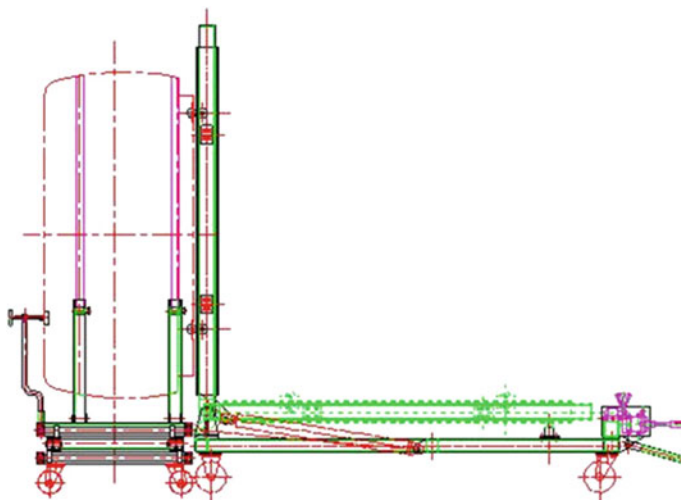
Fig. 36.13 Connect with the repair bracket
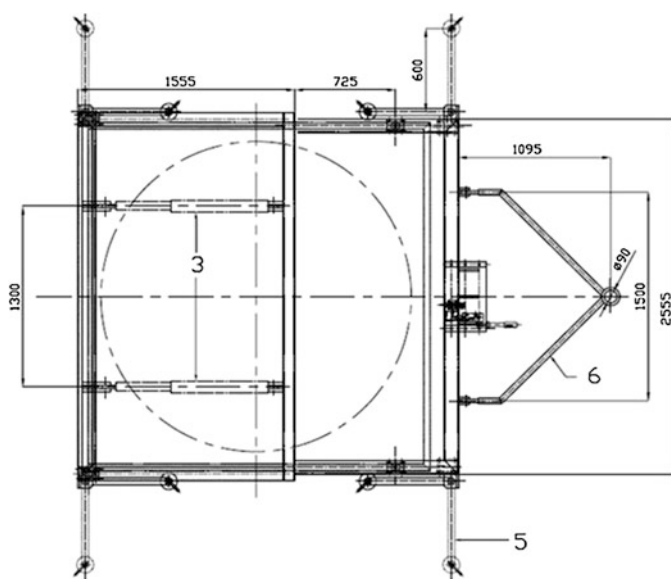
Fig. 36.14 Inlet cowl repair frame chassis structure

Inlet cowl repair frame chassis structure: Two wheels and two directional wheels have brakes and shock absorption; the entire brackets are with four ground organization. See Fig. 36.14.

Chapter 37
Study of the Ant-Colony-Algorithm-Based Optimal Scheduling of Shipboard Helicopter Maintenance Resource

Ke-nan Teng, Jun-liang Li, Lei Wang and Quan Liu

Abstract For the particularity of the maintenance of shipboard helicopter with finite resource, the optimized scheduling model of shipboard helicopter maintenance resource is put forward. By using the ant colony algorithm, the simulating calculation proves that the method uses the pheromone update to enhance search capability of ants to the optimal path, which solves the resource shortage problem well and reduces the maintenance cycle.

Keywords Shipboard helicopter maintenance · Resource constraint · Optimized resources · Shortest time

37.1 Introduction

China becomes stronger day by day and Chinese Navy offshore tasks more frequently, shipboard helicopter can, its role more prominent and its in-ship time longer. However, since the current support system is still the shore-based three-level system—"primary level," "intermediate-level," and "base level", the ship cannot take much air material spare parts; in addition, due to the uncertainty and emergency of the tasks on ship, the harsh natural environment increases the probability of equipment failure and the safeguard ability of shipboard helicopter is weak. How to solve the maintenance problem with limited resource under the current maintenance system and reduce the maintenance time is very crucial.

K. Teng · J. Li (✉) · Q. Liu
Naval Aeronautical Engineering Institute, Yantai, 264001 Shandong, China
e-mail: 343601858@qq.com

L. Wang
Qingdao Technological University Qindao College, Qingdao, Shandong, China

37.2 The Mathematic Model of Shipboard Helicopter Maintenance

37.2.1 Maintenance Resources Assumption

According to the characters of aviation maintenance, assuming that universal tools of repairing parts satisfy the requirement of repairing, the number of special tools designed by repair spare parts. Therefore, the maintenance resources this paper studied are the spare material parts carrying with the ship and exclude the maintenance tools and equipment, etc.

37.2.2 Basic Maintenance Unit Assumption

Assume the maintenance team as a basic support unit which has capability of completing primary-level and intermediate-level tasks.

37.2.3 Maintenance Work Procedure and Order

Literature [1] in resource-constrained model introduces the concept of maintenance unit importance, which means the process sequence of priority strategy. For example, according to current situation, shipboard helicopter repair work is mainly divided into mechanical, ad hoc, electronics, ordnance, and sonar system, which is a complicated system engineering, mutual restriction and involved, each system has certain correlation with others. Since helicopter maintenance work can be divided into mechanical system M_1, ad hoc system M_2, ordnance system M_3, electronic system M_4, and sonar system M_5. Then, system maintenance projects coding order in work order which restricted by physical logic, the time required for completion of each maintenance project show as Eq. (37.1):

$$D = \begin{pmatrix} d_{11} & \cdots & d_{1n} \\ \vdots & \ddots & \vdots \\ d_{51} & \cdots & \end{pmatrix} \tag{37.1}$$

Among them, $i = 1, 2, 3, 4, 5$, respectively each system, $j = 1, \ldots, n$ represents the maintenance projects of each system.

Taking mechanical and ad hoc system as an example to establish correlation matrix, the expression is as Eq. (37.2):

$$M_{12} = \begin{pmatrix} \delta_{11}^{12} & \cdots & \delta_{1n}^{12} \\ \vdots & \ddots & \vdots \\ \delta_{n1}^{12} & \cdots & \delta_{nn}^{12} \end{pmatrix} \tag{37.2}$$

Among them, $\delta_{ij}^{12} = 1$ or $\delta_{ij}^{12} = 0$.

So when considering any maintenance project, only need to consider the relevant four incidence matrixes can determine its priority and correlation between system maintenance, such as mechanical system only consider M_{12}, M_{13}, M_{14}, and the M_{15}. Therefore, important degree function is set up as and θ_{ij}, $\theta_{ij} = 1/4 \sum \delta_{jz}^{ik}$ where $i = 1, 2, 3, 4, 5$, $j = 1, \ldots, n$, $k = 1, 2, 3, 4, 5$, and $k \neq i$, $z = 1, \ldots, n$.

Then, a maintenance work can be expressed as a node type (activity-on-node, AON) directed network [2], and there are 2 types of constraints: one kind is the logic of project between constraint, expressed in AON the arrows in network; another kind caused the resource constraints of limited resources and limited the same time each task demand for resources cannot be more than the supply of resources. Assume that the task contains J projects, need to k kinds of renewable resources, the supply of resources for k is R_k, the time limit for a project j is p_j, the deadline for j is the d_j, the demand for the resources of k is r_{jk}, for all its tight before project set is p_j, project marked the beginning of time S_j, end time is C_j, the project from the moment $t = 0$ begin to execute, complete set the latest time for $T = \sum P_j$; All projects executing in time t marked as set I_t, and can use the project accomplishment time vector represent the project schedule $S = (C_1, C_2, \ldots, C_j)$. Therefore, the RCPSP can be described as

$$\min f(s). \tag{37.3}$$

s.t

$$S_j \geq C_h, \quad \forall j, h \in P_j. \tag{37.4}$$

$$\sum_{j \in I_t} r_k \leq R_k, \quad \forall k, t. \tag{37.5}$$

Equation (37.3) is the objective function of the shortest project time, Eq. (37.4) is the restraint relationship of project, and Eq. (37.5) is resource constraints. For the classic RCPSP, the goal is to minimize the total project time and limit resource for a project.

37.3 The Ant-Colony-Algorithm-Based Optimal Scheduling Model of Shipboard Helicopter Maintenance Resource

Ant colony algorithm is the foraging behavior of ant colony using pheromone bionic, has been widely applied to various combinatorial optimization problem, and is applied in solving RCPSP [3]. In general, the ant colony algorithm uses the schedule generation mechanism, expands local schedule step by step to generate a complete feasible project schedule, and gets the best solution by repeated search.

In the RCPSP ant colony algorithm, the ant search starting from the first task iterates through all the tasks and accomplishes the search after arrived J [4].

$$P_{ij}^k(g) = \begin{cases} \dfrac{\tau_{j(g)^\alpha} \eta_{ij}^\beta}{\sum_{h \in D_i^k} \tau_{j(g)^\alpha} \eta_{ij}^\beta}, & j \in D_i^k \\ 0, & j \notin D_i^k \end{cases} \quad (37.6)$$

In Eq. (37.6), τ_{ij} is the pheromone information, η_{ij} is heuristic information, α and β are to control the weight of 2 class information parameters. Generally said the ant heuristic information in the search can make use of visual information in the decision-making. In the RCPSP, generally with precedence rules to construct the heuristic information, the most common is the latest completion (latest finish, LF) time, the completion of the task j at the latest time for L_j, and the heuristic information can be represented as follows:

$$\eta_{ij} = \max_{h \in D_i} L_h - L_j + 1. \quad (37.7)$$

The pheromone update is the key of the ant colony algorithm, including the pheromone volatilization and accumulation. Pheromone volatilization and cumulative general can adopt the following mechanism:

$$\tau_{ij}(g + 1) = (1 - \rho) \sum_{k=1}^m \tau_{ij}^k(g) + \theta_{ij} \, \Delta\tau_{ij}(g). \quad (37.8)$$

$$\Delta\tau_{ij}(g) = \rho/f. \quad (37.9)$$

There, ρ represents for pheromone volatilization rate, f is the objective function value after ant complete a full search. When the ant k from the first project searches step by step to the j project, it would constitute a complete.

Table 37.1 The parameters

α	β	ρ	m
0.2	2.5	0.1	9
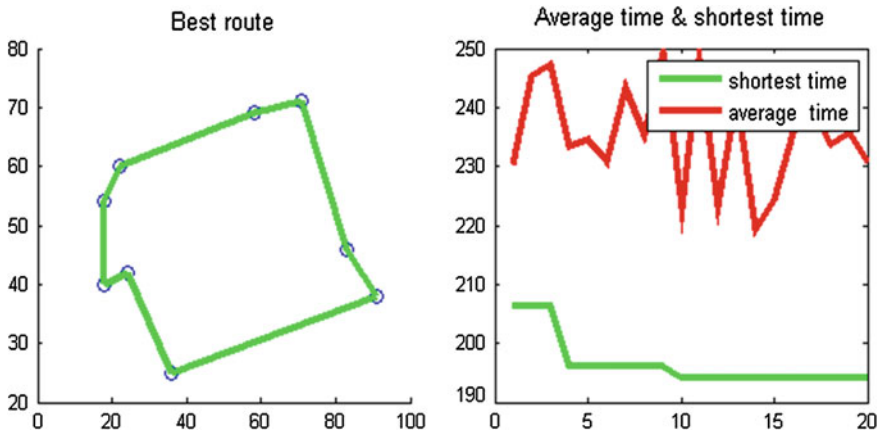
Fig. 37.1 The calculation results

Table 37.2 Comparison of other algorithms

	Shortest time (min)	Computing time (M/S)
Scan tine algorithm	211	108.26
Ant colony algorithm	195	98.33

37.4 Numerical Examples Analysis

The parameters of the matrix D and M only in specific calculation process should not be given in the paper, selecting 9 maintenance projects distribution in five system.

Ant colony algorithm is a kind of adaptive, positive feedback, distributed simulation optimization calculation method; it is in solving the complex combinatorial optimization problem certain advantages, and good combination of α, β, ρ has better solution quality and good stability, but in the improper selection of ant parameter of ant colony algorithm, faster convergence to the local optimum and slow convergence of the algorithm are greatly affected.

In that, the parameters in the scope $0.1 \leq \alpha \leq 0.3$, $3 \leq \beta \leq 6$, $0.01 \leq \rho \leq 0.3$, the algorithm has better overall performance, reaches the optimal solution and global optimal approaching, and at the same time, needs less iteration, not easy to fall into local optimal, results in the stagnation of algorithm [5].

In this paper, the values of the parameters show as Table 37.1

Calculated by software of MATLAB, the result shows as Fig. 37.1.

By comparing with other algorithms to verify the correctness and superiority, the result shows as Table 37.2.

37.5 Conclusion and Outlook

The model can realize the shortest time optimization under limited resources condition, improve the efficiency of maintenance, and also can improve the integrity rate of the shipboard helicopters. The model of maintenance tasks presented in this paper is simple; in order to present the actual maintenance work, the more complexity model of maintenance work be further studied.

References

1. Sun B-C, Jia X-S, Wang Y-B (2012) Study of the ant-colony-algorithm-based rush-dispatch of maintenance and support resources. Res Des 6:37–41 (in Chinese)
2. Chen Q-H (2007) Military operations research on equipment. National Defense Industry Press, Beijing (in Chinese)
3. Shou Y-Y, Fu A (2010) Multi-colony ant algorithm for multi-objective resource constrained project scheduling. J Zhejiang Univ 44(1):51–55
4. Merkle D, Middendorf M, Schmeck H (2002) Ant colony optimization for resource constrained project scheduling. IEEE Trans Evol Comput 6(4):333–346
5. Jiang L-Y, Zhang J, Zhong S-H (2007) Analysis of parameters in ant colony system. Comput Eng Appl 43(20):31–36 (in Chinese)

Chapter 38
Retracted: The Uncommanded Autofeather System Research of Turboprop Aircraft

Bai-ping Yang

Abstract As a part of turboprop, the autofeather system is to detect the power loss of any engine, trim the power of the opposite engine, and signal aircraft to feather the failed engine propeller. This work analyzes the composition of autofeather system, principle of system control, and the main influential factors of the auto-feather unit (AFU) and provides measures to deal with the uncommanded auto-feather events and low torque light flashing events, reducing the probability of the uncommanded autofeather and low torque light flashing events.

Keywords Uncommanded autofeather · Torque · AFU · EEC · Low torque · Power up trim

38.1 Foreword

In recent years, with the rapid development of regional air transport, regional aircraft also ushered flourish. As a turboprop aircraft, the short-range regional aircrafts are in favor of the growing number of users.

As a superior performance aircraft, domestic certain type of civil aircraft has fully opened the domestic market. With the continuous increase in sales, the aircraft also exposed some problems, especially uncommanded autofeather and low torque light flashing events [1], which greatly affect the operational safety of

An erratum of the original chapter can be found under DOI 10.1007/978-3-642-54233-6_79

B. Yang (✉)

AVIC Xi'an Aircraft Industry Company LTD, Xi'an 710089, China
e-mail: qinglongdragon@163.com

the aircraft, giving users greater economic losses, and also affect the reputation of civil aircraft.

This paper analyzes the composition and control principle of autofeather system, the occurrence of uncommanded autofeather events and the low torque light flashing events during takeoff and takeoff roll, and a lot of testing and data analysis [2–7], to determine the root causes of failure, and propose effective solutions and improved methods to reduce the probability of such a failure.

38.2 Autofeather System

38.2.1 The Composition and the Function of the Autofeather System

The engine autofeather system consists of the engine torque shaft, torque sensor, autofeather armed light, and autofeather unit (AFU). When the system is armed, the AFU captures the loss of torque and sends a feathering command to the local propeller system and an up trim command to the opposite engine's electronic engine control (EEC) [8].

38.2.2 Torque

As an important parameter of autofeather system, the torque is determined by the torque sensor, measuring the ratio between the fixed torque shaft signal (blue line) and the movable torque shaft signal (red line) in Fig. 38.1. The resulting pulse position modulated signal information (phrase shift) is then extracted for use in the AFU logic and converted to a DC signal to provide a calibrated signal as a voltage ratio between the output torque signal and the reference torque.

38.2.3 Principle of Autofeather System

The operating principle of control system of autofeather system is shown in Fig. 38.2.

To achieve the function of autofeather system, the system should be armed with the following conditions [8]:

(1) Autofeather line is connected;
(2) Engine power selects "TO/GA";
(3) Twin power lever angle is greater than 63°;
(4) Twin torque is greater than 46 %;
(5) Autofeather armed light goes on.
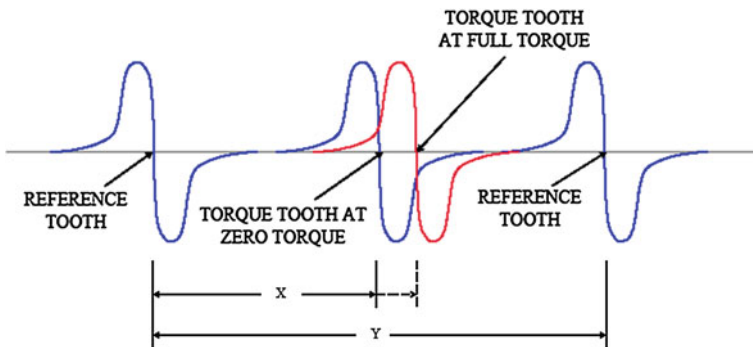
Fig. 38.1   Torque sensor signal
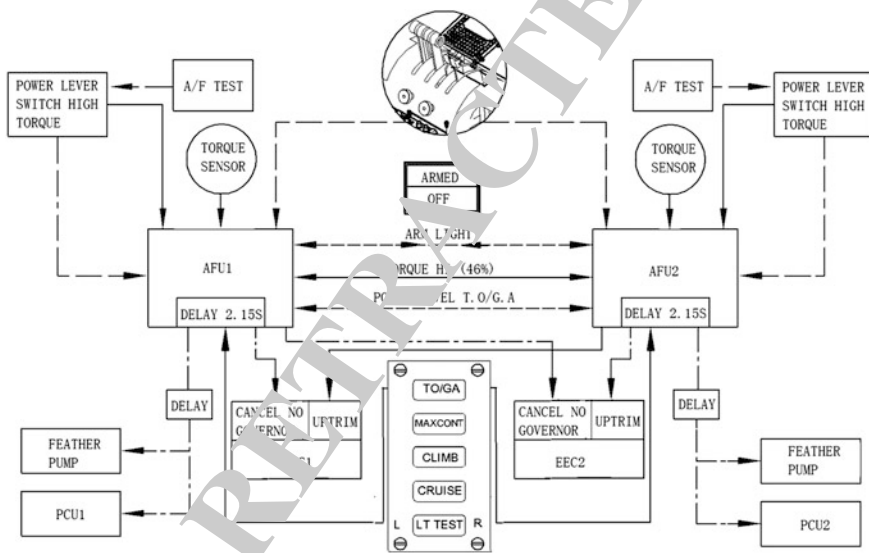
Fig. 38.2   Autofeather system schematic

The autofeather system is in armed mode with the above conditions. When the either side of the engine torque is less than 22 %, the AFU of failure side will send an up trim signal immediately to EEC unit of the other side to increase the engine power by 10 %. In the meantime, the AFU triggers the failed engine's propeller to feather after the duration of 2.15 s for low torque signal.

38.3 Failure Analysis of Autofeather System

38.3.1 Failure Symptoms of Autofeather System

The main failures of autofeather system are as follows:

(1) The failed engine feathers automatically when the torque signal of the failure engine lasts more than 2.15 s, and the power of the other engine increases by 10 %. The low torque light of the failed engine is always bright;
(2) The failed engine does not feather with the low torque light flashing, because the duration of low torque signal is less than 2.15 s. The power of the other engine increases by 10 %.

38.3.2 Failure Analysis

According to the principle of autofeather system, the main influencing factors of triggering autofeather and power up trim events are No.1 torque sensor, AFU, and circuit failure.

(1) No.1 torque sensor

No.1 torque sensor provides a signal to the AFU. The AFU determines whether the engine torque is less than 22 % and then decides whether to issue an alarm signal of low torque and to excite autofeather events. False low torque signal will force the AFU to emit low torque warning signal and trigger uncommanded autofeather.

(2) AFU

In the armed condition, if the torque signal from the No.1 torque sensor is less than 22 %, AFU sends a power up trim signal to the other engine and a low torque signal to the low torque light. If low torque signal lasts more than 2.15 s, the autofeather command is issued to trigger the uncommanded autofeather. If the input signal of power or torque is interrupted, the output signal of AFU will be affected.

(3) Circuit failure

Poor connection of circuit between the No.1 torque sensor and AFU can result in low torque signal. The AFU will receive intermittent torque signal and treat as a low torque signal to trigger uncommanded autofeather events.

Through the above analysis, it can be found that the No.1 torque sensor has a high reliability and less impact on autofeather light flashing or low torque fault, and the contact failure of circuit can be improved by applying conductivity enhancement solution and increasing the thermal shrinkable sleeve to the connection of plugs and sockets. Therefore, this work will focus on the impact analysis of the input signal to the output signal to the AFU.

38.4 Experiment Analysis

38.4.1 Experiment Method

In order to analyze the effect of power and torque signal interruption to the low torque and autofeather output signal of AFU, an autofeather control box is used in test to control the interruption signal of power and torque to the AFU, and a oscilloscope is used to observe the low torque and power up trim output signals.

The system test schematic is illustrated in Fig. 38.3.

To verify low torque and power up trim output signal, the power and torque signal are controlled by the signal generator. Experimental input parameters and aircraft state are shown in Table 38.1.

38.4.2 Experimental Results

38.4.2.1 Power Interruption Comparison: Armed and Unarmed

(1) The repetitive interruptions durations of 10 ms cannot generate a low torque output pulse for AFU (see No. 1, 2 of Table 38.1 and No. 1, 2 of Table 38.2).
(2) Although a signal pulse may be present on the autofeather relay drive output, repetitive pulses are not seen for interruption durations of 60 ms.
(3) Following an AFU power interruption, an output pulse is observed on the low torque and autofeather relay drive output irrespective of the armed status.
(4) An up trim request is sent to the opposite engine when the AFU is armed.
(5) Neither condition results in an uncommanded autofeather.

38.4.2.2 Unarmed Power Interruption Comparison: Low Torque with Up Trim

(1) The up trim output a shorter pulse following a 60 ms power interruption (see No. 1 of Table 38.1 and No. 1 of Table 38.2).
(2) There is no difference in the repetitive output pulse between the low torque and up trim outputs.

38.4.2.3 Armed Power Interruption Comparison: Low Torque with Up Trim

(1) The up trim does not output repetitive pulses for interruptions of 60 ms whereas repetitive pulses can be shown on the low torque output for interruptions of 60 ms (see No. 2 of Table 38.1 and No. 2 of Table 38.2).

Fig. 38.3 System test schematic
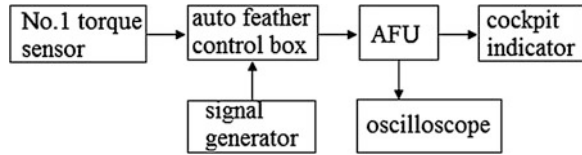
Table 38.1 Low torque test

No.	Signal interruption	Signal state	Arming state	Power condition
1	Power	10 × 60 ms@duty cycle	Unarmed	Cruise
		10 × 200 ms@duty cycle		
2	Power	10 × 60 ms@duty cycle	Armed	Take off
		10 × 200 ms@duty cycle		
3	Torque	10 × 30 ms@duty cycle	Unarmed	Cruise
		10 × 200 ms@duty cycle		
		10 × 500 ms@duty cycle		
4	Torque	10 × 10 ms@duty cycle	Armed	Take off
		10 × 30 ms@duty cycle		
		10 × 200 ms@duty cycle		
		10 × 500 ms@duty cycle		

Table 38.2 Power up trim test

No.	Signal interruption	Signal status	Armed state	Power condition
1	Power	10 × 60 ms@duty cycle	Unarmed	Cruise
		10 × 200 ms@duty cycle		
2	Power	10 × 60 ms@duty cycle	Armed	Take off
		10 × 200 ms@duty cycle		
3	Torque	10 × 30 ms@duty cycle	Unarmed	Cruise
		10 × 200 ms@duty cycle		
		10 × 500 ms@duty cycle		
4	Torque	10 × 10 ms@duty cycle	Armed	Take off
		10 × 30 ms@duty cycle		
		10 × 200 ms@duty cycle		
		10 × 500 ms@duty cycle		
		1 × 10 s@duty cycle		

(2) The repetitive pulses are observed on the up trim signal and low torque output for interruptions of 200 ms.

(3) Neither condition resulted in an uncommanded autofeather.

38.4.2.4 Torque Interruption Comparison: Armed and Unarmed

(1) The number of observed low torque pulses does not correspond to the number of interruptions below the 500 ms interruption rate when the system is armed (see No. 3, 4 of Table 38.1 and No. 3, 4 of Table 38.2).
(2) There are no transitions of the autofeather relay drive output when the AFU was armed for interruptions of 500 ms or less.
(3) There was no low torque or autofeather relay drive output transitions when the AFU was unarmed.
(4) Low torque output pulses were only present when the AFU was armed.
(5) Only the 10 s torque signal interruption with the AFU armed resulted in an autofeather event.

38.4.2.5 Unarmed Torque Interruption Comparison: Low Torque with Up Trim Output

None of the torque signal interruptions had any effect on the AFU outputs when the AFU is unarmed (see No. 3 of Table 38.1 and No. 3 of Table 38.2).

38.4.2.6 Armed Torque interruption comparison: Low Torque with Up Trim Output

(1) No AFU output transitions were observed on the up trim output for torque interruptions of 500 ms or less (see No. 4 of Table 38.1 and No. 4 of Table 38.2).
(2) AFU output transitions were observed on the low torque output for torque interruptions of 10 ms and above.
(3) The low torque light is seen to come on about 4 s before the autofeather armed light whereas the AFU up trim output occurs at the same time as the armed light.
(4) Only the 10 s torque signal interruption with the AFU armed resulted in an autofeather event.

38.4.2.7 Low Torque Output Compared to Up Trim Output

(1) The up trim output exhibits a better resistance to generate output pulses as a result of repetitive power interruptions up to a rate of 200 ms (see No. 1, 2, 3, 4 of Table 38.1 and No. 1, 2, 3, 4 of Table 38.2).
(2) The up trim output does not generate pulses as a result of a torque signal interruption less than 500 ms when the AFU is armed.
(3) When armed, the up trim signal only reacts if the torque signal has been continually lost for the duration of 2.15 s.

38.4.2.8 Power Interruption Compared to Torque Signal Interruption

(1) Power signal interruptions of 200 ms generate pulses on the AFU low torque and up trim output s for all configurations (see No. 1, 2, 3, 4 of Table 38.1 and No. 1, 2, 3, 4 of Table 38.2).
(2) The autofeather relay device output pulses are only generated as a result of power interruptions.
(3) Torque signal interruptions only generate pulses on the low torque output when the AFU is armed.
(4) Only a torque interruption of 10 s resulted in an autofeather event.

38.4.3 Solution

It can be concluded that the AFU does not result in an uncommanded autofeather events for all test conditions except for a torque interruption of 10 s resulting in an autofeather event per design when the AFU is armed, and only AFU power interruptions result in short pulses at the AFU relay drive output when the interruption rate is 200 ms or above. Meanwhile, experimental results indicate that either repetitive power interruptions or repetitive torque interruptions of the AFU can result in the low torque light flashing in the cockpit. Based on the survey results, the AFU is redesigned and two filters are added to the AFU output terminal of low torque and power up trim signal filtering the boring pulses to eliminate effect of such pulse signals generated by the system for the aircraft indicating system and improving the flight quality.

38.5 Conclusion

With the development of aviation industry, turboprop aircraft, as a superior performance turboprop regional aircraft, will bloom in more and more markets and fly all over the world. Any flaws will affect the aircraft's reputation and operations. The autofeather system analysis and optimization of AFU can effectively reduce the probability of uncommanded autofeather and low torque light flashing events, eliminating the effect of such a pulse signal generated by the aircraft on the indicating system, reducing the risk of single flight, and laying the strong foundation for the continued operation of the aircraft.

References

1. Vessella V (2012) PW127 J on XAC aircraft uncommanded autofeather investigation. Pratt & Whitney, Canada, pp 15–18
2. Takashisa K (2003) Aircraft engine sensor/actuator/component fault diagnosis using a bank of Kalman filters. In: NASA/CR-2003-212298, 2003
3. Zedda M, Singh R (2002) Gas turbine engine and sensor fault diagnosis using optimization techniques. J Propul Power 18(5):1019–1025
4. Xiao H, Xue Q, Lian X et al (2005) Engine fault diagnosis techniques of component characteristic un-known engine. J Propul Power 20(5):746–750 (in Chinese)
5. Zhang S (2004) A review of aero engine control system. J Aerosp Power 19(3):375–382 (in Chinese)
6. Wnag Y, Sha Y-D (2007) Aero engine fault diagnosis techniques summarization. J Shenyang Aerosp Univ 24(2):11–14 (in Chinese)
7. Dai W-Q, Yao W-Z (2003) Failure mode, effects and criticality analysis. Aircr Des 1:76–80 (in Chinese)
8. P & WC (2012) Maintenance manual. Pratt & Whitney Publication Center, Canada, pp 512–513

Chapter 39
Avionics System Fault Diagnosis Methods Based on the Probabilistic Causal Network

Yuxin Wang, Tianwei Zhang, Wei Zhou and Bin Ru

Abstract This paper applies the parsimonious covering theory and the causal network model to the multiple-fault diagnosis of an avionic system. Firstly, the paper introduces the meaning of the avionics system fault diagnosis and the basic content of the fault diagnosis; Next, it briefly introduces the basic theory of the parsimonious covering theory and the causal network model, summarizes the methods of the multiple-fault diagnosis research, and puts forward the causal strength calculation method depending on the fuzzy algorithm of multiple attribution judgment. Finally, based on the causal network structure method of the fault tree, it gives the corresponding structure rules and specific examples, and the difficulty of multiple-fault diagnosis modeling in avionic system is successfully solved. The validities of the methods presented in the thesis are verified by the application of the algorithms in the multiple-fault and correlative fault diagnosis of an avionic system.

Keywords Avionic system · Multiple-fault diagnosis · Parsimonious covering theory · Causal network

Y. Wang (✉) · T. Zhang · W. Zhou · B. Ru
School of Aeronautics, Northwestern Polytechnical University,
Xi'an 710072 Shaanxi, China
e-mail: wangyuxin1219@126.com

T. Zhang
e-mail: ztw@nwpu.edu.cn

W. Zhou
e-mail: wisemanguo@gmail.com

B. Ru
e-mail: hitlerrb@126.com

39.1 Introduction

Avionics system is an important part of aircraft, the normal operation of the system is not only related to constituting the quality of the system hardware and software, but also to the system environment, system composition, characteristics, structure, operation level, and maintenance level, so we must pay attention to the fault situation's study [1, 2].

When the avionics system failure occurs, due to its own multilateral and complex structure, making the fault does not generally exist in isolation; usually between them, there is interdependence and have reciprocal influence.

39.2 The Basic Content of Multiple-Fault Diagnosis

The so-called fault's characteristic refers to the correlation and inclusive between the system failure, which generally can be divided into two kinds: single fault and multiple faults.

The basic process of multiple-fault diagnosis is shown in Fig. 39.1.

39.3 The Parsimonious Covering Theory and the Causal Network Model

39.3.1 The Parsimonious Covering Theory

The parsimonious covering theory is a try to clarify the basis diagnosis expert system with induction reasoning the theory. It describes diagnosing the problem as a tetrad

$$P = <D, M, R, M^+ > \tag{39.1}$$

.

Among them, $D = \{d_1, d_2, \ldots, d_n\}$ indicates the failure limited non-empty set; $M = \{m_1, m_2, \ldots, m_p\}$ indicates signs of finite set are not empty; $R \subseteq D \times M$ indicates defined ordered subset relationship in the $D \times M$; $M^+ \subseteq M$ indicates signs of the known collection.

39.3.2 The Causal Network Model

Although the parsimonious covering theory for induction reasoning diagnosis problem which using symbols causal relationship provides the theoretical
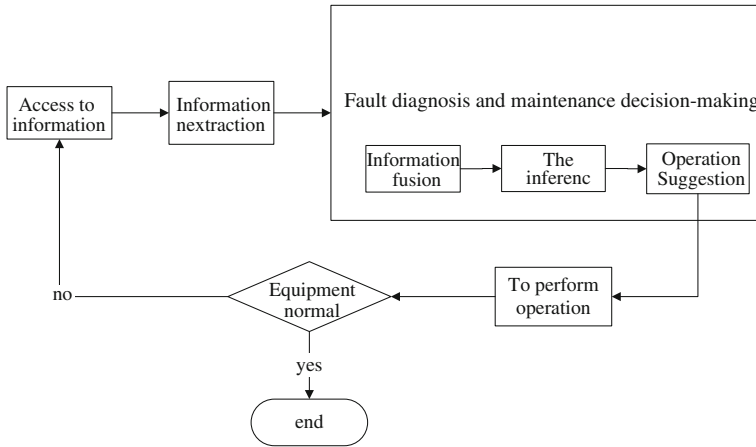
Fig. 39.1 Multiple-fault diagnosis process

foundation, the parsimonious covering theory just uses the symbols and rules as the basis of diagnosis reasoning, rather than in digital form of probability of the existence of knowledge [3, 4]. In order to solve this problem, we must bring the probable knowledge in the parsimonious covering theory and establish the analogous model [5].

The overall process of the causal network model is shown in Fig. 39.2.

39.4 Avionics System Fault Diagnosis Methods Based on the Probabilistic Causal Network

The fault tree is a common reliability, safety analysis, and diagnosis model. Its constructive thought is a typical thought of hierarchical structure. As follows, it mainly introduces the method of the probabilistic causal network structure based on the fault tree [6, 7].

According to Boeing 777 handbook of isolation fault tree model, on the basis of fuzzy theory and analytic hierarchy process [8], we can put forward the causal strength of the algorithm based on the method of fuzzy multiple attribute evaluation.

Maintenance of causal strength of expert advice u_1, conclusion maintenance history u_2, and design expert opinion u_3 constitute the implications of causal strength value judgment property set, denoted as:

$$U = \{u_1, u_2, u_3\} \tag{39.2}$$
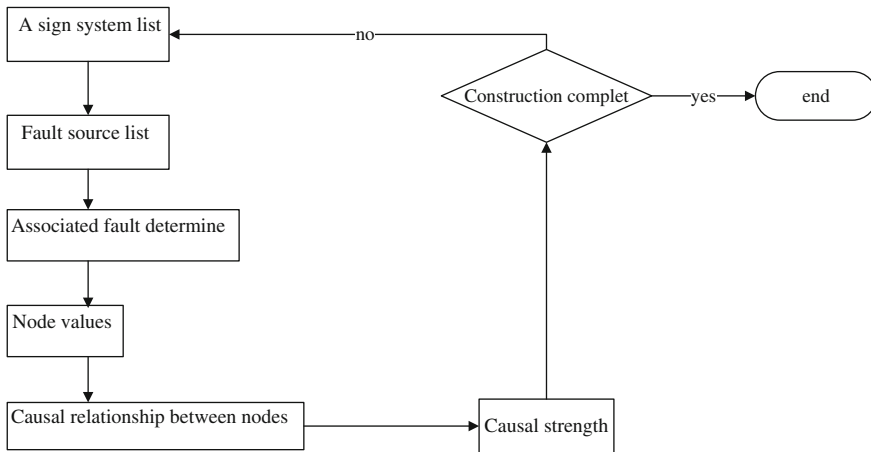
Fig. 39.2 The overall process of the causal network model

The expert points constitute the evaluation standard set several grades V, denoted as:

$$V = \{v_1, v_2, \ldots, v_M\} \quad (M \text{ is the total number of levels}) \tag{39.3}$$

The size of M can be determined depending on the accuracy and the corresponding in the practical application.

The causal strength can be obtained by (39.1) and (39.2) [9]: Fuzzy evaluation matrix

$$R' = \begin{bmatrix} r_{11} & \ldots & r_{1n} \\ r_{21} & \ldots & r_{2n} \\ r_{31} & \ldots & r_{3n} \end{bmatrix}. \tag{39.4}$$

(U, V, R') is known as the avionics causal strength fuzzy multiple attribute evaluation model of fault diagnosis. It uses analytic hierarchy process confirming the weight of expert advice U_1, concludes maintenance history U_2, and designs expert opinion U_3. According to the above methods, we can obtain the weight value and fuzzy evaluation matrix transformation [9]:

$$R = W \cdot R' = (w_1, w_2, w_3) \cdot \begin{pmatrix} r_{11} & \ldots & r_{1n} \\ r_{21} & \ldots & r_{2n} \\ r_{31} & \ldots & r_{3n} \end{pmatrix} = (r_1, r_2, \ldots, r_n) \tag{39.5}$$

39.5 The Example of the Avionics System Fault Diagnosis

Based on the Boeing 777 aircraft fault isolation manual and we build the wing (part) in electronic fault causal network based on the method of fault tree probabilistic causal network construction, which is shown in Fig. 39.3.

The link between the nodes is below: (Table 39.1).

We choose five aircraft design experts, five aircraft maintenance and troubleshooting historical records. With the fuzzy multiple attribute evaluation method, we calculate the causal strength (there are 17 unknown causal strengths).

The weight

$$W = (w_1, w_2, w_3) = (0.637, 0.258, 0.105) \tag{39.6}$$

$$R = W \cdot R' = (w_1, w_2, w_3) \cdot \begin{pmatrix} r_{11} & \cdots & r_{1,17} \\ r_{21} & \cdots & r_{2,17} \\ r_{31} & \cdots & r_{3,17} \end{pmatrix} \tag{39.7}$$

According to the above formulas, the causal matrix [9] as follows:

$$\begin{pmatrix} & c_1 & c_2 & c_3 & c_4 & c_5 & c_6 & d_1 & d_2 & d_3 & d_4 & d_5 \\ m_1 & 0.3758 & 0.7244 & 0.5083 & & & & & & & & \\ m_2 & 0.4382 & & 0.5245 & 0.1308 & & & & & & & \\ m_3 & & & 0.3940 & 0.5232 & & & & & & & \\ m_4 & & 0.6917 & 0.4197 & & 0.0983 & 0.7409 & & & & & \\ c_1 & & & & & & & 0.6681 & 0.4979 & & & \\ c_3 & & & & & & & & & 0.8204 & 0.3550 & 0.5515 \end{pmatrix}$$

$M^+ = \{m_2, m_3\}$, based on simple rules ICGS algorithm and minimum coverage, calculating second floor the minimum cover sets are: $\{c_3\}, \{c_4\}$, to solve their relative likelihood degrees, respectively.

The result is following:

$$L(\{c_3\}) = L_1(\{c_3\}) \cdot L_2(\{c_3\}) \cdot L_3(\{c_3\}) = 0.206653 * 0.2853 * 0.0000576$$
$$\approx 3.3960 * 10^{-6}$$
$$\tag{39.8}$$

The same can be:

$$L(\{c_4\}) = L_1(\{c_4\}) \cdot L_2(\{c_4\}) \cdot L_3(\{c_4\}) = 0.06843456 * 1 * 0.0000909$$
$$\approx 6.2207 * 10^{-6} \tag{39.9}$$

Obviously, $L(\{c_4\})$ is larger, so when calculating the second floor, the best solution is c_1. Because the c_4 upper has no source node, for any $L < 1$, according to the total of $\{c_3\}$ of reasoning, its relative likelihood degree is less than $L(\{c_4\})$. So for $M^+ = \{m_2, m_3\}$, in accordance with minimum cover of the contracted standards covers the solution according to the possibilities in the order: $\{c_4\} > \{c_3\}$.
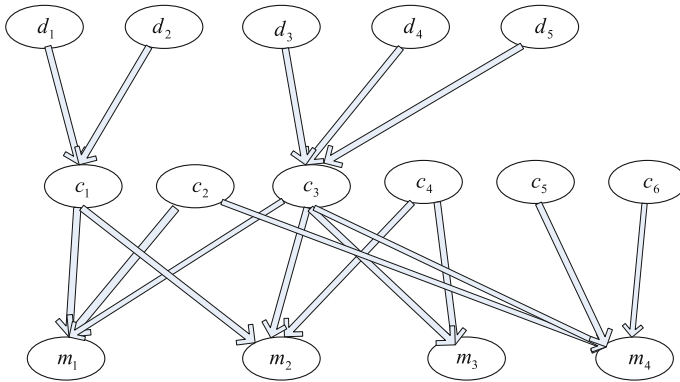
Fig. 39.3 The wing (part) electronic causal network fault

Table 39.1 p_i 和 effect (p_i)

Source node	Signs of the node	Source node	Signs of the node
d_1, d_2	c_1	d_3, d_4, d_5	c_3
c_1	m_1, m_2	c_2	m_1, m_4
c_3	m_1, m_2, m_3, m_4	c_4	m_2, m_3
c_5	m_4	c_6	m_4

The descriptions of the nodes are below: d1: Pressure sensor signal errors; d2: Hydraulic system pressure problems; d3: Incentive Control Center component failures; d4: Actuator / sensor failures; d5: Line faults; c1: Hydraulic system control problems; c2: Left aileron power control component failures; c3: Central incentive control module transmission faults; c4: Left flaperon power control component failures; c5: Center power supply component failures; c6: Spiral operated valve line faults; m1: Left aileron power control unit command errors; m2: Right flaperon power control unit command errors; m3: Right flaperon feedback power control unit problems; m4: Left aileron power control unit spiral tube valve failures. The probability value of each component is obtained from the reliability data

39.6 Conclusion

Through the example, compared with the traditional method of the avionics, the multiple-fault diagnosis based on the probabilistic causal network has the following two advantages: (1) Its accurate fault diagnosis is more efficient. When failure associated more coupling conditions, the network structure is more intricate. The customary fault diagnosis method is time-consuming and laborious. But, the method that described in this paper can indicate the source of trouble quickly through the calculation of reasoning, accurate, and efficient diagnosis task; (2) it identifies several possible faults collection and quantitative ordering. In traditional fault diagnosis, it is necessary to carry out in accordance with the fault isolation manual and maintenance manual step by step, which cannot good use the troubleshooting history data and expert inspection; But, this method can sort all diagnostic solution sets that based on giving all possible solution sets under the guidance of causal network, the reliability data, troubleshooting history data, and expert inspection, so as to realize the quantitative output of fault diagnosis.

To sum up, the example has verified the causal network based on the probabilistic in the avionics fault diagnosis method is more scientific and effective, and can satisfy the demands of multiple fault and associate faults diagnosis.

References

1. Wang Y, Yu H (2008) The onboard computer system. National Defence Industry Press, Beijing (in Chinese)
2. Feng P (2008) The development of China's large aircraft's airborne equipment thinking. J Aviat 29(3):681–685 (in Chinese)
3. Guo XJ (2008) Fault diagnosis model of aircraft avionics system board. In: Control and decision conference, pp 587–590
4. Ma C, Zhu D, Shi H (2009) Diagnostic method of causal network model based on swarm intelligence algorithm. In: International workshop on intelligent systems and applications (ISA 2009)
5. Boukhris I, Elouedi Z, Benferhat S (2013) On the modeling of causal belief networks. In: 5th international conference on modeling, simulation and applied optimization (ICMSAO 2013)
6. Liu B (2008) The fault tree and fault dictionary method combined with computer interlocking system fault diagnosis. J Railway Commun Signals 12(4):7–12 (in Chinese)
7. Chenhu W, Li J, Hu F (2011) Fault tree synthesis for an avionic network. In: International conference on transportation, mechanical, and electrical engineering (TMEE, 2011)
8. Xixiang C, Qiu J, Liu G (2010) Based on fuzzy comprehensive evaluation's analytic hierarchy process and method of the test equipment selection. Acta Armamentarium 31(1):68–73 (in Chinese)
9. Laifu L (1997) The mathematical model and mathematical modeling. Beijing Normal University Press, Beijing (in Chinese)

Chapter 40
Multiple Performance Parameters Fault Prediction Method Based on Gamma Process and Resemblance Coefficient

Wei Li, Yuying Liang, Jinyan Cai and Guolong Zhang

Abstract A 20kHz signal board of radar is the research object and the circuit board reliability analysis is made by using performance degradation reliability theory. The rule of radar circuit board performance degradation in the electric impact environment was concluded with the testing data. Aiming at the insufficient of the multiple performance degradation parameters fault prediction method existing, a new method based on resemblance coefficient is present. The new method combine the signal processing technology with the performance degradation theory. The resemblance coefficient fused the multiple performance parameters degradation characteristics, so the multi-feature extraction difficulties of multiple performance parameters has been solved. Then, the Gamma process is used to describe resemblance coefficient degradation for modeling, extrapolated life information of the product, and finally, validity of this method was proved by the testing data.

40.1 Introduction

At present, most fault trend forecasting methods based on degradation date only consider one single degradation measure of products, while in actual project, products often have multiple performance parameters. There are two ways to solve the multiple performance parameters reliability evaluation problems that mentioned above. One is assuming multiple performance parameters are independent;

W. Li (✉) · Y. Liang · J. Cai · G. Zhang
Department of Electronic and Optical Engineering, Ordnance Engineering College, Shijiazhuang 050003, China
e-mail: evenstar1213@sina.com

then, the system can follow the tandem approach. This method is simple and fast, but the analysis is not comprehensive enough and the result has large errors. Another is fully considered the correlation between performance parameters, such as joint state-space method and probability density method [1, 2]. These methods taken the correlation between the parameters into account fully, but when the amount of characteristic parameter is large, modeling is difficulty and the amount of calculation become large.

To solve these problems, from the statistical analysis and signal processing angles, fault trend forecasting method based on the data of multiple performance parameters degradation is researched in this paper. In environmental stress of electric shock and others, accelerated degradation test for the signal board with 18 V 20 kHz of a certain type of radar is conducted. We analyze the test results deeply and summed the general rules of board degradation under the electrical impact. Then, the signal processing theory is creatively introduced to the failure prediction of electronic equipment with high reliability and long life and the methods and procedures of failure prediction for electronic equipment is designed. Firstly, method of determine the characteristic of multiple performance parameter is given. Then through the introduction of signal processing techniques, failure prediction based on single performance parameter degradation data is expanded. Failure prediction of multiple performance parameter degradation data based on resemblance coefficient is proposed. The effectiveness of the algorithm is shown with test data.

40.2 Failure Prediction Methods Based on Degradation Modeling

Because modern electronic equipment is characterized by high reliability and long life, usually, little or no failures occur in the accelerated test failure. The traditional method is no longer applicable to the failure prediction of the electronic equipment with high reliability and long life. Studies show that most products can be traced back to the potential performance degradation process of the product. Starting from the failure mechanism of the product, by analyzing the correlation of product failure and law of degradation, information of performance fully associated with life can be accessed. Modeling and analyzing the accelerated degradation test data, we can get the reliability of the product under rated working under stress [3, 4].

The precise relationship between the failure of electronic product and the measure of performance degradation can be created using degradation model and degradation data. Then, lifetime can be inferred and predicted. There are two requirements to establish the relationship between the measure of degradation $X(t)$, lifetime distribution, and reliability function $R(t)$: a model describing performance degradation process and the failure threshold D.

Assuming m samples were put out randomly from all the products and the degradation track of a single sample degradation measure varying with time was denoted as $d(t)$, $t > 0$, then the obtained degradation data of the ith sample at the t_j time is as follows:

$$X_{ij} = d(t_{ij}, \theta_i) + \varepsilon_{ij}$$

where $i = 1, 2,\ldots, m$, $j = 1, 2,\ldots, n$, $d(t_{ij}, \theta_i)$ is the practical degradation track of the ith sample at the t_j time and $\varepsilon_{ij} \sim N(0, \sigma_\varepsilon^2)$ is measurement error. In the current work of investigating the modeling of accelerated degradation, the model of a stochastic process with independent increments is used to describe the product's performance degradation processes. For most products with performance degradation, degradation process can be described by the following models, where the first three models are most widely used as follows:

$$\text{Wiener process model: } X(t) = \mu t + \sigma W(t)$$

$$\text{Gamma process model: } \Delta X(t) \sim Ga(vt, \ u)$$

$$\text{Cumulative damage model: } X(t) = \sum_{k=0}^{N(t)} S_k$$

$$\text{Random variable model: } X(t) = g(t; \Theta)$$

$$\text{Marginal distribution: } X(t) \sim f(\theta_1(t), \ldots, \theta_n(t)).$$

Since Wiener process [5] can describe the performance degradation process of many typical products and has excellent statistical analysis characteristic, it is one of the most basic and most widely used models that modeling and analyzing reliability based on performance degradation. Gamma process is a nonnegative and strictly monotonic stochastic process. It can describe the performance degradation process which is strictly monotonic, such as fatigue process, corrosion process, and wear process. Cumulative damage model, also known as shock model, is suitable for performance degradation process that occur because cumulative impact and minor damage.

Let the product failure threshold be D. The lifetime T is the performance degradation measure become D for the first time. Take the increasing degradation process for example, $T = \inf\{t \mid X(t) > D\}$.

The steps of fault prediction algorithm based on the degradation model steps are as follows:

Step 1: Collect the performance degradation data of test samples at the time $t_1, t_2,\ldots, t_n$. For the ith sample, degradation data is (t_j, X_{ij}) $(i = 1, 2, \ldots, m, j = 1, 2,\ldots, n)$.

Step 2: Select appropriate degradation track model based on the trend of performance degradation curve the trend of changes of the amount of degradation in unit time.

Step 3: Estimate the parameter of performance degradation model θ using the collected performance degradation data.

Step 4: deduce the life characteristics, using $T = \inf\{t \mid X(t) > D\}$, according to the degradation track model obtained in Step 2, for given failure threshold D.

40.3 Failure Prediction of Multiple Performance Parameter Degradation Data Based on Resemblance Coefficient

In recent years, many scholars undertook detailed investigation of the assessment methods of equipment performance degradation, such as logistic regression, feature maps, CMAC neural network, support vector machine, hidden Markov process [6–9] and so on. The core idea of these studies is to describe the equipment performance degradation using the difference and degree of membership between the current data of equipment and the normal data of equipment. Inheriting this idea, through combining resemblance coefficient method with performance degradation theory, failure prediction of multiple performance parameter degradation data based on resemblance coefficient was proposed.

40.3.1 The Concept and Algorithm of Resemblance Coefficient

Resemblance coefficient is used in feature extraction of signal parameters. During the feature extraction, the high-dimensional vector of the measurement space is mapped into scalar of the feature space scalar directly [10, 11]. The mapping is parallel to the projection of a function on another.

Definition 1 Assuming there are two one-dimensional continuous real functions $f(x)$ and $g(x)$, then coefficient is as follows:

$$C_{\mathrm{rc}} = \frac{\int f(x)g(x)\mathrm{d}x}{\sqrt{\int f^2(x)\mathrm{d}x}\sqrt{\int g^2(x)\mathrm{d}x}} \tag{40.1}$$

C_{rc} is the resemblance coefficient of $f(x)$ and $g(x)$, where $f(x)$ and $g(x)$ are not always zero. This formula gives the difference degree between the trends of the two functions and also can be said the likeness of image or outline.

Sampling $f(x)$ and $g(x)$ with the sampling theorem, signed as $S_1(i)$ and $S_2(j)$

$$f(x) = \sum \left[S_1(i) \cdot \sin c(x - i \cdot T) \right] \tag{40.2}$$

$$g(x) = \sum \left[S_2(j) \cdot \sin c(x - j \cdot T) \right] \tag{40.3}$$

where T is the sampling period and $\sin c()$ is the sampling function. And the discrete formula of the resemblance coefficient can be got.

Definition 2 Assuming there are two one-dimensional discrete signal $\{S_1(i), i = 1, 2,\ldots, N\}$ and $\{S_2(j), j = 1, 2,\ldots, N\}$, coefficient:

$$C_r = \frac{\sum S_1(i) S_2(j)}{\sqrt{\sum S_1^2(i)} \sqrt{\sum S_2^2(j)}} \tag{40.4}$$

C_r is the resemblance coefficient of $S_1(i)$ and $S_2(j)$, called discrete resemblance coefficient, where $f(x)$ and $g(x)$ are not always zero.

This formula can be obtained by the Cauchy–Schwartz inequality:

$$0 \le \left| \int f(x) g(x) dx \right| \le \sqrt{\int f^2(x) dx} \sqrt{\int g^2(x) dx}$$

as well as the following:

$$0 \le |C_{\mathrm{rc}}| \le 1 \tag{40.5}$$

Accordingly, for discrete resemblance coefficient C_r:

$$0 \le \left| \sum S_1(i) S_2(j) \right| \le \sqrt{\sum S_1^2(i)} \sqrt{\sum S_2^2(j)}$$
$$0 \le |C_r| \le 1 \tag{40.6}$$

It can be shown from the definition that when the two signals are proportional, C_{rc} and C_r to the maximum value 1, when the two signals are orthogonal, the resemblance coefficients arrive the minimum value 0. When the difference between trend curves of two signals is large, the values of C_{rc} and C_r are small. With the two curves become more and more similar, the values of C_{rc} and C_r values gradually increase until the two signals are proportional or same. Resemblance coefficient depends primarily on two signals' trend or outline.

With this idea, the plurality of characteristic parameters of the equipment status data was stored in the waveform during monitoring process. The signal waveform at the initial time was taken as the standard waveform data. The daily monitoring data were set as the intermediate-state data. The performance of the equipment was evaluated through the difference between the waveforms.

40.3.2 Method for Parameter Selection and Fault Prediction

For degenerate complex electronic products, performance information can be reflected by the waveform monitored during the test process. The change in the

signal waveform contains the changes of signal frequency, phase, and amplitude change information. Therefore, the introduction of resemblance coefficient can give the change information of various characteristic parameters and can be used to describe the change in performance of complex electronic products. This paper takes C_{rc} and C_r as the major parameters of product's performance degradation.

The process of failure prediction algorithm based on resemblance coefficient is shown in Fig. 40.1, where the portion in the dotted rectangle is the collection and pretreatment of the monitoring data of product performance, in order to fit formulas and calculations. In the actual operation, the waveform is sampled at the acquisition time by the sampling theorem to obtain a discrete signal. Expression (40.4) in mainly used to calculate the resemblance coefficient another key factor of getting a curve of lifetime reliability is combing resemblance coefficient with performance degradation theory effectively. The algorithm is as follows:

Step 1: Suppose there are n samples. Then, collect performance monitoring signal of the samples at the time t_1, t_2,…, t_m. Pretreat these signals and calculate the resemblance coefficient of n samples at each time between standard signal and performance detection signal by expression (40.4) C_{i1}, C_{i2},…, C_{in}, $i = 1, 2,…, m$;

Step 2: Observe degradation regularity of the test data and select the appropriate degradation model for modeling.

Step 3: Estimate the parameters of degradation model based on resemblance coefficient.

Step 4: After getting the estimated value of the parameters of random degradation model based on resemblance coefficient, for given failure criterion C_{Df}, first passage time T obeys a certain distribution and the distribution of product life can be known.

Step 5: According to $R(t) = 1 - F(t)$, we can get relationship between the resemblance coefficient and the reliability index. Also the predicting value of each characteristics of product's lifetime can be obtained.

40.4 Example Analysis

Take accelerated degradation data of the signal board with 18 V 20 kHz of a certain type of radar under electronic impact as an example. There were eight samples during the test and data were detected each 24 h. The performance parameter was degenerate obviously after 2,040 h and test was end up. The test data are shown in Fig. 40.2.

The function of the circuit is signal generation and amplification, providing 18 V 20 kHz sinusoidal signal for the next level. The signal can have a certain margin when it was used. For a sinusoidal signal, usually there can be DC component, amplitude, frequency, and phase four characteristic values. According to the role they played in equipment, the phase was not considered.
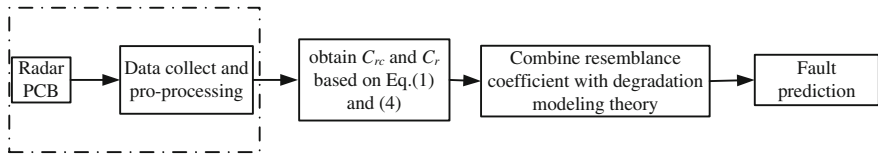
Fig. 40.1 Performance reliability analysis flow diagram based on RC
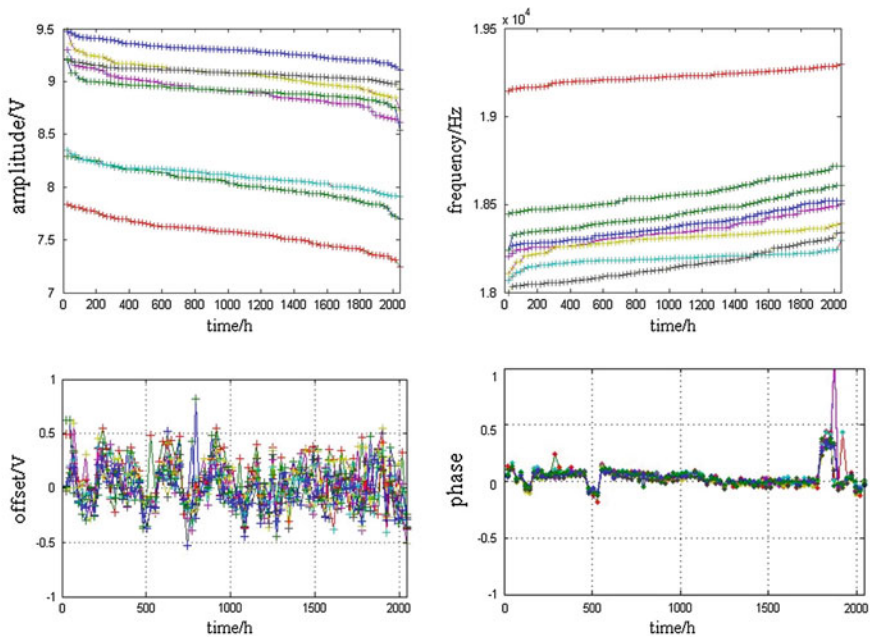
Fig. 40.2 Performance testing data

As can be shown from Fig. 40.2, there is no obvious outlier. In the frequency test, in the numerical way or the way of degradation trend, the curve of sample data at the top has obvious difference from other samples. The amplitude data curve of the same sample is at the bottom of the FIG and different to other samples either, so these sample rest data were excluded.

The detecting signal at one time is $X(t) = A \sin(2\pi f) + C$. A sequence was get after sampling by the sampling theorem $f_s \geq 2f$, usually $f_s = 4f$ in engineering, and $f_s = 80$ kHz in here. The resemblance coefficient of each time can be calculated. The resemblance coefficient of each sample at each time is shown in Fig. 40.3.

It can be shown from Fig. 40.3 that the degeneration process of the resemblance coefficient is strictly monotonous. Modeling by the Gaussian process, parameters can be estimated through Gauss iterative method. The estimated parameters of

Fig. 40.3 Degradation data of resemblance coefficient
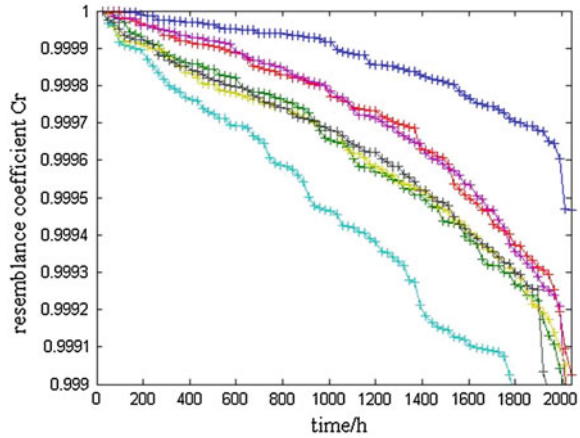
Gaussian process are the following: shape parameter $v = 2.5847 \times 10^{-5}$ and scale parameter $u = 0.2193$.

For failure fault identification of complex electronics, in the case of no given failure criterion, in addition to monitoring signals in practical, simulation method can be used. In [13], damage tests were carried out for each device on the circuit board and the mechanism of injury and sensitive device were identified. In this paper, the key component parameters were set into fail threshold. Simulating in PSpice, the waveforms were obtained. And then through the resemblance coefficient method, $C_{Df} = 0.9821$ was got. Figure 40.4 shows the waveform after compression of the time axis. In the actual analysis, it can be elongated for detailed observation and analysis.

By the characteristic of gamma process, the product's lifetime approximately obeys *BS* distribution [12]. That is,

$$F(t, D) \approx \Phi\left[\frac{1}{\alpha}\left(\sqrt{\frac{t}{\beta}} - \sqrt{\frac{\beta}{t}}\right)\right], \quad t > 0$$

where $\Phi(\cdot)$ is standard normal distribution, $\alpha = \sqrt{u/D}, \beta = D/vu$.

The reliability function of the circuit board can be obtained by the above formula:

$$R(t) = 1 - F(t)$$
$$= 1 - \phi\left[\sqrt{\frac{0.9821}{0.2193}}\left(\sqrt{\frac{0.2193 \times 2.5847 \times 10^{-5} \times t}{0.9821}} - \sqrt{\frac{0.9821}{0.2193 \times 2.5847 \times 10^{-5} \times t}}\right)\right]$$

The reliability curve of random degradation model based on resemblance coefficient is shown in Fig. 40.5.

When $t = 20{,}000$ h, the reliability $R(20{,}000) = 0.9998$. It shows that 99.98 % of the lifetimes of circuit board samples are more than 20,000 h.

Fig. 40.4 Standard signal of 18 V 20 kHz signal generation
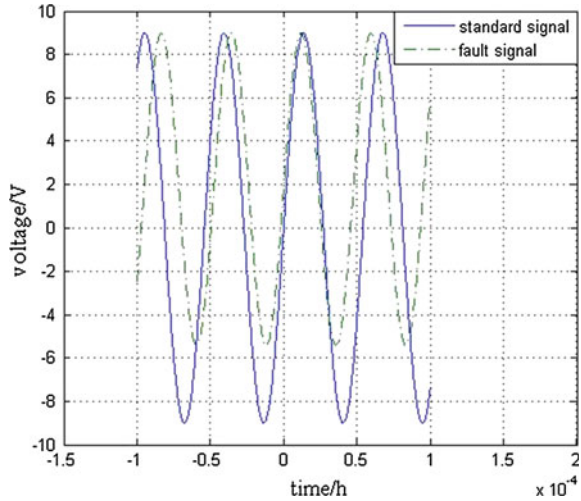
Fig. 40.5 Reliability curves
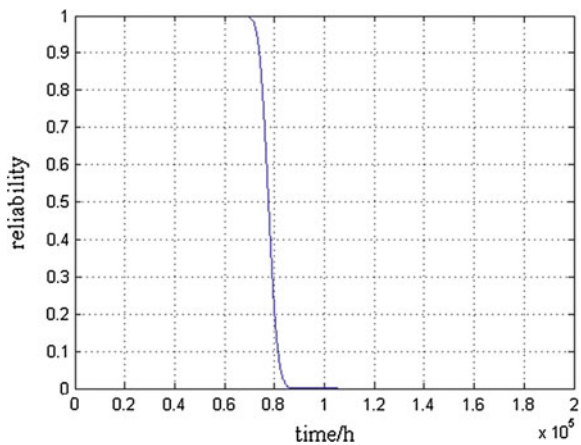
Furthermore, according to the "General failure analysis and simulation system of radar equipment," the average lifetime of that board is 6.9371×10^5 h, which is almost one order of magnitude higher than the lifetime gotten by the resemblance coefficient method. Through deeply analysis, the main sources of error are as follows:

1. The components used in the test are civil, which have some differences from the military ones in quality.
2. The input voltage, temperature, and humidity of the radar board in the test are normal working stress, but the frequency of electric shocks is 0.2 Hz, which is far higher than the frequency usually used. That also shows that the electric shock plays a significant role in affecting the lifetime of the circuit board;
3. The test is random.

40.5 Conclusion

In this paper, from signal feature extraction angle, the degradation law of circuit board with multiple performance parameters degradation data was investigated and used. Thus, the problem of fault prediction of multiple performance parameters degradation data was solved. The reliability assessment algorithm of reliability of multiple performance parameters degradation data based on signal process was proposed, namely resemblance coefficient method. For electronic equipment with complex output characteristics, the change in the waveform of the output signal can reflect the change in its performance, so feature extraction of complex signal and fault prediction of electronic equipment with complex output characteristics can be achieved by resemblance coefficient method. That method is suitable for reliability assessment of electronic products with periodic signal output characteristics. One difficulty of this method is the determination of the fail threshold. The degradation failure signal was got by circuit simulation in PSpice. And then, the failure threshold of resemblance coefficient was extracted in degradation failure. There may be some deviation between that and the actual failure threshold.

References

1. Lu S, Lu H, Kolarik WJ (2001) Multivariate performance reliability prediction in real-time. Reliab Eng Syst Saf 72:39–45
2. Wang Y (2009) Research on electronic products reliability analysis based on performance degradation data (in Chinese). Ordnance Engineering College (2009)
3. Jayaram JSR, Girish T (2005) Reliability prediction through degradation data modeling using a quasi-likelihood approach. Proceedings annual reliability and maintainability symposium. New York, pp 193–199
4. Chen Z, Zheng H (2005) Lifetime distribution based on degradation analysis. IEEE Trans Reliab 54(1):3–10
5. Peng B (2010) Research on reliability modeling methods based on Wiener process (in Chinese). National Defense Science and Technology University, Changsha
6. Duer S (2012) Examination of the reliability of a technical object after its regeneration in a maintenance system with an artificial neural network. Neural Comput Appl 21(3):523–534
7. Xia L, Fang H, Zhang H (2013) HMM based modeling and health condition assessment for degradation process. Control and Decision Conference (CCDC), Guiyang, pp 2945–2948
8. Jin Y, Hu Y, Huang J, Zhang J (2012) Application of support vector regression to vulnerability assessment of electronic devices illuminated or injected by high power microwave (in Chinese). High Power Laser Particle Beams 24(9):2145–2150
9. Casoetto N, Djurdjanovic D, Mayor R et al (2003) Multi-sensor process performance assessment through the use of autoregressive modeling and feature maps. SEM J Manuf Syst 22(1):64–72
10. Sarker BR (1996) Resemblance coefficient in group technology: a survey and comparative study of relational metrics. Comput Ind Eng 30(1):103–116
11. Qu Z, Huang G, Cheng Y, Gao J (2012) A method for radar signal modulation recognition based on multiple characteristic parameters (in Chinese). Electron Optics Control 9(11):31–38

12. Park C, Padgett WJ (2005) Accelerated degradation models for failure based on geometric Brownian motion and gamma processes. Lifetime Data Anal 11:511–527
13. Tan Z (2009) Theory modeling and experimental study of electromagnetic damage on electronic system (in Chinese). Ordnance Engineering College, Shijiazhuang

Chapter 41
Stress Analysis of Cracked Metallic Aircraft Structure Adhesively Repaired with Composite Patch

Weiguo Su, Lan Zou, Zhitao Mu and Xudong Li

Abstract A stress analysis model is developed to characterize adhesive stress distribution of adhesively bonded composite repair structures involving material nonlinearity. The finite element analysis (FEA) is conducted to validate the present closed-form solutions. The numerical results indicate that the analytical solutions and their simplifications correlate very well with the nonlinear finite element computations. The present mathematical techniques and analysis approaches are critical to the successful design, analysis, and implementation of bonded repairs.

Keywords Adhesively bonded composite repair · Analytical model · Adhesive stress · FE model

41.1 Introduction

Fatigue damage is often found on metal structural components of aircraft subjected to fatigue loading. This raises a number of problems, including the ability of the aircraft's structure to maintain damage tolerance and flight safety [1–4]. In order to extend the service life of an aging aircraft, the cracked components must be replaced or repaired. A repair method using composite patches to reinforce the cracked structure has been proved to be very promising due to the high stiffness, high strength, and light weight of the composite patch [5]. To efficiently apply this technology and increase the durability of damaged structures, stress analysis for

W. Su (✉) · Z. Mu · X. Li
Qingdao Campus, Naval Aeronautical and Astronautical University,
Siliu Middle Road. 2, Qingdao 266041, China
e-mail: suweiguo1985@126.com

L. Zou
Qingdao University, Ningxia Road. 308, Qingdao 266061, China

this type of bonding structure must be conducted. The difficulty arises from the fact that a plane stress metallic panel under in-plane loading would develop highly complicated 3-D stresses if composite patches are bonded to its surfaces either symmetrically (double-sided) or asymmetrically. It is difficult to obtain analytical solutions for such a bonded composite repair due to geometrical and material nonlinearity, shear-lag effect, bending effect, and edge effect.

In this study, the nonlinear analytical method of adhesive stress for a double-sided crack patching analysis is presented, in which elastic–plastic characterization of the adhesive is involved. The nonlinear finite element analysis (FEA) including the effect of adhesive plasticity is performed to verify the above analytical solutions.

41.2 Stress Analysis of Bonded Patch Repair

Figure 41.1 shows a typical two-sided patch repair configuration which has three constituents: the cracked plate, the adhesive, and the composite patch. The sheet is subjected to remote uniaxial stresses. The stresses of adhesive can be calculated explicitly using the conventional 1-D theory of bonded joints with the following simplifying assumptions:

- The out-of-deflection will be ignored due to the symmetric repair.
- Two boundary conditions of simple reinforcement strips of cross section AA′ and BB′ in Fig. 41.1 are under strain condition as shown in Figs. 41.2 and 41.3.
- The metallic plate and composite patch are linearly elastic materials, and the adhesive is modeled as an elastic-perfectly plastic material.

The analysis with elastic–plastic characterization of the adhesive is presented in this section. Referring to Fig. 41.4, the basic differential equations are as follows:
Horizontal force equilibrium:

$$\frac{\mathrm{d}N_p}{\mathrm{d}x} - \tau^{(A)} = 0$$
$$\frac{\mathrm{d}N_s}{dx} + \tau^{(A)} = 0 \tag{41.1}$$

Adherend stress–strain relations:

$$\frac{\mathrm{d}u_p}{dx} = \frac{N_p}{E_p' t_p}$$
$$\frac{\mathrm{d}u_s}{\mathrm{d}x} = \frac{N_s}{E_s' t_s} \tag{41.2}$$
$$E_{s,p}' = \frac{E_{s,p}}{1 - v_{s,p}^2}$$
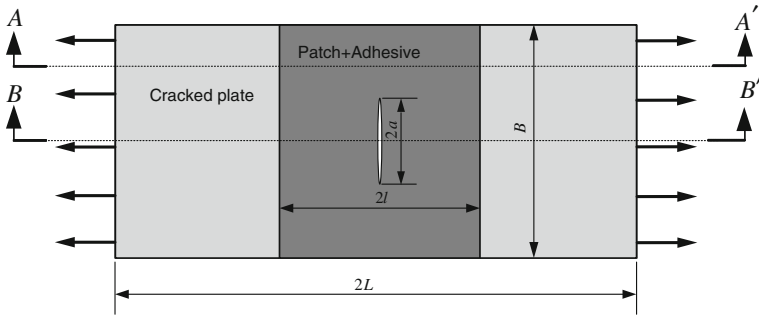
Fig. 41.1 Geometry of a two-sided adhesively bonded composite repair structure
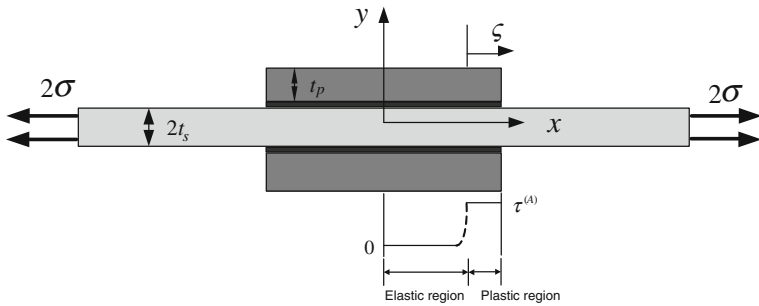
Fig. 41.2 The first-kind boundary condition A–A′
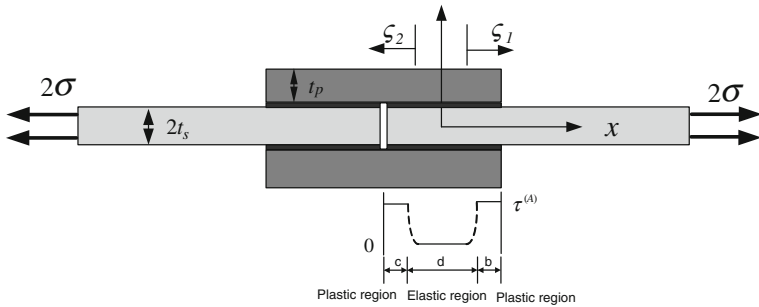
Fig. 41.3 The second-kind boundary condition B–B′

Adhesive elastic stress–strain relation:

$$\tau^{(A)} = G_A \gamma^{(A)} = -\frac{G_A}{t_A}(u_s - u_p) \tag{41.3}$$

where u is the longitudinal displacement of the adherend; N is the load per unit width; τ and γ are the shear stress and strain; E, t, and G are the extensional

Fig. 41.4 Load analysis
acted on the unit volume
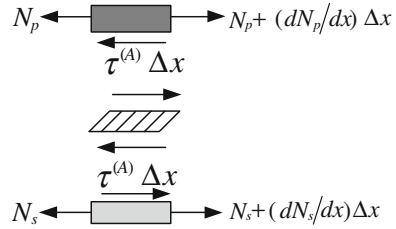
modulus, thickness and shear modulus, respectively; the subscripts and super-
scripts s, p, and A denote the substrate, patch, and adhesive, respectively.

The differential equation governing the adhesive shear–strain distribution fol-
lows by differentiation of Eq. (41.4)

$$\frac{d^2\gamma^{(A)}}{dx} - \beta_A^2 \frac{\tau^{(A)}}{G_A} = 0 \tag{41.4}$$

where

$$\beta_A^2 = \frac{G_A}{t_A}\left(\frac{1}{E_p' t_p} + \frac{1}{E_s' t_s}\right) \tag{41.5}$$

Integration leads to the following general solutions for adhesive elastic and
plastic response, respectively.

$$\gamma^{(A)} = \begin{cases} A\sinh(\beta_A x) + B\cosh(\beta_A x) & \left|\tau^{(A)}\right| < \tau_Y^{(A)} \\ \frac{\beta_A^2 \tau_Y^{(A)}}{2G_A}x^2 + Cx + F & \left|\tau^{(A)}\right| = \tau_Y^{(A)} \end{cases} \tag{41.6}$$

The constants A and B are evaluated from the boundary conditions I and II.

41.2.1 The First-Kind Boundary Condition

(1) Elastic analysis of the adhesive
   The boundary conditions for a doubler will be given by

$$\begin{aligned} \tau^{(A)}(0) &= 0 \\ N_s(l) &= P \\ N_p(l) &= 0 \end{aligned} \tag{41.7}$$

Thus, the adhesive elastic shear–stress distribution can be expressed as follows:

$$\tau^{(A)} = -\frac{G_A \sinh(\beta_A x)}{\beta_A t_A \cosh(\beta_A l)} \cdot \frac{\sigma_\infty}{E_s'} \tag{41.8}$$

(2) Elastic–plastic analysis of the adhesive

The boundary conditions are expressible in the form

$$\gamma^{(A)} = -\frac{\tau_Y^{(A)}}{G_A} = -\gamma_Y^{(A)} \quad x = d \quad \text{and} \quad \varsigma = 0$$

$$\frac{\mathrm{d}\gamma^{(A)}}{\mathrm{d}x} = \frac{\mathrm{d}\gamma^{(A)}}{\mathrm{d}\varsigma} \qquad\qquad x = d \quad \text{and} \quad \varsigma = 0 \tag{41.9}$$

Thus, the adhesive elastic–plastic shear–stress distribution can be expressed as follows:

$$\gamma^{(A)} = -\frac{\gamma_Y^{(A)}}{\sinh(\beta_A d)}\sinh(\beta_A x) \qquad\qquad |x| \leq d$$

$$\gamma^{(A)} = -\gamma_Y^{(A)}\left[1 + \frac{\beta_A}{\sinh(\beta_A d)}\varsigma + \frac{\beta_A^2}{2}\varsigma^2\right] \quad |x| > d \tag{41.10}$$

where d is determined from the transcendental Eq. (41.11).

$$\frac{\beta_A \cdot d \cdot \tanh(\beta_A d) - 1}{\tanh(\beta_A d)} = \beta_A l - \frac{1}{\beta_A t_A \gamma_Y^{(A)}} \cdot \frac{\sigma_\infty}{E_s'} \tag{41.11}$$

41.2.2 The Second-Kind Boundary Condition

(1) Elastic analysis of the adhesive

New boundary conditions must be employed and they are given by

$$N_s(0) = 0$$
$$N_p(0) = P$$
$$N_s(l) = P$$
$$N_p(l) = 0 \tag{41.12}$$

Thus, the adhesive elastic shear stress distribution can be expressed as follows:

$$\tau^A = \frac{G_A \sinh(\beta_A x)}{\beta_A t_A} \cdot \frac{\sigma_\infty}{SE_s'} - \frac{G_A \cosh(\beta_A x)}{\beta_A t_A \sinh(\beta_A l)} \cdot \frac{\sigma_\infty}{E_s'}\left[1 + \frac{\cosh(\beta_A l)}{S}\right] \tag{41.13}$$

(2) Elastic–plastic analysis of the adhesive

If the adhesive undergoes plastic deformation, the boundary conditions are expressible in the form

$$\gamma^{(A)} = -\frac{\tau_Y^{(A)}}{G_A} = -\gamma_Y^{(A)} \quad x = -\frac{d}{2}$$

$$\gamma^{(A)} = -\frac{\tau_Y^{(A)}}{G_A} = -\gamma_Y^{(A)} \quad x = \frac{d}{2}$$

$$\frac{d\gamma^{(A)}}{dx} = \frac{d\gamma^{(A)}}{d\varsigma} \qquad\qquad x = -\frac{d}{2}$$

$$\frac{d\gamma^{(A)}}{dx} = \frac{d\gamma^{(A)}}{d\varsigma} \qquad\qquad x = \frac{d}{2}$$

(41.14)

Thus, the solution of the adhesive shear strain can be expressed as

$$\gamma^{(A)} = -\frac{\gamma_Y^{(A)}}{\cosh(\frac{\beta_A d}{2})}\cosh(\beta_A x) \qquad\qquad -\frac{d}{2} \leq x \leq \frac{d}{2}$$

$$\gamma^{(A)} = \gamma_Y^{(A)}\left(\frac{\beta_A^2}{2}\varsigma_1^2 - \beta_A \tanh(\frac{\beta_A d}{2})\varsigma_1 - 1\right) \quad 0 \leq \varsigma_1 \leq c$$

$$\gamma^{(A)} = \gamma_Y^{(A)}\left(\frac{\beta_A^2}{2}\varsigma_2^2 - \beta_A \tanh(\frac{\beta_A d}{2})\varsigma_2 - 1\right) \quad 0 \leq \varsigma_2 \leq b$$

(41.15)

where *b, c, d* is determined from the Eqs. (41.16) and (41.17).

$$c = \frac{1}{t_A \beta_A^2 \tau_Y^{(A)}} \cdot \frac{\sigma_\infty t_s}{E_p' t_p} - \frac{\tanh\left[\frac{\beta_A(l-b-c)}{2}\right]}{\beta_A}$$

(41.16)

$$b = \frac{1}{t_A \beta_A^2 \tau_Y^{(A)}} \cdot \frac{\sigma_\infty}{E_s'} - \frac{\tanh\left[\frac{\beta_A(l-b-c)}{2}\right]}{\beta_A}$$

(41.17)

41.3 FE Results and Validation

To verify the present closed-form formulation, the FEA is conducted using the commercial FEA package ABAQUS. It is noted that all nonlinear properties of the repairs can be modeled in the FEA package. Using symmetry, the finite element model of a quarter of repaired panel is generated using plane stress quadrilateral elements. Figures 41.5 and 41.6 show the two boundary conditions of repairs for the FE. The properties of the materials are given in Table 41.1.

The adhesive shear stress and shear strain distributions predicted by analytical approach and FE models with far-field stresses in tension of 40 and 80 MPa are shown in Figs. 41.7, 41.8, 41.9, and 41.10. It can be shown that the present results are in good correlation with the finite element results either under elastic or under ductile response except very close to the ends of adhesive layer. This is because the adhesive analytical shear stress solution does not satisfy the traction-free boundary condition of zero shear stress at the ends of the adhesive layer.

Fig. 41.5 The first-kind
boundary condition for FE
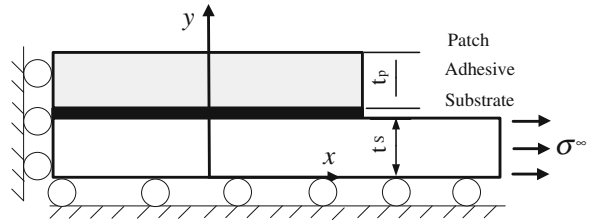
Fig. 41.6 The second-kind
boundary condition for FE
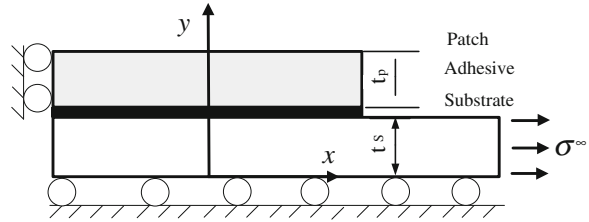
Table 41.1 Material
properties of LY12CZ, T300/
E51, and J150

LY12CZ	T300/E51	J150
$E = 73.8$ GPa	$E_1 = 136.2$ GPa	$E = 2.9$ GPa
$v = 0.33$	$E_2 = E_3 = 9.5$ GPa	$G = 1.09$ GPa
$t = 3.0$ mm	$G_{12} = G_{23} = 6.9$ GPa	$v = 0.33$
	$v = 0.33$	$t = 0.2$ mm
	$t = 0.1$ mm per ply 15 unidirectional(0°)plies	$\tau_Y^{(A)} = 10$ MPa
		$\gamma_{max}^{(A)} = 0.028$

Fig. 41.7 Adhesive shear
stress distribution of BC I
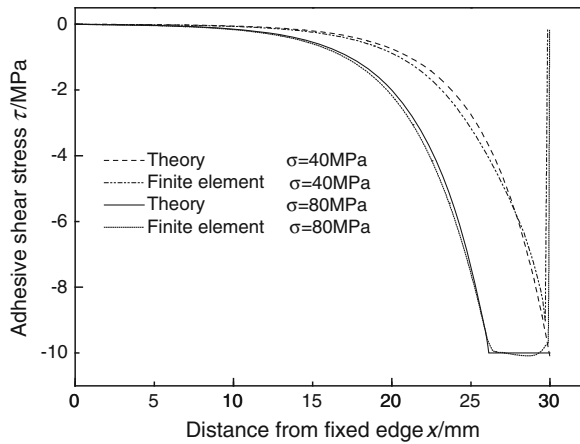
Fig. 41.8 Adhesive shear stress distribution of BC II
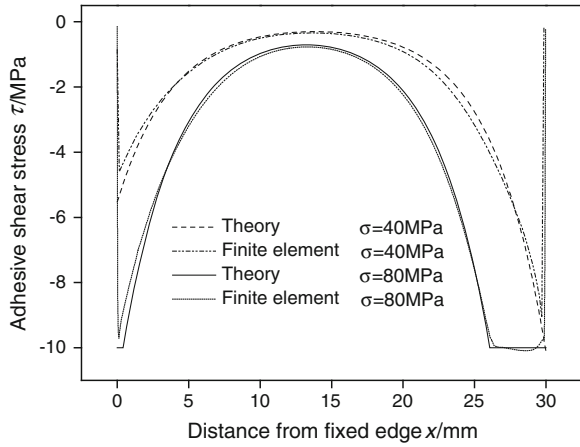
Fig. 41.9 Adhesive shear strain distribution of BC I
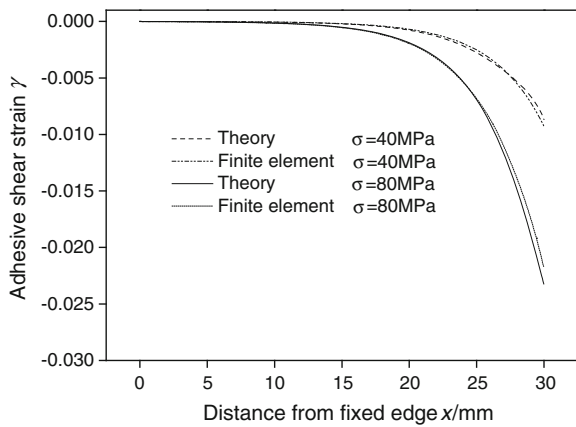
Fig. 41.10 Adhesive shear strain distribution of BC II
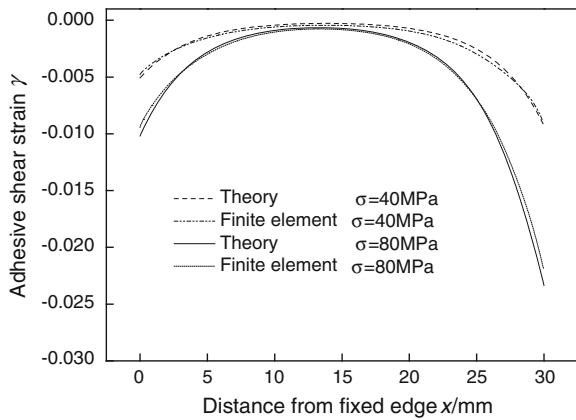
   The adhesive stress and strain distributions near the patch-free edge of the first
BC and the second BC are approximately the same by comparing Figs. 41.7 and
41.8. For a long overlap, there is no interaction between the overlap end and the
skin interruption end. The adhesive shear stress decays exponentially within these
transfer zones and becomes zero outside them. To the second BC, the adhesive
strain near the skin interruption end is always larger than the strain near the
overlap end, as shown in Fig. 41.8. The adhesive at the end of overlap will first
undergo plastic deformation due to shears with the increase in far-field-applied
stress.

41.4 Conclusion

Stress analysis method for adhesive stresses in two-sided crack patching including
effects of adhesive plasticity is developed. The derived analytical solutions and
their simplifications for the double-sided composite patch repairs correlate well
with the nonlinear FEA. The present analysis approaches would be of importance
in the successful design, analysis, and implementation of adhesively bonded
composite repairs.

References

1. Baker AA (1984) Repair of cracked or defective metallic aircraft components with advanced
   fibre composites. Comp Struc 2:153–234
2. Jones R, Callian RJ, Aggarwal KC (1983) Analysis of bonded repair to damaged fiber
   composite structures. Eng Fract Mech 17:37–46
3. Wang CH, Rose LRF (1999) A crack bridging model for bonded plates subjected to tension
   and bending. Int J Solids Struct 36:1985–2014
4. Naboulsi S, Mall S (1996) Modeling of cracked metallic structure with bonded composite
   patch using three layer technique. Comp Struct 35:295–308
5. Wang QY, Pidaparti RM (2002) Static characteristic and fatigue behavior of composite
   repaired aluminum plates. Comp Struct 56:151–155

Chapter 42
Dissimilar Redundancy Structure Design for Carrier Landing Guidance Computer and Reliability Analysis

Wenling Zhong, Wenhai Wu, Gaofeng An, Jian Ren and Shoumiao Yu

Abstract The guidance system is very important to the security of automatic carrier landing for carrier-based aircraft, while its guidance computer is the control center of this system. For enhancing the security and reliability of the system, avoiding general hitch, and serious consequence taken from it, dissimilar redundancy technology could be applied on the system design. From the practical requirements for security of carrier landing, the structure of the guidance computer has been studied, with dissimilar redundancy technique, and a kind of simplified reliability model has been applied on reliability analysis. This study shows that the designed structure can satisfy the security and reliability design requirements of the carrier landing system.

Keywords Dissimilar redundancy · Landing guidance computer · Reliability · Carrier-based aircraft

42.1 Introduction

The guidance computer is the control center of the automatic landing guidance system for carrier-based aircraft, not only to achieve the real-time control of flight for the carrier-based aircraft, but also to manage the carrier-based aircraft and other equipments on the carrier; its reliability plays a key role on the carrier landing [1]. Reliability and fault tolerance are the important factors that should be concerned in the structure design of the system, both software and hardware. In order to improve the performance and security of the landing guidance system, redundancy techniques are usually used to the component and system design [1, 2].

W. Zhong (✉) · W. Wu · G. An · J. Ren · S. Yu
Naval Aeronautical Engineering Institute Qingdao Branch, Shandong, China
e-mail: 1535516602@qq.com

In order to improve the reliability of the guidance computer, some measures should be taken on the features of software and hardware [2, 3]. In order to resolve the random failure of hardware, the redundancy technology usually be used, so the same process runs through the N identical hardware channels, these measures are more effective to improve the reliability of the hardware [2, 4]. However, if occurrence errors from the software and hardware design or specification, the purpose of fault tolerance could not be realized if only duplication of resources, as these errors can occur at the same time, the same failure will be caused at the same operation object or unit of work; it is impossible to detect and separate this kind of error, when we use the monitoring method through the cross-channel checking between every redundancy, and the system itself will ignore the common failure, which could bring catastrophic consequences [2, 5, 6].

In order to avoid the above serious consequences that caused by common failures, we can use another design technique of dissimilar redundancy. It is based on the independent design and development, both hardware and software should be developed by completely independent-working group, with different languages and different development tools, and should be run on different processors, so that the each channel's failure cannot occur at the same time with the same signal, the so-called common failure can be avoided [7].

42.2 The Structure Design of Landing Guidance Computer

42.2.1 The Function Requirement of the Landing Guidance Computer

The landing guidance computer will integrate the information from landing guidance radar, integrated navigation system, photoelectric sensors and sensors from other relative systems, transmit the guidance information/instruction to the carrier-based signal transmitter station, platform of landing guidance and instruct device of landing, and guide the carrier-based aircraft landing securely. The function structure of the computer is shown in Fig. 42.1.

42.2.2 The Reliability Requirements of Landing Guidance Computer

There is no Chinese standard requirement for the design of landing guidance computer. Based the requirements for safety and reliability of aircraft on GJB 3819-99 3.1.20.2 [8], the failure rating of the aircraft mission which caused by the failure of control system generally should be no more than 10^{-5}. The requirement based on GJB2023-94 3.6.3, the failure rating of the aircraft mission which cased
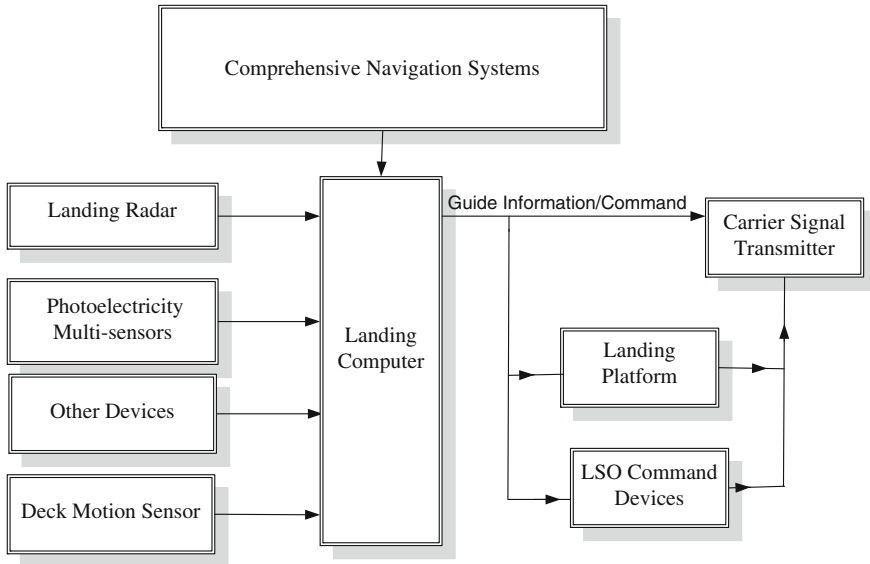
Fig. 42.1 The function structure chart of landing guidance computer

by the failure of computer generally should be no more than 10^{-6}/flight hours; the rating of the aircraft loss should be no more than 10^{-8}/flight hour. According to the actual situation of carrier-based aircraft landing, the requirement for failure rating of the landing guidance computer mission should be no more than 10^{-6}/h; the failure rating when landing by automatic should be no more than 10^{-8}/h.

42.2.3 The Basic Structure of Landing Guidance Computer

The landing guidance computer should have three identical computer channels which major controlled by digital, they are the left, middle, right channel, each channel has three branches, the guidance computer has nine CPUs, each channel using the ARINC 629 data bus to communication. The structure of guidance computer is shown in Fig. 42.2. Each branch includes three printer circuit board modules: processor module, input/output module (I/O interface Unit), and power supply module (no shown). Each channel has one processor, and their each hardware interface of processor and peripheral circuits is different, respectively, AMD29050, MOTOROLA 68040, INTEL 80486 processor. The software of each channel is designed using different compiler. Input/output module contains three APINC 629 terminals, of which only two for receiving, one for transmission/reception, control the data flow between the ARINC 629 bus and processor. The power module provides +5, +15, and −15 V power and has the ability to protect the external power interrupted.
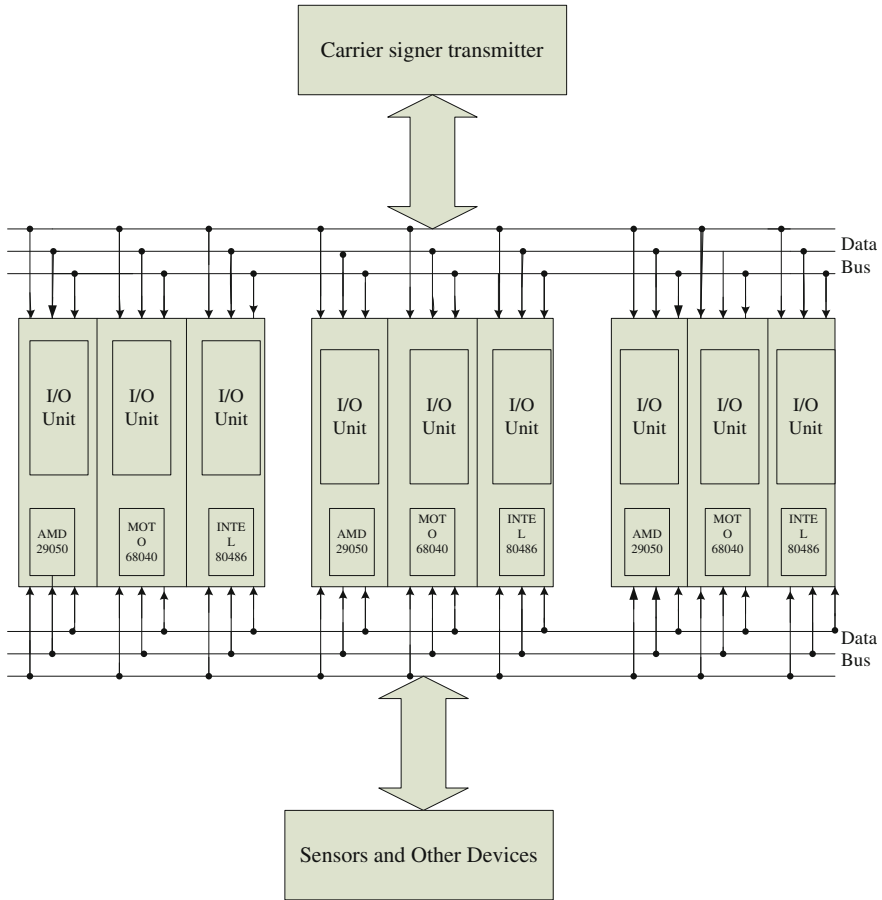
Fig. 42.2 The system structure chart of guidance computer

42.2.4 The Operation of Landing Guidance Computer

When the guidance computer is in the operation, processors receive and process the information of all the sensors system independently. The computer hardware interfaces and buses are divided into three groups (left, middle, right), though each channel can simultaneously monitoring three groups of bus, but only transmit data to its own group bus, once the transmission error occurs in one group bus, it will not affect the normal operation of the other two groups [9].

The three branches of each computer channel are allocated for the instruction branch, spare branch, and monitor branch. The instruction branch transmits all the data to its specified ARINC 629 bus, while the other two branches mainly perform monitoring functions and management tasks of branch redundancy, once the instruction branches failure, tasks will be replaced by spare branch. Any one of the

remaining two branches' failure again will cause the computer to disconnect the output.

The branches in each channel are working together; exactly the same input data are used to calculate by control law, three channels are working in an asynchronous manner. Modal, sensor status, and balance data of integrator are exchanged between them to ensure that the work of each channel does not produce differences. The key output parameters are calculated by each instruction branch and send to the specified ARINC 629 bus. Their own data are used by each instruction branch and send to the corresponding ARINC 629 bus.

42.2.5 Dissimilar Redundant Technology of the Landing Guidance Computer System

The dissimilar unit of central processing is used by three branches of each channel; different processor has different interface circuit and different ADA compiler. Since the three CPUs use different instructions, this can avoid common failure at the level of instruction; furthermore, the three CPUs have different structures, three groups were divided to design independently, so it is not all the same from the use of chips to the structure of computer, the dissimilarity are used to ensure the common failure rating of the hardware system to be minimized. Dissimilar redundant computer includes digital computer which has three channels. Each channel includes two modules, by CPU, I/O, and bus interfaces between the modules. This can overcome the common failure which is brought using the same manufacture's hardware equipment.

The dissimilar processor modules of the three branches are identical in function. At the initial time of the system running, each PFC selects a dissimilar branch as the instruction branch. Each PFC accepts input data from the three redundant ARINC 629 data bus, ARINC 629 bus is time-multiplexed system which can be connected to several terminals and at the same time only allow one terminal send data. After one terminal finish sending the data, three different timing protocols are used to ensure whether the other terminals have the opportunity to send data on the bus, after this the terminal can send the data again.

42.3 Reliability Analyses on Landing Guidance Computer System

Since the failure rating of electronic products generally obey exponential distribution, so it is assumed that all the system's hardware failure rating, which is constant, obeys exponential distribution; After the software put into use, the failure rating, which is constant, probability can be assumed to obey exponential distribution [5].

Table 42.1 Failure rating of each branch's component

Component name	Power	CPU	I/O interface unit	Software
Failure rating (10^{-4}/h)	1.0×10^{-3}	1.2	1.0	6.0

Table 42.2 The failure rating of single-branch, single-channel, and the whole system

Component name	Branch	Channel	Guidance computer
Failure rating (/h)	8.2×10^{-4}	2.0×10^{-6}	1.2×10^{-11}

According to the reliability references like MIL-HDBK-217, GJB/Z 299A-91, and relevant experience [5, 6], the failure rating of each branch's component is shown in Table 42.1.

Assuming that the failure rating of power, CPU, I/O, and software is λ_1, λ_2, λ_3, λ_4, then the reliability of entire computer system $R_S(t)$ and MTBF is that:

$$R(t) = \left[1 - (1 - e^{-\lambda_1 t})^3\right] \times \left[1 - (1 - e^{-\lambda_2 t})^3\right]$$
$$\times \left[1 - (1 - e^{-\lambda_3 t})^3\right] \times \left[1 - (1 - e^{-\lambda_4 t})^3\right] \tag{42.1}$$

$$\text{MTBF} = 1/(3\lambda_1 + 3\lambda_2 + 3\lambda_3 + 3\lambda_4) \tag{42.2}$$

$$\lambda_S(t) = -R'_S(t)/R_s(t) \tag{42.3}$$

According to formula (42.1) to (42.3), we can calculate the failure rating of mission performance λ and the rating of loss $\lambda_s(1)$, the failure rating of single-branch, single-channel, and the whole system is shown in Table 42.2.

About the similar redundancy systems, each channel is the same, each branch in the channel is similar, when the common failure occurs, the three branches fail at the same time, while the reliability of the system is reduced to the level of a single branch (8.2×10^{-4}/h), and it cannot reach the requirements. Dissimilar redundant technology greatly improves the reliability of the main guidance computer. In the mandate period, the rating of the mission failure should be no more than 10^{-6}/h, and the rating of automatic landing failure should be no more than 10^{-8}/h.

42.4 Conclusions

The system uses dissimilar redundancy technology, three sub-channels of dissimilar hardware are embedded in each redundant channel which is running parallel each other, so the redundant structure is formed which has high fault tolerance and high survivability.

The design of the system has the following advantages:

1. The structure of the system is simple, can expanded easily. Using the opening style of the criteria, standardized design of the module, simple and high-coverage monitor determines the failure of the channel, avoid the data transmission in cross-channel, this can make the structure of the system specification, simple and scalable good.
2. The safety of the system is grate. The dissimilar redundant technology is used by the design of system structure, redundancy unit separated in position to avoid the failure in common zone; separating in function, use the dissimilar hardware, control/monitoring functions, the design team of hardware/software, compilers, and so on, let the failure of one unit cannot affect the work of the other units.
3. The fault tolerance of the system is good. Using distributed structure, each device has the capabilities of intelligent processing. The self-test capabilities of the system have been expanded. Each device has the capability of partial failure prediction, so the system has strong fault tolerance.

References

1. Wu WH, Lv XT, Qu ZG (2012) Soft-fault study on carrier landing guidance system (in Chinese). Flight Dyn 30(1):1–2
2. Gao L (2012) Study on robust adaptive control applied in automatic career landing (in Chinese). Aviation Engineer Academy of Navy, QindDao
3. Pradhan, DK (1996) Fault tolerant computer system design. [S.l]: Prentice Hall PTR, Englewood Cliffs
4. Wu WH (2007) Synthesized flight control system (in Chinese). Aviation Industry Press, Beijing, pp 218–224
5. Wu WH (2009) Cheng Chuan Jin translates. The introduction of synthesized flight pilot system (in Chinese). Aviation Industry Press, pp 131–139
6. Yuan Yuan CHE (2011) E-commerce simulation platform and design (in Chinese). J Pedagogical Acad 13(2):53–55
7. Chen ZJ (2005) Dissimilar Redundancy Flight Control System Computer (in Chinese). Aviat J 5(3):320–327
8. GJB3819-99 Manual Pilot aircraft automatic flight control system and stability enhancing System. Control Enhancing System General Standard (in Chinese)
9. Dinesh Kumar U, Qinghua L (2010) Reliability, maintain and service guarantee—life cycle method (in Chinese). Electron Industry Press, Beijing, pp 65–68

Chapter 43
Fault Diagnosis of Rolling Bearing Based on Fisher Discrimination Sparse Coding

Chengliang Li, Zhongsheng Wang and Chan Ding

Abstract In response to mechanical fault in feature extraction problem, this paper presents a Fisher discrimination sparse coding method. This method is achieved by optimizing an objective function that includes two steps. First, this objective function works well in denoising where signals need to be reconstructed. Second, another objective function is added to the sparse coding framework, the discrimination power of the Fisher discriminative methods with the reconstruction property, and the sparsity of the sparse representation that can deal with the fault signal which is corrupted. Finally, the feature is extracted. In rolling bearing fault classification experiments, the new method improves the accuracy of classification.

Keywords Feature extraction · Sparse coding · Fisher discrimination

43.1 Introduction

Mechanical fault diagnosis is essentially the problem of pattern recognition, and feature extraction of signal has an important influence on the accuracy of fault diagnosis [1]. At present, many features that are used in the fault diagnosis of mechanical equipment include time domain, frequency domain, or time–frequency domain methods [1–3]. These methods often are the corresponding calculation methods based on the different characteristics; each feature value is reflected on a dynamic equipment characteristic, and this inherent computational property has

C. Li (✉) · Z. Wang
Northwest Polytechnical University, Xi'an, People's Republic of China
e-mail: licous@mail.nwpu.edu.cn

C. Ding
Xi'an Aerospace Precision Electromechanical Institute, Xi'an, People's Republic of China

limitation to extract useful diagnosis information. So, we need to extract multiple characteristic value in practical fault diagnosis; then, the high-dimensional features are need to be optimization. The feature extraction methods mentioned above have certain limitations [4].

Sparse coding method can be applied to feature extraction, parameter estimation, image recognition, failure diagnosis and so on [5]. Liu et al. [4] proposed that an adaptive feature extraction method, which is based on shift invariant sparse coding, has been used in bearing fault signal feature extraction. Zhu et al. [6] proposed a classify method which is based on sparse kernel mapping for improving the traditional sparse representation performance in low dimensions. Chen et al. [7] focus on the difficult problems which extracted pulse component of bearing vibration signal in strong noise environment, compressed sensing and K-SVD method combined. The research greatly enriched the sparse coding method and its application in fault diagnosis. However, based on the fault diagnosis and in order to improve the sparse features in discriminant information, class information needs to be added in learning phase.

In response to mechanical fault in feature extraction problem, this paper presents a Fisher discrimination sparse coding method. First, this objective function works well in denoising where signals need to be reconstructed. Second, another objective function is added to the sparse coding framework, the discrimination power of the Fisher discriminative methods with the reconstruction property, and the sparsity of the sparse representation that can deal with the fault signal which is corrupted. Finally, the discriminative feature is extracted, and capable of robust classification with a sparse representation of fault signals. In the rolling bearing fault classification experiments, the new method improves the accuracy of classification.

43.2 Fisher Discrimination Sparse Coding Method

43.2.1 Sparse Coding

The SC is based on linear generative model; one input signal set $X = [x_1, x_2, \ldots, x_M]^T$ can be represented by sum of the weighted basis functions and additive noise.

$$X = Ds + \varepsilon = \sum_{k=1}^{K} d_k s_k + \varepsilon \tag{43.1}$$

where $D \in \mathbf{R}^{M \times K}$ is the overcomplete dictionary, $M \ll K$, d_k is basis function or atom. Dimension number of basis functions can be much greater than input signal, $s = [s_1, s_2, \ldots, s_K]^T$ is the sparse representation for input signal. ε is always white noise. According to Eq. (43.1) expression, sparse coding needs to solve two

problems: (1) Find the overcomplete dictionary which can adaptive all patterns. (2) Solve the sparse representation of input signal when fix the dictionary: the objective function is as follows:

$$\min_{\boldsymbol{D},\boldsymbol{s}} J_1(\boldsymbol{D},\boldsymbol{s}) = \|\boldsymbol{X} - \boldsymbol{Ds}\|_F^2 + \lambda_1 \|\boldsymbol{X}\|_1 \tag{43.2}$$

According to the Eq. (43.2), solving the sparse representation of signal is the same goal between the two problems. For the first problem, sparse representation can capture the signal main feature basis function. For the second problem, sparse from the principle of simplicity pattern recognition makes reasoning process subsequent to simple. Focusing on the Eq. (43.2) optimization, scholars put forward different and feasible calculation method [8].

43.2.2 Fisher Discrimination Sparse Coding Algorithm

The sparse coding algorithm is the classic with the minimum signal reconstruction error as the objective function; obtaining the sparse representation basis, but sparse coding that do not have discrimination, the fault diagnosis of rolling bearing is not suitable for this. In order to make the information, signal is introduced into the optimization of sparse coding algorithm and can be extracted with the discriminant information. Fisher criterion is used for maximizing the distance between the different fault samples and minimizing the same fault sample distance. In this paper, the Fisher discriminant analysis criterion is introduced to the learning target function.

$$\max_{\boldsymbol{D},\boldsymbol{s}} J_2(\boldsymbol{D},\boldsymbol{s}) = F(\boldsymbol{s}) - \lambda_1 \sum_{i=1}^{K} \|s_i\|_0 - \lambda_2 \sum_{i=1}^{K} \|x_i - Ds_i\|_2^2 \tag{43.3}$$

The first term is Fisher discriminant power, used to enhance the sparse representation of coefficients $\boldsymbol{s}$. The concrete representation of $F(\boldsymbol{s})$ is as follows:

$$F(\boldsymbol{s}) = \frac{S_B}{S_W} = \frac{\left\| \sum_{i=1}^{C} M_i (m_i - m)(m_i - m)^T \right\|_2^2}{\sum_{i=1}^{C} \delta^2} \tag{43.4}$$

where $m_i = \frac{1}{M_i} \sum_{s \in C_i} s$ is the mean value in feature space for C_i class, $\delta^2 = \frac{1}{M_i} \sum_{s \in C_i} \|s - m_i\|_2^2$ is the variance value in feature space for C_i class. S_B is the mean between any two different fault samples and can be expressed as the distance in different class. S_W is expressed as the divergence of every kind of fault sample point. $\lambda_1 > 0$ is the penalty term of sparsity, and $\lambda_2 > 0$ is penalty of the reconstruction term. In this paper, we proposed an algorithm similar to orthogonal matching

pursuit and inspired by the simultaneous sparse approximation algorithm, and the pursuit algorithm can be summarized as follows:

1. Initialize the residue matrix $R_0 = X$, the iteration counter $t = 0$;
2. Choose the atom from the dictionary, D, that maximizes the objective function:

$$g = \arg \max_{g \in D} J_2 \left(g^T R_t, \lambda_1, \lambda_2 \right)$$

3. Determine the orthogonal projection matrix P_t onto the span of the chosen atoms and compute the new residue. $R_t = X - P_t X$
4. Increment t and return to step 2 until t is less than to a predetermined number.

43.3 Fisher Discriminant Sparse Coding Applicate in Fault Diagnosis

Training phase: the input is composed by training set that composed by rolling bearing signal, overcomplete dictionary, label information, λ_1, and λ_2. Then, the overcomplete dictionary is updated, and the eigenvalue is computed by FSC method. Using the extracted features train classifier, finally, FSC output trained classifier and updated overcomplete dictionary for test phase.

Test phase: The input is the test set project on the update overcomplete dictionary, then the test feature are computed. Diagnosis result can be output while the features input the classifier (Fig. 43.1).

43.4 Experiment

43.4.1 Experiment Set

The vibration data chosen are the test data of rolling element bearings from Case Western Reserve Lab (CWRU) [9]. This data set has been analyzed by a number of other researchers and considered as a benchmark. The test stand of rolling element bearings is shown in Fig. 43.2. On the left was a 2-hp, three-phase induction motor. A dynamometer (right) was connected to the motor through a torque sensor (center) by self-aligning coupling. The bearings under test were the ones on the drive end side supporting the motor shaft. Single-point faults were introduced to the bearings using electro-discharge machining with fault diameters of 0.007, 0.014, 0.021, and 0.028 in. Among these four fault diameters, SKF 6205-2RS JEM deep groove ball bearings were used for the first three tests, and NTN bearings were used for the last test. Vibration signals were collected using a 16-channel DAT recorder at a sampling frequency of 12 kHz.
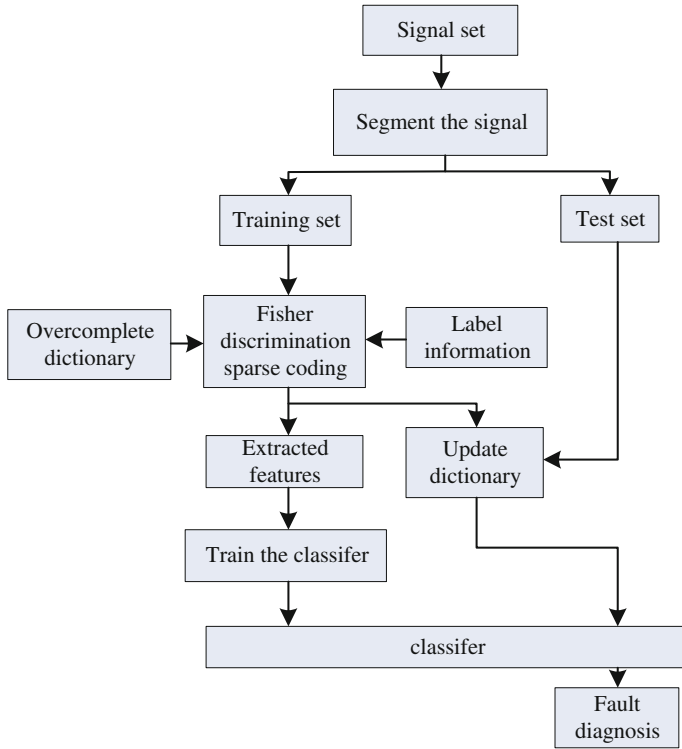
Fig. 43.1 The flowchart of fault diagnosis

Fig. 43.2 Schematic diagram of the test stand
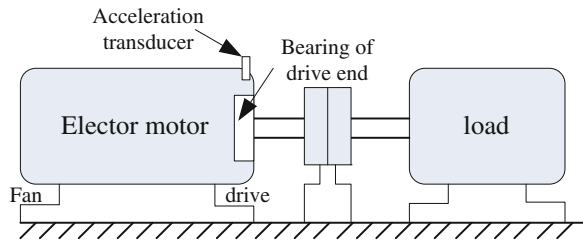
In our experiments, each data set was truncated into time-series with a 256-point window block; after segmentation, the normal data and fault data in each condition are 400. Total is 25,600. Atoms of dictionary are composed by Haar wavelet and Gabor wavelet, atomic length is 256, and the number of each wavelet basis is 1,024 and orthogonal. Sparse penalty weight is 5 and Fisher discrimination penalty weight is 1 from experience (Fig. 43.3).

First, in order to test the discriminability of the formulated sparse features, one normal condition and three fault conditions under 0 hp are analyzed. The data set is shown in Table 43.1. To diagnose all the 16 classes of bearing conditions, half
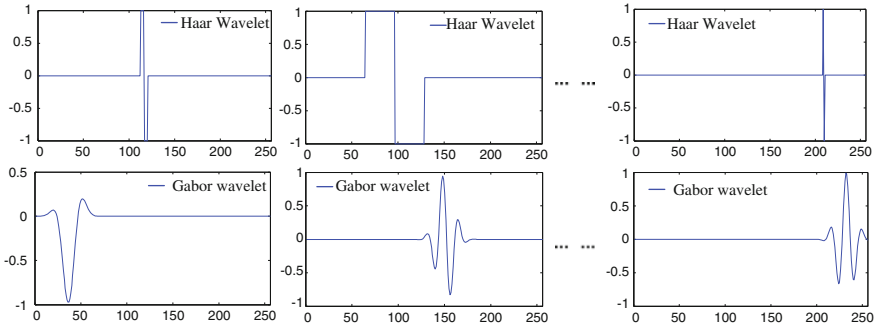
Fig. 43.3 Haar wavelet and Gabor wavelet

of the sparse features were randomly selected as the training set, and all the sparse features were set to be classified. The same test routine was carried out 20 times to get the averaged error rates of classification. As shown in Table 43.2, the low classification error is achieved by using extracted features. The highest classification error rate is 0.36 %. According to the result, the extracted feature is discriminability and can be used to do fault diagnosis.

In order to verify this method better discrimination than other methods, another experiment is implementation. The sparse features is extracted in a variety of conditions. The total number of feature vectors is 25,600. Half of the sparse features were randomly selected as the training set, and all the sparse features were set to be classified. The same test routine was carried out 20 times to get the averaged error rates of classification. The experiment results are shown in Table 43.3.

Compared with other methods, in literature [10], the feature set was composed by the statistical characteristics in time domain, the statistical characteristics of wavelet package transform coefficients, the energy characteristics of decomposition frequency band; a distance evaluation technique was used to select the superior features from the 98 features; the support vector machines ensemble were used to do the classification job. Totally, 7 classes of bearing conditions under the four motor loads were also set to be classified, and the classification accuracies ranged from 97 to 99 % for testing. In literature [4], dictionary and coefficient are learned by shift invariant sparse coding method, feature vectors can be formulated by counting the number of nonzero entries in the sparse activations of each atom. And the classifier also is LDA. Rolling bearing in 0.021″, @6:00 has the highest error rate 5.98 %. The average classification error for all classes is 1.24 %. And the highest error rate of FSC method is 3.63 %, and the average classification error for all classes is 0.71 %. It verifies that the new feature is more discrimination.

Table 43.1 Fault-bearing data description under load 0 hp

Fault diameter	Inner	Ball	Outer		
			Center @6:00	Vertical @3:00	Opposite @12:00
0.007″	I070	B070	O0760	O0730	O07120
0.014″	I140	B140	O1460	–	–
0.021″	I210	B210	O2160	O2130	O21120
0.028″	I280	B280	–	–	–

Table 43.2 Classification performance of the sparse features

Fault diameter	Normal	Inner	Ball	Outer		
				Center @6:00	Vertical @3:00	Opposite @12:00
0	0	–	–	–	–	–
0.007″	–	0	0.10	0	0	0
0.014″	–	0	0.36	0	–	–
0.021″	–	0	0	0.35	0	0.15
0.028″	–	0	0	–	–	–

Training set half of the sparse features under motor load 0 hp
Test set all the sparse features under motor load 0 hp

Table 43.3 Classification performance of the sparse features

Fault diameter	Normal	Inner	Ball	Outer		
				Center @3:00	Vertical @12:00	Opposite @6:00
0	0	–	–	–	–	–
0.007″	–	0	2.48	0	0	0
0.014″	–	1.31	0.15	0.05	–	–
0.021″	–	0	3.63	2.45	2.45	1.30
0.028″	–	0	0	–	–	–

Training set half of the sparse features under motor load 0, 1, 2, and 3 hp
Test set all the sparse features under motor load 0, 1, 2, and 3 hp

43.5 Conclusion

Focus on the feature extraction problem of rolling bearing, a new extraction method is presented. This method adds the Fisher discriminant criterion into sparse coding framework to reconstruct and denoise the original signal. Most importantly, the extracted feature is more discriminative and more conductive to the classification. In experiment, CWRU benchmark used to verify that the new feature is more discriminative and more suitable for fault diagnosis of rolling bearing.

References

1. He Z, Chen J, Wang T Theory and application of mechanical fault diagnosis. Higher Education Press first edition
2. Jiang H, He Z, Duan C, Chen X (2005) Wavelet construction based on lifting scheme and incipient fault feature extraction. J Xi'an Jiaotong Univ 39(5)
3. Jiang H, Dou D, He Z (2011) A new method for identifying ultrasonic echo signal features using adaptive second generation wavelet. J Northwest Polytechnical Univ 29(1)
4. Liu HN, Liu CL, Huang YX (2011) Adaptive feature extraction using sparse coding for machinery fault diagnosis. Mech Syst Signal Process 25(2):558–574
5. Shi J, Jiang Z Elastic net sparse coding-based sparse object recognition. Acta Aeronaut et Astronaut Sin 34(5):1129–1139
6. Zhu Q, Yang Y, Huang M (2013) Bearing fault diagnosis based on a kernel-mapping sparse representation classification. J Vib Shock 32(11):30–34
7. Chen X, Du Z, Li J, Li X, Zhang H (2013) Compressed sensing based on dictionary learning for extracting impulse components. Signal Process 6 (online)
8. Lee H, Battle A, Raina R, Ng AY (2006) Efficient sparse coding algorithm. In: Proceedings of conference on neural information processing system, 2006
9. The Case Western Reserve University Bearing Data Center. Bearing data center fault test data [EB/OL]. http://www.eecs.cwru.edu/laboratory/bearing (2011-01-01)
10. Lei Y, He Z, Zi Y (2008) A new approach to intelligent fault diagnosis of rotating machinery. Expert Syst Appl 35(4):1593–1600

Chapter 44
The Influence of Interceptive Position on Adhesive Area in Cellular Sandwich Board Patch Repair Method

Hai Tao Wang and Mo Wu

Abstract This text summarizes cellular sandwich board's development and application and sums up its damage mode and repair method in terms of air applications. We put forward a method of researching the relationship between interceptive position and adhesive area when the cellular sandwich board gets damage and is mended by patch repair method.

Keywords Cellular sandwich board · Patch repair · Interceptive position · Adhesive area

44.1 Introduction

Cellular sandwich board has been widely used [1] with problems of maintenance. When the damage area does not exceed a certain value, we can use the patch repair method to repair it [2]. In the cellular sandwich board maintenance process, every time the damage location and size are different, so are the bonding areas of the corresponding section round be case wall [3]. How to cut round at damage parts? How different are the areas when bonding in different position? Whether can we ignore the impact of these differences? These are realistic problems and have not related to any literature and material. This article mainly revolves around determining the local positioning and the patch size to study.

H. T. Wang (✉) · M. Wu
Northwestern Polytechnical University, 127 Youyixi Road, Xi'an, Shaanxi, People's Republic of China
e-mail: whaitao@nwpu.edu.cn

M. Wu
e-mail: wumo550136009@qq.com
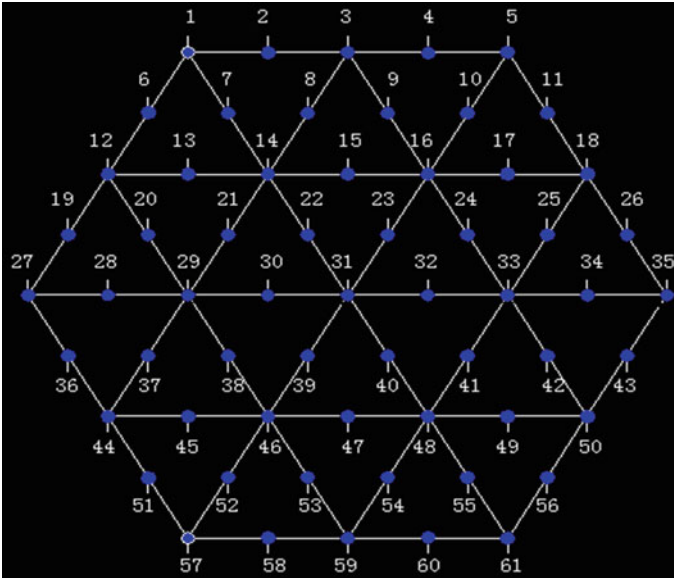
Fig. 44.1 The symbolic position of the center

44.2 The Design of Experiments and Establishment of the Steps

44.2.1 The Control of the Relative Positions in the Model

Our study the position of interceptive round, in fact, is studying which region of honeycomb core is the center of interceptive round located in. The center of interceptive round will situate in some honeycomb core or the sideline practically, and every honeycomb core is equivalent to study as long as the relative is the same because of the hexagonal symmetry. Thus, we need not consider the position of the interceptive round and the honeycomb core but just need to take the relative position into account so that simulate all situation of practical application [4]. In actual project, the center can be everywhere, which means that we should perform thousands of different experiments to faultlessly imitate all situations. We take both the accuracy and feasibility of the experiment into account and conclude some symbolic position, as shown in the chart below. As a result, we just need to work on the experiments in the 61 conclusive positions (Fig. 44.1).

Our experiments provided evidence when the center located at 1, 5, 57, and 61, the sizes of honeycomb core wall lines are the same, and the shapes of space are definitely symmetrical. Therefore, we can get the equivalent size of the wall line when the center of interceptive round is located at the symmetrical point in hexagon. So, we can further simplify the experiment to the research of 19 points,
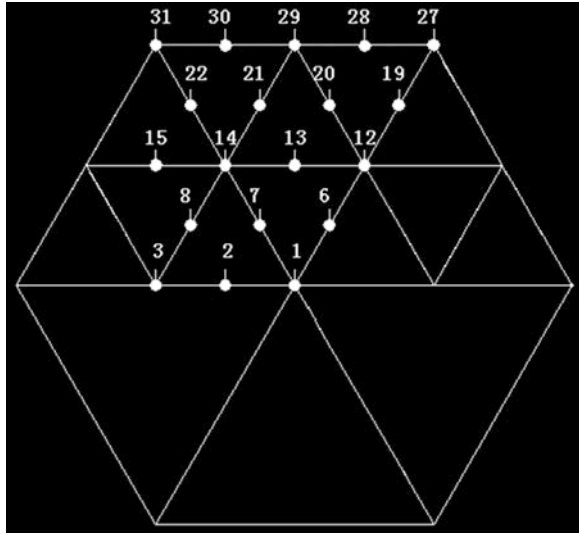
namely the research of the sizes when the centers lie in points of 1, 2, 3, 6, 7, 8, 12, 13, 14, 15, 19, 20, 21, 22, 27, 28, 29, 30, and 31 (Fig. 44.2).

With the method above, the control of the relative position can be taken.

44.2.2 Experiment Process

Main parameter:
n the proportion to control relative size
R the radius of the interceptive round
r the inradius of the hexagon
N the padding proportion selected in software

We can learn from geometric knowledge that:

$$n = R/r \tag{44.1}$$

$$N = 16.364 * 10/n = 163.64/n \tag{44.2}$$

Experiment procedure:

1. determine $n = 5$ as the proportion of this experiment and work out that the padding proportion $N = 163.64/n = 32.728$.
2. Calculate $r = 450/n = 90$. Draw the hexagon used to be the symbolic framework with inradius of $r = 90$. Move the hexagon into the circle and make the two centers coincident.

Fig. 44.3 The corresponding filled pattern in the center of Circle-1
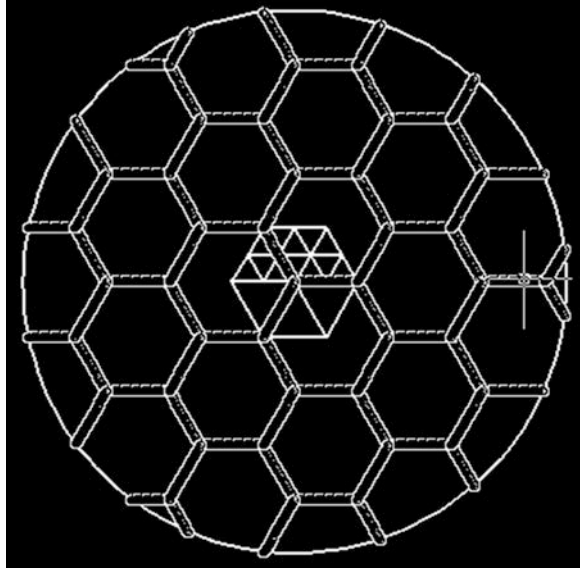
3. Choose "Honey" as the padding pattern in the AutoCAD software and make the proportion 32.728. Choose "appointed original point" in "origin of padding pattern." Make the original point coincide with the center of Circle-1. Choose round as the boundary to fill in and we can get the result shown as the chart (Fig. 44.3).
4. Choose all of the comb lines that come from filling and remove them to the blank of drawing panel.
5. Choose the comb line and detach it into the separated.
6. Upload Autolisp software.
7. Choose all of the detached lines and run Autolisp so that we can figure out the overall length: 6,740.64001.
8. Record 6,740.64001 into the corresponding blank of the Circle-1's center with $n = 5$ in Excel. Repeat the 3–7 processes 19 times and work out all of the data of the 19 points.

We have completed the data collection in the case of $n = 5$ so far.

44.3 The Experiments' Data Statistics and Processing

44.3.1 The Analysis of Extremum Deviation and Tendency

After we finish the statistics of the 19 points data, we need to expand them to initiatory 61 points. The 19 points take different weight. For instance, point 1 shares data with point 2, 3, 4. So, if we manage the data with just 19 points, there

Fig. 44.4 Extremum
deviation
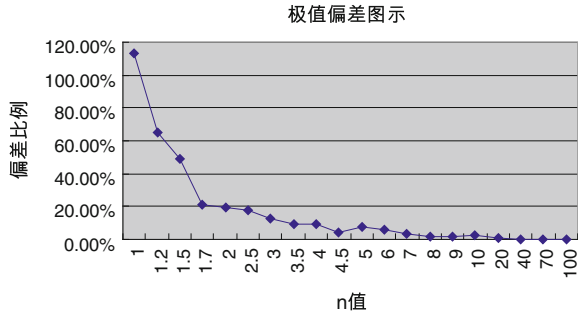
must be inconformity with practical situation. We expand to actual 61 points
instead of considering the weight of each point for convenience. Thus, we cannot
only obtain the data result but also the position which each point corresponds with.

Extremum deviation = (maximum − minimum)/average value, and we can
figure out the chart (Fig. 44.4).

The meaning of extremum deviation is to determinate the patch's maximum
with different position of interceptive round as the comb size, and interceptive area
is the same. The larger the extremum deviation, the greater influence the different
interceptive position has to different n. So, the extremum deviation, from one
aspect, indicates the importance of the determination of the interceptive round's
position. The extremum deviation is 5.50 % when $n = 6$. Therefore, we can infer
that the extremum would be less than 5.50 % if "n" is greater than 6 from the chart
above. The proportion is very small. If there is not strict requirement of the patch
repair accuracy when $n > 6$, we can overlook the influence of the patch area which
the interceptive round's position brings [5].

44.3.2 Extremum Deviation of the Center Located at Different Points

The selection of this experiment is $R = 450$ as a research model. In order to reflect
all-size situations, we need to transform absolute sizes to relative ones. Relative
deviation = (local value − the average value of the same n)/n. Relative devia-
tion's signification is similar to extremum's, and they both indicate the influence of
interceptive round's position to the area of patch [6]. However, relative deviation
is clearer to express the value of every points in the experiment to extremum one.
The signification of every relative deviation's minimum: the possible proportion
between the minimum of patch area and the average one with random position of
interceptive round in the same group [7]. Here, we statistics the minimum of
relative deviation of every group in the experiment and obtain the chart
(Fig. 44.5).

Fig. 44.5 The minimum of relative deviation
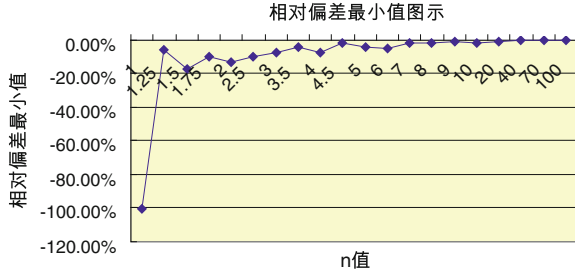
This chart indicates the conclusion of extremum deviation: the proportion of deviation tends to decay with the amplification of "*n*," but repetition occurs in some area.

44.4 Summary

1. When $n \leq 1.15$, we need to amplify the radius of interceptive round and make $n > 1.15$
2. When $1.15 < n < 2$, we should chose point 31 in charts 2–1 as the center of interceptive round. In other words, we should make the center of scathing interceptive round coincide with the one of hexagon where the damage area locates in.
3. When $2 \leq n \leq 6$, we determine the center with the method of point collection according to the principle of proximity.
4. When $n > 6$, interceptive round's position has little influence on paste area, and we can ignore it.
5. The proportion of deviation tends to decay with the amplification of "*n*," but repetition occurs in some area.

References

1. Liu X, Gao X (2005) Present situation and prospects of composite honeycomb panels. China Wood-based Panels 10:22
2. Li XZ (1997) Honeycomb composite materials. Southwest Pulp Pap 3:166
3. Fan QX (1998) Honeycomb sandwich composite. Beijing Inst Light Ind 16(2):77–81
4. Zhang G, Dai G (2000) Honeycomb sandwich composite material and its application. Fiber Compos 2:25–27
5. Zeng J, Zhao Y, Pan Z (2005) Damage forms and repairing methods of aircraft's sandwich structure composite components. Aviat Maintenance Eng 3:36–37
6. Sun H, Yan H, Fu S, Ling Y, Gu Z (2001) Research on filling repair for honeycomb sandwich structures. Aerosp Mater Technol 1:37–39
7. Xu J, Zhang K (1998) Repair decision composite patch bonding. Aviat Maintenance Eng 4:33–34

Chapter 45
Review of Teardown Process of Foreign Aircraft

Haijiao Yu, Zhi Wang, Haiping Song and Jun Xue

Abstract Due to various reasons, aircrafts are currently being operated to their design life and often beyond. In order to assess the true condition of structures of aging aircraft operated beyond their design life, structural teardowns have become more common in the aviation industry over the past decade. The present work presented the purpose and significance of aircraft structural teardown, reviewed the foreign aircraft structural teardowns over this decade, and illuminated a typical structural teardown process step-by-step. Finally, it gave a prospect to further development of the structural teardown of the aircraft.

Keywords Aging aircraft · Structural teardown · Nondestructive inspection

45.1 Introduction

Due to various reasons, aircrafts are currently being operated to their design life and often beyond. Safely sustaining the ever-increasing numbers of aging aircraft bring an ever-increasing requirement to determine the true condition of service-aged aircraft structural components. Meanwhile, actual damage status such as cracks and corrosions of structure of aircrafts reached their design life is also needed for the life extension subject. Based on experience over the past decade, one of the most important approaches available to precisely determine the damage state of a given structure is by a "teardown inspection" of that structure. Teardown inspection, as defined in Advisory Circular (AC) 25.571-1D, is "the term used for the process of disassembling structure and using destructive inspection techniques or visual (e.g., magnifying glass and dye penetrant) or other nondestructive (e.g., eddy current,

H. Yu (✉) · Z. Wang · H. Song · J. Xue
Beijing Aeronautical Technology Research Center, Beijing 100076, People's Republic of China
e-mail: yunzeyu2000@163.com

ultrasound) inspection techniques to identify the extent of damage, within a structure, caused by fatigue, corrosion, and accidental damage [1]."

Teardown data fidelity is highly dependent on the processes developed and implemented to gather the data. Improper procedure selection often results in the destruction or degradation of teardown findings, while incorrect implementation of procedures frequently results in increased scatter in the teardown data, which lead to false, invalid, and unilateral teardown results. Therefore, proper procedure selection is a powerful guarantee to obtain authentic and valid teardown inspection data.

Thus, based on purpose and significance of the aircraft structural teardown, the present work reviewed the foreign aircraft structural teardowns over this decade and illuminated a typical structural teardown process step-by-step. Finally, it gave a prospect to further development of the structural teardown of aging aircraft.

45.2 Purpose and Significance

At the present time, the population of in-service aging aircraft continues to increase. As the time goes, the aging problem getting more and more extrusive, and the safety risks of aircraft continually increased [2]. Meanwhile, as the training program establishing requirement, assessment on the damage state of an aircraft after a known period of usage is also required. Thus, the true damage state of aircraft structure must be comprehended, and the corresponding structural maintenance plan must be developed. Thus, teardown inspection, which permits making a thorough inspection of each component, including components that would not normally be addressed during routine maintenance because of their inaccessibility, to assess its condition, is considered [3]. That is the first main goal of teardown inspection.

The second goal of structural teardown inspection is to determine the actual damage status such as cracks and corrosions of aircraft structures reached their design lives, providing support for aircraft life extension. Yet other purposes of teardown inspection are to assess and correct current damage prediction model and validate the effectiveness of nondestructive inspection (NDI) method [4].

45.3 Aircraft Structural Teardowns over this Decade

45.3.1 Concerned Criterion and Requirements

Prior to early 2000s, structural teardowns were primarily performed by original equipment manufacturers (OEMs). Therefore, the processes used and the data generated by these teardowns was held proprietary, making the information unavailable to the public. In the early to mid-2000s, the demand for teardowns performed by government entities continued to increase. Since then, structural teardowns performed by government agencies have become popular. Even with

this trend, limited information is still available to the general public due to security restrictions on military teardowns. The Federal Aviation Administration (FAA) is the only government agency to fully disclose structural teardown processes and result to the general public.

Aviation developed countries such as the USA and the UK have paid much attention on aircraft structural teardown inspection and put forward specific requirements in corresponding standard and criterion. Presently, three documents serve as the governing policy on structural teardown for American general, commercial, and military aviation: FAA, AC 23-13A [5] and 25.571-1D [1] address the uses of structural teardown, while MIL-STD-1530C [6] addresses teardown inspection and evaluation techniques for military aircraft. The UK military aviation engineering policy and regulation JAP-100-01A [7] also prescribed as follows: The teardown of a full-scale fatigue test specimen airframe at the conclusion of testing is normally required for completion of fatigue and damage tolerance qualification, and teardown of a high-life aircraft is normally required for life extension activities. These documents do provide information on when to perform structural teardowns and the desired end goals. However, none of them prescribes a teardown inspection process or provides guidance specifically on the desired data to be captured from structural teardown. This lack of guidance led to inconsistency between teardown programs, which resulted in a wide variety of teardown processes and types and amounts of data captured from program to program. In addition, inter-agency sharing of successful teardown procedures is often lacking, which limited the study of lessons learned from previous individual teardowns and the development of teardown techniques.

The United States Air Force (USAF) Academy's Center for Aircraft Structural Life Extension (CAStLE) was tasked by the 77th Aeronautical System Wing, Wright-Patterson Air Force Base (AFB), Ohio, to prepare a handbook that documents procedures for planning and executing an aircraft structural teardown program. The resulting handbook was published as "USAFA-TR-2008, Procedures for Aircraft Structural Teardown Analysis" in early 2008 [8]. And then, they also drafted some teardown process protocols documenting practices and lessons learned, namely "USAFA-TR-2009-01," "USAFA-TR-2009-06," "USAFA-TR-2010-03," and "USAFA-TR-2010-04." However, they cannot be obtained by general public till now.

45.3.2 Case of Aircraft Structural Teardown

A very large number of teardown programs have been executed worldwide in recent years. These include: A-10, AV-8B, B-2, B-52, B-727, C-5, C-17, C-130, C-141, C/KC-135, EC-135, F-15, F-16, F-22, F-111, KC-130, P-3, T-37, T-38, VC-10, and numerous civil and general aviation aircraft [9–11].

In the USA, teardown inspections were performed at the end of fatigue testing of all the full-scale testing aircrafts, including military or civil aircrafts. In these

programs, many NDI findings were validated. The estimation of deficiencies found in full-scale fatigue tests of F-16A, F-16C, and F-22 indicated that about one-third of the deficiencies were found during the subsequent teardown inspections [12, 13].

Besides, as the USAF main combat aircraft in service, F-15 had an original design life of 4,000 flight hours, which was then extended to 8,000 and 9,000 flight hours combining fatigue tests according to the military operational requirement. After fatigue tests, the aircrafts were removed to teardown tasks, during which a great plenty of cracks were detected [14, 15].

To meet the requirements of operational until 2025 of F-15C and 2035 of F-15E, the life extension tasks are executed by USAF. As part of life extension program, an F-15C, an F-15D, an F-15E, and six F-15C/D aircrafts were planned executing for teardown inspection [15, 16]. Among them, teardown inspections of F-15C (81-0044, 6,233 flight hours, 9,400 equivalent hours) and F-15D (82-0048, 6,318 flight hours, 9200 equivalent hours) were completed, and a great plenty of valuable information was obtained.

45.4 Typical Teardown Steps

Planning and executing a teardown program, the first thing is to develop the program frame, defining all the tasks and processes to be implemented as part of that structural teardown. It is important to recognize that no one standard set of teardown process or program structure will meet the goals and objectives, or requirements of every structural teardown. The structure of a teardown program and particularly teardown process should be tailored to meet the specific requirements of the planned structural teardown.

A typical teardown program task flow includes identify purpose and requirements, identify teardown subjects and extract, disassembly, clean parts and remove coatings, NDI, prioritize NDI indications, failure analysis, and analyze and report findings. The steps will be common among different program structures, but the detailed processes may vary significantly.

45.4.1 Identify Purpose and Requirements

There are a wide variety of reasons why a teardown program may be required or desired. For instance, the USAF Aircraft Structural Integrity Program (ASIP) Standard [11] requires that an assessment of damage state be conducted at the conclusion of full-scale durability and damage tolerance testing. However, these tests are generally based on assumed load spectra, and their effectiveness is waiting for validating yet. As a result, a teardown program conducted on an aircraft removed from service after a period of known operational usage still provides the most reliable data to validate these models on the one hand. On the

other hand, the teardown data obtained after these tests can be used for identifying critical structural details, establishing inspection intervals, and providing evidence for aircraft life extension.

The most important decisions to be made in any teardown program are what type of findings will the program be focusing upon and what degree of fidelity will be required in these findings. It will drive all program tasks and impact the budget and the schedule. One should consider that the required fidelity must be tied back to the purpose of the teardown program. If the goal is to validate damage prediction models, there should be consideration of what minimum size findings would be useful for such validation. Since damage tolerance analysis begins from the rouge flaw size, 1.27 mm for most structure (0.127 mm for cold-worked holes and 0.5 mm for durability analysis), there may be no utility in data for cracks that are dramatically smaller.

45.4.2 Identify Teardown Subjects and Extract

The selection of the teardown subject is more important since it will address the utility of teardown data. The most important two aspects of subject selection are considerations of service history and the separation of those subjects from surrounding aircraft structure.

Known Service History Regardless of the teardown program purpose, the findings obtained will need to relate back to the applicable service history. Depending upon the damage mechanism, the relevant service history of a selected teardown subject may be in terms of operational hours, ground air ground (GAG) cycles, number of certain mission types flown, calendar time, or a combination of factors. Therefore, the program requirements are essential in identifying an appropriate teardown subject or at least ensuring the subject chosen is accompanied by a complete set of relevant service history.

Extract Teardown Subjects After the subject aircraft has been selected for a teardown program, the next task is to remove the components that constitute the focus of the program. A key consideration is to avoid inducing incidental damage by the extraction process itself. Such incidental damage would cloud the inspection results and waste program resources as it would ultimately need to be distinguished from damage incurred during service. For smaller aircraft, subassemblies may be extracted directly from the airframe with minimal special provisions. Larger airframes, such as transports and bombers, require additional considerations. In such structure, the weight involved with the individual extracted components, as well as the dependency of one section of structure to support the weight of another, requires significant preparation prior to any section and component extraction. In these cases, the aircraft OEM is often a useful resource to provide component weight data, support requirements, and plans to stabilize the remaining structure as component assemblies are removed. Support and

stabilization requirements often dictate the order in which component assemblies are removed from a given teardown aircraft.

Prior to making any of the section cuts, a detailed cut plan should be developed and approved by the program manager. This plan not only includes the aforementioned stabilization requirements but also ensures the inclusion of all teardown subjects.

45.4.3 Disassembly

After extraction, the component/section disassembly should be executed and make preparations for the subsequent NDI.

Component disassembly for teardown programs differs from that of aircraft maintenance. When fasteners are removed during structural maintenance operations, it is customary to oversize or in some way refinish the bore of the fastener hole to prepare for fastener replacement. In contrast, for structural teardown analysis, the hole bores are often primary targets of the investigation, preserving the condition of the hole bore while removing the fastener is of paramount importance. Any damage induced during the disassembly process will create the extra task of distinguishing that damage from the operational damage data sought by the program. Since disassembly results in the creation of separate parts and the exposure of many faying surfaces, part identification, tracking, and documentation take on additional importance during this task. Before beginning the disassembly of an extracted component, the teardown subject parts must be identified, and each part should be tracked with a part log of appropriate identifying data.

45.4.4 Clean Parts and Remove Coatings

To prepare a subject part for initial visual inspections and damage photographic documentation, the surfaces should be cleaned to remove all loose grease, sealant, dirt, and particles. Specific guidance for cleaning can be found in Technical Order (TO) 1-1-691, Aircraft Weapons Systems Cleaning and Corrosion Control, Appendixes E-2 and E-3 [17].

To complete surface preparation for NDI methods such as close visual, fluorescent penetrant, and eddy current inspections, it is important that all coatings be removed from parts after the initial visual inspections. There are two general categories of coating removal processes: chemical removal and media removal. The selection and mix of removal process will depend on the criticality or fidelity of the required analysis, the NDI methods that will be subsequently applied and local or regional environment regulations.

Chemical stripping is the method of choice for removal of sealant, topcoat, and primer, as these processes result in chemically clean surfaces, which are optimum

for accepting penetrant inspection. Properly applied chemical stripping will not modify the component substrate surfaces as will often occur with many mechanical stripping methods. Many of the conventional organic topcoats and primers can be readily removed using processes defined in TO 1-1-8, Application and Removal of Organic Coatings, Aerospace and Non-Aerospace Equipment [18], Chap. 2. Nylon bristle brushes and nonmetallic scrapers can be used to facilitate coating removal.

Media blast coating removal methods, while attractive for their environmental reasons, are not recommended for use in detailed teardown programs. Because they are mechanical stripping processes that can modify substrate surfaces and therefore negatively impact the performance of subsequent NDI processes. Thus, they are only recommended for use on noncritical parts where inspections methods will be applied that are not affected by surface modification (i.e., eddy current inspections).

45.4.5 NDI

Selection of the NDI method to employ depends on many factors, such as component geometry, size, and material type; surface condition including coatings, plating, and finishes; expected damage, location, orientation, and type of interest; part criticality; detection fidelity (capability); cost [19].

To optimize resources and manage cost and schedule risk, a tiered approach, which focuses program resources in proportion to the structural criticality of the parts, should be implemented. Accordingly, the NDI method recommendations based on part category and/or criticality are as follows:

1. Fracture critical, durability critical, mission critical, safety-of-flight components: close visual inspection, bolt-hole eddy current, eddy current surface scan, fluorescent penetrant inspection, enhance visual inspection, and magnetic particle inspection.
2. Noncritical load-bearing components: close visual inspection, fluorescent penetrant inspection, limited bolt-hole eddy current or eddy current surface scan, and magnetic particle inspection.
3. Secondary, nonload bearing components: close visual inspection.

45.4.6 Prioritize NDI Indications

In each of the teardown tasks, a single teardown aircraft may generate many extracted assemblies. Of these extracted assemblies will result in one or more teardown subject parts. Each part will need to be prepared for NDI by cleaning and coating removal. NDI of each part may result in multiple NDI indications.

Each NDI indication must be considered for further failure analysis investigation. However, investigating all indications by failure analysis techniques may be an unacceptable burden on both schedule and fiscal program constraints. Therefore, prioritization is a powerful tool in any program to ensure finite program resources are best focused on achieving desired results.

Hence, program requirements often serve to prioritize the extraction order of assemblies from a teardown aircraft. Such priority would naturally carry through the subsequent tasks of disassembly, coating removal, and NDI.

45.4.7 Failure Analysis

Metallographic failure analysis is a destructive failure analysis technique, wherein the specimen is sectioned and broken in parts to identify and visualize the indications identified by the various NDI techniques. If the indication is verified as a defect, then it is necessary to analyze the root cause and failure mode of the defect. Since USAF's emphasis gradually transferred from finding and fixing damage to current anticipation and management of damage, complete and detailed characterization of these findings is a vital result for any teardown program. This detailed characterization includes the type, origin, propagation mechanism, propagation path, propagation rate, final size, and final shape of the damage. Such data are necessary to establish the database required to support predictive model validation, develop and/or modify preventive maintenance schedules, and evaluate the remaining life of the aircraft fleet.

Failure analysis must always be performed by a trained failure analysis engineer/technician who is fully conversant with failure mechanisms and features. Before a report can be finalized based on fractographic evaluation, it is necessary for a second failure analysis engineer to review and evaluate the data independently as a verification of the findings.

The specific tasks associated with conducting a proper failure analysis investigation on a given NDI indication are as follows: visual examination, enhanced examination of the NDI indication site, specimen preparation, crack opening, scanning electron microscopy, corrosion product evaluation, and fracture surface corrosion product removal. After the analysis of an NDI indication has been completed, the details of the finding should be fully documented, the NDI indications should be depicted, the failure analysis results should be summarized, and the damaged photographs should be gathered.

45.4.8 Analyze and Report Findings

After teardown inspection, the teardown data should be analyzed in concert with different program goals and the teardown analysis report should be completed.

The teardown and failure analysis data can be used in correlation of non-NDI indications and findings, inspecting assets other than the teardown article to understand the nature of damage found, the fidelity of the operational fleet NDI procedures, fatigue life prediction model validation, reparability of the findings, and corrosion prevention and control programs [20].

The results of a teardown program have many uses in fleet management activities. For damage found during the teardown program, the fleet manager must understand the nature of the finding, if the damage is systemic and should be expected in most of the fleet or anomalous and only occurring in the teardown article. Systemic damage requires a fleet-wide solution, whereas anomalous damage does not have fleet-wide implications. Once the correct decision on teardown findings is made, the information can be accurately used for fleet management.

Meanwhile, there are further considerations that incidental damage should be reported and tracked in any teardown program. These damage reports should be reviewed by program leadership in order to judge the impact on remaining program tasks. Reports of incidental damage should include, at minimum, the location, type, extent, and cause of the damage as well as a detailed photographic record. The location should be given in terms of part number and aircraft coordinates.

45.5 Further Development of Structural Teardown

Aircraft structural teardowns can offer evident for fleet management decision, supply validation for damage prediction, provide guidance for aircraft life extension, and validate the level of NDI techniques, it thereby should be strive to develop. Some foreign countries have early startings and possess many cases to be referred. However, due to the proprietary limitation, confidential requirement, and other reasons, limited information was shared between government agencies, OEMs, and administrators/operators. Thus, the study of lessons learned from individual teardowns and the development of teardown techniques were confined, and recurring problems with past teardown programs continue to occur on new teardown programs. Without published processes and results, lessons learned cannot be ascertained and absorbed by the teardown community as a whole.

Through the literature survey of available teardown cases, the following recurring problems have been identified: lack of definition in goals and objectives, lack of planning prior to execution, requirements not rigidly defined, and not all teardown processes fully documented. These common problems have resulted in increased teardown cost, increased schedule and capacity requirements, and degradation in fidelity or destruction of valuable teardown data. To solve these problems, the communication of different organizations should be facilitated. If a universally accepted structural teardown process was adopted that provided recommendations based on lessons learned from previous teardown programs, the

recurrence of these problems could be drastically reduced or even eliminated. In addition, structural teardown is a technical data collection process; therefore, a defined, repeatable process is desired to minimize errors and scatter in the resulting data set.

References

1. U.S. Department of Transportation, Federal Aviation Administration: Damage Tolerance and Fatigue Evaluation of Structure. Advisory Circular, AC 25.571-1D (2011)
2. Tong YC (2001) Literature review on aircraft structure risk and reliability analysis. Aeronautical and Maritime Research Laboratory. Report Aeronautical and Maritime Research Laboratory, Defence Science and Technology Organisation, DSTO-TR-1110
3. Findlay SJ, Harrison ND (2002) Why aircraft fail. Mater. Today 5:18–25
4. Laubach M (2008) Destructive evaluation of four aircraft representative of the general aging aircraft fleet. SAE International, New York
5. U.S. Department of Transportation, Federal Aviation Administration: Fatigue, Fail-Safe, and Damage Tolerance Evaluation of Metallic Structure for Normal, Utility, Acrobatic, and Commuter Category Airplanes. Advisory Circular, AC 23-13A (2005)
6. Department of Defense, United States: Aircraft Structural Integrity Program. Standard, MIL-STD-1530C (2005)
7. Command of the Defense Council, UK Military Aviation: Joint Air Publication, JAP-100-01A (2001)
8. Shoales GA (2009) Procedures for aircraft structural teardown analysis: development of a best practices handbook. In: 25th international conference on aeronautical fatigue symposium. Springer, Heidelberg, pp 329–353
9. Arunachalam SR, Shah SR, Fawaz SA, Shoales GA (2010) C/KC-135 teardown analysis program. Center for Aircraft Structural Life Extension, US Air Force (2010)
10. Molent L, Dixon B, Barter S, White P, Mills T, Maxfield K et al (2009) Enhanced teardown of ex-service F/A-18A/B/C/D centre fuselages. In: 25th international conference on aeronautical fatigue symposium. Springer, Heidelberg, pp 123–142
11. Tomblin J, Salah L, Hoffman D (2012) Durability and aging of composite aircraft structures. In: Pochiraju KV, Tandon GP, Schoeppner GA (eds) Long-Term Durability of Polymeric Matrix Composites, Chap. 13. Springer, Heidelberg, pp. 513–548
12. Babish CA (2007) Implications of usage severity and variability based on a case study. In: 24th international conference on aeronautical fatigue symposium. Springer, Heidelberg, pp 445–457
13. Moore BGCD (2007) Aircraft structural integrity and the F-22. 2007 USAF structural program conference palm springs
14. Reid PA, Lane JD (2010) Certifying the F-15C Beyond 2025. 2010 USAF aircraft structural integrity program conference
15. McFarland J, Currie D (2010) Moving forward with ASIP on the F-15. 2010 USAF aircraft structural integrity program conference
16. Alpaugh A (2010) F-15C/D structural disassembly and analysis support projects. 2010 USAF aircraft structural integrity program conference
17. Robins Air Force Base (2003) Cleaning and corrosion prevention and control, aerospace and non-aerospace equipment. Technical Order, WR-ALC/LEET, TO 1-1-691
18. Robins Air Force Base (2007) Application and removal of organic coatings, aerospace and non-aerospace equipment, change. Technical Order, AFRL/MLS-OR, TO 1-1-8

19. Shoales GA, Fawaz SA, Walters MR (2009) Complication of damage findings from multiple recent teardown analysis programs. In: 25th international conference on aeronautical fatigue symposium. Springer, Heidelberg, pp 187–207
20. Lucas KA, Duffield MJ (2009) Service history analysis and teardown evidence—key elements for structural usage monitoring of an aging fleet. In: 25th international conference on aeronautical fatigue symposium. Springer, Heidelberg, pp 1135–1153

Chapter 46
Flight Operations Quality Assurance Based on Clustering Analysis

Zhuo Sun, Cunbao Ma, Wen Li and Chunnan Shen

Abstract Flight operations quality assurance (FOQA) can be applied to monitoring and analyzing the data recorded in a flight to improve line operations and safety. In view of the requirements of FOQA and the shortage of general data processing algorithms, clustering analysis and density-based spatial clustering of applications with noise (DBSCAN) algorithm are studied depending on data mining, and FOQA based on clustering analysis is presented. The process of flight data analysis is discussed with this algorithm. The practicability and universality of DBSCAN algorithm is validated by the clustering analysis instance of an abnormal data during takeoff.

46.1 Introduction

With the rapid development of civil aviation, there is an increasing emphasis on flight safety. Almost 70 % of aviation accidents are caused by flight operation errors depending on the statistical analysis of international accidents from 1981 to 2001 [1]. Therefore, in order to ensure high level of safety, flight operation monitoring method must be developed. In order to prognosticate the incipient symptom of a fault and improve the flight safety, the FOQA system is implemented for the flight data analysis. Based on these, a reasonable user maintenance schedule could be worked out to reduce production cost.

Z. Sun (✉) · C. Ma · W. Li · C. Shen
School of Aeronautics, Northwestern Polytechnical University,
Xi'an 710072 Shaanxi, China
e-mail: sunzhuo0224@126.com

With the statistical analysis method, traditional FOQA technique is effective to discover the factors that might cause deviation [2]. However, it relies on predefined characteristic values of some parameters under given conditions and cannot deal with obscure failures effectively.

Partitioning the data into groups depending on rules determined by the data characteristics [3], the clustering analysis is an effective data processing method and has been widely used in numerous applications like machine learning situations, pattern recognition, and image processing. Using the algorithm of density-based spatial clustering of applications with noise (DBSCAN), the FOQA based on clustering analysis is developed to identify anomalous data or flights by grouping the flight data into clusters, avoid subjective effects and enhance processing ability for obscure failures.

In this article, the clustering analysis and DBSCAN algorithm are researched in depth. And the FOQA based on clustering analysis is presented. The process of flight data analysis is discussed depending on this method.

46.2 Clustering Analysis and DBSCAN Algorithm

46.2.1 Clustering Analysis

Some definitions are as follows:

Definition 1 Let data object X be consisted of m attributes (sampling points), define X as m-dimensional vector, denoted by $X = (X_1, X_2, \ldots, X_m)$, where X_i is the ith attribute of X, m is the dimension of data space.

Definition 2 Let Y be considered as n m-dimensional data points, then define Y as a row vector of dimension $n * m$, denoted by $Y = (Y_1, Y_2, \ldots, Y_n)$, where $Y_i = (Y_{i1}, Y_{i2}, \ldots, Y_{im})$, and Y_{ij} is the jth attribute of the ith data point [3, 4].

Definition 3 Assume that n m-dimensional data points $(X_1, X_2, \ldots, X_n)$ are given, and let $d(i, j)$ be the quantified expression for the similarity of two points (i and j). Then, define difference matrix [5] as the lower triangular matrix of dimension $n * n$ with $d(i, j)$, denoted by

$$\begin{bmatrix} 0 & & & & \\ d(2,1) & 0 & & & \\ d(3,1) & d(3,2) & 0 & & \\ \vdots & \vdots & \vdots & & \\ d(n,1) & d(n,2) & \cdots & \cdots & 0 \end{bmatrix}. \tag{46.1}$$

where $d(i, j)$ is non-negative, $d(i, j) = d(j, i)$, $d(i, i) = 0$, and $d(i, j)$ tends to 0 with the increase in the similarity between i and j.

Definition 4 Let X_i, X_j be m-dimensional data point, define the Euclidean distance [6] $d(i, j)$ is

$$d(i,j) = \left(\sum_{k=1}^{m} \left| x_{ik} - x_{jk} \right|^2 \right)^{\frac{1}{2}} \tag{46.2}$$

where Euclidean distance $d(i, j)$ will not be influenced by the coordinate transformation.

Clustering analysis is to group a given collection of unlabeled patterns into meaningful clusters based on similarity. The patterns within a valid cluster are more similar to each other than those belonging to a different cluster [7].

In density-based clustering analysis, a specific cluster is represented by the central point of it. The number of points in a certain region with a given radius is computed as the density. Based on the density, whether to group these points is determined. Therefore, this method can be used to find arbitrary-shaped clusters with joining high-density regions and handle noise or outliers well [8].

46.2.2 DBSCAN Algorithm

A. Algorithm description

DBSCAN algorithm is a typical density-based clustering method. In this algorithm, the cluster is discovered by acquiring the density of points' neighborhood. The neighborhood of each point is defined as the circle with a given radius, and this radius is denoted as Eps. Some definitions are introduced as follows:

Definition 1 If the Eps-neighborhood of a point contains at least a minimum number (MinPts) of points, then define the point as a core point, shown in Fig. 46.1a.

Definition 2 If the Eps-neighborhood of a point contains less than MinPts of points, then define the point as a border point, shown in Fig. 46.1a.

Definition 3 A point p is directly density-reachable from a point q with respect to Eps and MinPts if p is within the Eps-neighborhood of q, and q is a core point.

Definition 4 A point p is density-reachable from a point q with respect to Eps and MinPts if there is a chain of points p_i, where $i = 1, 2, …, n$, and p_{i+1} is directly density-reachable from p_i; q is p_1 and p is p_n, shown in Fig. 46.1b.

In data set D, DBSCAN algorithm starts with an arbitrary point p and acquires all points density-reachable from p with respect to Eps and MinPts which is called region queries. If p is a core point, the cluster C is yielded with respect to Eps and MinPts. Then, these unlabeled points in cluster C are visited, and their corresponding density-reachable neighborhoods are checked. The process will continue
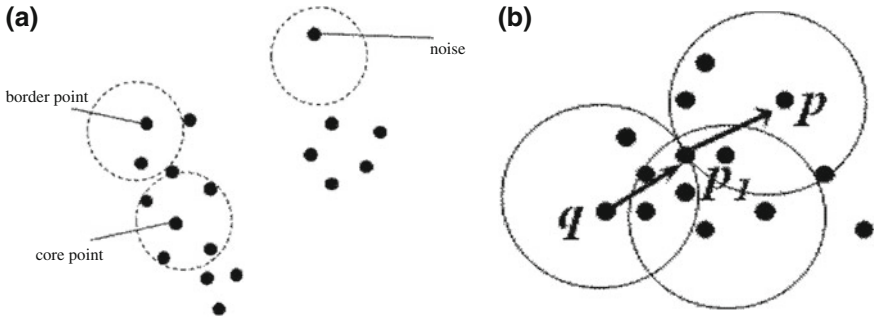
Fig. 46.1 Basic definitions in DBSCAN. **a** Core points and border points. **b** p is density-reachable from q

recursively until no new points can be added to this cluster. Other clusters are yielded using the same step. If p is a non-core point, no points are density-reachable from p, and the next point of the data set is visited. At last, those points that are not belonging to any clusters are taken as noise. The DBSCAN algorithm can be used to handle data sets with noise well, and it is not influenced by the order of input data [9], the steps in detail are shown in Fig. 46.2.

B. Parameter Determination

From the description of DBSCAN algorithm above, it is known that the result of clustering analysis is effected by Eps and MinPts. The selection methods of two parameters are discussed, and their influence on the result is presented.

The determination of the two parameters was based on sensitivity analysis. In data set D, assume integer k and measure the distance between all points and their kth nearest point called the k-dist distance. These distances are sorted in descending order to draw k-dist map, where X-coordinate is sorted sequence of points, and Y-coordinate is their corresponding k-dist distances [7, 10]. Let p be an arbitrary point, Eps be its k-dist distance, and MinPts be $k + 1$, then those points whose k-dist distances are not more than Eps are core points. Therefore, the largest k-dist distance in the most intensive clusters region is considered as the ideal value of Eps. Assume that data set D is given, and k is known as $k = 4$, then the 4-dist map is drawn, and the value of Eps is determined, as shown in Fig. 46.3.

Figure 46.4 depicts the comparison results from DBSCAN for various Eps and MinPts. In Fig. 46.4, it is observed that the results are more sensitive to the value of Eps than MinPts. Therefore, set MinPts be a constant here, and the clustering result is controlled by adjusting Eps.

Fig. 46.2 Flow chart of DBSCAN algorithm

46.3 Flight Operations Quality Assurance Based on Clustering Analysis

46.3.1 Description of the algorithm

According to the data recorded in flight data recorder (FDR) and quick access recorder (QAR), the flight data can be grouped into the closest cluster during a normal flight. While failures occur, some data can deviate from any clusters and be

Fig. 46.3 4-dist map of data set *D*
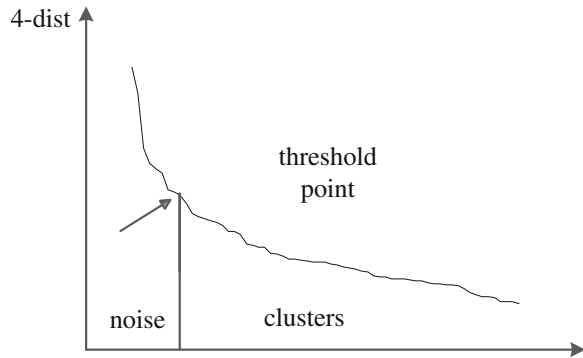
Fig. 46.4 Comparisons of the number of noise for various Eps and MinPts
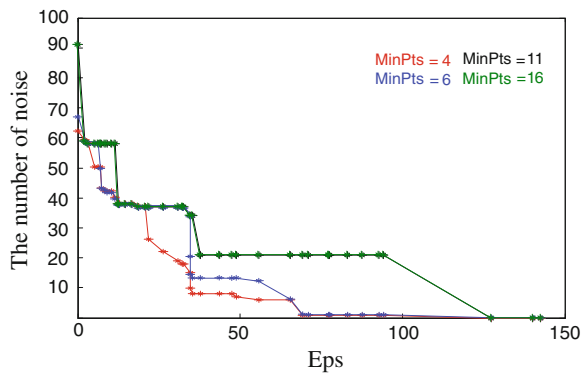
taken as noise. Therefore, FOQA based on clustering analysis is presented to group the flight data, identify the abnormal data, and improve flight safety. The flow chart is shown in Fig. 46.5.

1. Data Preparation

   (a) Data conversion
   For different flight phases, time series flight data are sampled at proper sampling intervals. The sampled discrete data are mapped to multidimensional data space and converted into vectors [11], which are easy to clustering analysis.

   (b) Data preprocessing
   The converted high-dimensional vectors are preprocessed to reduce random effects such as the environment condition breaking. Preprocessing method is explained as follows:

   Let $D = \{x_1, x_2, \ldots, x_n\}$ be a data set in m-dimensional space, where x_{ij} is the value of the ith flight data at sample time j, $D' = \{x'_1, x'_2, \ldots, x'_n\}$ be a normal flight data set, where x_{ij}' is the normal value of the ith flight data at sample time j. Then,

Fig. 46.5 Flow chart of clustering analysis-based flight operations quality assurance
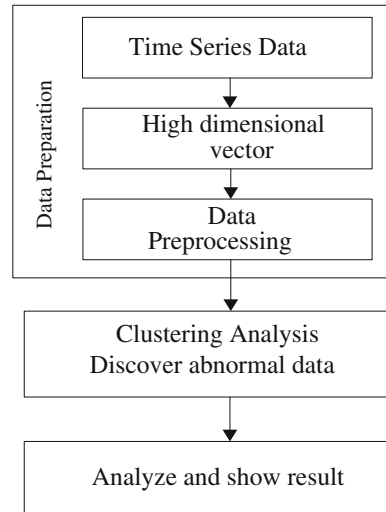
$$\Delta x_{ij} = x_{ij} - x'_{ij}. \tag{46.3}$$

Data set S, which is consisted of Δx_{ij}, tends to {0} without abnormal data; otherwise, it has exponential distributions. Therefore, abnormal flight data can be identified by discovering noise points of Data set S.

2. Clustering Analysis

After data preparation, high-dimensional vectors are processed by the DBSCAN algorithm. The flow is shown in Fig. 46.6.

In Fig. 46.6, it is first to determine monitoring items and demands, such as the monitoring rate of situations exceeding the limits. Next, it is necessary to analyze data type and select proper distance formula to compute the distance between two points. Then, the values of two important parameters (Eps, MinPts) are determined depending on history data, personal working experience, and specific requirements from the airlines. The flight data are analyzed with the DBSCAN algorithm, and the clustering results are discussed and shown.

3. Result processing

The FOQA database [12] is built with basic theory, expert knowledge, and history events. According to the results of the cluster analysis, these outliers or abnormal data are used to match knowledge stored in the FOQA database. If a match is found, the associated knowledge is considered to be active. Otherwise, the database is updated by the new data.
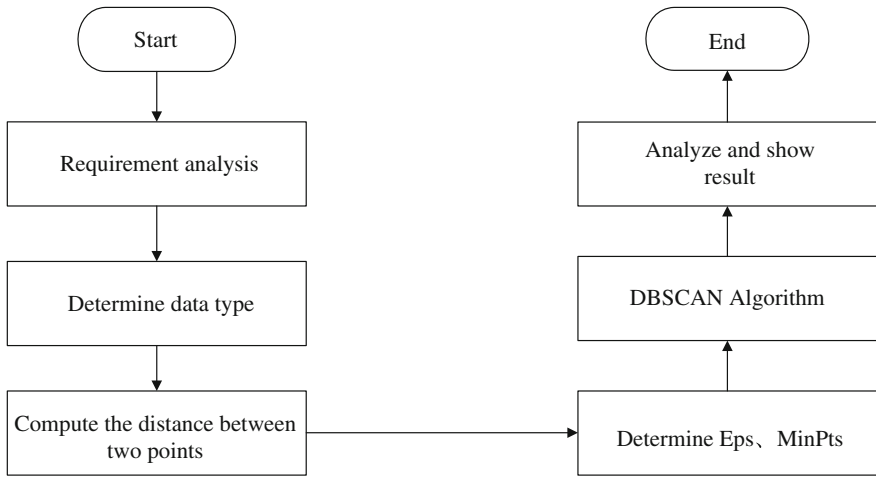
Fig. 46.6 Flow chart of DBSCAN algorithm-based data processing

46.3.2 Example of Abnormal Flight

One example is presented in detail during the takeoff phase. The ID of three flights is 04400, 70444, and 22208, where flight 70444 and 22208 are normal, and flight 04400 is abnormal. The analyzing process of radio altitude is taken for an example to explain FOQA based on clustering analysis. The changing curve of the radio altitude within 90 s after takeoff is indicated in Fig. 46.7.

Firstly, the flight data are preprocessed. The time series data are sampled at 1 s intervals and converted to multidimensional vectors. The difference between abnormal data and the normal ones is made as the array x.

Then, the important parameter, Eps, is selected by drawing 5-dist map of x and determined to be 42. Next, the array x is processed with DBSCAN algorithm, and the results are two row vectors: class and point, shown as follows:

class =

```
 1   1   1   1   1   1   1   1   1   1  1  1  1  1  1  1  1  1   1   1  1
 1   1   1   1   1   1   1   1   1   1  1  1  1  1  1  1  1  1   1   1
 1   1   1   1   1   1   1   1   1   1  1  1  1  1  1  1  1  1   1   1
 1   1   1   1   1   1   1   1   1  -1  2  2  2  2  2  2  2  2  -1  -1
-1  -1  -1  -1  -1  -1  -1  -1  -1  -1
```

Fig. 46.7 The change curve of the radio altitude
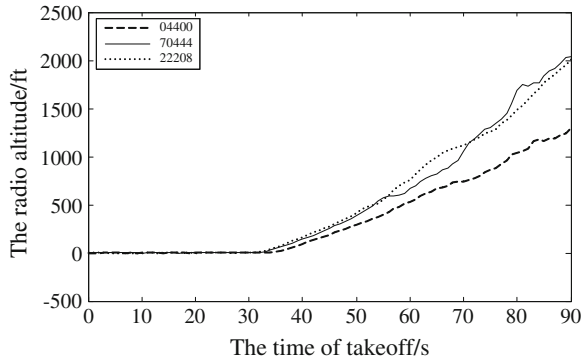
point =

1	1	1	1	1	1	1	1	1	1	1	1	1	1	1	1	1	1	1	1
1	1	1	1	1	1	1	1	1	1	1	1	1	1	1	1	1	1	1	
1	1	1	1	1	1	1	1	1	1	1	1	0	0	0	0	0	1	0	1
1	1	0	1	0	0	0	0	0	−1	0	0	0	0	1	0	0	0	−1	−1
−1	−1	−1	−1	−1	−1	−1	−1	−1	1

where class is the type of cluster: cluster 1 and cluster 2, point is the type of points in the clusters: 1 is core point, 0 is border point, and −1 is noise. From the results, it is observed that the 91 points are grouped to two clusters, and the abnormal points are discovered after 79 s by continuous noises.

The flight data, including pitch angle and thrust, are analyzed using the same steps. The results indicate that the trust is normal, but pitch angle is anomalous after 79 s, and the climb rate is low with the same trust. Furthermore, the difference of the climb rate increases with the time.

After data analysis, the information is matched with the knowledge in the FOQA database, and a match is found. As a result, lifting rate is lower than the normal flights during takeoff.

46.4 Conclusions

The clustering analysis and DBSCAN algorithm are studied depending on the characteristics of FOQA. This algorithm is applied to FOQA, and FOQA based on clustering flight is presented. The practicability and universality of DBSCAN algorithm are validated by the clustering analysis instance of an abnormal data during takeoff.

References

1. Xiaoli L (2002) Human factor accident/incident classification standard and classified statistical report on human factor accident/incident of China Civil Aviation in recent twelve years. J China Saf Sci J 12(5):55–62 (in Chinese)
2. Lijuan H, Zheng L, Yu W (2011) A concise course book on SPSS statistical analysis. Electronic Industry Press (in Chinese)
3. Yan C (2011) Application of data mining. Tsinghua University Press, Beijing (in Chinese)
4. Keyun H, Fengzhan T, Houkuan H (2008) Application of data mining. Tsinghua University Press, Beijing (in Chinese)
5. Heng Z (2005) Study on some issues of data clustering in data mining. Xi'an Electronic and Engineering University, Xi'an (in Chinese)
6. Mikawa K, Ishidat T, Goto M (2011) A proposal of extended cosine measure for distance metric learning in text classification. In: IEEE international conference on systems, man, and cybernetics (SMC), pp 1741–1746
7. Shuhua R, Fan A (2011) K-means clustering algorithm based on coefficient of variation. In: 4th international congress on image and signal processing, pp 2076–2079
8. Shah GH (2012) An improved DBSCAN, a density based clustering algorithm with parameter selection for high dimensional data sets. In: Proceedings of the 5th international conference on machine learning and cybernetics
9. Budhi GS, Adipranata R, Sugiarto M (2011) Pengelomopokan Sunspot Pata Citra Digital Mahatari Menggunakan Metode Clustering DBSCAN. In: Seminar Nasional Aplikasi Teknologi Informasi
10. Vijayalakshmi S, Punithavalli M (2010) Improved varied density based spatial clustering algorithm with noise. In: IEEE international conference on computational intelligence and computing research-ICCIC
11. Chaojiang H, Lie C, Quanfa Y (2012) Application of FDR system. National Defense Industry Press (in Chinese)
12. Zhipeng L, Shangjun L, Chunpeng Z (2005) Study of a flight data based expert system. J Aircr Des 2:52–58 (in Chinese)

Chapter 47
Experimental Investigation on Aluminum Plate Damage Monitoring Based on Acoustic–Ultrasonic Technique

Lei Zhang and Mingliang Zhu

Abstract It is important to monitor the condition and detect the damage of structures in order to insure aviation equipment safety and reduce maintenance cost. For damage monitoring of aircraft structures, elastic wave propagation approach is briefly discussed, in which the acoustic–ultrasonic technique can be used to identify the additional reflections generated from seeded cracks. In this article, based on acoustic–ultrasonic technique, theoretical and experimental studies are performed to explore the characteristics of the Lamb wave produced in the aluminum plate for aeronautic use. Various comparing experiments and theoretical studies are performed on the aluminum plates with and without artificial crack damage. Mainly, short-time-root-mean-square (STRMS) method and wavelet reassigned scalogram analysis are applied to investigate the propagation and time-frequency characteristics of the Lamb wave. By analyzing the features of corresponding Lamb wave signals, the qualitative damage identification method is developed. And this work provides technical support for the innovation of maintenance pattern from time-based maintenance to condition-based model.

Keywords Damage monitoring · Acoustic–ultrasonic technique · Lamb waves · Short-time-root-mean-square (STRMS) · Wavelet reassignment scalogram

47.1 Introduction

Acoustic–ultrasonic technique is a new damage detection technique which was proposed by American scholars in the early 1970s and 1980s [1, 2]. The technology uses a piezoelectric transducer to stimulate interrogation pulse stress wave

L. Zhang (✉)
Beijing Aeronautical Technology Research Centre, Beijing 100076, China
e-mail: Lei_zhang76@126.com

M. Zhu
Huaxia Hanhua Chemical Equipment Corporation, Beijing 100120, China

on the material surface and receives stress wave signal by piezoelectric sensor on the other parts of the same surface. Then, the stress wave factor that reflects the efficiency of the instant pulse wave propagation can be determined by signal analysis [3]. Consequently, the mechanical properties of materials or the changes of defects and damage can be characterized. As a new technique of structural damage detection and completeness of dynamic evaluation, the key of acoustic–ultrasonic technique is to extract and quantify the information about the properties of materials that are included in the modeling stress wave. So, it is very suitable for quantitative detection of relevant parameters of the structure and mechanical properties. Since the technique was founded, it has been attracting great interest. Extensive research works have been carried out, and many important results have been reported by many research institutions and universities, such as United States NASA Lewis Research Center, Washington University, Johns University, Hopkins University, MIT as well as the former Soviet Union, Canada, Denmark, etc. [4].

According to plate wave theory [5], acoustic–ultrasonic technique excites Lamb waves in thin plate. Therefore, it is important for acoustic–ultrasonic technique to analyze the Lamb wave rationally and effectively, to explore the information about the detected objects. This article focuses on LY12CZ aviation aluminum. That is to waveform analysis and modal analysis method to study the Lamb wave properties in aluminum. The properties of Lamb wave propagation time-frequency are also discussed. Besides, the damage simulation for the aluminum plates with and without damage is compared and analyzed.

47.2 The Lamb Wave in Acoustic–Ultrasonic Technique

Lamb wave is a kind of guided waves, which is a plane strain wave generated in the free board. The upper- and lower-surface traction force is zero. And the wave equation is the Rayleigh–Lamb equation [6], the expression is as follows:

Symmetric mode

$$\frac{\tan k_s b}{\tan k_l b} = -\frac{4k_0^2 k_1 k_s}{\left(k_0^2 - k_s^2\right)^2} \tag{47.1}$$

Antisymmetric mode

$$\frac{\tan k_s b}{\tan k_l b} = -\frac{\left(k_0^2 - k_s^2\right)^2}{4k_0^2 k_1 k_s} \tag{47.2}$$

$$k_l^2 = \left(\frac{\omega}{c_l}\right)^2 - k_0^2, \quad k_s^2 = \left(\frac{\omega}{c_s}\right)^2 - k_0^2 \tag{47.3}$$

where k_0 is the wave number along the horizontal direction of the plate, b is the 50 % of the plate thickness, ω is angular frequency, c_l is the longitudinal wave velocity, and c_s is the shear wave velocity.

Multimodal and dispersion properties of Lamb wave are determined by wave equation. However, each mode has different order, which is the most important characteristics of Lamb wave [7].

47.3 The Methods of Analyzing Lamb Wave Analysis

47.3.1 Lamb Wave Propagation Properties Based on Short-Term-RMS Signal (STRMS)

Wave propagation is the process of energy propagation, so analyzing energy can understand the properties of wave propagation. Signal root-mean-square (RMS) analysis is a method commonly used in the energy analysis where RMS signal indicates the amount of total energy. And short-time-root-mean-square (STRMS) analysis is to divide the total energy of the signal through the entire time history into short signal by timing sequence and calculating the RMS value. STRMS reflects the energy properties of short signal. For example, it can reflect the energy propagation properties by lining up the signal energy through timing sequence. Lamb wave is a multimodal elastic wave. Each modal wave has frequency range and dispersion, so the average propagation velocity and properties should be measured in terms of energy propagation. This article analyzes the propagation properties of Lamb wave with STRMS.

47.3.2 Lamb Wave Time-Frequency Properties Analysis Based on Scale Redistribution Spectrum of Wavelet

Group velocity is energy propagation velocity of different modal Lamb wave. And group velocity dispersion curve is the distribution of energy in the frequency thickness—time plane. Therefore, there is a corresponding relation between Lamb wave group velocity dispersion curves and their time-frequency distribution and time-frequency properties [4]. Here, the time-frequency properties of Lamb wave were discussed with excellent scale redistribution spectrum of wavelet.

Let $f(t)$ be a finite energy function, namely $f(t) \in L^2(R)$. Then, it can be unfolded based on the wavelet which is called continuous wavelet transfer (CWT). The expression is:

$$W_f(a,b;\psi) = \langle f(t), \psi_{a,b}(t) \rangle = \frac{1}{\sqrt{a}} \int f(t)\psi_{a,b}(t)\,dt, \quad (a > 0) \qquad (47.4)$$

wherein, the functions group $\psi_{a,b}(t)$ stems from the basic wavelet function generated through dilation and translation. And a is conversion factor, the factor $\frac{1}{\sqrt{a}}$ is used to ensure conservation of energy; b is position parameters.

According to equidistant of the wavelet transform, there is no information loss in wavelet transform, which means that the transformation is the conservation of energy, as the following equation:

$$\int \left| f(t)^2 \right| \mathrm{d}t = \frac{1}{C_\psi} \int a^{-2}\,\mathrm{d}a \int \left| W_f(a,b;\psi) \right|^2 \mathrm{d}b \qquad (47.5)$$

$SG_f(a,b;\psi) = \left| W_f(a,b;\psi) \right|^2$ can be defined as scale spectrum which resembles to short-time Fourier transform spectrum. And scale spectrum can be regarded as a constant relative bandwidth spectrum. In order to improve the readability of scale spectrum and to eliminate interference terms effectively, Ref. [8] proposed the method of redistribution scale. The algorithm is as follows:

$$RSG_f(a,b;\psi) = \int\int (\hat{a}/a)^2 SG_f(a,b;\psi)^* \delta(\hat{b} - b'(a,b))\delta(\hat{a} - a'(a,b))\mathrm{d}a\mathrm{d}b$$
$$(47.6)$$

wherein,

$$b'(a,b) = b - \mathrm{Re}\left\{ a \frac{W_f(a,b;\psi')W_f^*(a,b;\psi)}{\left| W_f(a,b;\psi) \right|^2} \right\} \qquad (47.7)$$

$$\frac{\omega_0}{a'(a,b)} = \frac{\omega_0}{a} + \mathrm{Im}\left\{ a \frac{W_f(a,b;\psi')W_f^*(a,b;\psi)}{2\pi a \left| W_f(a,b;\psi) \right|^2} \right\} \qquad (47.8)$$

47.4 Experimental Study

47.4.1 Introduction of the Experiments

Equipments include Agilent 33120 A arbitrary waveform generator, PAII broadband acoustic emission preamplifier and broadband main amplifier, PCI9812 high-speed acquisition cards, and computers. Transmitting and receiving transducers are Φ 8 mm $\times$ 0.4 mm piezoelectric film. The excitation signal is 5 cycles sine pulse signal modulated by Hanning window, and the peak value is 10 V. The sampling frequency of acquisition system is 2 MHz, and each sampling time is 0.5 s. STRMS analysis is carried out by the received signal with every 10 sampling site as a unit.

Scheme I used 2024-T3 aluminum plate whose size is 715 mm $\times$ 475 mm $\times$ 3.5 mm. The piezoelectric sheet was arranged on the same side of the aluminum plate, located at A (365,400), B (365,350), C (365, 250). The piezoelectric crystal plate at site serves as the excitation source and the other two as receiver sensors. Excitation frequencies are 250 and 350 kHz, respectively.

Scheme II used two aluminum plates whose size is 475 mm × 300 mm × 3.5 mm. Make a transparent slot simulated crack defects on one of them, and the slot size is 30 mm × 1 mm. If using the lower left corner of the plate as the coordinate origin, the defect center coordinates are (225, 140) with an included angle 135° to bottom. Three sensors, 1#, 2# and 3#, are arranged around the defect. And ligature between 2# and 3# divided defect slot equally and perpendicularly. The spacing between sensors is 30 mm. Ligature between 1# and 2# parallel to the defect slot with a 20-mm space. The arrangement of the 3 sensors of good aluminum resembles to defect aluminum. Excitation frequencies are 175 and 350 kHz, respectively.

47.4.2 Results and Discussion

47.4.2.1 The Basic Properties of Lamb Wave in Aluminum Plate

According to STRMS principle, the maximum amplitude of STRMS sequence of the signal point corresponds to the moment when the center of Lamb wave energy goes through center position of the sensor. And the amplitude of the wave energy represents the strength of Lamb wave. Figure 47.1 shows the STRMS analysis results of Lamb wave signal in scheme I. The following propagation properties of aluminum plate can be obtained from the figures. At low-frequency excitation, aluminum plate Lamb wave mainly includes two modes: A_0 and S_0. And amplitude ratio of A_0 mode and S_0 mode Lamb wave goes up with the decrease in excitation frequency. In Fig. 47.1a, the maximum amplitude of S_0 first to reach is lower than that of A_0. In Fig. 47.1b, the maximum amplitude of S_0 is nearly twice of that of A_0. In other word, Lamb wave energy transits gradually from A_0 to S_0 when the excitation frequency increases.

47.4.2.2 Analysis About Propagation Properties of Lamb Wave

Figure 47.2 shows the STRMS analysis results of Lamb wave signal in scheme II. It can be indicated that the first Lamb wave energy of S_0 and A_0 will reduce if the propagation path is defective in a short-distance communication process. But, the decreasing amplitude of A_0 is smaller than that of S_0. When the receiving sensor is directly facing the damage on the both sides (path 2 ↔ 3), STRMS amplitude of first wave of S_0 will go down to 1/10 of no damage [(3) in Fig. 47.2a] while STRMS amplitude of first wave of A_0 declines to only about 1/2 [(3) in Fig. 47.2b]. The oblique damage (path 1 ↔ 3), amplitude of first wave of S_0, is about 1/2 [(2) in Fig. 47.2a] and that of A_0 first wave is 1/5 [(2) in Fig. 47.2b]. Consequently, S_0 Lamb wave modes are more sensitive to simulation damage. When damage is not on the transmission path (the path 1 ↔ 2), first wave of A_0 and S_0 are essentially unchanged [(1) in Fig. 47.2a, b].
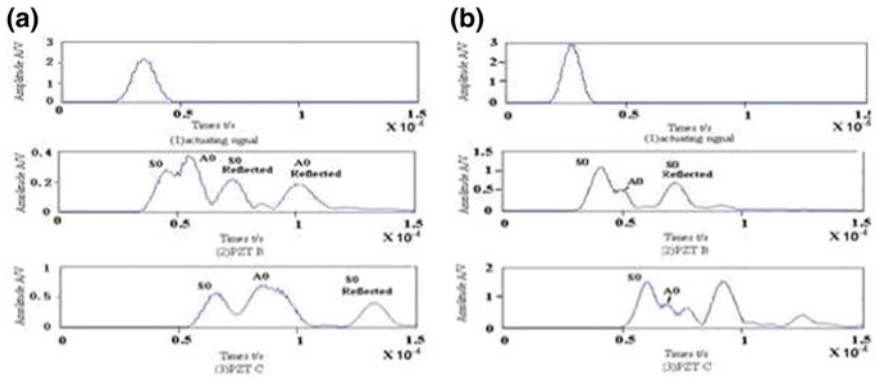
Fig. 47.1 STRMS analysis of Lamb wave. **a** 250 kHz. **b** 350 kHz

(1) path 1 ↔ 2

(2) path 1 ↔ 3

(3) path 2 ↔ 3
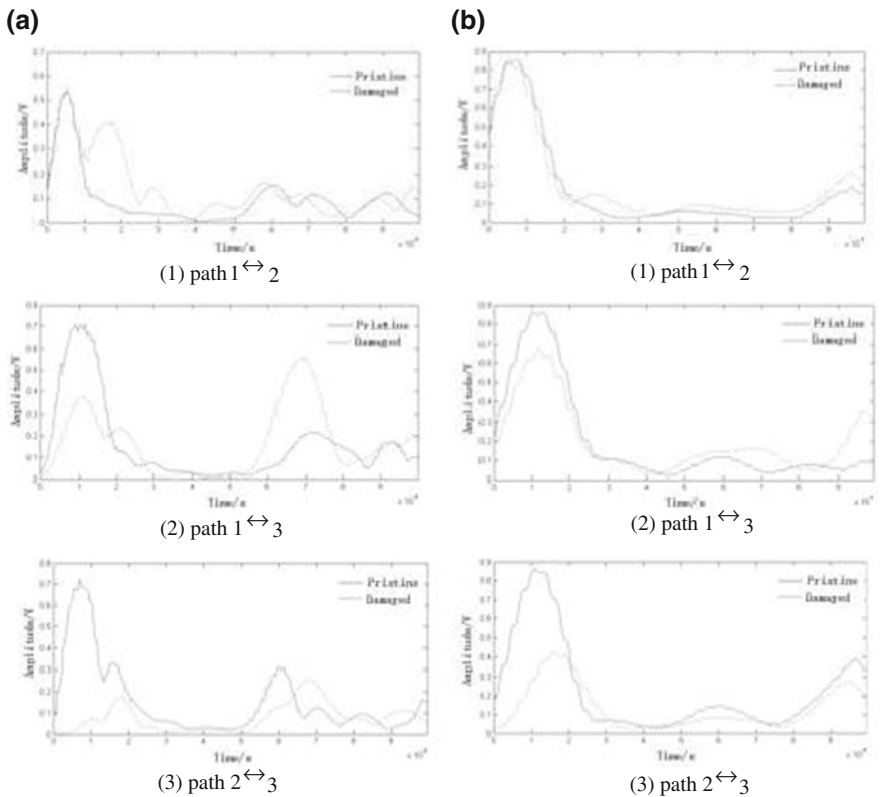
Fig. 47.2 STRMS analysis of Lamb wave for scheme II. **a** 350 kHz. **b** 175 kHz

(a)

(1) path 1 ↔ 2

(2) path 1 ↔ 3

(3) path 2 ↔ 3

(b)

(1) path 1 ↔ 2

(2) path 1 ↔ 3

(3) path 2 ↔ 3
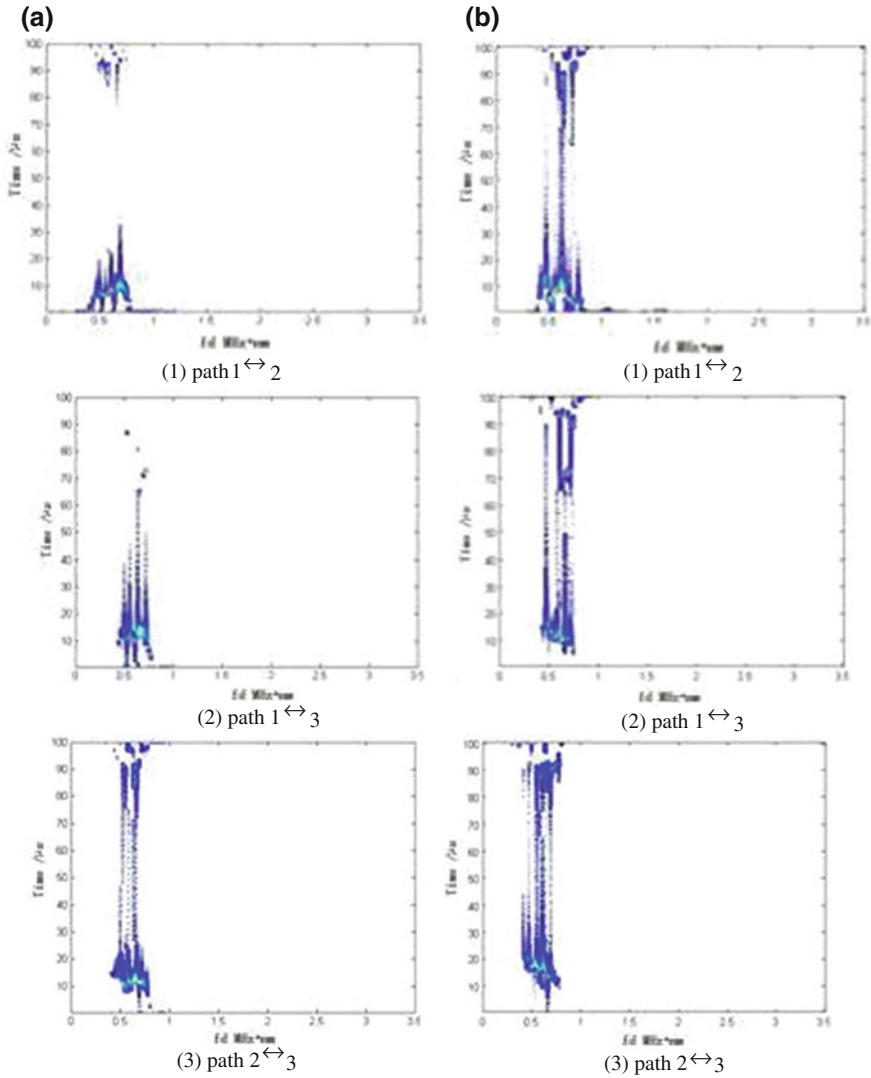
Fig. 47.3 Wavelet reassigned scalogram analysis of Lamb waves at 175 kHz. **a** Pristine plate.
b Damaged plate

47.4.2.3 Analysis About the Time and Frequency Properties of Lamb Wave

Figures 47.3 and 47.4 show the analysis results of Lamb wave redistribution scale wavelet time-frequency spectrum under different excitation frequencies in aluminum plate.

(a)   **(b)**

(1) path 1 ↔ 2   (1) path 1 ↔ 2

(2) path 1 ↔ 3   (2) path 1 ↔ 3

(3) path 2 ↔ 3   (3) path 2 ↔ 3
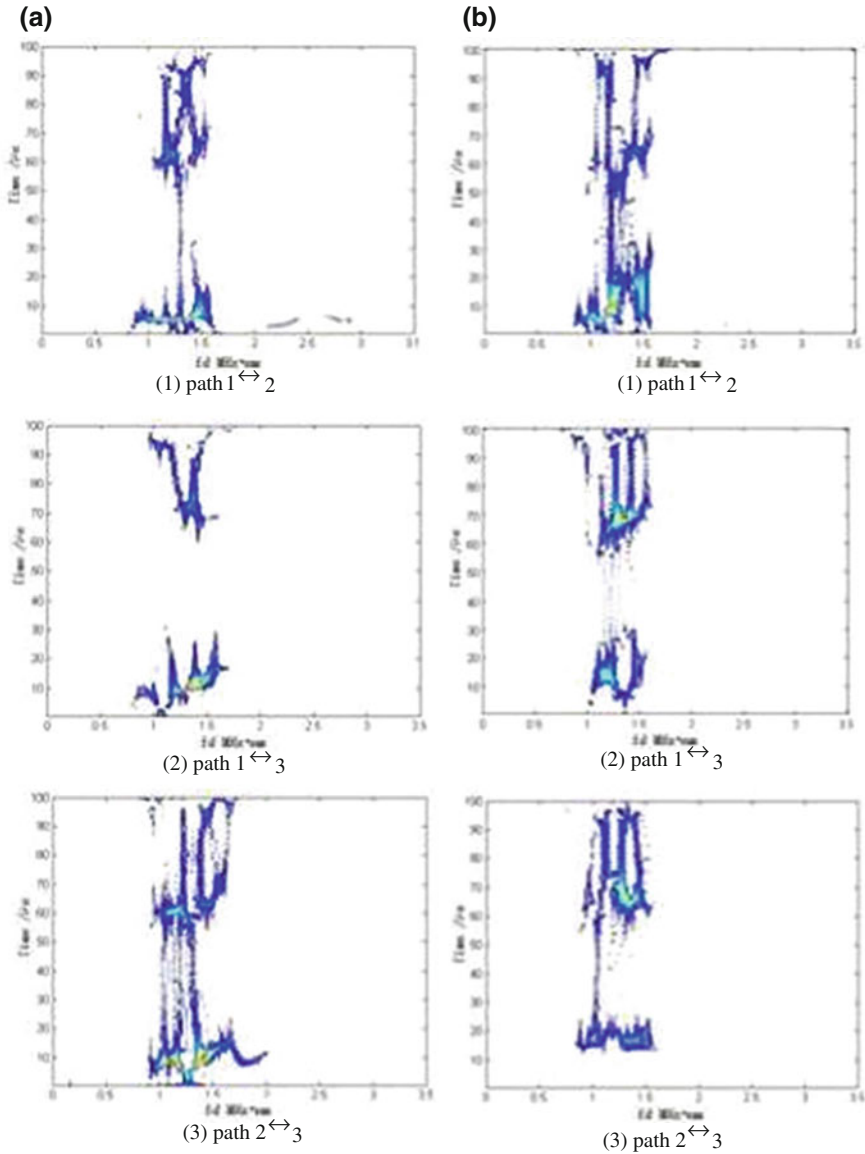
Fig. 47.4 Wavelet reassigned scalogram analysis of Lamb waves at 350 kHz. **a** Pristine plate. **b** Damaged plate

According to time-frequency distribution of energy, energy distribution within Lamb wave changes due to the presence of simulation damage. In case of no damage, the distribution of Lamb wave energy is more concentrated and pure. And the Lamb wave energy transmitted takes up a large proportion directly in the total

energy of the signal which manifests as that the red area represents the highest energy value always appears in the first conveyed wave group in the result of no damage scale redistribution of the energy spectrum [(b) of Figs. 47.3 and 47.4]. However, the Lamb wave contains more information which is received by simulation-damaged aluminum plate. The graph on scale redistribution Lamb wave wavelet spectrum of simulation-damaged aluminum plate indicates a new energy ingredient which is caused by the presence of the simulation damage, such as scattering, diffraction, and other Lamb wave energy. And these ingredients are unable to distinguish in STRMS analysis which reflects excellent time-frequency analysis results of wavelet scale redistribution spectrum in the Lamb wave signal analysis.

It can also be seen from the figures, when the defects are on directly conveyed transmission path, energy goes down significantly since the large attenuation of Lamb wave signal. And the higher Lamb wave frequency is, the greater the energy drops. This is because that the higher frequency leads to shorter wave length of Lamb which shows more sensitive to damage and greater attenuation.

47.5 Summary

STRMS and spectrum of wavelet scale redistribution were used to study Lamb wave propagation properties, time–frequency properties, and modal properties of undamaged aluminum plate and damaged aluminum plate under different excitation conditions. The following is the valuable conclusions.

1. Under low-frequency excitation, Lamb wave in the aluminum plate mainly consists of two kinds of modes A_0 and S_0. Lamb wave energy transited gradually from A_0 to S_0 with the increase in excitation frequency.
2. According to propagation properties, S_0 modal Lamb wave is more sensitive to simulation damage than A_0 mode.
3. According to time-frequency distribution of energy, new energy component shown in Lamb waves of damaged aluminum reflected as the graph in the spectrum of wavelet scale redistribution. And these ingredients are unable to distinguish in STRMS analysis which reflects excellent time-frequency analysis results of wavelet scale redistribution spectrum in the Lamb wave signal analysis.
4. When the defects are on directly conveyed transmission path, attenuation of Lamb wave signal and decreasing amplitude are large. And the higher Lamb wave frequency is, the greater the energy drops.

References

1. Vary A (1988) The acousto-ultrasonic approach. In: Duke JC Jr (ed) Acousto-ultraxonics theory and application. Plenum Press, New York, pp 1–21
2. Kautz HE, Lerch BA, Tribolet RM (1991) Preliminary investigation of acousto-ultrasonic evaluation of metal matrix composites specimens. Mater Eval 49(5):607–612
3. Tong GS, Sun LX (1999) A review and prospect of problems in stress wave factor technique. J Vibr Meas Diagn 19(4):320–326 (in Chinese)
4. Thomsen JJ, Lund K (1991) Quality control of composite material by neural network analysis of ultrasonic power spectra. Mater Eval 49(5):594–600
5. Liu ZQ (1999) Guided waves in ultrasonic nondestructive testing. NDT 21(8):367–369 (in Chinese)
6. Rose JL (1999) Ultrasonic waves in solid media. Cambridge University Press, New York
7. Zheng XM, Gu XH, Shi LF et al (2003) Time-frequency analysis of Lamb waves. Acta Acustica 28(4):368–374 (in Chinese)
8. Aguer F, Flandrin P (1995) Improving the readability of time-frequency and time-scale representations by the reassignment method. IEEE Trans Sig Process 43(5):1068–1089

Chapter 48
Rolling Bearing Fault Diagnosis Based on 1.5-Dimensional Spectrum

Xueli Zhang and Hongkai Jiang

Abstract Signal de-noising and extraction of useful signal feature are significant problems in the work of scientific research. Higher-order cumulants (HOC) have a strong ability of noise reduction. However, the increase in the order number of HOC will lead to the increase in computation. This will bring great difficulties to practical application. This paper introduces the knowledge of 1.5-dimensional spectrum, which results from the HOC. 1.5-dimensional spectrum is actually a simplified calculation method of HOC. It also remains the HOC's excellent characteristic which can suppress the additive Gaussian noise. Consequently, 1.5-dimensional spectrum can be well applied in engineering practice. Meanwhile, the Hilbert transform is also introduced simply in this paper. The simulation signals and rolling failure data are processed with the 1.5-dimensional spectrum and Hilbert transform, respectively. The comparison results confirm the practical value of 1.5-dimensional spectrum.

Keywords Rolling bearing · Fault diagnosis · Higher-order cumulants · 1.5-dimensional spectrum

48.1 Introduction

Recently, studies on mechanical failure diagnosis have obtained promising results. It is an active area of current research. In the diagnosis, the most critical issues is the principle of feature extraction of failure, for example, what approach would be taken and which sensitive signal should be extracted so that the most effective

X. Zhang · H. Jiang (✉)
School of Aeronautics, Northwestern Polytechnical University,
Xi'an 710072, Shaanxi, China
e-mail: jianghk@nwpu.edu.cn

X. Zhang
e-mail: zxl2013@mail.nwpu.edu.cn

real-time monitoring and diagnosis will be achieved. All of these would be the key of the modern failure diagnosis and monitor.

Higher-order cumulant (HOC) [1] is a new technology which rapid developed recently. It receives increasing attention as an important toll for processing non-Gaussian signal and nonlinear signal as well as the blind signal. It can extract the coupling characteristics between signals and the nonlinear characteristics of the detection systems; moreover, it is insensitive to Gaussian noise. Theoretically, HOC can eliminate the influence of noise completely.

However, the computation of the higher-order statistics will increase with the increase in its rank. This has brought great difficulties to the practical application. Because of this disadvantage, many scholars tried to find the simplified method of HOC. Recently, some scholars introduce an ideology, which is called dimensionality reduction, to project the high-order spectrum into the one-dimensional frequency space by the way of slice. Therefore, the conception of 1.5-dimensional spectrum [2] is obtained.

48.2 Higher-Order Cumulants

The definition of HOC was given by introducing the characteristic function [3], for a single random variable x, the HOC C_k is defined as:

$$C_k = \frac{1}{j^k} \frac{\mathrm{d}^k \psi(\omega)}{\mathrm{d}\omega^k} \Big|_{\omega=0} \quad k = 1, 2, \ldots, n \tag{48.1}$$

where

$$\psi(\omega) = \ln \phi(\omega) \tag{48.2}$$

$$\phi(\omega) = \int_{-\infty}^{\infty} f(x) \exp(j\omega x)\mathrm{d}x = E[\exp(j\omega x)] \tag{48.3}$$

$\psi(\omega)$ is called the first characteristic function of the random variable x, $\phi(\omega)$ is called the second characteristic function of the random x.

48.3 1.5-Dimensional Spectrum

The 1.5-dimension spectrum was first proposed by Giannakis and Mendel [4]. It is defined as the Fourier transform of third-order cumulants diagonal slice; hence, it not only retains the advantage of high-order cumulants which can suppress Gaussian noise, but also simplifies the calculation [5]. The 1.5-dimensional spectrum also can enhance the low-frequency components.

For a signal $x(t)$, its third-order cumulant is $c_{3x}(\tau_1, \tau_2)$, and the diagonal slice is $c_{3x}(\tau, \tau)$, $(\tau_1 = \tau_2 = \tau)$, we define the Fourier transform of the diagonal slice as 1.5-dimensional spectrum $C(\omega)$:

$$C(\omega) = \int\limits_{+\infty}^{-\infty} \left[\int\limits_{-\infty}^{+\infty} x(t)x^2(t+\tau)\mathrm{d}t \right] \mathrm{e}^{-j\omega\tau}\mathrm{d}\tau \qquad (48.4)$$

The 1.5-dimensional spectrum has the following properties [4].

1. If $x(t)$is a n times real harmonic signal that the mean is zero and the basic frequency is ω_0. When $|\omega_m| < |\omega_l|$, there is

$$C(\omega_m) > C(\omega_l) \qquad (48.5)$$

$(\omega_m = m\omega_0, \ m = \pm 1, \pm 2, \ldots, \pm n, \ \omega_l = l\omega_0, \ l = \pm 1, \pm 2, \ldots, \pm n)$

2. If $x(t)$ is a zero-mean Gaussian noise, there is

$$C(\omega) = 0 \qquad (48.6)$$

3. If $x(t)$ is a zero-mean random noise, it is uncorrelated in any two different time, and the probability density function is symmetric distribution, then there is

$$C(\omega) = 0 \qquad (48.7)$$

4. If $x(t)$ is the harmonic signal, $\omega_m, \omega_p, \omega_q$ are three harmonic components, if $\omega_m \neq \omega_p + \omega_q$, there is

$$C(\omega) = 0 \qquad (48.8)$$

In summary, 1.5-dimensional spectrum can enhance low-frequency components and also has a particularly effect in weaker low-frequency component extracting. The 1.5-dimensional spectrum is an important tool in modern signal processing.

48.4 Hilbert Transform

Hilbert transform is an important tool of signal analysis. For a real causal signal $x(t)$ or $x(n)$, there is Hilbert transform relationship between their real part and imaginary part of Fourier transform, the frequency response, and phase response.

By Hilbert transform, we can construct the response signal, it contains only positive frequency components, and thereby, the sampling rate of the signal was reduced [6].

Given a set of continuous vibration signal $x(t)$, the Hilbert transform $y(t)$ is defined as:

$$y(t) = \frac{1}{\pi} \int_{-\infty}^{\infty} \frac{x(\tau)}{t-\tau} d\tau = \frac{1}{\pi} \int_{-\infty}^{\infty} \frac{x(t-\tau)}{\tau} d\tau = x(t) * \frac{1}{\pi t} \qquad (48.9)$$

The analytic signal, which constituted by Hilbert transform, contains only the positive frequency components and is two times of the original signal's positive frequency components.

48.5 Experimental Results' Comparison

48.5.1 Simulation Results

A modulation source, a centered impulse response simulation carrier signal $x(t)$ is constructed to simulate the rolling bear failure response signal:

$$x(t) = \sum_{i=1}^{42} \left(e^{-\zeta 2\pi f_1(t-i/f_{ou})} \sin 2\pi f_1(t - i/f_{ou}) \right) \sqrt{1 - \zeta^2} \qquad (48.10)$$

The carrier center frequency of $x(t)$ is $f_1 = 40$ Hz, damping ratio is $\zeta = 0.01$, $f_{ou} = 30$ Hz. With the sampling frequency which is 1,600 Hz for discrete sampling, the length of the data is 2,048.

The time-domain chart and frequency-domain chart of the simulated signal are showed in Fig. 48.1. The result that processed by the 1.5-dimensional spectrum is showed in Fig. 48.2, the result that processed by Hilbert transform is showed in Fig. 48.3.

From Figs. 48.1, 48.2, and 48.3, 1.5-dimensional spectrum is significantly better than the Hilbert transform for this signal feature extraction. In Fig. 48.2, the 30 Hz impact signal is extracted, and the frequency is clear, noise canceling effect is good; while in Fig. 48.3, Hilbert transform did not extract the 30 Hz impact signal, and the noise reduction effect is not obvious.

48.5.2 Bearing Fault Analysis of Experimental Results

A set of actual experimental data is showed, the sampling frequency is 12,800 Hz, and this can be used to prove the above conclusions.
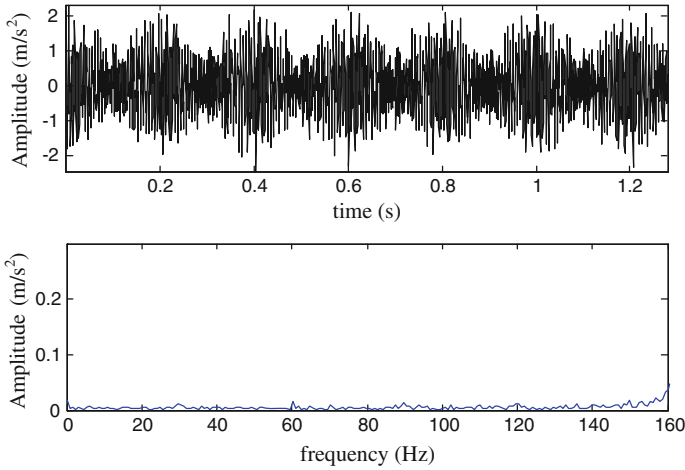
Fig. 48.1 Time-domain chart and frequency-domain chart of the simulated signal
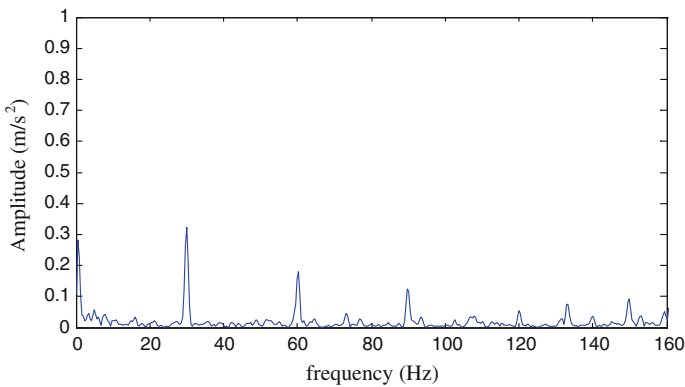
Fig. 48.2 Result of 1.5-dimensional spectrum

The time-domain chart of the original signal is shown in Fig. 48.4. The frequency-domain chart of the original signal is shown in Fig. 48.5. The result which the original signal is processed by 1.5-dimensional spectrum is showed in Fig. 48.6. The result which the original signal is processed by Hilbert transform is showed in Fig. 48.7.

From Figs. 48.4, 48.5, 48.6, and 48.7, a result that 1.5-dimensional spectrum and Hilbert transform are all the feature extraction methods is confirmed. Any of them can be used to extract feature of the failure signal. But, using 1.5-dimensional spectrum, the frequency will be more clearer, and the noise reduction capability of 1.5-dimensional spectrum is better than the Hilbert transform.
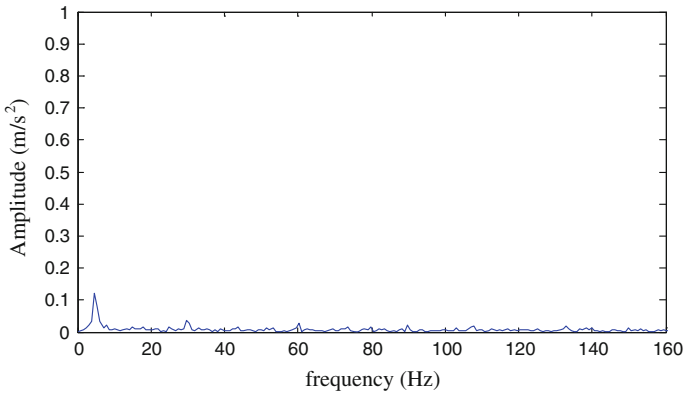
Fig. 48.3 Result of Hilbert transform
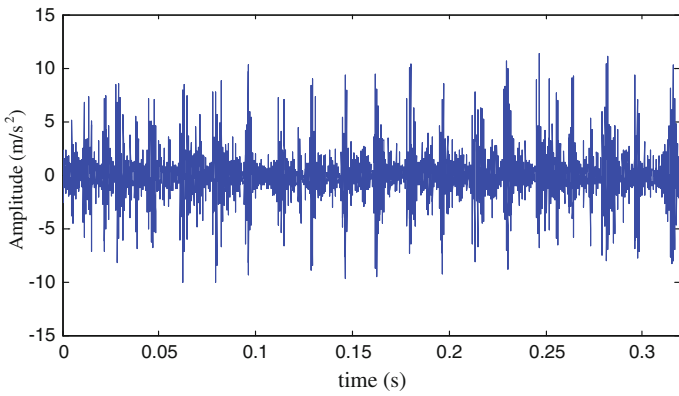
Fig. 48.4 Time-domain chart of the original signal
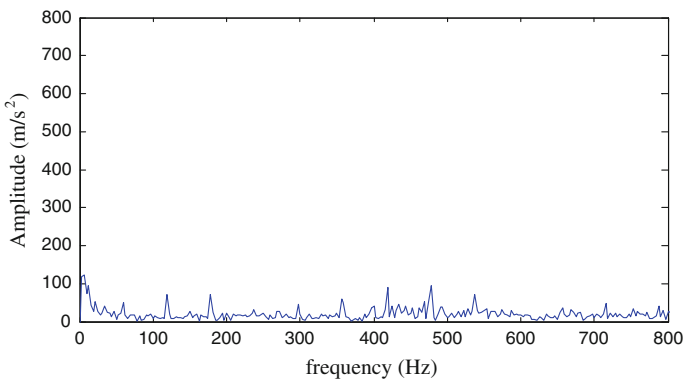
Fig. 48.5 Frequency-domain chart of the original signal
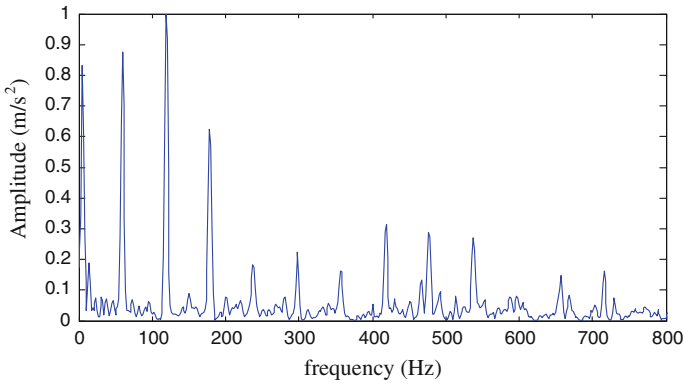
Fig. 48.6 Result of 1.5-dimensional spectrum
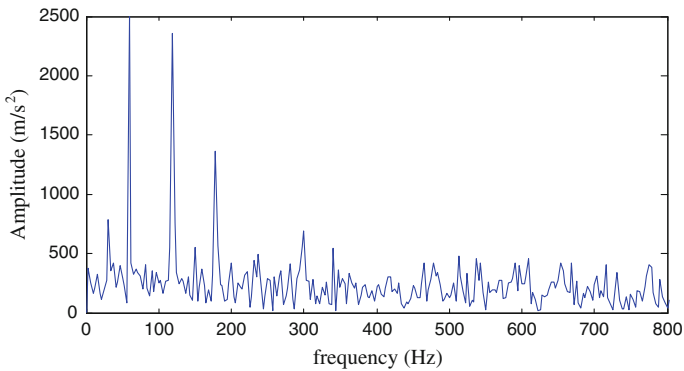
Fig. 48.7 Result of Hilbert transform

48.6 Conclusion

The knowledge about 1.5-dimensional spectrum is introduced in this paper. The 1.5-dimensional spectrum is actually a simplified calculation method of the HOC. It remains the HOC's excellent capability that can suppress the Gaussian noise simultaneously. These entirely make 1.5-dimensional spectrum, which is well used in practical application. At the end of the paper, two sets of data are analyzed with the two methods, respectively. The results would confirm the practical value of 1.5-dimensional spectrum.

References

1. Renping S, Xinna H, Hongyu L, Xu Y (2008) Fault detection and diagnosis of gear system based on higher order cumulants. J Chin J Mech Eng 44(6):161–168 (in Chinese)
2. Yangyu F, Baoqi T, Ke X, Jiuhao S, Jincai S, Yaan L (2002) Feature extraction of ship-radiated noise by $1\frac{1}{2}$-spectrum (in Chinese). J Acta Acustica 27(1):71–76
3. Renping S, Xinna H, Hongyu L, Hu J (2008) A more refined fault detection and diagnosis of gear system based on higher order cumulants (HOCs). J Northwest Polytech Univ 26(2):259–264 (in Chinese)
4. Yaan L, Xian F, Yangyu F, Jiangguo H (2004) Extraction of low frequency line spectrum of ship radiated noise based on the $1\frac{1}{2}$ D spectrum (in Chinese). J Acta Armamentarii 25(2):239–241
5. Hongkai J, Yong X, Xiaodong W (2013) Rolling bearing fault detection using an adaptive lifting multiwavelet packet with a $1\frac{1}{2}$ dimension spectrum. J Meas Sci Technol 24:125002 (10 pp) (2013)
6. Guangshu H (1997) Digital signal processing: theory algorithm and implementation. Tsinghua University Press, Beijing, pp 120–124 (in Chinese)

Chapter 49
Research on Semi-active Suspension Vibration Control Using Magneto-Rheological Damper

Haidong Shao and Hongkai Jiang

Abstract A novel semi-active vibration control technique using magneto-rheological (MR) damper is presented in this paper for researching the key points that help realize the control of semi-active seat suspension. Bingham model is applied to establish for MR damper in this method, and the dynamics simulation on vehicle seat semi-active suspension system is carried out. In the case of random input of the Grade B road, the vibration characteristics of vehicle seat are analyzed and the effect of spring stiffness, damping, and vehicle speed on the vibration damping characteristic is discussed as well. Simulation results show that the semi-active suspension has a higher damping performance than passive suspension. PID control strategy is introduced to the semi-active suspension; the maximum acceleration decreases obviously to around 40 % compared with passive suspension that confirms that the effect of control strategy has played well.

Keywords MR damper · Semi-active suspension · Vibration control · PID

49.1 Introduction

In the past two decades, noise and vibration have been a major problem in many human activities and domains such as airplanes, satellites, cars, and bridges. In particular, in the automotive industry, people have paid more and more attention to the car's driving safety and comfort. To solve this problem, better technology and

H. Shao · H. Jiang (✉)
School of Aeronautics, Northwestern Polytechnical University,
Xi'an 710072, Shaanxi, China
e-mail: jianghk@nwpu.edu.cn

H. Shao
e-mail: hdshao@mail.nwpu.edu.cn

Fig. 49.1 Simplified model
with MR damper
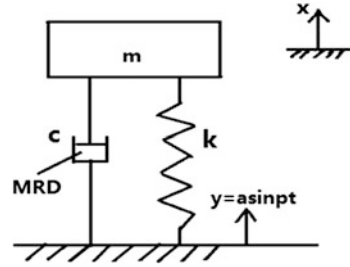
device are required. To increase the adaptability of vehicle to various types of
roads, controllable dampers, such as magneto-rheological (MR) dampers, are
invented to improve the suspension performance. On the other hand, semi-active
vibration control technique has been widely used in vehicles, aviation, aerospace,
and other fields in recent years [1]. Obviously, vehicle semi-active vibration
suppression system based on MR dampers has become the focus and it has great
potential for development [2]. The seat as one part of decreasing vibration of
vehicle is easy to be improved and has great influence on the vibration perfor-
mance. Consequently, considering vehicle seat MR semi-active suspension control
not only has a very high theoretical research value, but also has a wide application
prospect.

49.2 Semi-active "Body-Seat" Suspension Dynamic Model

Generally, the motion of cab floor makes the seat vibrate, acceleration sensors
collect acceleration signal to the controller, through a certain control algorithm,
and controller outputs appropriate control current to the MR damper, thereby
generating an appropriate damping force to suppress the impact from the cab floor
effectively. Nowadays, the focus of the "Body-Seat" model is the treatment of the
human body; single degree of freedom model is analyzed mainly in this paper; that
is, the human body is seen as a particle. As shown in Fig. 49.1, let the movement
of supporting is a harmonic function [3]:

$$y = a \cdot sinpt \tag{49.1}$$

The differential equations of motion of the system can be written as

$$m\ddot{x} + c\dot{x} + kx = ky + c\dot{y} \tag{49.2}$$

where m, c, k, $\ddot{x}$, $\dot{x}$ and x represent the sprung mass, damping coefficients, stiff-
ness, acceleration, velocity, and displacement, respectively.

Fig. 49.2 Grade B road,
$v = 40$ km/h simulation
curve of vertical
displacement
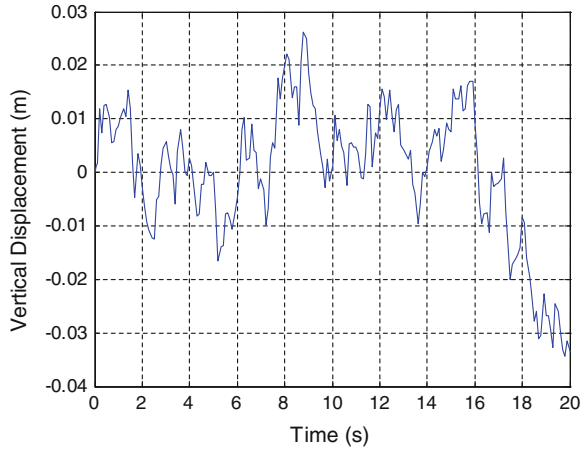
49.3 Simulation Modeling of Seat Vibration Suppression System

49.3.1 Simulation of the Excitation Signal

Road surface roughness is the most important reason making the cab floor vibrate. Choosing random excitation as road excitation on the wheel in this paper, the excitation of wheel from the road can be expressed by

$$\dot{x}_g = -2\pi f_0 x_g + 2\pi n_0 \sqrt{G_q(n_0)v_0}\,\omega \tag{49.3}$$

where x_g, f_0, n_0, $G_q(n_0)$ and v_0 represent road vertical displacement, the cutoff frequency, reference frequency, the road power spectral density function, and speed, respectively. ω is white noise which is distributed uniformly, and its mean is 0.

A mathematical description of road surface roughness is established which is the model of integral white noise. Take $v = 40$ km/h for example, the excitation signal of pavement vertical displacement is given in Fig. 49.2.

49.3.2 Simulation Modeling of the MR Damper

In engineering application, MR damper is controlled by changing the impressed current. Studies show that when impressed current is zero, magnetic fluid yield stress can be approximated to zero, when the impressed current is large, the magnetic fluid yield stress increases more slowly [4]. The relationship between impressed current and yield stress can be written as

Fig. 49.3 Simulation curve
of current
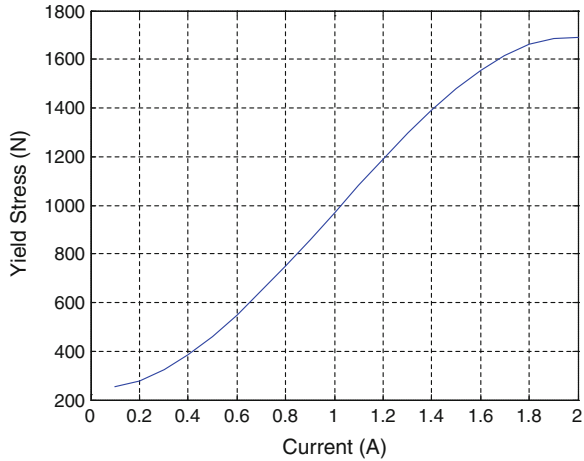
$$\tau_y = C_1 I^3 + C_2 I^2 + C_3 I + C_4 \qquad (49.4)$$

where C_1, C_2, C_3 and C_4 are all the coefficients related to the performance of MR fluid. Simulation diagram of impressed current and yield stress are established, and the result is given in Fig. 49.3.

Currently, Bingham model is commonly used for both theory research and engineering design of MR damper. Studies have shown that the relationship between stress and strain can be written as

$$\tau = \tau_y \mathrm{sgn}\left(\frac{\mathrm{d}u}{\mathrm{d}t}\right) + \eta \frac{\mathrm{d}u}{\mathrm{d}t} \qquad (49.5)$$

where τ_y, τ, η and $\frac{\mathrm{d}u}{\mathrm{d}t}$ represent stress, strain, viscosity, and flow velocity, respectively. On the basis of this model, the output of damping force from MR damper can be written as

$$F = f_c \mathrm{sgn}(\dot{x}) + C\dot{x} \qquad (49.6)$$

where f_c is function about MRF yield and C is the damping coefficient which is related to the structure of MR damper. As shown in Fig. 49.4, Bingham model is established based on the related data.

49.4 PID Control Strategy and Simulation Results

Recently, semi-active feedback control methods such as the conventional PID controllers and the fuzzy PID controllers have been applied to the MR damper for a base isolation system by Ang et al. [5]. Usually, the main controlled variable is chosen as the acceleration, displacement, and velocity in vibration system. In this
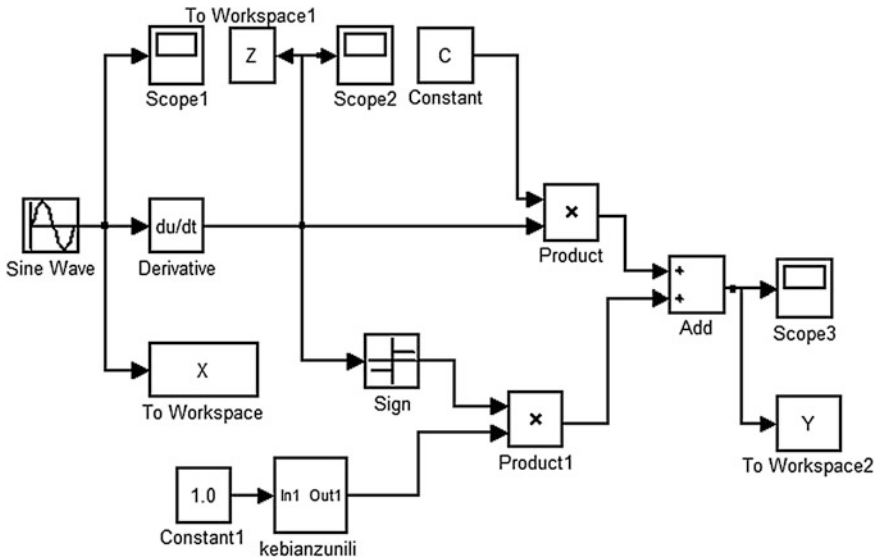
Fig. 49.4 Bingham simulation mode

Fig. 49.5 Grade B road,
$v = 50$ km/h seat
displacement
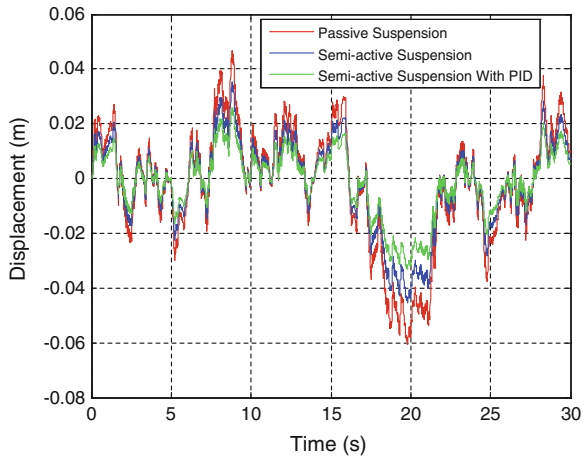
paper, vibration displacement and vibration acceleration are selected, respectively, to test the vibration damping effect. Simulation results are shown in Figs. 49.5, 49.6 and 49.7.

As shown above, it is found that semi-active suspension has a higher damping performance than the passive suspension. When PID control is introduced, the maximum acceleration decreases to around 40 % compared with passive suspension.

Fig. 49.6 Grade B road,
$v = 50$ km/h seat acceleration
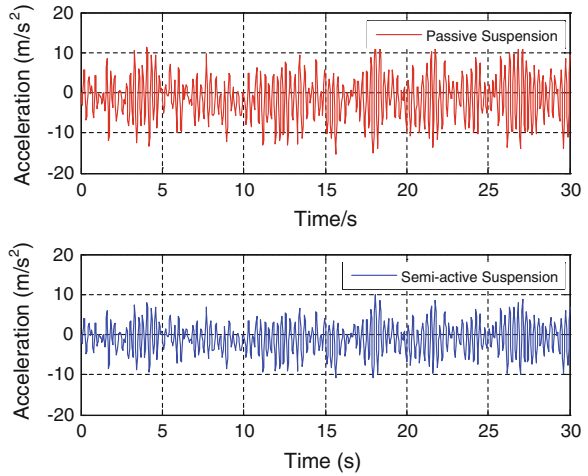
Fig. 49.7 Grade B road,
$v = 50$ km/h seat acceleration
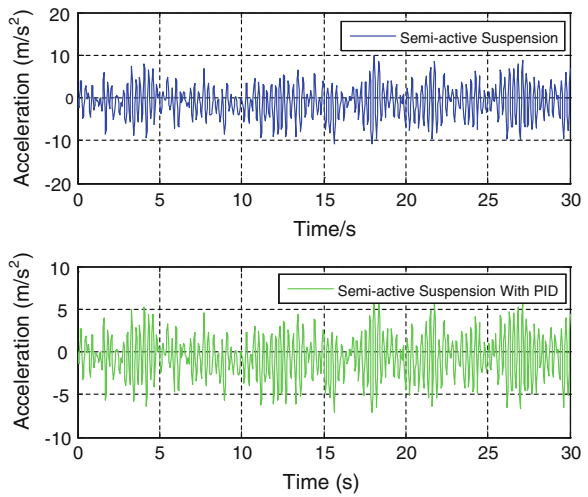
49.5 Conclusion

In this paper, the conventional PID controller as one of the semi-active feedback control methods is proposed and applied to smart dampers for the damping of single degree of freedom system. The simulation results are demonstrated and analyzed, which prove the following conclusions:

1. Application of mixed programming technology for seat vibration model and the simulation calculation makes the modeling and simulating flexibly and truthfully.

2. Comparing passive suspension and semi-active suspension, it is found that semi-active suspension has a higher damping performance than the passive suspension. Using semi-active control technique can effectively improve the damping performance of suspension system, improving the driving stability and comfort.

3. When PID control algorithm is introduced to semi-active suspension, the damping effect is more prominent. In practical application, it is suggested to increase damping and reduce the spring stiffness appropriately to the extent permitted in order to achieve the best effect of vibration reduction.

It is finally remarked that the proposed method has been widely used in aviation and aerospace, especially in aviation maintenance. This issue will be considered as a second phase of the current work.

References

1. Karkoub M, Zribi M (2006) Active/semi-active suspension control using MR actuators. Int J Syst Sci 37:19–23
2. Uwe R, Oskar S (2005) Optimal and robust damping control for semi-active vehicle suspension In: Proceedings of 5th Euromeeh nonlinear dynamics conference, pp 195–197
3. Wen B (2007) Mechanical vibration (in Chinese). Metallurgical Industry Press, Beijing pp 25–27
4. Kim Y, Langari R, Hurlebaus S (2009) Semi-active nonlinear control of a building with a MR damper system. Mech Syst Signal Process 23:14–21
5. Ang KH, Chong G, Li Y (2005) PID control system analysis, design and technology. IEEE Trans Control Syst Technol 13:37–44

Chapter 50
Aeroelastic Response Analysis of a Typical Airfoil Section with Control Surface Structural Nonlinearities

Baihui Liu, Lihui Guo and Kang Li

Abstract In this paper, a typical airfoil section with control surface freeplay is studied. A type of friction nonlinearity in flap degree is designed to suppress the effect of freeplay nonlinearities. The Roger rational function fitting method is adopted to deduce the approximative expressions of the time-domain aerodynamic force, based on the coefficient matrices of unstationary aerodynamics in simple harmonic motion. The equations of motion are solved using the fourth-order Runge–Kutta numerical integration technique to provide time-history solutions of the aeroelastic response. The result shows that the adopted friction nonlinearities can effectively impair the airfoil nonlinear motion and prevent the aeroelastic response from various nonlinear behaviors when the airspeed is under the linear flutter speed.

Keywords Aeroelastic response · Structural nonlinearities · Flutter · Limit cycle oscillation

50.1 Introduction

Flutter is an aeroelastic dynamic instability phenomenon. Many experiments, whether performed in wind tunnels or in flight, have shown phenomena, such as limit cycle oscillation (LCO) and chaotic vibration, which are not predictable from linear theory. So it is deeply necessary to study nonlinear aeroelastic dynamics.

B. Liu (✉) · L. Guo · K. Li
Ameco Beijing, No.2 Capital Airport Road, Chaoyang District, P.O.Box 563
Beijing 100621, People's Republic of China
e-mail: liubaihui@ameco.com.cn

L. Guo
e-mail: guolihui@ameco.com.cn

K. Li
e-mail: likang@ameco.com.cn

A lot of theoretical and numerical studies devoted to nonlinear flutter control of aeroelastic system. Some researches [1] used the center manifold theory and normal form method or harmonic balance method on the cubic structural nonlinearities airfoil. Conner et al. [2]. performed numerical and experimental studies on the nonlinear aeroelastic characteristic of a typical section wing with control surface freeplay. Lee et al. [3] investigated a two-dimensional aeroelastic system with freeplay using a point transformation technique. Lee and Kim [4] studied LCO and chaotic motion of a missile control surface with freeplay using a time-domain analysis. And Bae et al. [5] studied the nonlinear aeroelasticity of an aircraft wing with freeplay and bilinear nonlinearity. Li et al. [6] adopted a cubic nonlinearity in pitch degree to prevent the aeroelastic response from divergence when the flow velocity is beyond the system critical flutter speed. Some other investigations [7, 8] were conducted for the aircraft aeroelastic system with friction nonlinearities. Mignolet et al. [8] showed that friction can indeed be an important stabilizing factor.

Because of the limitation of the manufacture technics, the freeplay nonlinearities remarkably exist. And this nonlinear aeroelastic problem could not be solved by the traditional linear aeroelastic analytical method. It makes engineering design more difficult. In previous researches, the effect of the freeplay on the nonlinear aeroelastic response was examined numerically and experimentally, but all these investigations did not provide a way to weaken this influence of structural nonlinearities. In this paper, based on the Conner's airfoil section and study, friction nonlinearity in flap degree will be adopted to weaken this effect of nonlinearities, thereby making this nonlinear problem regress to a linear or approximately linear problem and simplify the engineering design.

50.2 Theoretical Analysis

In this paper, a typical airfoil section with control surface freeplay studied by Conner et al. [2] is adopted. Figure 50.1 shows the structural system consists of 3 ° of freedom namely the plunge (h), the pitch (α), and the flap (β). The control surface moment rotation relationship considering freeplay nonlinearity in the control surface is illustrated in Fig. 50.2.

To weaken the effects of freeplay nonlinearities, a type of friction nonlinearity in flap degree is designed to regress to a linear or approximately linear problem. This friction is illustrated in Fig. 50.3. Theoretically, the torque between airfoil and control surface is shown in Fig. 50.4 and can be expressed as

$$M_\beta = K_\beta(\beta)\beta = \begin{cases} k_{\beta 1}(\beta - \delta) & \beta > \delta \\ M_0 & e < \beta < \delta \\ k_{\beta 1}\beta & -e \leq \beta \leq e \\ -M_0 & -\delta < \beta < -e \\ k_{\beta 1}(\beta + \delta) & \beta < -\delta \end{cases} \tag{50.1}$$
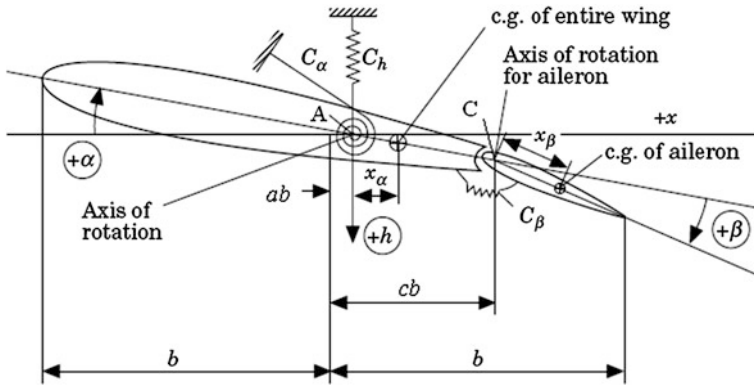
Fig. 50.1 3 d.o.f. airfoil with structural nonlinearity

Fig. 50.2 Freeplay nonlinearity
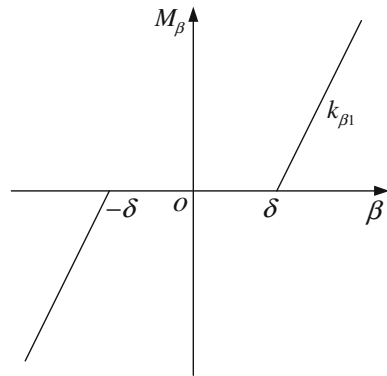
Fig. 50.3 Friction nonlinearity
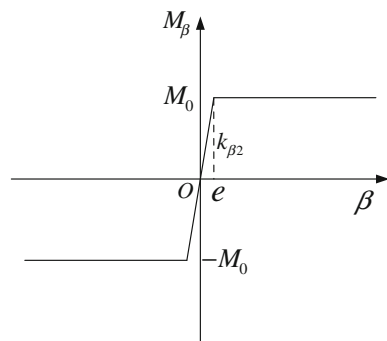
Fig. 50.4 Structural
nonlinearity
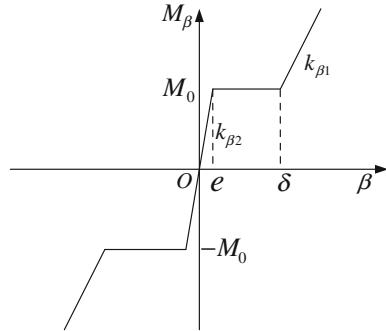
where δ is the freeplay angle and e is the deflection angle of friction. $k_{\alpha 1}$ and $k_{\beta 2}$ are the structural stiffness and stiffness of the added friction in the control surface, respectively. The motion equation of the 3 d.o.f. nonlinearity airfoil system is

$$M\ddot{x} + B\underline{x} + K(\beta)x = Q \tag{50.2}$$

$x = \{h\ \alpha\ \beta\}T$ is the displacement vector, and M and $K(\beta)$ are the mass matrix and nonlinear stiffness matrix

$$M = \begin{bmatrix} m_T & S_\alpha & S_\beta \\ S_\alpha & I_\alpha & I_\beta + S_\beta(bc - ab) \\ S_\beta & I_\beta + S_\beta(bc - ab) & I_\beta \end{bmatrix} \tag{50.3}$$

$$K(\beta) = \begin{bmatrix} K_h & 0 & 0 \\ 0 & K_\alpha & 0 \\ 0 & 0 & K_\beta(\beta) \end{bmatrix} \tag{50.4}$$

where m_T is the total mass (per unit) of wing-aileron and support. S_α and S_β are the static moments of wing per unit length of wing-aileron (relative to A) and aileron (relative to C). I_α and I_β are the moments of inertia per unit length of wing-aileron and aileron about A and C. The structure damping matrix B is

$$B_{\mathbf{mod}} = \begin{bmatrix} 2m_h\omega_h\varsigma_h & 0 & 0 \\ 0 & 2m_\alpha\omega_\alpha\varsigma_\alpha & 0 \\ 0 & 0 & 2m_\beta\omega_\beta\varsigma_\beta \end{bmatrix} \tag{50.5}$$

where $m_i(i = h, \alpha, \beta)$ represents the modal mass for each degree of freedom (per unit span), $\omega_i(i = h, \alpha, \beta)$ is the coupled natural frequency, and $\zeta_i(i = h, \alpha, \beta)$ is the measured damping ratio, which is obtained by experiment. From the structure damping matrix, it can be obtained as $B = (\Lambda^T)^{-1}B_{\mathrm{mod}}(\Lambda)^{-1}$.

The unsteady aerodynamic force and moments in incompressible flow $Q = [LM_\alpha M_\beta]^T$ are given by Theodorsen T [9]. And these moments are dependent on Theodorsen's function $C(k)$, where k is the reduced frequency of harmonic oscillation.

In this paper, the Roger rational function fitting method is adopted to deduce the time-domain generalized aerodynamic force matrix. The unsteady aerodynamic force matrix Q is

$$Q = q_d Q(k, M_\infty) x \qquad (50.6)$$

where q_d is the dynamic pressure. After the Roger rational function fitting method is adopted, it can be obtained in time domain as

$$Q(k, M_\infty) = P_0 + P_1 \frac{b}{V} s + P_2 \left(\frac{b}{V} s\right)^2 + \sum_{m=1}^{4} \frac{E_m s}{s + \frac{V}{b} \gamma_m} \qquad (50.7)$$

where P_0, P_1, P_2, E_m $(m = 1, \ldots, 4)$ are all the real coefficient matrixes, which can be deduced by the coefficient matrixes of unstationary aerodynamics in simple harmonic motion on few reduced frequencies. γ_1, γ_2, γ_3, γ_4 are all positive constants, which are usually adopted by the experience. $s = \mathrm{i}k = sb/V$, b is the airfoil semi-chord and V is the free stream velocity. The following aerodynamic state variable is imported.

$$X_{am} = \frac{s}{s + \frac{V}{b} \gamma_m} X, \quad m = 1, 2, \ldots, 4 \qquad (50.8)$$

Then, the state-space method is adopted to express Eq. (50.2), and the state-space model is

$$\begin{Bmatrix} \dot{X} \\ \ddot{X} \\ \dot{X}_{a1} \\ \vdots \\ \dot{X}_{a4} \end{Bmatrix} = \begin{Bmatrix} 0 & I & 0 & \cdots & 0 \\ -\bar{M}^{-1}\bar{K} & -\bar{M}^{-1}\bar{B} & q_d\bar{M}^{-1}E_1 & \cdots & q_d\bar{M}^{-1}E_4 \\ 0 & I & -\frac{V}{b}\gamma_1 I & \cdots & 0 \\ \vdots & \vdots & \vdots & \ddots & \vdots \\ I & I & 0 & \cdots & -\frac{V}{b}\gamma_4 I \end{Bmatrix} \begin{Bmatrix} X \\ \dot{X} \\ X_{a1} \\ \vdots \\ X_{a4} \end{Bmatrix} \qquad (50.9)$$

where $\bar{M} = M - q_d \left(\frac{b}{V}\right)^2 P_2$, $\bar{B} = B - q_d \frac{b}{V} P_1$, $\bar{K} = K - q_d P_0$.

50.3 Presentation of Results

The values for the system parameters are taken from Conner et al. [2] and listed in Table 50.1.

By using the fourth-order Runge–Kutta numerical integration method, Eq. (50.9) can be solved. To perform a transient response analysis of nonlinear aeroelastic systems, it is required to specify an initial disturbance to excite the nonlinear

Table 50.1 The value for the system parameters[a]

Parameter	Value	Parameter	Value
Elastic axis, a	−0.5	K_α	37.3
Semi-chord, b	0.127	$K_{\beta 1}$	3.9
Span, s	0.52	$K_{\beta 2}$	3,900
Hinge line, c	0.5	K_h	2,818.8
Total mass, m_T	3.393	ζ_α	0.01626
Chord, l	0.254	ζ_β	0.0115
I_α (per span)	0.01347	ζ_h	0.0113
I_β (per span)	0.0003264	δ	2.12^0
Density, ρ	1.225	M_0	0.037

[a] The units of the with dimension in the above table are all using the standard kg, m, s unit

system. This can be achieved by a one-cycle oscillation of the control surface with 0.1 rad of amplitude. A small time step of 0.0001 s is set in the process of numerical integration.

In both Conner's experimental and numerical results, five types of motion were observed during the transition of freeplay nonlinear responses. These five types of motion are classified as damped decay (the airspeed below $V/V_f = 0.18$ where $V_f = 24.35$ m/s is the linear flutter speed, which is obtained by v-g method.), periodic LCO (the airspeed increases up to $V/V_f = 0.35$), intermittent chaos (the airspeed is in the neighborhood of $V/V_f = 0.55$), nearly harmonic LCO (the airspeed is further increased beyond $V/V_f = 0.55$), and flutter (the airspeed reaches $V/V_f = 1$).

Those motions are best illustrated via a phase trajectory diagram as shown in Fig. 50.5. A flap phase trajectory figure for freeplay at $V/V_f = 0.27, 0.49$, and 0.73 corresponding to the periodic LCO region, the intermittent chaos region, and the nearly harmonic LCO region is presented in this figure. Figure 50.6 shows the flap phase trajectory for the linear system. When the airspeed is below the flutter speed, the system will converge; contrariwise, the system will diverge. These two figures reveal that the freeplay nonlinearity will likely have a significant effect on the response of the system. It makes the aeroelastic response more complex than the linear system.

By way of validating the arithmetic of this paper, the transient responses at $V/V_f = 0.27$ and 0.73 corresponding to the periodic LCO region and the nearly harmonic LCO region will be computed. The comparison of these transient responses within an arbitrary one-second-window time computed by MATLAB (use numerical expression in the following figures) with the experimental data and the Conner's numerical results are shown in Figs. 50.7 and 50.8. It can be seen that both this paper's numerical results and Conner's numerical results slightly over-predict the oscillatory amplitude. And there are some phase lags between this paper's and Conner's numerical results. The cause is these two numerical results adopts two different methods to deduce the time-domain generalized aerodynamic

Fig. 50.5 Flap phase trajectory of the freeplay
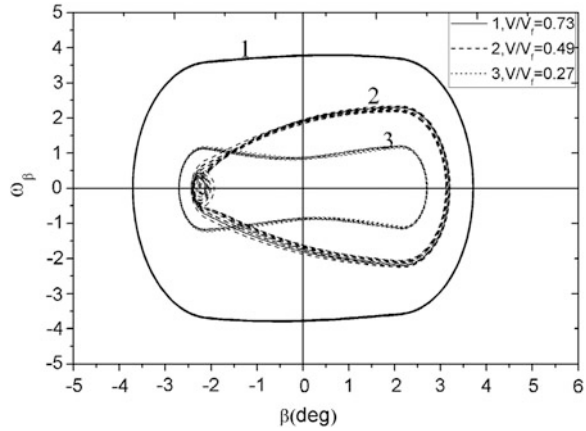
Fig. 50.6 Flap phase trajectory of the linear
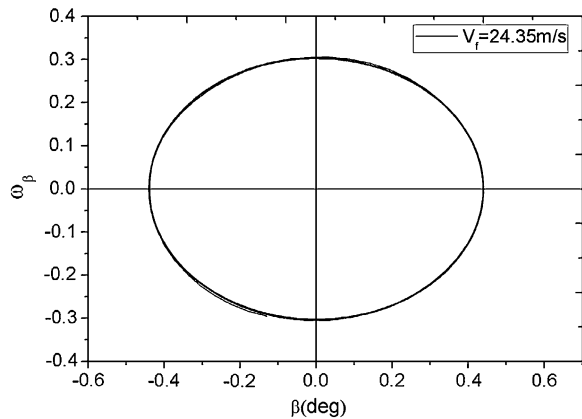
force matrix. Overall, the correlation among these sets of results is acceptable. It indicates that the arithmetic of this paper is credible.

Based on the freeplay nonlinear model, a type of friction nonlinearity in flap degree is designed to reduce the nonlinear behaviors shown in Fig. 50.4 and expressed in Eq. (50.1). It shows the aeroelastic response becomes convergent after applying the friction, when the airspeed is under the linear flutter speed. For instance, at the airspeed $V = 20$ m/s, Fig. 50.9 shows the friction nonlinearity can impair the airfoil motion to divergence and prevent the complex aeroelastic response of freeplay nonlinearity.

When the airspeed is nearly linear flutter speed ($V = 24$ m/s in Fig. 50.10), it may produce the approximate linear response. This means the project of adding the friction nonlinearity is useful.
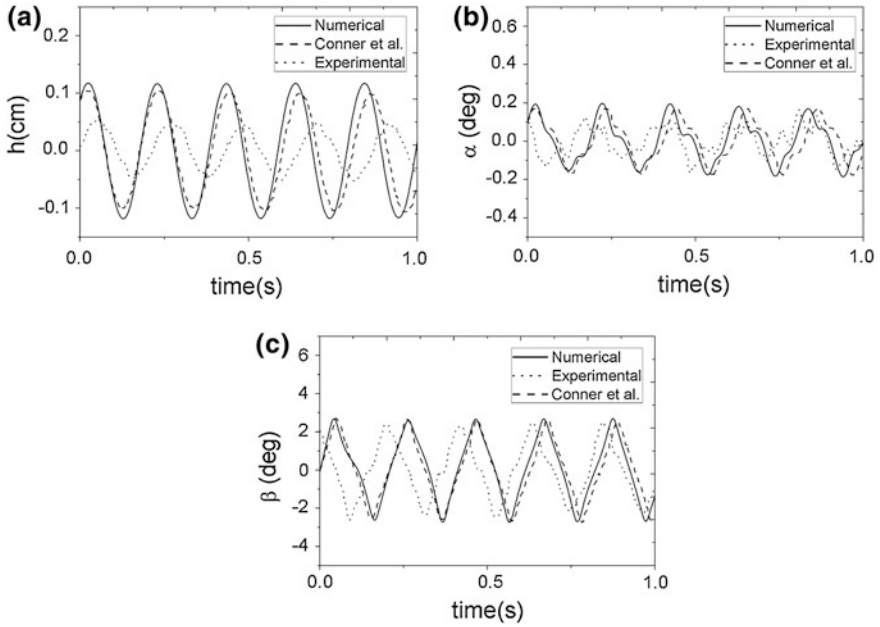
Fig. 50.7 Time history for low-frequency LCO, $V/V_f = 0.27$
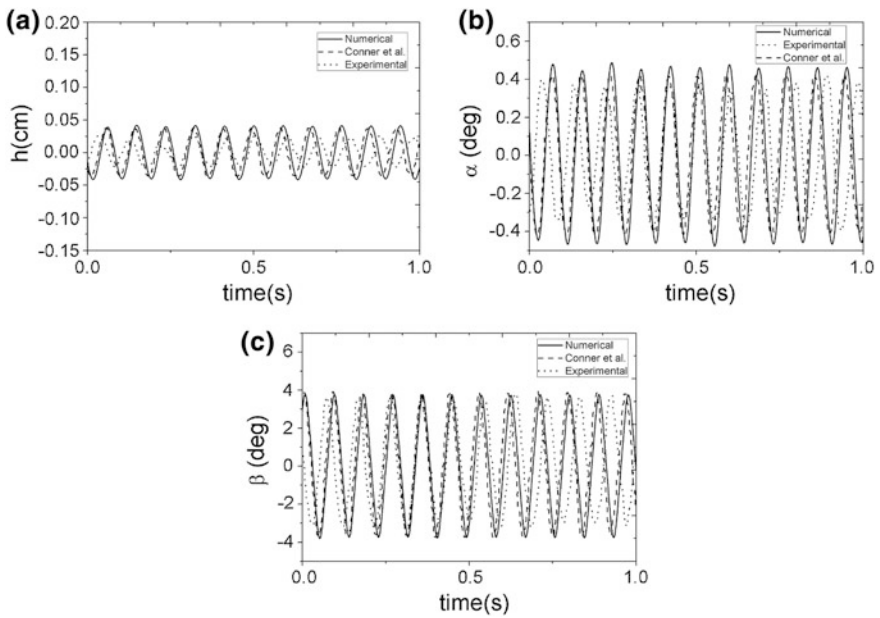
Fig. 50.8 Time history for high-frequency LCO, $V/V_f = 0.73$
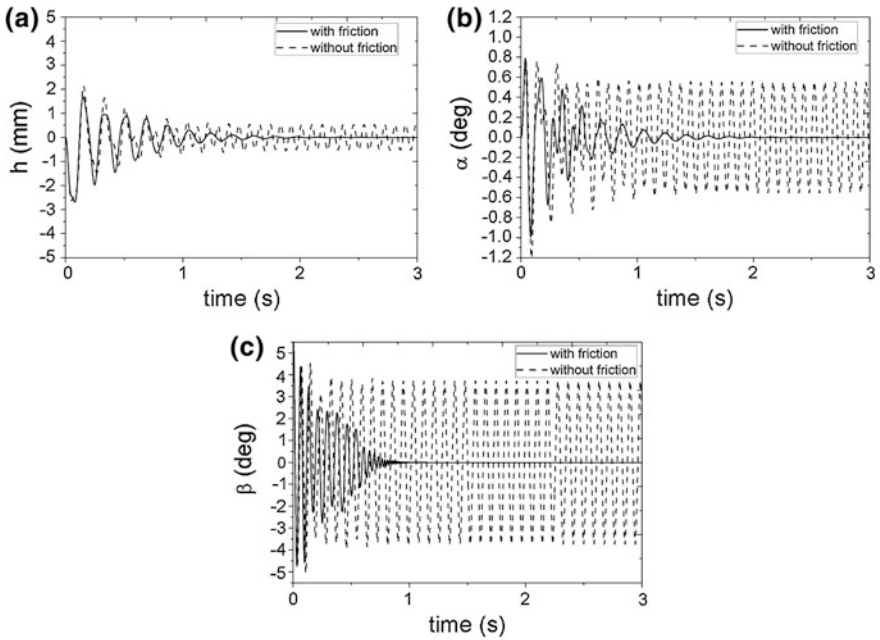
Fig. 50.9 Aeroelastic response with (*solid*) and without (*dash*) friction at $V = 20$ m/s
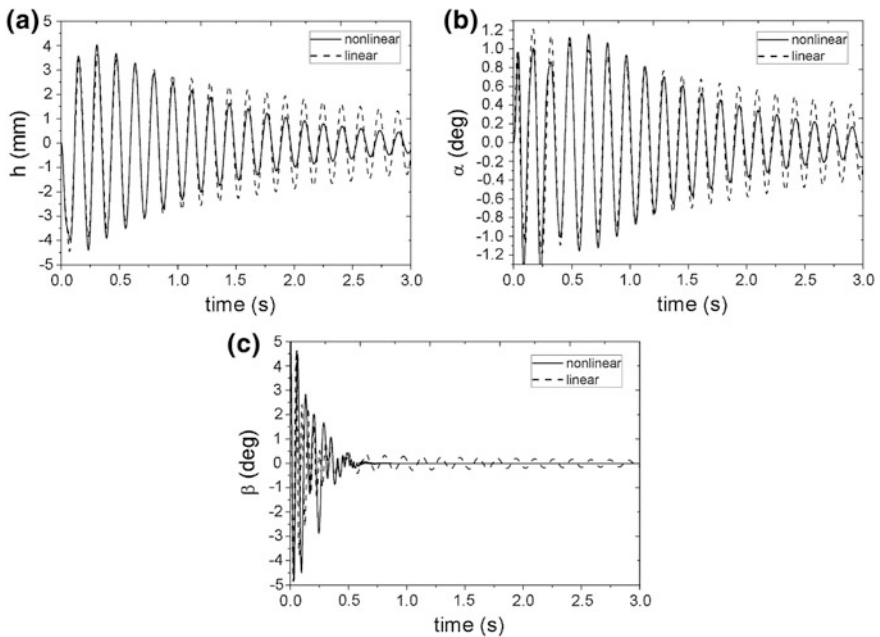
Fig. 50.10 Aeroelastic response with (*dash*) and without (*solid*) nonlinearities at $V = 24$ m/s
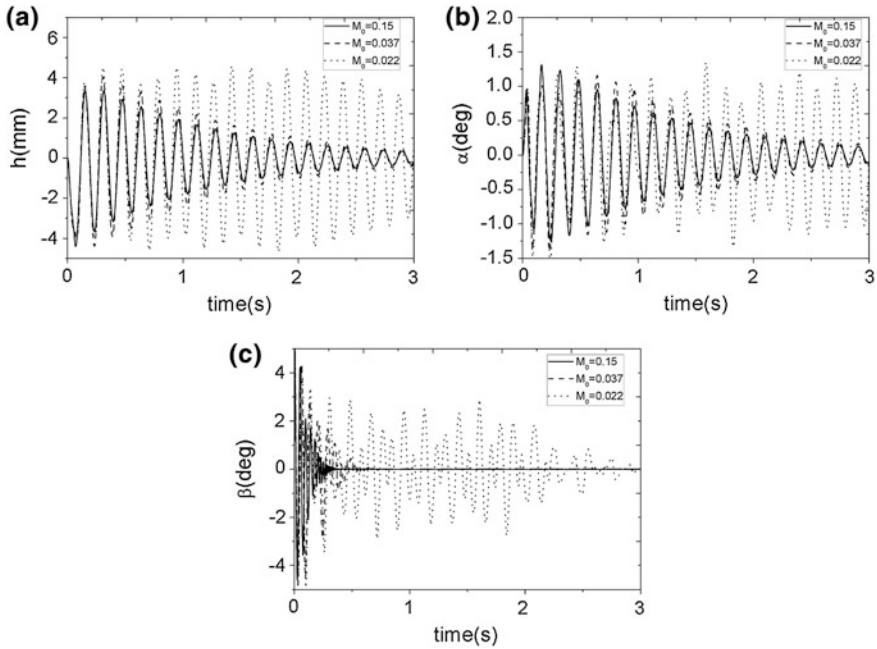
Fig. 50.11 Aeroelastic response at $V = 24$ m/s, $M_0 = 0.15$ (*solid*), $M_0 = 0.037$ (*dash*), and $M_0 = 0.022$ (*dot*)

Fig. 50.12 The flutter speeds V_f of the different M_0
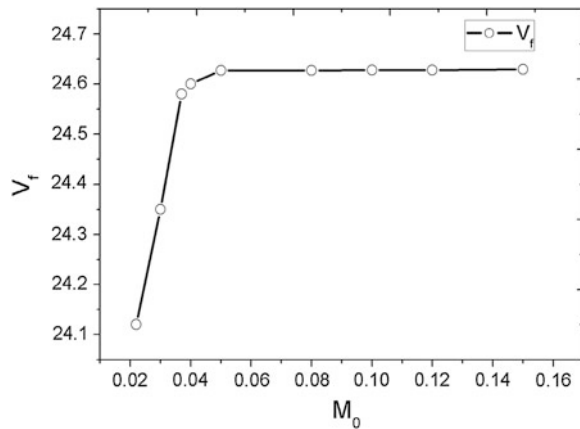
If the friction nonlinearity is adopted, the initial torque M_0 may have a significant effect on the system's stability. So the value of M_0 will be vital. Figure 50.11 shows the different aeroelastic responses with different initial torque M_0. It can be observed that the system with $M_0 = 0.022$ needs more time to

converge. In addition, the response amplitude is obviously bigger than the others. So it means to depress the nonlinear system to converge; it has to be $M_0 \geq 0.022$. It also shows that the value of M_0 can barely affect the rate of converging, while the value of M_0 is larger than 0.037.

The flutter speeds of the different M_0 are presented in Fig. 50.12. When the value of initial torque M_0 reaches a certain value, the flutter speed will slightly change, which is good for engineering.

50.4 Conclusions

The nonlinear aeroelastic response of airfoil section with freeplay and friction-combined nonlinearities in flap is studied in this paper. First, it reveals that the friction nonlinearity can effectively suppress the airfoil nonlinear motion and prevent the aeroelastic response from various nonlinear behaviors when the air-speed is under the linear flutter speed. Second, the friction can weaken the influence of the freeplay nonlinearity and make the airfoil produce the approximately linear movement. Third, the system with nonlinearity will be convergent when the initial torque M_0 can reach a certain value and the airspeed is under linear flutter speed. And if the type of friction is confirmed, the value of M_0 can barely affect the rate of converge, while the value of M_0 is larger than a certain value.

References

1. Li D, Xiang J (2008) Chaotic motions of an airfoil with cubic nonlinearity in subsonic flow. J Aircr 45:1457–1460
2. Conner MD, Tang DM, Dowell EH, Virgin LN (1997) Nonlinear behavior of a typical airfoil section with control surface freeplay. J Fluids Struct 11:89–109
3. Lee BHK, Liu L, Chung KW (2005) Airfoil motion in sub-sonic flow with strong cubic nonlinear restoring forces. J Sound Vib 281:699–717
4. Lee I, Kim SH (1995) Aeroelastic of a flexile control surface with structural nonlinearity. J Aircr 32(4):868–874
5. Bae JS, Inman DJ, Lee I (2004) Effects of structural nonlinearity on subsonic aeroelastic characteristics of an air-craft wing with control surface. J Fluids Struct 19(6):747–763
6. Li DC, Guo SJ, Xiang JW (2010) Aeroelastic dynamic response and control of an airfoil section with control surface nonlinearities. J Sound Vib 329:4756–4771
7. Sinha A, Griffin JH (1983) Friction damping of flutter in gas turbine engine airfoils. J Aircr 20(4):372–376
8. Mignolet MP, Agelastos AM, Liu DD (2003) Impact of frictional structural nonlinearity in the presence of negative aerodynamic damping. A03–24940
9. Theodorsen T (1935) General theory of aerodynamic instability and the mechanism of flutter. NACA Report 496:291–311

Chapter 51
Support Drilling Device for B747-400 STA2521 Modification

Qinglu Hao and Degong Wei

Abstract Based on CATIA, this paper designs a set of support fitting drilling device for B747-400 STA2521 modification. During aircraft modification, using this drilling device can improve work efficiency of STA2521 support fitting holes drilling under the premise of accurate holes position and quality, reduce manpower consumption effectively, at the same time, shorten the processing time, and improve work efficiency, finally contribute aircraft overhaul TAT.

Keywords B747-400 · Support fitting · Drilling device · CATIA · Ergonomics

51.1 Introduction

Aircraft overhaul is an important means to ensure aircraft airworthiness, and the quality of aircraft overhaul is the key to make sure the flight safety. Key path of Aircraft overhaul will directly affect production schedule and turn around time (TAT); also, production process and high-quality requirements directly give influence to aircraft TAT. During aircraft overhaul, if any production conflicts occur due to some special technical requirements by specific tasks, production coordination between each production action will be difficult, even make aircraft delayed, so reducing aircraft overhaul key path duration will make overhaul process more smooth and manpower allocation more reasonable and finally make

Q. Hao (✉)
Beijing Aircraft Maintenance and Engineering Corporation (AMECO), Capital Airport, Beijing 100621, China
e-mail: haoqinglu@ameco.com.cn

D. Wei
Civil Aviation University of China, Jinbei Road 2898, Dongli District, Tianjin 300300, China
e-mail: zihan_1001@163.com

TAT shortened and optimize MRO resource configuration, then benefit MRO economic results [1]. B747-400 STA2521 support fitting modification is a key path in aircraft overhaul.

This paper analyzes the disadvantages of traditional processing methods of support fitting drilling for B747-400 STA2521 modification and designs a set of support fitting drilling device by CATIA software [2] to assist the support fitting drilling on the premise to guarantee quality.

51.2 Analysis of the Support Fitting Drilling of STA2521 Modification

The support fittings of horizontal stabilizer joints with fuselage on B747-400 STA2521 distributed on both sides of fuselage and connected with frame and skin with bolts, as shown in Fig. 51.1; these fittings play an important supporting role in aircraft structure reinforcing. In B747-400 STA2521 modification, task requests both sides support fittings replacement; on different B747-400 aircraft, the position of holes on these support fittings is slightly different, so new holes have to be drilled based on holes on the original support fittings.

To guarantee the replacement of the new support fittings, the dimensional and location accuracy of the holes on the new support fittings must be same with holes on the original support fittings. Through the observation and analysis [3] of the modification, shortcomings of the traditional processing method were found, such as holes drilling took very long time, multiple clamping required, large manpower consumption, imprecise locations and damage of the support etc.

The traditional processing method is shown in Fig. 51.2. Aluminum plates were used as a transition template, firstly clamping the aluminum plate with one face of the original support fitting, then drill corresponding holes on the aluminum template, finally clamping the aluminum plate with the corresponding face of the new support fitting, and drill new holes, each surface needs to be drilled according to the above method.

This approach has some obvious shortcomings:

(1) Whole drilling process requires repeated clamping, so it will have a great cumulative error. Compared with the old support fittings, dimensional and location accuracy of the holes on new support fittings cannot be guaranteed.
(2) To accomplish the support fittings hole drilling work, at least 3 persons are required to work 6-7 days, lots of manpower consumed, and work efficiency is quite low.
(3) By this traditional holes drilling process, human errors will happen easily if any mistake occurs; there is no guarantee to drill the new support fitting in one time; it may be required to rework; worst case is to scrap the drilled support fitting due to holes position deviation and it will seriously influence Aircraft overhaul schedule and TAT and also bring economic loss to MRO.

Fig. 51.1 Support fitting
installation locations

Fig. 51.2 Traditional
drilling methods
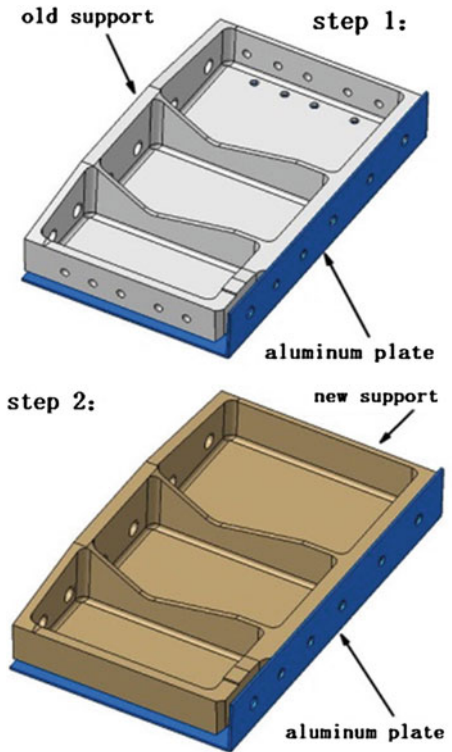
51.3 The Scheme Design and Physical Design for Support Fitting Drilling Device

51.3.1 The Scheme Design

The material of the support fitting is 7075-T6 aluminum alloy and its weight is 4.68 kg; analysis on the support fitting found that the support fitting has regular shape and modest size, and its 26 holes distributed on the four sides of the support fitting with four kinds of diameters: 15.3, 13.6, 12.7 and 10.0 mm.

The designed drilling device can compensate the shortcomings of traditional processing method effectively, and the designed drilling device consists of following five parts: base for support fitting, hole positioning plate, top wire, positioning pin and compression screw. Using CATIA software to model and assemble the parts, the design scheme [4] is shown in Fig. 51.3.

Using the device as following steps:

Step 1 Install the original support fitting to the base.
Step 2 Insert positioning pin to holes and the corresponding holes on positioning plate, tighten the top wire on positioning plate.
Step 3 Remove original support fitting, load the new support fitting in and tighten the clamp screw.
Step 4 Drill new holes in turn according to positioning the piece.

51.3.2 The Physical Design

The base for installing the support fitting: It is the main structure of the device, carrier of the support fitting and holes positioning plate. Its structure is shown in Fig. 51.4, and the shape of the base is a rectangular shell. In order to facilitate holes positioning plate movement to adjust position, there are 5-mm wide grooves in the four sides of the base, the threaded holes are also designed on the four sides of the base, and its diameter is 5 mm.

The positioning pin: The positioning pin that inserts into the corresponding holes is used to locate position of the positioning plate. To save material, positioning pins were designed with four kinds of diameters to meet different holes requirements, as shown in Fig. 51.5.

51.3.3 Comparison of Two Kinds of Drilling Methods

Through application in actual production, effect of the drilling device is good and time-consumption is reduced, and laborious process becomes relatively easy.
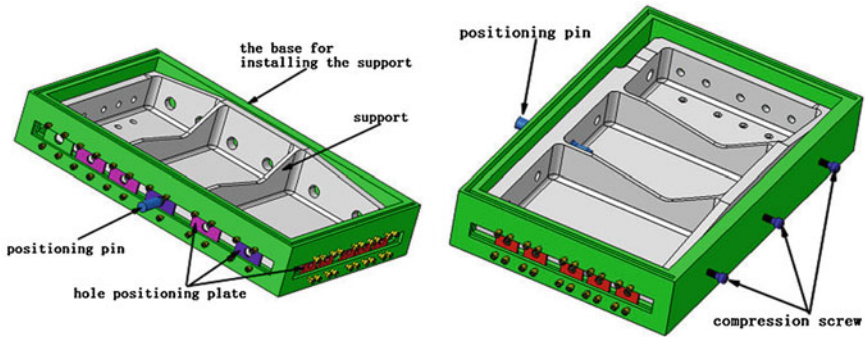
Fig. 51.3 Overall scheme 3D figure

Fig. 51.4 The base for installing the support
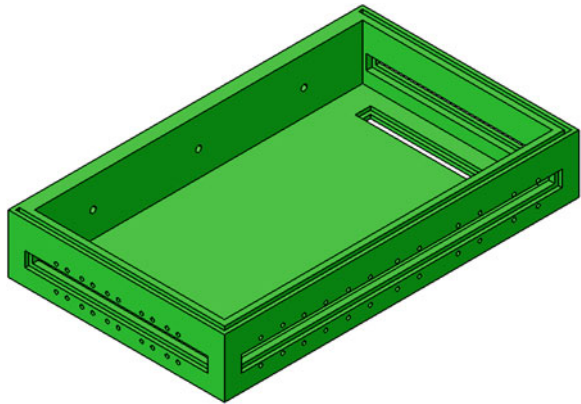
Compared with the traditional processing method, its advantage lies in the following:

(1) Aluminum transition template is not necessary, so extra investment is reduced;
(2) No multiple clamping required in whole process;
(3) Working time is shorten from 7 to 3 days;
(4) Manpower is reduced from 3 to 2 ea persons; compared with the traditional processing method, manpower consumption reduced by 70 % greatly.

51.4 The Man–Machine Engineering Simulation of the Drilling Mechanism

Ergonomics [5] is to study the coordinative relation between human, machine and environment. The research on human behavior ability, operating factors, operation space limitations, etc. will guide the design and transformation of work toolings,
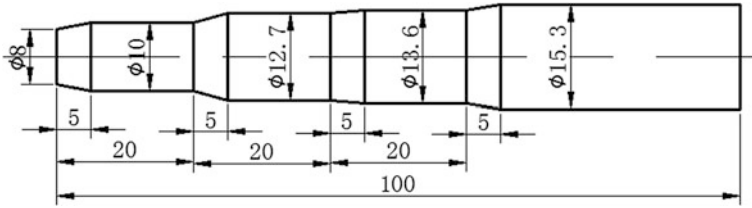
Fig. 51.5 Positioning pin

Fig. 51.6 Drilling device simulation
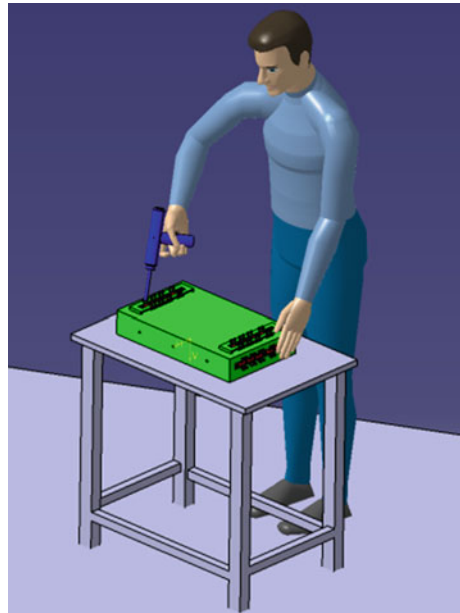
working mode and work environment, and it aims at making the production operation more efficient, safe, health and comfortable.

As shown in Fig. 51.6, DELMIA [5] is used to simulate the process, which using the drilling device, Delmia/Human module [5] analyze various postures on the human body, testing the reachability of the various positions of human; accessibility analysis of the final score reached 6 points. It is shown that drilling device is easy to operate, and whole process becomes more comfortable and convenient with good man–machine interface.

51.5 Conclusions

The application of the drilling device on B747-400 STA2521 modification reduces manpower consumption greatly, improves the support fitting hole processing quality, shortens support fitting hole drilling processing time. Quick and accurate holes drilling purpose were achieved, and it significantly contributes aircraft overhaul TAT by shortening production time of key path work.

References

1. Yong C (2006) Civil aircraft maintenance cost analysis and evaluation. Nanjing: Nanjing University of Aeronautics and Astronautics (in Chinese)
2. Shan Y, Xie L (2004) CATIA V5 mechanical design applications. Tsinghua University Press, Beijing (in Chinese)
3. Wang L, Chen T (2008) Mechanical design. Harbin Institute of Technology Press, Harbin (in Chinese)
4. Zhang H, Zheng Y (2008) New mechanical design manual. People's Posts and Telecommunications Press, Beijing (in Chinese)
5. Sheng Y, Sheng J (2009) DELMIA man–machine engineering simulation tutorial. Mechanical Industry Press, Beijing (in Chinese)

Chapter 52
Development of Nondestructive Testing for Aeronautical Composite Structures

Hui Jiang, Huayuan Zhu, Jie Yu and Kai Zhang

Abstract Structural defects or damage in composite materials are difficult to be found during manufacturing and in service. Nondestructive testing (NDT) has become an important engineering approach in the sphere. During these years, many composite material NDT approaches were researched and applied, such as acoustic microscope, NMR, μCT, ultrasonic, eddy current testing, penetrant, X-ray radiation, and so on. By comparing and analyzing, these approaches' advantages and disadvantages were pointed out, and their applicability in aviation sphere and the developing foreground were presented ultimately.

Keywords Composite · NDT approach · Aviation · Development

52.1 Introduction

Composite materials are more and more commonly used in airplanes in recent years. Composite structures working without fatal damage are fairly important to flying safety. But during composite material manufacturing, the pore, the inclusion, the crack, or delaminating may occur on or within the material because of short shot, manual operating, surroundings, loading, impact, etc. The processing involves composite material's quality. In order to ensure the fine performance of the composite material, it is quite important to find material defects in time by nondestructive testing (NDT) approaches.

Since 1970s in the twentieth century, the technology of NDT for composite materials has been studied and applied to the involved regions. In early years, almost all the NDT approaches for composites came from those for metal [1–5].

H. Jiang (✉) · H. Zhu · J. Yu · K. Zhang
Qingdao Branch, NAAU, No.2 Siliu Middle Road, Qingdao, Shandong Province, China
e-mail: aloe111@sina.com

After about 30-years research, many new approaches appeared, which satisfied the requirements and specialties of composite materials and structures.

52.2 Approaches Based on Mechanics

52.2.1 Manual Checking

Visual inspection and knocking: These two approaches were the earliest and simplest ones for composites and are still in use. With the help of optical fiber, video camera, computer, and endoscope, people were able to detect, record, and analyze structures away from the object or even the inner parts unreachable or unseen [4, 6].

By visual checking, we are able to find color changing, surface scratch, surface crack, bloated, orange peel surface, concave, shrink, etc. By knocking, we are able to find delaminating and pore in sheet laminate.

52.2.2 Penetrating

Penetrating is an age-old but widely used approach in metal NDT. In recent years, it has been applied in composite structures tentatively. With the help of fluorescent powder and red dye, penetrating became more sensitive (up to 10^{-6} mm crack on surface) and practical [7]. But it was only fit for surface crack, loosen, inclusion, etc.

52.3 Approaches Based on Acoustic Technology

52.3.1 Acoustic Vibration Testing

The acoustic vibration testing is also called mechanical impedance analysis approach. It was designed just for composite laminate, cellular structures, and foam structures. The theory of acoustic vibration is to make the object vibrate by exerting outer acoustic vibration and then to analyze the parameters of vibration such as amplitude, frequency, time consumption, and impedance. These parameters relate to the structure and character of the object, and therefore, we are able to judge the quality of the material. Two branches of this approach are acoustic impedance and resonance.

Staveley Company presented a comprehensive acoustic vibration testing equipment named as Sonic Bondmaster. It had five operating modes—mechanical impedance analysis, resonance, scan frequency continual wave, frequency
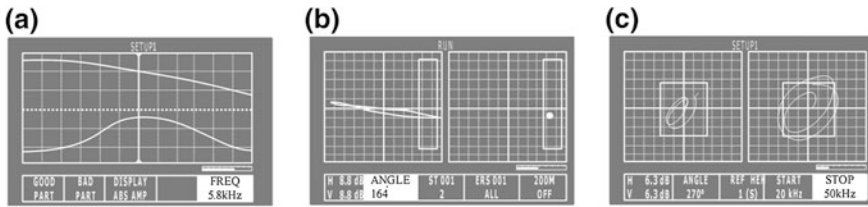
Fig. 52.1 Operating modes of Sonic Bondmaster. **a** Mechanical impedance analysis. **b** Resonance testing. **c** Scan frequency continual wave

choosing pulsant wave, and radio frequency testing—as shown in Fig. 52.1. The most proper mode would be chosen according to the object and our requirement. It had attracted the attention of composite NDT circle widely [8].

52.3.2 Ultrasonic

Defects in the material can be detected by comparing resonance and the initial wave of ultrasonic through the damaged structure. Ultrasonic can be applied in detecting delamination, pore, crack, and inside foreign substance in composite structure. Furthermore, it can estimate the density, lamina thickness, fiber direction, modulus of elasticity, and the change in size or shape.

Because of high acoustic resistance of epoxy matrix, scatter properties, and small thickness of the laminates, it is not easy to get apparently ultrasonic signal from noise. People have made many efforts to choose ultrasonic probe and proper dose of wave. Nowadays, ultrasonic testing is becoming a major NDT approach for composites, which has been developed and divaricated into pulse echo, ultrasonic penetrate, resonance ultrasonic testing, etc. [6, 9].

ICI Fiberite Company carried out NDT for complicated composite structures, such as polymer foam and honeycomb structure, with 9-shaft C-scan equipment. Boeing Group studied and found that ultrasonic can not only test defects but also can give the strength properties after damage [7]. Robert and his associates presented an online testing system that could emit laser pulse and produce ultrasonic in composite materials. This system had been used in standoff online monitor in composite solidification [1, 8]. American ABB AMDATA Company initiated an graphic ultrasonic equipment that can sample full waveform and has a quite higher discriminating ability than normal peak sampling system. It has adopted synthetic aperture focusing technique (SAFT) patent technique [10]. Sonix Company had a more sophisticated system named scan acoustic microscope (SAM), which could perform even with higher discriminating ability. Quatro Company introduced a resonance ultrasonic NDT system (RUS), which can estimate elastic properties in 3D [11].

52.3.3 Acoustic Emission (AE)

This is a promising approach in composite materials NDT and NDE. Most objects will emit sound wave under outer action (mechanical load, temperature, and electromagnetic wave). Such sound wave presents some kind of structural change inside the composite material. Most of them are so weak that only by sensitive electronic equipment can we perceive the change.

Investigators of Leuren University in Belgium had found that in most circumstances, AE serves fine in testing and judging fiber cracking and peeling off between fiber and matrix during the study on XA fiber. In the Sherbrooke University and the Toronto University in Canada, optical fibers that conducted microsensors of AE were embedded in composite materials [5]. In 1990s of last century, US Digital Wave Company developed a sophisticated AE testing system—Model AE—which had attracted the attention of many large airplane manufacturing companies, as shown in Fig. 52.2 [12].

52.3.4 Acoustic–Ultrasonic (AU) or Stress Wave Factor (SWF)

The acoustic–ultrasonic approach works as follows: firstly, impulse stress wave is aroused on the object surface by piezoelectric transducer or laser irradiation. And then, stress wave comes from microstructure in the material (defects and damage zone) and reaches receiver (piezoelectric sensor or laser interferometer) on the same or the other side after many echoes or wave mode changing. Ultimately, the received signal is analyzed and the parameter indicating the mechanical characters (strength or stiffness) of the material is obtained, named as SWF. The bigger the SWF is, the stronger the material strength or structure is, i.e., few defects exist.

The main NDT method used in ICI Company was just AU approach. Quatro Company supplied an NDT equipment named resonate ultrasonic spectrum (RUS), which could analyze mechanical character such as shear modulus and Poisson ratio with the precision at 0.5 % [2, 13, 14].

52.3.5 Acoustic Microscope

In order to detect minor defects in composite materials, such equipment has been developed since 1970s of last century. It was said that this approach is quite effective to low energy impact defects in carbon/epoxy laminate. The resolving power is high up to 5 μm. Three types of acoustic microscope are the following: scan laser acoustic microscope (SLAM), scan acoustic microscope (SAM), and C-scan acoustic microscope (C-SAM) [3, 10].
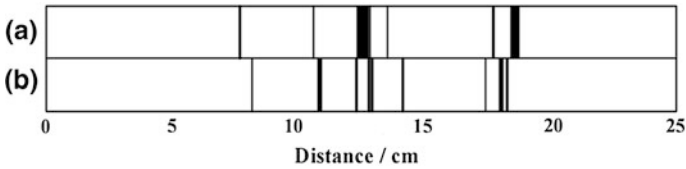
Fig. 52.2 Comparison of modal AE location and microscope location. **a** Location of crack by microscope. **b** Location of crack by modal AE

Sonix Company made a SAM system, which is the most sophisticated high-resolving power acoustic microscope so far. It could give sectional character parameters, especially the depth of defects by B-scan analysis after A-scan. Another SAM system made by Sonix was Sonix Flex SCAN-C^TM). It was a flexible precise water-immersion C-scan supersonic system [10]. Sonoscan Company presented Grindosonic Mksi testing machine which could detect elastic modulus, stiffness modulus, environment damage, etc. [2].

52.4 Approaches Based on Electricity and Electromagnetism

52.4.1 Eddy Current Testing

This is a classic metal testing method. Experiments in recent years proved that eddy current is fit for carbon composites for carbon fiber has some low electrical conductivity (750–800 Ω in 25 °C). Because of skin effect, it is in favor of impact damage detecting that current centralizes near the component surface, without contacting the object surface.

Robert Gordon University developed Nortec NDT25-1 and Nortec 19eH, which could scan the component surface under the control of computer. In order to get a high signal-to-noise ratio, they used commercial 5 mm Staveley ferrite probe [6].

52.4.2 Microwave Testing

Microwave means the electromagnetic wave between infrared and radio wave which can easily penetrate epoxy matrix. But when the wave barges up against discontinuous interphase such as pores, inclusion, unbonded zone, or crack, some of the energy will be scattered or reflected and the amplitude and phase of the wave will be changed. By comparing the wave penetrated or came back from the body with the referenced wave before contacting the body, the information about defects in the body structure will be got.

It was reported that the USA used 300 Hz wave to detect glass fiber reinforced plastic on solid missile engine [7]. Lu [15] had measured pore defect in different composite materials and proved that electromagnetic NDT theory for metal presented by Rockwitz was fit for composite too.

52.4.3 Nuclear Magnetic Resonance (NMR)

An NMR spectrum shows the resonant frequencies of the different protons contained in a sample and is used to determine a chemical species concentration. The intensity of the signal and its area are proportional to the number of protons that emit that signal. The resin rheologic behavior could be studied using an NMR technique, such as the viscosity, the concentrations, and the humidity.

Dow Chemical Company invented TA Instruments based on NMR spectrum analysis. The viscosity of the epoxy vinyl ester resins was successfully tested on specimens containing styrene concentrations [16]. SWRI Company made an NMR probe which can indicate internal humidity of composite [5]. ICI Company had thoroughly investigated NMR approach for composites [3].

52.5 Approaches Based on Optical Theory

52.5.1 Infrared Thermal Wave Imaging (ITWI)

ITWI can plot isothermal on the heated body of component based on heat conduction, thermal diffusion, or the change in thermal capacity. Composite materials have a high thermal impedance; their heat conduction and balancing are very slow, which induces high temperature gradient near the defects in the structure [5, 10]. The nearer the defect lies to the component surface, the higher the temperature gradient is, so ITWI is fit for composite materials, especially sheet laminate.

The most widely used pocket ITWI is Video Therm 2000 made by ISI Group in the USA. DeltaTherm^{TM} 1000 stress-detecting machine made by US Stress Photonics Company is another characteristic ITWI with sensitive infrared video camera [6, 10, 17].

52.5.2 X-ray Radiation

X-ray radiation NDT is one of the most usual approaches in composites defects testing. It is a very good approach in detecting tridimensional defects such as pores and inclusion. But it is difficult to find delamination in composites for only when the interstice lies in parallel direction to the rays can we notice its existence.

Eric H. Jordan developed a method for measuring strain on internal surfaces of optically opaque objects using synchrotron X-ray radiation. Small (20 micron) metal markers were embedded in a plane of interest inside of the object. The special properties of synchrotron X-ray radiation were used to form images of these markers before and after mechanical loading. The radiographs were optically enlarged and then measured to determine the change in marker spacing. Strain was then computed by differentiation of the measured marker coordinates. Calculations showed that if the markers were 5 diameters apart, the strain errors were less than 1 % [18]. In China, Li et al. developed an X-ray inspection method of wavelet image enhancement based on soft threshold [19, 20].

52.5.3 Microcomputed Tomography (μCT)

Microcomputed tomography (μCT) is a nondestructive method to obtain geometrical information about the internal microstructure of an object. It was originally designed for medical purpose but was equally applicable to the three-dimensional (3D) measurement and analysis of other materials such as composite structures.

The most commonly used μCT is based on X-rays. The transmitted X-rays are recorded on a two-dimensional detector that measures the different intensities of the beams, where intensities vary due to the X-ray absorption of the different materials along the beam path. Basically, high-density materials absorb more X-rays than low-density materials. In order to obtain 3D image representations, a number of 2D X-ray projections are recorded. Using appropriate image reconstruction algorithm, a 3D object can be generated.

Except X-ray μCT, there are photon μCT, antielectron μCT, nuclear magnetic resonance μCT, microwave μCT, ultrasonic μCT, etc.

An express real-time X-ray μCT system was developed by Lockheed Company, which could read the thickness of metal laminates in the rate of 25×10^6/h with the accuracy of $\pm 2.54 \times 10^{-3}$mm. A real-time system had been manufactured by Digiray Company, which could present 3D image of C/epoxy, metal matrix, pottery matrix, and other composites. [21].

52.5.4 Laser Digital Imaging

Laser holography is an optical approach for composite NDT. The laser reflected from the surface of composite structure and the other from reference surface will interfere, and the interference pattern includes all the optical information of the composite structure.

Impose load on the composite components by heating, pressurizing, or sonic vibrating. Under outer load, the feeble surface displacement (about several
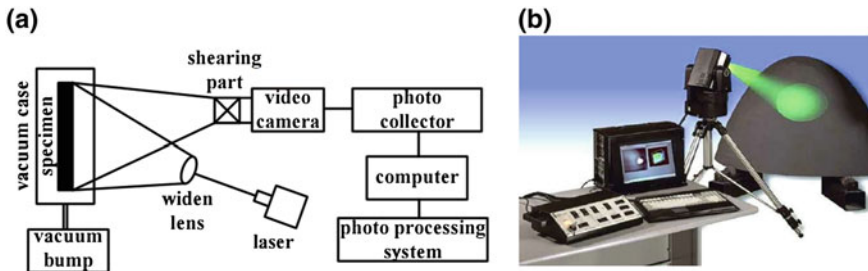
Fig. 52.3 LDSSPI. **a** LDSSPI system. **b** LDSSPI equipments

wavelengths) will cause apparent optical change in holograph. Because holography is highly sensitive, the experiment system should keep far from vibration, noise, and temperature gradient.

Laser digital shearography speckle pattern interferometry (LDSSPI) is another composite NDT approach via laser and computer technology, which has been developed for about 10 years. It comes from the theory of laser shearography presented by Professor Hung [22]. At first, we must get the static image of sample surface under the laser and get the second stress image after imposing load on the sample and then lay the two images together and get interference pattern. After analyzing the pattern, defects can be found, as shown in Fig. 52.3.

The Aerospace Research Institute of Materials and Processing Technology in China made YZ200 instrument based on the theory of LDSSPI [17]. The Institute of Aeronautical Materials invented a handset of Electronic Shearography (ES-NDT) and applied it in detecting GFRP and foam structures [10]. American LTI Company presented a series of Laser Digita Shearography systems such as LTI-5100HD [23–25].

52.6 Comparison of NTD Approaches and Their Future

In the actual operating of NDT for composite structures, the above approaches are chosen according to different fiber, matrix, structure, and other requirements. Sometimes, two or three approaches are applied to one structure in order to gain more accurate and adequate information (Table 52.1).

Because of the diversity and complexity of NDT technology, there is quite a gap between composite NDT requirements and approaches available so far, especially in China. Acoustic microscope, AU, AE, μCT, and microwave seem to be promising NDT technologies for composites. These good approaches are not widely used in engineering because of their high cost and complicated operating procedures. If we could cut down the manufacturing cost some day and make them more flexible and suitable for outdoor or production line using, our airplanes with so many composite materials will be more safe and reliable.

Table 52.1 Comparison of NDT approaches for aviation composites

Approach	Range of Application	Advantage	Disadvantage
Mechanic			
Visual inspection	Surface obvious defects	Fast, easy to operate, low cost	Surface inspecting only, dependent on person
Knocking	Sheet laminates	Easy to record and automate, low cost	Time waste, point checking, only fit for delamination
Penetrant	Surface defects	Easy, practical, rapid	Requiring pre-cleaning, pollution
Acoustic			
Acoustic vibration testing	Hollow defects in thick laminate, large scale testing	Simple operating, non-coupling agent	Depending on geometry of object and acoustic pulse character
Ultrasonic	Inner defects, mechanical characters measuring	Rapid, reliable, flexible, precise	Dead zone existence, high acoustic resistance of composites, difficult to distinguish signal from noise
Acoustic–ultrasonic (AU)	Delamination, hair-like defects group, evaluation of structural integrity	Reliable, precise	Noise influence, offline
Acoustic emission (AE)	Damage during loading	Dynamic detecting, only need AE sensor, online testing	Difficult to distinguish signal from noise
Acoustic microscope	Microscopic defects	Precise, efficiency	Little specimen
Electric and electromagnetism			
Eddy current testing	Carbon fiber composite	Low cost, no contact, real-time monitor, colorful imaging	Difficult to read and determine signals, fit for superficial or shallow defects
Microwave testing	Crack, pore, delamination, unbonded etc.	Low attenuation, sensitive	Only fit for macroscopic defects
NMR	Wet absorbability, viscosity	3D imaging, rheologic behavior measure	High cost, low efficiency, offline

(continued)

Table 52.1 (continued)

Approach	Range of Application	Advantage	Disadvantage
Optical			
Infrared thermal wave imaging	Little component, low surface radiation ratio	Sensitive, colorful real-time imaging	Expensive, long time heating, sensitive to circumstance temperature
X-ray radiation	Inclusion (especially metal inclusion), unbonded, surface microcrack	High sensitivity, real-time monitoring, testing the whole body	Harmful to operator, offline
μCT	Internal microstructure	High resolving power, large section body, 3D imaging, precise	Harmful to operator, high cost, low efficiency, offline
Laser digital imaging	Delamination, unbonded, maldistribution of resin	High speed, no touching, imaging, large scale components like radome, rotor blade	Sensitive to vibration, offline

References

1. Robert E, Green JR (1987) Nondestructive characterization of material properties. Mech Eng 268
2. MacRae M (1993) Details without damage: NDT methods "find fault" with composite materials. Adv Compos 4:28–34
3. Lei N, Gao L (1994) Advances in NDT for composite materials. Solid Rocket Technol 6:74–78 ((in Chinese))
4. Guan W (1996) Advances in nondestructive testing. Technique Intelligence of China and Oversea 8:4–5 (in Chinese)
5. Xu T (1996) Advances in NDT for composite materials. Astronaut Mater Process 2:63–66 (in Chinese)
6. Jian Z (1995) Nondestructive testing of low energy impact defects in CFRP. Aeronaut Manuf Eng 9:24–26 (in Chinese)
7. Liu H (2003) Nondestructive testing for composite materials. Nondestr Test 12:631–634 (in Chinese)
8. Li Z (2000) Nondestructive testing of advanced composites. Astronaut Mater Process 5:28–31 (in Chinese)
9. Liu Z (2003) Ultrasonic inspection and mechanical testing of fiber placed composites. Nondestr Test 9:441–446 (in Chinese)
10. Chen J (2002) Comprehensive nondestructive testing technology for composites and their components. Nondestr Test 6:253–256 (in Chinese)
11. Lian J (1999) Research on NDT for composite and loading experiment. Nondestr Test 6:11–14 (in Chinese)
12. Prosser WH et al (1995) Advanced waveform-based acoustic emission detection of matrix cracking in composite. Mater Eval 53:1052
13. Vary A (1990) Acoustic–ultrasonic in nondestructive testing of fiber reinforced plastics composites. Elsevier Appl Sci 28:1–54
14. Geng R, Jing P (2012) Up-to-date NDT technology for aviation equipment. Aeronaut Manuf Technol 1:55–59 (in Chinese)
15. Lu R et al (2001) Electromagnetic NDT theory and its application in composite. GFRP Compos 2:40–41 (in Chinese)
16. Hubert P (2005) Processing variability in low-cost VARTM aeronautical structures. In: Proceedings of the 26th international SAMPE Europe conference. SEBO SAMPE Europe Business Office, Paris, pp 385–390
17. Chen G (2005) Study on the digital imaging evaluation of composite bonding defects. Nondestr Test 27:121–122 (in Chinese)
18. Jordan EH (1996) Measurement of strain at interior points using synchrotron radiation. In: AIAA, pp 17–124
19. Hu B (2012) Carbon fiber composites X-ray digitization of real-time imaging detection technology. Aeronaut Manuf Technol 18:83–85 (in Chinese)
20. Li J, Han Y, Wang L (2008) Study on X-ray inspection for composite materials. J Projectiles Rockets Missiles Guidance 2:215–217 (in Chinese)
21. Schell JSU, Dawsey P (2005) Fabric architecture investigation by micro-computed tomography (µCT). In: Proceedings of the 26th international SAMPE Europe conference. SEBO SAMPE Europe Business Office, Paris, pp 92–97
22. Hung YY (1992) Shearography: a new optical method for strain measurement and nondestructive testing. Opt Eng 3:391–395

23. Hung YY (1996) Shearography for non-destructive evaluation of composite structures. Opt Lasers Eng 24:164–166
24. Hung YY, Chen YS, Liu L, Huang YH, Luk BL, Wu CML, Chung PS (2009) Review and comparison of shearography and active thermography for nondestructive evaluation. Mater Sci Eng R 64:73–112
25. Tu J (011) Studies on laser shearographic NDT of honeycomb sandwich structure (in Chinese). Nanchang Hangkong University, Nanchang

Chapter 53
Design and Experimental Research of Microquantity Lubrication Device Used in the in situ Cutting of Aircraft Titanium Alloy Structural Damage

Kun Gao, Lehua Qi, Dazhao Yu and Jun Luo

Abstract Contrapose the question existing in that compound droplets generator used in the laboratory is not suitable for field, this paper design and manufacture a new device based on gas driving, and using the device for a titanium alloy drilling test. Experiment shows that wet minimal quantity lubrication (Wet MQL) can be used in in situ cutting due to its good lubricating effect, and without damage to electrical equipment of aircraft. The designed generator of compound droplets is suitable for field use for a simple structure, wide range of parameter adjustment, and easy to carry.

Keywords Damage repair · Drilling of titanium alloy · Wet MQL · Lubrication device

K. Gao · L. Qi (✉) · J. Luo
School of Mechatronic Engineering, Northwestern Polytechnical University,
Xi'an 710072, China
e-mail: qilehua@nwpu.edu.cn

K. Gao
The First Aeronautical College of Air Force, Xinyang, 464000 Henan, China
e-mail: gk2009154@sina.com

J. Luo
e-mail: luojun@nwpu.edu.cn

D. Yu
Naval Aeronautical and Astronautical University, Yantai, 264001 Shandong, China
e-mail: ytyudazhao@aliyun.com

53.1 Introduction

The reparation of the aircraft titanium alloy structural damage is increasing with the time passing when the more quantum of the titanium alloy is using in the airframe of military aeroplane. The reparation of titanium alloy structural damage is the special difficulties of the aircraft structural reparation. In particular, clean up the damage hole, drilling the riveting hole, and manufacturing the patch on the damage point are the most difficult tasks. The reason is dry cutting technology is pick up in order to control the corrosion proceeding of the airframe and security of the all electrical devices in the aeroplane. The physical property of the titanium alloy including high hardness, low conductivity for heat, and low cutting property gives rise to the high difficulty for manipulation, low life of cutting tool, and low cutting quality [1]. The reasons above affect the reparation efficiency of the titanium alloy structural damage. Wet MQL for the titanium alloy structural damage is proposed for enhancing the reparation quality and improving the repair speed of the titanium alloy structural damage.

Wet MQL is a green cutting technology, which uses the microscale oils as the lubricant, uses appropriate amount water as coolant, and then atomizes them to compound droplets in the condition of high-pressure draught. The experiment shows that the cooling effect of compound droplets lubrication is better than the minimal quantity lubrication (MQL), and the manipulation is easier than cryogenic minimal quantity lubrication (cryogenic MQL) and cold air technology as wet MQL has no use for subzero storing device and the protectors. Wet MQL technology adapts the outside environment, which is hand operation predominates. The value of practice and military is outstanding when wet MQL is used in the reparation of the aircraft titanium alloy structural damage. The compound droplets generator mainly constitutes by peristaltic pump and frequency generator for getting more than ten to dozens of ml/h steady flows of lubricant oil. Therefore, it is hardly used in the outside as the complex construction needs air supply and power supply.

A portable wet MQL generator driven by compressed air is designed to getting tiny, continuous steady, and adjustable lubrication oil. The compound droplets obtained by the designed generator are better cooling and lubricant effect, and it is no effect to the electrical equipment in the aircraft. The designed generator is the basis of compound drop lubrication technology used in the aircraft metal body milling and drilling application.

53.2 The Structure and Operational Principle of the Generator

The structure of the designed generator is shown in Fig. 53.1, and it is comprised of generator and spray nozzle. The interior of generator is three hydraulic and air circuits of oil, water, and air. It is used to supply of oil and water and flow control.

The spray nozzle is two-double, and the function of the spray nozzle is atomized the mixture of water and oils. It is portable as there is a handle in the shell of the generator and a rubber mat in the bottom to protect the thin-gage skin.

The operating principle is as follows: The compressed air and its pressure 0.6 ∼ 0.7 MPa entered the airtight cavity by air inlet hole 6 between upper cover and base 13, and then, the air is passed the external layer of double-deck pipeline 7 and spouted by the external layer of two-layer spray nozzle. The compressed air comes from *a* and *b*, is reduced the pressure to 0.1 ∼ 0.5 Mpa by reducing valves 4 and 9 (the pressure can be read by pressure gages 3 and 10), and entered the oil and water container. Then, oil and water are pressed into themselves pipeline and mixed in three exchanges connector 8 and finally entered the internal layer of double-deck pipeline 7 and nozzle. The flow of oil and water can be adjusted by flow adjust bolt 2 and 12 of throttle valve. In the front of nozzle, the mixture is atomized by compressed air and spurted to cutting area. The proportion of oil and water can be adjusted independently, and the generator can be converted into a MQL generator when close the water circuit.

53.3 Oil, Water Adjustment, and Scaling

53.3.1 Flow Adjustment

The proportion of oil and water is (5 ∼ 10): 100 [2] in wet MQL, so the different adjustment is needed for the two different flows. The formula (53.1) represents the rate flow which the liquid flow past the annular rift, when the flow is adjusted.

$$q = \frac{\pi d \delta^3}{12 \, \mu l} \Delta p \qquad (53.1)$$

q—quantity of flow; δ—width of annular rift; μ—the kinetic viscosity of liquid; d—diameter of pipeline; l—length of the pipeline; Δp—the pressure difference, the pressure is calculated in the container.

From the formula, changing the Δp and δ can influence q, but the range of the two variables is different, changing δ can influence the q more. The adjustment of δ cannot maintain the liquid steady and accurate when the flow is little. In order to overcome this weakness, the adjustment of water flow selects the approach of fixed the container pressure and adjusts the reducing valve; the adjustment of oil flow selects the approach of fixed the orifice and adjusts the container pressure.

53.3.2 Scaling

The application amount of water and oil in MQL is too little, especially the application amount of lubricating oil is less. It is very difficult to display. Consequently, the quantity of water and oil is measured by scaled container, and it can be transformed into quantity of flow further. In the experiment, the air pressure is fixed at 0.2 Mpa, the knob of the reducing valve 12 in Fig. 53.1 turns $0 \sim 5/8$ circumferences, and the flow of water is shown in Fig. 53.2. If we fix the knob 2 in a certain position, then the reducing valve 3 is adjusted as shown in Fig. 53.1, the pressure of the container is $0.1 \sim 0.5$ Mpa, and the flow of oil (castor oil, 20 °C) is shown in Fig. 53.3. The degree of the knob is 3/8 which can content the most requirement of the lubrication.

When the scale of the knob is confirmed, the flow of oil and water can be controlled to content the different requirement of the cutting an drilling lubricating parameter.

53.4 The Experiment of Cooling Lubricating Effect

Drilling a crack arresting hole on the aeroplane of titanium alloy skin is a common technique for outside crack reparation. In order to examine the cooling lubrication effect of the designed wet MQL generator, the comparison of cutting experiment is selected, which include the drilling force, the working life of the drill which affect working strength and reparation efficiency in the dry cutting and the device of wet MQL.

53.4.1 The Experiment Approach

The devices of the experiment are vertical drilling machine (Z525), tool microscope (Nikon, MM400), dynamometer (Kistler, 9272), and system of data

Fig. 53.2 Flow graph of
water
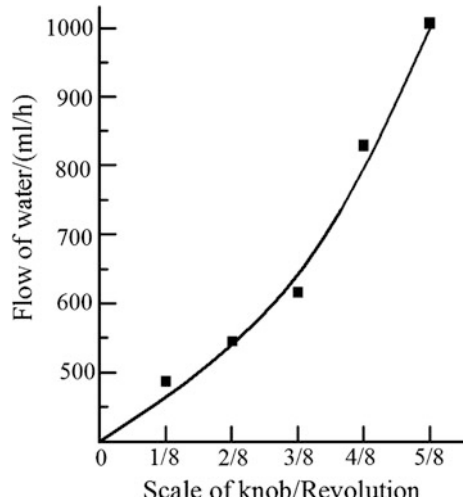
Fig. 53.3 Flow graph of oil
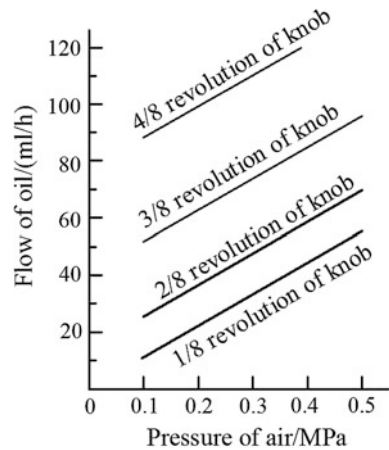
collection. The drill is the standard spiral drill. Its material is high-speed steel
(W6Mo5Cr4V2Al), its diameter is 4 mm, and vertex angle is 135°. The aviation
titanium alloy Ti6Al4V (TC4) is selected in the experiment, which thickness is
2 mm.

The pressure of compressed air is 0.6 Mpa. The castor oil (without any addi-
tive) can be chosen as lubricating oil, which pressure is 0.3 Mpa and rate of flow is
60 ml/h. The pressure of water is 0.2 Mpa, and rate of flow is 600 ml/h. The
rotation rate of drill n is 500 rpm, the feed f is 0.05 mm/r, and the angle between
the axis of drill and nozzle is 45°.

Fig. 53.4 Compare of
cutting force
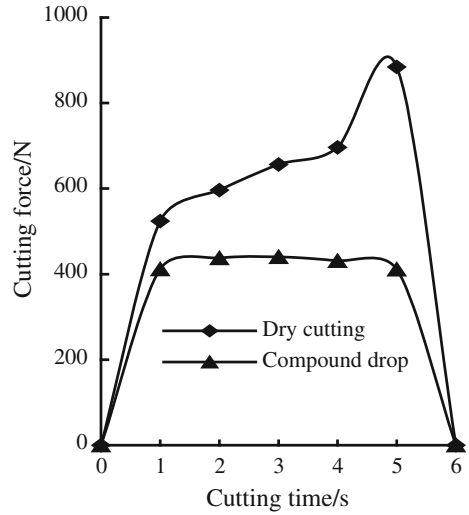
Fig. 53.5 Compare of tool
wear
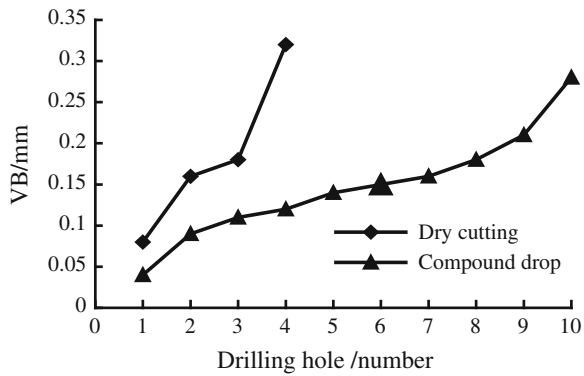
53.4.2 Experiment Results

Figure 53.4 shows the drilling force in the two lubricating conditions. Figure 53.5
shows the relation of working life of the drill and the quantity of drilling holes.
Figures 53.4 and 53.5 show that the cutting resistance of wet MQL is smaller and
steady; however, the drilling force is increased with cutting procedure in the
course of dry cutting. When wet MQL is selected and the average flank wear *VB* is
0.3 mm, the drill can make more than 10 holes. By contrast, only four holes can be
obtained in dry cutting. When wet MQL is selected, the obvious vestige can be
seen around the drilling hole, but oil stains hardly can be found in the work piece
surface after the water is evaporated. Wet MQL can reduce the corrosion of
aircraft body caused by left coolant liquid and ensure the safety of electric
accessory in the aircraft. It is very important to the fly security.

53.5 Conclusions

1. Designed and manufactured wet generator give the approach of the adjustment of oil supply and water supply and demarcate the flow scales. The generator is simple-structured, portable, and adapted the outside.
2. The experiment is used the titanium alloy skin drilling, and it is validated that the cooling effect of wet MQL is better. It can be reduced the cutting force and increasing the work life of the tools. It is a right technology for the cutting of the titanium alloy structure to cooling and lubrication.

Reference

1. Eo Ezugwu, Wang ZM (1997) Titanium alloys and their machinability review. J Mater Process Technol 6(8):262–272
2. Liu J, Zhang C, Zhang C (2011) Lubricating properties of the aqueous solution of castor oil polyoxyethylene ether (in Chinese).Tribology 31(3):240–248

Chapter 54
Study on the Evaluation of Engine Performance Based on Hybrid Optimization Algorithm

Zhao Kai and Li Benwei

Abstract To solve the lack of ability to evaluate engine performance based on single parameter, the method of evaluating engine performance based on multiple parameters is studied. This paper uses hybrid optimization algorithm and classical particle swarm optimization algorithm to obtain the weights of multiple parameters by analyzing the test data of a type of engine. The comparative study shows the hybrid optimization algorithm is superior to the classical particle swarm optimization (PSO) in the calculation result. Finally, the engine performance index of each overhaul is calculated.

Keywords Aircraft engine · Multi-parameter weights · Comprehensive evaluation · Particle swarm optimization · Simulated annealing algorithm

54.1 Introduction

The continuous performance monitoring of aero-engine is an effective method to judge whether the engine can run stability. At present, the method based on single parameter test in the aero-engine performance monitoring is used mostly. The advantage of this method is that the processing technology is mature, and the result is visual and intuitionistic. But the engine is a complicated and huge system, and the operation environment is complex and changeable, so the test method based on single parameter often has the weaknesses, which are problems reflected singly, evaluation conclusion fuzzily or even contradictorily and cannot fully reflect the overall performance of the engine. Evaluation method based on multi parameters is the development of evaluation method based on single parameter. It considers

Z. Kai (✉) · L. Benwei
Department of Airborne Vehicle Engineering, NAAU, Yantai 264001 Shandong, China
e-mail: 254657425@qq.com

the importance of multiple parameters in the evaluation systematically. It has the characteristics of comprehensive, reasonable and accurate, so it is more reasonable to judge the conclusion.

To solve the weight problem of multi-parameters in evaluation system, this paper proposes the method of improved hybrid optimization algorithm to evaluate engine performance. Hybrid optimization algorithm can combine the complementary advantages of different algorithms, and the global searching ability of modern intelligent algorithm is combined with the local searching ability of traditional optimization algorithm, which has global convergence. In this paper, the global searching ability of particle swarm optimization algorithm is combined with the local searching ability of simulated annealing algorithm, namely the adaptive particle swarm optimization algorithm based on simulated annealing. This method can calculate the weights of parameters quickly and accurately in the engine performance evaluation system, and the effect is obvious.

54.2 Theoretical Basis

54.2.1 Particle Swarm Optimization

Particle swarm optimization (PSO) is a kind of intelligent optimization algorithm put forward based on birds preying behavior by Kennedy [1] and Eberhart [2] in 1995. It can be used to solve the optimization problem of multi-parameters better, and it is an effective global optimization method. In the particle swarm optimization algorithm, each particle has a fitness function to judge their position, and a speed value to determine their flying direction and distance. Finally, the particle swarm will follow the current best particle to search in the solution space. Each particle will replace their velocity and position according to the following formulae [3, 4].

$$v_{i,j}(t + 1) = wv_{i,j}(t) + c_1 r_1 (p_{i,j} - x_{i,j}(t)) + c_2 r_2 (p_{g,j} + x_{i,j}(t)) \qquad (54.1)$$

$$x_{i,j}(t + 1) = x_{i,j}(t) + v_{i,j}(t + 1) \qquad (54.2)$$

In the formulae: $i, j = 1, 2, \ldots, d$ (d is the search space); t is the iteration number; w is inertia weight; c_1 and c_2 are positive learning factor; r_1 and r_2 are uniformly distributed random numbers between 0 and 1; $p_{i,j}$ is the location of optimal solutions found by the particle itself (p_{best}); $p_{g,j}$ is the location of optimal solutions found by the whole group (g_{best}).

Particle swarm optimization algorithm has the advantages of simple rules, small amount of calculation, high efficiency, high precision, fast convergence and easy programming, but it is poor for the optimization problem of discreteness, easily falls into local extreme point, and in the later period becomes slow convergence, low precision etc. [5–7].

54.2.2 The Simulated Annealing Algorithm

The simulated annealing algorithm (SA) is a random optimization method developed in early 1980s. It simulates the thermodynamic process of high-temperature metal cooling and is widely used in combinatorial optimization problems. Firstly, the SA determines the initial temperature during the optimization, selects an initial state randomly and observes the objective function value of the state. Secondly, a small disturbance is attached on the current state, and the objective function of the new state value is calculated. Finally, the better point is accepted by the probability 1, and the worse point is accepted to be the current point by the probability Pr, until the system becomes cool. The SA method can converge to the global optimum with the probability 1 in value, in the conditions that the initial temperature is high enough, and the temperature drop is slow enough. Because it accepts the worse point with small probability, it has the ability to jump out the optimal solution. SA is a greedy algorithm, and random factors are introduced into its searching process. It can accept a worse solution than the current solution with a certain probability, so it may jump out of the local optimal solution and get the optimal global solution. The process of the classic SA is as follows [8]:

Step 1: Initialize annealing temperature T_k ($k = 0$) and generate a random initial solution x_0;

Step 2: Repeat the following operation in the temperature of T_k, until get the balanced state of temperature T_k;

    1. Generate a new feasible solution x' in the solution of x field;
    2. Calculate the difference Δf of objective function $f(x')$ and objective function $f(x)$;
    3. Accept x' according to the probability $\min\{1, \exp(-\Delta f/T_k)\} > random$ [0, 1], where $random$ [0, 1] is a random number of interval [0, 1];

Step 3: The annealing operation: $T_{k+1} := CT_k, k :\leftarrow k + 1$, where $C \in (0, 1)$. If it meets the convergence criteria, the annealing process ends, otherwise turn to step 2.

SA is a random optimization algorithm. Being the extension of local search algorithm, it may not need to find global optimal solution, but the approximate optimal solution problem can be found more quickly. It is different from the local search that SA selects the cost value state with a certain probability in the field. If the parameter is set properly, the calculation of SA is faster than exhaustive search method.

The advantages of SA are simple calculation process, strong universality and robustness. It is suitable for parallel processing and can be used for solving complex nonlinear optimization problem; the disadvantages are slow convergence, long running time and the performance of the algorithm relating to the initial value and the sensitivity of parameters.

54.2.3 Multi-objective Adaptive Particle Swarm Hybrid Optimization Algorithm Based on Simulated Annealing

The hybrid optimization algorithm is the algorithm contains more than two different optimization algorithms and can realize the complementary advantages of different algorithms. The global searching ability of modern intelligent algorithm is combined with the local searching ability of traditional optimization algorithm, which has global convergence. In this paper, the adaptive particle swarm optimization algorithm has an advantage of global optimization, and the characteristic of SA local optimization is obvious. So combining the advantages of these methods, the optimal weight of each parameter can be calculated in the engine performance evaluation system.

In the standard PSO algorithm, the inertia weight is usually decreased linearly by the number of iteration, but in order to simulate the real state better, the inertia weight cannot be reduced to zero. In the early stage of the algorithm, it searches in the whole space, so as to ensure the global convergence. With the continuous increase in the number of iterations, in order to guarantee the convergence of the algorithm and the convergence precision, incorporating the simulated annealing mechanism, to improve the performance of the algorithm, thereby effectively balances the global and local convergence [9]. Adaptive particle swarm optimization algorithm based on simulated annealing is as follows:

1. Initialize each particle, set the annealing initial temperature T_star, the end temperature T_end, the current temperature T_cur, the cooling coefficient C, the learning factor C_1 and C_2, and the particle number n;
2. Generate n random initial solution or give n initial solution and generate n random initial speed, generate the new position of the particles according to the current position and velocity;
3. Calculate the fitness value of the new location of each particle;
4. To a certain particle, if the particle's fitness value is better than the individual extreme p_{best}, set the current fitness value to be p_{best};
5. Find out the global extreme g_{best}, according to the individual extreme p_{best}, of each particle;
6. Replace its speed according to the formula (54.4) and limit it to v_{max};
7. Replace the current position according to the formula (54.5) and limit it to x_{max};
8. Take the standard particle swarm learning factor to replace speed in the early stage of iterations; in the later stage, according to the principle of simulated annealing, calculate the difference ΔE of the current fitness and the last fitness; if $\Delta E \leq 0$, the optimal value of the individual is replaced to be the current particle fitness; then according to the Metropolis standards, if $\exp(-\Delta E/T\text{rand}) > rand$, rand as the random number in (0, 1) also accepts the current solution to be the new value and adjusts the cognitive function c_1; otherwise, refuse it, and x_{k+1} is still x_k.

$$c_1 = c_1 \times \exp(-t\_cur/t\_star) \times \text{rand} \qquad (54.3)$$

where c_1 is cognitive function; c_1 is the initial value of the cognitive function.

It can be analyzed by the formula (54.3), c_1 gradually becomes smaller with the temperature decreasing, while c_2 gradually increases with the temperature decreasing, so as they realize the dynamic adjustment of the global and local search ability of particle.

The adjustment formula of inertia weight is as follows:

$$W = W_{\max} + (w_{\max} - w_{\min}) \times (i - 1)/(iwa - 1) \qquad (54.4)$$

where w is the inertia weight; $w_{\max}$ is the maximum of inertia weight; $w_{\min}$ is the minimum of inertia weight; iwa is the step number of the inertia weight adjustment.

9. If the result satisfy the termination condition of calculation, the algorithm stops; otherwise, turn to step (2).

54.3 Experiment Verification

The data of this paper are a part of the test data of Ref. [10]. This paper selects the platform main performance parameters ΔF, Δsfc, T_3, T_4, ΔS and full afterburner air excess coefficient ALF. ΔF is the difference of thrust and its corresponding upper limit of acceptance curve; Δsfc is the difference of fuel consumption and its corresponding acceptance curve upper limit; and ΔS is the difference between the slip and lower limit of slip acceptance curve.

In order to facilitate the engine performance evaluation, the parameters of the engine are normalized, and the concept of efficacy function is introduced as follows. Let the engine performance matrix to be $[Z] = [Z_1, Z_2, \ldots, Z_n]$, where k_1 performance parameters are hoped to be as large as possible (such as F), k_2 performance parameters are hoped as small as possible (such as T_3, T_4, sfc), k_3 performance parameters are hoped as middle as possible (such as ΔS, ALF), and $k \leq n$. Every target Z_i is given a certain function coefficient (the score) d_i [d_i is a number in $(0, 1)$]. When the target gets the most satisfactory value, set $d_i = 1$; when the target gets the worst value, set $d_i = 0$. According to the analysis of engine performance acceptance standard, the Z value can be found when $d_i = 1$ and $d_i = 1$, namely the upper and lower limits of performance Z_i. Usually, use the upper and lower boundary of the acceptance curve or statistics extreme of a certain number of engine performance to be the upper and lower limits of performance. The function described the relationship between d_i and Z_i is called the effect function [10].

Because the distance between the upper and lower limits of the performance parameters is small, the effect function is approximated as a linear function according to the small deviation theory. With the efficacy function method, each performance parameters can be calculated to be the corresponding efficacy

function. Finally, the comprehensive parameters reflected the overall performance change trend of the engine can be calculated by using these efficacy functions.

Comprehensive weighted method is also called the weights of comprehensive parameters of algorithm. It can calculate the engine performance comprehensive index quantitatively and expressed by the following formula [11]:

$$\left.\begin{aligned} Q(t) &= \frac{\sum_{s=1}^{m} r_s \cdot d_s(t)}{\sum_{s=1}^{m} r_s} \\ s &= 1, 2, \ldots, m \end{aligned}\right\} \tag{54.5}$$

where m is the number of monitored parameters of the engine, r_s is the weight value of parameter, it reflects the importance of the parameter when monitored state is estimated, $d_s(t)$ is the function value of monitored engine parameter, it is the value of each engine parameter after dimensionless. The weights of different parameters can be determined by experience or optimization algorithm generally. And $0 \leq d_s(t) \leq 1$; $0 \leq r_s \leq 1$.

Use the comprehensive index to characterize the performance of engine. When the engine performance is normal, the comprehensive index value must be as large as possible, and the discrete degree of the comprehensive index values should not be great in the normal work; when the deterioration or failure of the engine performance happens, the comprehensive index value must be as small as possible, and the discrete degree of the comprehensive index values should not be great in the fault stage. Composite index can be obtained to distinguish whether the performance of engine is normal, or used to describe the degradation rate of performance when the engine runs normally. Therefore, the variation range of comprehensive parameter is: $0 \leq Q(t) \leq 1$. When the engine failed, $Q(t) = 0$; when the engine is in an optimal working state, $Q(t) = 1$. Therefore, the values of $Q(t)$ can be used for monitoring the state of engine.

Literature [1] records three test data of engine overhaul. The third overhaul data of engine performance are worse than the first overhaul, so they meet the conditions of comprehensive index method, and the date can be calculated in accordance with the above methods. Therefore, the corresponding effect function of multiple parameters in the first and third overhaul, in the largest state of a certain turbofan engine, is shown in Table 54.1.

The optimization criterion function is selected in this paper as follows:

$$f = (Rn + Rf)/|un - uf| \tag{54.6}$$

where un is the average value of comprehensive index value $Q(t)$ at the normal state of the engine, Rn is the variance value. uf is the average value of comprehensive index value $Q(t)$ at the failure state of the engine, Rf is the variance value. From Eq. (54.6), it can be seen that the smaller the value f is, the better the comprehensive index value reflects whether the engine performance is normal or not, the more reasonably the weight is. So f is selected as the optimization criterion function to evaluate the weight.

Table 54.1 Effect function of two engine overhaul

Parameters	df	$dsfc$	dt_3	dt_4	d_s	$dalf$
First overhaul	0.68	0.41	0.52	0.41	0.81	0.53
Third overhaul	0.50	0.32	0.48	0.43	0.91	0.47

54.3.1 Determine the Parameters of Weight Based on the Hybrid Optimization Algorithm

Use the improved hybrid optimization algorithm to calculate weights of parameters and set the initial value as follows: the number of the population particles $N = 30$, the strength parameter $c_1 = c_2 = 2.05$, the maximum number of iterations $M = 200$, the number of dimensions $D = 6$. The result of calculation is the weight of each parameter, and then substituted into the formula (54.6),

$$Q(t) = 1.0000 \times df + 0.7919 \times dsfc + 0.6492 \times dt_3 + 0.3237 \times dt_4 + 0.1557 \times d_s$$
$$+ 0.6057 \times dalf)/3.5262$$

The optimization criterion function is $f = 0.0254$.

In Fig. 54.1, the red chain line is the result of the hybrid optimization algorithm; the blue line is the result of the classical PSO.

Then, comprehensive weighting value of the corresponding test data engine of each overhaul can be calculated by using the hybrid optimization algorithm, and the formulae are as follows:

The first overhaul,

$$Q_1(t) = \left(\begin{array}{l} 1.0000 \times 0.68 + 0.7919 \times 0.41 + 0.6492 \times 0.52 \\ \qquad + 0.3237 \times 0.41 + 0.1557 \times 0.81 + 0.6057 \times 0.53 \end{array} \right) \Big/ 3.5262$$
$$= 0.54509613748511145142079292155862 \approx 0.5451.$$

The second overhaul,

$$Q_3(t) = \left(\begin{array}{l} 1.0000 \times 0.50 + 0.7919 \times 0.32 + 0.6492 \times 0.48 \\ \qquad + 0.3237 \times 0.43 + 0.1557 \times 0.91 + 0.6057 \times 0.47 \end{array} \right) \Big/ 3.5262$$
$$= 0.46241875106346775565764846009869 \approx 0.4624.$$

The weights are substituted into the formula (54.6) to calculate the engine performance index of other overhauls Table 54.2.

Fig. 54.1 The results of optimization algorithms
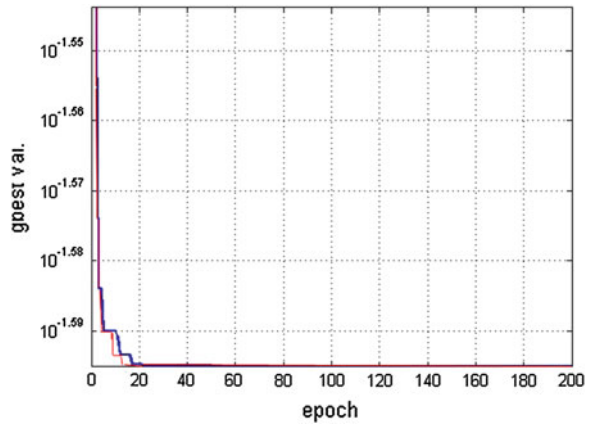
Table 54.2 Use comprehensive weighted method (CWM) to calculate the engine overhaul data

	Maximum stage			Intermediate stage		
Overhaul	1	2	3	1	2	3
CWM	0.5451	0.5364	0.4624	0.4881	0.4273	0.3783

54.4 Conclusions

In order to solve the question that how to calculate the parameters weight of engine performance in the comprehensive evaluation system, this paper uses the hybrid optimization algorithm to search multi-objective optimization and compares its result with the result of PSO calculation. Finally, the results of experiment show that the hybrid optimization algorithm can get better optimal solution of the problem quickly than using classical particle swarm optimization algorithm.

References

1. Kennedy J, Eberhart R (1995) Particle swarm optimization. In: IEEE international conference on neural networks, Perth, Australia, 1995:1942–1948
2. Eberhart R, Kennedy J (1995) A new optimization using particle swarm theory. In: Proceedings of the sixth international symposium on micro machine and human science, Nagoya, Japan, 1995:39–43
3. He X, Liu Y, Zhao X (2012) Performance deterioration evaluation of compressor fouling based on evolving neural network. Aeroengine 38(2):41–45 (in Chinese)
4. Wu H, Zhang L (2011) Application of one improved pso algorithm in the boiler-turbine coordinate control. Electr Power Sci Eng 27(10):53–56 (in Chinese)
5. Nie R, Zhang W, Li G, Liu X (2011) A more useful AHMOPSO (adaptive hybrid multi-objective particle swarm optimization) algorithm. J Northwest Polytechnical Univ 29(5):695–701 (in Chinese)

6. Gai feng (2011) A speed improved particle swarm optimization and its application. Modem Comput 10(19):3–6 (in Chinese)
7. Luo G, Liu B, Song D (2011) Hybrid particle swarm optimization in solving aero-engine nonlinear mathematical model. Gas Turbine Exp Res 24(2):5–8 (in Chinese)
8. Wang L, Hong Y, Zhao F, Yu D (2008) A hybrid algorithm of simulated annealing and particle swarm optimization. Comput Simul 25(11):178–182 (in Chinese)
9. Yu H, Huichao L, Zhijuan W (2012) Strategy of adaptive simulated annealing particle swarm optimization algorithm. Appl Res Comput 29(12):4448–4450 (in Chinese)
10. Li J, Tao Z (1994) Statistical analysis and prediction of aeroengine deterioration. J Aerosp Power 7(2):173–176 (in Chinese)
11. Jinhai H, Shousheng X (2003) Performance monitoring and fault diagnosis of aeroengine based genetic algorithm. J Propul Technol 24(3):198–200 (in Chinese)

Chapter 55
The Design of the Aircraft Supportability Evaluation System

Jiang Zhi, Song Dong and Ren Han

Abstract With the increasing complexity of aircraft system, it is more difficult to analyze and design the supportability of equipment. Aiming at this problem, this paper designed an aircraft supportability evaluation system, which is based on DEA and other assessment algorithm. Firstly, this paper gives the system's functional components and establishes the assessment software process of aircraft supportability scheme. Then, the DEA model algorithm of the evaluation system is introduced in detail. Finally, the paper applies evaluation system to analyze different supportability schemes. Moreover, the optimal supportability scheme is obtained.

Keywords Supportability scheme · Data envelopment analysis (DEA) · Evaluation system

55.1 Introduction

Supportability design of equipment should be taken into consideration in the process of new equipment development so that it has a high level of post-deployment readiness and has the ability to compete with foreign advanced equipment in the aspect of the comprehensive efficiency. However, with the increasing complexity of aircraft equipment, it is more difficult to analyze and design the supportability of equipment. Supportability design has become the bottleneck of equipment design. Obviously, it is imperative to provide an effective tool for developing a more comprehensive and systemic computer-aided analysis software for the next generation, which is aimed at improving the level of operational readiness and reduce life cycle costs [1].

J. Zhi (✉) · S. Dong · R. Han
School of Aeronautics, Northwestern Polytechnical University, Xi'an 710072, China
e-mail: jiangzhi457@163.com

Aircraft supportability evaluation system is aimed at solving supportability requirements and provides a balance means between these requirements and system design. Besides, it is the bridge and link to contact the equipment design and supportability system design. It is designed to achieve the aircraft supportability evaluation procedures of mathematical models and assess the effectiveness of the aircraft supportability schemes and provide simple tools for decision makers.

55.2 Aircraft Supportability Evaluation System Components

According to the assessment process of aircraft supportability scheme, the main function modules of designed aircraft supportability evaluation system include system login module, a database management module, DEA evaluation module, Stochastic frontier analysis (SFA) evaluation module, user management module, etc. Specific functional modules are shown in Fig. 55.1.

Database management module is used to provide supportability scheme view, search, add and modify features, affordable comprehensive analysis of the choice of indexes and data maintenance functions. DEA/SFA evaluation modules, providing the use of DEA/SFA model for calculation and analysis, include index data preprocessing, processed data for assessment calculations, and the final output results to determine valid value of the different options. Management module is used for user management.

The SQL Server2000 is used for the system background database. Microsoft Visual Studio 2008 (programming language adopts C#) is used for interface development. Considering the powerful computing capabilities of MATLAB, MATLAB programming is used for algorithm design (principal component analysis and mathematical envelopment analysis).

55.3 DEA Model and Algorithm Design

DEA model often uses C2R constant returns to scale model and BC2 variable returns to scale model. This paper adopts C2R model. The linear programming methods are used to measure multi-input and multi-output efficiency problem of supportability scheme [2, 3]. Model is as follows:

Suppose there are n supportability schemes, there are m kinds of input index, and s kinds of output index for each supportability scheme. Set up

$$X_j = \left(x_{1j}, x_{2j}, \ldots \ldots, x_{mj}\right), \tag{55.1}$$
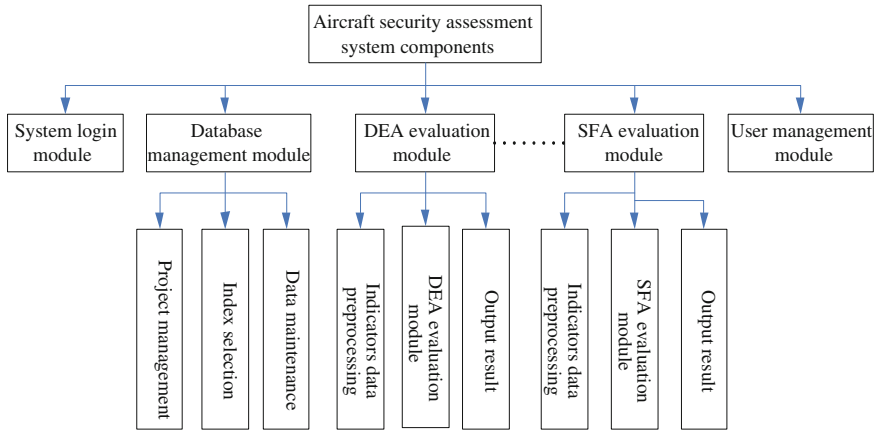
Fig. 55.1 Aircraft supportability evaluation system components

$$Y_j = \left(y_{1j}, y_{2j}, \ldots\ldots, y_{sj}\right)^T, \quad (j = 1, 2, \ldots\ldots, n);$$ (55.2)

Respectively, they are the j-th input vector supportability schemes and output vectors.

$$\left(D_\varepsilon^T\right) \begin{cases} \min\left[\theta - \varepsilon\left(\hat{e}^T S^- + e^T S^+\right)\right], \\ \displaystyle\sum_{j=1}^{n} X_j \lambda_j + S^- = \theta X_0 \\ \displaystyle\sum_{j=1}^{n} Y_j \lambda_j + S^+ = Y_0 \\ \lambda_j \geq 0, \ j = 1, 2, \ldots\ldots, n \\ S^- \geq 0, \ S^+ \geq 0 \end{cases}$$ (55.3)

Among them, θ is the relative efficiency of supportability schemes for the value; $S^- = \left(S_1^-, S_2^-, \ldots, S_m^-\right)$ is the slack variables which m item inputs; $\lambda = (\lambda_1, \lambda_2, \ldots, \lambda_n)$ is a combination of factors of n DMU; $e^T = (1, 1, \ldots, 1)_{1 \times s}$, $\hat{e}^T = (1, 1, \ldots, 1)_{1 \times m}$; ε is a small positive number (general admission $\varepsilon = 10^{-6}$). For each DMU, according to the linear programming model, we can find the optimal solution that is also known as supportability schemes relative efficiency index [4], we can get:

1. If $\theta^0 < 1$, j_0 is a non-DEA effective supportability schemes;
2. If $\theta^0 = 1$, $\hat{e}^T S^{-0} + S^{+0} > 0$, j_0 is only weakly DEA efficient supportability schemes;
3. If $\theta^0 = 1$, $\hat{e}^T S^{-0} + S^{+0} = 0$, j_0 is a DEA efficient supportability schemes.

Fig. 55.2 Aircraft supportability evaluation software process
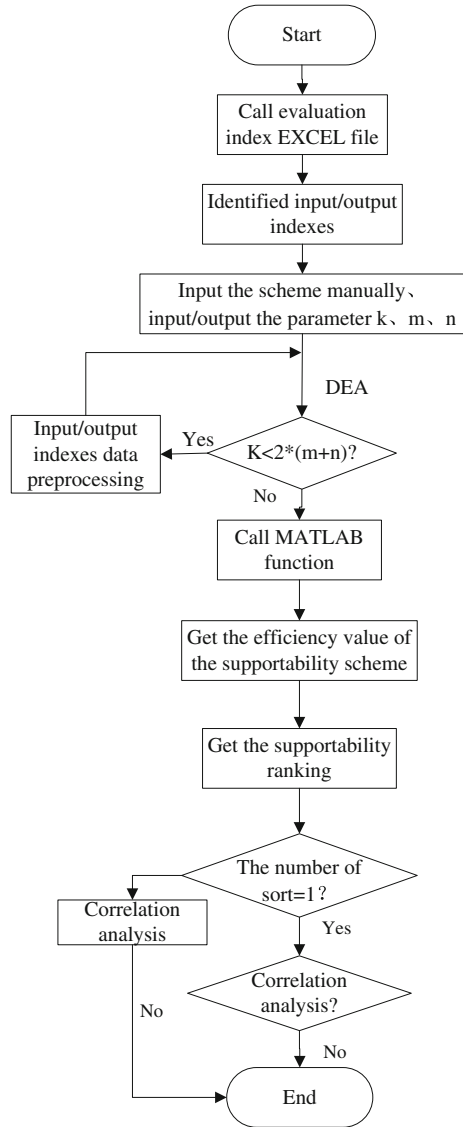
55.4 Aircraft Supportability Evaluation Software Process

Aircraft supportability evaluation software process is shown in Fig. 55.2. The EXCEL file, which preserves multiple options of supportability schemes, is used for input. Then, the supportability indexes, which supportability schemes provide, are used for the input data preprocessing. The input and output indexes are

determined after calculating. Then, the indexes are made through the DEA model to evaluate. Firstly, the input and output indexes are judged whether they should be preprocessed. If so, the indexes are input to the preprocessing unit; if not, the indexes are got into the DEA model assessment using the MATLAB program directly. Then, the efficiency for each supportability schemes is obtained, and each supportability scheme is sorted according to the size of the efficiency value. Finally, the supportability scheme assessment outcome based on the approach of DEA is obtained.

55.5 Systems Running Instance and Analysis

The evaluated supportability schemes should be imported to determine the input and output indexes. Manual input the number of supportability schemes, input and output indexes, which are used to determine whether preprocess the data [5].

55.5.1 Original Data

An aircraft's five proposed Performance Evaluation of Maintenance Support System basic data are shown as follows: I_i ($i = 1$, 2) stand for input indexes, where I_1, equipment disrepair rate; I_2, equipment repair rate; and O_j ($j = 1, 2, …, 17$) stand for the output indexes, where O_1, technical personnel allocation rate; O_2, technical personnel competent rate; O_3, management personnel allocation rate; O_4, management personnel competent rate; O_5, equipment types matching rate; O_6, equipment number configured rate; O_7, repair instruments, equipment, and facilities species matching rate; O_8, repair instruments, equipment, and number of facilities configuration rate; O_9, type of technology matching rate; O_{10}, technical data rate of the number of configurations; O_{11}, technical data types matching rate; O_{12}, technology configuration data rate; O_{13}, funding in place rate; O_{14}, efficient use of funds; O_{15}, personnel participating in the training rate; O_{16}, equipment intact rate; O_{17}, instruments, equipment, facilities, and good rate, as shown in Table 55.1.

55.5.2 System DEA Evaluation Module

The module is required to complete the assessment calculation of DEA method and then is sorted based on scheme evaluation results. "The simplified input indexes" and "simplified output indexes" are completed for the input and output indexes PCA by the C# calling MATLAB in principal component analysis procedures; "Evaluation results display" will display the calculation results and ranking results by calling the MATLAB DEA program.

Table 55.1 Supportability schemes evaluation parameters

Input indexes	I_1	I_2							
Scheme 1	0.25	0.25							
Scheme 2	0.25	0.25							
Scheme 3	0.4	0.4							
Scheme 4	0.15	0.2							
Scheme 5	0.35	0.3							
Output indexes	O_1	O_2	O_3	O_4	O_5	O_6	O_7	O_8	O_9
Scheme 1	0.85	0.5	0.9	0.9	0.9	0.85	0.85	0.85	0.85
Scheme 2	0.85	0.95	0.9	0.9	0.9	0.85	0.85	0.85	0.85
Scheme 3	0.9	0.6	0.7	0.5	0.6	0.8	0.7	0.6	0.7
Scheme 4	0.95	0.9	0.9	0.9	0.8	0.95	0.8	0.9	0.9
Scheme 5	0.7	0.7	0.8	0.6	0.7	0.9	0.8	0.7	0.7
Output indexes	O_{10}	O_{11}	O_{12}	O_{13}	O_{14}	O_{15}	O_{16}	O_{17}	
Scheme 1	0.85	0.5	0.7	0.7	0.75	0.75	0.75	0.8	
Scheme 2	0.85	0.95	0.7	0.7	0.75	0.75	0.75	0.8	
Scheme 3	0.7	0.5	0.8	0.7	0.7	0.7	0.9	0.7	
Scheme 4	0.8	0.95	0.9	0.8	0.9	0.9	0.8	0.9	
Scheme 5	0.9	0.8	0.8	0.9	0.8	0.8	0.7	0.8	

Table 55.2 Simplified input–output index data

Input indexes	Scheme 1	Scheme 2	Scheme 3	Scheme 4	Scheme 5
X_1	1.5026	1.5026	3.9896	0.3109	2.6943
Output indexes	Scheme 1	Scheme 2	Scheme 3	Scheme 4	Scheme 5
Y_1	5.4418	6.4060	0.1758	8.1411	4.8353
Y_2	2.5998	3.2367	5.5935	7.1147	6.4553
Y_3	4.9181	5.1154	6.2104	6.6662	2.0899
Y_4	3.6697	6.5002	5.1295	4.7138	4.9868

55.5.2.1 Index Preprocessing of the Input and Output Indexes

After the original data going through index preconditioning (principal component analysis), the final input and output indexes are determined, as shown in Table 55.2.

55.5.2.2 DEA Analysis Results

The final input and output indexes are determined according to calculating and analysis. Results are shown in Fig. 55.3. Comprehending the above result, the Scheme 4 has the highest overall efficiency value.
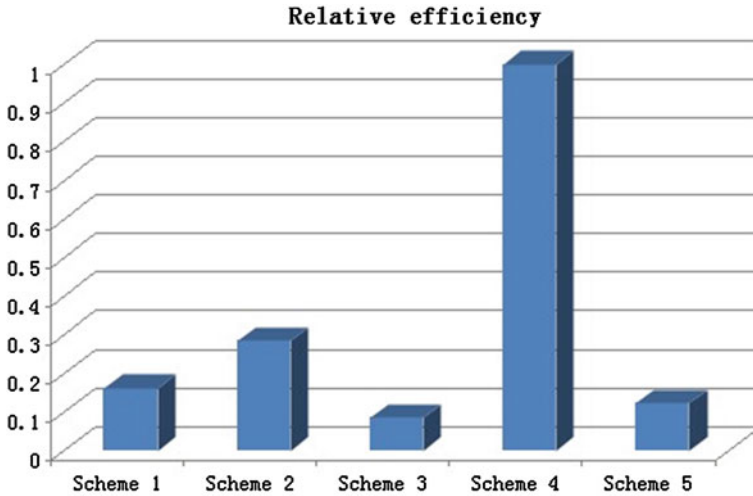
Fig. 55.3 The histogram of the EDA method to evaluate the results

55.6 Conclusion

This paper describes the function components of the aircraft supportability evaluation system. The DEA model, which is the main function module of the system, is analyzed emphatically. Subsequently, the aircraft supportability evaluation system software process is established. With the aircraft supportability evaluation system different schemes are assessed and analyzed. The optimal supportability scheme is obtained according to the assessment result. Of course, in addition to the DEA model evaluation algorithm, many evaluation algorithms can be applied to the aircraft supportability evaluation system. In the future course of the study, different models should be studied and integrated the use of the aircraft in order to improve the assessment of different supportability schemes accuracy and feasibility.

References

1. Liu Z-W, Deng S (2003) Review on the evaluation of engineering design methods of complex system. Syst Eng Electron 25(12):P1487–P1491 (in Chinese)
2. Li M, Chen G (2003) Research and application of the data envelopment analysis (DEA). China Eng Sci 5(6):P88–P90 (in Chinese)
3. Wang Q (2008) Further study of the DEA method. Tianjin University (in Chinese)
4. Charnes A (1985) Sensitivity and stability analysis in DEA. Annals of OR 139–156
5. Charnes A, Cooper WW, Rhodes E (1978) Measuring the efficiency of decision making units. Eur J Oper Res 6(2):P429–P444

Chapter 56
Composite Patch Bonded Repair Simulation and Optimization of the Lap Joints

Xinjun Wang, Yongchao Dai and Feibo Huang

Abstract In this paper, the finite element method is applied to optimize the stress distribution of the adhesively bonded composite patch for repairing of a cracked metal plate. A three-dimensional finite element model was created and simulated, a finite element procedure is programmed to find the optimized parameters of the composite patch, and the optimized parameters are listed for convenient application. The simulated result shows that the directions of the plies and the distance between the lap joints could affect the adhesive stresses distribution greatly, and compared with the single lap joint case, the maximum shear stress of the recommended multi-joints case could reduce more than 80 %.

Keywords Bonded repair · Finite element · Simulation · Optimization

56.1 Introduction

Externally bonded composite patches have proved to be an effective method for repairing metal and nonmetal aircraft structures. Compared with ordinary mechanically fastened method, the adhesively bonded patch offered many advantages, which include greater strength to weight ratios, lower cost, fewer task time and improved fatigue behavior. This method was firstly proposed by Baker [1] in 1970s, when Baker and his colleagues in the aeronautical and maritime research laboratory of the Royal Australian air force began to study adhesively bonded repair application for solving old aircraft metal structure repair problem, then adhesive bonded repair method was applied to repair many military aircraft

X. Wang (✉) · Y. Dai
The First Aeronautic Institute of the Air Force, Xinyang 464000, china
e-mail: knightwxj@163.com

F. Huang
The military representative office of China's Air Force, Guangzhou 510405, china

such as F/A-18, F-16, F-111, C-141 and C-130, commercial aircraft such as L1011 and DC-10 [2, 3], the use of this new method have obtained significant military and economic benefits. Soon some research has also been conducted by a lot of scholars in China. Reissner–Mindlin theory is used by Bai [4] to create finite element model of the bonded structure; they studied the factors affecting repaired effects such as diameter and thickness of the patch; the simulation result shown that the thickness is what affects the repair effect the most. Zhao and Wang [5] analyzed the thickness of the plate and the shear modulus of the adhesive; the result shown that the composite patch must have enough stiffness to ensure a reliable repaired patch. Zhu [6] created 6 patch models with different shape; the simulated result shown that at the angular point of the patch exists stress concentration; an arc angular patch is recommended to replace the right angle patch. Yan et al. [7] studied the influences of the adhesive properties, and the study result shown that using the adhesive with higher modulus of elasticity could lead to more severe uneven stress distribution. In practical project application, thick patch and adhesive with high elasticity modulus are often selected in order to improve quality of the repaired structure, as analyzed above; it can decrease the stress-intensity factor, but it also lead to unevenly distributed shear stress, as a result interface debonding often occured at the end of the patch. Recently, scholars found that reasonably designing the direction of the plies and setting more steps can decrease stress concentration [8]. Based on the existing research results, finite element models must be created in order to get optimized parameters though numerical simulation method, but this method is not easy to use in practical working condition. So, this paper developed a three-dimensional finite model to solve the adhesively bonded problem, the orientation of plies and the length of patch steps are considered as the key factors affecting stress concentration. Based on frequently used material in aircraft repair work, a finite element computing procedure is programmed with variational design parameters; at last, a parameter table for practical repair work is recommended according to simulation result.

56.2 Establish the FEM Model

The general configuration of the adhesively bonded repair model is shown in Fig. 56.1; a thin plate with a through thickness crack is subjected to a uniaxial remote load σ, and in order reinforce the cracked plate, a composite patch is adhesively bonded at one side or both sides. Suppose the stress in the plate is σ, the width of the patch is W_P, the length is L_P and the thickness is t_P. According to the result of Quaresimin and Ricotta [9], it is effective to set more than one steps on the patch to ease stress concentration.

Figure 56.2 demonstrates the plate bonded with three symmetric stepped patches. Figure 56.3 demonstrates the plate being bonded at only one side.

Here, we suppose the crack length is $2a$, L_i mean the length of the stepped patch i, the material and geometric is listed in Table 56.1.

Fig. 56.1 Cracked plate repaired by composite patch
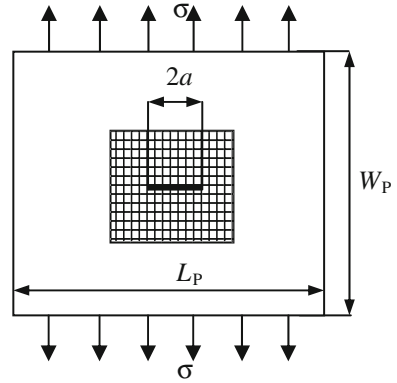
Fig. 56.2 Plate bonded with symmetric stepped patches
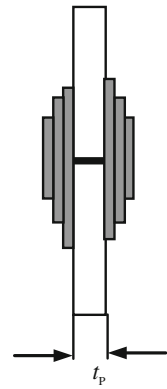
Fig. 56.3 Plate bonded with unilateral patches
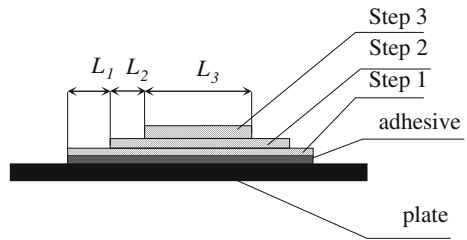
For the bonded patch with more than one step, suppose that step k includes m plies composites, so the stiffness of the step k can be computed by the following formula where subscript 1 means the ply 1 of the step k.

$$E_o^k t_o^k = \sum_{l=1}^{l=m} E_l t_l \tag{56.1}$$

Because the bending moment effects cannot be neglected for aluminum alloy plate bonded with unilateral patches, it is best to use 3D finite element model

Table 56.1 Material and geometric parameter

Component	Mechanical property	
Aluminum plate	Elasticity modulus E (Gpa)	71.02
	Poisson ratio V	0.33
Adhesive	Elasticity modulus E (Gpa)	2.158
	Poisson ratio V	0.35
Composite patch (carbon/epoxy)	Elasticity modulus E (Gpa)	$E_1 = 181$
		$E_2 = 10.3$
		$E3 = 10.3$
	Shear modulus G (Gpa)	$G_{12} = 7.17$
		$G_{13} = 7.17$
		$G_{23} = 3.78$
	Poisson ratio V	$V_{12} = 0.28$
		$V_{13} = 0.28$
		$V_{23} = 0.3$

which can compute combined effects of stretch and bending moment [10], so here we use 3D finite element to simulate the stress state of the adhesively bonded model and the meshed figure is illustrated in Fig. 56.4. The plate and adhesive layers are modeled by isotropic element solid185; the composite layers are modeled by anisotropic element solid186; both solid185 and soild186 are 20 nodes three-dimensional nonlinear finite element. The direction and thickness of plies of composite steps are configured by command SECTYPE in ANSYS, and the stress-intensity factor are computed by command CINT.

56.3 Result Analysis

Bonded repairs function by transferring some portion of the load to the reinforced composite patch through the adhesive bond layer; in order to enhance the cracked plate, the bonded patch must be thick enough, but this may result in the failure of adhesive layer because of nonuniform shear stress. Hence, we shall focus on the simulated result of the shear stress distribution considering different patch design scheme and try to find the best composite patch design parameters which would reduce the maximum shear stresses.

56.3.1 Simulated Result of Single-Step Case

The most common bonded repair case is single-step patch where every composite ply has the same length; in order to reduce the maximum shear stress, we should firstly compute the stress distribution by finite element analysis procedure.
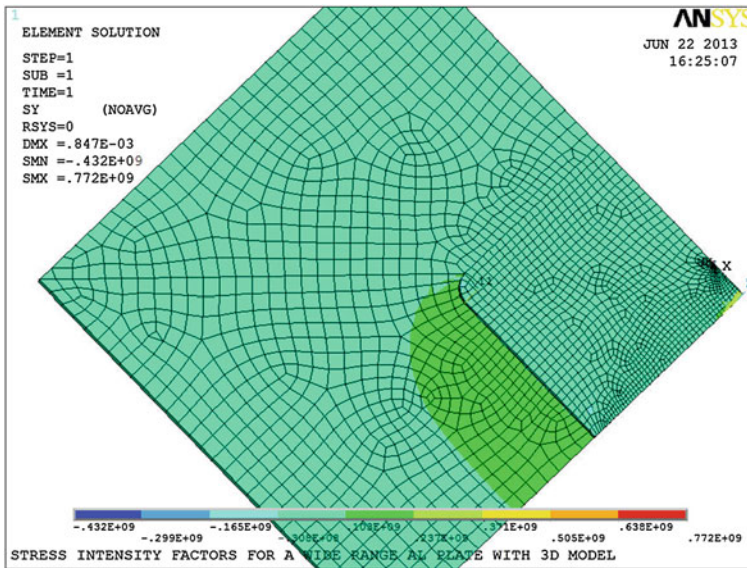
Fig. 56.4 Finite element model meshed by 3D elements

Suppose the thickness of the aluminum plate is 3.0 mm and the thickness of the composite patch is 1.6 mm which include 10 plies and every ply has the same direction perpendicular to the crack. Considering the symmetry of the bonded structure, we just need to model 1/4 of the bonded plate; the font of the crack was set perpendicular to axis y, using ANSYS12 programme; the simulated finite element result is shown in Fig. 56.5. Clearly, the maximum shear stress located at the lap joints, and it is consistent with the experience that the bonded patch may often fail at the patch end. According to Fracture Mechanics theory [11], the stiffness of the plate is $E_P t_P$; the stiffness of the patch is $\sum_{l=1}^{l=m} E_l t_l$; then at the bonded sector, the stiffness is $E_p t_p + \sum_{l=1}^{l=m} E_l t_l$; the maximum stiffness gradient located at the lap joints results in the maximum shear stress. So we can infer that if we decrease the stiffness at the lap joints, the shear stress may decrease also.

56.3.2 Simulated Result of Multi-Step Case

As analyzed above, if we reasonably design the patch with more than one step, the stiffness gradient at the lap joints could decrease and the shear stress could distribute more evenly. So we firstly consider a simple design scheme; the patch is bonded with uniformly distributed steps; the patch steps is evenly spaced and every step has the same stiffness. The simulated result shows this uniform multi-step patch can reduce the maximum stress concentration, but the stress
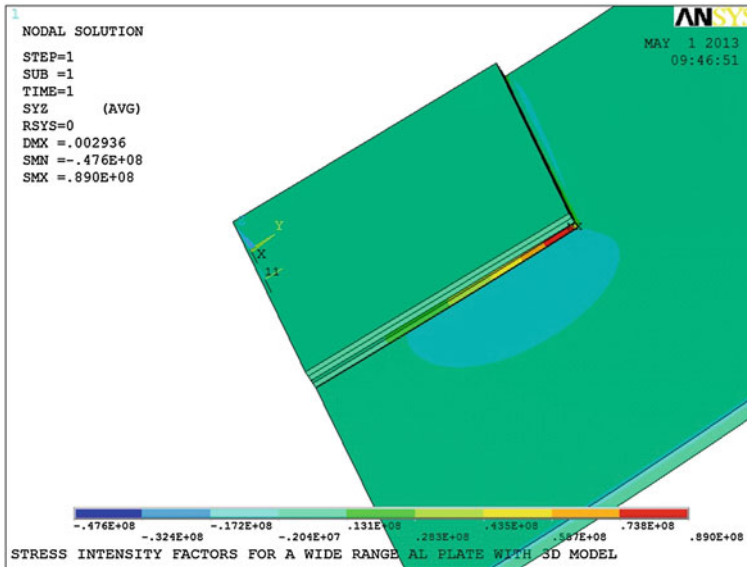
Fig. 56.5 Shear stress distribution figure of the patch with one step

concentration is still significant. In order to reduce the shear stress concentration, the parameters of the uniform patch are used as the starting point; a finite element procedure is programmed to run on ANSYS12 which could compute the maximum shear stress with different patch parameters by changing thickness and interval of the step and directions of the plies; the optimized result is shown in Table 56.2 when step number is 3, 4, 5 and 6, the shear stress distribution is illustrated in Fig. 56.6.

The result shown that the shear stress distributed evenly when the step number is 5 or 6; the maximum shear stress decreases nearly 80 % from 46.7 MPa with 3 steps to 11.3 MPa with 6 steps.

56.3.3 Recommended Parameters for Different Bond Mode

Considering allowable time and operating personnel in actual repair process, it cannot afford to create finite element model and run simulated computing program. So it is helpful to provide recommended parameters for common repair case; the following recommended parameters are optimized by finite element procedure on ANSYS with variational thickness and interval of the step and directions of the plies. Various authors [10, 12] showed that the thickness of the patch is what affected the maximum shear stress the most, so we firstly use finite element programme to find the best thickness of the patch by changing thickness parameters of plates and patch. Suppose the thickness of the cracked aluminum alloy is t_p, the

Table 56.2 The maximum shear stress of different step numbers

Step numbers	Ply direction of different steps	The maximum shear stress (MPa)
3	[+45, −45] [0, 90, 0, 90] [0, 90, 0, 90]	46.7
4	[+45, −45] [0, 90] [0, 90, 0, 90] [0, 90]	23.5
5	[+45, −45] [0, 90][0, 90] [0, 90] [0, 90]	11.8
6	[+45, −45] [0, 90] [0, 90] [0, 90] [0] [0]	11.3
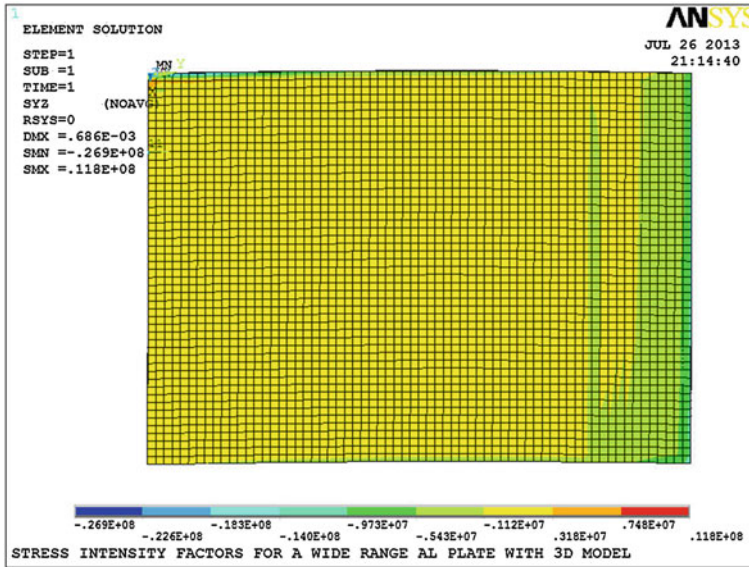
Fig. 56.6 Shear stress distribution figure of the patch with five steps

Table 56.3 Recommended parameters for unilateral patches

Plies of one side	Number of steps	Length of every step (mm)	Number and direction of plies
4.3 * t_p	1	2.0	2(−45/45)
	2	3.0	2(0/90)
	3	6.0	2(0/90)
	4	4.0	2 * t_p − 5 (0/90)
	5	2.0	2.3 * t_p − 6 (0/90)
	6	2a + 20	3(0/90/0)

simulated result shown that for unilateral bonded mode, the best thickness of the composite patch is 4.3 * t_p, for symmetric bonded mode, the recommended thickness is 2.8 * t_p to both sides, and the recommended length and number of the bonded patch step are shown in Table 56.3 for unilateral patch and Table 56.4 for

Table 56.4 Recommended parameters for symmetric patches

Plies of one side	Number of steps	Length of every step (mm)	Number and direction of plies
$2.8 * t_p$	1	3.0	1(0)
	2	4.0	2(0/90)
	3	3.0	$t_p - 1(0/90)$
	4	1.5	$t_p - 2(0/90)$
	5	$2a + 26$	$0.5 * t_p(0)$

symmetric patch. Compared with one step case, simulation result shown that using these recommended parameters, the maximum of the adhesively bonded patch could decrease more than 80 %, so the multi-step patch could bear more load.

56.4 Summary

The study has been made in aim to determine the optimized parameters of the bonded composite patch for reducing shear concentration. The obtained results allow us to deduce the following conclusions:

- The reduction in the maximum shear stress by the multi-step composite patch is 80 %, which improve the load-bearing capability of the plate.
- The stiffness of the bonded patch layers is a key factor which determine the maximum shear stress of the bonded area.
- The maximum shear stress often located at the lap joints, using multi-step patch can decrease stiffness gradient at the lap joints and decrease maximum shear stress as well.

References

1. Baker AA (1987) Fiber composite repair of cracked metallic aircraft components practical and basic aspects. Composites 18:293–307
2. Baker AA (1984) Repair of cracked of defective metallic aircraft components with advanced fiber composites-an overview of Australian work. Compos Struct 2:153–181
3. Alias MN, Brown R (1993) Corrosion behavior of carbon fiber composites in the marine environment. Corros Sci 35:31–54
4. Bai J (2001) The optimal analysis of patch bonding parameters in composite repairing technique. Mech Sci Technol 20:748–750
5. Zhao L, Wang Z (2011) The study of stress intensity factor of cracked metallic structure repaired with adhesive bonding composite patch. Aircr Des 30:50–67
6. Zhu X (2011) Optimization research of composite patch shape based on residual strength. J Civ Aviation Flight Univ Chin 22:8–11
7. Yan Z, You M, Yu H (2006) Influence of elastic modulus of adhesive on the stress and strain distribution in aluminium single lap joint. J Aeronaut Mater 26:39–42

8. Kaye RH, Heller M (2002) Through-thickness shape optimization of bonded repairs and lap-joints. Adhes Adhes 22:7–21
9. Quaresimin M, Ricotta M (2006) Stress intensity factors and strain energy release rates in single lap bonded joints in composite materials. Compos Sci Technol 66:647–656
10. Meo M, Thieulot E (2005) Delamination modeling in a double cantilever beam. Compos Struct 71:429–434
11. Knott JF (1973) Fundamentals of fracture mechanics. Butterworths, London
12. Wang CH, Rose LRF, Callinan R (1998) Analysis of out-of-plane bending in one-sided bonded repair. Int J Solids Struct 35:1653–1675

Chapter 57
Multidimensional Flexibility Measurement of Ship-Based Aircraft Maintenance Support Organization Based on Structure Entropy

Qiaoli Mi, Tingxue Xu, Hui Wang and Jikun Yang

Abstract Uncertain changes are the principal factors influencing the operation and support of ship-based aircraft. On the basis of analyzing the definition of flexibility and the flexible characteristics in the maintenance support organization, a three-dimensional measurement frame is established. The three dimensionalities, which are responding speed, robust flexibility and adaptable flexibility, are respectively measured by the efficient entropy, quality entropy and changing entropy. And then the comprehensive flexibility measurement method and steps are presented. Lastly, the example studied verifies the feasibility and practicability, and the measurement results of two organizations are evaluated and contrasted. Consequently, the flexibility measurement and optimization of the maintenance support organization can be realized effectively.

Keywords Flexibility · Maintenance support · Structure entropy

57.1 Introduction

With the rapid development of building the digitized and informational forces in the worldwide military field, the large-scale support systems are been transformed to the high-agility, accurate and reliable support systems. The support models of the

Q. Mi (✉) · H. Wang · J. Yang
Department of Graduate Students' Brigade, NAAU, Yantai 264001 Shandong, China
e-mail: 14717mql@163.com

H. Wang
e-mail: 1781599519@qq.com

J. Yang
e-mail: 13583533630@139.com

T. Xu
Department of Ordnance Science and Technology, NAAU, Yantai 264001 Shandong, China
e-mail: xtx-yt@163.com

military forces around the world, such as the USA, Russia, Denmark, have been developed in the direction of centralized control and decentralized implementation. At the same time, some flexible thoughts of equipment maintenance support adapting to the joint operation are advanced, such as the logistic support being serviceable at peacetime and wartime, the rapid and mobile emergency support, and visually remote support [1–3]. For example, according to the accrual requirements, the US armed forces have build some new support organizations, such as maintain command in war zone, expeditionary maintain command, and support battalion.

In the air-sea battle, as the main equipment of naval air combat, ship-based aircraft is equipped with the operational capabilities of attacking aerial, surface, underwater, and ground targets. It is the key force of despoiling and maintaining the air-sea supremacy. The fast changing information in the informational battlefield will make the operational missions more variable, so the external conditions of the maintenance support may be uncertain constantly when the ship-based aircraft breaks down. Besides, the current maintenance support organizations of ship-based aircraft are relatively dispersed geographically and managerially, as a result, it is difficult for them to achieve the high efficiency of maintenance support. Imitating the example of the theories and practices of building flexible maintenance support organizations in the USA, Russia, and other military powers, it is an inexorable trend to establish flexible maintenance support organizations of ship-based aircraft. Consequently, the flexible maintenance support, maintaining the status quo or dynamically changing the organization structures, will be provided for the ship-based aircraft.

57.2 Flexibility Connotation

The concepts of flexibility, adaptability, and robustness are not only connected, but also distinguishing, as in the literatures [4–6]. From the systematic point of view, adaptability refers to the ability of responding to the foreseeable changes, while robustness is respected to the extent of maintaining the normal level under disturbances. Here, they are contrasted from some aspects, such as the changing type, driving factor, responding state, and expected target, as shown in Table 57.1.

The responding types of flexible system to the external changes can be basically reflected in two aspects. On the one hand, possessing insensitivity and the ability of resisting the changes, flexible system can maintain the status quo. On the other hand, the system should coordinate its internal elements to cope with the external uncertainties better. As a result, the flexibility definition of maintenance support organization can be summarized as follows.

When facing the uncertain changes of outside world, flexibility of the maintenance support organization refers to not only the buffering capacity of resisting changes and keeping stability, but also the reaction capability of adjusting the structure fast and effectively to respond to the changes. According to Table 57.1, the adaptability and robustness, respectively, reflect the two respects of flexibility, so the two capabilities of flexibility can be called as robust flexibility and adaptable flexibility here.

Table 57.1 Contrast of flexibility, adaptability, and robustness

Options		Adaptability	Robustness	Flexibility
Correlation		Responding capability to the uncertainties of external changes		
Distinctions	Changing type	Foreseeable	Unforeseeable	Uncertain (foreseeable or unforeseeable)
	Driving factor	External factors	Internal factors	Combining internal and external factors
	Responding state	Passive changing	Maintaining the status	Responding subjectively and initiatively
	Expected target	Adapting to changes	Against changes	Achieving the optimal balance of system and uncertainties

57.3 Multidimensional Measurement Frame

The flexible maintenance support organization of ship-based aircraft is a complex organization, having multi-nodes connecting with each other and involving multi-factors in human–machine-environment engineering under the constraint of multi-conditions. Its flexibility should be analyzed and measured from multiple perspectives. Firstly, the flexibility of the maintenance support organization is reflected by the responding speed to the uncertain changes. Secondly, it is shown by the robust flexibility that can still maintain the normal functions under the disturbance of uncertainties. Thirdly, it is represented by the adaptable flexibility that can achieve the best support efficiency according to adjusting the structure rapidly. Referring to [7], a three-dimensional flexibility measurement frame of maintenance support organization for ship-based aircraft is established, including responding speed, robust flexibility, and adaptable flexibility, as shown in Fig. 57.1.

The coordinates of the three-dimensional flexibility measurement frame are corresponding to the responding time, static quality, and dynamic change. The responding time of organization indicates the time interval from the moment of receiving the changes to that of adopting response activities. Static quality indicates that the organization achieves the coordination of nodes and support activities maintaining the status quo, while the dynamic change indicates that the organization responds to the changes of support requirements and tasks by dynamically changing its structure.

57.4 Measurement Method Based on Structure Entropy

Entropy is a concept used to measure the intent of uncertainties in many fields. In system engineering, it represents the quantification description of the status complexity and the order degree. The concept of structure entropy is proposed by applying it to measure the uncertainties of systemic organization structure [8, 9].

Fig. 57.1 Three-dimensional flexibility measurement frame
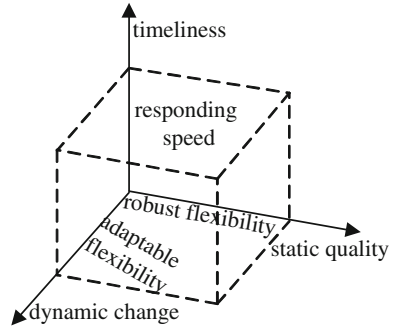
Evidently known, higher the order degree of an organization is, smaller the structure entropy is, otherwise, larger the structure entropy is.

57.4.1 Comprehensive Measurement of Flexibility

According to the above theory, structure entropy can judge the organization stability by measuring the uncertainty of organization structure. Therefore, flexibility measurement of ship-based aircraft maintenance support organization can be accomplished by calculating its structure entropy. Here, the static order degree and dynamic changing entropy are used to measure and evaluate the three aspects of organizational flexibility. Denoting the responding speed of the maintenance support organization by T, robust flexibility by R, and adaptable flexibility by A, the comprehensive flexibility measurement formula of it can be expressed as the following form:

$$F = \alpha T + \beta R + \gamma A, \tag{57.1}$$

where α, β, and γ, respectively, express the weight of responding speed, robust flexibility, and adaptable flexibility. And the weight can be determined by the weighting methods such as expert scoring method, principal component analysis, and entropy weighting.

57.4.2 Measurement of Responding Speed

Efficient entropy is used to measure the uncertainties of information flow timeliness among nodes, denoted by H_1. As a result, the responding speed of ship-based aircraft maintenance support organization, denoted by T, can be measured by efficient entropy.

The total number of the nodes in the ship-based aircraft maintenance support organization is N. If there is a directed information flow between arbitrary two

nodes, i and j, there is a connection between them, and the number of the connections is called as connection length, denoted by L_{ij}. Microstate is the microscopic state of the organization structure that may appear or go through, and the amount of microstate is the total passing number of the current state evolving to another state, denoted by S_1, and it satisfies $S_1 = \sum_{i=1}^{N} \sum_{j=1}^{N} L_{ij}$ $1 \leq i,\ j \leq N$.

Efficient entropy of the connection refers to arbitrarily longitudinal two nodes, i and j, it can be calculated by:

$$H_1(ij) = -p_1(ij) \log_2 p_1(ij), \qquad (57.2)$$

where $p_1(ij) = L_{ij}/S_1$ is the realization probability of the microstate about the connection of i and j.

Therefore, the responding speed can be calculated by:

$$T = 1 - H_1/H_{1m}, \qquad (57.3)$$

where H_1 is the total efficient entropy and satisfies the following form:

$$H_1 = \sum_{i=1}^{N} \sum_{j=1}^{N} H_1(ij), \qquad (57.4)$$

and H_{1m} is the maximum efficient entropy and satisfies the following form:

$$H_{1m} = \log_2 S_1. \qquad (57.5)$$

57.4.3 Measurement of Robust Flexibility

The robust flexibility can be measured by the quality in structure entropy, which reflects the response extent in the information flow among the nodes. The uncertainties measurement of organization structure is called quality entropy, denoted by H_2. The number of the nodes directly connecting to i is called connection span, denoted by k_i, $i = 1, 2, \ldots, N$. Defining the amount of quality microstate by $S_2 = \sum_{i=1}^{N} k_i$, the uncertainties measurement of making mistakes in the information flow can be realized by quality entropy, which satisfies the following form:

$$H_2(i) = -p_2(i) \log_2 p_2(i), \qquad (57.6)$$

where $p_2(i)$ is the realization probability of the microstate about the node i, and it satisfies $p_2(i) = k_i/S_2$.

Therefore, the robust flexibility can be calculated by:

$$R = 1 - H_2/H_{2m}, \qquad (57.7)$$

where H_2 is the total quality entropy and satisfies the following form:

$$H_2 = \sum_{i=1}^{N} H_2(i), \qquad (57.8)$$

and H_{2m} is the maximum quality entropy and satisfies the following form:

$$H_{2m} = \log_2 S_2. \qquad (57.9)$$

57.4.4 Measurement of Adaptable Flexibility

The adaptation of the adaptable flexibility can be expressed by the capability of information reconfiguration and the efficiency of local information circulation. Therefore, the adaptable flexibility can be measured according to the dynamic entropy, called changing entropy, and denoted by H_3. Larger the changing entropy is, lower the adaptable flexibility is. Otherwise, higher the adaptable flexibility is, more sensitive the organization is.

Defining the connection minimum of the two nodes i and j in the same layer as the horizontal connection length, denoted by F_{ij}, the microstate amount is $S_3 = \sum_{i=1}^{N} \sum_{j=1}^{N} F_{ij}$.

For F_{ij}, the number of the connections from i is called the initiative connection number, denoted by f_1, while the number of the first-step connections from i is called valid initiative connection number, denoted by f_2. And the number of the rest connections is called changing connection number, denoted by f_3. The realization probability of the changing microstate can be defined $p_3(ij) = f_3/S_3 = (f_1 - f_2)/S_3$.

The changing entropy of arbitrary two nodes i and j in the same layer satisfies the following form:

$$H_3(ij) = -p_3(ij) \log_2 p_3(ij). \qquad (57.10)$$

Therefore, the adaptable flexibility can be calculated by:

$$A = 1 - H_3/H_{3m,} \qquad (57.11)$$

where H_3 is the total changing entropy and satisfies the following form:

$$H_3 = \sum_{i=1}^{N} \sum_{j=1}^{N} H_3(ij), \qquad (57.12)$$

and H_{3m} is the maximum changing entropy and satisfies the following form:

$$H_{3m} = \log_2 S_3. \qquad (57.13)$$

57.5 Illustrative Example

On the basis of support system in our navy, the maintenance level of ship-based aircraft can be divided into three levels, which are depot level, intermediate level, and grassroots level. And the management system is performed hierarchically according to the jurisdiction and function of the organizations. The hierarchical structure shown in Fig. 57.2 is a typical frame of ship-based aircraft maintenance support organization, where the first layer is the depot-level support organization, including the maintenance support command department, maintenance depot, and so on. The second layer is the intermediate-level support organizations, including the maintenance shop, storage, branched support management department, and equipment storage. The third layer is the grass-roots level support organizations, including maintenance team, emergency team, spare parts store, and so on. According to the three-dimensional measurement method and calculation steps, the flexibility of the maintenance support organization shown in Fig. 57.2 can be measured.

The first step is calculating the timeliness of the organization, called responding speed to the external certainties. The results of connection length and microstate amount are shown in Table 57.2.

From Eqs. 57.2–57.5 and the results in Table 57.2, the amount of microstate is $S_1 = 24$. The total efficient entropy is $H_1 = 3.989$. And the maximum efficient entropy is $H_{1m} = 4.585$. Therefore, the responding speed is $T = 0.130$.

The second step is calculating the quality of the organization, called robust flexibility. The results of connection span and microstate amount are shown in Table 57.3.

From Eqs. 57.6–57.9 and the results in Table 57.3, the amount of microstate is $S_2 = 20$. The total quality entropy is $H_2 = 3.209$. And the maximum quality entropy is $H_{2m} = 4.322$. Therefore, the robust flexibility is $R = 0.258$.

The third step is calculating the adaptable flexibility. The results of connection length, changing connection amount, and microstate amount are shown in Table 57.4.

From Eqs. 57.10–57.13 and the results in Table 57.4, the microstate amount is $S_3 = 80$. The total changing entropy is $H_3 = 3.497$. The maximum changing entropy is $H_{3m} = 6.322$. Therefore, the adaptable flexibility is $A = 0.447$.

The fourth step is calculating the comprehensive flexibility. The weight values can be gained by combining the expert scoring method and entropy weight method [10]. The weight value of the responding speed, robust flexibility, and adaptable flexibility, respectively, is $\alpha = 0.329$, $\beta = 0.365$, and $\gamma = 0.306$. By the Eq. 57.1 and the results gained previous, the comprehensive measurement of flexibility is $F = \alpha T + \beta R + \gamma A = 0.274$.

The results above indicate that the alone or comprehensive flexibility of maintenance support organization shown in Fig. 57.2 is not enough. Therefore, an optimal organization structure shown in Fig. 57.3 is constructed based on the thought of flexible organization. In the optimal organization, the complexity is

Fig. 57.2 A typical
maintenance support
organization
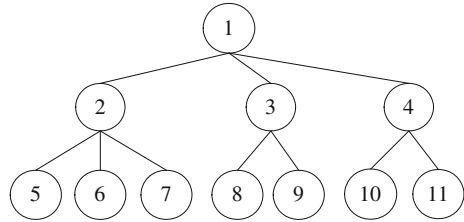
Table 57.2 Calculation of responding speed

L_{ij}	Nodes	Length amount	$P_1(ij)$	Microstate amount
1	1–2, 1–3, 1–4, 2–5, 2–6, 2–7, 3–8, 3–9, 4–10, 4–11	10	1/24	10
2	1–5, 1–6, 1–7, 1–8, 1–9, 1–10, 1–11	7	1/12	14

Table 57.3 Calculation of robust flexibility

k_i	Connection nodes	Nodes amount	$P_2(i)$	Microstate amount
1	5, 6, 7, 8, 9, 10, 11	7	1/20	7
3	1, 3, 4	3	3/20	9
4	2	1	1/5	4

Table 57.4 Calculation of adaptable flexibility

L_{ij}	f_3	Nodes	Connection amount	$P_3(ij)$	Microstate amount
2	1	2–3, 2–4, 3–4, 5–6, 5–7, 6–7, 8–9, 10–11	8	1/80	16
4	3	5–8, 5–9, 5–10, 5–11, 6–8, 6–9, 6–10, 6–11, 7–8, 7–9, 7–10, 7–11, 8–10, 8–11, 9–10, 9–11	16	3/80	64

Fig. 57.3 An optimal
organization structure
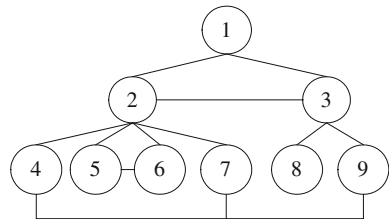
reduced, while the horizontal communication and cooperation of the nodes in the
same layer is enhanced.

According to the flexibility measurement method, the results of two organi-
zation structure, as shown in Figs. 57.2 and 57.3, are contrasted in Table 57.5.

Table 57.5 Contrast of flexibility measurement results for two organizations

Options	H_1	T	H_2	R	H_3	A	F
Organization in Fig. 57.2	3.989	0.130	3.209	0.258	3.497	0.447	0.247
Organization in Fig. 57.3	2.798	0.873	3.013	0.641	2.425	0.515	0.679

From the results in Table 57.5, the responding speed of the optimal organization in Fig. 57.3 increases from 0.130 to 0.873, the robust flexibility increases from 0.258 to 0.641. While the adaptable flexibility increases from 0.447 to 0.515, and comprehensive flexibility increases from 0.247 to 0.679. Consequently, the flexibility of the optimal ship-based aircraft maintenance support organization is exceeded to the prior.

57.6 Conclusion

Enhancing the flexibility of the ship-based aircraft maintenance support organization can shorten the maintenance time, reduce maintenance costs, and enhance the maintenance efficiency. Based on the analysis of the definition of flexibility, a multidimensional measurement model is the establishment of the ship-based aircraft maintenance support organization, so the comprehensive flexibility measurement is effectively analyzed. And the detailed calculation methods and steps are given. By contrasting the two organizations before and after being optimized, the results indicate that the flexibility of the optimal organization is superior to the original one apparently. At the same time, it points out a direction of optimizing the flexibility of organization structure, that is, on the premise of ensuring the management and coordination function of support command department, reducing the complexity, and strengthening the combination of horizontal interaction and vertical communication. Accordingly, sufficient flexibility will be possessed by the ship-based aircraft maintenance support organization.

References

1. Gebauer J, Lee F (2012) Enterprise system flexibility and implementation strategies: aligning theory with evidence from a case study. Inf Syst Manage 25:71–82
2. Jeffrey J, Mortensen DR (2011) Developing flexible command and control of airpower. Air Space Power J 25(1):53–63
3. Mcclaflin SW (2012) System provides flexible, realistic squad training. Infantry 101(2):41–43
4. Qi YB (2010) Research on supply chain flexibility evolution and the relationship between supply chain flexibility and performance (in Chinese). Jilin University, Jilin
5. Joseph OA, Sridharan R (2011) Analysis of dynamic due-date assignment models in a flexible manufacturing system. J Manuf Syst 30:28–40

6. Cheshmehgaz HR, Desa MI, Wibowo A (2013) A flexible three-level logistic network design considering cost and time criteria with a multi-objective evolutionary algorithm. J Intell Manuf 24(2):277–293
7. Huang MM (2007) Research on flexible resource constrained optimal scheduling problems (in Chinese). Wuhan University of Technology, Wuhan
8. Xu JH, Yang B, Chu X (2010) Application of structural entropy in aviation equipment support capability system of non-war military operations (in Chinese). Aviat Maintenance Eng 4:57–59
9. He XJ, Wu YY (2011) Analysis of supply chain system stability based on network structure entropy. In: International conference on mechatronic science, electric engineering and computer. Jilin, pp 1326–1330
10. Han H, Li JF, Sui H (2011) Research on multi-scheme supportability evaluation based on entropy weight TOPSIS method (in Chinese). Command Control Simul 33(3):61–64

Chapter 58
Lifetime Prediction Based on Degradation Data Analysis with a Change Point

Haowei Wang, Tingxue Xu and Jikun Yang

Abstract To predict the lifetime based on degradation data analysis has been widely studied. The accuracy of lifetime prediction largely depends on whether the degradation model is appropriate or not. For some products, there is a change point in the degradation process, and the entire degradation process can be divided into two phases by the change point. Motivated by an example of resistors, we studied the difference of several modeling approaches with nonlinear gamma and wiener process. The result indicated that modeling the process after the change point obtained more reasonable estimations in the example.

Keywords Lifetime prediction · Degradation model · Changepoint

58.1 Introduction

With the development of engineering and science technology, more and more products with long lifetime and high reliability have emerged. Lifetime prediction based on degradation data analysis is a dramatic method to obtain the lifetime information, which can provide valuable guideline for preventive maintenance [1]. The accuracy of lifetime prediction largely depends on whether the degradation

H. Wang (✉) · J. Yang
Department of Graduate Students' Brigade, NAAU,
Yantai, 264001 Shandong, China
e-mail: 13583533630@139.com

T. Xu
Department of Ordnance Science and Technology, NAAU,
Yantai, 264001 Shandong, China

model is appropriate or not. For some products, there may be more than one degradation processes subsequently in their lifetimes, for example, the Carbon-film resistors may undergo a sharp degradation process before reaching a stably increasing degradation process [2]. From a practical view, modeling the stably increasing degradation process can more precisely predict the lifetime than that of modeling the entire degradation process. Motivated by the degradation data of the Carbon-film resistors, we focused on studying the difference of the two modeling approaches by comparing their prediction results.

Gamma process and Wiener process are two well known stochastic processes and have been widely applied in the field of degradation process modeling [3–7]. We adopted the two stochastic processes to model the degradation data.

58.2 Models

58.2.1 Gamma Process

Unlike the wiener process, a gamma process is specified to model the degradation data which is strictly increasing. A gamma process $Y(t)$ has independent, nonnegative increment $\Delta Y(t)$ that follows a gamma distribution as $\Delta Y(t) \sim \text{Ga}(\alpha \cdot \Delta\Lambda(t), \beta)$ here $\Delta\Lambda(t) = \Lambda(t + \Delta t) - \Lambda(t)$, β is a constant scale parameter and α is a shape parameter. According to the additivity of the gamma distribution, it can be deduced that $Y(t)$ follows the distribution $\text{Ga}(\alpha \cdot \Lambda(t), \beta)$. The probability density function (pdf) of $Y(t)$ is expressed as

$$f_g(Y; \alpha\Lambda(t), \beta) = \frac{\beta^{\alpha \cdot \Lambda(t)}}{\Gamma(\alpha \cdot \Lambda(t))} Y^{\alpha\Lambda(t)-1} \exp(-Y\beta). \tag{58.1}$$

Let ξ be the first passage time of the $Y(t)$ to the failure threshold l, then the reliability function of $Y(t)$ can be given by

$$P(\xi > t) = P(Y(t) < l) = \int_0^l \frac{\beta^{\alpha \cdot \Lambda(t)}}{\Gamma(\alpha \cdot \Lambda(t))} Y^{\alpha \cdot \Lambda(t)-1} \exp(-Y\beta)$$
$$= \frac{\int_0^{l_\beta} y^{\alpha \cdot \Lambda(t)-1} \exp(-y)\,\mathrm{d}y}{\Gamma(\alpha \cdot \Lambda(t))} \tag{58.2}$$

where $l_\beta = l \cdot \beta$, $y = Y \cdot \beta$. Substitute the incomplete gamma function $\Gamma(a, z) = \int_z^\infty y^{a-1} \exp(-y)\mathrm{d}y$ into (58.2) the cumulative distribution function (cdf) of ξ be obtained as

$$F(t) = \frac{\Gamma(\alpha \cdot \Delta\Lambda(t), l_\beta)}{\Gamma(\alpha \cdot \Delta\Lambda(t))}. \tag{58.3}$$

With (58.3), the exact pdf of ξ for a gamma process can be derived, but the exact pdf is too complex to practical applications. For mathematical convenience, Park and Padgett provided an approach that the pdf of ξ can be approximated by a form of the Birnbaum–Saunders (BS) distribution. And when the gamma process is non-stationary, the BS distribution can also be obtained by a time transformation as $z = \Lambda(\xi)$,

$$f_{BS}(z) = \frac{1}{2\sqrt{2}ab}\left[\left(\frac{b}{z}\right)^{1/2} + \left(\frac{b}{z}\right)^{3/2}\right]\exp\left[-\frac{(b-z)^2}{2a^2bz}\right], \tag{58.4}$$

where $a = 1/\sqrt{l_\beta}$ and $b = l_\beta/\alpha$. The expression of the mean lifetime can be deduced from (58.4) as $\hat{\xi}_{BS} = \Lambda^{-1}(\hat{z}) = \Lambda^{-1}((l \cdot \beta + 0.5)/\alpha)$.

58.2.2 Wiener Process

To be capable of modeling the nonlinear degradation process, the extensions of wiener process have been prevailingly studied. Let $\Lambda(t)$ be a monotonically increasing function of time t and $\Lambda(0) = 0$. Then, the non-homogeneous wiener process $X(t)$ can be written as

$$X(t) = \mu \cdot \Lambda(t) + \sigma \cdot B(\Lambda(t)), \tag{58.5}$$

where $B(\cdot)$ is the standard Brownian motion, denoted as $B(t) \sim N(0, t)$, μ is the drift parameter and σ is the diffusion parameter. It is well known that the degradation increment follows a normal distribution as the following form $\Delta X(t) \sim N(\mu \cdot \Delta\Lambda(t), \sigma^2 \cdot \Delta\Lambda(t))$, where $\Delta\Lambda(t) = \Lambda(t + \Delta t) - \Lambda(t)$. Let constant value l be the failure threshold, the lifetime ξ is equal to the time when $X(t)$ firstly reaches the failure threshold. So, the lifetime ξ of product can be described as $\xi = \inf\{X(t) \geq l\}$.

For a Wiener process, it is well known that the first passage time z follows an inverse Gaussian distribution, where $z = \Lambda(\xi)$. The pdf of z is

$$f_w(z; \mu, \sigma, l) = \frac{l}{\sqrt{2\pi\sigma^2 z^3}}\exp\left[-\frac{(l - \mu z)^2}{2\sigma^2 z}\right]. \tag{58.6}$$

Substituting $z = \Lambda(\xi)$ into (58.6), the pdf of ξ can be obtained.

58.2.3 Reaction Rate Model

To predict the lifetime of a product from accelerated degradation data, the relationship between the acceleration variables (e.g., use rate, temperature, voltage, or pressure) and the parameters of degradation model must be established so that the

values of the parameters at normal use stress level can be extrapolated. Reaction rate model, such as power law model, Arrhenius model, is the mathematical expression of the relationship. However, which of the parameters depends on acceleration variables and which is irrelevant to acceleration variables are required to determine. There were widely acceptable assumptions on the relationship between parameters and acceleration variables [8]. As far as a gamma degradation model, the assumption is that the shape parameter α is a function of acceleration variables, while the scale parameter β is irrelevant to acceleration variables. For a wiener degradation model, it is assumed that the drift parameter μ is a function of acceleration variables, while the diffusion parameter α is irrelevant to acceleration variables. Suppose that the acceleration variable is temperature T_i and the function of acceleration variables $\varphi(T_i)$ is the Arrhenius reaction rate model, then for a gamma degradation model

$$\alpha(T_i) = \exp(\gamma_1 - \gamma_2/T_i), \quad \beta(T_i) = \beta \tag{58.7}$$

and for a wiener degradation model

$$\mu(T_i) = \exp(\gamma_3 - \gamma_4/T_i), \quad \sigma(T_i) = \sigma \tag{58.8}$$

where γ_1, γ_2, γ_3, γ_4 are positive coefficients.

58.3 Parameters Estimation

In order to apply the degradation models to practical examples, statistical methods for the parameters estimation are required. We obtained the estimations of parameters by maximum likelihood estimation method. Suppose that constant stress accelerated degradation test is carried out to obtain degradation data. Let T_0 be the normal use stress level, T_k be the kth accelerated stress level, y_{ijk} be the ith measurement of the jth sample at the kth accelerated stress level, t_{ijk} be the ith measuring time of the jth sample at the kth accelerated stress level, $\Delta y_{ijk} = y_{ijk} - y_{(i-1)jk}$ be the degradation increment, where $i = 1, 2, \ldots, n_1; j = 1, 2, \ldots, n_2; k = 1, 2, \ldots, n_3$.

For a gamma degradation model, the degradation increment follows a gamma distribution as $\Delta y_{ijk} \sim \mathrm{Ga}\big(\exp(\gamma_1 + \gamma_2/T_k) \cdot \Delta\Lambda(t_{ijk}), \beta\big)$ and the likelihood function synthesizing all the observed data is

$$
\begin{aligned}
L(\gamma_1, \gamma_2, \beta) = \prod_{i=1}^{n_1} \prod_{j=1}^{n_2} \prod_{k=1}^{n_3} & \frac{\beta^{\exp(\gamma_1 - \gamma_2/T_k) \cdot \Delta\Lambda(t_{ijk})}}{\Gamma(\exp(\gamma_1 - \gamma_2/T_k) \cdot \Delta\Lambda(t_{ijk}))} \\
& \cdot \Delta y_{ijk}^{\exp(\gamma_1 - \gamma_2/T_k) \cdot \Delta\Lambda(t_{ijk}) - 1} \cdot \exp\big(-\Delta y_{ijk}\beta\big).
\end{aligned}
\tag{58.9}
$$

For a wiener degradation model, there is a relationship as $\Delta y_{ijk} \sim N\big(\exp(\gamma_3 + \gamma_4/T_k) \cdot \Delta\Lambda(t_{ijk}), \exp(\gamma_5 + \gamma_4/T_k) \cdot \Delta\Lambda(t_{ijk})\big)$ and the likelihood function synthesizing all the observed data is

$$L(\gamma_3, \gamma_4, \gamma_5) = \prod_{i=1}^{n_1}\prod_{j=1}^{n_2}\prod_{k=1}^{n_3} \frac{1}{\sqrt{2\pi \exp(\gamma_5 + \gamma_4/T_k) \cdot \Delta\Lambda(t_{ijk})}}$$
$$\cdot \exp\left[-\frac{\big(\Delta y_{ijk} - \exp(\gamma_3 + \gamma_4/T_k) \cdot \Delta\Lambda(t_{ijk})\big)^2}{2\exp(\gamma_5 + \gamma_4/T_k) \cdot \Delta\Lambda(t_{ijk})} \right]. \tag{58.10}$$

As described in [3], empirical studies show that the expected deterioration of $y(t)$ is often proportional to a power law. Thus, the $\Lambda(t)$ can be expressed as $\Lambda(t) = t^c$ where c is a positive coefficient. Besides, an exponential time transformation was found in the literature [9], expressed as $z = \Lambda(t) = 1 - \exp(-d \cdot t^\lambda)$ where d, λ are positive coefficients. We specified $\lambda = 0.5$ as Carey and Koenig [10] did. The unknown coefficients can be estimated by substituting $\Lambda(t)$ into (58.9) and (58.10), respectively.

To evaluate the goodness-of-fit of the degradation models, the Akaike information criterion (AIC) was adopted as the measure of comparing different models. The AIC statistics is calculated as

$$\mathrm{AIC} = -2 \times (\max \ell) + 2m. \tag{58.11}$$

where m is the number of estimated model parameters and max ℓ is the maximized log-likelihood. When there are several candidate models, the one with the smallest AIC can be considered as the best-fitting model.

58.4 Example Analysis

Shiomi and Yanagisawa obtained the accelerated degradation data of Carbon-film resistors, which is also explicitly given in Table C.3 by Meeker and Escobar. There were total 29 resistors in a constant stress ADT, where 9 samples were observed at 83 °C, 10 samples were observed at 133 °C, and the rest 10 sample were observed at 173 °C. All the samples were simultaneously observed every time at $t_0 = 0$, $t_1 = 0.452$, $t_2 = 1.03$, $t_3 = 4.341$ and $t_4 = 8.084$ (in 1,000 h). It was assumed that the normal use temperature was 50 °C and the threshold value for percent increase in resistance was $l = 5$. The sample numbered 27 was omitted in our example, because its degradation data is not strictly increasing and the gamma process is expected to model the degradation data.

To illustrate the degradation path of resistors, the degradation data was plotted in Fig. 58.1. It can be seen that the resistances of the samples at three different stress levels uniformly show a sudden augment at the beginning of the ADT, and then reach a stably increasing process. We assumed that there was a change point
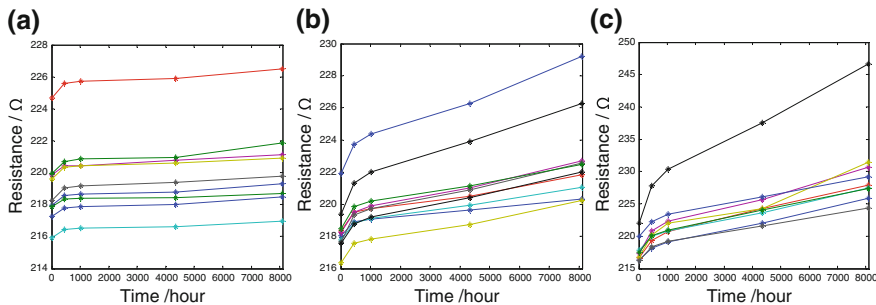
Fig. 58.1 The degradation data of resistors at (**a** 83 °C, **b** 133 °C, **c** 173 °C)

Table 58.1 The estimations of the models no. 1–8 with AICs

Case	Models	$\Lambda(t)$	Estimations				AIC
			$\gamma_1(\gamma_3)$	$\gamma_2(\gamma_4)$	$\beta(\sigma)$	$c(d)$	
1	Gamma	t^c	10.642	3,642.020	6.025	0.466	9.782
2	Gamma	$1 - \exp(-d \cdot t)$	10.451	3,334.277	3.111	0.200	109.987
3	Wiener	t^c	10.377	4,375.421	0.236	0.551	127.355
4	Wiener	$1 - \exp(-d \cdot t)$	11.748	4,276.306	1.999	0.201	202.367
5	Gamma	t^c	11.134	4,124.156	7.806	0.793	−17.322
6	Gamma	$1 - \exp(-d \cdot t)$	14.483	4,093.253	7.833	0.022	−10.794
7	Wiener	t^c	10.571	4,860.741	0.085	0.887	76.951
8	Wiener	$1 - \exp(-d \cdot t)$	14.582	4,771.589	5.010	0.015	79.389

that separates the entire degradation process into two different phases. Because the change points were far from the failure threshold, the former phase had little effect on the result of lifetime prediction. It may be more appropriate to model the latter phase than the entire degradation process. In the example, the change point is approximate near the time t_1, and the time span between t_1 and t_4 can be considered as the stably increasing phase. For simplification, 8 modeling approaches were denoted as case 1 to case 8. Note that the case 1 to the case 4 used all the degradation data and the case 5 to the case 8 used the degradation data at t_1 to t_4. All the estimations were obtained as in Table 58.1.

From the AICs of Table 58.1, it can be concluded that a gamma process with $\Lambda(t) = t^c$ modeled the degradation data best. Thus, we adopted the estimations of case 1 and case 5 to predict the lifetime of the resistor at 50 °C. In case 1, the estimations of the shape parameter were computed as $\alpha_0 = 0.534$, the mean of lifetime can be obtained as $\hat{\xi}_{BS} = 5.991 \times 10^6$ h. However, we obtained $\alpha_0 = 0.196$ and $\hat{\xi}_{BS} = 8.015 \times 10^5$ h in case 5. It can be seen that the estimation of lifetime in case 1 is much bigger than that in case 5. The estimation in case 5 is more reasonable from the engineering experience and industrial knowledge. The pdf curve, the reliability curve, and the mean lifetime curve of the resistor deduced from case 1 to case 5 are illustrated in Figs. 58.2 and 58.3, respectively.
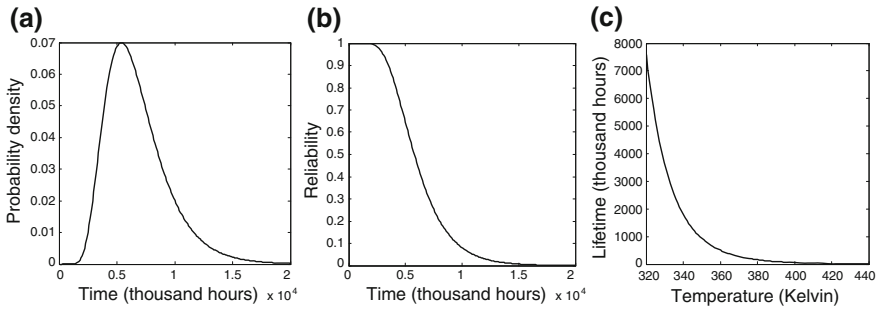
Fig. 58.2 The predictions from case 1 (**a** pdf, **b** reliability curve, **c** mean lifetime curve)
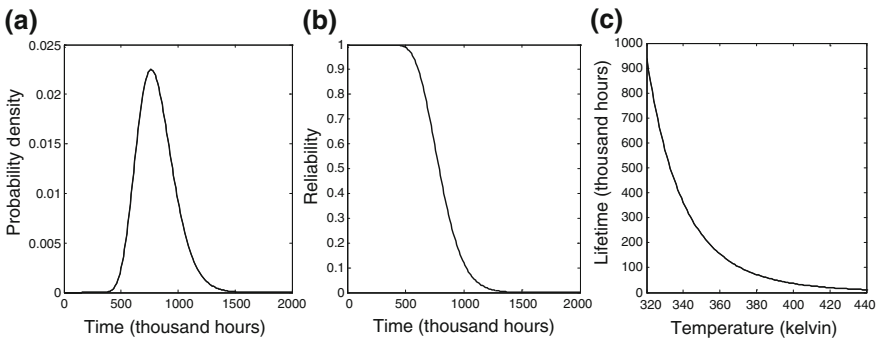
Fig. 58.3 The predictions from case 5 (**a** pdf, **b** reliability curve, **c** mean lifetime curve)

58.5 Summary

When there is a change point in the degradation process, modeling the process after the change point may be more reasonable than modeling the entire degradation process because the process after the change point reaches a stable degradation phase.

References

1. Xia X (2012) Forecasting method for product reliability along with performance data. J Fail Anal Prev 12:532–540 (in Chinese)
2. Meeker WQ, Escobar A (1998) Statistical methods for reliability data. Wiley, New York
3. van Noortwijk JM (2009) A survey of the application of gamma processes in maintenance. Reliab Eng Syst Safety 94:2–21
4. Wang X (2010) Wiener processes with random effects for degradation data. J Multivar Anal 101:340–351 (in Chinese)
5. Padgett WJ, Tomlinson MA (2004) Inference from accelerated degradation and failure data based on Gaussian Process Models. Lifetime Data Anal 10:191–206

6. Lawless JF, Crowder MJ (2004) Covariates and random effects in a Gamma Process Model with application to degradation and failure. Lifetime Data Anal 10:213–227
7. Escobar LA, Meeker WQ (2006) A review of accelerated test models. Stat Sci 552–577
8. Park C, Padgett WJ (2005) Accelerated degradation models for failure based on Geometric Brownian Motion and Gamma Processes. Lifetime Data Anal 11:511–527
9. Whitmore GA, Schenkelberg F (1996) Modelling accelerated degradation data using Wiener Diffusion with a time scale transformation. Lifetime Data Anal 3:27–45
10. Carey MB, Koening RH (1991) Reliability assessment based on accelerated degradation: a case study. IEEE Trans Reliab 40:499–606

Chapter 59
Maintenance and Support Management for Type Certification Flight Test of Large Civil Aircraft

Kang Feng and Xiping Zhang

Abstract Based on the flight test support characteristics of large civil aircraft, this paper summarizes and analyzes the research results and practical experiences of maintenance and support management of ARJ21-700 aircraft during its type certification flight test stage. These management experiences ensure the quality, safety, and efficiency of flight test; aiming at the problems occured during flight test support, this article presents some suggestions and advices for flight test integrated support to further integrate flight test support resources, improve flight test support efficiency, reduce the risk caused by human errors, promote type certification flight test of ARJ21-700 aircraft, and provide references for flight test maintenance and support of C919 large passenger aircraft and other civil aircraft.

Key Words Civil aircraft · Flight test · Maintenance and support management

59.1 Introduction

Chinese civil aviation industry has entered rapid development stage, the type certification flight test of ARJ21-700 aircraft is near the end, and C919 large passenger aircraft is being developed. The flight tests of civil aircraft consist of applicant R&D flight test and type certification flight directed by the authority. ARJ21-700 is China's first civil aircraft to conduct type certification flight test fully in accordance with airworthiness documents (such as CCAR-25), and the flight test process is very complicated and strict. Therefore, during the flight test of ARJ21-700 aircraft, maintenance, and support management not only the guarantees for quality and safety of the flight test, but also plays an important role in certification.

K. Feng (✉) · X. Zhang
73 P Box, Xi'an, China
e-mail: huangbingyin@163.com

59.2 Flight Test Maintenance and Support Environmental Characteristics of Civil Aircraft

There are big differences between maintenance environment and management environment for initial airworthiness and course operation of civil aircraft, and these bring new challenges to maintenance and support activities.

59.2.1 Low Technical Maturity of Aircraft and Systems

With the adoption of a great deal of new technologies and new products, the characteristics of the new developed test prototype are highly complicated system technology, high level of integration, but low technical maturity. Thus, during flight test, a lot of design technology defects and problems of manufacturing technologies and quality are constantly exposed.

59.2.2 Complex Technology and High Risk of Flight Test Subject

CCAR-25 has proposed strict check requirements for all systems of test prototype, all functional and performance indexes of aircraft should be verified, the limit flight of test prototype should be assessed, and a lot of different ground tests should be conducted, but many test items have very high risk, such as natural icing test, high crosswind test, minimum control speed test, and flutter test.

59.2.3 Complex and Changeable Aircraft Configuration

In order to meet the requirements of different flight test subjects, the configurations of test prototypes are quite different, and due to the different flight test tasks, the factory configuration condition between each aircraft has big differences; at the same time, each test prototype needs to be modified based on test mission progress to guarantee testing requirements of flight test. For the avionic system of ARJ21-700 aircraft, its software version has experienced nine upgrades during flight tests. With the exposure of design defects, a lot of trouble shootings, engineering changes, and upgrades of software occured, the aircraft configuration becomes complex and changeable.

59.2.4 Incomplete Maintenance and Support Resources

During flight test stage of the aircraft, all kinds of publications were quite incomplete, the integrity and correctness of the contents should be perfected through verification of flight test, and the guidance effect was low; the ground support equipment was incomplete, many equipment had defects, and some general tools could not meet the requirements of special tasks; the support of spare parts involves many suppliers both at home and in aboard, so some spare parts cannot be supplied in time.

59.2.5 Different Maintenance Environment for Multi-area Flight Tests

The test prototype is required to do flight test under various special environmental conditions around the country, such as high temperature and humidity, high cold, high crosswind, natural icing flight tests, and the functional and reliability flight test involves multi-area, multi-airspace, and multi-course flight tests.

59.3 Flight Test Maintenance and Support Management Characteristics of Civil Aircraft

The flight test maintenance and support environmental characteristics of civil aircraft present new challenges to maintenance management and higher requirements to maintenance and support personnel. In the maintenance and support of ARJ21-700 aircraft, based on the flight test maintenance and support environmental characteristics of civil aircraft, the flight test unit drew on flight test experiences of military aircraft, launched the exploration and research on maintenance and support management of civil aircraft and made positive progresses.

59.3.1 Flight Test Maintenance and Support Mode of Civil Aircraft

The integrated analysis and selection of maintenance system are based on maintenance objective, mission, and environment. The characteristics of new technology, the unfixed status, and complex and changeable flight test subjects determine differences between the maintenance and support mode during flight test and airline operation.

During the flight test initial stages of ARJ21-700 aircraft, by drawing on the success experiences of military aircraft flight test support, two elite and high-efficiency maintenance group and management group were established. The maintenance group, with maintenance team as the core, is divided into three subjects: mechanical, electrical and avionics, and responsible for flight support, daily maintenance, periodic check, troubleshooting, information acquisition, and evaluation and check tasks. The core maintenance personnel are relatively fixed, other maintenance personnel can be flexibly deployed, and the advantages of this arrangement are as follows: the maintenance personnel will become highly skilled technical experts and are familiar with the technical status. A management and support group is responsible for technical, quality, plan and dispatch, and equipment support, and plays a role in document preparation, supervision and control, and support and coordination.

This maintenance and support mode promotes the integration of flight test management systems of civil aircraft and military aircraft, and especially, it has a positive significance in allocation of maintenance and support resources, personnel training and control of quality and safety.

59.3.2 Technical Management of Maintenance and Support

ARJ21-700 aircraft adopts a great deal of new technologies, processes, and equipment, but the design and maintenance technical document is far from perfect; therefore, the strengthening of technical management becomes especially important.

59.3.2.1 Preparation of Maintenance and Operation Document

Due to the preparation lag of part of the design initial maintenance document and design personnel are lack of outfield maintenance and support experiences, the initial maintenance document is lack of some contents, inaccuracy, or poor operability, consequently the maintenance group must deeply analyze the design initial maintenance document, and combine with maintenance practical experiences to conduct maintenance process, safety analysis, and revise the maintenance job file to form maintenance operation sheet.

59.3.2.2 Research on Failure Law

In view of hundreds of times software and hardware failures happened during flight tests, the maintenance group launched a maintenance method research based on failure cases, and prepared troubleshooting instruction manuals by analyzing failure causes, summarizing failure law and troubleshooting experiences; established failure

information bank, launched systematic failure statistic analysis, from this foundation, some methods suited flight test outfield were established, such as failure quick-isolation, software defect positioning and data general interpretation; and launched failure effects and hazardous analysis, maintenance safety analysis and optimize work contents and workflow to improve the flight test efficiency.

59.3.3 Maintenance and Support Quality and Safety Management

Quality and safety are always the core of maintenance and support management for maintenance crew. The maintenance department focuses the following three aspects to launch quality and safety management during flight test of ARJ21-700 aircraft.

59.3.3.1 Implementation of Detailed Configuration Management

During flight test of civil aircraft, the aircraft baseline has not determined, and different flight test stages have different baselines. The instrumentation and modification of flight test prototype are required according to different flight test missions and stages, and thus, the aircraft design baseline is changed; therefore, the configuration management in flight test stage is much more complicated. The maintenance department established strict control system and control flow to ensure the control of the configuration according to each configuration management item.

The hold of configuration is controlled and managed according to design technical document. The installation, failure, exchangeable parts, life cycle, and maintenance period of the product are especially controlled. During flight test, the design department needs to issue software and hardware technical changes of hundreds technical status, or issue temporary operation limitation, although the technical changes are usually implemented by development unit, but the maintenance department must strictly supervise, corporate with design department to implement, conduct onboard check and test to ensure their proper implementation.

The configuration status of flight test mission is controlled according to flight test documents, including modification status of aircraft, and installation of a great deal of instrumentation sensors. Different flight test missions have different flight test configurations, and the maintenance department should strictly implement mission configuration control according to flight test mission sheet.

The hold of configuration is controlled and managed according to failure influences. During flight test of civil aircraft, the minimum flight permission list has not established, many failures cannot be eliminated temporarily, and mission flight or air failure flight test verification is required, so the maintenance department must conduct failure influence analysis and risk evaluation, and control it according to the strict approval procedure.

59.3.3.2 Maintenance Quality Management

Under the guidance of quality system of flight test facility, the maintenance department has established strict maintenance job quality control system, which includes the preparation and approval system of maintenance job card, quality recheck and inspection system, aircraft maintenance quality on-site examination system, major maintenance activity and maintenance quality evaluation system and quality reward and punishment system. The establishment of these systems has improved the maintenance quality.

59.3.3.3 Safety and Risk Management

During flight test of ARJ21-700 aircraft, a risk management team has been established by maintenance department to launch maintenance and support safety and risk management.

This team organizes relative personnel to analyze all the maintenance activities during maintenance crew preparation before and after flight, ground test, periodic maintenance, disassembly and assembly transportation, looks for hazard source and does analysis and evaluation, and determines the risk level according to risk matrix and establishes risk countermeasures.

There are many risk test subjects during flight test, and the maintenance department launches risk analysis and formulates check contents and requirements of risk subjects and emergency plan. In view of the significant changes in maintenance activity, for example, the civil aircraft is required to do flight test at special environmental condition (such as high plateau, high cold, natural icing, high temperature and humidity, and high crosswind), the maintenance and support condition should be changed according to different test environmental conditions; therefore, the maintenance department needs to launch special investigation and risk evaluation and formulate corresponding safe work system.

59.4 Suggestion on Improvement of Civil Aircraft Flight Test Maintenance and Support

After more than four years of explorations and practices since August 2013, the flight test support team has already safely guaranteed 4,000 h of flights, successfully completed a series of risk subjects, and gradually established and perfected the flight test maintenance and support system of civil aircraft, but there are still some links that restrict the maintenance and support efficiency that need to be further improved.

59.4.1 Further Establishment of General Flight Test Support Concept

For the large civil aircraft, the information integration level is higher, the cross-link of each system is much more, and the safety, comfort, and economy requirements for that are higher. Take ARJ21-700 as an example, as the advanced commercial aircraft abroad, the system integration level is high, the avionic, flight control, engine, and landing gear systems can be functionally cross-linked, and the flight management, performance optimizing, and integrated control can be realized; the signal source is maximally shared between systems, and bus technology is adopted in data exchange between systems. Therefore, an integrated support concept must be established, and communication and coordination, information share, and resource allocation with each test participating unit should be strengthened.

59.4.1.1 Need for Shortening Flight Test Period and Reducing Flight Test Cost

The maintenance cost for initial airworthiness is much larger than that of continuous airworthiness for large civil aircraft, but at the same time, it also has much bigger adjustable space. Applying the integrated flight support concept to reasonably arrange flight test mission will not only satisfy the flight test requirements in initial airworthiness, but also improve the efficiency and reduce flight test cost.

Take the jacking up of ARJ21-700 aircraft as an example, Table 59.1 presents the support resources related to the jacking up of ARJ21-700 aircraft. Generally, before the jacking up of the aircraft, basically a plenty of fuel is in fuel tanks and must be fully defueled. Estimate that there is 4 tons of residual fuel in fuel tanks before each jack-up (the full load fuel of ARJ21-700 aircraft is 10 tons), and according to "Circular on the Raise of Aviation Oil Factory Price by National Development and Reform Commission" issued on December 12, 2012, the price of 3# aviation oil is 5,990 RMB/ton, so the loss of fuel for each jacking up of aircraft is up to 23,960 RMB; the total man-hours of maintenance personnel are about 30 h * person; now there is four test prototypes in flight test center, but only two special hangers, and some support resources, such as power supply truck, towing vehicle, and fuel and defuel truck, are in short supply.

In a word, jacking up of the aircraft takes time, energy, and money. During the work arrangement, if consult information from different test participants, use integrated support method, and strive to do work which needs twice or multiple jacking at the same time, or arrange tests related with engine or APU power-on before jack-up of the aircraft, and consume some fuel, in that case, the flight test cost can be greatly reduced and support efficiency can be significantly raised.

Table 59.1 Support resources related to jacking up of ARJ21-700 aircraft

Item	Vehicle	Maintenance	Location	Equipment	Man-hours
Quantity	One defueling truck, one power supply truck, and one towing vehicle	10 persons	Hangar	4 jacks	3 h

59.4.1.2 The Need for Integration of Flight Test Resource and Reduction of Error

There are many repetitive works in flight test support, if apply a integrated support idea to systematic plan the work, the flight test resources can be intensively used, and working period can be greatly shortened. For example, many functional tests related to dynamic/static pressure need KTS-2000 digital air data test instrumentation, and it takes more than 1 h to connect the KTS-2000 test instrumentation to airtightness check equipment, and the hangar will be occupied, so if some functional tests related to air data can be done in an integrated manner, a lot of time and support resources can be saved.

The human error prevention research shows that during the operation of simple and repetitive mission, the frequency of human error is about 1/100–1/1,000. That is to say, during the monotonic, simple and repetitive operational and technical work, one big or small mistake might be happen in every 100–1,000 operations, and this can be regarded as an innate error constant of human. In this sense, the risk of human error will be reduced with each decrease in repetitive work.

59.4.2 Strengthen the Construction of Flight Test Maintenance and Support Information Platform

Flight test maintenance and support is a systematic engineering, involves the personnel and resources in various aspects, including design, instrumentation and modification, test, engineering, maintenance, and ground support. Without a high efficient information exchange platform, the maintenance and support management will be deep in water.

Practices show that many unavailing works are caused by low efficient communication and coordination. During the early days of flight test of ARJ21-700 aircraft, some confused situation has occurred, some maintenance personnel even did not know their recent work plan, and the material, equipment, and personnel were always allocated and dispatched in working field. The best work time was often missed until the working condition was ready, and the maintenance personnel need to work overtime to complete the mission. In some situation, a key condition was found that it could not meet the requirements even at the last minute, and as a result, the work could not launch and all the previous efforts were wasted. Therefore, a flight test information platform must be established and

perfected. This platform should be based on computer network to build the flight test support information database. In addition to a detailed record of state parameters, such as aircraft maintenance record and different kinds of limitation conditions, this database also needs to integrate with other information involving design, modification, instrumentation, engineering, maintenance, and ground support to form an effective feedback loop.

The flight test support information database is the health record of aircraft, and through it, all test participants can clearly understand the current state of the aircraft and judge from this to properly arrange the mission process; the dispatching part can optimize and integrate the current support plan and even introduce intelligent analysis software to make overall plans. In this way, the repetitive aircraft jack-up problems mentioned above can be clearly improved. The work for test participants will be more proper organized and planned, and the operating efficiency will be significantly enhanced.

59.4.3 Advance the Reform on Professional Competency Division of Maintenance Personnel

Now, the maintenance subjects of ARJ21-700 can be divided into three subjects: mechanical, special equipment, and avionic, and this follows the military subject set mode, and during the initial state of flight test, this mode realizes the buffering and transition of flight test support resources of military and civil aircraft, but from a long-term perspective, the reform of professional competency division is inevitable.

For the large civil aircraft, the high integration and interconnection of avionic information make the contradiction among three subjects more distinct in maintenance and support. The initial airworthiness and continuous airworthiness have different maintenance items and propose different requirements for skill and quality of maintenance personnel. During the initial airworthiness stage, the maintenance personnel need to face many unknown failures, corporate with others to complete more tests, check and maintain more equipment and instrument, and should have a wide range of knowledge, so the workload is very heavy. In the current support mode, the subjects are divided too precise, so technical personnel master singular skill and have relative obscure understanding of cross-link area between avionic system and other systems and lead to some latent defects and work obstacles.

For example, in April 2010, the ISI display could not simulate air state when integrated spare instrument (ISI) functional test was conducted on ARJ21-700 A/C 103. ISI was maintained by special equipment subject, and the maintenance personnel of special equipment subject carefully checked the baffle and line connection for many times, but still could not eliminate the failure, and then, they exchanged the ISI of A/C 101–A/C 103, but the failure still existed. The design personnel checked the lines and found that the CVR (sound recorder) of A/C 103

has already removed, and CVR and ISI share a common air–ground signal, the air–ground signal of ISI is transmitted from CVR, but the CVR has not installed; as a result, the failure that air–ground simulation could not be transformed naturally happened, and at last, the CVR was reinstalled in the aircraft and the failure was eliminated. It costs one precious day to eliminate the failure. In this case, ISI belongs to special equipment subject, and CVR belongs to avionic subject, but for the common cross-link air–ground signal, the personnel of two subjects were not clear; consequently, this failure occurred and affected the work progress.

From an integrated support angel, in order to improve the support efficiency and resultant force of maintenance personnel in initial airworthiness of civil aircraft, neither the support mode of military aircraft nor the support mode of civil aircraft in continuous airworthiness state cannot be mechanically applied, by drawing on the reform experiences, the authors suggest that the work of special equipment subject can be divided and merged into mechanical subject and avionic subject, and the name mechanical subject is changed as electromechanical subject. The new established electromechanical subject and avionic subject should be further integrated, and for the basic and cross-link work, such as power supply out of aircraft, should be mastered by personnel of two subjects.

Through the integration of subject and integration of maintenance personnel resources, the work time pressure for maintenance personnel is reduced; the interconnections among many subjects are integrated within the subject, from the human error prevention angle, that is, the number of saw-tooth in "SHEL" model is reduced, and the human error risk is significantly decreased.

59.4.4 Reliability-centered Maintenance Theory

The reliability-centered maintenance (RCM) is established based on the design characteristics, operating function, failure mode, and consequence analysis of the equipment, and the biggest characteristic of this theory is that it proceeds from the severe degree of failure effect, strives to avoid or reduce failure consequences, and changes traditional concept preventing the failure itself according to the technical characteristics of failures.

During the initial airworthiness stage, maintenance department and development department can collaborate effectively through integrated flight test support platform, and much information in integrated flight test support database can become the important data resource for preventative maintenance. Under the support of integrated flight test support database, through the reliability-centered maintenance analysis, the maintenance plan is further optimized to provide references for periodic maintenance and on-condition maintenance, to reduce the excessive maintenance and improve integrated flight test maintenance efficiency.
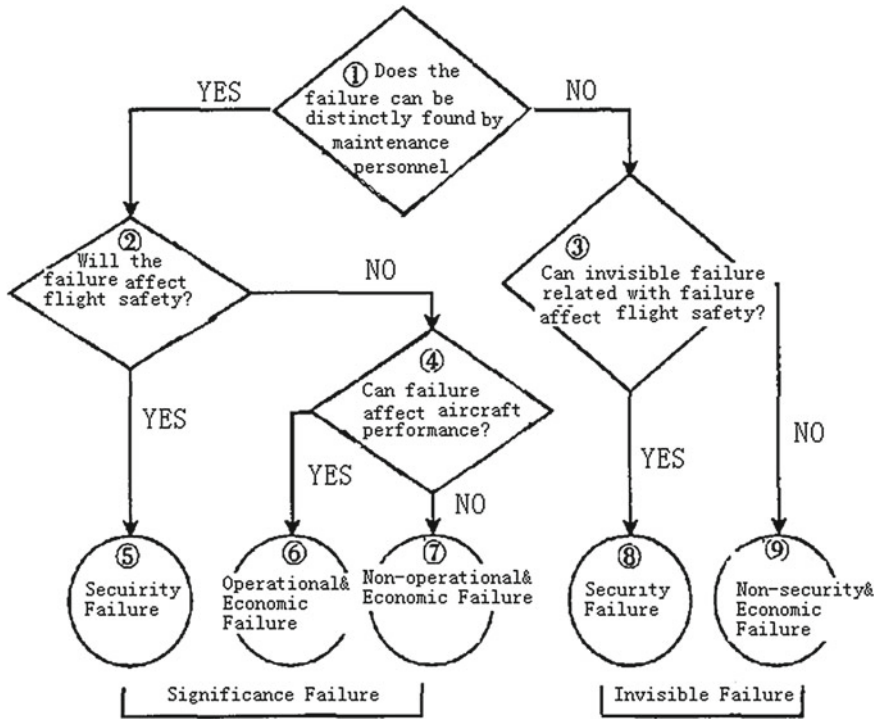
RCM Flow

59.5 Conclusion

Developing large aircraft is China's strategic decision and "state will," and our country has already poured enormous manpower and material resources, through these years' efforts, and China has already established type certification flight test maintenance and support management system of large civil aircraft, but compared with airworthiness requirements (such as CCAR-25), there are still many new methods and new technologies needing to be dug and discovered in the civil aircraft type certification flight test maintenance and support area.

It is believed that the type certification flight test maintenance and support management level for China's civil aircraft will certainly be improved through continuous accumulation and innovation, and these efforts will not only create conditions for scientific research flight test and airworthiness certification of ARJ21-700 aircraft, but also provide references for flight test maintenance and support of C919 large passenger aircraft and other civil aircraft, and realize the long-cherished dream of "China's large aircraft flying in the sky as early as possible."

Chapter 60
Impact Analysis and Evaluation Method of Military Aerotransport Transport Capability

Zhifeng Xie, Weigang Niu and Xuan Liu

Abstract In this paper, through the research of military aerotransport usage, it especially analyzes the key influencing factors of transport capability. They are range ability and load, sortie generation rate, operational availability, and mission reliability. The paper, respectively, presents the calculation model of transport capacity for single voyage and multiple voyages. Besides, through two examples of relief material delivery by IL-76 and C-17, the transport capacity calculation model is verified. And, it analyzes the main causes of transport capacity gap between IL-76 and C-17. This research provides the theoretical foundation to transport capacity evaluation in flight test phase and the further study of operational effectiveness evaluation.

Keywords Transport capability · Influencing factors · Military aerotransport · Multiple voyages

60.1 Introduction

In the information-oriented modern war, these traits such as sudden, fast rhythm, high strength, and large material consumption put forward higher requirements for rapid response, mobile, and continuous operation ability to combat troops. Lift capacity has gradually become an important factor in determining the outcome of war to some extent. Military aerotransport is fast, long-range, and mobile. These characteristics make it become the pillar of rapid deployment in the forepart war, the main tool of logistics and long-range support in middle war, an important force of maneuver transfer, and timely retreat in the late period of the war. But in the

Z. Xie (✉) · W. Niu · X. Liu
Chinese Flight Test Establishment, Xi'an 710089, Shaanxi, China
e-mail: zhifeng423@163.com

field of military aircraft effectiveness evaluation, mainly for the fighter plane, the bombers, and helicopters, there is a few studies about evaluation of transport capacity for military aerotransport.

Transport capacity is the ability to perform tactical transport task via military aerotransport. It is one of the important factors for fighting and use efficiency. With the rapid development of the domestic military aerotransport, the evaluation method of transport capacity has become a problem to urgently solve in flight test phase. Through the research of military aerotransport usage and analysis of main influence factors, this paper establishes the calculation model of transport capacity to lay theoretical foundation for further research about combat effectiveness evaluation.

60.2 Influencing Factors

60.2.1 Transport Performance Index

The relation curve of load and range ability is the most important parameters for transport capacity of single sortie. Large load, long-range aerotransport undoubtedly have a greater transport capacity for single sortie. Therefore, the load and range ability capability is a key target to seek for aerotransport deviser. According to the Jane's Aircraft Handbook (2007–2008) and the data of United States defense research center [1, 2], Fig. 60.1 shows the curve of load and range ability about foreign several typical military aerotransport. From the figure, we can obviously see difference of each type of aerotransport load and range ability. The maximum load capacity of C-17 is 77.3 tons; the range ability is 4,630 km in full load and without air refueling; the maximum range of no-load is 8,700 km; the maximum range after air refueling is 11,600 km.

But in the actual process to perform task, due to the difference of the goods type and range ability, the aerotransport transport capacity is different. For example, the aerotransport standard load is 40 tons, using to load support equipment, its average load capacity only can reach 28 tons, even making full use of warehouse space.

60.2.2 Operational Availability

Operational availability refers to proportion of the military aerotransport uptime in the support system. It is an availability parameter which is related to uptime and downtime for use effect evaluation and reflects the probabilities to be deployed at any time. It is a linear relationship between military aerotransport transport capacity and operational availability. The operational availability index associated

Fig. 60.1 The relation curve
of load and range ability
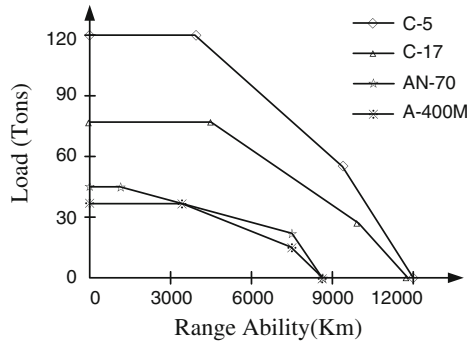
with corrective maintenance time, preventive maintenance time, and delay time. It
is expressed as:

$$\text{AO} = \frac{\text{Up Time}}{\text{Up Time} + \text{Down Time}} = \frac{T_M + T_{R\&A} + T_N}{T_M + T_{R\&A} + T_N + T_{CM} + T_{PM} + T_{ALD}} \quad (60.1)$$

Hereinto:

T_M Mission time
$T_{R\&A}$ Reaction time and Alert time
T_N Not operating time
T_{CM} Corrective maintenance time
T_{PM} Preventive maintenance time
T_{ALD} Delay time.

Base on calculation model of operational availability, we must reduce downtime
of military aerotransport to improve the operational availability. Thus, we must
make the failure rate to be low, corrective and preventive maintenance to be less, and
delay time which is caused by spare parts and personnel to be short. So operational
availability is comprehensive reflection of reliability, maintainability, testability
level, and efficiency of support system, but also related to use of support system.

According to statistics data of relevant literature [3, 4], the distribution of
operational availability is shown in Fig. 60.2 about American typical military
aerotransport from August 2004 to July 2005.

60.2.3 Sortie Generation Rate

Sortie generation rate refers to the number of times that each aerotransport can be
dispatched every day in the use and repair support scheme. It is directly related to
the specific tasks and maintenance support ability. The measurement model is:

$$R_{SG} = \frac{T_{FL}}{T_{DU} + T_{TA}} \quad (60.2)$$

Fig. 60.2 Operational
availability statistics curves
of USA typical aircraft
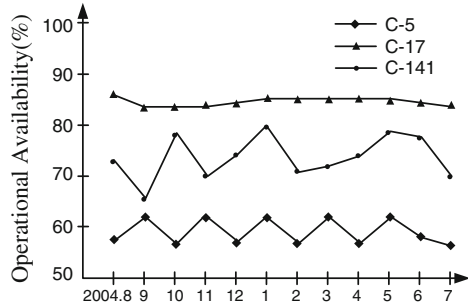
Hereinto:

T_{FL} The plane of each calendar time hours, generally 24 or 12 h
T_{DU} The average time each task
T_{AT} Turn around time (including the lay time).

Therefore, there is an important significance to improve sortie generation rate via reducing the preparation and handling time.

For example, in relief process of Wenchuan earthquake, C-17 has taken off about 6 h to arrive at Chendu from Guam for delivery of relief supplies, and unloading goods spends 2 h. But IL-76 has taken of about 2 h from a city to Chengdu, and unloading time is 4 h. In comparison, in high-strength transport task, IL-76 transport capacity is much lower than C-17 because of loading and unloading efficiency.

60.2.4 Mission Reliability

Aerotransport is mainly used for the implementation of transport task. So when the mission is successful, transport capacity can be reflected. Characterization of mission reliability is:

$$R_M = e^{(-t/T_{MTBCF})} \tag{60.3}$$

$$T_{MTBCF} = 2T/\chi^2(\alpha, 2r + 2) \tag{60.4}$$

Hereinto:

t Typical task time
T_{MTBCF} Mean time between critical failures
T The cumulative time of flight
r The cumulative number of serious fault
α Significant levels of selected, generally take 0.2.

Through the statistics of mission reliability data about a certain type aircraft from 1998 to 2005, the cumulative flight hours are 11,749 h and the critical fault

times are 31. Calculation result of mean time between critical failures is 320.7 h. Based on the above data, the mission reliability is 0.978 for completing 7 h mission.

60.3 Evaluation Model of Transport Capacity

60.3.1 Maximum Transport Capacity of Single Voyage

Maximum transport capacity of single voyage refers to the maximum transport capacity of a plane and a voyage in the ideal state [5]. It generally is the largest product of range ability and load from the relation curve of load and range ability. The relation curve is described by three consecutive line segments. As shown in Fig. 60.3, points (r_1, p_1), (r_2, p_2), (r_3, p_3), and (r_4, p_4) are known and the relation curve can be expressed to a piecewise function, as follow:

$$\begin{cases} p - p_1 = \frac{p_2 - p_1}{r_2 - r_1}(r - r_1) & r_1 \leq r \leq r_2 \\ p - p_2 = \frac{p_3 - p_2}{r_3 - r_2}(r - r_2) & r_2 \leq r \leq r_3 \\ p - p_3 = \frac{0 - p_3}{r_4 - r_3}(r - r_3) & r_3 \leq r \leq r_4 \end{cases} \tag{60.5}$$

Transport capacity curves are expressed by following formula, where C is a constant.

$$C = r \cdot p \tag{60.6}$$

According to the physical significance, the intersection point of the relation curve and transport capacity curves is the maximum transport capacity values of single voyage, such as Point 5 in Fig. 60.3. And at point 5, the relation curve is tangent with one of transport capacity curves. Through the above formulae, several typical aerotransport maximum transport capacities of single voyage are given in Table 60.1.

60.3.2 Transport Capacity of Multiple Voyages

Transport capacity of multiple voyages is usually used to characterize transport capacity of a kind of aircraft or an air fleet. Transport capacity evaluation of multiple voyages is generally divided into remote transportation and short-range transportation.

In remote transportation, transport capacity index is turnover ability of goods at unit time, and the unit is tons kilometer per day. It is related to aircraft load (p), range ability (r), sortie generation rate (R_{SG}), operational availability (AO),

Fig. 60.3 Physical method of maximum transport capacity of single voyage
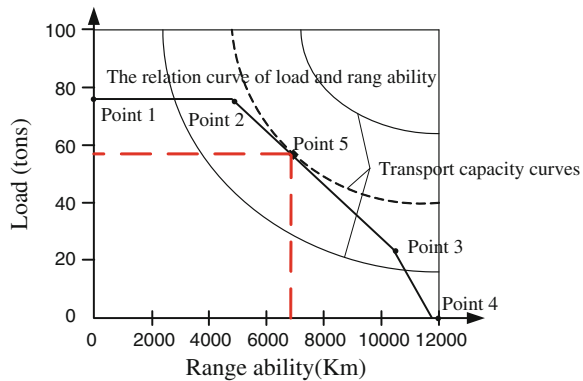
Table 60.1 Maximum transport capacity of single voyage

Type	Maximum load (ton)	Maximum transport capacity (kton km)	Corresponding load (ton)	Corresponding range ability (km)
C-5	120	548	83.7	6,549.2
C-17	77.3	372	58.1	6,414.4
IL-76	47	147	27.2	5,420.6
A-400M	37	142	26.5	5,370.4

mission reliability (R_M), and fleet size (S). A kind of aircraft multiple voyages transport capacity calculation model is:

$$\text{Transport Capacity} = r \times p \times R_{SG} \times AO \times R_M \times S \qquad (60.7)$$

Short-range transportation mainly refers to capability of tactical transport in close quarters. It is related to aircraft load or airdrop weight (P_{MAX}), sortie generation rate (R_{SG}), operational availability (AO), mission reliability (R_M), and fleet size (S). Because short-range transport mainly is executed in theater of operations, the range ability is shorter. Therefore, transport capacity index mainly reflect the turnover capacity of total materials. At this state, a kind of aircraft multiple voyages transport capacity calculation model is:

$$\text{Transport Capacity} = p_{\max} \times R_{SG} \times AO \times R_M \times S \qquad (60.8)$$

Then, transport capacity of an air fleet is sum of some kinds of aircraft transport capacity.

In flight test phase, load and range ability select the actual value of aerotransport at different transport task to evaluate the transport capacity of new type aircraft.

Combined with the flight test, using the daily information of reliability, maintainability and supportability reckons the average sortie generation rate, operational availability, mission reliability of typical transport task time to calculate transport capacity of different typical transport task.

60.4 Calculation Examples and Analysis

60.4.1 Examples of Calculation

This paper uses C-17 and IL-76 aircraft transport examples to verify transport capacity evaluation model.

Example 1: In August 2005, the United States New Orleans suffered Katrina hurricane, two C-17 aerotransports took off from Edwards Air Force Base in California which loaded with 80 tons relief materials, passed 4 h to the disaster area of 2,720 km outside. The loading and unloading time is about 4 h.

Example 2: In April 2013, Sichuan Ya'an suffered earthquake which is seven on the Richter scale, two IL-76 aerotransports took off from Beijing Nanyuan airport which loaded with 52 tons relief materials. After 2 h and 40 min, it arrived to Sichuan Qionglai of 1,580 km outside. The loading and unloading time is about 6 h.

It, respectively, calculates sortie generation rate of two kinds of aerotransport through sortie generation rate calculation formula.

$$\text{C-17}: R_{\text{SG}} = \frac{T_{\text{FL}}}{T_{\text{DU}} + T_{\text{TA}}} = \frac{24}{8 + 4} = 2$$

$$\text{IL}: R_{\text{SG}} = \frac{T_{\text{FL}}}{T_{\text{DU}} + T_{\text{TA}}} = \frac{24}{5.3 + 6} = 2.12$$

In view of the above situation, using transport capacity calculation model of remote transport, C-17 and IL-76 transport capacity of carrying relief materials, respectively, is:

$$\text{Two C-17}: \text{Transport Capacity} = r \times p \times R_{\text{SG}} \times \text{AO} \times R_{\text{M}} \times S$$
$$= 357.6 \, \text{ktons km day}^{-1}$$

$$\text{Two IL-76}: \text{Transport Capacity} = r \times p \times R_{\text{SG}} \times \text{AO} \times R_{\text{M}} \times S$$
$$= 121.2 \, \text{ktons km day}^{-1}$$

60.4.2 Comparative Analysis

The above result shows that the transportation capacity of IL-76 is less than C-17. Main parameters of two type aircrafts are shown in Table 60.2.

As can be seen from Table 60.2, the main reasons that transport capacity IL-76 is less than C-17 and the improvement measures are as follows:

Table 60.2 Main parameters of two type conveyer

Main parameters	IL-76	C-17
Hold size	20 × 3.46 × 3.4 m	26.83 × 5.49 × 4.11 m
Maximum load	47 tons	77.3 tons
Turnaround time (include loading and unloading)	6 h (in example)	3.5 h (in example)
Operational availability	0.71	0.83
Mission reliability	0.98	0.99

(a) Design of IL-76 hold size is less than C-17 aerotransport; the maximum load weight is only 60.8 % of C-17.
(b) The C-17 military aerotransport does not affect unloading and parts of ground works when its engine is running. And the performance of loading and unloading establishments which are laid in floor is better than IL-76. So its turnaround time (include loading and unloading time) is less than the IL-76. We can adopt higher efficiency establishments and more perfect loading scheme to reduce turnaround time of IL-76.
(c) C-17 has the advantages of operational availability and mission reliability. We can improve reliability, maintainability, testability, and supportability level of IL-76 to improving operational availability and mission reliability.

Through the improvement measures, the turnaround time of IL-76 in example can be reducing to 4 h. And mission reliability and operational availability is the same as C-17. Then sortie generation rate is 2.58 times a day. Transport capacity of two IL-76 aerotransports can be increased to 174.1 ktons km day^{-1}.

60.5 Conclusions

This paper analyzes the influencing factors of transport capacity and establishes the calculation model to evaluate transport capacity of single voyage and multiple voyages, through the study of foreign military aerotransport usage. The result of example calculation shows that the accuracy of the factor analysis and transport capacity calculation model. At the same time, the research of influencing factors and calculation model not only settles theoretical foundation for evaluation of transport capacity, provides the gist for future predication and evaluation of military aerotransport fighting efficiency, but also affords the auspice for logistics planning and military materials transportation.

References

1. Jackson P (2007) Jane's all the world's aircraft 2007–2008. Cambridge University Press, Cambridge
2. Bexfield JN (2001) C-17 COEA case study. IDA Document D-2688, 2001.9
3. Pendley SA (2006) Factors and interactions that affect air force C-17 aircraft mission capable rates. Department of the Air Force, Air University, 2006.12
4. Curtin NP (2001) Updated readiness status of U.S air transport capability. GAO-01-495R
5. Anderton GL, Berney IV ES, Mann TA, Kent Newman J, Alex Baylot E, Miller DK, Mason Q (2008) Joint rapid airfield construction (JRAC) 2007 technology demonstration. ERDC/GSL TR-08-17, 2008.7

Chapter 61
Applied Design Optimization of Nose Landing Gear Cabin Structure of Airplane

Wei Tian and Qin Sun

Abstract Based on structure dynamics finite element method (FEM) numerical analysis, and optimal design methods, this paper analyzed the finite element modeling of cabin structure of nose landing gear and discussed optimal design of structural parameter. The main research work conducted included the following: Finite element discretization of structure of nose landing gear, construction of finite element model, optimal variable design, optimal design for component dimension parameter of structural low-order frequency property in numerical value technique frame, lightest structural weight under low-order frequency restriction conditions, and best geometrical stiffness structure distributing. The thesis introduced in details the structure dynamic characteristic finite element mesh adopted in performance calculation as well as the structure numerical optimal theory and discussed every detail of optical design for numerical value of intrinsic dynamic characteristics and the optimal analysis results. At the end of the paper, the author proposes the conclusion of the research.

Keywords Cabin structure of nose landing gear · Dynamic finite element model · Lower-order frequency property · Optimal design · Numerical analyze

61.1 Introduction

An airplane taxiing down the runway suffers from random low-amplitude loadings which pass through landing gear to airframe structural, forming dynamic-load working environment of the part structure. According to structure dynamics design, stiffness distributing design is required, to keep the intrinsic frequency

W. Tian (✉) · Q. Sun
School of Aeronautics, Northwestern Polytechnical University, Aeronautics Building A407, Laodong Road, Xi'an 710072 Shaanxi, China
e-mail: tianwei@nwpu.edu.cn

away from the working environment frequency, thus to ensure the technological performance demands of structural endurance. The thesis studied cabin structure of nose landing gear of certain type, and developed intrinsic frequency property optimal design. In consideration of mechanism load low-frequency property of cabin structure of nose landing gear, the author constructed a dynamic finite element parameter, made an optimal design, adjusted the structure rigid distributing and component parameter, reached the best structure rigid distribution for low-order and high-order frequencies property and lightest structure weight, and thereafter enhanced structural dynamics qualities and realized engineering application [1–3].

61.2 The Main Goal of this Paper

The main goal of this paper is to develop an intrinsic low-order frequency characteristics based optimal design method for a cabin structure of nose landing gear of certain type. The study relies on the numerical results obtained from the ANSYS finite element analysis and a design optimization software system. Numerical model is constructed by finite element discretizing of the cabin structure of nose landing gear. The low-order frequency property of the cabin structure is optimized based on the results of the parametric study [4–6]. In addition, the best geometrical stiffness structure distribution and the lightest structural weight are obtained under low-order frequency restriction conditions. The main research work conducted included the following:

1. A comprehensive overview of structural dynamic methods and its application in analysis of structural natural frequency and mode of vibration are given in the sense of numerical calculation. Furthermore, the parameter optimization theory and the corresponding optimization module of ANSYS software are summarized [7].
2. The finite element model of the cabin structure of nose landing gear is constructed using ANSYS software. The displacement mode selection of finite element, the discretization of the structure, the connection of different components as well as the constraints and boundary conditions are prescribed in detail.
3. The proposed method can be used directly for the optimization of the cabin structure with the minimum weight as its object and the first-order natural frequency as its constraints. For the given cabin structure, optimization design of the intrinsic frequency characteristics is carried out by incorporating the low-frequency properties of mechanical loading and the low-order frequency characteristics of the nose landing gear. The optimal stiffness distribution and the minimum weight of the cabin structure are obtained by adjusting the component geometry parameters and thus the stiffness distribution mode, which insure the high quality of the structural dynamics.

4. The dynamic loading capabilities before and after the optimization are shown to indicate the usage of the proposed optimization process. Additionally, numerical results are given to illustrate the improvement of the loading capability, the stress development, and the performance of the cabin structure by using the proposed optimization process.

61.3 The Feature Analysis of the Force Transmission in the Structures

The cabin structures mainly absorb the random jounce or impact loads transmitted from the nose landing gear when the airplane taxies or lands on the runway. From the connections between nose landing gear strut, its brackets, nose cabin structure, and the framing member, we can see that the jounce or impact loads in the Y direction act directly on the connection brackets through the axles, struts, and supporting point axles as is shown. The base of connection base is directly mounted on the two side wall panels, and through the connections among side wall panels, air inlet and airframe, the loads are transmitted to all of the nose landing gear cabin structure. The moments resulted from the loads in the Y direction can be balanced by the internal forces in the fore and the aft supporting point axles. The jounce or impact loads from the runway in the X direction is similar to the one in the Y direction that is the force is transmitted directly to the connection brackets through the strut system (along the X direction). The resulting moment is as well balanced by the internal forces in the fore and the aft supporting point axles. The loads in the Z direction are transmitted to the brackets by the landing gear strut and act on the brackets by the strut sleeve in the brackets axle. But it can result in transverse load effect in the negative stiffness direction of side wall panel of cabin. So the strengthened ribbons in the base of the brackets should be designed so as to diffuse the force distribution patterns in the negative load directions.

Figure 61.1 shows full extension working sketch of nose landing gear.

61.4 Finite Element Modeling of Cabin Structure

The cabin of nose landing gear is mounted to the forward fuselage. The cabin structure system is basically comprised of fuselage section, inlet, the cabin of nose landing gear, and the fuselage skin. Considering the thin-walled characteristic of the cabin structure, the skin, the web plate, the flange, and the rib, the displacement modes for shell structure are adopted in this paper. The finite element model is comprised of 44,136 four-node shell elements of ANASYS (Shell 63) with element thickness of 20 mm, as shown Fig. 61.2

The joining and mounting connections among different components are indicated with asterisk. In this paper, the element-based node coupling technique of
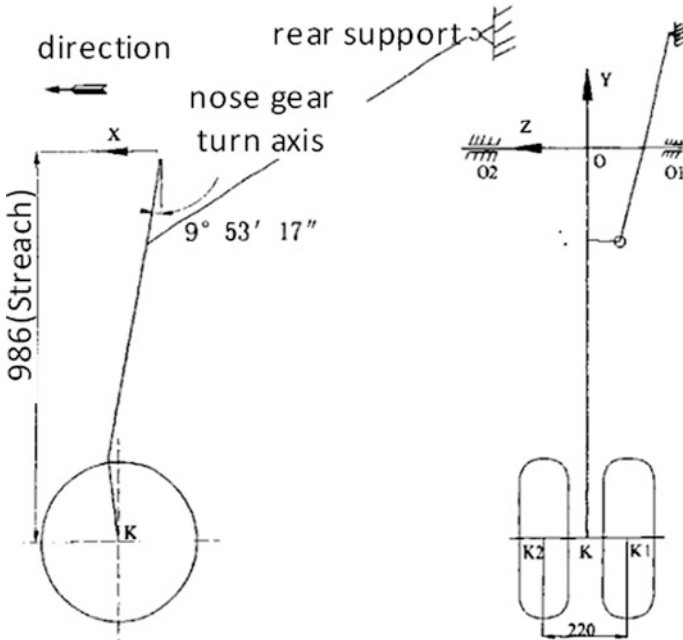
Fig. 61.1 Full extension working sketch of nose landing gear

Fig. 61.2 The cabin of nose landing gear build-up (include fuselage skin) finite element mesh
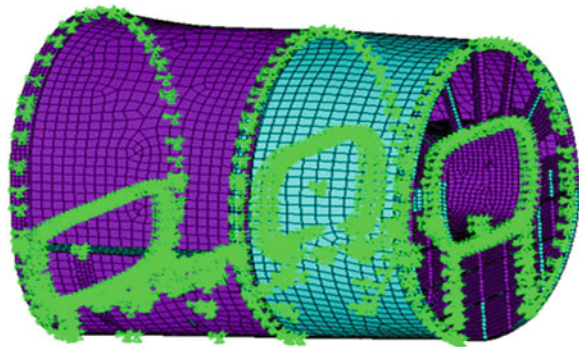
ANASYS is adopted. A completely displacement coordination (all known as node coupling) is used to simulate the riveted joint behaviors of different nodes. For example, to establish the connection between fuselage and skin, these nodes belong to the skin and the flange are coupled together by using the node coupling technique. The general riveting joint space of 20–30 mm are selected in accordance with the engineering situation. This coupling technique is used to simulate the connections between the fuselage frame and the skin, the inlet, the cabin of nose landing gear, and various auxiliary patch components.

Due to the complexity of the rear fuselage structure, it is difficult to take into account the displacement support stiffness of the cabin transferred from the fuselage. However, the neglecting of this kind of support will lead to the decrease in the natural frequency characteristics. Considering the optimization design performed in this paper can be increased the cabin structure's frequency; it is appropriate to apply a clamped support boundary condition to approximate the actual situation, which to a certain degree will enlarge the solution of natural frequency of the cabin [8–10].

61.5 Results of Optimal Design

Based on the fundamental work of the preceding, this thesis takes the weight of cabin structure of nose landing gear as the target of optimal design and the first-order intrinsic frequency of the structure as the constraint condition and applies the optimal design module of ANASYS to carry out iterative calculation of numerical optimal design. The optimal design of cabin structure of nose landing gear can be indicated in the following expressions.

$$\begin{cases} \min W = \min \sum S_i v_i & S_i \text{ is surface dimension of each FEM element } i \\ & v_i \text{ is its thickness,} \\ \text{s.t.} f_1 \geq 60 \,(\text{Hz}) & f_1 \text{ is first-order intrinsic frequency of the structure,} \\ 1 \leq v_i \leq 10 \,\text{mm} & \text{range of design variable } i. \end{cases}$$

This paper adopts the optimized design module of the ANASYS system for iterative computation of numerical optimization design. Table 61.1 shows ten of the design variables, their original design dimensions, and the corresponding design optimization results.

Table 61.2 provides the numerical solutions and optimization results of natural vibration characteristics of the original structure and also gives the weight optimization results.

The results listed in Table 61.2 show that parameter optimization for the cabin structure of the nose landing gear reduces the weight of the structure by 3.06 % and also significantly enhances the natural vibration characteristics of the structure (where it is guaranteed that the primary frequency vibration of the structure is in a flexural mode in the vertical plane and the natural frequency of the structure increases by 12.5 % approximately) [11, 12].

In order to compare the carrying capacity of the cabin structure of the nose landing gear before and after its optimization, Fig. 61.3 shows the stress distribution nephograms of the fore frame under the design ultimate load before and after optimization [13, 14]. After comparison of the design ultimate loading stress before and after optimization of the cabin structure of the nose landing gear, it can be seen that the internal force distribution of each component changes as the stiffness distribution of the structure changes after optimization, but no change is found in the main transmission line of structural internal force (i.e., no change

Table 61.1 Table captions should variable of optimal design resolution

Order	Name	Design variables identify	Numerical value of original design	Design variable codomain (mm)
1	Fore frame-web	rk1d	4	1.59
2	Fore frame stiffner flange	rk1	2.5	1.50
3	Lateral 1 frame-web	rdk1d	3.5	4.21
4	Lateral 1 stiffner flange	rdk1b	3	1.59
5	Lateral 2 frame-web	rdk2d	3.5	2.07
6	Attached box 1	rfk1	2	1.11
7	Strengthened spar	rbk	1.5	3.05
8	Strengthened panel 1	rfklj1	1.5	1.75
9	Inlet thick wall	rjhm	2.5	1.39
10	Fuselage skin	rmp	1.5	1.16

Table 61.2 Numerical solutions and numerical optimization results of natural vibration characteristics of the structure

Definition	Modal shape at 1st order frequency (Hz)	Modal shape at 2nd order frequency (Hz)	Design weight
Original design	53.165	61.48	98
Optimization design	59.81		95

occurs at the position where the maximum stress appears); also, the difference in stress level before and after optimization is not quite significant. These findings reflect the characteristics of the parameter optimization design: There is no change in either the connection relations or the position relations among the components of the structure, and also no major change in the weight of the structure; the only change exists in the parameter of geometric stiffness of the structure. However, such parameter change has a great impact on the overall stiffness distribution of the structure and can significantly improve the natural frequency characteristics of the structure (See Table 61.2).

61.6 Design Analysis and Conclusion of Results of Numerical Solutions for Natural Vibration Characteristics and Calculation Results of Optimal Design

Here is the analysis and conclusion of the optimal design after comparing with the results in the table:

(a) From the numerical solutions for overall vibration mode of the structure, it can be seen that the finite element modeling in this thesis is correct, which complies with concepts of engineering structural design.

Fig. 61.3 Equivalent stress nephograms of the fore frame before and after optimization. **a** Before optimization, **b** after optimization
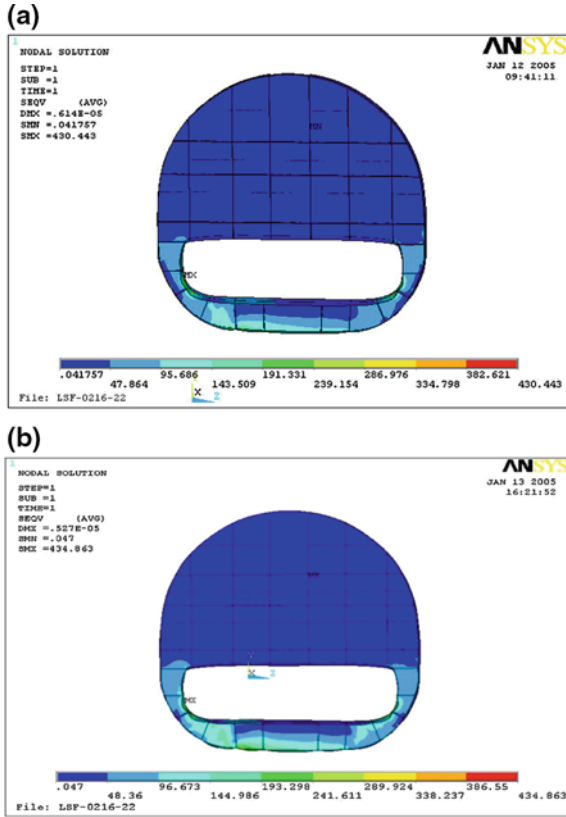
(b)   From the optimal solution results of this paper, it can be seen that the structural stiffness distribution of the original design is basically reasonable, and the internal force distribution of the original design still needs to be checked by numerical calculation.

(c)   The numerical optimal model is reasonable, and the numerical results conform to engineering concepts; when the process conditions are moderated to a certain extent, the stiffness distribution of the original design will become more reasonable; the weight will be reduced to some degree, by 3.06 % compared with the weight of the original design.

(d)   Due to lack of stiffness constraint condition of the rear body, the intrinsic frequency of the actual structure is generally lower than the calculation result, which, however, will not affect the comparability of results before and after optimization.

References

1. Walker N, Philbin DA, Fisk AD (1997) Age-related differences in movement control: adjusting submovement structure to optimize performance. J Gerontol Ser B: Psychol Sci Soc Sci 52:40–53
2. Pu X, Liu X, Qiu F et al (2004) Novel method to optimize the structure of reticulated porous ceramics. J Am Ceram Soc 87:1392–1394
3. Chu DN, Xie YM, Hira A et al (1996) Evolutionary structural optimization for problems with stiffness constraints. Finite Elem Anal Des 21:239–251
4. Xie YM, Steven GP (1997) Basic evolutionary structural optimization. Springer, London
5. Fleury C, Braibant V (1986) Structural optimization: a new dual method using mixed variables. Int J Numer Meth Eng 23:409–428
6. Fadel GM, Riley MF, Barthelemy JM (1990) Two point exponential approximation method for structural optimization. Struct Optim 2:117–124
7. Ha SK, Keilers C, Chang FK (1992) Finite element analysis of composite structures containing distributed piezoceramic sensors and actuators. AIAA J 30:772–780
8. Svanberg K (1987) The method of moving asymptotes—a new method for structural optimization. Int J Numer Meth Eng 24:359–373
9. Xie YM, Steven GP (1993) A simple evolutionary procedure for structural optimization. Comput Struct 49:885–896
10. Toropov VV (1989) Simulation approach to structural optimization. Struct Optim 1:37–46
11. Barthelemy JF, Haftka RT (1993) Approximation concepts for optimum structural design—a review. Struct Optim 5:129–144
12. Hale AL, Dahl WE, Lisowski J (1985) Optimal simultaneous structural and control design of maneuvering flexible spacecraft. J Guidance Control Dyn 8:86–93
13. Kicinger R, Arciszewski T, Jong KD (2005) Evolutionary computation and structural design: a survey of the state-of-the-art. Comput Struct 83:1943–1978
14. Perez RE, Behdinan K (2007) Particle swarm approach for structural design optimization. Comput Struct 85:1579–1588

Chapter 62
Study on Comprehensive Evaluation for Civil Aircraft Cockpit Display Ergonomics During Flight Test

Hai-jing Song, Fei-min Li and Lv Bao

Abstract The ergonomics comprehensive evaluation of aircraft cockpit plays a key role in the efficiency of pilot–cockpit system and flight safety, especially for display equipments. Several standards and norms related to the ergonomics design and evaluation techniques of aircraft cockpit were established; however, there was not an operational and systemic evaluation method. Aiming at this issue, the process integrating modified Delphi, modified analytical hierarchy, membership function, and fuzzy evaluation method were proposed to solve display ergonomics certification. The inevitable fuzziness and subjectivity of ergonomics evaluation were taken into account to acquire and analyze expert opinion, finally realizing the quantitative evaluation of qualitative indexes. This method was applied in ARJ21-700, and the results proved the validity of this study and also be used as the evaluation guidance for other civil aircraft.

Keywords Cockpit ergonomics · Display equipment · Index system · Weight factors · Index value pretreatment · Quantitative evaluation

62.1 Introduction

With the development of airplane, the unsafe events caused by cockpit ergonomics have been more and more prominent, and then cockpit ergonomics becomes the key factor in improving pilots' performance and reducing work load. The pilot is always exposed to the highly intensive environment full of lots of information from electronic equipment when performing a task, which requires that display equipments must make good performance to ensure safety [1]. So, the display

H. Song (✉) · F. Li · L. Bao
Chinese Flight Test Establishment, Xi'an 710089, China
e-mail: shjaj@163.com

ergonomics is closely related to flight safety and efficiency. Besides, flight test is an important means to reflect the ergonomics level of the real test aircraft, to meet the demand of civil aircraft urgently; this research is necessary and meaningful.

Currently, the ergonomics study is common in foreign countries; however, considering the differences in pilot physical at home and abroad, these researches could be only for reference partly [2]. The study in China shows that lots of methods are proved in ergonomics designing, but few in ergonomics evaluating [3]. Meantime, there is not a set of operational evaluation index system and evaluation standards and many ergonomics problems exist in how to perform ergonomics evaluation. This paper focuses on how to construct a set of operational evaluation index system, comprehensively reflecting the airliner cabin display ergonomics characteristics; this study can provide the key technical support for the evaluation of display ergonomics during the flight test of civil aircrafts. Similar studies in China had not been developed previously in flight test.

Aiming at this issue, the integrated evaluation method was proposed, which then was applied in ARJ21-700, and the results proved the validity of this study and also be used as the evaluation guidance for other civil aircraft.

62.2 The Thought of this Paper

The basic thinking of the research is as follows: First, it should establish the evaluation index system through modified Delphi method; then apply modified analytical hierarchy process to determine weight coefficient of each index, membership function to quantize index value, and fuzzy evaluation method to achieve the ultimate operable evaluation result; and finally, present and discuss an example at last to verify the effectiveness of the proposed method (see Fig. 62.1).

62.2.1 Establishment of the Evaluation Index System

Because the cockpit involves lots of ergonomics problems, and the quantitative analysis cannot be used in many ergonomics factors, such as pilot emergency response, safety, and screen information layout [4]. Thus, the evaluation and improvement of the ergonomics evaluation can only be made by aviation specialists and experienced pilots depending on their plenty of experience and intuition through the vague concepts and synthetic judgment ability formed in practice.

Therefore, the actual evaluation of index system is often less scientific, comprehensive, and normative; this paper applied specialists' consistency and confidence to modify Delphi to establish the ergonomics evaluation index system. The specific procedure can be described as follows:
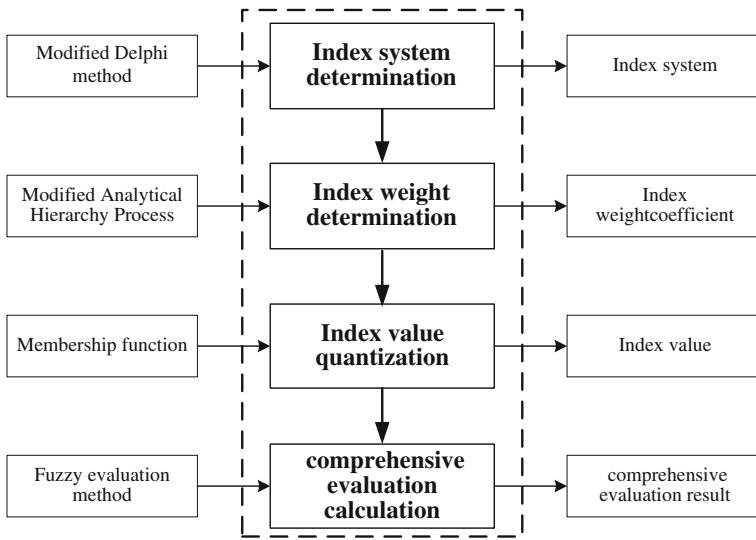
Fig. 62.1 The research frame of display ergonomics

Step 1: Form a coordination group

The coordination group consists of 4–8 persons with senior engineer, intermediate engineer, and special senior engineer, respectively. The major tasks are to draw up the research topic, determine the consultant specialists, write the questionnaires to consultant specialists, organize the consult work, and collect and process statistics.

Step 2: Determine the consultant specialists

Selecting the specialist is the key point of modified Delphi, a specialist with certain professional knowledge, rich practice experience, much dynamic information, and willing to participate should be chosen. The number of the consultant specialists should be 10–30 [5].

Step 3: The first round of specialists consulting

According to studies and analysis of available standards, specifications, and relative literatures for civil aircraft ergonomics design and evaluation, a more comprehensive evaluation system which have four levels were initially determined after seeking relative specialists for opinions, as shown in Fig. 62.2.

Based on the indexes determined in U_k, the first round specialist consulting list was studied out to require each specialist telling out the impact level of index on display ergonomics through their knowledge and experience, where the impact level has a "5-point Likert scale," from 1 to 5, representing "not very big," "general," "big," "very big," and "great" in turn. The consistency opinion can be defined as no less than two-thirds specialists (about 67 %) give the judgment above "big," where the "big" means the impact level which the index has to display ergonomics, this parameter can be named as P_{33}.
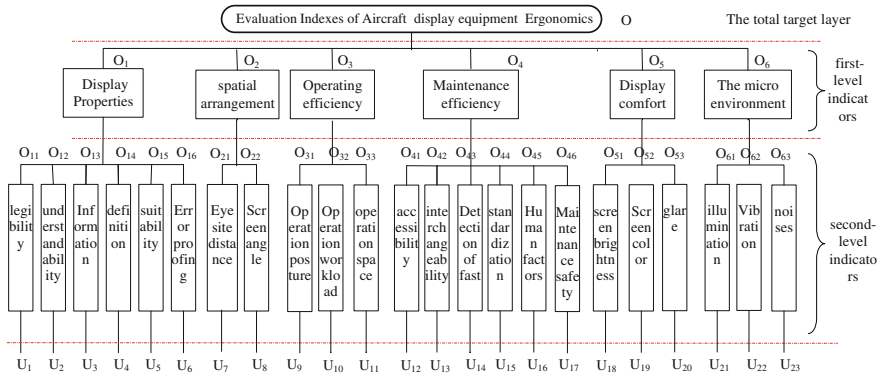
Fig. 62.2 The index system frame of display ergonomics evaluation

Step 4: The second round of specialists consulting

The specialist inquiry forms reclaimed from the first round were processed and analyzed, and then, the consistency opinion, average value, and its distribution of each index were given to the specialists in second round, and the specialist evaluated each index based on the feedback again.

Meanwhile, the specialists should give their confidence on their evaluation of the impact level which the index has on the display ergonomics. The confidence level is a "1–5" point scale, with "lower," "low," "general," "high," "higher," respectively. Data show that if the group confidence ranking (GCR) was not lower than 3, the consulting results should be close to the real subjective judgment.

Step 5: Screening the evaluation indexes

Usually, several parameters have been used to analyze the results:

1. The degree of concentration:

$$\overline{E}_i = \sum_{j=1}^{5} E_j m_{ij}/d \quad (i = 1, 2, \ldots, n) \tag{62.1}$$

2. The degree of discretion:

$$\sigma_i = \left[\sum_{j=1}^{5} m_{ij}(E_j - \overline{E}_i)^2 / (d - 1) \right]^{\frac{1}{2}} \tag{62.2}$$

3. The degree of coordination:

$$V_i = \sigma_i/\overline{E}_i \tag{62.3}$$

Generally speaking, the specialists' opinion would become mutual assent after two rounds, as shown in Table 62.1.

Table 62.1 The comparison of index results of two rounds

Target layer	Level indicators	The first step				The first step				GCR
		E_i	σ_i	V_i	P_{33}	E_i	σ_i	V_i	P_{33}	
Display properties	Legibility	3.35	1.03	0.31	3.00	3.39	0.94	0.28	3.00	4.13
	Understandability	2.83	0.65	0.23	2.00	3.04	0.56	0.18	3.00	4.00
	Information	2.30	1.02	0.44	2.00	2.43	0.66	0.27	2.00	3.91
	Definition	3.48	1.04	0.30	3.00	3.26	0.75	0.23	3.00	4.04
	Suitability	3.13	0.76	0.24	3.00	2.91	0.73	0.25	3.00	4.00
	Error proofing	3.09	1.04	0.34	3.00	3.22	0.80	0.25	3.00	4.04
Spatial arrangement	Eye site distance	3.04	1.02	0.34	3.00	3.22	0.52	0.16	3.00	4.04
	Screen angle	3.30	0.93	0.28	3.00	3.22	0.85	0.26	3.00	4.17
Operating efficiency	Posture	3.26	1.01	0.31	3.00	3.30	0.63	0.19	3.00	3.96
	Workload	3.48	0.99	0.29	3.00	3.83	0.72	0.19	4.00	4.09
	Space	3.17	1.15	0.36	3.00	3.17	0.49	0.15	3.00	4.04
Maintenance efficiency	Accessibility	3.17	0.83	0.26	3.00	3.17	0.65	0.20	3.00	3.78
	Interchangeability	2.91	1.00	0.34	2.00	2.39	0.50	0.21	2.00	3.91
	Detection of fast	2.70	0.70	0.26	2.00	2.26	0.54	0.24	2.00	3.91
	Standardization	2.96	0.98	0.33	2.00	3.09	0.60	0.19	3.00	3.83
	Human factors	3.22	1.04	0.32	2.00	2.78	0.74	0.26	2.00	3.91
	Safety	3.09	0.90	0.29	2.00	3.13	0.81	0.26	3.00	3.91
Display comfort	Screen brightness	3.22	1.04	0.32	3.00	3.91	0.67	0.17	4.00	4.04
	Screen color	3.13	0.97	0.31	3.00	3.13	0.55	0.18	3.00	3.96
	Glare	3.04	0.93	0.30	3.00	3.78	0.60	0.16	4.00	4.09
The micro environment	Illumination	3.00	0.95	0.32	2.00	3.09	0.73	0.24	3.00	3.96
	Vibration	3.09	1.08	0.35	2.00	2.78	0.80	0.29	2.00	3.83
	Noises	2.87	0.97	0.34	2.00	2.43	0.66	0.27	2.00	3.96

Therefore, the evaluation index system could be selected according to the specialists' opinion in the second round; meantime, the confidence degree of specialists also should be above "3." Therefore, on the basis of the statistical results, 17 final indicators were screened from the established 23 in first step.

62.2.2 Determination of Index Weight Coefficient

The determination of weight coefficient is the core problem to making evaluation index system operational [6]. This paper presents "three-scale" based modified AHP to determine the index weight coefficient. The three-scale AHP is a kind of simplified method on traditional thought, reducing numbers of comparisons between indexes and meeting the consistent requirement automatically, with a strong operability. The process of determining the index weight factors can be divided into four steps:

Step 1: Establishing the judgment matrix C (get from experts' judgments)

$$c_{ij} = \begin{cases} 1 & \text{Index } i \text{ is more important than } j; \\ 0 & \text{Index } i \text{ has equal importance with } j; \quad \forall i,j \\ -1 & \text{Index } i \text{ is less important than } j; \end{cases} \quad (62.4)$$

Step 2: Finding optimal transfer matrix D

$$d_{ij} = \frac{1}{m} \sum_{k=1}^{m} (c_{ik} - c_{jk}) \ \forall i,j \quad m \text{ is the order of } C \quad (62.5)$$

Step 3: Obtaining consistent matrix Q

$$q_{ij} = \exp(d_{ij}) \quad \forall i,j \quad (62.6)$$

Step 4: Calculating the eigenvector of the biggest eigenvalue in Q, then unitized eigenvector as index relative weight coefficient a_i

In practical work, in order to weaken disturbance of human factor and define the judgment matrix more objectively and accurately, $d(d > 1)$ experts should be invited simultaneously to give judgment on the same problem and then synthesize a relative ideal value from all the results.

62.2.3 Quantization of Evaluation Index Value

Usually, many ergonomics indexes, such as visual accessibility, comfort, and security, are described by natural language variables, so these indexes have not been standardization ones. Therefore, the index values obtained from MD should be normalized to make sure that all indexes meet the normalization, dimensionless terms, and be commensurability.

Therefore, all the characteristic values of indexes should be changed to [0, 1] before applying this evaluation index system, that is, we should quantize the index characteristic values firstly. The key problem of quantizing is to construct membership functions for indexes one by one [7]. The methods for qualitative indexes and quantitative indexes separately can be described as follows:

Step 1: Quantify characteristic values of quantitative indexes

In the index system of display ergonomics evaluation, there are following types of qualitative indexes.

1. The bigger the value is, the better the index, such as readability and explicitness of display information, and appropriate functionality of device. The memberships function for quantizing this type of index can be expressed:

$$\mu_i = \begin{cases} 1 & x_i \geq M_i \\ \dfrac{x_i - m_i}{M_i - m_i} & m_i < x_i < M_i \\ 0 & x_i \leq m_i \end{cases} \tag{62.7}$$

2. The smaller the value is, the better the index, such as pilots' technical workload and noisy environment. The quantization membership function for this type is:

$$\mu_i = \begin{cases} 1 & x_i \leq M_i \\ \dfrac{M_i - x_i}{M_i - m_i} & m_i < x_i < M_i \\ 0 & x_i \geq m_i \end{cases} \tag{62.8}$$

3. Index of moderate value, which means the value cannot be too big or too small. For example, size of some devices, color and illumination inside cockpit. The membership function is:

$$\mu_i = \begin{cases} \dfrac{2(x_i - m_i)}{M_i - m_i} & m_i \leq x_i < \frac{M_i + m_i}{2} \\ \dfrac{2(M_i - m_i)}{M_i - m_i} & \frac{M_i + m_i}{2} \leq x_i \leq M_i \\ 0 & x_i > M_i, \ x_i < m_i \end{cases} \tag{62.9}$$

4. Interval-type index, whose value should be at a fixed interval for the best, such as the stroke range of devices like pedals, control stick, throttle lever, the regulation range of devices like seat, and the view requirements of inner and outer vision field. The membership function for interval-type index is:

$$\mu_i = \begin{cases} 1 - \dfrac{q_{i1} - x_i}{\max\{q_{i1} - m_i, M_i - q_{i2}\}} & x_i < q_{i1} \\ 1 & x_i \in [q_{i1}, q_{i2}] \\ 1 - \dfrac{x_i - q_{i2}}{\max\{q_{i1} - m_i, M_i - q_{i2}\}} & x_i > q_{i2} \end{cases} \tag{62.10}$$

where x_i is the characteristic value of u_i; M_i and m_i is the upper and lower limit for x_i; $[q_{i1}, q_{i2}]$ is the optimum stable interval; μ_i is the membership degree of u_i.

Step 2: Quantify characteristic value of qualitative index

For the indexes difficult to obtain quantitative values, such as the comfort level inside the cockpit, communications accuracy, and so on, the evaluators can only give qualitative estimates and judgments. Therefore, it is better to apply linguistic variables and fuzzy numbers to deal with this type of indexes, overcoming the inaccuracy and ambiguity of evaluators' judgments.

Table 62.2 Evaluation results of ARJ21-700 ergonomics indexes

Target layer	Sub target layer			Index layer		
	Name	Weight	Membership	Name	Weight	Membership
Evaluation results of ARJ21-700 ergonomics indexes	Display properties	0.17	0.6546	Legibility	0.27	1.0000
				Understandability	0.13	0.0000
				Definition	0.23	0.7142
				Suitability	0.16	0.5143
				Error proofing	0.21	0.6574
	Spatial arrangement	0.20	0.7443	Eye site distance	0.45	0.8033
				Screen angle	0.55	0.6961
	Operating efficiency	0.20	0.7557	Posture	0.33	0.4820
				Workload	0.42	1.0000
				Space	0.25	0.7065
	Maintenance efficiency	0.16	0.6962	Accessibility	0.36	1.0000
				Interchangeability	0.30	0.5631
				Safety	0.34	0.4921
	Display comfort	0.14	0.5501	Screen brightness	0.39	0.7000
				Screen color	0.26	0.6326
				Glare	0.35	0.3215
	The micro environment	0.13	1.0000	Illumination	1.00	1.0000

62.2.4 Determination of the Comprehensive Evaluation Model

The comprehensive evaluation model used in this paper is as follows [8]:

$$B = A * R = (B_1, B_2 \ldots, B_m)$$

The column vector of B can be expressed:

$$b_j = (w_1 \hat{*} r_{1j}) \breve{*} (w_2 \hat{*} r_{2j}) \breve{*} \ldots \breve{*} (w_p \hat{*} r_{pj}) \quad (j = 1, 2, \ldots, m) \tag{62.11}$$

Assume the evaluation grade as

$$J = (j_1, j_2, \ldots j_m)'$$

The evaluation results can be expressed as

$$W = B \times J \tag{62.12}$$

62.3 Case Studying

On the above basis, the ergonomics evaluation index system of ARJ21-700 display equipment was investigated roundly. According to research dates provided by pilots and maintenance personals of ARJ21-700, the weight coefficient of each

index was calculated through AHP method described in Sect. 62.2.2; the membership grade of each index was gained by formula described in Sect. 62.2.3; the results were shown in Table 62.2.

Based on the analysis results, the index system is operational and can be directly applied in fuzzy comprehensive evaluation to obtain the result to judge ergonomics level.

From Table 62.2, we can see that the display ergonomics of ARJ21-700 can be calculated from the index layer and sub target layer, the final evaluation value was 0.7296, which reflects the level and defects of ARJ display ergonomics. Clearly, the layout and operating efficiency of display equipment make good performance, but the amenity requires compensation.

62.4 Conclusion

The establishment of the evaluation index system, the index weight coefficient and the evaluation index value, the key problems of the display ergonomics comprehensive evaluation index system were deeply studied in the paper. From the case results, we can conclude that the index system research method is more reasonable, scientific, and accurate.

1. Considering the specialists' consistence in opinion and confidence, the establishment of index system becomes very scientific and practical, realizing the operable index system.
2. The inevitable fuzziness and subjectivity of ergonomics evaluation were taken into account to acquire and analyze experts' opinion, making the quantitative evaluation of qualitative indexes.
3. This method was applied in ARJ21-700, and the results proved the validity of this study and also be used as the evaluation guidance for other civil aircraft.

References

1. Li YX, Yuan XG (2004) Design and realization of synthesis assessment system for cockpit ergonomics. Comput Appl Res 21(9):264–265 (in Chinese)
2. Guo YJ (2002) Comprehensive evaluation theory and methods. Press of Science and Technology, Beijing, pp 41–46 (in Chinese)
3. Chen XJ, Liang L (2003) The methods and applications of system evaluation. Press of University of Science and Technology of China, Hefei, p 58 (in Chinese)
4. GJB1062-91 (1991) General requirements of human engineering design for military visual displays
5. Linstone HA, Turoff M (1975) The Delphi Method: techniques and applications, Advanced Book Program. Addison-Wesley, Massachusetts, pp 3–10

6. GJB/Z201-2001 Human engineering design manual for military equipment and facilities
7. Chen W (2000) Correct recognition of analytic hierarchy process. Ergonomics 6(2):32–35 (in Chinese)
8. Lu J (2009) Practical fuzzy mathematics. Press of Science and Technology, Beijing, pp 73–77 (in Chinese)

Chapter 63
Repair of Shot Peening on Fatigue Properties of High-Strength TC18 Titanium Alloy for Aviation

Dongxing Du, Daoxin Liu, Dinggen Xiang, Baoli Meng and Xiaohua Zhang

Abstract In this paper, the machining texture and shot peening (SP) on the fatigue properties of a high-strength TC18 titanium alloy for aviation were studied. The surface texture, surface morphology, hardness distribution, and residual stress characteristics of fatigue specimens were analyzed by using scanning electron microscopy (SEM), micro-hardness tester, and X-ray diffraction residual stress analyzer. The results showed that the fatigue life of the axial texture processing was 27 % lower than that of the axial polishing specimens (BM). But circumferential texture processing was 72 % lower than that of BM. It was attributed that the fatigue cracks was initiation easily by circumferential texture processing. Then, SP technology was induced to repair the fatigue life of the circumferential texture processing specimens. Compared with the BM specimens, the fatigue life of SP specimens increased approximately 12 times. That was attributed to the depth of compressive residual stress field induced by SP.

Keywords TC18 titanium alloy · Machining · Surface texture · Shot peening · Fatigue properties

63.1 Introduction

Ti5Al5Mo5V1Cr1Fe called TC18 in China is a novel high-strength titanium alloy in recent years. It is employed in aviation industry because of its remarkable characteristics: high-strength-to-weight ratio, outstanding toughness and hardenability,

D. Du · D. Liu (✉) · D. Xiang · X. Zhang
Institute of Corrosion and Protection, College of Aeronautics,
Northwestern Polytechnical University, Xi'an 7l0072, China
e-mail: liudaox@nwpu.edu.cn

B. Meng
Xi'an Aircraft International Corporation, Xi'an 710089, China

excellent welding performance, and good fatigue performance, so it has been applied for machining landing gear and other aircraft structures [1–4]. However, by the effect of alternating bending fatigue, like landing gear, it is prone to fatigue failure for the main load-bearing structural parts [3, 4].

In the manufacturing process, various mechanical processing textures will inevitably be introduced on the surface of the load-bearing structural parts, which are equivalent to the induced machining notches. When the aircraft parts are subjected to alternating fatigue loading, the notch stress concentration is easily led to fatigue fracture and then to catastrophic aircraft accidents [4–6].

The shot peening (SP) technology is an effective method to improve the fatigue properties of aerospace structures [7–11], whether it is possible to repair the fatigue failure problem caused by the machining texture. Therefore, this paper carried out the investigation on SP repair of fatigue failure for high-strength titanium alloy TC18 caused by machining texture.

63.2 Materials and Research Methods

63.2.1 Experimental Material

The experimental material is TC18 high-strength titanium alloy, with following chemical composition (in mass percent, %): 5.1Al, 5.1V, 5.1Mo, 0.93Cr, 0.98Fe, 0.021C, 0.15O, 0.02N, 0.0027H, and the balanced Ti. The heat treatment was as follows: The material was annealed at 840 °C for 1 h and then furnace-cooled; Furthermore, it was also annealed at 750 °C for 1 h and then air-cooled; at last, it was annealed at 600 °C for 2 h and then air-cooled. The tensile properties of TC18 titanium alloy are $\sigma_b = 1,220$ MPa (tensile strength), $\sigma_{0.2} = 1,160$ MPa (0.2 % offset yield strength), $\delta = 17.0$ % (elongation), and $\psi = 48.2$ % (reduction in area).

63.2.2 Research Methods

The specimen was utilized by *No.* 100 mesh sandpaper to machining along the axial and circumferential textures, which are parallel to the axial direction of the specimen and perpendicular to that of the specimen, respectively.

To simulate the working condition that sliding rail of aircraft landing gear components was subjected to bending fatigue, the PQ-6 type rotary bending fatigue testing machine was used for fatigue test. The test condition has the frequency of 50 Hz, stress ratio R of −1, and room temperature environment. The sharp and dimension of the fatigue specimen is shown in Fig. 63.1.
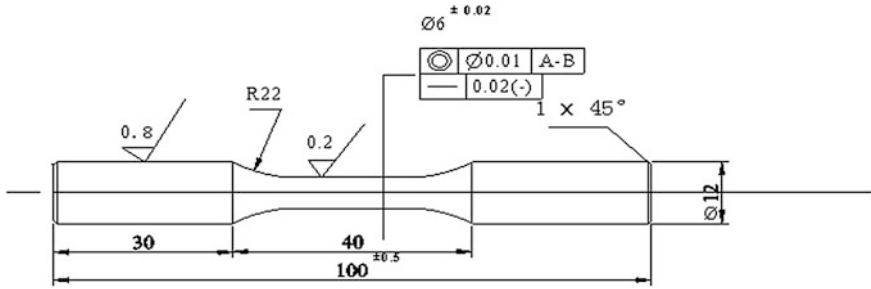
Fig. 63.1 Schematic diagram of fatigue specimen (unit mm)

The SP process was carried out with S110 shot steel, 0.20 mmA SP intensity, and 100 % SP coverage.

JSM-6390A scanning electron microscopy (SEM) was used to analyze the machining textures. An HV-1000 micro-hardness instrument was used to determine the Knoop micro-hardness of the specimen with a load of 0.98 N and loading time of 20 s. The residual stress was measured by D/MAX 2200 PC-type computer-assisted X-ray stress analyzer, with the following methods [11]: the roll method, fixing Ψ_0 scan method (Ψ_0 selected as 0°, 10°, 20°, 30°, respectively), the FWHM for determining peak, Cu ($K\alpha$) target radiation, tube voltage 40 kV, tube current 30 mA, parallel beam technology, and irradiation area 2 mm × 2 mm. Delaminating method was used to measure the residual stress distribution.

63.3 Results and Discussion

63.3.1 Fatigue Life

Figure 63.2 shows the results of fatigue tests on TC18 titanium alloy in different surface states. Fig. 63.2 clearly shows that the machining surface textures decreased the fatigue life of the axial polishing specimen (based material—BM) of the TC18 alloy. The fatigue life of the axial texture and circumferential texture specimens decreased to 27 and 72 % than that of the BM, respectively. That was attributed to the high-strength titanium alloy sensitively to machining notch.

The repair effect of the SP technology is obvious, and then, the SP fatigue life is increased about 12 times than the BM fatigue life. As it is known to all, the turning processing is an important machining process of key aircraft components such as landing gear. When the turning process brought the texture problem, the SP can greatly repair it. So, it will provide a way to improve the fatigue properties of the turning aircraft parts.
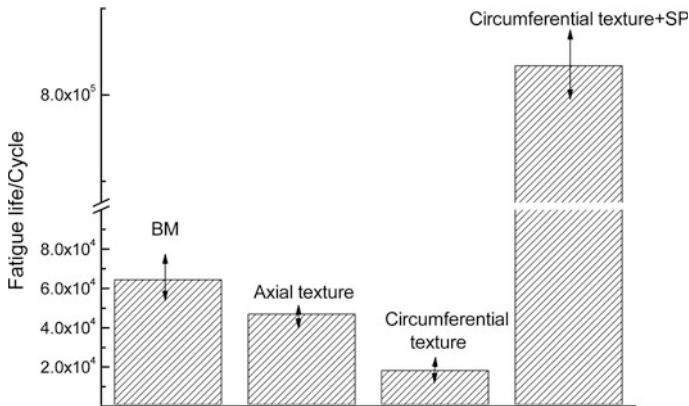
Fig. 63.2 Histogram for comparing with fatigue lives of different surface state specimens at 650 MPa stress level

63.3.2 Micro-characteristic of Surface Texture Orientation

Figure 63.3 illustrates the macroscopic and microscopic morphology of the different surface states. As shown from the figure, there are no obvious mechanical processing traces on the surface of the axial polishing (BM) specimens. However, in Fig. 63.3c–f, it can be obviously seen the machining feature of the axial and circumferential texture. As shown in Fig. 63.3g, h, for the SP treatment on the specimen of circumferential texture, macroscopic and microscopic surface morphology can be seen that the SP pits cover the circumferential texture traces.

63.3.3 Cross-sectional Hardness

Figure 63.4 shows the cross-sectional hardness distribution under the surface of different machining states. As can be seen, surface hardness of the circumferential texture after SP presents the gradient distribution, and the hardened layer is about 150 μm. However, the surface hardness of the axial texture, the circumferential texture, and the axial polished specimen is changed little, and the values of hardness are quite to the substrate.

63.3.4 Surface Residual Stress

Figure 63.5 shows the results of residual stress distributions along the depth in the surfaces of the different surface states. As shown from Fig. 63.5, there has the same distribution rule in the surface of axial polishing, axial and circumferential
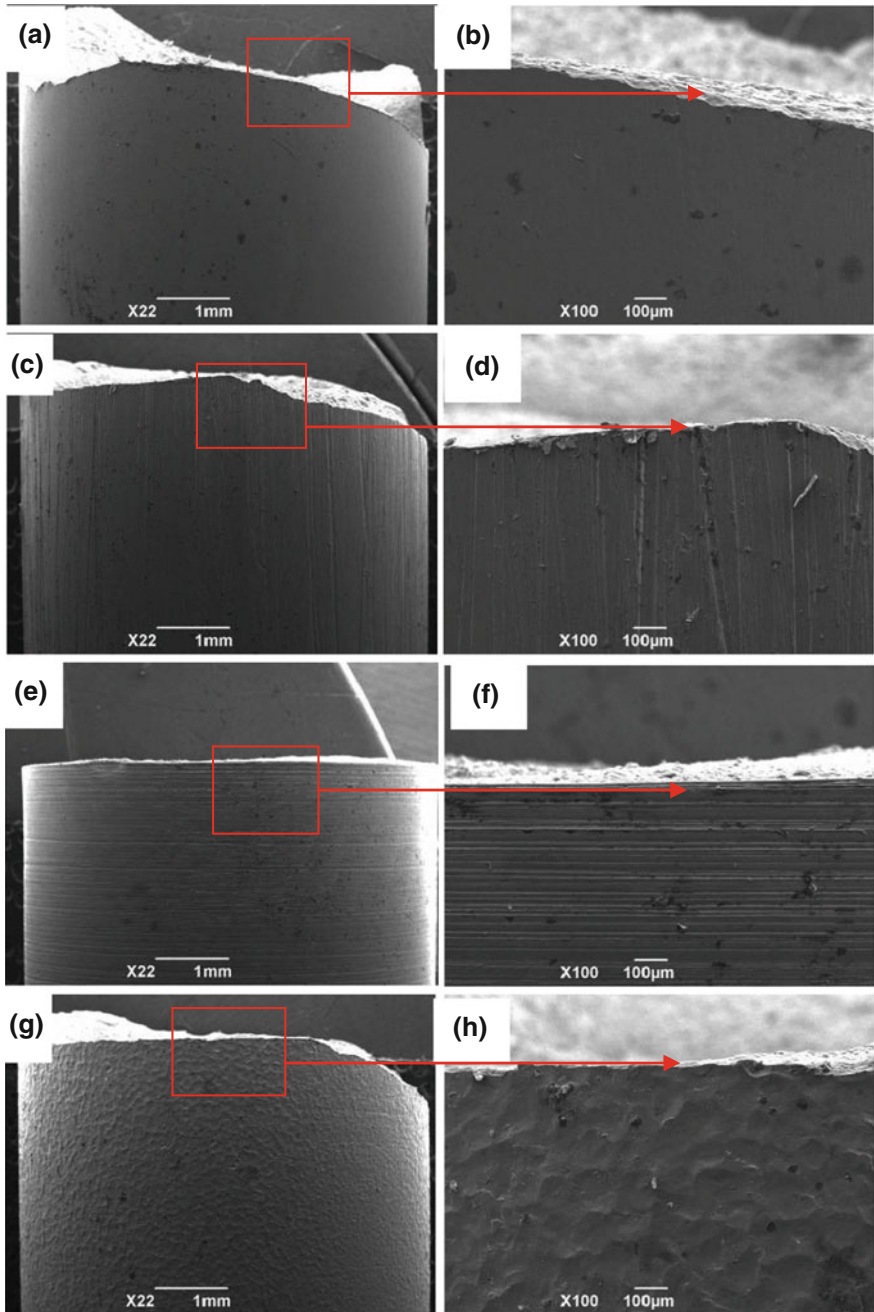
Fig. 63.3 The surface topography of fatigue specimens with different surface states
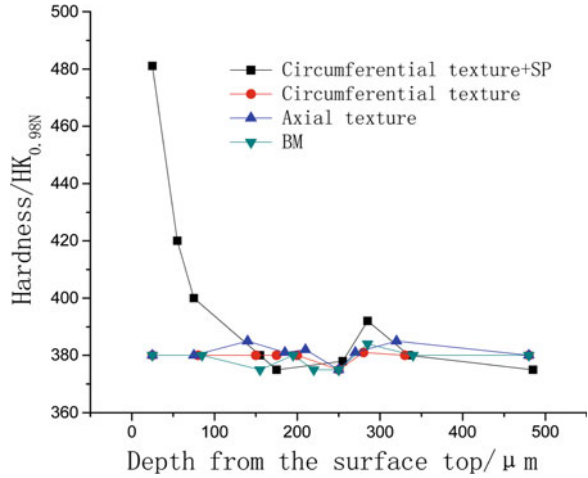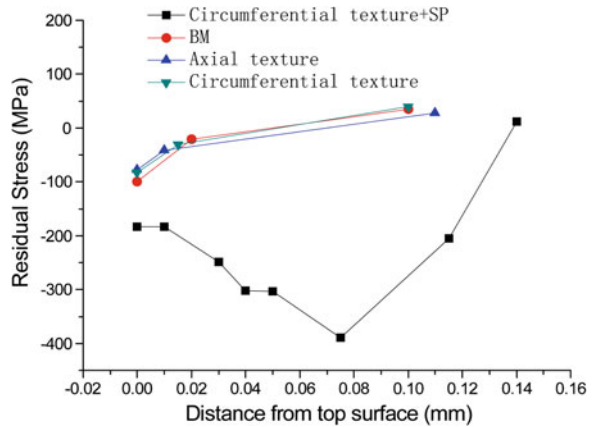
texture specimens. The maximum residual compressive stress at the very surface
was induced by machining, and the value was about -100 MPa. While the cir-
cumferential texture specimens after SP treatment, residual compressive stress was
formed as a gradient field, gradient increasing first and then decreasing. The depth
of SP residual stress field layer was approximately 150 μm, and surface residual
compressive stress was at -182.83 μm. In addition, the maximum residual com-
pressive stress (the value of -389 MPa) of SP at 75 μm underneath the
subsurface.

63.4 Discussion

The fatigue life of TC18 titanium alloy can be significant increased by SP treatment (Fig. 63.2). It mainly attributes to the surface residual compressive stress, which prevents fatigue crack initiation and delays fatigue short crack propagation (promoting crack closure) introduced by SP (Fig. 63.5). There have beneficial effects on surface work hardening (Fig. 63.4) caused by SP. It promotes fatigue crack initiation by surface roughness increasing and surface damage. When the effects of favorable factors outweigh than those of the adverse factors, SP can significantly increase the fatigue life of TC18 titanium alloy.

Therefore, SP can be utilized to improve the fatigue life of the axial high-strength titanium alloy parts and repaired that of the circumferential texture parts induced by turning process.

63.5 Conclusion

In this paper, to solve the problem of the manufacture of aircraft landing gear with high-strength titanium alloy materials TC18, machining textures and SP technologies have been investigated, main conclusions are as follows:

1. The machining texture orientation has great effect on the rotating bending fatigue life of the high-strength titanium alloy. The fatigue life of axial texture parts was reduced 27 % lower than that of the axial polishing parts, and the life of circumferential texture was 72 % lower than that of the axial polishing parts.
2. The effect of the repairing on fatigue life of machining parts by SP was obvious, and the fatigue life was increased about 12 times than that of the base material. It mainly attributes to the surface residual compressive stress, which prevents fatigue crack initiation and delays fatigue short crack propagation (promoting crack closure) introduced by SP.

References

1. Ulutan D, Ozel T (2011) Machining induced surface integrity in Titanium and Nickel Alloys: a review. Int J Mach Tool Manuf 51:250–280
2. Boyer PR, Briggs RD (2005) The use of β Titanium Alloys in the Aerospace Industry. J Mater Eng Perform 14:681–685
3. Wang X, Gao Y, Wang Q et al (2012) Effect of re-shot-peening on the fatigue life of TC18 Titanium Alloy. J Mater Eng (2):67–71 (in Chinese)

4. Javidi A, Rieger U, Eichlseder W (2008) The effect of machining on the surface integrity and fatigue life. Int J Fatigue 30:2050–2055
5. Suraratchai M, Limido J, Mabru C et al (2008) Modelling the influence of machined surface roughness on the fatigue life of Aluminium Alloy. Int J Fatigue 30:2119–2126
6. Wang CY, Xi WJ (2012) Investigation on notch sensitivity of TC18 Titanium Alloy. Rare Metal Mater Eng 41:663–666
7. Zhang XH, Liu DX (2009) Effect of shot peening on fretting fatigue of Ti811 Alloy at elevated temperature. Int J Fatigue 31:889–893
8. Liu DX, He JW (2001) Effect of shot peening factors on fretting fatigue resistance Titanium Alloy. Acta Metall Sin 37:156–160 (in Chinese)
9. Xie L, Jiang C, Lu W (2011) Investigation on the residual stress and microstructure of (TiB + TiC)/Ti–6Al–4V composite after shot peening. Mater Sci Eng, A 528:3423–3427
10. Mylonas GI, Labeas G (2011) Numerical modelling of shot peening process and corresponding products: residual stress, surface roughness and cold work prediction. Surf Coat Technol 205:4480–4494
11. Du DX, Liu DX, Meng BL et al (2013) Effects of pretreatment and HVOF sprayed cermet coating on fatigue properties of TC21 Titanium Alloy. Sci China Technol Sci 56:1029–1037

Chapter 64
The Confirmation of FDR Parameter Set for UAV

Liu Changwei and Zhang Ruifeng

Abstract Flight data recorder (FDR) is equipped on all manned aircrafts almost. The parameter set used in vehicle maintenance, flight training assessment, and flight accident investigation is standardized. Given the difference of design, employment, and maintenance between UAV and manned aircraft, the FDR parameter set for manned aircraft is not appropriate for UAV. In this article, a new parameter set for UAV is presented, including four supplementary parameters specialized for UAV. This new set can be the reference for design and can improve the safety of UAV.

Keywords Flight data recorder · UAV · Safety · FHA

64.1 Introduction

Flight data recorder (FDR) is auto-recording equipment for flight data. It is crucial for flight accident investigation because the precise cause of accident can be determined by the data. These data could also be used in the flight maintenance and quality control, flight training assessment, and other aspects. Flight data are imperative to increase airworthiness consistently, and thus, the use of FDR has been expending over time.

CAA published the first standard [1] of FDR in 1957. All aircrafts whose weight exceeds 12,500 pounds and service ceiling higher than 25,000 ft must be equipped with crash-safe FDR. As more problems are encountered throughout the service,

L. Changwei (✉) · Z. Ruifeng
Beijing Aeronautical Engineering Technology Research Center, Beijing 100076,
People's Republic of China
e-mail: liuchangwei@netease.com

Z. Ruifeng
e-mail: thisway030217@163.com

the protection standard has been improved over time. According to the rules of the standard, manned aircrafts must fly with FDR.

There are two basic requirements for a FDR system. One is the survivability from light accident, and the other is a comprehensive parameter set.

The parameter set for manned aircrafts is determined by numerous flight accidents and maintenance experience, and the rationality, the systematicness, and the completeness of parameter set of actual FDR norm are proved fully by practice [2].

From the practice, we can see that the parameter set can be divided into six parts. The first one consists of aerodynamic parameters, such as altitude, air speed, attitude, angle of attack, and angel of sideslip. The motion of the aircraft and the surrounding atmosphere condition can be deduced from these data.

The second part is the engine data, including rotor speed, exhaust gas temperature, and fuel consumption rate. One can deduce the operational status and the emergency alarm of engine from these data.

The third part is the control input data, including the stick input, the steering input, the flap/slat control, and speed brake. These data present the overall input from pilots.

The fourth part is aircraft configuration data. It comprises the deflection of aileron, rudder, and elevator, the position of landing gear, etc. If the aircraft uses fly-by-wire flight control, the key value of every phase of each channel is also recorded for denoting the details of whole control system response.

The fifth part is the status and alarming of other important airborne equipment, including electrics, hydraulic, navigation, and environment control. These data indicate the status and failure of these equipments.

The sixth part is peripheral information, such as GMT, index of flight, takeoff weight, and synchronous token. All these data serve as the reference of validity of flight data.

These six categories of data present the running status of aircraft and airborne equipment, and they can satisfy the requirement of maintenance, flight training assessment, and flight accident investigation.

In recent years, with the ever-increasing progress of computer, communication, navigation, and control technology, UAV is under rapid development. They are qualified for some kind of missions, such as dangerous, stuffy, long range, and long airborne time, which were carried out manually. With the improvement of the functionality and capability of UAV, these vehicles are widely used in scout, surveillance, strike, and relay missions. Because of these characteristics, UAV has been increasing in weight, range, and cost, resulting in a higher requirement for safety of the whole system. So UAV's FDR becomes important for maintenance, flight training assessment, flight accident investigation, and airworthiness development.

At present, no fixed standard exits, which defines the parameter set to be recorded for UAV. Neither in the countries that have sophisticated aeronautic technology such that the USA, Russia, and Israel nor in China. The reason comprises three aspects. First of all, the safety of crews does not need to be taken into account, thus resulting in a lower overall safety requirement than the manned counterparts, and the need of relating research is less urgent. Secondly, the rapid

development of UAV and the discrepancy among each type make a uniformed standard of FDR difficult. The last one is that most early and current UAV types are small in size, coupled with simple functions, mostly disposable missions such as target drone or suicidal attacker, so there is no need for FDR in this case. All these factors cause scarce usage of FDR in UAV, let alone the standardization of UAV's FDR parameter set.

Nowadays, the obvious trend of UAV lies in larger size, longer endurance, and higher artificial intelligence. It may feature both scout and strike capability, such as the "Predator." For example, the "Global Eagle" has a huge fuselage, long endurance and range. For these huge UAV, the requirement of their safety and mission reliability is increasing steadily. UAV's tasks include not only military operations, but also non-military applications, so its operating airspace has some overlap with the civil and general aviation, and a more strict safety standard is needed from a point of view of air traffic and airworthiness. The demand of health management and application assessment by FDR is exigent, and the standardization of FDR's parameter set should be completed soon so as to satisfy the demand in safety and maintenance.

64.2 UAV Safety Assessment

UAV's key feature is that it is unmanned. It requires a comprehensive safety assessment to select its FDR's parameter set. The workflow of the assessment is recommended by ARP4761 [3], which performs the functional hazard analysis (FHA). The process is as follows: the functions of aircraft and its systems are arranged first, and then, the failure model should be extracted and the hazards of failure models should also be determined. At last, the parameter set is finalized with regard to the hazards.

According to the workflow of FHA, the functions and components of UAV system are clarified first. UAV system can be divided into two relatively independent parts: The first is ground equipment, including ground control stations and communication equipment. The ground control station is responsible for the selection of flight stage, route, and course. The maneuvering strategy and load factor control are also performed by the ground equipment. The communication equipment is responsible for transforming data, voice, vision signal, and the payload (such as surveillance equipment) of UAV between ground control station and UAV. The second part of UAV system is the UAV's ontology. The UAV's ontology features several backup communication equipments, besides the engines, flight control, electric, navigation, and autopilot system, which all aircrafts have in common. These equipments can communicate with ground stations through UHF, VHF, and even through the satcom with multiple frequencies and modulations. The link of communication can be directly lined between UAV and ground station or relayed by other airborne vehicles. The typical protocol of UAV system [4] is shown in Fig. 64.1.
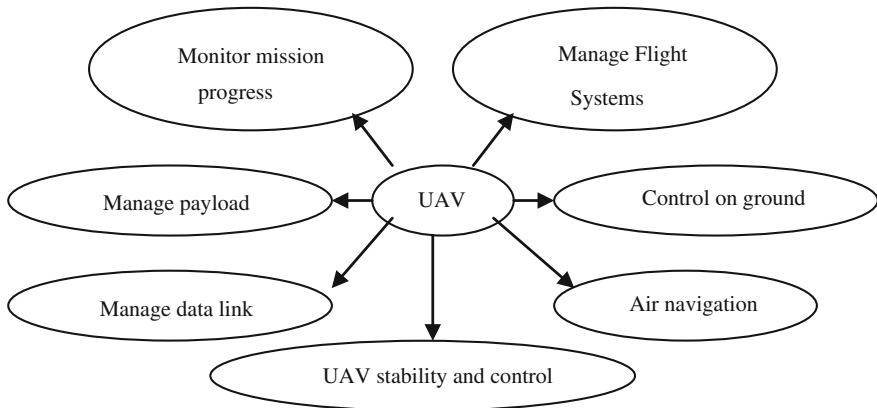
Fig. 64.1 Typical protocol of UAV system

UAV's workflow is executed in a standardized order. First step is uploading flight plan, which includes the setting of route, frequency, channels, and the encryption method of communication. Then, instructions of starting engine, taxing, takeoff, rocket-assisted, or catapult launch are sent by the ground station. After takeoff, UAV will climb up and join the route according to the intended procedure. On the arrival of the desired airspace, the UAV will execute the scout, surveillance, and investigation missions. If needed, the UAV's maneuver can be controlled by the ground stations. When air-traffic systems are involved, the voice communication will relay by UAV to link air-traffic controllers and UAV's controllers. If the UAV is about to leave the control area of one ground control station, the control will be taken over by others. During the mission, reasonable data communication mode is chosen by mission manager on UAV to transform the detected info and devices on UAV to ground control station. After the completion of the mission, UAV will land or touch down by arresting barrier.

In the whole process, function hazards are mainly embodied in three aspects. The first thing to consider is the hazard of losing self-test ability. Both software and hardware of communication, flight control, navigation, and mission management are all under self-test supervision in real time. Once failure occurred, or contact between UAV and ground control stations lost, the flight must be terminated according to a predefined emergence mode. If a false alarm occurs, the wrong decision will be made, which has negative effects on the safety and mission reliability. The second is hazard of executive control failures from ground stations. UAV should avoid losing contact with ground stations or getting in danger due to complex environment. In order to avoid communication occlusion of mountain or adverse weather, ground stations should change the route of UAV provisionally. So coordination between UAV and ground stations is imperative. If any of these hazards happens, UAV will be led astray. The third is the hazard of losing airborne mission computer safety–critical software function [5]. This software is. It is

because of the "unmanned" characteristic. Correct execution of tasks relies on the information stream between UAV and ground stations. Response and delay to control command depend on the communication, navigation, and intelligent task management. Emphasizes on reliability, real time and normalized response place great demands on reliability and higher quality of software [6]. Once the software fails, UAV would be in danger instantly, even crash.

Analysis above suggests that FDR parameter set of UAV should append relating information according to its workflow and function hazards, based on manned aircrafts.

64.3 Catalog of UAV's FDR Parameter Set Need to be Appended

Besides six parts of FDR parameter set of manned aircrafts, following data should be appended.

First, the data to append consist of the commands from ground station received by UAV and the response to command from UAV. This information includes the engine start, taxi, takeoff, selection of route or course of flight, the maneuver, mission plans, payload control, distributed routing of investigation information, index of landing field and landing command, and target distribution. One important thing needs to be addressed is that this information is generated and received by UAV, not by ground stations. That is to say, we should know what it hears, what it will do, and what it has done with the FDR data.

Secondly, information of working condition monitoring and fault isolation of airborne devices should be taken into account. UAV determines the status of airborne systems through runtime self-test, regulates its mission, and makes emergency operation according to the results, so low false alarm rate is obligatory, especially the key systems such as communication, navigation, and fly control. Not only should the data of every channels, but also test results and decision of each segment be recorded, so as to reduce the false alarm rate.

The third thing is the information of software branch judgments. These data represent how computers deal with the calculation and decision within its safety critical software. They are firsthand to determine the failures and faults of software. This information will be good to increase the reliability of software and play a role of pitching pile in software test. According to the experience of software engineering, the failures in highly integrated and extremely complex airborne software cannot be completely eliminated only by testing, serving as a complement. DO178B should be strictly carried out throughout the whole life expectancy to guarantee its airworthiness. Software deficiency rate deduction method is ameliorated in practice.

The fourth thing includes commands and information created in ground control stations. In the narrow sense, ground station does not belong to UAV, but in view

of its core position in UAV system, it is very important for correct and safe UAV operating. So the operating information of ground control station should be recorded with UAV synchronously. These data include control instructions, communication, manual control, usage of payload, and emergency handling. They should be processed with data download from UAV after flight.

These data are proposed according to characteristics of UAV and can reflect real conditions and the transient of decision making of UAV comprehensively, thus improving its safety.

64.4 Summary

According to the characteristics of UAV, its FDR should record additional information to satisfy these features. All four types of data discussed above basically cover these requirements. Together with the traditional six parts of parameters, these new types of parameters present the process of UAV's software and hardware and are competent for FDR's tasks. UAV will achieve a better safety with this material basis.

References

1. Yang L, Shu P (2013) The development of aviation records review and future trends. Civil aviation administration aviation safety technology center, Beijing. http://123.127.67.23/castcdata/webedit/UploadFile/2007420111039998.pdf. Accessed 12 Nov 2013 (in Chinese)
2. Boeing. Aviation Safety, Boeing Commercial Airplanes (2011) Statistical summary of commercial jet airplane accidents-worldwide Operations 1959–2010. Seattle
3. ARP4761 (1996) Guidelines and methods for conduction the safety assessment process on civil airborne systems and equipment. Society of automotive engineers, Inc., Warrendale, PA
4. Evans AR (2006) The hazards of unmanned air vehicle integration into unsegregated airspace. The University of York, York
5. Nordhoff S (2012) DO-178C/ED-12C the new software standard for the avionic industry: goal, changes and challenges. SQS Software Quality System AG. Stollwerckstrasse 11, 51149 Cologne, Germany
6. Schultz T (2009) Meeting DO-178B software verification guidelines with coverity integrity center. Coverity, Inc., San Francisco

Chapter 65
Investigation of Characteristics of New Helicopter Maintenance and Impact on Current Domestic Maintenance Work

Min Zhou, Zhi-hui Ge, Ke-xue Yan, Rong Huang and Wei-gang Wang

Abstract As the maintainability and reliability of new helicopter have been greatly improved, the domestic users directly realize some new characteristics of maintenance work. The investigation of characteristics and impact of new helicopter maintenance on the current domestic maintenance work are performed in this paper. Firstly, the analytical results show that the troubleshooting work becomes simpler; condition-based maintenance (CBM) and "changing parts maintenance" have become the inevitable trend for new helicopter maintenance. Secondly, for the impact on maintenance work, the current system of maintenance work and profession division is facing challenge; some maintenance profession has been marginalized; on the contrary, there are some new vacancy profession for maintenance should be filled. Finally, some suggestions of maintenance theory, technology method and maintenance system are brought forward.

Keywords New helicopter · Maintenance · Characteristic · Impact

65.1 Introduction

As well known, the work of helicopter maintenance engineer is to inspect, maintain and repair the various electrical/electronic, mechanical and structural components of helicopters. They should carry out routine preflight checks to ensure that the helicopter is safe. More detailed inspections are also carried out on each helicopter, where each component is examined and tested for damage and faults. Where problems are detected, helicopter maintenance engineers assess whether the component can be repaired or if it needs to be replaced entirely.

M. Zhou (✉) · Z. Ge · K. Yan · R. Huang · W. Wang
Beijing Aeronautical Technology Research Center, Beijing 100076,
People's Republic of China
e-mail: minzhou1981@163.com

Recently, some new types of helicopter have been equipped at home; through the operation and maintenance of new helicopter, the users have directly felt with the rapid development of helicopter technology, especially with improvements in the maintainability and reliability of new helicopter, so that the first-line maintenance work is also reduced and the labor intensity is reasonably reduced. At the same time, the users also directly realize that the new helicopter maintenance process and method have gradually changed [1]. The main objective of this study is to widely investigate the characteristics of new helicopter and impact on the current domestic maintenance work.

65.2 The Characteristics of New Helicopter Maintenance

The transition from time-based maintenance (TBM) to condition-based maintenance (CBM): With the development of the high-precision sensor, data processing and component monitoring technology, the health and usage monitoring system (HUMS) has gradually been a standard feature of the new helicopter [2], which uses specialized software designed to identify trends or anomalies in key helicopter systems, allowing them to be assessed and corrected. In flight, pilots can view and monitor this data via the pilot interface panel and make informed decisions. After each flight, all HUMS flight data are downloaded to the ground station (as shown in Fig. 65.1). Anomalies in helicopter performance are detected and reported to maintenance instantly, allowing immediate responses to potential issues. Providing users' maintenance department an in-depth view of the health of each helicopter before and after each flight ensures that the fleet of helicopter is always ready for service [3, 4]. As a result for extensively using of HUMS, which assists in the transition from TBM to CBM, there is an increasing trend to use HUMS to facilitate CBM approaches to achieve maintenance burden reductions and make the maintenance work becomes more scientific, and the ultimate goal of helicopter CBM programs of new helicopter is to conduct maintenance only on the evidence of need.

"Changing parts maintenance" has become the main repair method. Seen from the perspective of troubleshooting method, there are two main troubleshooting method, one is to recover the function of fault components by maintaining work, the other is to entirely replace faulty components. In the new helicopter, the reliability level of key component of flight safety has become more higher, such as composite flexible rotor head and main structure of helicopter body, which almost never makes problem, so that users rarely need to carry out maintenance work; moreover, the condition monitoring and CBM have been the main maintenance methods for new helicopter. When these systems or parts malfunction, the built-in-test system (BIT) of helicopter can provide information of fault detection, fault isolation and fault location, so that fault detection and location work become more accurate and simpler; moreover, as the design of line replaceable unit (LRU) and line replaceable module (LRM), so the troubleshooting work becomes simpler; in
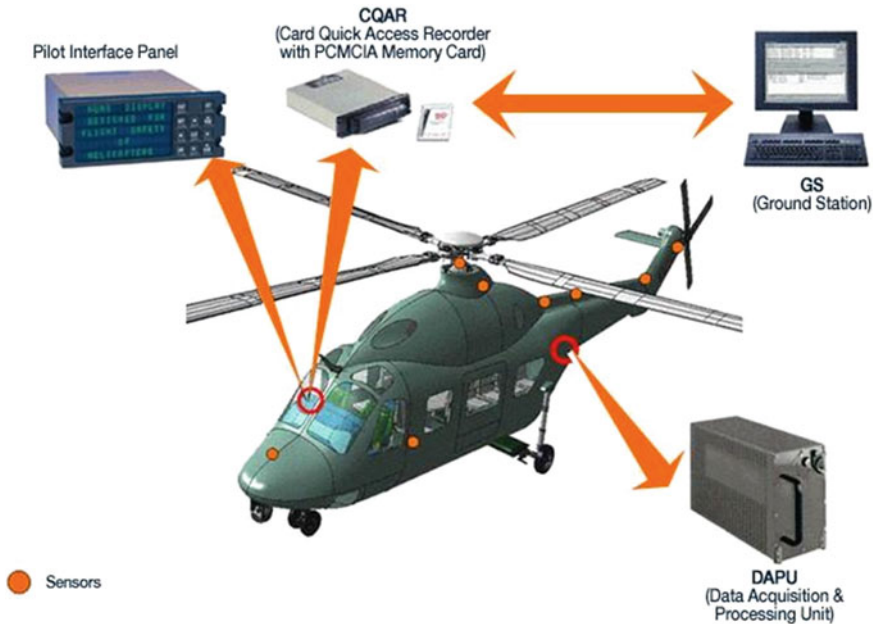
Fig. 65.1 The health usage monitoring system (*HUMS*) in the helicopter

the maintenance practice, the failure of equipment function and performance are recovered by users with the tools and equipment, and these traditional sense of the maintenance work has gradually become history and that "cannibalization maintenance to confirm the fault" and "changing parts maintenance for troubleshooting work" have become the main maintenance way of new helicopter.

For example, the new composite rotor blade has been a standard feature of the new helicopter, not only the flight performance of composite rotor blade is enhanced but also the maintainability is enhanced, such as the requirement for improved resistance to sand erosion and the need for enhanced resistance to impact damage, all these through provision of role fit protection or as a capability of the basic blade design to be achieved; as a result, strong emphasis was placed on the incorporation of a robust blade trailing edge structure and a mechanically fastened tip. If the blade tip structure was damaged, outfield maintenance crew would no longer need to replace the whole rotor and simply change a new detachable tip.

In addition, the maintenance method of "changing parts maintenance" has reduced the requirement any less dependent on the traditional troubleshooting ability of maintenance crew; on the other hand, requirement of aircraft material reserve, detection and calibration equipment is greatly increased.

The new requirement for ability of maintenance engineer: New helicopter with complicated body structure and high technical equipment, and the requirement for technical ability of maintenance engineer also become more higher, and this representation is very conducive to emphasize the difficulty and importance of

maintenance. But the truth is, which seems not very accurate. In general, due to using advanced equipment, the maintenance burden and requirement of traditional troubleshooting ability have been reduced.

For the outfield maintenance of new helicopter, users should focus on the ability to efficient routine maintenance work and condition judgment; while for the infield maintenance, users should focus on the new ability to data processing and fault diagnosis. In addition, for new helicopter maintenance work, the users should not only consider the new requirement for maintenance engineer quality but also to need to take into account the increment of overall ability of maintenance crew.

65.3 The Impact on Current Domestic Maintenance Work System

The current maintenance work and profession division are facing challenge. At present, due to the integration, degree of helicopter technology and system become more and more higher; as a result, the maintenance profession also develops in the directions of integration, but the current profession division is difficult to meet the maintenance requirements of new helicopter, and the current maintenance system cannot make the maintenance work bring into full play.

For the new helicopter has been in service, users have clearly divided the systems, components and parts of new helicopter in accordance with previously mentioned the four maintenance profession division. Obviously, for the new helicopter, if the maintenance profession continues to be divided into mechanical, ordnance, ad hoc and radio profession, the systems of new helicopter would not be effectively covered with current maintenance division. For these systems, components and parts involve multiprofession, which can not be divided into a separate profession field. So that the phenomenon of cross and integration of technology and profession is an indisputable reality.

Such as the fly-by-wire technology, in a fly-by-wire system, the pilot's control stick movements are converted to electronic signals and transmitted to computers. The computers determine how to move the actuators at each control surface to provide the best response. The computers also enhance performance by issuing commands without the pilot's knowledge to stabilize the helicopter and perform other tasks. It is clear that fly-by-wire technology includes fly control system, electrical source system and engine etc., which relates to traditional mechanical and ordnance and ad hoc profession; the traditional mechanical profession cannot work by himself, so that the traditional division is facing challenge.

In addition, as the same maintenance system of fixed wing aircraft, current domestic helicopter maintenance system is also divided into infield work and outfield work. The outfield work is responsible for the daily maintenance and flight support of helicopter; the infield work is responsible for regular check, inspection and maintenance work of helicopter. The maintenance crew is a unit to organize

outfield maintenance, and the air mechanic is appointed responsible person of maintenance crew in accordance with the current domestic helicopter maintenance regulations. But in the infield practice, maintenance crew is constituted by fixed mechanical engineer and non-fixed ordnance, ad hoc and radio engineers; maintenance crew can not effectively work in the organization, personnel management and coordination. In addition, because of the profession work responsibility interface is clear, even in the same helicopter, the maintenance engineer also works with the non-interference principle; all these phenomena are not beneficial to improve the maintenance work of new helicopter.

Some maintenance profession has been marginalized. Among the domestic helicopter maintenance system, in addition to the four traditional maintenance profession, there are also some other maintenance profession, such as processing machinery, accessories maintenance and oil joint; these types of work used to be called the repair profession. Due to the widespread use of new technology and new material, the maintainability and reliability of new helicopter have been greatly improved; these simple repair professions have been almost nonexistent in new helicopter maintenance system, such as parts manufacture and soft and hard pipe production work have no implementation chance.

There are some new vacancy profession for maintenance should be filled. With the development of helicopter technology, there are some new maintenance profession with clearly profession character, such as software maintenance, winch operator and data processing, but these professions are still blank in the current domestic maintenance profession division [5]. So that there is the need to increase some new maintenance profession, which mainly inculdes the composite maintenance, software maintenance, data processing and flight parameters judgment. To improve the maintenance system of new helicopter and keep enhancing the core ability to maintenance, users should demonstrate the requirement of new maintenance profession and then research the scheme of supplementary profession for new helicopter.

65.4 The Suggestions

Strengthening the research on the scientific theory of helicopter maintenance: The scientific helicopter maintenance is a scientific summary based on the practice of helicopter maintenance activities [6], which involves operation and maintenance etc. As the face of helicopter maintenance changes, the maintenance theory should be dynamic enough to keep pace with the advanced maintenance theory. In order to guide effectively, the development of helicopter maintenance science, designer and users should deeply research fault rule and maintenance initiatives of new helicopter; moreover, designer and users also should carry out the research of new material maintenance technology, new maintenance method, green maintenance technology and independent maintenance technology; based on these research, the

front maintenance team can effectively master the scientific theory of maintenance and technology.

Further enrichment of the maintenance technology method: At present, with the development of new maintenance technology, there has been fairly constant research devoted to reduce the front maintenance burden, and many applications of new support system of maintenance have been realized. Such as wireless maintenance technology and integrated maintenance support system, the maintenance support system includes links production control, quality control, tech supply, decision support system, network library of manufacturers' technical data, electronic logbook and flight records, which can effectively enhance the ability of front line to manage maintenance events at the platform, and which can provide the decision and technology support for higher level analysis of fleet management. For wireless maintenance technology, which is a wireless net set in a limited field environment, the users can get information of maintenance instantly through the wireless net; moreover, the wireless server can transmit logbook data from flight line back to PC and QC instantly, realize the network maintenance management and effectively reduces the "Off Aircraft" maintenance time of the maintain crew.

Improvement of the current maintenance work system: To keep pace with the development of new helicopter, the maintenance level of front line should be improved, and the users' core maintenance ability should be enhanced. Relaying on the new maintenance support technology, users should make great efforts to develop maintenance management innovation and realize the networking and information management of helicopter equipment, maintenance personnel and security facilities; moreover, users should do efforts to explore new helicopter equipment maintenance organization model, optimize maintenance process, reduce maintenance work links and improve the current 3-level maintenance of domestic helicopter to 2-level maintenance.

65.5 Summary

The investigation of characteristics and impact of new helicopter maintenance on the current domestic maintenance work are performed in this paper. As a whole, CBM and "changing parts maintenance" have become the inevitable trend for new helicopter maintenance, and the current domestic maintenance work system can not keep pace with the development of new helicopter and new technology. These changes of maintenance work are inevitable; in order to make sure these changes develop in the right direction and enhance the key ability to maintenance, the domestic users and manufacturer should do more.

References

1. Li W (2012) The impact of new technology for helicopter maintenance. Int Aviat 595:75–81
2. Draper A, Gourlay J (2003) The operational benefits of health and usage monitoring systems in UK military helicopters. DSTO HUMS 17:18–25
3. Butcher SW (2000) Assessment of condition-based maintenance in the department of defense. In: Corporate RIDGE (ed) Logistics Management Institute Report LG903B1
4. US Joint Helicopter Safety Implementation Team (2013) Health and usage monitoring systems toolkit. In: International Helicopter Safety Team (ed)
5. Information, http://easa.europa.eu/rulemaking/technical-publications.php
6. Zhang ZM (2011) Flight test helps to set up efficient maintenance. Int Aviat 578:71–82

Chapter 66
The Requirement Analysis of Aviation Equipment Maintenance and Supportability Under the Two-level Maintenance System

Jilong Zhong, Jilian Guo and Zhuojian Wang

Abstract Based on the data of specific airborne equipment, PRICE model is adopted to analyze the impacts of different maintenance concepts for maintenance and supportability costs and operational availabilities. The costs of different maintenance concepts differ a lot with the result of calculations, which will also place a great impact on the equipment operational availability. To further cost estimate and analyze the three-level (level-III) and two-level (level-II) maintenance concepts, the program under a two-level Maintenance System has an advantage on using economics.

Keywords Maintenance concept · Maintenance and supportability cost · PRICE model · Two-level maintenance

66.1 Introduction

Over the last 20 or 30 years, various countries adopt the three-level Maintenance System for aviation equipment, namely Organization, Intermediate, and Depot three levels. Of course, there will be some differences with the name among countries. However, since 1990s, the United States and some European countries took a lead in aviation reform and exploration, which affects greatly on the maintenance mode of aviation equipment, resource requirements, and even the equipment fight force.

J. Zhong (✉) · J. Guo · Z. Wang
Air Force Engineering University, Xi'an, China
e-mail: z_jilong@sina.cn

J. Guo
e-mail: guojilian@aliyun.com

Z. Wang
e-mail: zhuojianw1974@sina.com

Based on a specific airborne equipment data, this paper attempts to analyze how the different Maintenance Systems (level-II or level-III) impact on the maintenance costs and operational availability using a quantitative way.

66.2 The Aviation Equipment Maintenance System

66.2.1 The Current Military Aviation Equipment Maintenance System

At present, Maintenance Systems of air force in China are divided into three levels with an enormous difference in the maintenance depth or detail. The maintenance level for the introduction to maintenance task is as follows:

1. Organization maintenance. Organization maintenance usually refers to the outfield and infield maintenance of the Flying Corps, operating by professionally trained personnel for on-site equipment. As the result of time and resource limitation, Organization maintenance is only limited by regular maintenance, judging and determining a fault, removing parts of equipment. The main tasks include (1) cleaning and lubricating equipment. (2) antirust and corrosion prevention. (3) performance monitoring and measurement. (4) electronic parts in site inspection. (5) system adjustment and calibration. (6) failure searching and isolation. (7) removing parts or components. and (8) equipment keeping and information record and transmission.
2. Intermediate maintenance. Intermediate maintenance usually refers to maintain the military aviation repair plant with personnel having a better technical capability than the one in Organization maintenance, equipped with all kinds of supporting equipment. And it is able to complete the work that the Organization maintenance cannot do. It provides technical support to the Organization maintenance at the same time. The activities in this are the following: maintenance, overhaul, measure, and inspect all equipment parts not belonging to plant or sale manufacturers' responsibility to repair.
3. Depot maintenance. Depot maintenance refers to maintenance in the aircraft factory with a greatest repair capability and can perform any repair work necessary to failure equipment, including the improving maintenance. The Depot maintenance usually includes equipment overhaul, large components repair, spare parts manufacturing, remaking or refitting, and some programs that cannot be completed in the Intermediate maintenance. In the multi-level structure, the general maintenance units provide technical support to several subordinate maintenance units [1].

66.2.2 US Air Force Two-level Maintenance System

US Air Force has long adopted the three-level Maintenance System. Aircraft is repaired by the Organization, Intermediate, and Depot three levels. In June 1992, US Air Force instructs that all the new weapon systems adopt the two-level Maintenance System, and encourage the implementation for current weapon. In December 1992, number 983 defense management review decision approves this program. In October 1, 1993, the selected engine and aviation electronic equipment formally start two-level Maintenance System.

Two-level maintenance refers to sending the equipment parts that cannot be repaired in the Organization to Depot without passing through the Intermediate maintenance. In fact, the Intermediate maintenance is canceled after the implement of two-level maintenance. At the same time, the meaning of Organization and Depot maintenance is also different from the meaning before. It transfers most repairing functions of Intermediate to Depot, and a few to Organization, which strengthens the Organization and Depot functions of original system. The benefits of this are [2] as follows:

1. Canceled the Intermediate maintenance, reducing the quantities of Intermediate maintenance support equipment, personnel, training task, and reservation of spare parts, so the costs are saved.
2. The cost of each failure decreases during the Depot maintenance; thus, the supply demand declines.
3. Limited funds for spare parts acquisition can support more individual systems, so the using availability increases, which means there will be more equipment or equipment will be more efficient.
4. Shorten the maintenance cycle.

Two-level maintenance has another two benefits of reducing managers in air force unit, and shortening the logistic support. According to the relevant information, the mean maintenance cycle of a set of typical electronic device will be shortened from the original 17 to 9.5 days. Based on the forecast, annul logistic funds of US Air Force could reduce $100 million or more after adopting two-level maintenance. According to air force material command program, there are about 3,000 engines and 500 aircrafts adopting two-level Maintenance System.

In order to meet the requirement of two-level maintenance, equipment in the design and use must meet the following requirements: First, optimize the life-cycle cost through properly grading maintenance during the program design; second, provide enough in-test capabilities during hardware design so as to provide line replaceable unit (LRU) list in time; and third, guarantee enough LRU without delay.

However, experts of maintenance Organization do not wish the equipment in accordance with the three-level Maintenance System design and manufacture forced to use two-level Maintenance System. They wish that the selected system will have a better maintenance and use economy through design. Thus, considering

canceling the Intermediate maintenance, inspection and support during new weapon design are necessary. After having done this, the costs and personnel technical requirement brought from Intermediate maintenance can be solved effectively.

F-22 aircraft design adopts two-level Maintenance System. Because the purpose of two-level maintenance and its study are both to make the late support workload minimized, so F-22 only needs 45 % maintenance personnel of F-15's. Deploying a flying squadron owned 24 F-15 aircrafts needs 17 C-141 transports, while F-22 only needs 8 C-141 transports [4]. In order to cancel the Intermediate maintenance of aviation electronic devices and engines, design of the F-22 aircraft comprehensively considers the improvement of failure judgment and repair capability.

Of course, two-level Maintenance System still exist many problems during its implementation. At present in US Air Force, especially in combat troops, there are many doubts for two-level maintenance. First, it will impact on the maintenance capability of combat troops because 90 % or more maintenance work was done by combat troops themselves before, but now the work was sent to Depot complete, which makes the combat troops lost the ability of failure judgment. Second, combat troops do not trust the repair quality of Depot maintenance. Third, aircrafts are often in frontline service. Once requiring frequently flying, the situation will be passive totally depending on Depot maintenance [6].

Using two-level maintenance, there is still risk of reducing readiness rate. Because of canceling the Intermediate maintenance, the overhaul work will depend more on transportation and supply function. This new dependency has become the "Lean Logistics" causes.

66.3 Example Analysis

It is an airborne radar system, mainly composed of three kinds of hardware, namely the LRU: processor, antenna, and a digital processing unit. This paper selects one of the LRUs to analyze, using the mainstream equipment life-cycle cost model PRICE to calculate [5].

66.3.1 The Maintenance Concepts of Three-level Maintenance System

PRICE model provides 28 kinds of basic maintenance concepts, basically covering all the possible maintenance concepts under the three-level system as is shown in following Table 66.1 [3].

Table 66.1 28 kinds of basic maintenance concepts

Number	The details of the maintenance concept
1	Discard LRU at failure
2	Replace modules at Organization—scrap bad modules
3	Replace modules at Intermediate—scrap bad modules
4	Replace modules at Depot—scrap bad modules
5	Replace modules at Organization—repair modules at Intermediate
6	Replace modules at Organization—repair modules at Depot
7	Replace parts at Intermediate
8	Replace modules at Intermediate—repair modules at Depot
9	Replace parts at Depot
10	Replace parts at Organization
11	Discard modules at failure
12	Isolate modules at Organization and repair modules
13	Isolate modules at Organization—repair modules at Intermediate
14	Isolate modules at Organization—repair modules at Depot
15	Replace modules at Depot—scrap bad modules
16	Replace modules at Organization—repair modules at Depot
17	Replace modules at Organization—repair modules at Depot
18	Replace modules at Intermediate—repair modules at Depot
19	Replace parts at Depot
20	Recheck LRU at Organization—scrap bad LRU
21	Recheck LRU at Organization—replace modules at Intermediate—scrap bad modules
22	Recheck LRU at Organization—replace modules at Depot scrap bad modules
23	Recheck LRU at Organization—replace parts at Intermediate
24	Recheck LRU at Organization—replace modules at Intermediate—repair modules at Depot
25	Recheck LRU at Organization—replace parts at Depot
26	Recheck LRU at Organization—replace modules at Depot scrap bad modules
27	Recheck LRU at Organization—replace modules at Intermediate—repair modules at Depot
28	Recheck LRU at Organization—replace parts at Depot

66.3.2 Basic Parameters Input

One LRU may consist of several modules, and one module may consist of several parts. The processor parameters in an airborne radar system are shown in the Table 66.2.

66.3.3 Deployment Parameters Input

The deployment of equipment decides its quantities, repair environment, transportation, and storage, which is the main cause of the cost of equipment support. The deployment input parameters of airborne radar system are as follows:

Table 66.2 Basic processor parameters

The parameter name	Value	The parameter name	Value
Mean time between failure (MTBF)	469	Contractor unit repair costs	855
LRU mean time to repair at Organization	1.57	Contractor module mean repair cost	361
LRU mean time to repair at Intermediate	1.57	LRU checkout test set cost	19,000
LRU mean time to repair at Depot	1.57	Module checkout test set cost	23,000
Module mean time to repair at Organization	3.19	LRU checkout test area	11
Module mean time to repair at Intermediate	3.19	Module checkout test area	0.5
Module mean time to repair at Depot	3.19	Test time	0.1
Mean time to repair on equipment	1	LRU weight	22
Number of module types	26	Module weight	2
Number of parts types	318	Parts weight	0.01
One LRU production cost	12,229	LRU storage volume	0.011
One module mean production cost	1,118	Module storage volume	0.0025
One part mean production cost	32	Parts storage volume	0.00006

1. Equipment support last for 10 years, the deployment time is 10.
2. For 10 years' support time, there will be 700 systems deployed. All systems will be deployed in the first year, so the last time for deployment is 1. Production cost and number is closely related, so defining a reference number is necessary, corresponding to the production cost. If equipment used in actual number is consistent with reference number, the production cost is corrected according to skilled curve. The slope of LRU, module, and parts skilled curve is 0.92.
3. System runs for 34 h per month, so running time is 34.
4. There are totally 20 Organization maintenance stations, 20 Intermediate maintenance stations, and 1 Depot maintenance station.
5. There are no supply stations for spare parts on equipment, and 20 Organization-level supply stations, and 1 Depot-level supply station.
6. The function of spare parts storage coefficient is to adjust spare parts numbers. The coefficient of LRU, module, and spare parts storage on equipment is 1.65, and Organization and Intermediate level are both 0, and Depot is 3, which are all the recommended value.
7. The transportation cost of Organization, Intermediate, Depot, and contractor is one way 1.28 yuan per kg. Transportation cost parameters are all 1.28.
8. Organization working hour is 56 h; Intermediate and Depot is 40 h. Working hour cost rate on equipment is 39.03 yuan, Organization and Intermediate is 63.38, and Depot is 71.83 yuan (the working hour cost rate data are provided by PRICE). CPI statistics is given by the model according to the recommended values without considering indirect management cost.

66.3.4 Estimation and Analysis

To compare maintenance and support cost impacts under different maintenance concepts, simplifying the calculation requirement is necessary. This paper thinks that:

1. After equipment has failure, it can always be correctly disassembled without mistakes. Or if mistakes are making, this paper thinks that there is no cost during disassembly, inspection, installation, and restoration.
2. The failure parts can always be repaired according to corresponding repair level, and they can always recover after repairing. Or if they cannot recover, we must send failure parts to a senior station for repairing, which is not considered costs during this process. Although that assumption and the actual situation differ, it has little effect.
3. When the failure parts are repaired on regular level, the maintenance will be done according to the identified maintenance concept. When we choose the policy of repair, if the parts can be repaired, we think there are no costs. When we choose the policy of disposition, we only need to calculate the costs of spare parts without repairing.

For the processor of airborne radar system, we adopt different programs. The support and repair costs and the results of corresponding availability estimation are shown in the Table 66.3.

We can see from the chart that the costs of different programs differ a lot. Among the 28 basic maintenance concepts in the Table 66.3, the minimum cost is on program 12, which is 2,996,000 yuan, namely replace modules at equipment and repair module at Organization. And the corresponding availability of device is high. At the same time, we know that the cost of program 13 is also very low, and its availability is high. If we pay more attention to availability, we can choose this solution, namely replace modules at equipment and repair module at Intermediate.

If further analysis of the composition of maintenance and support costs, we can see that program 12 only needs initial spare parts with 2 LRU and 45 parts during its cycle (10 years), not need the subsequent parts. In contrast, if we choose the higher cost maintenance concept, such as program 1, namely directly scrap failure LRU at equipment, the spare parts will come to 149 LRU initial spare parts and 440 LRU subsequent spare parts. The cost of it is so high that the device cannot be supported. Of course, it is a limiting case, and it cannot occur normally.

The cost-effectiveness is defined as the ratio between repair cost and availability. And we assume that the value of best cost-effectiveness program is 100. The cost-effectiveness of different program is shown in the Table 66.4.

From the Table 66.4, the highest cost-effectiveness value is program 12, namely replace modules at equipment and repair module at Organization. The second one is program 10, namely disassemble the parts at equipment and replace the part at Organization. In the actual situation, maintenance concept can be selected according to this.

Table 66.3 The support and repair cost corresponding to different maintenance concepts

Maintenance concept	The support and repair cost	Availability	Maintenance concept	The support and repair cost	Availability
1	1,664.5	0.9257	15	605.7	0.9802
2	442.0	0.9970	16	344.3	0.9999
3	462.9	0.9928	17	368.0	0.9970
4	502.6	0.9783	18	371.1	0.9928
5	333.4	0.9970	19	497.6	0.9802
6	334.4	0.9970	20	1,476.1	0.9356
7	313.4	0.9928	21	474.4	0.9966
8	337.7	0.9928	22	505.0	0.9857
9	360.7	0.9783	23	324.4	0.9966
10	300.7	0.9970	24	348.7	0.9966
11	418.7	0.9999	25	361.6	0.9857
12	299.6	0.9994	26	591.1	0.9864
13	309.7	0.9999	27	382.3	0.9966
14	310.6	0.9999	28	482.1	0.9863

Table 66.4 The cost-effectiveness of different maintenance concepts

Maintenance concept	Cost-effectiveness
12	100
10	101
13	103
14	104
7	105
23	109
5	112
6	112
8	113
16	115
24	117
25	122
9	123
17	123
18	125
27	128
11	140
2	148
3	156
21	159
28	163
19	169
22	171
4	171
26	200
15	206
20	526
1	600

Table 66.5 Six kinds of maintenance concept under two-level maintenance

Maintenance concept	The details of the maintenance concept
7	Replace parts at Intermediate
9	Replace parts at Depot
10	Replace parts at Organization
12	Isolate modules at Organization and repair modules
13	Isolate modules at Organization—repair modules at Intermediate
14	Isolate modules at Organization—repair modules at Depot

66.3.5 Analysis of Maintenance Concept Under Two-level Maintenance System

If maintenance activity is divided by two-level system, the work of Intermediate level will be assigned to Organization and Depot levels. We do not consider to directly scrapping maintenance policy, because the failure parts are impossible to be directly scrapped without repair at Depot. If needed, they can be scrapped at Organization. So among the 28 maintenance concepts, program 12, 13, and 14 can be seen as the maintenance concept under two-level Maintenance System, as shown in the Table 66.5.

Now, we analyze the Tables 66.3 and 66.4. The six maintenance concepts under two-level Maintenance System take lower costs and higher availability than other programs. In particularly, the top five highest cost-effectiveness programs in the Table 66.4 are all programs under two-level Maintenance System. It is not an accident. It shows that two-level Maintenance System can indeed improve the equipment's economy. At least for the device like this processer in this paper is so.

66.4 Conclusion

For the same equipment, the cost of different programs differs a lot. And this will place a significant impact on equipment availability. So how to choose the reasonable maintenance concept is one of the key factors to reduce support cost. Through cost estimation and analysis of three-level and two-level system, we can get the result that two-level Maintenance System usually has better economics.

References

1. PRICE whitepaper_V1.1_031804_single. PRICE Corp, 2005.6
2. PRICE executive-overview_final 1-26. PRICE Corp, 2005.3
3. PRICE Background. PRICE Corp, 2002.6

4. Parametric Estimating Handbook. PRICE Corp, 2004.5
5. Li J, Guo J, Yan S (2010))Research on the means of cost evaluation for maintenance and support based on maintenance level analyzing. In: 9th China equipment management association LCC committee. NUDT Press, Shanghai, pp 169–173 (in Chinese)
6. Yan S, Guo J (2010) An analysis of the influence of equipment reliability on M&S cost in multi-theater deployments. Int J Plant Eng Manage 15:217–221 (in Chinese)

Chapter 67
Modeling in Aircraft Battle-Damaged Repair System

Shufeng Huang, Zhixian Hu and Yuanyuan Wu

Abstract It is an important guarantee of regaining aviation force effectiveness by implementing repair effectively on the battle-damaged plane. The study of the battle-damaged plane to repair has always been one of the most core issues focused on by the equipment support personnel. Aircraft battle repair system is a complex artificial system. Taking aircraft battle-damaged repair system as an object, this paper analyzed the concept and composition of the aircraft battle-damaged repair system. Then, adopting state space analysis method, the paper studied and established state-space model of the aircraft repair system. This model can be used as a framework for building repair demand analysis model, the repair system structure model, the repair process model, and effectiveness evaluation model.

S. Huang (✉)
The Military Logistics and Technology Equipment Department of National Defense University of PLA, Beijing 100091, China
e-mail: cnxahsf@126.com

Z. Hu
Beijing Aeronautical Engineering Technology Research Center, Beijing 100076, China

Y. Wu
Foreign Language Department of Academy of Armored Forces Engineering, Beijing 100072, China

S. Huang
Repair Plant of Unit 95965, Gucheng 253801 Hebei, China

67.1 Introduction

Local war under the condition of future informatization, the aircraft repair task will be more heavy, and the effect is more obvious. Therefore, the meaning of guaranteeing the damaged plane quickly "renewable" is more important [1]. At present, the construction about aircraft damage repair power has made some achievements, such as strengthening the theoretical research, technology development, and planning research. But the study on the process and ability of the aircraft damage repair still stays in the qualitative methods phase according to the operation principle the usual maintenance support system and the historical experience. It is lack of scientific and systematic quantitative analysis methods, for example, lacking the method calculating repair agencies capacity in wartime which is critical to aircraft repair system, and lacking the model aircraft quantity change law with the time, etc. [2]. Therefore, it is necessary to analyze and research the aircraft battle repair system, applying the system science theory, adopting the combination of qualitative and quantitative methods, thus to provide a theoretical support for building efficient aircraft battle repair system.

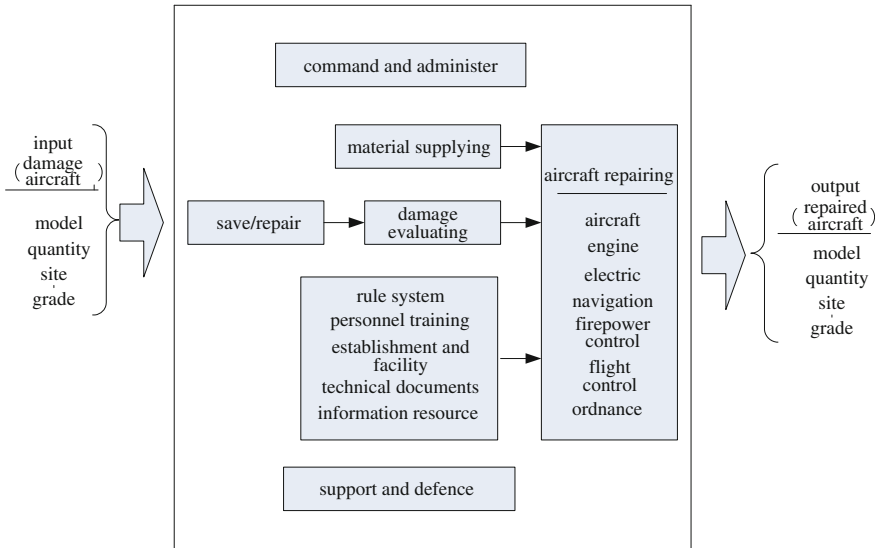## 67.2 Analyzing Aircraft battle-damaged Repair System

67.2.1 Concept of Aircraft battle-damaged Repair System

The aircraft battle-damaged refers to all kinds of damage the aircraft flying in the air or parking on the ground suffers. It also includes those events happening in the way of aircraft scheduled task, such as random failure, debilitating failure, accident, human error, lack of maintenance supplies, and environmental changes [3].

In "the language of the Chinese people's liberation army," the definition of the battle-damaged aircraft repair is to quickly repair the aircraft suffering battle-damaged within the scope of the battlefield, mainly to repair its structural damage, making its restore technology condition to perform the task in a short time.

Aircraft battle-damaged repair system is the union of organic whole formed by a number of interrelated and interacting elements (subsystems), existing in aircraft maintenance support system, in order to make the battle-damaged aircraft back rapidly to state of technology for performing the task, and sustaining aviation combat ability to the highest degree. Aircraft battle-damaged repair system is composed of personnel, material resources, financial resources technology elements, etc. needed by aircraft battle-damaged repair. It has the property of general system, such as integrity, collection, level-oriented, purposeful, and correlation characteristics, and is an open complex system [4, 5].

The goal that aircraft battle-damaged repair system achieves is to repair the damaged aircraft, devoting them into battle again, to maintain and restore aviation combat effectiveness, by repairing the battle-damaged aircraft with repair quantity

Fig. 67.1 The composition of the aircraft battle-damaged repair system

and repair rate of meeting the need of combat mission. Function of the system is to complete the mission, making the battle-damaged plane quickly return to the state of technology to perform the task, including performing certain tasks or saving his life. Input of the system is the battle-damaged plane, and the output is a repaired plane.

67.2.2 Composition of Aircraft Battle-Damaged Repair System

Aircraft battle-damaged repair system is an important part of equipment maintenance support system, according to the function division, aircraft repair system consists of some subsystems such as assessing battle-damaged, rescue and evacuation, material support, command management, defense, and principles, and methods making them play a role, as shown in Fig. 67.1.

67.3 The General Idea of Aircraft Battle-Damaged Repair System Modeling

The essential purpose of aircraft battle-damaged repair system modeling is to quantitatively analyze work efficiency of the system, namely under the given constraint conditions (resources, time, environment) how to make the battle-damaged

equipment repaired greatest number. So the process, how the battle-damaged air-craft can be changed to useful aircraft in repair system, makes up the main line of the system we care state. Through system analysis, the input of aircraft battle repair system includes the battle-damaged equipment, waiting to evacuate equipment and rescue force, both parts of the input have a great influence on the work efficiency of repair system. This study, therefore, not only must forecast needing to repair and evacuate equipment, but also must accurately evaluate ability of repair organization under different conditions, so that reasonably assign repair assignment, and maxi-mize the efficiency of the entire repair system.

Based on the above consideration, this paper studied and established state-space model of the aircraft battle-damaged repair system by using the state space analysis method [6]. Selected number of repairing aircraft as state variables of aircraft repair system reflects the status of the repair system, by studying the system's repair ability (repair process) and the number of battle aircraft and its distribution situation(equilibrium process), establishing the relationship of the system output (the amount of repaired aircraft) along with the change in time (system state model).

67.4 State-Space Model of Aircraft Battle-Damaged Repair System

67.4.1 State Vector of System

Assuming the system input is $x_i(t)$: the number of type i battle-damaged aircraft into the system in t moment; assuming the system output is $y_i(t)$: the number of type i repaired aircraft t moment.

Consequently, $y_i(t)$ ($i = 1, 2,...m$) can completely describe work state of the aircraft battle repair system, among them, the m is the type number of the aircraft being repaired. And, $y_i(t)$ is a set of independent variables, so it can be the system state variables, that is:

$$Y(t) = \begin{bmatrix} y_1(t) \\ y_2(t) \\ \vdots \\ y_m(t) \end{bmatrix}$$

Here, $Y(t)$ is the state vector of system.

67.4.2 State-Space Model of System in the Form of Dispersing

Theory analysis and practical experience show that the basic factors affecting aircraft repair system state changing are the following: one is the system's ability to repair wounds plane, namely the repair process, and the other is the number and distribution of the battle-damaged plane, namely the equilibrium process. Considering the practice demand for discrete form of mathematical model, this article established the discrete form of state-space model of the plane battle repair system by analyzing both the processes.

67.4.2.1 Repair Process

To repair aircraft via the battle-damaged repair system, the battle-damaged aircraft from an unuseful state into a useful state, the process is known as the repair process. Assuming $\beta_i(t)$ is the on schedule repair rates of type i plane, namely the system average repair rate of the type i plane during the at time t to $t + 1$ time. So, at time $t + 1$, the numbers of repairing type i plane are equal to the system time t, the numbers of the repairing type i plane plus during time t to $t + 1$ of the numbers of repairing type i plane, namely

$$y_i(t + 1) = y_i(t) + \beta_i(t) \cdot x_i(t) \quad i = 1, 2, \ldots, m \qquad (67.1)$$

In wartime, after repair scheme is determined, the aircraft repair system structure also is determined. So the maximum repair capacity of the system is a certain value, assuming the certain value is $Q_i(t)$. $Q_i(t)$ shows the number of repairing type i plane at full working capacity during the time t to $t + 1$.

As a result, when the system inputs $x_i(t) \leq Q_i(t)$, $\beta_i(t) = 1$;

When the system inputs $x_i(t) > Q_i(t)$, $\beta_i(t) = Q_i(t)/x_i(t)$, namely

$$\beta_i(t) = \begin{cases} 1 & x_i(t) \leq Q_i(t) \\ Q_i(t)/x_i(t) & x_i(t) > Q_i(t) \end{cases} \qquad (67.2)$$

In general, $x_i(t)$ and $\beta_i(t)$ should be broken down repairing quantity and the repair rates of repair agencies at all levels repairing the type i plane in the system, and calculated, respectively. Among them, $j = 1, 2, \ldots k$ is repair organization level contained in the system, generally takes $k \leq 4$, respectively, corresponding to grade four repair mechanism.

67.4.2.2 Equilibrium Process

It is named as equilibrium process that predicts the number of battle aircraft entering repair system and the allocation process of the all levels rescue agencies in the system. In a limited action time, the ratio of the number of aircraft needing

to repair and the operational time is called the repair flow, with the repair flow intensity $\lambda(t)$, aircraft/day as unit. Repair flow intensity reflects the number status of the unit's battle-damaged plane in operation time. Obviously, when calculated on daily, there is $x(t) = \lambda(t)$. Battle-damaged aircraft mainly includes random failure and battle-damaged, so this paper considered two kinds of causes to repair flow intensity.

Battle-damaged aircraft mainly includes random failure and battle-damaged, so this paper considered two kinds of causes to repair flow intensity.

1. Repair flow intensity of the type i aircraft due to random failure reasons

If calculated on combat operations process day by day, the average daily repair flow is

$$\lambda_{i0}(t) = N_i(t - 1) \cdot (1 - P_i(t)) \cdot \omega_{i0} \qquad (67.3)$$

where

$\lambda_{i0}(t)$ means the number of the type i failure plane in the day t;
$N_i(t - 1)$ means the initial number of the type i failure plane joining battle in the day t;
$P_i(t)$ means the battle-damaged probability of the type i in the day t;
ω_{i0} means the average failure flow intensity of the type i plane, namely the fault number of every single plane in a flight hour.

2. Repair flow intensity of the type i plane because of battle-damaged

According to the above parameters defined, at the t day of battle, repair flow intensity of the type i plane because of battle-damaged is

$$\lambda_{i\delta}(t) = N_i(t - 1) \cdot P_i(t) \qquad (67.4)$$

where $\lambda_{i\delta}(t)$ means repair flow intensity of the type i plane because of battle-damaged.

By (67.3) and (67.4), we can obtain the general repair flow intensity of the type i plane on the day t $\lambda_i(t)$:

$$\lambda_i(t) = \lambda_{i0}(t) + \lambda_{i\delta}(t) \qquad (67.5)$$

3. The probability of the type i plane entering the level j repair agency

By (67.3), (67.4) and (67.5), we can get the gross of daily needing to repair the failure or the battle-damaged planes. However, these battle-damaged planes do not wholly repaired by one level or a repair body, but according to the repair time needed for each aircraft and emergency departments at different levels of tasks, distributed to different levels of repair departments, or even to deduct irreparable

plane. So in the equilibrium process, we should not only study the number of the battle-damaged plane and also must study the distribution of aircraft repair time.

Research shows that the repair time of damaged equipment in wartime obeys exponentially [3]. Assume that τ, the repair time of the battle-damaged aircraft obeys exponential distribution, its distribution function is $P(\tau) = 1 - \exp(-\tau/\tau_i)$ where τ_i means mathematical expectation the type i plane repair time and $P(\tau)$ means the probability of the repairing plane falling into a time interval $[0, \tau]$.

1. Due to random failure, the probability of the type i plane entering the level j repair agency

According to task division of the repair agency, needing to be repaired plane entering the level j repair agency needs to be deducted the plane in the top level of repair agencies. So the probability of the type i plane entering the level j repair agency is

$$
\begin{aligned}
P_{ij0}(t) &= \left[1 - \exp\left(-\tau_{\varphi j}(t)/\tau_{i0}\right)\right] - \left[1 - \exp\left(-\tau_{\varphi(j-1)}(t)/\tau_{i0}\right)\right] \\
&= \exp\left(-\tau_{\varphi(j-1)}(t)/\tau_{i0}\right) - \exp\left(-\tau_{\varphi j}(t)/\tau_{i0}\right)
\end{aligned}
\tag{67.6}
$$

where τ_{i0} is the mean repair time of the type i fault plane; $\tau_{\varphi(j-1)}(t)$ is the maximum repair time of the level $j - 1$ repair agency; and $\tau_{\varphi j}(t)$ is the maximum repair time of the level j repair agency.

2. Due to battle-damaged, the probability of the type i plane entering the level j repair agency

Like above, expression can be written directly:

$$
P_{ij0}(t) = \exp\left(-\tau_{\varphi(j-1)}(t)/\tau_{i\delta}\right) - \exp\left(-\tau_{\varphi j}(t)/\tau_{i\delta}\right)]
\tag{67.7}
$$

In the above expression, $\tau_{i\delta}$ is the mean repair time of the type i battle-damaged plane.

In wartime, random failures generally also are repaired in accordance with the mode of repairing battle-damaged aircraft (changing parts, merging, etc.). So when calculating, it could take $P_{ij0}(t) = P_{ij\delta}(t)$.

3. Considering the task division of repair departments at different levels, the calculation model of the repair flow intensity.

In wartime, when organizing to repair the damaged plane, according to the result of evaluating the plane battle-damaged, the preliminary estimates repair work hours and, then according to the specific situation and the division of labor, distribute to different repair departments.

So when considering task partitioning of repair departments at different levels, on the day t, the repair flow intensity of the type i aircraft entering different levels of repair departments after equilibrium processing is as follows:

$$
\lambda_{ij0}(t) = \lambda_{i0}(t) \cdot P_{ij0}(t) = N_i(t-1) \cdot (1 - P_i(t)) \cdot \omega_{i0} \cdot P_{ij0}(t)
\tag{67.8}
$$

$$\lambda_{ij\delta}(t) = \lambda_{i\delta}(t) \cdot P_{ij\,\delta}(t) = N_i(t-1) \cdot P_i(t)P_{ij\,\delta}(t) \qquad (67.9)$$

The total repair flow intensity of t entering aircraft battle-damaged repair system is as follows:

$$\lambda_i(t) = \sum_{j=1}^{K} \left(\lambda_{ijo}(t) + \lambda_{ij\delta}(t) \right) \qquad (67.10)$$

where K is the number of repair departments' level in the aircraft battle-damaged repair system.

67.4.2.3 Repair Ability

About calculating ability of different levels emergency repair departments, their working hours can be taken as the limiting conditions, number of aircraft repaired can be taken as the main calculation content, the staff technical proficiency, supplies, spare parts supply and other factors can be taken as the correction coefficient to modify the results of calculation.

1. The repaired number of the level j repair department repairing the type i aircraft every day

$$q_{ij}(t) = n_{ij} \cdot \tau_{\varphi j}(t) \cdot k_{uj} \cdot k_{cj} / \overline{\tau}_{\varphi j}(t) \qquad (67.11)$$

where

$q_{ij}(t)$ is the repaired number of the level j repair department repairing the type i aircraft on the day t;
n_{ij} is the number of the professional repair team allocated to the type i aircraft by the level j repair department;
$\tau_{\varphi j}(t)$ is the number of repair hours provided by repair team of the level j repair body;
k_{uj} is the time utilization coefficient of the level j repair body;
k_{cj} is the coefficient of staff technical proficiency at the level j repair body;
$\overline{\tau}_{\varphi j}(t)$ is the mean repair time of the level j repair body repairing a aircraft.

2. The repaired number of the type i aircraft every day, considering wastage of the repair organization

In the fighting, at all levels of repair institutions may be attacked by an enemy. When considering the damage, the number of the type i aircraft repaired by the aircraft repair system on the day t is

$$Q_i(t) = \sum_{j=1}^{K} B_j \cdot q_{ij}(t) \cdot \left(1 - \sum_{d=1}^{t} f_j^d\right) \tag{67.12}$$

where

K is the level number of the repair institutions contained in the aircraft battle repair system;

B_j is the number of the level j repair institution owned in the aircraft battle repair system;

f_j^d is the loss rate of the level j repair agency on the day d.

Taking (67.2), (67.8)–(67.12) into (67.1), then we get,

$$y_i(t+1) = \begin{cases} y_i(t) + \sum_{j=1}^{K} N_i(t-1)\left[P_i(t)P_{ij\delta}(t) + (1 - P_i(t)) \cdot \omega_i(t) \cdot P_{ijo}(t)\right] & \lambda_i(t) \leq Q_i(t) \\ y_i(t) + \sum_{j=1}^{K} B_j \cdot n_{ij} \cdot \tau_{\varphi j}(t) \cdot k_{uj} \cdot k_{cj} \Big/ \overline{\tau}_{\varphi j}(t) \cdot \left(1 - \sum_{d=1}^{t} f_j^d\right) & \lambda_i(t) > Q_i(t) \end{cases}$$

$$\tag{67.13}$$

By the above expression, the number of aircraft repaired can be obtained at time $t + 1$ in the aircraft battle repair system.

67.5 Analyzing Influence Factors of System

Through the (67.13), it can be found that there are five parameters directly affecting the output of the system after given repair level of the aircraft battle repair system. The composition and change in these parameters had a great influence on the aircraft battle repair system.

1. Battle probability of aircraft $P_i(t)$ and distribution of its repair hours $P_{ij}\delta(t)$, $P_{ij0}(t)$

$P_i(t)$ is higher, the ability of aircraft repair system needs to be higher. $P_i(t)$ is related to such factors as object, style, and strength of the operation. Strength of the operation is more intense, and the operational capability of enemy is stronger, so $P_i(t)$ is higher. Among different operating patterns, aircraft battle-damaged rate changed a lot, such as the battle-damaged rate to attack ground targets is higher than air defense combat whereas the change in repair time distribution $P_{ij\delta}(t)$ and $P_{ij0}(t)$ has a direct influence on the optimal allocation of the system resources and the task.

2. B_j, the number of the level j repair institution owned in the aircraft battle repair system

The number of repair institutions allocated directly determines the ability of the aircraft battle repair system. Therefore, repair demand must be predicted according to the combat mission, and repair organization and its quantity must be scientific

allocated. B_j generally be determined by the next higher level equipment maintenance support headquarters.

3. n_{ij}, the number of the professional repair team allocated to the type i aircraft by the level j repair department;

n_{ij} is commonly used to optimize system internal different levels repair departments and is determined by the aircraft battle repair command at the same level. The main basis of optimizing is prediction results for quantity and degree of various aircraft wounds. Therefore, it is basis to optimize repair department internal composition, support resources configuration, and to increase the efficiency of repair, that the research on the laws of the battle-damaged under different operating patterns.

4. $\tau_{\varphi j}(t)$, the number of repair hours provided by repair team of the level j repair body;

$\tau_{\varphi j}(t)$ is determined by the operation requirements and the task division of different levels of repair departments. The basic principles of determining $\tau_{\varphi j}(t)$ are to meet the requirements of operations. Under the premise, the principles of task partitioning are balanced repair, namely make all levels of the battle-damaged repair agencies to work at full capacity as possible and make the whole system in the shortest possible time to repair the most aircraft.

5. The time utilization coefficient K_{uj} and technical proficiency K_{cj} of the level j repair agencies

   K_{uj} and K_{cj} reflect the working strength and personnel training level of repair agencies. The level of training higher, technical proficiency is higher, so repair agencies to repair efficiency is higher.

67.6 Conclusion

Using state space analysis method, the paper studied and established the state-space model of repair process, equilibrium process, and emergency repair and analyzed the influence factors of the aircraft battle-damaged repair system based on the model. The model founded in this paper provided a basis for quantitative analyzing the aircraft battle repair system and provided a technical support for the aircraft battle repair simulation. It can be taken as a system framework for studying repair demand analysis model, the repair system structure model, process model, and effectiveness evaluation mode.

References

1. Hu F, Su H, Huang X (2006) Significance of Aircraft battle-damaged Repair in modern war(in Chinese). The technology and development of aviation equipment support. Publishing Company of National Defence Industry, Beijing, pp 71–75

2. Zhang J (2003) Aircraft battle repair and its development trend (in Chinese). Air Force Equipment 7:12–13
3. Academy of Military Science of PLA (2011) Military language of PLA(in Chinese). Publishing Company of Military Science, Beijing, p 12
4. Yuan D (2004) Research on concept model of Aircraft battle-damaged Repair(in Chinese). Air Force Engineering University, Xi'an
5. Zhang J (2001) Engineering science of aircraft battle-damaged repair(in Chinese). Publishing Company of Aviation Industry, Beijing
6. Wang Y (2007) Systems engineering science(in Chinese). Publishing Company of Higher Education

Chapter 68
Support Capacity Evaluation of Aviation Equipment Support Unit Based on Factor Analysis

Fu Yin, Shenjian Yao and Jinfeng Lv

Abstract The capability of support units to support aviation equipment is an important part of combat effectiveness of Air Force, whose support capability has a direct effect on whether the task of aviation equipment support can be accomplished well or not. Therefore, it is necessary to evaluate it scientifically. Based on the construction of capacity evaluation index system of support units, this paper comprehensively evaluates the support capacity of nine units with the system analysis software SPSS through factor analysis. According to each unit's support capacity, we can rank their overall scores and give a comparative analysis. Then, we can find each unit's support capacity presents an imbalanced trend. The scores of each unit demonstrate the direction and key points of future training. So equipment office can carry out a targeted training aiming at each unit's weakness in order to effectively promote a balanced development of their support capacity.

Keywords Factor analysis · Aviation equipment · Support unit · Support capability

68.1 Introduction

Any advanced weaponry and material, especially high-tech weapons owned by modern Air Force, has to be given technical support in order to be available under the background of modern war. The operational effectiveness of the Air Force's aviation equipment depends on equipment support units' comprehensive support capacity, which is an important part of Air Force's combat effectiveness. Evaluating each unit's support capacity, helping decision-making departments to

F. Yin (✉) · S. Yao · J. Lv
Department of Foundation, The First Aeronautic Institute of the Air Force, Xinyang 464000 Henan, China
e-mail: yinfu_017@163.com

scientifically make decisions by evaluation result, and adopting effective measures to improve weak links in aviation support units are significant to enhance aviation equipment support units' support capacity in wartime.

At present, there are many evaluation methods used to evaluate support units' support capacity, such as neural network method [1], fuzzy evaluation [2, 3], analytic hierarchy process (AHP) [4], gray predication [5], and so on, which play a positive role in the evaluation of support units' support capacity. But they also have disadvantages. For example, the factors are not comprehensive and the result is imprecise. For the evaluation of support units' support capacity, the task is a complicated system engineering. Lots of factors need to be taken into account. If all the factors are evaluated, the task must be difficult. Thus, a technology called "dimensionality reduction" will be needed, in which a few "abstract" variables can show the basic information of the factors. Factor analysis method is a statistical analysis technique in which the latent variables are evaluated by the explicit variables and the abstract factors are assessed by the specific indexes. There are two advantages to evaluate the support capacity of a support unit through constructing evaluation model on the basis of the factor analysis [6, 7]. One is that the evaluation result is quite objective, because the factor analysis method uses the contribution rate of the variance of each factor consisting of the original variables as weight. The other is to change the multivariate into a small number of new factors and determine the major factors reflecting the support capacity of the aviation equipment support units, which benefits the decision-making section to know the current situation and the potential of the support capacity of each unit, and thus provide the basis for developing corresponding measures. This paper uses the factor analysis method to comprehensively evaluate the support capacity of the aviation equipment support units.

68.2 Establishment of the Evaluation Index System

68.2.1 Analysis of the Influencing Factors

Many aspects including the collection and deployment of the support resources as well as the command and management of the technical support need to be supported by the aviation equipment support units, which are onerous, demanding, and critical tasks. According to the reality of the aviation equipment technology, factors influencing the support capacity are the followings:

Resources support capacity. The support resources of the unit are the material basis of the aviation equipment technical support, and the support activity cannot be carried out without them. The resources mainly include human resource, material resource, information resource, and financial resource which are an organic and indispensable whole. We mainly consider whether the type and quantity of the resources can meet the need of the support task and whether they

can ensure the success of the support activity. Therefore, the influencing factors of the resources support capacity mainly take the human resource support capacity, the material resource support capacity, the information resource support capacity, the financial resource support capacity, and the resource management capacity into account.

Maintenance support capacity. It is the main content of the technical support of the unit both in peacetime and wartime. The maintenance support capacity directly influences the accomplishment of the support task. The maintenance support is a complex activity in which all kinds of maintenance support power coordinate with each other, so it has to be managed powerfully. In wartime, battlefield damage repair is a major approach to recover the fighting capacity of the equipment, which can maintain the continuous combat capacity of the army. Therefore, the influencing factors of the equipment maintenance support capacity mainly consider the maintenance management capacity, the effectiveness of the maintenance activity, and the battlefield damage repair capacity [8].

Command capacity. Command over the equipment technical support is an important content of the equipment support activity. Only by means of scientific and effective command, can we coordinate the support units effectively to carry out the support activity scientifically and reasonably, and thus to fulfill the support task. The command activity of the technical support involved not only the commander and his object, but also the command method. The command over the equipment technical support includes not only the command over the support and the defense activity, but also the mobilization of the equipment support [9]. Hence, the influencing factors of the command capacity chiefly consider the commanding and decision-making capacity, the commanding and support capacity, the defense capacity as well as the capacity of the mobilization and support of the equipment.

68.2.2 Evaluation Index System

For the evaluation of aviation material support units' support capacity, the task is a complicated system engineering. Its evaluation index system should include every aspect of support units' support activities. According to the analysis on factors affecting aviation material support units' support capacity, we can follow the principles of science, system, operation, and dynamic which construct index system, and refer to the research results of military material support capacity evaluation [10–13] to initially design support capacity evaluation index system of aviation material support units. In order to ensure the rationality of designed index, avoid repeated information among indexes, and design aviation material support units' support capacity evaluation index system survey questionnaire, we can use expert survey method to choose from initial designed index. And by expert survey, we can choose aviation material support units' support capacity evaluation index system, as shown in Table 68.1.

Table 68.1 Aviation material support units' support capacity evaluation index system

	One-level index	Two-level index	Sign
Aviation material support units' support capacity evaluation index system	Resource support capacity	Manpower resource support capacity	X_1
		Material resource support capacity	X_2
		Information resource support capacity	X_3
		Financial resource support capacity	X_4
		Resource management capacity	X_5
	Maintenance support capacity	Maintenance management capacity	X_6
		Maintenance activity effectiveness	X_7
		War injury do rush repairs capacity	X_8
	Command capacity	Command decision-making capacity	X_9
		Command support capacity	X_{10}
		Defend capacity	X_{11}
		Material mobilization capacity	X_{12}

68.3 Basic Principles and Implementing Steps of Factor Analysis

Factor analysis method was put forward in 1904 by British psychologist Charles Spearman. The aim for him to put forward this method was to explain statistics analysis of intelligence test score. At present, factor analysis method is successfully applied in many fields. Factor analysis method is a statistics method which changes several test indexes into few comprehensive indexes. When multivariable statistics problems are dealt with, the reflected formation may overlap since the variables made up of samples are many and there may be certain relativity among variables. By the research on several variables' related factor matrix or covariance matrix, factor analysis can find less comprehensive variables which can reflect as much original variable information as possible among many variables of test data.

Suppose: There are n samples and p indexes are tested in each sample, recorded $x = \begin{pmatrix} x_{11} & \cdots & x_{1p} \\ \vdots & \ddots & \vdots \\ x_{n1} & \cdots & x_{np} \end{pmatrix}$. There is strong relativity among p indexes. In order to research and eliminate the effect caused by the difference of tested variables and

the difference of order of magnitude, we can suppose the variable dealt with by standardization is 0 and variance is 1. Here, we use X to show original variable and the variable dealt with by standardization and use $F_1, F_2,\ldots, F_m (m < p)$ to show standardized common factors. If: (1) $X = (X_1, X_2,\ldots,X_p)'$ is testable vector quantity, its average vector quantity $E(X) = 0$, covariance matrix $\mathrm{cov}(X) = \sum$, and covariance matrix is equal to related matrix; (2) $F = (F_1, F_2, \ldots, F_m)'$ $(m < p)$ is un-testable variable, its average vector quantity $E(F) = 0$, and covariance matrix $\mathrm{cov}(F) = 1$, that is, each component of F is independent from one another; (3) $\varepsilon = (\varepsilon_1, \varepsilon_2, \ldots, \varepsilon_m)'$ is independent from F, $E(\varepsilon) = 0$, and ε's covariance matrix Σ_ε is diagonal matrix

$$\mathrm{cov}(\varepsilon) = \Sigma = \begin{pmatrix} a_{11}^2 & \cdots & 0 \\ \vdots & \ddots & \vdots \\ 0 & \cdots & a_{pp}^2 \end{pmatrix}, \text{ that is, each component is independent from}$$

one another, the mathematics expression of factor model is:

$$\begin{cases} X_1 = a_{11}F_1 + a_{12}F_2 + \cdots + a_{1m}F_m + \varepsilon_1 \\ X_2 = a_{21}F_1 + a_{22}F_2 + \cdots + a_{2m}F_m + \varepsilon_2 \\ \quad\vdots \\ X_p = a_{p1}F_1 + a_{p2}F_2 + \cdots + a_{pm}F_m + \varepsilon_p \end{cases} \tag{68.1}$$

Factor model is expressed by matrix: $\mathbf{X} = \mathbf{AF} + \varepsilon$. In it, $\mathbf{A} = (a_{ij})_{p \times m}$ is factor matrix which will be evaluated, called factor loading matrix. a_{ij} is called No. i's loading in No. j factor, which shows the importance of No. i in No. j factor. Special factor ε_i is only connected with variable X_i, which represents the character of corresponding variable and has no connection with other variables.

The implementing steps of factor analysis are as follows: (1) make original variable standardized and look for related matrix, and analyze the relativity of variable; (2) variance analysis; (3) look for initial common factor and factor loading matrix; (4) use rotation method to make variable factor have stronger explanation; (5) calculate the score of variable factor; (6) have comprehensive evaluation according to the score. Figure 68.1 shows the process of factor analysis on aviation material support units' support capacity.

68.4 Analysis and Application

68.4.1 Data Handling and Variance Analysis

Suppose there are nine support units to take part in evaluation and sample data are evaluation statistics data of material support capacity of each unit in a certain Air Force station given by experts, as shown in Table 68.2. Non-dimensionalize

Fig. 68.1 The process of
factor analysis on aviation
material support units'
support capacity
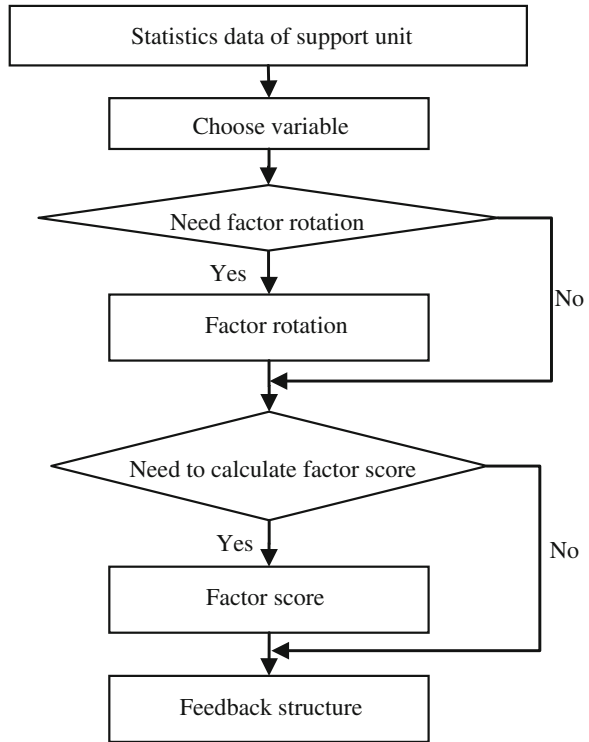
Table 68.2 Original data of support units

Unit	X_1	X_2	X_3	X_4	X_5	X_6	X_7	X_8	X_9	X_{10}	X_{11}	X_{12}
1	80	85	81	79	93	85	89	90	86	82	80	71
2	76	82	80	84	83	80	79	86	87	78	75	80
3	88	94	91	90	87	86	89	84	85	80	71	74
4	71	75	73	78	78	70	72	78	72	75	73	76
5	75	79	69	71	72	75	69	71	70	71	76	80
6	79	80	82	75	72	69	72	75	80	81	78	82
7	78	80	84	70	75	84	75	78	76	72	82	76
8	82	84	78	75	84	72	86	74	80	90	86	80
9	78	76	81	73	75	69	84	90	81	80	78	80

original data representation (68.2) to eliminate the inconformity of dimension among indexes and the difference of quantity.

$$X_j^* = \frac{X_j - E(X_j)}{\sqrt{D(X_j)}}, (j = 1, 2, \ldots, n) \tag{68.2}$$

Then carry out KMO sample measure and Bartlett spherical test on standardized data. The result of KMO is 0.776, which is more than the standard 0.7.

Bartlett spherical test shows that the applicability of factor analysis test has pasted. Then carry out total variance decomposition. The result is shown in Table 68.3.

From Table 68.3 and characteristic value scree plot (Fig. 68.2), we can know that the former factor variables comprehensively include enough information expressed by 12 evaluation indexes in original data and accumulation variance reaches to 88.9 % (more than 85 %). Therefore, we can make sure that the number of common factors picked up is 4.

68.4.2 Factor Loading and Factor Score

Factor variables in factor loading analysis matrix which are gained after they are handled by variance maximum rotation method have more specific meaning. Factor variables that have high loading distribute in several key evaluation indexes regularly, which shows that there is clear structure relationship among them. Table 68.4 is factor loading matrix after rotating.

In order to observe and study each unit's material support capacity level and have analysis and comprehensive evaluation to it, we can adopt regression method to get factor score function. Table 68.5 is factor score function coefficient matrix. According to factor score function coefficient matrix, we can get factor score function:

$$\begin{cases} F_1 = 0.392X_1 + 0.352X_2 + \cdots + 0.162X_{12} \\ F_2 = -0.196X_1 - 0.221X_2 + \cdots - 0.02X_{12} \\ F_3 = -0.056X_1 + 0.061X_2 + \cdots - 0.504X_{12} \\ F_4 = 0.072X_1 - 0.029X_2 + \cdots - 0.092X_{12} \end{cases} \qquad (68.3)$$

What should be paid attention to is that X in the above formula has not been original variable yet, but variable after being standardized. According to the above formula, we can calculate each unit's corresponding score of each common factor and evaluate and rank different common factors. At last, we need to calculate different units' comprehensive performance scores. The calculating method is to use the proportion of which each common factor's variance contribution rate in Table 68.3 occupies four common factor's accumulative variance contribution rate as weight number, make every common factor score have weighted average, and calculate each unit's final score. The formula is as follows:

$$F = 0.34F_1 + 0.29F_2 + 0.21F_3 + 0.16F_5 \qquad (68.4)$$

After calculating, we can get nine units' comprehensive scores, as shown in Table 68.6. From it, we can see each support unit's advantage and disadvantage in each index.

The result analysis: According to Table 68.4, we can see that X_1, X_2, X_3, and X_4 in the first component loading response are larger, which shows that each support

Table 68.3 Explained total variance

Elements	Initial characteristic value of number			Pickup quadratic sum loading			Rotation quadratic sum loading		
	Total	Variance (%)	Accumulation (%)	Total	Variance (%)	Accumulation (%)	Total	Variance (%)	Accumulation (%)
1	6.298	52.479	52.479	6.298	52.479	52.479	3.663	30.525	30.525
2	1.997	16.641	69.120	1.997	16.641	69.120	3.056	25.464	55.989
3	1.205	10.044	79.164	1.205	10.044	79.164	2.226	18.547	74.537
4	1.169	9.743	88.907	1.169	9.743	88.907	1.724	14.370	88.907
5	0.766	6.386	95.293						
6	0.350	2.913	98.205						
7	0.173	1.439	99.644						
8	0.043	0.356	100.000						
9	2.383E−16	1.986E−15	100.000						
10	1.426E−16	1.188E−15	100.000						
11	−7.092E−17	−5.910E−16	100.000						
12	−2.900E−16	−2.417E−15	100.000						

Pickup method: main component analysis
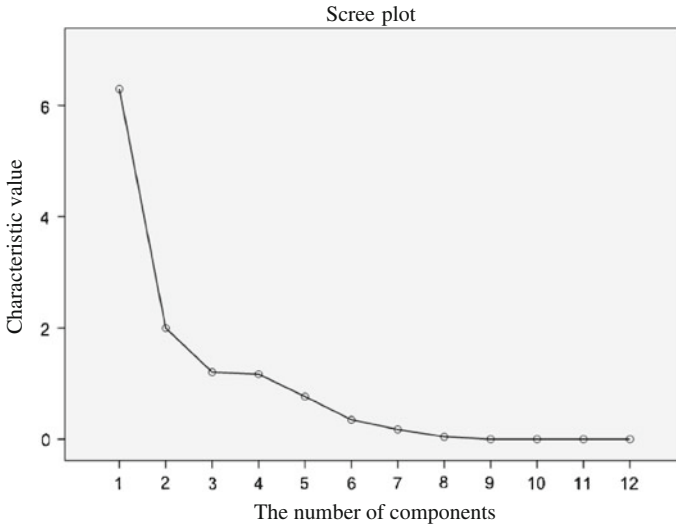
Fig. 68.2   Characteristic value scree plot

Table 68.4   Rotation component matrix

	Component			
	1	2	3	4
Manpower resource support capacity	0.936	0.175	0.128	0.128
Material resource support capacity	0.897	0.154	0.355	−0.097
Information resource support capacity	0.736	0.312	0.187	−0.124
Financial resource support capacity	0.563	0.457	0.151	−0.585
Resource management capacity	0.383	0.656	0.518	0.093
Maintenance management capacity	0.421	0.084	0.839	−0.130
Maintenance activity effectiveness	0.537	0.723	0.256	0.228
War injury do rush repairs capacity	−0.010	0.870	0.270	−0.211
Command decision-making capacity	0.522	0.768	0.066	−0.052
Command support capacity	0.479	0.509	−0.341	0.551
Defend capacity	−0.012	−0.012	−0.044	0.976
Material mobilization capacity	−0.100	−0.289	−0.890	0.065

resource is the basis to finish aviation material technology support. If they want to finish aviation material technology support task with high quality, they must perfect the supply system of support resource. X_5, X_7, X_8, and X_9 in the second component loading response are larger, which shows that the quality of aviation material specific maintenance task is main part of aviation material support units' support capacity. When support units carry out aviation material technology support, they should truly implement each system and measure, promote aviation material technology support capacity, and meet the requirement of high quality

Table 68.5 Component score coefficient matrix

	Component			
	1	2	3	4
Manpower resource support capacity	0.392	−0.196	−0.056	0.072
Material resource support capacity	0.352	−0.221	0.061	−0.029
Information resource support capacity	0.250	−0.056	−0.049	−0.075
Financial resource support capacity	0.137	0.099	−0.142	−0.368
Resource management capacity	−0.080	0.198	0.201	0.111
Maintenance management capacity	0.067	−0.186	0.443	0.042
Maintenance activity effectiveness	0.011	0.223	0.024	0.147
War injury do rush repairs capacity	−0.296	0.483	0.020	−0.115
Command decision-making capacity	0.024	0.289	−0.147	−0.059
Command support capacity	0.112	0.212	−0.280	0.232
Defend capacity	−0.020	−0.029	0.133	0.600
Material mobilization capacity	0.162	−0.020	−0.504	−0.092

Table 68.6 Each unit's scores and sequence

Unit code	Factor 1	Factor 2	Factor 3	Factor 4	Total score	Total score sequence
1	−0.25963	1.32315	1.59394	0.70586	0.736436	1
2	−0.13849	0.87352	−0.35365	−0.96735	−0.02749	5
3	2.0493	0.04289	0.59698	−1.27354	0.634586	2
4	−1.39269	−0.09687	0.02807	−0.84775	−0.63708	8
5	−0.63785	−1.63217	0.09474	−0.21701	−0.70179	9
6	0.45044	−0.54947	−1.43565	−0.07606	−0.31451	7
7	−0.15103	−1.13789	1.19123	0.66224	−0.02222	4
8	0.79443	0.07761	−0.7676	1.93056	0.446895	3
9	−0.71449	1.09923	−0.94807	0.08304	−0.11484	6

when using aviation material. X_6 in the third component loading responses is larger, which shows that it is important to mobilize the enthusiasm of each level command and maintenance personnel. All of these tell us that we should use all kinds of motivation methods to mobilize support personnel's work enthusiasm when support units carry out aviation material support work.

From Table 68.6, the score of each unit points out the direction and importance of future training. The less the factor's score in the table is, the more it shows that support unit has disadvantage in this index. Material office can carry out pertinent training which aims at each unit's weak link. For example, if the disadvantage of support unit 1 and 4 is that the score of support resource factor is low, they should strengthen resource support in the follow-up work, do logistics work well, and enrich each support resource. The disadvantage of support unit 2 and 3 is that personnel's work enthusiasm is not high. They should strengthen to motivate personnel in the follow-up work. By motivation, personnel's work positivity and initiative can be improved. The disadvantage of support unit 5 and 7 is that first-

line work quality in maintenance is not high. They should strengthen daily practice, improve maintenance skills, and at the same time, strengthen supervision during the process of maintenance to ensure high quality of maintenance in the follow-up work. The disadvantage of support unit 6, 8, and 9 is that management work has weak link. They should strengthen management during the process of maintenance in the follow-up work.

68.5 Conclusion

The evaluation of aviation material support units' support capacity has been affected by many factors. This paper constructs evaluation index system of aviation material support units' support capacity, eliminates the impact of the relativity of many variables, calculates weight to evaluate factors, simplifies the complexity of aviation material support units' support capacity evaluation, and evaluates support units' support level objectively and fairly. The result shows that each unit's support level is not balanced. We suggest material department adopts effective measures to strengthen each unit's weak link to improve each unit's material support capacity according to evaluation results.

References

 1. Yin G, Liu Y (2007) Research on evaluation model of tank firepower performance using BP network. Fire Control Command Control 32(11):105–107 (in Chinese)
 2. Yang P (2001) Fuzzy evaluating model of guarantee capability of equipment and technology of missile army. Mod Defence Technol 29(4):39–41 (in Chinese)
 3. Hu Z, Zheng D (2008) Evaluation for equipment technology supporting ability based on fuzzy method. Ordnance Ind Autom 27(1):10–11 (in Chinese)
 4. Sun R, Jia M, Dong H (2012) The causal analysis of aviation equipment technical support quality based on the AHP. J Naval Aeronaut Astronaut Univ 27(6):679–683 (in Chinese)
 5. Yu Z, Meng F (2009) Purpose of military equipment performances forecast for the operation requirement analysis based on GM(1,1) model. Command Control Simul 31(4):46–47 (in Chinese)
 6. Liu G (2009) Application of factor analysis in a synthetic evaluation of flying ability. College Math 25(4):151–154 (in Chinese)
 7. Linghu C, Liu Y, Zhang C, Sun D, Wang J (2008) Application of vehicle equipment support training estimate by factor analysis. Sci Technol Eng 8(18):5336–5340 (in Chinese)
 8. Zhang Z, Wang J (2002) Introduction to equipment and technical support (in Chinese). Military Science Press, Beijing
 9. Zhao T, Wang L (2005) Equipment and technical support science of command. The PLA Press, Beijing (in Chinese)
10. Zhang W, Hua X (2007) Study on evaluation of technical support capability for radar equipment. Radar Sci Technol 6:419–421 (in Chinese)
11. Chen Z, Yang J, Wu Y, Ke Z (2009) Evaluation of missile weapon system support ability based on blurring theory. Ship Electron Eng 9:56–59 (in Chinese)

12. Zhang L, Leng X, Wang P (2010) Evidence theory model of warship equipment technical supporting ability evaluation based on combined weight. Fire Control Command Control 8:162–164 (in Chinese)
13. Sun P, He G, Cheng G, Zhu F (2011) Design support capability evaluation of surface to air missile based on grey system. Mod Defence Technol 39(5):162–165 (in Chinese)

Chapter 69
Research on Security Monitoring and Health Management System of UAV

Gongcai Xin, Weilun Chen and Jie Li

Abstract The purpose of security monitoring and health management system is to synthesize equipment detection, fault diagnosis, and maintenance management into a whole to establish an integrative maintenance management and support platform based on information of unmanned air vehicle (UAV) system and ultimately to realize the autonomous logistics (AL) support. Some functions to realize are: performing security monitoring and failure early-warning for the whole process of UAV involving takeoff, flight, and recovery; continuously recording the telemetry data during flight as well as the equipment operation and maintenance information and integrating these data for performance degrade trend analysis, life-time cumulating, and remaining life forecasting, to diagnose potential failures and provide maintenance suggestion; and providing information integrated management for the whole UAV system.

Keywords Unmanned air vehicle · Security monitoring · Prognostic and health management · Autonomous logistics

69.1 Introduction

Unmanned air vehicle (UAV) is a new-type armament which is used to carry out real-time observation of foe position day and night and perform target location and artillery adjustment for the operational and tactical missile. But, UAV systems are just equipped in our army for a short period, and the number of UAV is quite few. In conclusion, the technical support for the UAV is just being in the initial stages yet, and the maintenance power is also quite weak. The reasons of the frequent

G. Xin (✉) · W. Chen · J. Li
Department of Aerial Instrument and Electric Engineering, The First Aeronautical Institute of Air Force, Xinyang 464000, China
e-mail: xingc2752@163.com

system failures and random failures for UAV system include: the small amount of equipment product, little knowledge for failure regulation, and the unstable equipment quality. Research on the security monitoring and health management system for medium-range UAV mainly aims at the problems, such as the unmanned drive of airplane, the inadequate ability of flight condition monitoring and trend prediction, and at requirement for more ability of security monitoring and failure early-warning.

The security monitoring for UAV mainly performs security monitoring and failure early-warning for the factors that influence the flight safe in the process of flight such as powerful horsepower for the emission flying-off process, presetting indication for the climb, and engine state in the process of flight. The health of UAV describes the ability of UAV sub-system and units to perform the design functions. The health management is defined as the management activities correlated directly with the health condition of UAV and mainly includes ending the bad condition of devices and carrying out failure prognosis and life forecast, to repair the failure parts and confirm the exactness of maintenance process. Ultimately, this security monitoring and health management system aims at the specialty of long-term storage and wartime application for UAV and enhances the capability of detection, diagnosis, and maintenance decision on earth, so as to realize upper air, long flight, more flight sorties, and reduce the whole cost of operation and maintenance support for UAV.

In this article, the system architecture model, function design, and key technique of UAV security monitoring and health management system are described.

69.2 System Architecture and Function Design

69.2.1 System Architecture

This general medium-range UAV mainly includes aerospace vehicle sub-system, control and navigation sub-system, integrated radio sub-system, and mission facility sub-system, and every sub-system themselves is consisted of some devices and parts. The topological structure map of UAV system must be build, so as to confirm the fault propagation path of devices. And on the foundation of this map, the structural model of management system UAV security monitoring and health is established, which can be seen in Fig. 69.1.

In which, the health management of system level mainly acquires the health state and its development trend of the whole UAV system, carries out maintenance decision based on the health condition of UAV, and then forms maintenance advice for the maintainers. The health management of sub-system level performs relativity analysis with all classes of condition data, solves the inconsistency for those data, then confines and isolates fault, and receives more reliable health information of sub-system. As the real-time actuator, the health management of device level acquires the sensor information of key parts, carries out fusion
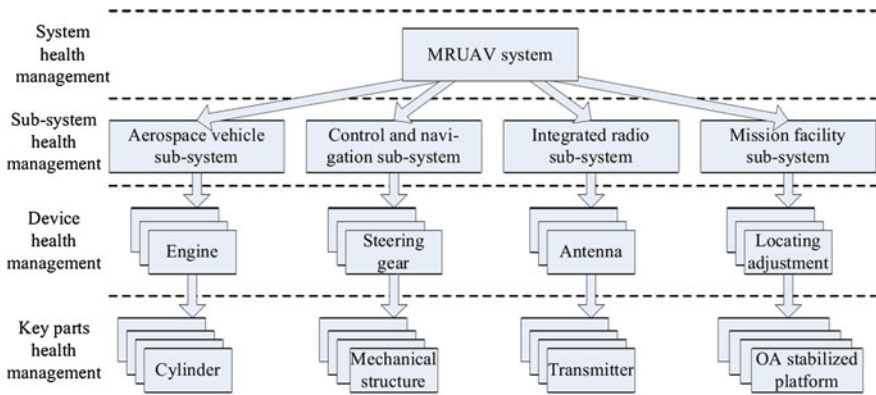
Fig. 69.1 Structure model of UAV's health management system

treatment to realize abnormality detection, enhanced fault diagnosis, health assessment, and life-time prediction. The health management of key parts' level actualizes security monitoring and fault early-warning through reading real-time sensor data of key parts and performing feature extraction for those data.

Thereby, this security monitoring and health management system for medium-range UAV adopts hierarchical fusion architecture and realizes abnormal data detection, fault diagnosis and prognosis, life-time prediction, and maintenance management with reasoning based on case. In which, the function of security monitoring is mainly involved with those devices and parts related with flight safe, and the function of health management should cover the key devices and parts for the whole UAV system. Thus, the logical reasoning framework of health management system for the whole UAV system can be seen in Fig. 69.2.

69.2.2 Function Design

The security monitoring and health management system can provide some functions including: (i) safety monitoring and fault early-warning for the whole process of UAV takeoff, flying, and recovery; (ii) continually tracking and recording the telemetry data for the whole process of flight and the operation, detection, and maintenance data of devices, and carrying out trend analysis based on performance degradation analysis and life-time accumulation, so as to diagnose the potential fault, predict the residual life, and present the maintenance advice; (iii) providing integrated management for the facility operation information, fault detection information, maintenance process, maintenance personnel, and allocation of maintenance resource. This system can be installed in the ground data terminal host computer, as well as in the military portable notebook alone; and the computer data interfaces are connected with the host computer to share the same
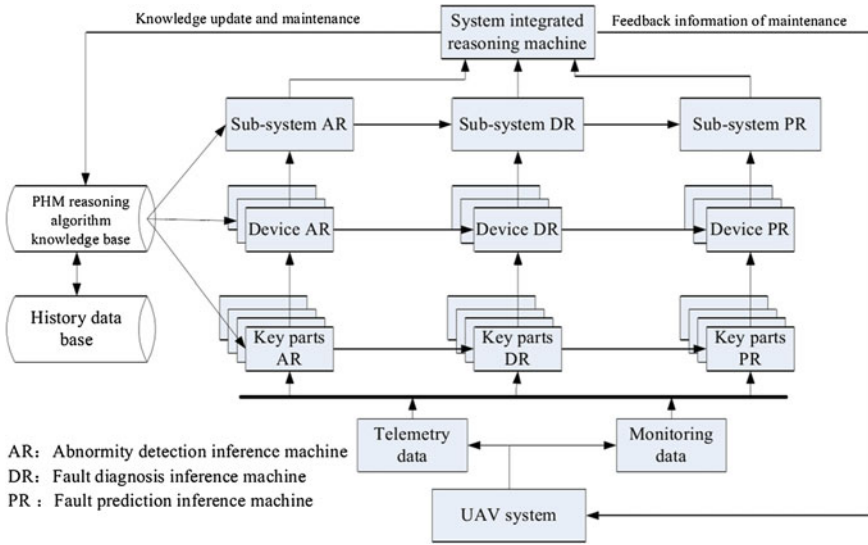
Fig. 69.2 PHM structure scheme of logical reasoning for UAV

database for system security test and evaluation, fault prediction, and health management based on telemetry data.

This UAV security monitoring and health management system functions can be divided according to three key points: diagnosis, prediction, and management. Thus, the function module design includes the following modules: System management module: The basic system functions consist of creating a new project, opening a project, user authority management, exiting the system safely, and so on;

Data maintenance module: The basic data maintenance functions consist of data backup, data restoration, data exporting/importing, and so on;

Information management module: The information management functions consist of importing the history data, device basic information, device maintenance information, maintenance personnel information, and some other functions inter-related with device operation maintenance.

Security monitoring module: security monitoring of flight status (the data analyses and early-warning which influence the security during flight), condition monitoring of takeoff (the presetting monitoring on the powerful horsepower and climb instructions during launching process), and condition monitoring on the surface (surface debugging and the monitoring and fault early-warning of air vehicle in the detection process).

Fault diagnosis module: fault detection, diagnosis, and location according to feature extraction and symptom analysis by reasoning machine.

Health management module: health condition evaluation, performance degradation analysis, health classification early-warning, and so on.

Life prediction module: life accumulation, life prediction, verifying the optimum maintenance occasions, and so forth.

Maintenance management module: constituting the maintenance schedule, management of maintenance parts, deployment of maintenance tasks, allocation of maintenance resource, and so forth.

69.3 Support Techniques

69.3.1 Information Acquisition of Flight Status

The information acquisition of flight status performs under the precondition that the normal operation status of UAV cannot be affected. It collects the flight status data and condition data of ground control station to do the analyses and mainly includes such steps as: optimizing the choose of acquisition point, converting the format of collected signals, design of acquisition circuits, and analysis and pretreatment of collected data. If the flight status data can be acquired accurately for real time and long time, the fault prediction and security warning will be realized; the missed alarm and false alarm will be avoided as well. The UAV telemetry data consist of a large number of flight status information; so through the acquisition of telemetry data, the raw data of flight status can be acquired, and no influences would be introduced to the flight during acquisition process. At the same time, the control commands sent by the UAV ground control station will be collected to check whether the air vehicle would be controlled to respond to the control commands.

The operation principle of acquisition circuit can be seen in Fig. 69.3. It includes telemetry and remote sensing signal demodulation module, frame/byte/bit synchronization module, and signal modulation module. In order to avoid that the isolation circuit influences the UAV system, isolation and cache circuits are added to prevent the UAV from abnormal situation. The acquisition circuit adopts the T joint structure to capture four kinds of signals from host observation and control terminal: frame synchronization, byte synchronization, bit synchronization, and data flow signal. Based on the byte synchronization signal, the transmitting and receiving signal flows will be dealt with to extract telemetry and remote sensing signals. The other key points are correspondingly few including synchronization locking signal, tracking gain, and so on; thus, they are acquired through direct connection.

69.3.2 Flight Status Estimation and Fault Prognosis

On condition of the treatment and analyses of acquired data, the movement tendency of flight status can be estimated correctly; the undetectable failures can be analyzed; and the probability of failure can be predicted. Meanwhile, the hazard
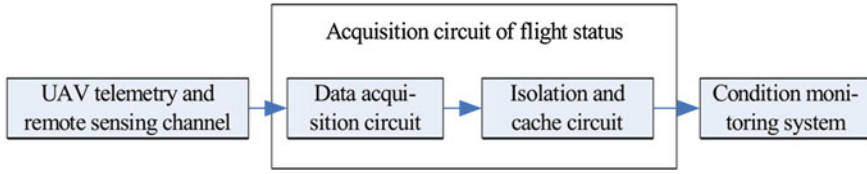
Fig. 69.3 Scheme of flight status acquisition circuit

degree of failure will be analyzed and predicted to provide safety-level alarm and corresponding emergency procedure. From the collected telemetry and remote sensing data, the UAV real-time flight status information and ground control information can be obtained to analyze the UAV engine, autopilot, attitude sensor system, operation state, and performance state of ground control station in a time interval; the developing trend will be estimated as well. Based on these, combined with intelligent prediction techniques, the possible failures can be predicted; criticality analysis will be carried out to give safety-level alarm. Therefore, the dynamic neural network will be adopted to process the status analysis and safety early-warning on flight data.

The Elman dynamic NN is employed in the flight status prediction module, its structure can be seen in Fig 69.4.

The mathematical expressions of this NN are expressed:

$$y(k) = g\left(w^3 \cdot x(k)\right) \tag{69.1}$$

$$x(k) = f\left(w^1 \cdot x_c(k) + w^2 u(k-1)\right) \tag{69.2}$$

$$x_c(k) = x(k-1) \tag{69.3}$$

where

$$y(k) = [y_{k1}, y_{k2}, \ldots, y_{km}] \tag{69.4}$$

$$x(k) = [x_{k1}, x_{k2}, \ldots, x_{kn}] \tag{69.5}$$

$$u(k-1) = \left[u_{(k-1)1}, u_{(k-1)2}, \ldots, u_{(k-1)r}\right] \tag{69.6}$$

$$x_c(k) = [x_{c1}, x_{c2}, \ldots, x_{cn}] \tag{69.7}$$

In which, k denotes the output vector set number; w^1, w^2, w^3, respectively, denotes the weight vector between through layer and bidden layer; input layer and bidden layer, hidden layer and output layer. $g(\cdot)$ is the transfer function of output neuron and the linear combination of intermediate-layer outputs; $f(\cdot)$ is the transfer function of intermediate-layer neuron and always adopts the S function. Generally, the Elman network weights are modified by BP arithmetic; the study index function adopts the sum of error square:
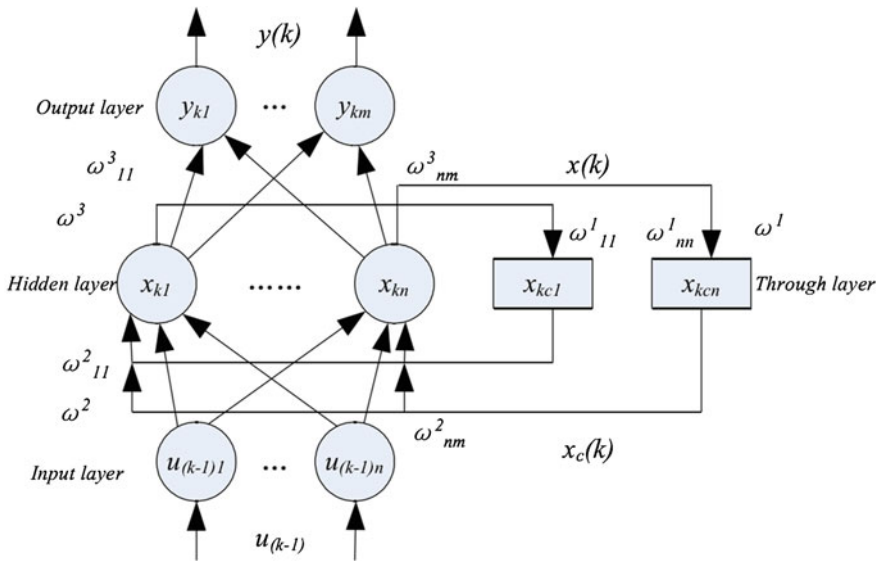
Fig. 69.4 The structure of Elman dynamic NN

$$E(w) = \sum_{k=1}^{n} [y_k(w) - \bar{y}(w)]^2 \tag{69.8}$$

where, $\bar{y}(w)$ is the target output vector.

With regard to the flight safety, the engine failures are the fatal factor of flight accidents. So, taking the oil cylinder temperature sensor as the example, the temperature change will be continuously monitored. In this way, the engine failure can be early-warned, and corresponding safety precautions will be advised to avoid the prang accidents.

The prediction module is built up following these steps:

1. The data pretreatment of remote sensing temperature will take place firstly;
2. Choosing the optimum time delay constant and embedding dimension m; then, the phase space of original time series is reconstructed;
3. Constructing the dynamic NN prediction module;
4. Training the NN with flight data and determining the NN model parameters;
5. Choosing some testing samples to verify the validity of the prediction module which is determined in step 4, if it can achieve the demands, then the prediction module is adopted; else if there is a large testing error, then go to step 4 to retrain the NN or step 3 to redesign the NN structure;
6. Using the real-time sensor data as the input, prediction module is employed to predict the oil cylinder temperature; and if the predicted value is excess, then alarm is giving immediately.

The whole process is realized through calling the NN toolbox of Matlab.

69.3.3 Life Accumulation, Prediction, and Maintenance Decision

In the engineering applications, the importance of life accumulation must not be ignored. On the basis of accumulated data collected during the operation time, the operation conditions and prospective performance degradation can be judged qualitatively and visually according to experiences. The mission time accumulation and operation time accumulation of device level are the key factors of armament performance degradation analysis and prediction and should be treated as important parameters to analysis and management. At present, the life prediction and the prediction-based maintenance decisions are gradually approved in the engineering application. The residual life is the time span between the moment when the product is detected and the moment of product failure. It means that the product residual time at some moment not only depends on its age but also on all the condition information until this moment. Recently, the mature residual life prediction models include: proportional hazard model, filtering model, and stochastic process deterioration model. Among them, the Kalman filtering model is quite applicable for the residual life prediction based on multimode information. The model expression and model parameter determination can be consulted from Refs. [1] and [2].

On the basis of filtering theory and probability statistics, the residual life prediction model can help the maintenance-operating personnel to confirm the residual life according to device condition information quantificationally. This method can preferably utilize the available condition information to predict the residual life; and with the accumulation of the condition information, the predicted mean residual life will be more and more close to the reality. Besides, the residual life density function can be achieved via the prediction model; then, with it, the assistant maintenance personnel can make maintenance decisions and confirm optimal maintenance interval considering the targets: reliability optimization and cost minimum.

69.4 Summary

The system of security monitoring and health management can realize the real-time acquisition, monitoring, and analysis functions of UAV flight data. Based on the above, the UAV system conditions and performance trend can be controlled; the fault premonitory analysis can be used to realize the pre-preparation and treatment of maintenance. The purpose of researching and developing this system is: to integrate the armament condition monitoring, fault diagnosis, and maintenance management into a whole; to construct a general maintenance management and support platform based on the information of UAV system; to provide the continuous operation data of UAV key parts for the research of UAV failure

mechanism and failure rule; and to offer the true data for the armament manufacture and improvement. The ultimate target is to enhance the armament operational readiness and maintenance support efficiency, to decrease the maintenance cost, and to realize the information-based autonomous logistics (AL) support of UAV system.

References

1. Chen L (2008) Research on CBM modeling and its application. Doctor's degree thesis, Ordnance Engineering College
2. Wan EA, van der Merwe R (2000) The unscented Kalman filter for nonlinear estimation. In: Proceedings of symposium on adaptive systems, signal processing, communication, and control Lake Louise, AB, Canada, Oct 2000

Chapter 70
Evaluation of Aircraft Electric Network Battle Damage Repair and Device Design

Houjun Yin, Dongchao Yan and Chuang Guo

Abstract Electric network mainly includes the aircraft power supply network, connection lines between airborne equipment, data bus and connectors. Based on the research of the aircraft electric network battle damage repair, this paper analysis the basic principles and of the damage repaired. Then, through the main frame design and model library building, the decision support system model of the aircraft electric network battle damage assessment and repair is established. Finally, this paper designs the software and hardware of the aircraft electric network damage repair test equipment and takes experimental verification with good effect.

Keywords Electric network · Battle damage · Assessment · Device design

70.1 Introduction

As the veins and nerves of the aircraft, electric network is manly composed of cable and all kinds of connecting device. Since it exits at every part of aircraft, it is easily damaged during the war. At present, the study of the electric network battle damage repair means a lot for reducing loss of war and maintaining the importance of continued flight capacity [1].

In this paper, the basic knowledge of the aircraft electric network battle damage repair is introduced, and it emphatically discusses the evaluation and simulation of the damage. This paper also gives the design of the electric network damage repair test equipment.

H. Yin (✉) · D. Yan · C. Guo
Air Force Engineering University, Xi'an 710038, China
e-mail: yhj120021@126.com

70.2 The Basic Theory of Aircraft Electric Network Battle Damage Repair

By using the aircraft electric network distribution characteristics, the damage can be decided the visible damage and hidden damage [2]. Visible damage can directly be seen by naked eye and equipment; hidden damage mainly in air combat maneuvering too hard, and the airplane was shot in the strong vibration caused by the need to pass the test equipment to find the point of failure.

The purpose of the electric network damage battle repair is to guarantee the aircrafts with the largest sortie, requirements under the harsh environment, the shortest period of time, the plane back to fight again. Therefore, there exist the basic principles and basic process accordingly.

70.2.1 The Basic Principle of Electricity Network Battle Damage Repair

In order to make rapid recovery of war-wounded combat aircraft, electric network battle damage repair work must be highlighted word a, 'quick'. So it should obey the following principle:

1. Exam tissue repair policy
2. To lower, not higher principles
3. Principle of temporary repairs.

70.2.2 The Basic Process Flow of Electricity Network Battle Damage Repair

Aircraft electric network battle wounds may come from the air and also may come from the ground. The ground damage is generally more serious. According to the principle of repair, aircraft with good air worthiness should be repaired firstly, such as plane attracted in air combat [3]. At this point, the aircraft warning system and flight information recorded reference system are very important for the use of electrical networks battle damage repair test equipment to find hidden point of failure.

We will express electric network fault location into three steps as a line in the school, two rough sentenced to three points. The implementation of the basic flow as the Fig. 70.1 is to repair the damaged electric network [4].

Fig. 70.1 Basic flow of electric network battle damage repair
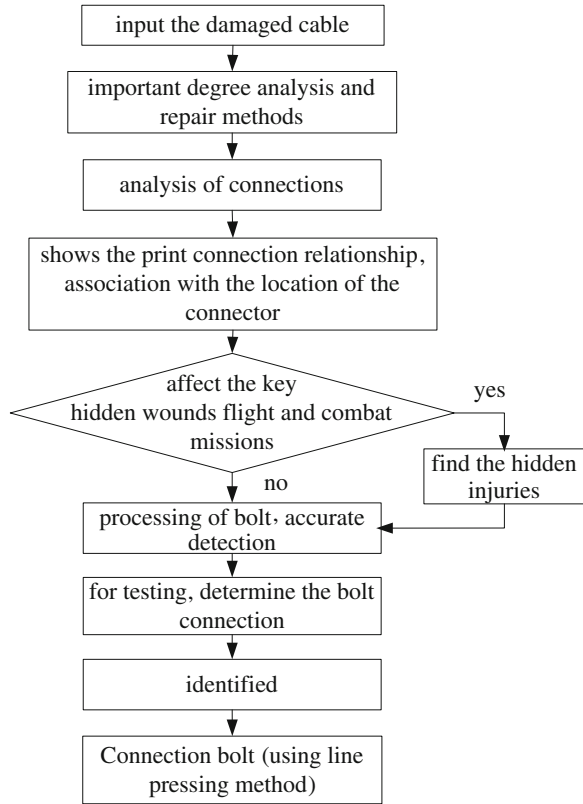
70.3 Aircraft Electric Network Battle Damage Repair Assessment

70.3.1 Overall Framework of Simulation System

Aircraft electric network battle damage mechanism simulation is using computer to simulate the aircraft under the condition of actual combat, by air-to-air, ground-to-air, air-to-ground, ground-to-ground and other weapons to fight. By making sure of the situation of aircraft electric network damage, it can solve basic problems in the study of aircraft electrical network battle damage repair. Through analysis, the physical model electric network battle damage, mathematical model of assault weapons and aircraft rendezvous after model of the bursting of the missile shell fragments scattering mathematical model, shrapnel hit to the plane mathematical model and mathematical model of aircraft damage deformation are all established [5]. Comprehensive analysis of domestic and foreign existing damage analysis of the development platform have to be prepared suitable for aircraft battle damage analysis of system software, which is to be able to run the above models.
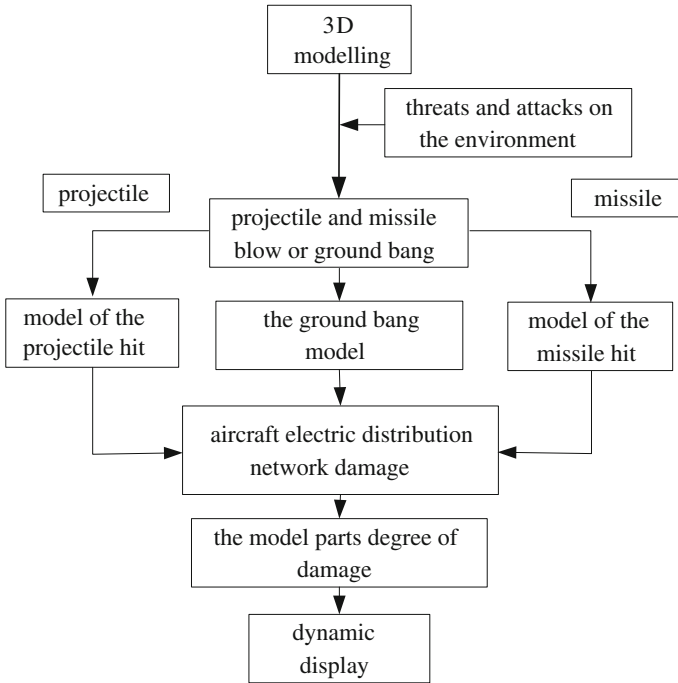
Fig. 70.2 Logical flowchart of battle damage mechanism simulation system

According to the results of the experiment of modifying model and dynamically displaying, the main research contents are shown as follows:

1. preliminary evaluation of the survivability of the plane,
2. predict of the model aircraft electric network battle damage in the future war,
3. to dynamically display the injuries, study different types of missile strikes initiation point distribution of the plane, the shrapnel on aircraft electric network damage degree and the scope,
4. determine the aircraft electric network battle damage rule.

Through the above researches, aircraft electric network battle damage analysis platform is built. Then, it can determine the mode of electric network battle damage and the damage mechanism [6]. This technology will help the repair work easier by providing the science support. First by using geometric modeling technology, 3d entity model of the aircraft is established separately; then, we build the model of air attack and ground attack. The exchange of information using data exchange technology is used to find the probability of various parts of the electric network and the injuries [7]. Finally, it dynamically shows that under the condition of the air combat aircraft electric network model of damage location and damage degree of damage. Logic flowchart is shown in Fig. 70.2.
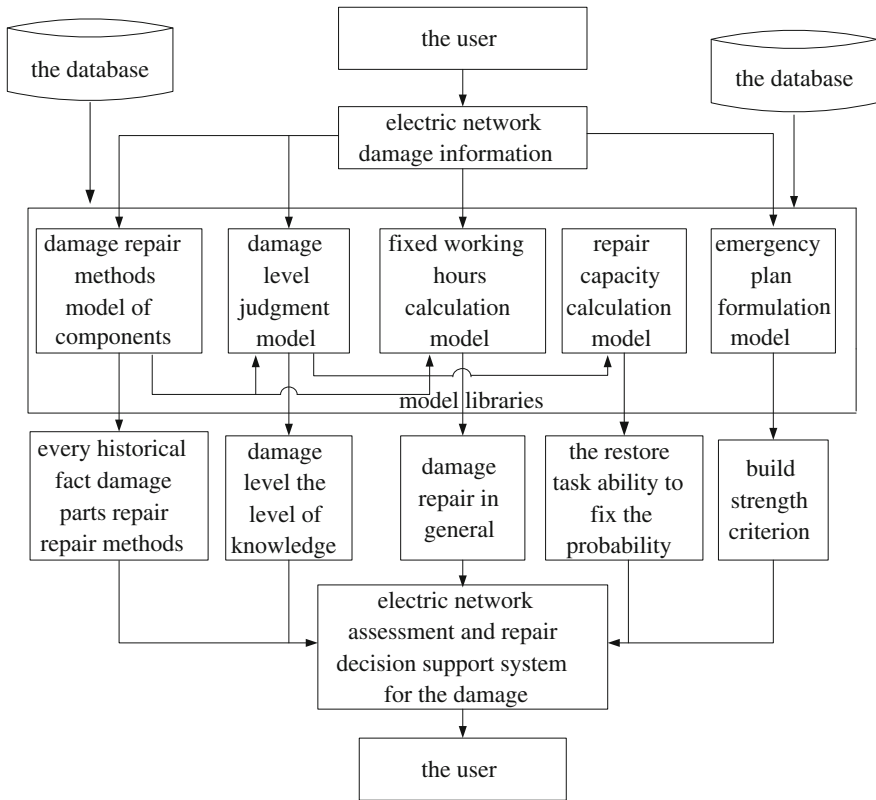
Fig. 70.3 Work process of the assessment and repair decision support system

70.3.2 The Establishment of Model Base and its Working Process

The main models in the model base are component damage repair method model, damage level estimation model, repair work calculation model performance computing model and repair program development model. The decision model system is the combination of each model [8].

Model library through the damage data input, output and combination of different unit operations, aircraft structure provides users with the injuries assessment; repair decision support information and work process are shown in Fig. 70.3.

Fig. 70.4 The principle
diagram of the system
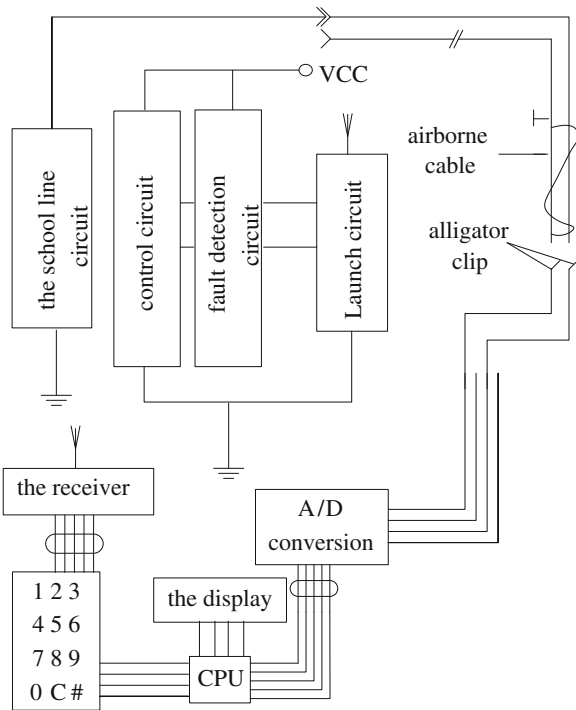
70.4 Design of Aircraft Battle Damage Repair Electrical Network Test Equipment

70.4.1 Hardware Design

Electrical network battle damage repair test equipment system composition principle is shown in Fig. 70.4. The master device is composed of two parts, respectively, in the main separation equipment at the cable and connector damage on electrical equipment. Which applied a signal from the wireless remote control for communication, the main function of battle damage repair electrical network test equipment is calibration line and fault location. The probe in turn is connected with the jack nailing. Controlling the remote computer cyclic scanning method is technically easy to implement.

Therefore, the hardware design is divided into the remote module design and fault locator module design.

Fig. 70.5 The flowchart of
system control
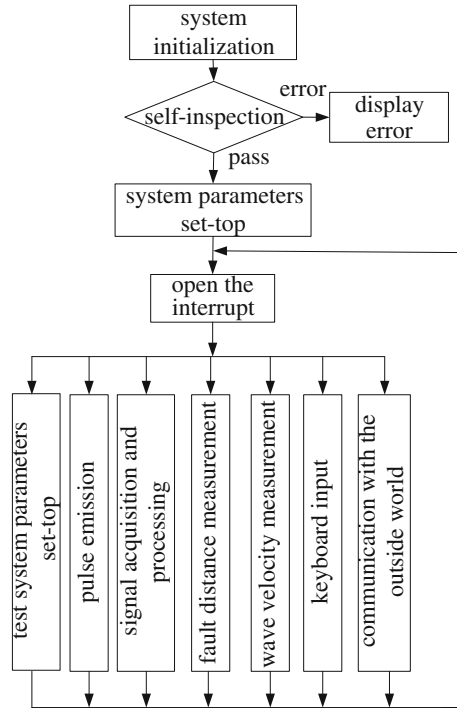
70.4.2 Software Design

The software design of electricity network battle damage test equipment consists of three parts: information analytical software, system control software, expert system software.

Information analytical software. Using the reflection of pulse legal position detection inevitably caused various kinds of electromagnetic interference, bringing errors to the fault location. Digital signal processing algorithms and wavelet transform for signal processing are used to eliminate these interference effects, to identify the point of failure and to improve positioning accuracy.

System control software. Under the management of the main program, the system control software can control the hardware circuit and finish the data acquisition, data transmission and terminal display. Logic flowchart is shown in Fig. 70.5.

Expert system software. Influenced by various factors, the reflection waveform collected is diverse and complex. In order to carry out the various features of the pulse correct judgment and finally to get accurate results, the instrument requires users to have expert level and experience. Expert system simplifies the process, reduces the demand for the consumer, can optimize the data processing, judges the fault types, and invokes the corresponding accurate positioning model; cable to test the final optimization results is given, and the test results are analyzed. The logic flowchart of expert system is shown in Fig. 70.6.

Fig. 70.6 The flowchart of expert system
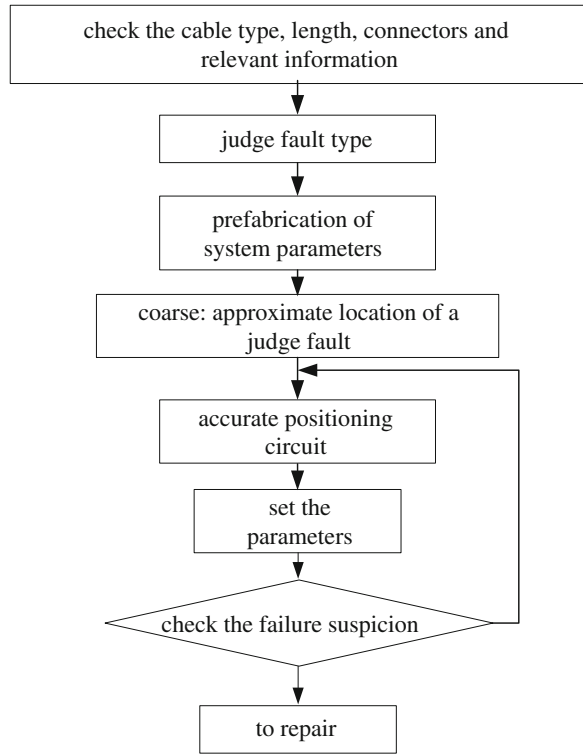
70.5 Experimental Verification

Finally, we developed the aircraft battle damage repair electrical network test equipment, taking the plane at the end of the cable connect to the data reception and processor, connecting to the other end to signal feedback device. The signal feedback device sends signal to the data reception and processor, thus accurating quickly cable failure is detected during the process of testing. The experimental results show that the device is a success.

70.6 Conclusions

Studying on aircraft electric network battle damage repair is the important part of the study of aircraft battle damage repair. The proposed simulation system aims to establish a visual plane to analysis the common platform of the damage. Build aircraft electric network assessment and repair decision support system model base. The damage for rapid assessment of the aircraft electric network and repair provides scientific judgment and guidance.

References

1. Yan D, Ma J (2008) Study on aircraft electric network battle damage repair. The Aviation Maintenance and Engineering, Beijing
2. Zhang J, Li W (2010) Research on methods for evaluating the design of aircraft combat resilience. Northeastern university, Shen Yang, pp 156–169
3. Yao W, Yao H (2008) The research of aircraft battle damage repair technology supporting system.The Air Force's First Institute of Aviation, Xinyang
4. Yao W, Cai K (2011) Research on information management and decision system of airplane battle damage repairing. The Air Force's First Institute of Aviation, Xinyang
5. Zhang J, Liu H (1997) To meet the need of the future-step up aircraft repair professional construction of the damage. The Air Force College Education, Beijing
6. Yu J, Yang B (1999) Cable fault detection technology and practical experience. Central China Electric Power, Wuhan, pp 51–52
7. Pan Q (2007) Design and development of composite aircraft battle damage repair simulation system. The Air Force's First Institute of Aviation, Xinyang
8. Zhao H (2005) Study on aircraft electric network battle damage. Air Force Engineering University Graduate Dissertation, Xi'an

Chapter 71
Brush Plating for Renovating the Piston of Wing Flap Motion Tube

Chengbao Xia, Baosheng Yang, Yunkui Gao and Minghua Chen

Abstract In order to solve the repairing problem of worn piston of wing flap motion tube, the technology of brush plating Ni–diamond composite coating on the surface of high strength steel 18Cr2Ni4WA has researched. A new repairing technology was proposed based on the failure analysis of worn piston of wing flap motion tube. Using this coating system of brushing, Ni–diamond composite coating, through reducing the electrode potential of cathode, the degree of cathode polarization would be increased and make the speed of forming nuclei faster than the speed of growth of crystal nucleus, so the adhesion between the coating and basis material was increased. When the thickness of repairing coating is up to 30 μm, the hardness of the coating achieves 780 (HV); the adhesive power was better, and the adhesion tests are as follows: coating not fall off; the bend test: coating not peel off; the cupping test: height of test is 5.1 mm; the wear resistance of the repairing coating and the basis material's approach. Tests have shown that qualified brush electroplating layer for repairing worn piston can be got through this kind of process.

Keywords Brush plating · Ni–diamond composite coating · Worn piston

71.1 Introduction

Wing flap motion tube, an important controlling part, is used to control the elevating and descending of plane, and the piston of it is the key part, which is made of high strength steel 18Cr2Ni4WA; its surface is treated by bluing. During the working process, the piston's top will be worn or scratched because of its reciprocating motion under high pressure. If the wear surpasses the stipulated fit

C. Xia (✉) · B. Yang · Y. Gao · M. Chen
The First Aeronautic Institute of Air Force, Xinyang, Henan, China
e-mail: xiachengbao1@163.com

internal 0.025–0.185 mm, the hydraulic oil will leak out. Further, its performance will be influenced, and flying will be threatened. In the past, we mainly polished [1] the piston's top φ22f7 that had been worn or scratched. Once the wear surpasses the stipulated tolerance 0.025–0.185 mm, it had to be deserted, which caused a heavy loss. In recent years, with the development [2] and deep research [3] of surface technology, such as brush plating, the better repair for piston φ22f7 is possible. So we researched brush plating on the surface of high strength steel 18Cr2Ni4WA. Through reducing electrode potential of cathode, increasing the degree of cathode polarization, this technology made nuclei forming faster than crystal nucleus growing. So the adhesion between coating and basis material was enhanced. We had examined the performance of repaired parts. The testing showed that the coating met the requirements by brush plating special Ni–diamond.

71.2 Technological Designs

71.2.1 Main Equipments

MS-100 Nanometer plating equipments; Fuel delivery pumps SYB-2; MK200 wore test HCC-8 thickness gauge; HVS-1000 microsclerometre.

71.2.2 Composition for Plating Solution

According to the request, the repaired coatings should have two basic functions: First, the adhesion should be bigger between working coating and basis material and the hardness of the repaired coatings should be high. Synthesizing to consider, the Ni–diamonded has been chosen. Its composition is as follows:

$NiSO_4 \cdot 7H_2O$ (CP) g/L	300
CH_3COOH (CP) mL/L	48
Na_2SO_4 (CP) g/L	20
NaCl (CP) g/L	20
$NH_2H_2SO_4NH_2$ (CP) g/L	0.1
Additive g/l	2.0
Diamond power (0.5 μm)	Right amount
Activating agent g/L	2.0
pH	3–4

In order to remove the oxidizing layer on the diamond powder, the powder needs to be boiled in nitric acid for 25 min or so and then wash it with distilled water until it is not acid and alkaline, and oven-dry it.

71.2.3 Technological Process

Polishing → washing → removing the oil → protecting partly → electrochemical corrosion → washing → activating with activating solution 2 → washing → activating with activating solution 3 → brush plating the repaired coating → washing → processing after plating → washing and drying.

Then *Preparation for renovating the surface*. Polish and wash the surface and its neighborhood with acetone and measure it precisely, meanwhile calculate the added thickness. The part not plated should be protected by vinyl perchloride adhesive solution and be dried by airing. Then, fix the piston on the platform; in the processing of plating, the part would be fixed, and the plating pen moved. Anode is made of graphite plate.

Electrical cleaning. Operating voltage: 14 V; electrode connection: join the plating pen to cathode and the piston to anode. The relative moving speed between the plating pen and the piston is 6–8 m/min. Electrical cleaning time: 40 s; wash it well with running water.

Activating. Activate the surface by applying activating solution 2 and 3 in turn. There are black carbides on the basis material's surface after it was processed by activating solution 2; you must remove the carbides by activating solution 3. If not, the adhesive power between the coating and the basis material will be greatly reduced by the carbides left on the surface. They can even result in the coating's peeling and falling off. Being activated by activating solution 3, the surface becomes silver gray, without black spots, not absorbing drops of water. Operating technology: voltage: 10 V for activating solution 2; 16 V for activating solution 3; electrode linkage: connect the pen with cathode, and the piston with anode; the relative moving speed: 8–12 m/min; electrical cleaning time: 30 s.

Brush plating special Ni as the transition coating. The special Ni is deposited fast. The safe thickness of the single coating is 2–5 micron [4]. And the coating has a strong binding force. Therefore, the special Ni was chosen.

Brush plating the Ni–diamond for renovating. With an inferior internal stress, the Ni–diamond coating still has strong hardness in a very high temperature. It is a good wear-resisting working coating. The technological parameters: voltage for plating: 12 V; electrode linkage: connect the pen with anode, and the piston with cathode; the relative moving speed: 10–25 m/min; factor of the power assumption: 0.162 A H/μm dm^2. When you measure it, you must spray water on the whole plated surface in case it is polluted, and the adhesion is influenced.

The processing after being plated. When the coating reaches the thickness as requested, you should stop plating and remove the vinyl perchloride layer. The coating should be burnished properly, with roughness Ra $\leq$ 0.1 μm. Then, clean

Table 71.1 The performance of the renovating coating

Program	Result	Standards
Thickness	30 μm	GB 4955-85
Hardness	780 (HV)	GB/T 4342-91
Adhesion	fine[a]	GB 5270-85
Height	5.1 mm	GB 5270-85
Wearability	0.115 mg/frequency	GB 5932-86[b]

[a] Bend test: no peeling
[b] Wear quantity of original part is 0.118 mg/time

the coating by well applying gasoline and spread red oil on it, and then it can be used again.

The quality of the repaired coating. Measure the thickness by KL-1 coulomb thickness gauge; measure the hardness by micro-hardness tester HVS-1000; and measure the adhesion by the BT-2. The results are as follows (Table 71.1).

71.3 Main Measures

Using bidirectional brush plating, reducing the internal stress of the repaired coating. The internal stress of the repaired coating relates to the change of crystal microstructure in the brush plating process.These changes include crystal lattice parameter,crystallite dimension and so on. Furthermore, the crystal lattice parameter of the repaired coating is not just the same with the internals; therefore, in the process of electrodepositing, because of the emission of atom produced on the surface, the acting force of changing crystal lattice parameters in the internal repaired coating would be produced; thus, the internal stress was produced. In view of this situation, technological method of turn and reversal alternately was adopted; the internal stress produced along forward direction with the reversal would cancel out each other and make the internal stress of the repaired coating reduce greatly. It was propitious to get a thicker repaired coating.

Improving intensity of polarization, increasing the adhesion of repaired coating. In the process of electrodepositing, the more the number of crystal nucleus, the more the bond strength of the repaired coating. Therefore, the additive was appended into electrolyte of brush plating, and deposition potential of the metal ion was reduced; more electrons would be gathered at the brush plating surface, the more crystal nucleus would be formed; the quantity of bonding point would be increased; therefore, the bond of the repaired coating with the original surface would be increased also.

Controlling temperature of electrolyte, increasing abradability of repaired coating. The effect that abradability was influenced by temperature of electrolyte is shown in Fig. 71.1. It indicates that the abradability of repaired coating would be improved as the rise in temperature; the abradability was the best at 50 °C. The reason lies in the fact that the grain content of diamond in the repaired coating

Fig. 71.1 Effect of temperature to abradability of repaired coating
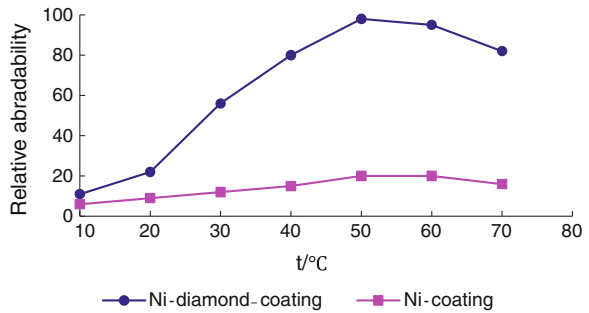
was the most at 50 °C, making the hardness repaired coating increased, and leading to improving of abradability of repaired coating. Therefore, the temperature of electrolyte was controlled about 50 °C.

71.4 Summary

This renovating method can strengthen the adhesion between the coating and the working coating, enhance the hardness of the repaired coating and make the fit surface more wear-resisting. As a result, it settles the problem of 18Cr2Ni4WA high strength steel that easily generate hydrogen embrittlement in the superficial treatment course. This simple technology, with stable performance, can be used well in renovating the aviation weaponry parts.

References

1. The First Research Institute of Air Force (1997) A manual of repairing planes' accessories. The First Research Institute of Air Force Press, Beijing, pp 362–366 (in Chinese)
2. Xu B, Liu S (2002) New technology of surface engineering. Mechanical Industry Press, Beijing, p 162 (in Chinese)
3. Tu W, Xu B (2003) Study on microstructure and co-deposition mechanism of n-Al2O3/Ni composite coating prepared by electro-plating. Mater Eng 7:31–35 (in Chinese)
4. Xu B, Zhu S, Liu S (1996) Surface engineering and maintenance. Mechanical Industry Press, Beijing (in Chinese)

Chapter 72
Maintenance Performance Evaluation Based on Matter Element Analysis of Aviation Maintenance

Lihai Peng, Liwan Zhang, Baomin Ji and Wengui Li

Abstract Maintenance effectiveness evaluation of aviation equipment is the era of information technology and new areas with the fresh concept of the maintenance revolution. Based on Extenics theory and other theory including entropy method based on gray relational analysis, the article constructed a frame of system to evaluate the performance of aviation maintenance ability which is not only suitable for helicopter repair. The paper analyzed evaluation model and framework by the numerical example drawn maintenance performance levels, modified similar assessment issues and promoted innovative maintenance theories and methods, which provides a new method and may has a good prospects of application.

Keywords Aviation maintenance · Matter element analysis · Entropy method · Performance evaluation · Gray relational

72.1 Introduction

Aviation maintenance performance is an important branch of aviation industry. How to improve the aviation repair ability plays an important role in the service life of the aircraft and flight safety. The paper try to establish effective evaluation and analysis of performance on deep understanding of aviation repair system. Based on system of performance is an important component in the simulation and practical assessment which has important significance for the aviation and play an important role in the evaluation.

L. Peng (✉) · L. Zhang · B. Ji · W. Li
Maintenance Researcher of Aviation, Mechanical Engineer, Hhehuan str. 5182, Shanxi 043000, China
e-mail: likewangyi27@126.com

L. Peng
Institute of Aviation, Beijing 100000, China

Aviation system demonstration means expansion expert appraisal, analytical reasoning, including simulation analysis, considering the environment and other factors; many scholars have conducted massive research for aviation maintenance efficiency who promoted the technical progress including the method of Genetic Algorithm, Neural Network, Particle Swarm Optimization, Support Vector Machine, Expert System, and so on [1–4]. Massive advanced techniques have been realized in the practice and application.

In the objective machinery world, things are intrinsically linked by modules and sub-units; their relationship may be described by matrix. Professor Cai Wen [5, 6] founded amusing theory called matter element and extension set to generate untraditional knowledge system; it introduces the concept of matter element to associate and to seek means of making mathematics evaluation. In this paper, matter element analysis theory was used through the establishment of multiple indicators of operational capability evaluation model; according to the classical matter element analysis steps, major parameter was acquired [7]. As an example, the repair system of capacity for helicopter was explored and maintenance performance was assessed.

72.2 Principle of Mathematical Models

Given the name of thing N which is consist by the characteristics C whose measure is v, using an ordered triple $R = (N, C, v)$ as basic element which can describe target things, also referred to matter-element. The elements of things including three partment: features and value, in this paper we call Matter-element. Assuming the thing N has many characteristics, we can use number of n such as $c_1, c_2, c_3, \ldots c_n$, and also the corresponding values $v_1, v_2, v_3 \ldots v_n$ to express its composition, at this time we call the matter element R N-dimensional matter element, which can be described as $R = (N, C, V) = (R_1, R_2, \ldots, R_n)'$, or, $R =$

$$\begin{bmatrix} N & c_1 & v_1 \\ & c_2 & v_2 \\ & \ldots & \ldots \\ & c_n & v_n \end{bmatrix}$$, in the formula, R means matter with N-dimensional, and R_i

$(i = 1, 2, \ldots, n)$ means sub-matter element.

72.3 Main Steps

72.3.1 Divide Classical Field

Assume N_j include evaluation number of j, C_i means characteristics of evaluation indicators of N_j, $Y_{ji} = \langle m_{ji}, n_{ji} \rangle$ $(i = 1, 2, \ldots, n)$ show the corresponding range which refer to C_i. And the date domains R_j rely on index evaluation; C_i is called

classical domain, it also correspond with N_j. At this time, R_j can be describe as follows:

$$R_j = (N_j, C_i, Y_{ji}) = \begin{bmatrix} N_j & c_1 & v_{j1} \\ & c_2 & v_{j2} \\ & \cdots & \cdots \\ & c_n & v_{jn} \end{bmatrix} = \begin{bmatrix} N_j & c_1 & \langle m_{j1}, n_{j1} \rangle \\ & c_2 & \langle m_{j2}, n_{j2} \rangle \\ & \cdots & \cdots \\ & c_n & \langle m_{jn}, n_{jn} \rangle \end{bmatrix} \quad (72.1)$$

72.3.2 Determine Section Domains

If N is expressed in all the evaluation level, Y_{N1}, Y_{N2},..., Y_{Nn} represent the number range of C_i ($i = 1, 2,..., n$), respectively, whose value correspond with N, and section domains can be describe as

$$R_p = (p, C_i, Y_{pi}) = \begin{bmatrix} p & c_1 & v_{p1} \\ & c_2 & v_{p2} \\ & \cdots & \cdots \\ & c_n & v_{pn} \end{bmatrix} = \begin{bmatrix} p & c_1 & \langle m_{p1}, n_{p1} \rangle \\ & c_2 & \langle m_{p2}, n_{p2} \rangle \\ & \cdots & \cdots \\ & c_n & \langle m_{pn}, n_{pn} \rangle \end{bmatrix} \quad (72.2)$$

Another way of saying, section domain can be considered at all levels of evaluation range.

72.3.3 Determine Matter Element to be Evaluated

Gather all monitored data and analysis results with the material or element as this,

$R_0 = \begin{bmatrix} p_o & c_1 & v_1 \\ & c_2 & v_2 \\ & \cdots & \cdots \\ & c_n & v_n \end{bmatrix}$ in the formulas, P_o as element to be evaluated, v_1, v_2,

$v_3...v_n$ represent the value of the thing C_i ($i = 1, 2,..., n$), which is linked separately with P_o, just to be evaluated relative to each index specific data.

72.3.4 Determine the Degree of Association with Things to be Assessed on Each Level of Each Index

Weight coefficient $\sum_{i=1}^{n} \omega_i = 1$, and

$$K_j(x_i) = \begin{cases} \frac{\rho(x_i, x_{oji})}{\rho(x_i, x_{oji}) - \rho(v_i, v_{oji})}, & \rho(x_i, x_{oji}) - \rho(v_i, v_{oji}) \neq 0 \\ -\rho(x_i, x_{oji}) - 1, & \rho(x_i, x_{oji}) - \rho(v_i, v_{oji}) = 0 \end{cases} \quad (72.3)$$

$$\begin{cases} \rho(x_i, x_{oi}) = \left| x_i - \frac{1}{2}(w_{oi} + b_{oi}) \right| - \frac{1}{2}(b_{oi} - w_{oi}) \\ \rho(x_i, x_{pi}) = \left| x_i - \frac{1}{2}(w_{pi} + b_{pi}) \right| - \frac{1}{2}(b_{pi} - w_{pi}) \end{cases} \quad (72.4)$$

Then calculate the degree of the correlation among the target dates [8]

$$K_j(p_o) = \sum_{i=1}^{n} \omega_i K_j(x_i). \quad (72.5)$$

72.3.5 The Assessment Level

From above-mentioned function formula, quantitative description of any element of the domain belongs to positive field, negative or zero bound three domains which can also be an element belonging to a domain with a correlation function value to distinguish different level [5]. If $K_j(p_o) = \max\{K_j(p_o)\}$ ($j = 1, 2,\ldots$, m), then the matter element which to be evaluated as P_o stand in class j.

72.4 Maintenance Performance Evaluation for Helicopter

72.4.1 Target of Evaluation

Learn from operational capabilities and related quantitative methods of research results [5], the attempt of systems analysis and theoretical ideas, which build descriptor, will be more reasonable and more quantitative since the repair efficiency of helicopter is part of its combat capability. With the rapid development of civil aircraft, support capability of aircraft became vital to us. The paper designs four sub-evaluation indexes, mainly for aviation maintenance of the main capabilities: reliability, security, economy, social welfare. The sub-index of corresponded evaluation contains a total of eleven under evaluations ,in this paper considered as follows:

Reliability B_1 Maintenance fault tolerance c_1, Maintenance intervals c_2, Equipment readiness c_3;
Security B_2 Accident rate c_4, Continuous safe working time c_5, Maximum working life c_6;
Economy B_3 Overhaul repair cost for one helicopter c_7, Parts cost recovery state c_8, Tools and equipment costs c_9;
Affordable B_4 Number of crew members c_{10}, State recovery rate c_{11}.

72.4.2 Assessment Framework to Build

Evaluation index value range, $A(90–100)$, $B(80–89)$, $C(70–79)$, $D(60–69)$, E(below 60), it means $N_j (j = 1, 2, 3, 4, 5)$. The section domains for them $c_1(0–100)$, $c_3(0–1)$, $c_4(0–1)$, $c_{11}(0–1)$, and dimensionless matter of c_2, c_5, c_6, write as $\bar{t} \cdot (0 \sim 1)$, dimensionless matter of c_7, c_8, c_9, write as $\bar{a} \cdot (0 \sim 1)$, c_{10} as $\bar{b} \cdot (0 \sim 1)$, $\bar{t}, \bar{a}, \bar{b}$ means reference value which selected a foreign helicopter maximum online evaluation, t as the time, a and b both as the existing evaluation value. From the corresponding classical field $A(90–100)$, $B(80–89)$, $C(70–79)$, $D(60–69)$, E(bellow 60), the range is evaluated by correspond evaluation value ratio.

So we come to the matrix

$$
R_1 = \begin{bmatrix} N_1 & c_1 & \langle 90 \sim 100 \rangle \\ & c_2 & \bar{t} \cdot \langle 0.9 \sim 1 \rangle \\ & c_3 & \langle 0.9 \sim 1 \rangle \\ & c_4 & \langle 0.9 \sim 1 \rangle \\ & c_5 & \bar{t} \cdot \langle 0.9 \sim 1 \rangle \\ & c_6 & \bar{t} \cdot \langle 0.9 \sim 1 \rangle \\ & c_7 & \bar{a} \cdot \langle 0.9 \sim 1 \rangle \\ & c_8 & \bar{a} \cdot \langle 0.9 \sim 1 \rangle \\ & c_9 & \bar{a} \cdot \langle 0.9 \sim 1 \rangle \\ & c_{10} & \bar{b} \cdot \langle 0.9 \sim 1 \rangle \\ & c_{11} & \langle 0.9 \sim 1 \rangle \end{bmatrix}, R_2 = \begin{bmatrix} N_2 & c_1 & \langle 80 \sim 89 \rangle \\ & c_2 & \bar{t} \cdot \langle 0.8 \sim 0.89 \rangle \\ & c_3 & \langle 0.8 \sim 0.89 \rangle \\ \cdots & \cdots & \cdots \\ & c_{11} & \langle 0.8 \sim 0.89 \rangle \end{bmatrix} \quad (72.6)
$$

$$
R_3 = \begin{bmatrix} N_3 & c_1 & \langle 70 \sim 79 \rangle \\ & c_2 & \bar{t} \cdot \langle 0.7 \sim 0.79 \rangle \\ & c_3 & \langle 0.7 \sim 0.79 \rangle \\ \cdots & \cdots & \cdots \\ & c_{11} & \langle 0.7 \sim 0.79 \rangle \end{bmatrix}, R_4 = \begin{bmatrix} N_4 & c_1 & \langle 60 \sim 69 \rangle \\ & c_2 & \bar{t} \cdot \langle 0.6 \sim 0.69 \rangle \\ & c_3 & \langle 0.6 \sim 0.69 \rangle \\ \cdots & \cdots & \cdots \\ & c_{11} & \langle 0.6 \sim 0.69 \rangle \end{bmatrix} \quad (72.7)
$$

$$
R_5 = \begin{bmatrix} N_5 & c_1 & \langle 0 \sim 59 \rangle \\ & c_2 & \bar{t} \cdot \langle 0 \sim 0.9 \rangle \\ & c_3 & \langle 0 \sim 0.9 \rangle \\ \cdots & \cdots & \cdots \\ & c_{11} & \langle 0 \sim 0.9 \rangle \end{bmatrix} \quad (72.8)
$$

Section domains can be write as:

$$
R_p = \begin{bmatrix} N_p & c_1 & \langle 0 \sim 100 \rangle \\ & c_2 & \bar{t} \cdot \langle 0 \sim 1 \rangle \\ & c_3 & \langle 0 \sim 1 \rangle \\ \cdots & \cdots & \cdots \\ & c_{11} & \langle 0 \sim 1 \rangle \end{bmatrix} \quad (72.9)
$$

Combined with expert parameters of a model comprehensive maintenance performance, design a matrix to be evaluated,

$$
R_0 = \begin{bmatrix}
N_0 & c_1 & 84.7 \\
 & c_2 & \bar{t} \cdot 0.852 \\
 & c_3 & 0.65 \\
 & c_4 & 0.734 \\
 & c_5 & \bar{t} \cdot 0.831 \\
 & c_6 & \bar{t} \cdot 0.715 \\
 & c_7 & \bar{a} \cdot 0.82 \\
 & c_8 & \bar{a} \cdot 0.89 \\
 & c_9 & \bar{a} \cdot 0.83 \\
 & c_{10} & \bar{b} \cdot 0.77 \\
 & c_{11} & 0.75
\end{bmatrix}
\tag{72.10}
$$

72.4.3 Using Entropy Method Based on Gray Relational Analysis to Determine the Weight Coefficient

Information entropy reflects the degree of disorder; system of the disordered degree will be small after the value is smaller. The information entropy can be used to evaluate the order degree and its utility of the system [9]. Using the extreme value method to normalize the judgment matrix, we can write as $U = (u_{ij})_{mn}$, and we write $u^{ij} = \frac{x_{ij} - x_{\min}}{x_{\max} - x_{\min}}$, the next step is to determine the entropy of the index H_i,

$$
H_i = -\frac{1}{\ln m}\left[\sum_{j=1}^{m} f_{ij} \ln f_{ij}\right]
\tag{72.11}
$$

In the formula, $i = 1, 2, 3,\ldots, n, j = 1, 2, 3,\ldots, n$, and

$$
f_{ij} = \frac{1 + b_{ij}}{\sum_{j=1}^{m}\left(1 + b_{ij}\right)}
\tag{72.12}
$$

Then, we calculate the entropy of the evaluation index $W = (w_i)_{1\times n}$:

$$
w_i = \frac{1 - H_i}{n - \sum_{i=1}^{n} H_i}
\tag{72.13}
$$

Lead into gray relational analysis to calculate correlation coefficient [10, 11],

$$
k_{0i}(j) = \frac{\min(\min \Delta_i(j)) + \beta \max(\max \Delta_i(j))}{\Delta_i(j) + \beta\max(\max \Delta_i(j))}
\tag{72.14}
$$

In the formula $\beta \in (0,1)$ and $\Delta_i(j) = |x_o(j) - x_i(j)|$, then, we combine the matter element way and gray relational analysis method to compute relative k

$$k_0 = \frac{k_{0i} - \min k_{0i}}{\max k_{oi} - \min k_{oi}} \tag{72.15}$$

According to entropy method to calculate the correlation degree, through a existed method and link formula (72.5), (72.9), (72.10), (72.12)–(72.15), reach the coefficient as

$$K_1(p_o) = \sum_{i=1}^{n} w_i K_1(x_i) = 1.23\overline{K}_0, \quad K_2(p_o) = \sum_{i=1}^{n} w_i K_4(x_i) = 1.05\overline{K}_0,$$

$$K_3(p_o) = \sum_{i=1}^{n} w_i K_1(x_i) = 1.34\overline{K}_0, \quad K_4(p_o) = \sum_{i=1}^{n} w_i K_4(x_i) = 0.95\overline{K}_0,$$

$$K_5(p_o) = \sum_{i=1}^{n} w_i K_5(x_i) = 1.17\overline{K}_0.$$

According to the matrix and existed date, we can appraise the C-class as the maintenance performance for the target helicopter which to be evaluated. But there need further research and investigation.

72.5 Conclusion

Based on the matter element model and extension analysis including gray relational, the article discussed a system of maintenance performance evaluation combined with entropy calculation and constructed performance evaluation model and framework for a certain type of equipment. It is similar to the problem solution which provides an efficient approach. In subsequent calculations, some of the course needs more accurate data to support and testify model validation. This method for calculation seems simple, the matrices are clarity, and the attractive model is relevance faithfulness and reliability. It may play an important role in validation of aviation maintenance efficiency.

References

1. Chen Y (2013) Comprehensive evaluation and forecast analysis of safety and quality in civil aviation maintenance. J Aviat Univ China 13(1):267–270
2. Tian X, Li H (2007) Application of AHP method to QTM system of aviation servicing company. J Nanjing Univ Aeronaut Astronaut (Soc Sci) 9(3):21–25 (in Chinese)
3. Cao W, Zhou T (2007) Application of neural network in the aviation repair in expert system. Sci Technol Consult Herald 5(4):157–159 (in Chinese)

4. Feng G, Liu W, Zhang X (2006) Evaluation of equipment repair quality based on BP neural network. Sci Technol Eng 9(6):1296–1299 (in Chinese)
5. Wen C, Chunyan Y (2013) Basic theory and methodology on extenics. Chin Sci Bull 58(13):1190–1199
6. Wen C, Yong S (2006) Extenics: its significance in science and prospects in application. J Harbin Inst Technol 38(7):1080–1085
7. Lee YC, Terashima N (2011) An extenics-based intelligent distance learning system. Int J Comput Sci Netw Sec 11:57–63
8. Chuan ZDL (2006) Modeling and control implementation of virtual maintenance simulation. J Beijing Univ Aeronaut Astronaut 32(7):843–848 (in Chinese)
9. Zhang G, Lu Y, Tu Q et al (1992) System reliability and maintain ability analysis and design. Beijing University of Aeronautics and Astronautics Press, Beijing
10. Zhou J, Lu F, Huang J (2011) Gas-path component fault diagnosis based on gray relational analysis for aero-engine. J Propul Technol 32(1):141–145 (in Chinese)
11. Wang Y, Wang H (2011) Analysis of aeronautical repair of human factors based on Grey theory. Ergonomics 17(3):60–64 (in Chinese)

Chapter 73
Evolution of Aircraft Maintenance and Logistics Based on Prognostic and Health Management Technology

Jing Dai and Haifeng Wang

Abstract This study discusses the new evolution of aircraft maintenance and logistics. After the introduction of motivation for evolution of aircraft maintenance and logistics, the conception and key technologies of prognostic and health management (PHM) are explained in detail. Key capabilities of future aircraft maintenance and logistics are proposed. Finally, the challenges to aircraft maintenance and autonomic logistics are illuminated.

73.1 Introduction

In recent years, with the rapid development of aeronautical science and technology, the modern aeronautics engineering systems become more and more complicated. Aircraft, helicopter, unmanned aerial vehicle, etc., are all expensive complex systems. Once this kind of system fails, the consequence is often catastrophic and will bring huge economic loss. Thus, it is very important to avoid failure of these systems while operating. The traditional method is to improve the reliability of the system through a large number of preplanned maintenance. However, on the one hand, the traditional maintenance method cannot avoid catastrophic failure, and on the other hand, it will lead to excessive repair, which will bring unbearable high life cycle support costs and may also introduce unanticipated failure by incorrect repair.

J. Dai (✉) · H. Wang
Chengdu Aircraft Design and Research Institute of AVIC, Chengdu 610091, China
e-mail: buaadaij@126.com

In order to solve the above problems, the concepts of condition-based maintenance and autonomic logistics (AL) were proposed. The main idea is to change the traditional passive reactive maintenance to active piloted maintenance and to realize the knowledge-oriented logistics system through comprehensive logistics demand, supply chain management, component reliability, safety, and a series of related information. As the supporting technology of AL, prognostic and health management (PHM) has gradually matured with the development of science and technology, which guarantees the realization of new maintenance and logistics methods, and is of great significance and influence on enhancing the combat effectiveness of weapon equipments.

73.2 Motivation for Evolution of Aircraft Maintenance and Logistics

For modern air combat, the importance of integrated logistics capability is the same as aircraft platform performance. The economic affordability and flexible capacity are all key factors for aircraft maintenance and logistics. Reducing aircraft maintenance and logistics links and enhancing line maintenance capability as well as convenient transportation maintenance equipment are urgent needs. Condition-based maintenance and two-level maintenance system extend the aircraft maintenance management from using stage to design and manufacture stage and bring a huge impact on the evolution of aircraft maintenance and logistics.

Under the traditional maintenance method, the depot maintainers are unsure what exact parts to order, and end up ordering more parts than they require, in the hope of receiving the few parts they actually need [1]. However, according to the actual health condition of equipments estimated by the PHM system, maintainers can timely understand when and which component will fail and then schedule a reasonable plan to purchase spare parts in advance to avoid purchasing unnecessary parts. It is very important that the right parts are present at the right workstation and at the right time for reducing spare parts storage costs and repair time.

The PHM is a new technology used by new planes, which can timely and accurately diagnose fault or predict the remaining useful life (RUL) of airborne equipments. Most of the failure of the airborne equipments can be isolated by the onboard self-test device, so that the original line maintenance does not have to rely on the ground device detection. And the PHM system can achieve integrated monitoring, information sharing and warning for the aircraft power system, fuel system, hydraulic system, environmental control system, etc., which extend the capability of line maintenance and promote the reform of the aircraft maintenance and logistics.

73.3 The Concept and Key Technologies of Prognostic and Health Management

73.3.1 Concept

The PHM concept is first introduced in the joint strike fighter (JSF). It is that the JSF AL system is a new supportability conception that can enable the airplane to be better utilized throughout the life of the platform and at a lower cost as compared with legacy aircraft. The basis of AL is the PHM system, which can realize the fault detection, isolation, diagnosis, and prognosis [2–4]. The concept of the PHM is shown in Fig. 73.1, in which the capabilities of the system to contain, prevent, detect, diagnose, respond to, and recover from conditions that may interfere with nominal system operations are all addressed [5].

In the PHM system, the system functions are defined and needed as follows:

1. Anomaly detection.
2. Failure detection.
3. Failure tolerance: an action to maintain intended function in the presence of failure.
4. Failure avoidance: an action to prevent a failure from occurring.
5. Failure prognosis: predicting the instant at which a component will fail or estimating the RUL.
6. Failure recovery: an action taken to recover the functions necessary to achieve existing or redefined system goals after a failure.
7. Failure response determination: selecting actions to mitigate a current or future failure.
8. Fault containment: preventing a fault from causing further faults.
9. Fault identification: determining the possible causes of off-nominal behavior.
10. Fault isolation: determining the possible locations of the cause of off-nominal behavior, to a defined level of maintenance.

73.3.2 PHM System Framework

The PHM system overall framework can be divided into two main parts: online part and off-line part, as shown in Fig. 73.2 [6]. For both the parts, the sensing, data collecting, state monitoring, diagnosis, prognosis, and decision making were all addressed and emphasized. At the same time, with the integration of the online PHM part and off-line PHM part, the advantages of both the online framework and off-line framework can be exerted, respectively. The PHM system output is the input of AL system, which ensures that the new type two-level maintenance and logistics system based on condition-based maintenance could be achieved.
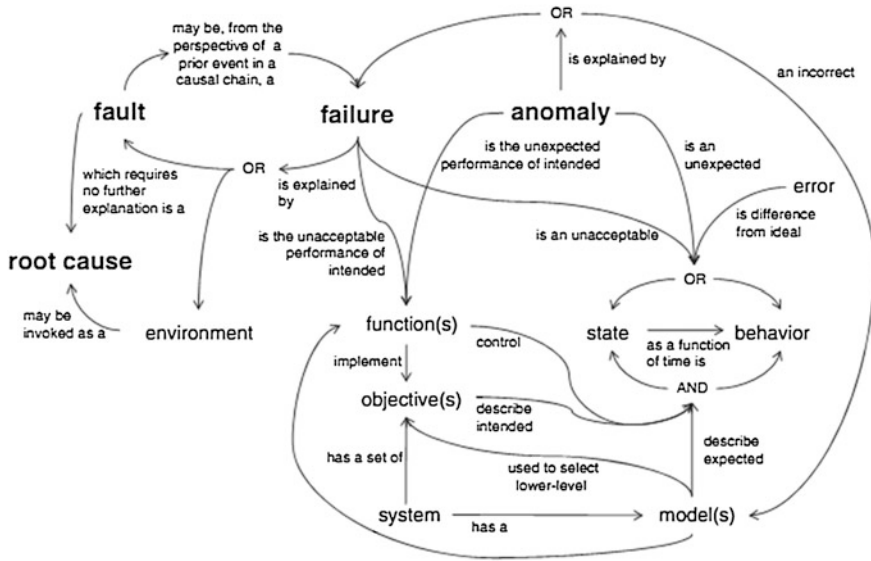
Fig. 73.1 Concept diagram of PHM [5]
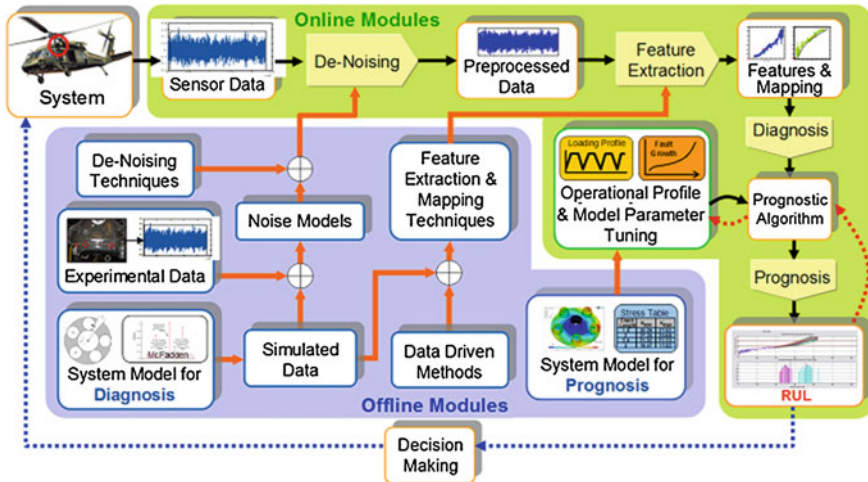
Fig. 73.2 PHM system framework (combined online and off-line architecture) [6]

73.3.3 PHM System Architecture

PHM system relies on the network platform, which consists of sensors, interface units, information processing units of airborne systems, and the software hosted in hardware to realize its function. The PHM system hardware architecture is
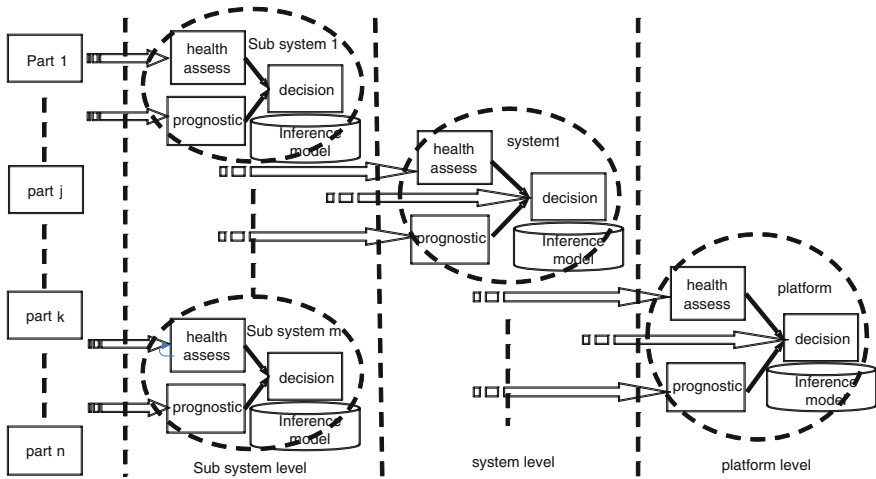
Fig. 73.3 PHM system software architecture

consistent with airborne system hardware architecture, and the software architecture is deployed according to the function requirement. As shown in Fig. 73.3, the scalable hierarchical software architecture of PHM system is suitable for airborne deployment. The system architecture consists of parts level, subsystem level, system level, and platform level, including health assessment, prognostic, and decision inference machine. The various components in the bottom of PHM function level could realize the data acquisition/processing, feature extraction, and state monitoring function, and the software modules are normally deployed in traditional equipment BIT parts. Subsystem-level, system-level, and platform-level inference machines are mainly to achieve health assessment, prediction, and decision function by receiving the output information from the lower-level reasoning machines. The inference machines could locate the fault, assess the health situation or the RUL of equipments, and generate the decision information, which is benefit for making equipment life more durable or equipment maintenance. According to function needs, the software modules could be deployed in the airborne equipments of subsystem level, system level, or platform level.

In the PHM system architecture, the key technologies are explained as follows:

1. Data Sensing and Acquisition. The first step in the PHM system is the data sensing and acquisition. The advanced sensor technology is applied to realize the data collection at all levels. Then, the monitoring data are transmitted through data bus to the data processing equipments, which implement the online data-driven processing late.
2. Data Preprocessing. In data acquisition and transmission, a lot of noise would be introduced, and the missing values existed in the data, which will bring a great challenge to data processing. Therefore, the preprocessing of monitoring data is necessary for PHM.

3. Feature Extraction and Selection. As a complex system, monitoring data of different subsystems are of multi-dimensions and are not suitable for directly analyzing online. And some of the data are useless for system health assessment and will bring extra computing burden for online processing. So feature extraction and selection are needed. By feature extraction, the representative features will be selected and enhanced for failure diagnosis and prognosis; especially for the failure prediction, the health index (HI) is usually extracted and fused to indicate the system degradation and health state.
4. State Monitoring. State monitoring is mainly used for judgment of the threshold of the key parameters to forecast the anomaly and underlying failure.
5. Health Assessment/Evaluation. Health assessment module receives the processed data from other units such as monitoring unit and other health assessment module. The main function of the health assessment unit is to evaluate the health state and estimate the probability of failure with the related data and information.
6. Fault Diagnostics. Based on a variety of health-state historical data, operating state, and maintenance recording data, the fault diagnosis realizes the fault location, isolation, and recovery when the state assessment alarms.
7. Fault Prognostics/Prediction. Fault prognosis is the outstanding capability for the PHM system. This unit integrates the information from the units above to evaluate and predict the health state of the targeting system. The prediction of parameters and RUL estimation are involved here. It could be achieved by high-performance and low-power embedded computing systems in real-time or off-line analysis systems according to system requirements.
8. Logistics Decision. Logistics decision is mainly based on the integration of the state monitoring, fault diagnosis, and prognosis, to release the reasonable and scientific maintenance strategies and guides. This decision should consider the available resources on ground and the aircraft mission requirement.

73.4 Key Capabilities of Future Aircraft Maintenance and Logistics

Due to the PHM system, future aircraft has a wide range of built-in-test (BIT) capability for airborne equipments, and the faults could be located to the line replaceable module (circuit board individual) level or the line replaceable component level. The PHM system could determine whether a fault is serious enough to warn the cockpit pilot by fault filtering, and the failure data of airborne equipments and the consumables state will be recorded. At the same time, the information will be transmitted to the ground station through the air-ground data link for maintainers to timely and accurately grasp the status of the aircraft. The maintainers could prepare well in advance and provide timely maintenance with knowing when and which parts failure and the consumables state accurately. The

diagnosis and prognostic capabilities of PHM system are very important for improving the repair efficiency, improving repair speed, and saving repair time.

The integrated maintenance information system is very important for future aircrafts, and the ground PHM capability is the core capability of the information system. When the aircraft returns to the station, the maintenance data card will be uploaded and sent to the maintenance department, and the data recorded in the maintenance data card will be downloaded to the integrated maintenance information system. If a failure occurs during the mission, the ground PHM system will find out the cause of the malfunction and propose the repair measure. It is very useful for battlefield repair. And through the integrated maintenance information system, remote repair support technology can be realized, which facilitates the sharing of maintenance technology resource. The expert could guide the battlefield repair and provide remote repair strategy and technical methods.

Providing an integrated scheduling capability would have the greatest impact on the daily operation of the maintenance facility. A master schedule incorporates requirements, parts, equipment, human resources, and program schedules. Without a schedule that integrates all major inputs, it is difficult, if not impossible, to manage facility capacity. Further, a comprehensive solution must have an integrated scheduling tool that will provide maintenance facilities with the process visibility to implement effective schedule performance monitoring [1].

Interactive Electronic Technical Manuals (IETMs) is a kind of important electronic technical data for aircraft maintenance, which is often displayed in portable maintenance aids (PMAs). PMA is the main interface between the maintenance with the aircraft, and it can upload or download data or software program, drive the aircraft system into test or maintenance model, and record maintenance work information. And the IETMs are a set of interactive repair procedure and can tell maintainers how to check and replace a component. Through the PMA and IETMs, the maintenance data, including the plane where a fault has occurred, how long repairs, parts usage, and so on, could be collected to plan, arrange inspection items, and arrange regular maintenance work. Also, within the life cycle management area is the requirement to provide tracking, management, and replacement of the limited life components in the asset. The historical maintenance data are used to project the effective life of those components that are limited by either time or exposure [1].

73.5 Challenges to Aircraft Maintenance and Autonomic Logistics

Lack of novel conception and technology is a challenge to China, and our technical storage in this respect is insufficient. Foreign countries have attached the great importance to new type maintenance conception and technology. By exploring the new conception PMA, IETMs, joint distributed information system (JDIS), professional knowledge on aircraft maintenance tools and means can be accumulated,

which could lay a foundation for the development of new aircraft maintenance and AL. In addition, the lack of design tools, approaches, software, and platforms decreases the development of science and technology for the modern aircraft maintenance and logistics.

The performance degradation of the PHM system and the integrated maintenance information system caused by the immature technology is another challenge. Nowadays, there is a big gap between the design of built-in-test technologies, real-time embedded computing for online processing, the integration of the data-driven and physics-based methods, and PHM system application. General interface, resource sharing, etc., are also problems, which should be solved in the development of the integrated maintenance information system.

73.6 Summary

Aviation maintenance is an important work to maintain and restore the combat capability of aircrafts, and the traditional maintenance and logistics method has been unable to meet the requirements of modern air combat. The new type maintenance and logistics method discussed in this study is a way to improve the mission reliability and maintenance of aircrafts. With the development of new type maintenance and logistics conception and technology, aeronautical equipments will be timely and appropriate and can be economically repaired.

References

1. A New Frontier in Military Maintenance and Repair. http://www.download.microsoft.com
2. Hess A, Fila L (2002) The Joint Strike Fighter (JSF) PHM concept: potential impact on aging aircraft problems. In: Proceedings of IEEE aerospace conference, vol 6. Big Sky, Montana, USA, pp 3021–3026
3. Zhang B (2008) Evolution and application of PHM technology. Meas Control Technol 23(2):5–7 (in Chinese)
4. Han G (2009) Prognostics and health management of avionics. Avionics Technol 40(1):30–38 (in Chinese)
5. Johnson Stephen B, Gormley Thomas J, Kessler Seth S, Mott Charles D, Ann Patterson-Hine, Reichard Karl M, Scandura Philip A (2011) System health management with aerospace applications. Wiley, The Atrium, Southern Gate, Chichester, West Sussex, United Kingdom
6. Vachtsevanos G, Lewis F, Roemer M, Hess A, Wu B (2006) Intelligent fault diagnosis and prognosis for engineering systems. Wiley, Hoboken, pp 284–354

Chapter 74
Honeycomb Structure Detection Using Pulsed Thermography

Zhi Zeng, Xiaoli Li, Chunguang Li, Zhigang Ye, Cunlin Zhang and Jingling Shen

Abstract Pulsed thermography is a nondestructive evaluation method, which has been qualitatively and quantitatively applied for different classes of materials to detect variety of defects. In this study, one-dimensional theoretical model of transient heat conduction under an instantaneous plane source is described for its application in the detection of honeycomb structures. Three kinds of honeycomb structures, including glass fiber-reinforced plastics (GFRP) honeycomb, carbon fiber-reinforced plastics (CFRP), and aluminum (Al) honeycombs, were used to demonstrate the detection ability, and the defects include most typical defects in honeycomb structures, such as disbonds, fluid ingress, and excessive adhesive. The image sequences were used for defect detection, and temperature decay analysis was helpful for the characterization of defect types.

Keywords Pulsed thermography · Honeycomb · GFRP · CFRP · Al

Z. Zeng (✉) · C. Zhang · J. Shen
Department of Physics, Capital Normal University, Beijing 100048, China
e-mail: zzh406@hotmail.com

Key Laboratory of Terahertz Optoelectronics, Ministry of Education, Beijing, China

X. Li
Beijing Waiteksin Advanced Technology Co. LTD, Beijing 100085, China

C. Li
China Academy of Civil Aviation Science and Technology, Beijing 100028, China

Z. Ye
Beijing Tianyihongyuan Science Technology Development Co. LTD,
Beijing 100142, China

74.1 Introduction

Honeycomb sandwich construction has been widely used for aircraft structures due to its lightweight, tailored stiffness and strength, superb fatigue resistance, and low manufacturing cost. Therefore, honeycomb sandwich structures have an increasing number of applications in aircraft manufacture, especially in some key parts such as trailing rudder and wing. Defects can inadvertently be produced in honeycomb structures either during the manufacturing process or in the course of the normal service life. The main defects include delamination within face sheet, core–face sheet disbond, and fluid ingress. Penetrated fluid in the honeycomb structures can cause problems, because moisture corrodes the honeycomb/skin bonding, causes delamination and weight increase, and further reduces the strength of the adhesive and affects structural integrity.

Due to the ever-increasing demands within the aerospace industry for cheaper, more efficient and cost-effective aircraft the industry is investing in the development of new testing and evaluation methods. Such methods are needed during the manufacture of the aircraft and during subsequent maintenance [1]. Pulsed thermography is a nondestructive evaluation method, which has been qualitatively and quantitatively applied for different classes of materials to detect variety of defects, such as corrosions and delamination in composite, metal [2]. Quantitative characterization in order to extract defect depth, size, and thermal properties has been proven effective in pulsed thermography [3–8]. In 1990s, Wayne State University used pulsed thermography to detect disbond and delamination in composite sample, and water ingress in honeycomb panel from three sides of the sample (front, back, and vertical) [9]. Laval University applied PPT method to detect honeycomb sandwich structure and show the water ingress in phase images [10]. In Russia, water ingress in aluminum, glass fiber, and carbon fiber honeycomb structures was experimentally studied using thermography with several kinds of lights source [11].

In this study, pulsed thermography was adopted, and three different honeycomb structures were used for a demonstration of detectability, and the defects include disbond, fluid ingress, and excessive adhesion.

74.2 Method

The principle and experimental setup of adopted pulsed thermography are shown in Fig. 74.1, the bottom surface of the detected sample is heated with a short pulse of light, and the sample surface is instantaneously heated to a high temperature. The generated heat at front surface propagates to the interior of the sample and leads to a continuous decrease in the surface temperature [2].

The general thermal diffusion equation is written as

Fig. 74.1 Sketch map of the transient heat conduction in a composite region
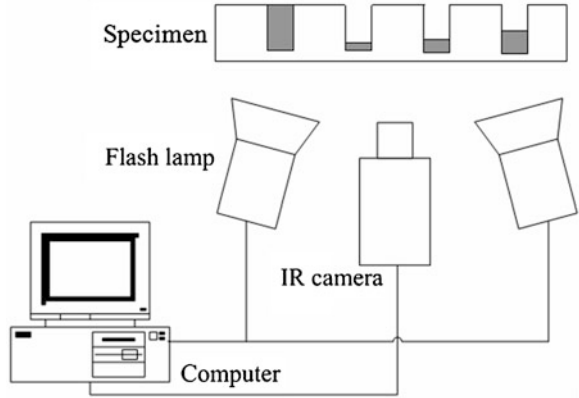
$$\nabla \cdot [\kappa \nabla T(r,t)] - \rho c_V \frac{\partial T(r,t)}{\partial t} = -f(r,t). \tag{74.1}$$

The one-dimensional solution of the Fourier equation for a Dirac delta function in a semi-infinite isotropic solid is given by [2]

$$\Delta T(t) = \frac{Q}{e\sqrt{\pi t}} \tag{74.2}$$

where Q is the input energy per unit area, and e is the thermal effusivity. An IR camera controlled by a PC monitors the time-dependent response of the sample surface temperature to the thermal impulse. When there is any subsurface defect or structure difference, the one-dimensional solution is given by [2]

$$\Delta T(t) = \frac{Q}{e\sqrt{\pi t}} \left[1 + 2 \sum_{n=1}^{\infty} R^n \exp\left(\frac{-n^2 L^2}{\alpha t}\right) \right] \tag{74.3}$$

where L is the defect depth, α is the thermal diffusivity, and R is expressed as [2]

$$R = \frac{e_1 - e_2}{e_1 + e_2} \tag{74.4}$$

where e_1 is the thermal effusivity of steel sample, which is a known value, and e_2 is the thermal effusivity of the filled fluids. The R coefficients of different filled fluids are different, which reflects in logarithmic temperature versus logarithmic time curves that the curves with bigger R have bigger deviation from sound area. Thus, different materials show different thermal diffusive properties in temporal domain, which could be used in material recognition.

74.3 Experimental Results

In this study, three honeycomb structures including GFRP, CFRP, and Al face sheets were used, and each of them have artificial defects. For GFRP sample, it exists several disbond defects between face sheet and core and excessive adhesion. For CFRP sample, only disbond defects exist. For Al sample, water ingress will be detected. In order to detect fluid ingress, those samples are injected with water or oil at certain locations.

The experimental temperature data were obtained by using EchoTherm flash pulsed thermographic system manufactured by TWI Inc (USA), and the schematic diagram is shown in Fig. 74.1. During the test, two 4.8 kJ flash lamps were triggered at $t = 0$ to deposit a thermal impulse on the sample's surface, the flash pulse duration is several milliseconds. The infrared camera, whose spectral range is from 7 to 8 μm with 20 mk thermal sensitivity and full frame size 320×240 pixels, was mounted on an hood, which allows about 350×250 mm area per capturing, and set at a 60-Hz sampling frequency to capture the temperature evolution of the detected surface.

74.3.1 GFRP Honeycomb Sample

One 280×210 mm GFRP sample, which is designed to have only one face sheet with 0.6 mm thickness, is manufactured with eight artificial defects including four delamination defects and four excess adhesive defects. For each type of defects, it has two different sizes. Before the experiment, the sample surface is painted with soluble black paint to increase the thermal emissivity, and different quantity and areas of oil and water are injected into four different locations.

The thermographic image at 4.5s is shown in Fig. 74.2, and all artificial defects are successfully detected. For those defects, only delamination defect is shown as bright area compared with sound area, and other defects including excess adhesive, oil and water ingress, appear darker than sound area. Excessive adhesive defect appears a little bit darker than sound area, and oil ingress at left dark column and water ingress at right dark column appear much darker. Though all defects are detected, it is necessary to judge what kind of defects it is in some situations. Temperature time plot is helpful to analysis the difference among different defects, and Fig. 74.3 compares the logarithmic curves corresponding to different defects. At defect interface, different defects have different heat reflective coefficients R; therefore, it causes different temperature drop rate as shown in Fig. 74.3. Qualitative recognition and quantitative characterization of defect type could be implemented [12, 13].

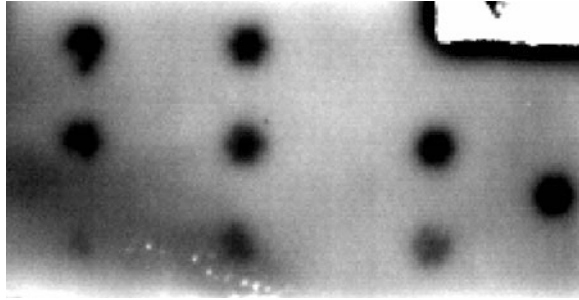**Fig. 74.2** Original image of GFRP honeycomb sample at 4.5s
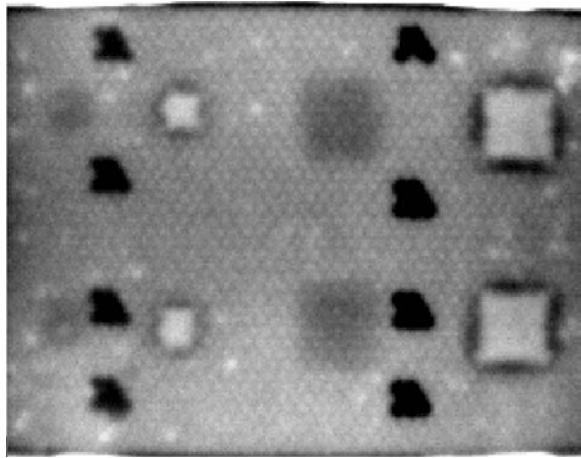
**Fig. 74.3** Logarithmic curves of GFRP honeycomb sample
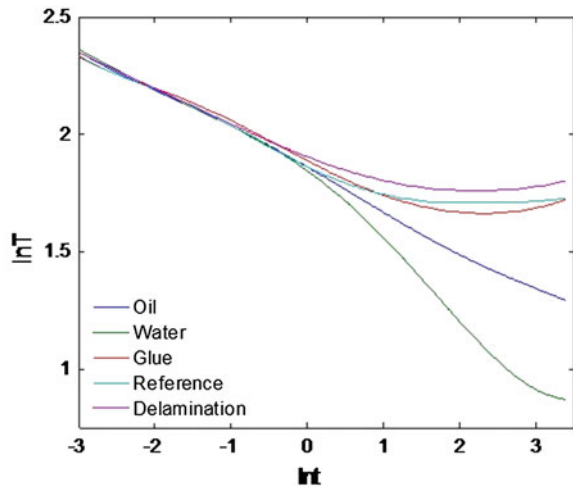
74.3.2 Al Honeycomb Sample

One Al honeycomb sample, which is also with only face sheet, is injected with different amount of water at nine different locations. At different locations, water ingress area is the same. The corresponding thermographic image at 0.2s is shown in Fig. 74.4, and all nine water ingress areas are detected. However, those areas show different gray levels, and water ingress areas with smaller quantities appear brighter than areas with bigger quantities because more heat is reflected from the interface between water and air.

Fig. 74.4 Original image of
Al honeycomb sample at 0.2s

Fig. 74.5 Original image of
CFP sample at 2.5s
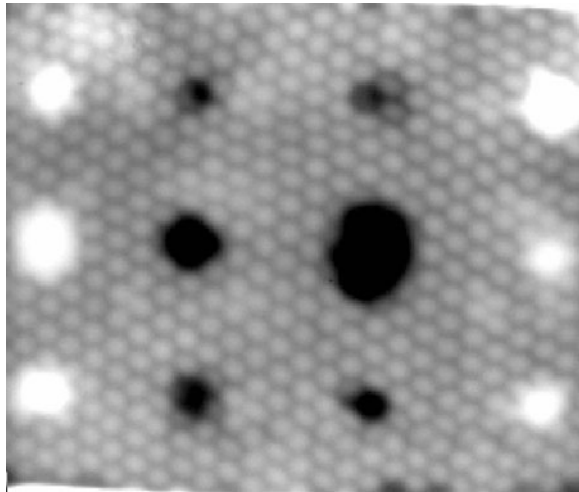
74.3.3 CFRP Sample

The CFRP honeycomb sample has several disbond areas, and it is injected with
different quantities of water at different locations. The thermographic result at 2.5s
is shown in Fig. 74.5, in which water ingress area appears as dark area, and
disbond areas are shown in as bright area. For water ingress areas, the area with
smaller water quantity shows bigger gray level than the area with bigger water
quantity.

74.3.4 Discussions

The above samples show that pulsed thermography could be used to detect typical
defects in honeycomb structures. It is harder to detect defects in honeycomb
structure with Al face sheet because Al material has very big thermal diffusivity, in

such a situation, the sampling rate of infrared camera should be set to a big value, and the early time thermographic images should be analysis for the detection of defects.

74.4 Conclusions

The main objective of this study was to examine the effectiveness of pulsed thermography to detect typical defects in honeycomb structures, such as disbond and fluid ingress, and it provided excellent results on all investigated samples. Through the analysis of thermographic images and temperature time curves, it is possible to recognize or characterize the defect type or property.

References

1. Avdelidis NP, Hawtin BC, Almond DP (2003) Transient thermography in the assessment of defects of aircraft composites. NDT&E Int 36:433–439
2. Maldague X (1993) Nondestructive evaluation of materials by infrared thermography. Springer, New York
3. Zeng Z, Li C, Tao N, Feng L, Zhang C (2012) Depth prediction of non-air interface defects in pulsed thermography. NDT&E Int 48:39–45
4. Zeng Z, Zhou J, Tao N, Feng L, Zhang C (2012) Absolute peak slope time based thickness measurement using pulsed thermography. Infrared Phys Technol 55(2–3):200–204
5. Zeng Z, Tao N, Feng L, Zhang C (2012) Specific value based depth prediction in pulsed thermography. J Appl Phys 112:023112
6. Sun JG (2006) Analysis of pulsed thermography methods for defect depth prediction. J Heat Transfer 128(4):329
7. Almond DP, Peng W (2001) Thermal imaging of composites. J Microsc 201:163–170
8. Shepard SM (2007) Thermography of composites, Material evaluation. July, 690–696
9. Han X, Favro LD, Thomas RL (1998) Thermal wave NDI of disbonds and corrosion in aircraft. In: The second joint NASA/FAA/DOD Conference on Aging Aircraft, NASA/CP-1999-208982, Part 1, pp 265–274
10. Maldague X, Marinetti S (1996) Pulse phase infrared thermography. J Appl Phys 79:2694–2698
11. Vavilov VP, Klimov AG, Shiryaev VV (2002) Active thermal detection of water in cellular aircraft structures. Russ J Nondestr Test 38:927–936
12. Chen D, Zeng Z, Tao N, Zhang C, Zhang Z Quantitative study of water ingress in pulsed thermography
13. Zhi Z, Ning T, Lichun F, Cunlin Z Hidden heterogeneous materials recognition in pulsed thermography. Review of Progress in Quantitative Nondestructive Evaluation 31:705–712

Chapter 75
Impact Damage Detection
on the Laminated Composite

Ming Li, Yingchun Xiao and Guoqiang Liu

Abstract Impact damage detection is critical for the utilization of composite materials. This paper investigates the applicability of active Lamb wave to composite damage monitoring. First, a time-reversal method has been adapted to guided-wave propagation to improve the detectability of local defects in composite plate structures. Second, a damage index (DI) method using a pair of sensors is introduced to generate index, which can be used to characterize the damage extent around the diagnostic path. Both of the methods proposed are validated through experimental studies in which different impact damages are generated by the falling a steel projectile on a laminated composite plate. The result showed that the methods may provide good correlation with the impact damage in the laminated composite plate.

75.1 Introduction

Compared to traditional metal material, the composite structure has been applied to many important engineering structure because of its high strength/stiffness-to-density ratio, easy to design, good fatigue performance, and corrosion resistance. Laminated structure is one of familiar composite and is always used to typical fuselage structure, by this way, the weight can be decreased 20–30 % [1]. Some research shows that the main threaten to composite is impact damage, which mainly comes from

M. Li (✉) · Y. Xiao · G. Liu
Aeronautics Science and Technology Key Laboratory of Full Scale Aircraft Structure
and Fatigue, China Aircraft Strength Research Institute, No. 86 of Dianzi 2nd Road,
Xi'an 710065 Shaanxi, China
e-mail: liakali@163.com

the process of manufacture and utility such as bird strike and tools dropping. Impact damage to the composite is beyond retrieve and will decrease the laminated composite strength [2].

Usually, in the practice, impact damage in the composite is always difficult to detect due to the anisotropy of the material, the conductivity of the fibers, the insulative properties of the matrix, and the fact that much of the damage often occurs beneath the top surface of the laminate, so it is important to ensure the aircraft structure safety by correct detection and estimation to the damage. Traditional nondestructive testing (NDT), such as x-radiographic detection and C-scan, tends to limited during the execution by the damage part, damage type, and personnel factor.

In the composite structural health monitoring (SHM) field, the SHM based on Lamb wave is regarded as the one of the most effective ways to the plate-like structure [3–6] and is becoming a hopefully tool to the local damage detection [7–9]. Lamb wave is a kind of mechanical waves, and its wavelength is in the same order of magnitude as the thickness of the plate. The various frequency components of Lamb wave travel at different speeds, and the shapes of wave packets change as they propagate through a solid medium due to its dispersive and multimodal natures. Therefore, such character is very suitable for damage detection. In Stanford University America, Professor Chang F K has made a good deal of research on it. In China, Yuan S F group has applied the time-reversal imaging method successfully on damage monitoring of composite structure [10–12]. Domestic and overseas academician even introduced some novel theory and means to improve the quality of Lamb wave, such as time reversal and phase array theory [13, 14].

This paper first introduces the Lamb wave transmission theory, then two means of damage detection on laminated composite are presented and researched. Experiment shows that different impact damage size on laminated composite plate can be detected and quantified by active Lamb wave and it will be a promising ways to monitor impact damage in composite.

75.2 Theory of Lamb Wave Propagation

Lamb wave is a type of guided-ultrasonic wave propagation between two parallel surfaces of a plate-like structure. It can be excited by surface mounted or imbedded piezoelectric actuators. From the wave theory, we know that there are two basic vibration modes of motion with respect to the wave type generated in the material, longitudinal waves and shear waves. Thus, Lamb wave arise from a coupling between shear and longitudinal waves reflected at the top and bottom of a plate. Lamb wave is a type of stress wave that arises from a coupling between shear and longitudinal waves reflected at the top and bottom of a plate.

There are two groups of waves, the symmetric waves (S) and the anti-symmetric waves (A), which satisfy the wave equation and the boundary conditions. The velocities of these waves depend on the frequency and the thickness of the plate

Fig. 75.1 The velocities of lamb waves depend on the frequency and the thickness of the plate (the dispersion relation), and there exist a finite number of symmetric modes (S_0, S_1, S_2,...) and anti-symmetric modes (A_0, A_1, A_2,...) that travel independently
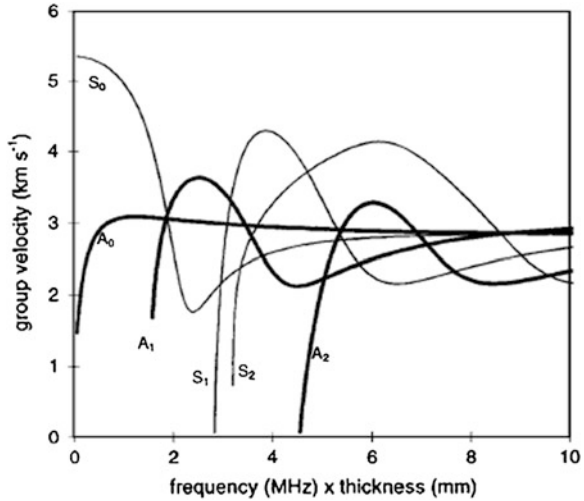
(the dispersion relation), and there exist a finite number of symmetric modes (S_0, S_1, S_2,...) and anti-symmetric modes (A_0, A_1, A_2,...) that travel independently. This phenomenon is so-called "dispersion effect" (Fig. 75.1). This effect shows that the phase velocity c_p and the group velocity c_g change with the frequency–thickness values.

The dispersion equation of Lamb wave is [15]

$$\frac{\tan(qh)}{\tan(ph)} = -\frac{4k^2 pq}{(q^2 - k^2)^2} \tag{75.1a}$$

$$\frac{\tan(qh)}{\tan(ph)} = -\frac{(q^2 - k^2)^2}{4k^2 pq} \tag{75.1b}$$

where $p^2 = (\omega^2/c_L^2) - k^2$, $q^2 = (\omega^2/c_s^2) - k^2$, c_L, and c_S denoting the velocity of longitudinal waves and shear waves, h denotes thickness of plate, $k = \omega/c_p$ denotes the wavelength, ω denotes the circular frequency, and c_p denotes the phase velocity. Equation (75.1a) denotes symmetric modes dispersion equation, and (75.1b) denotes anti-symmetric modes dispersion equation.

75.3 Lamb Wave for Damage Detection

When Lamb wave is generated from a transmitter and travels through a region where there is a change in material properties due to damage, wave scattering occurs in all directions. The damage can be considered as a wave-scattering source and measured generating dispersion curves—user's manualscattered wave at sensors will be utilized to investigate the damage. For a given set of N distributed

Fig. 75.2 Every *imaging point* can be calculated by a particular pixel (or focal point) to the amplitude of the scattered signal received by the pair of sensors in the network
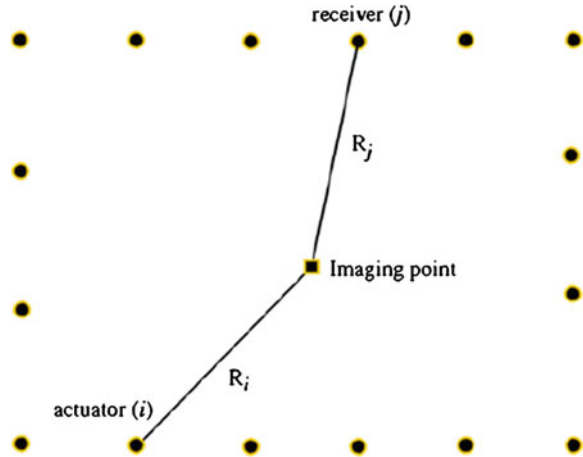
sensors, the response of the healthy structure is collected. Assuming damage has occurred in the structure, the response of the damage structure is collected for the same set of N distributed sensors. The scattered or difference response is assumed to contain the scattered waves only coming from the damage-no reflected waves from structural boundaries.

75.3.1 Time-Reversal Imaging

In time-reversal acoustics, every burst of sound diverging from a source and possibly reflected, refracted, or scattered by any propagation media—there exists in theory a set of waves that can be exactly reconstructed at the source location if a response signal measured at a distinct location is time reversed (literally the time point at the end of the response signal becomes the starting time point) and reemitted to the original excitation location, as if time were going backward. Regard the wave packet as the study object, all of them traveling at different speeds concurrently converge at the source point during the time-reversal process, compensating the dispersion.

Based on the principle of the time-reversal method that yields a stronger signal, an imaging method can be developed. A coarse image can be first constructed by relating the contrast at a particular pixel (or focal point) to the amplitude of the scattered signal received by all the sensors in the network. From this coarse image, approximate locations of structural damages or scatters can be determined. Then, a refined image can be generated by reconstructing, from the same set of measured responses, an image by modifying the aperture values according to the ratio of the scattered amplitude to the on-target incident amplitude.
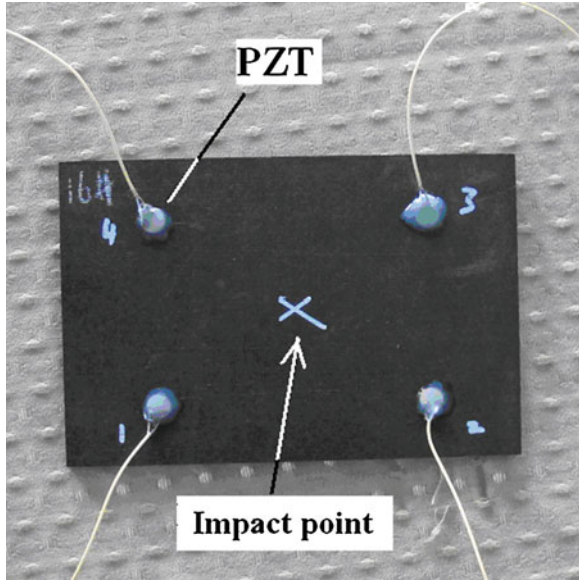
Consider a distributed network consisting of N active sensors, their positions
being denoted as (x_i, y_i), $i = 1, 2,..., N$. The contrast S at a particular location or
imaging pixel (x, y) can be expressed as, referring to Fig. 75.2 for notations

Table 75.1 Impact energy and damage area for specimens

Specimen no.	Impact energy (J)	Damage area (mm^2)
1	19.0	569
2	19.0	512
3	18.7	428
4	16.6	422
5	18.0	393
6	17.0	381
7	16.5	340
8	17.1	315
9	10.3	162
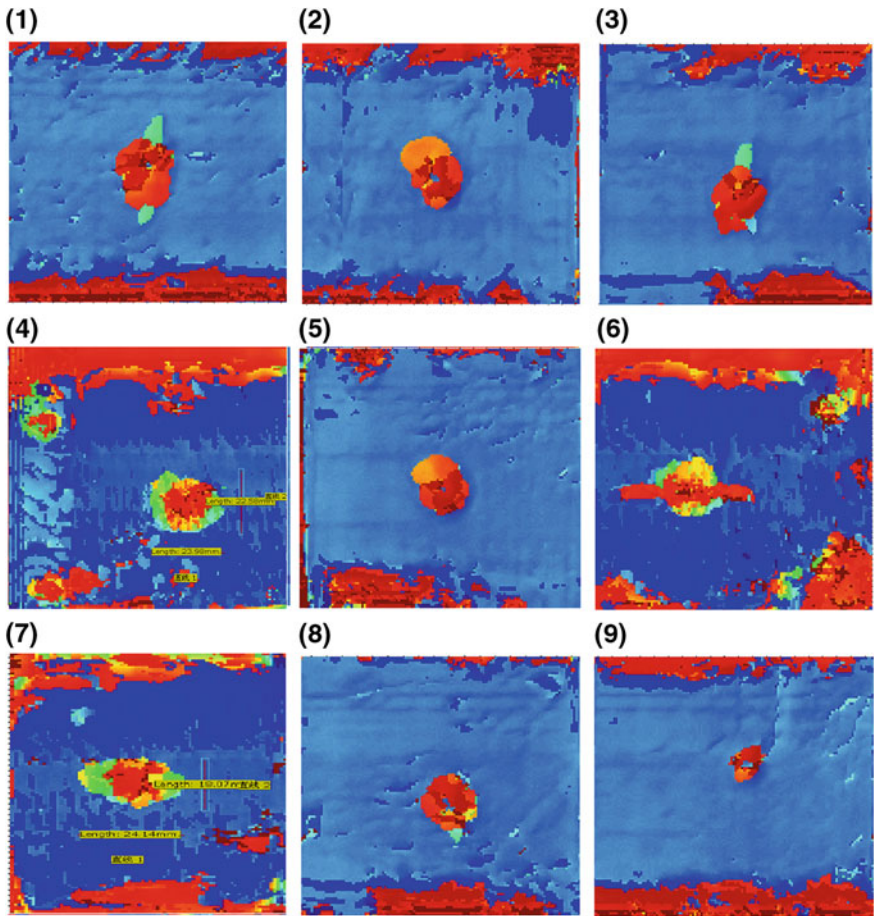
Fig. 75.5 The C-scan result of impact damage
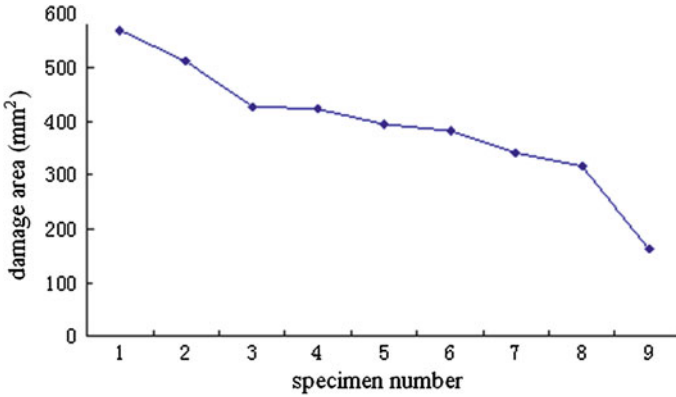
Fig. 75.6 Damage area trend of the specimens

$$S(x, y) = \sum_{i=1}^{N} \sum_{j=1}^{N} A_{ij} f_{ij}^{(s)} \left(\frac{R_r + R_t}{c_g} \right) \tag{75.2}$$

where $f_{ij}^{(s)}$ denotes the received scattered signal by sensor j due to the excitation of sensor i. Parameters R_r and R_t denote, respectively, the distances between sensors i and j and the imaging pixel (x, y). The parameter c_g denotes the group velocity of the controlled signal in the structure, which may vary significantly with the center frequency. Parameters A_{ij} refer to the appropriate aperture weighting to each sensor pair, which in the simplest case would be equal to unity for uniform aperture weighting.

75.3.2 Damage Index

Ihn and Chang find that the S_0 mode is sensitive to cracks in metal structure, while the A_0 mode is sensitive to disbond in composite structure [16]. Mode extraction can be achieved via disperse curve and time-of-flight [17, 18].

The damage index (DI) is defined as the ratio of the scatter energy contained in the S_0 mode wave packet to the baseline energy contained in the S_0 mode wave packet. This ratio can be obtained by the time integration of the power scatter spectral density within the S_0 time window at a specified frequency, which then can be non-dimensionalized by baseline information such that

$$DI = \left(\frac{\int_{t_0}^{t_i} |S(\omega_0, t)|^2 dt}{\int_{t_0}^{t_i} |B(\omega_0, t)|^2 dt} \right)^{\alpha} \tag{75.3}$$
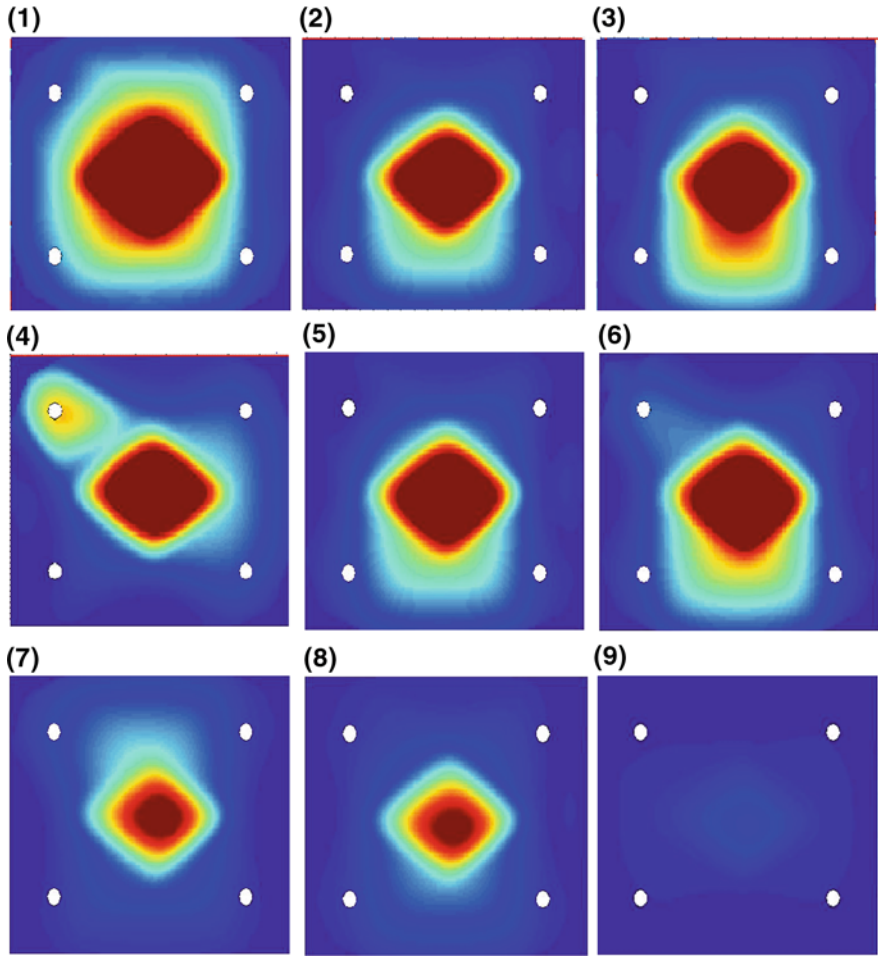
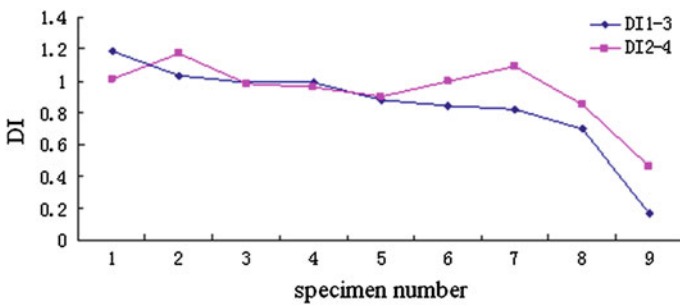**Fig. 75.7** Imaging result of impact damage based on time reversal

Fig. 75.8 DI trends of the specimens

where S denotes the time-varying spectral amplitude of the scatter signal, B denotes the time-varying spectral amplitude of the baseline signal, ω_0 denotes the actuation frequency of Lamb wave, t_i and t_0 denote the upper bound and lower bound of the fundamental mode in the time domain, respectively. α is the gain factor, $0 < \alpha \leq 1$. $\alpha = 0.5$ was taken for this study.

75.4 Experiment and Analysis

A composite plate with dimension of $200 \times 200 \times 2.3$ mm is selected as the test specimen. The layup of this composite laminate contains 24 plies stacked according to the sequence [45/0/-45/90/0/45/0/-45/0/45/90/-45]s. As Fig. 75.3 shows four piezoelectric sensors and actuators were surface mounted on the plate and a square monitor network with side length of 120 mm is formed.

The impact damage is generated on the composite plate by falling down a steel projectile from the impact shooter as shown in Fig. 75.4. Several impact tests were repeated varying the impact energy from 10.3 to 19 J. The data collection using the active-sensing system was performed before and after the impact test.

The damage image of every plate by time reversal was made and compared with C-scan, at the same time, the DI of diagnostic paths 1–3, 2–4, was used for detection of the impact damage too.

The impact energy and damage area of the test specimens are showed in Table 75.1.

The C-scan result of impact damage is showed in Fig. 75.5, the trend of damage area is showed in Fig. 75.6. Figure 75.7 shows the imaging by time reversal, and Fig. 75.8 shows the DI of diagnostic paths.

From the Fig. 75.5, we can find that the damage is minified with the decrease in the impact damage and the result of imaging by time reversal reflects the change of damage correctly; while in Fig. 75.8, two DIs of diagnostic path accord with the trend of damage area closely.

75.5 Conclusions

Two active Lamb wave methods were presented for monitoring impact damage in the laminated composite plate: imaging method using multiple actuator–sensor paths and the DI method using a single actuator–sensor path. The imaging method can visualize scattering locations and estimate size/location of various areas impact damage; the DI approach can achieve a damage expansion trend curve by appropriate mode selection. The result showed that imaging by time reversal is more effective in quantifying localize impact damage, while the DI is more suitable for reflecting the damage expansion trend.

References

1. Du SY, Guan ZD (2008) Strategic considerations for development of advanced composite technology for large commercial aircraft in China (in Chinese). J Acta Materiae Compositae Sin 25(1):1–10
2. Zhang XJ, Zhang BP (2010) Damage analysis of composite laminate under low- velocity. J Aeronaut Comput Tech 40(3):68–70 (in Chinese)
3. Michaels JE (2008) Detection, localization and characterization of damage in plates with an in situ array of spatially distributed ultrasonic sensors. J Smart Mater Struct 17:1–15
4. Xu BL, Giurgiutiu V (2007) Single mode tuning effects on lamb wave time reversal with piezoelectric wafer active sensors for structural health monitoring. J Non-destr Eval 26:123–134
5. Holmes C, Drinkwater BW, Wilcox PD (2008) Advanced post-processing for scanned ultrasonic arrays: application to defect detection and classification in non-destructive evaluation. J Ultrason 48:636–642
6. Purekar A, Pines DJ (2002) A phased array sensor actuator array for detecting damage in 22D structures. In: Denver 43rd AIAA/ASME/ASCE/AHS/ASC structures, structural dynamics and materials conference, AIAA, Denver
7. Giurgiutiu V, Cuc A (2005) Embedded NDE for structural health monitoring, damage detection, and failure prevention. J Shock Vib Dig 37(2):83–105
8. Su Z, Ye L, Lu Y (2006) Guided lamb wave for identification of damage in composite structures: a review. J Sound Vib 298(4):753–780
9. Wang CH, Rose JT, Chang FK (2004) A synthetic time-reversal imaging method for structural health monitoring. J Smart Mater Struct 13(2):415–423
10. Wang Q, Yuan SF (2009) Time reversal imaging method for composite delamination monitoring. J Acta Materiae Compositae Sin 26(3):99–104 (in Chinese)
11. Qiu L, Yuan SF, Zhang XY (2010) Shannon complex wavelet and time reversal focusing based multi-damage imaging method on composite structures. J Acta Materiae Compositae Sin 27(2):101–107 (in Chinese)
12. Wang Q, Yuan SF (2009) Baseline-free imaging method based on new PZT sensor arrangements. J Intell Mater Syst Struct 20(14):1663–1673
13. Wang CH, Rose JT, Chang FK (2004) A synthetic time-reversal imaging method for structural health monitoring. J Smart Mater Struct 13(2):415–423
14. Giurgiutiu V (2005) Tuned Lamb wave excitation and detection with piezoelectric wafer active sensors for structural health monitoring. J Intell Mater Syst Struct 16:291–305
15. Viktorov IA (1967) Rayleigh and lamb waves. Plenum Press, New York
16. Ihn JB, Chang FK (2004) Detection and monitoring of hidden fatigue crack growth using a built-in piezoelectric sensor/actuator network: I. Diagnostics. J Smart Mater Struct 13:609–620
17. Pavlakovic BN, Lowe MJS (2001) A system for generating dispersion curves—user's manual for disperse v.2.0
18. Lowe MJS, Pavlakovic BN, Cawley P (2001) Guided wave NDT of structures: a general purpose computer model for calculating waveguide properties. In: Proceedings of the 3rd international workshop on structural health monitoring, Stanford, pp 880–888

Chapter 76
Study of the Application
of Super-Capacitors in Diesel Cold Start

Jianfei Liu, Tao Ning, Shihong Cao and Fucai Zhang

Abstract This paper introduces a diesel cold system composed of super-capacitors in parallel with lead-acid batteries. When used to start the diesel engine, the system can effectively improve the cold start performance of diesel engines, reduce the impact on lead-acid batteries during the start-up process, and extend the working life of lead-acid batteries.

Keywords Super-capacitor · Lead-acid battery · Diesel engine · Cold start

76.1 Introduction

At present, the diesel engine mainly uses lead-acid batteries as the start-up power. However, due to the poor performance of lead-acid batteries under low-temperature conditions, it is very difficult to start diesel engines at low temperatures. Due to its own limitations, lead-acid battery has a number of unsolvable inherent defects, such as large size, short working life, and poor performance under low-temperature conditions, thereby making diesel engines often unable to be started at low temperatures. This paper proposes the use of super-capacitors in parallel with lead-acid batteries to start the diesel engine. Before start, the super-capacitors are charged by the lead-acid batteries first, and then together, they both serve as the power supply to start the diesel engine. At the moment of start-up, instantaneous high current provided by the super-capacitors can assist lead-acid batteries to easily start the diesel engine, which solves the difficulty in diesel cold start and effectively improves the electric start-up performance of the diesel engine and the application state of lead-acid batteries.

J. Liu · T. Ning (✉) · S. Cao · F. Zhang
General Logistics Department of PLA, Construction Engineering Research Institute,
Xi'an 710032 Shaanxi, China
e-mail: 105294054@qq.com

76.2 Comparison of Features of Super-Capacitor and Lead-Acid Battery

Super-capacitor is an electrochemical device depending on electrolyte polarization for energy storage, and a transition between batteries and normal capacitors. It is highly reversible in terms of storage mechanism, allows rapid charging and discharging of high current, and features long life and average number of charge and discharge exceeding 400,000 times. In addition, it also boasts a wide range of operating voltage and temperature (-41–65 °C) [1]. Using super-capacitors to provide the instantaneous high current required for diesel start can avoid frequent high-current discharge of lead-acid batteries and thus extend battery life. Moreover, in the event of insufficient performance of lead-acid batteries under low-temperature conditions, the diesel engine can also be easily started.

Since the conditions of use of diesel engines vary significantly in China, GJB-235A requires that diesel power plants with power not greater than 250 kW should be successfully started within 30 min at the ambient temperature of -40 °C [2]. Lead-acid battery voltage has a negative temperature coefficient, and its optimum operating temperature is 25 °C. At -40 °C, the electricity of lead-acid batteries drops by about 50 %. Therefore, diesel engines started by lead-acid batteries often encounter start-up difficulties under low-temperature conditions. Continuous start-up (lead-acid batteries have to frequently discharge high current) of the engine for a long time at low temperatures is bound to affect the working life of batteries.

Compared with lead-acid batteries, super-capacitors can be charged to any voltage value within the range of their rated voltage and release almost all of the energy stored when discharging. In contrast, lead-acid batteries can only work in a narrow voltage range, and its electric power cannot be over-charged or fully discharged. Super-capacitors can frequently release energy pulses and be charged, while frequent charging and discharging will reduce the life of or even damage lead-acid batteries. Super-capacitors allow thousands of charge and discharge cycles, while lead-acid batteries can tolerate only hundreds of cycles. In addition, super-capacitors are barely affected by temperature, while lead-acid batteries change significantly with temperature. Due to their large capacitance and small resistance, super-capacitors can provide great instantaneous starting power and starting torque. Therefore, using super-capacitors to meet the peak power demand of diesel engines is a better choice.

Figure 76.1 shows the voltage change curve of super-capacitors in natural discharging. After super-capacitors are charged to 28 V and placed for 600 h, the voltage drops to 14 V, suggesting that the super-capacitor has better performance in energy storage, but cannot store electric power for a long time. As shown in Fig. 76.2, after placed for 2,000 h, 24-V lead-acid battery only drops to 21.5 V. It thus can be shown that lead-acid battery has longer electric power storage and can store energy ten times more than super-capacitors. Therefore, this paper proposes to start diesel engines with lead-acid battery in parallel with super-capacitors.

Fig. 76.1 Voltage change *curve* of super-capacitors in natural discharging
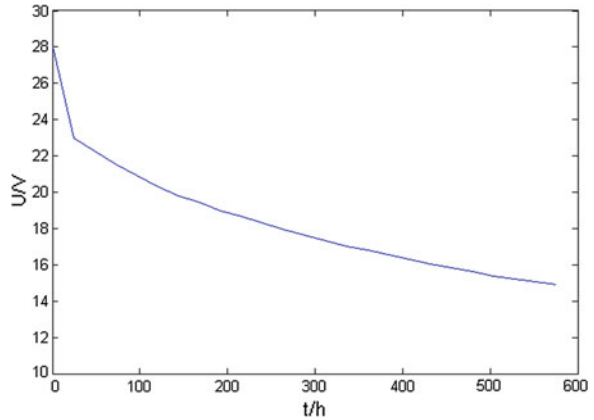
Fig. 76.2 Voltage change *curve* of lead-acid batteries in natural discharging
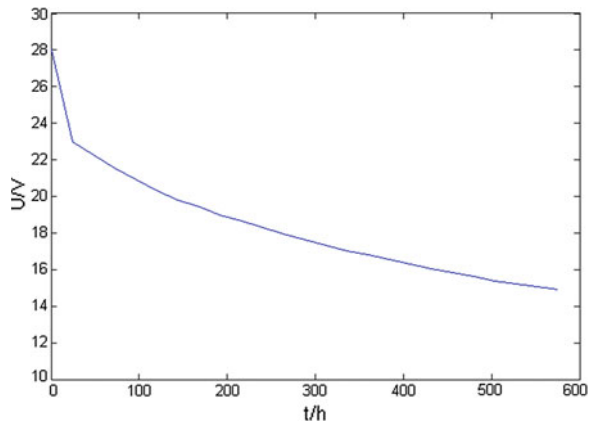
On the one hand, lead-acid battery can store electric power for a long time; on the other hand, at low temperatures or when lead-acid battery has only a little electric power, super-capacitors can ensure the smooth diesel start.

76.3 Application Test of Super-Capacitors in Diesel Cold Start

At the moment when the diesel engine is started, the motor's speed is zero and no electric potential is induced, so the starting current is calculated as: $I = E/(RM + RS + RL)$, where E is the non-load terminal voltage of lead-acid batteries, RM is the armature resistance when the motor is started, RS is the internal resistance of lead-acid batteries, and RL is line resistance. Since RM, RS, and RL are close to zero [3], the starting current at this time is very high.

Fig. 76.3 Instantaneous
voltage waveform at the
moment of diesel engine
start-up by lead-acid batteries
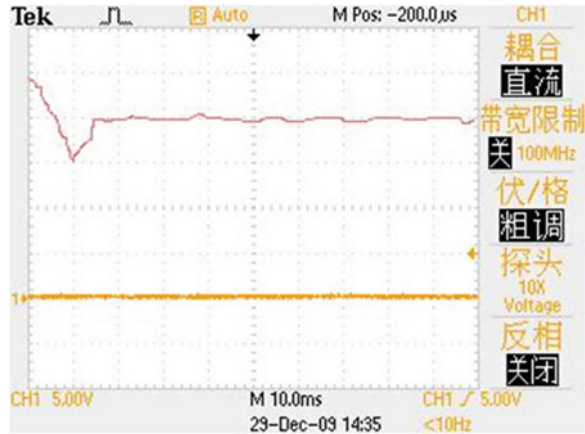
76.3.1 Test Results at Normal Temperature and Analysis

Figure 76.3 shows the lead-acid battery voltage waveform during start-up. 24-V, 60-Ah lead-acid batteries were used to start a diesel power plant, and the voltage of lead-acid batteries dropped from 23.6 V to about 10.2 V at the moment of start-up. Figure 76.5 shows the corresponding current waveform during start-up. It can be shown that instantaneous starting current was up to 260 A. The damage of such a high discharge rate to the lead-acid battery is very serious, thereby affecting its life.

When super-capacitors were used in parallel with lead-acid batteries to start the engine, the voltage waveform of the engine's start-up process is shown in Fig. 76.4, while the current waveform is shown in Fig. 76.6. Compared with Figs. 76.3 and 76.5, the starting instantaneous voltage dropped to 15.4 V, much higher than 10.2 V when only lead-acid batteries were used; starting current was increased from 260 to 490 A. It can be shown that the minimum voltage and the maximum current appear at the same time. Calculation shows that the starting instantaneous power output was increased from 2.6 to 7.5 kW, while the steady voltage during start-up was increased from 14.7 to 19.4 V.

When super-capacitors were used in parallel with lead-acid batteries to start the diesel engine, the super-capacitor's equivalent series resistance was much smaller than the internal resistance of lead-acid batteries. Thus, at the moment of starting, about 80 % of the starting current was provided by the super-capacitor, while batteries only provided 20 % of the current, thereby effectively reducing the polarization of the plate for lead-acid batteries, preventing the internal resistance of lead-acid batteries from rising and improving the steady voltage during start-up. Most importantly, the decrease in the polarization of the plate for lead-acid batteries could not only prolong the working life of lead-acid batteries, but also eliminate the impact of frequent start-up on the battery life, which could greatly reduce diesel engine maintenance. Therefore, the starting system composed of

Fig. 76.4 Instantaneous voltage waveform at the moment of diesel engine start-up by lead-acid batteries in parallel with super-capacitor

Fig. 76.5 Instantaneous current waveform at the moment of diesel engine start-up by lead-acid batteries
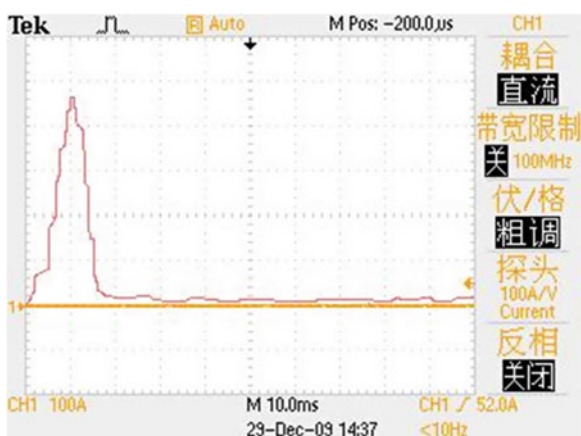
Fig. 76.6 Instantaneous current waveform at the moment of diesel engine start-up by lead-acid batteries in parallel with super-capacitors
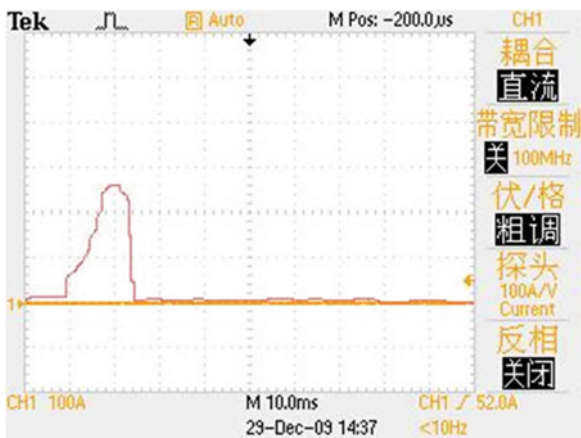
super-capacitors in parallel with lead-acid batteries can discharge instantaneous high current and store electric power for a long time, thereby greatly improving the engine start-up performance at low temperatures.

76.3.2 Cold Start Test

In order to enable diesel engines to adapt to a wider range of environment, the authors conducted a cold start test by adopting the low-temperature test method in GJB1488-92 [4]. The monomer specifications of the super-capacitor adopted in the test were 2,400 F and 2.7 V. 12 super-capacitors were connected in series and then used in combination with lead-acid batteries to form the system to test the low-temperature start-up performance of the diesel engine. During the experiment, the ambient temperature was lowered to -41 °C, and the test was conducted after incubation for 12 h. At that time, the voltage of the lead-acid batteries in parallel with the super-capacitors was 24.75 V. After artificial heating of the engine for 12 min, the first start-up succeeded. Afterward, the voltage dropped to 23.22 V, and then the second start-up also succeeded. After 6 consecutive hours of freezing without any measures taken, 4 continuous start-up attempts with only lead-acid batteries all failed, and the engine speed at that time dropped significantly, indicating that the engine would by no means be started. Subsequently, super-capacitors in parallel with lead-acid batteries were used again for start-up, and the first three attempts all failed. However, the voltage slightly dropped, and then the fourth attempt succeeded. The test results have fully demonstrated that the super-capacitor can significantly improve the engine's low-temperature start-up performance.

76.4 Conclusion

Above is feasibility analysis on the application of super-capacitors combined with lead-acid batteries in the diesel cold start. Super-capacitors already have a wide range of industrial applications. For example, it is used combined with batteries in the electric starting system of various automobile engines; it is also used as the DC operating power for high-voltage switchgear, braking energy recovery, and start-up accelerate power of electric-drive armored vehicles and electric starting system of military vehicles, as well as uninterruptible power supply system of important users and wind and solar power generation systems [5]. These facts have sufficiently proved the good performance of super-capacitors. It can be predicted that with the constantly deepening of applications of super-capacitors in parallel with batteries in diesel cold start, super-capacitors will greatly improve the performance, expand the applicable scope, and enhance the reliability of diesel power plants.

References

1. Zhang Bing-li (2009) Study on the application of super-capacitor in a new starting system of automobile engine. J Hefei Univ Technol 32:1648–1651
2. Liu Shu-guo (1998) The design of cold starting for Moblie generator with Air cooling diesel engine. Mobile Power Station & Vehicle 1:15–18
3. Xin W (2006) Application of super capactor in auto startup. Int Electron Elem 5:57–59
4. Tian Rui (2012) On High-low Temperature test method of a certain type of military Power Van. Equipment Environ Eng 1:102–104
5. Liang Q et al (2006) Analysis on the feasibility of aerial DC ground supply of the super capacitor combined with batteries. Battery 1:30–31

Chapter 77
Characterization of Fretting Fatigue Behavior of TiN/Ti Coating on Ti-811 Alloy at Increased Temperature

Xiaohua Zhang, Feng Pan and Dinggen Xiang

Abstract A TiN/Ti composite coating has been prepared on a Ti-811 titanium alloy substrate by an ion-assisted arc deposition (IAAD) technique. The composition distribution, microhardness, ductility, tribological properties, and fretting fatigue resistance (FFR) at increased temperature of the coating have been investigated. The results indicate that the IAAD technique can be used to prepare a TiN/Ti composite coating with high hardness, good ductility, excellent bonding strength, and high load-bearing capability. The TiN/Ti composite coating can improve the resistance to wear and fretting fatigue (FF) of the Ti alloy at 350 °C because of the good toughness and high bonding strength of the IAAD TiN/Ti composite coating with excellent lubrication of Ti particles in the coating.

Keywords Titanium alloy · Fretting fatigue · Ion-assisted deposition · Increased temperature

77.1 Introduction

Titanium alloys have been widely used in manufacturing the fans, compressor disks, and blades of advanced aircraft engines [1]. However, titanium alloys are very sensitive to fretting fatigue (FF) damage due to their low thermal conductivities and high coefficients of friction, which may affect the safe reliability of the aircraft engine compressor [2, 3]. Hence, the development of surface modification techniques to improve the fretting fatigue resistance (FFR) of titanium alloys is vital for their safe use in advanced aero-engines with high reliability and long

X. Zhang (✉) · F. Pan · D. Xiang
Corrosion and Protection Research Laboratory, Northwestern Polytechnical University, Xi'an 710072, China
e-mail: yhzhangxh@nwpu.edu.cn

usable life [4–7]. To improve the FFR of titanium alloys at increased temperature, it is necessary to devise other effective surface treatment methods.

TiN coating leads to superior abrasion resistance, a low coefficient of friction, high temperature stability, and high hardness. TiN coating is thus widely used in many industries. Research has indicated that the tribological and fretting wear performances of metals may be improved by a TiN coating [8]. In this paper, the FF behavior of the Ti-811 alloy with TiN/Ti composite coating was studied.

77.2 Experimental Procedures

FF specimens and fretting pads were obtained from Ti-811 titanium alloy bars ($\varnothing$ 16 mm). Ti-811 alloy is almost all α-phase and contains 7.9 % Al, 1.0 % Mo, 0.99 % V, 0.05 % Fe, 0.1 % C, 0.01 % N, 0.001 % H, 0.06 % O, and balance, Ti. The material was treated by double annealing (910 °C for 1 h, cooled in air, 580 °C for 8 h, cooled in air). The resulting microstructure is an equiaxial α-phase and intergranular β-phase. The mechanical properties of the alloy are as follows: $\sigma_b = 931$ MPa, $\sigma_{0.2} = 890$ MPa, $\delta = 23$ %, and $\Psi = 46$ %.

A PIEMAD-03 multifunction apparatus was used to prepare the ion-assisted arc deposition (IAAD) coatings. The IAAD target used in this study consisted of 99.5 % Ti. The specimen was finely ground using 1200 grit SiC paper and ultrasonically cleaned with acetone. Before deposition, the surface of the specimen was cleaned with a 1 keV Ar ion beam in a flux of 20 μA/cm^2 for 20 min. To improve the bonding strength between the coating and substrate, a high-energy assisting ion beam was used to bombard the surface of the coating during deposition. The coating deposition processing parameters were arc current: 100 A, bias voltage: -200 V, and N$_2$ pressure: 0.5 Pa.

An HITACHI S-570 scanning electron microscope (SEM) was used to investigate the morphology of the TiN/Ti coating. A GDA750 glow-discharge spectrometer was used to determine the elemental distribution in a cross section of the coating. An XRD-700 X-ray diffraction analyzer was used to analyze the phases of the coating. An HV-1000 microhardness instrument was used to measure the Knoop microhardness of the coating with a load of 0.245 N and loading time of 20 s. The ductility of the coating was estimated using a multi-impact tester with a total number of 1×10^4 impacts. The maximal impact load that resulted in cracking of the coating was defined as the critical ductility load.

The wear resistance of the coating at increased temperature was evaluated using a ball on disk machine with a rotating ball and a fixed disk. The ball was made of Ti-811 titanium alloy. The diameter, the surface roughness R_a, and the hardness HK$_{25}$ of the ball were 4.75 mm, 0.05 μm, and 346, respectively. The disk, made of the Ti-811 titanium alloy, had a diameter of 30 mm, a thickness of 8 mm, and a surface roughness R_a of 0.05 μm. The wear tests were conducted under a 5 N load at a temperature of 350 °C, which simulated the conditions of aircraft engine compressors.
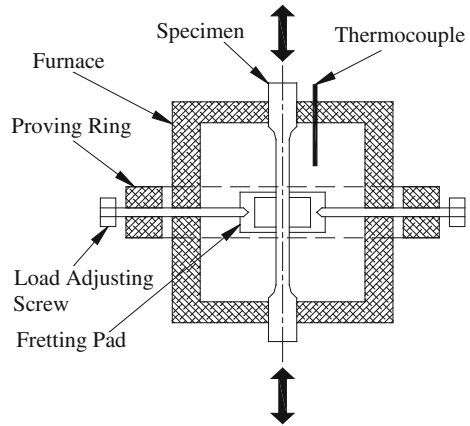
A PLG-100C high-frequency fatigue machine was used to conduct FF tests. A schematic drawing of the FF test setup is shown in Fig. 77.1. The load was set in pull–pull mode. The contact state between the pad and the specimen was flat to flat, with a rectangular contact area of 2 mm × 6 mm. Relative slip between the specimen and pad was introduced by the difference in elastic deformation between them. The contact stress of the pads with the specimen was 85 MPa, which was loaded by using a stressing ring. The span length between the fretting bridge foots was 15 mm. The slip was approximately 36 μm for an axial loading force of 500 MPa in sinusoidal form at 110 Hz with a stress ratio of 0.1. The FF life was taken as the average value of three specimens. An electrical resistance furnace was used for heating, and the temperature was controlled at 350 ± 1 °C using a feedback temperature controller with a rectifier and a K-type thermocouple.

77.3 Results and Discussion

Figure 77.2 shows the SEM morphology of the IAAD TiN/Ti coating surface. Many particles with different diameters can be seen on the surface of the IAAD TiN/Ti coating. These particles were formed from the freezing of target drips composed mainly of Ti.

Figure 77.3 shows the XRD pattern of the TiN/Ti coating, with a 2θ scan from 20° to 80°. The TiN/Ti coating shows preferential orientation in the (200), (111), and (220) crystal planes. Among these crystal planes, the (200) plane is the most highly preferential orientation due to the bombardment effect of the assisting ion beam on the coating.

Figure 77.4 shows the elemental distribution over a cross section of the IAAD TiN/Ti coating. The thickness of the TiN/Ti coating is 6 μm. The percentages of Ti and N at the coating surface are 40 and 42 %, respectively. To improve the

Fig. 77.2 Micrograph of a TiN/Ti film
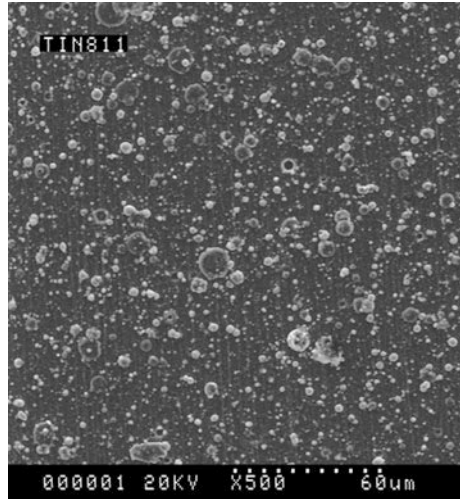
**Fig. 77.3** XRD pattern of TiN/Ti coating
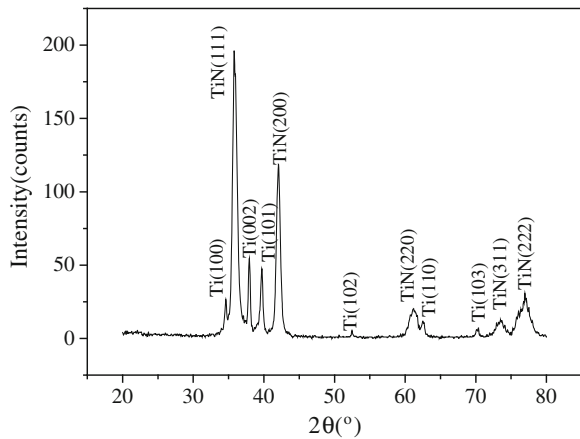
ductility of the TiN coating and the bond strength between the coating and substrate, a pure Ti interlayer (approximately 3 μm) was deposited between the substrate and the TiN coating. The nitrogen content was seen to increase gradually on going from the Ti coating to the TiN coating, and thus, the hardness of the TiN/Ti coating gradually decreased with increasing depth of the coating and its deformability was improved concomitantly, which was favorable for its tribological and mechanical properties. The mixing interface of the coating element and the substrate element was obtained by the bombardment of the assisting ion beam during the initial deposition stages of the coating, which improved the bond strength between the coating and substrate.

Fig. 77.4 Element content distribution curves of TiN/Ti coating
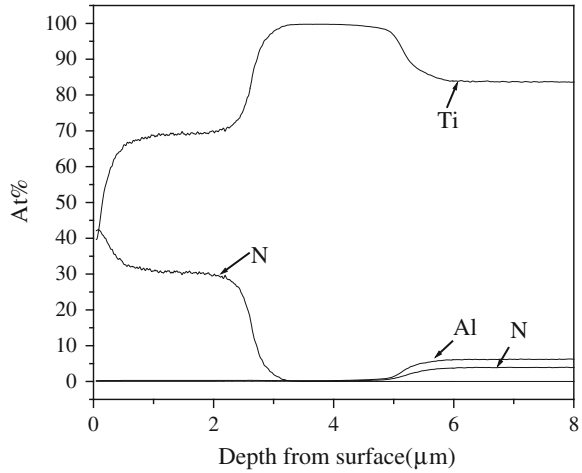
**Fig. 77.5** Impact morphology of TiN/Ti coating
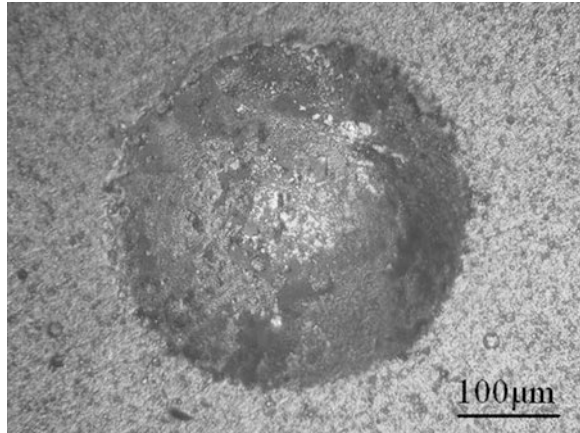
The microhardness test yielded a value of HK_{25} 2,362 for the IAAD TiN/Ti coating, which is a factor of 6.8 higher than that of the Ti-811 alloy substrate. The high hardness of the coating resulted from the ceramic phase of the TiN.

The multi-impact test indicated that the IAAD TiN/Ti coating had very good ductility and high bonding strength. The coating did not crack and delaminate even if the substrate was impacted to collapse under the maximum load of the tester (Fig. 77.5).

Figure 77.6 compares the coefficient of friction of the Ti-811 titanium alloy and the IAAD TiN/Ti coating as a function of friction time at 350 °C. The results indicate that the coefficient of friction of the Ti-811 alloy substrate was 0.55 at the beginning of the experiment and 0.45 at the end. The IAAD TiN/Ti coating reduced the coefficient of friction of the Ti-811 alloy substrate surface from 0.55 to 0.4. The wear resistance of the Ti-811 alloy was improved by the IAAD TiN/Ti

Fig. 77.6 Comparison of friction coefficient of TiN/Ti coating and Ti-811 alloy at 350 °C
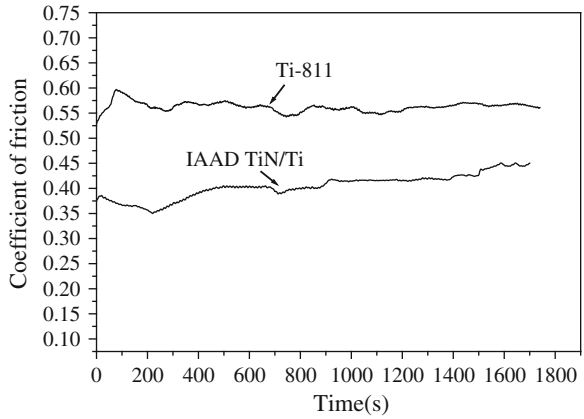
Fig. 77.7 Fretting fatigue lives of Ti-811 alloy and TiN/Ti coating at 350 °C
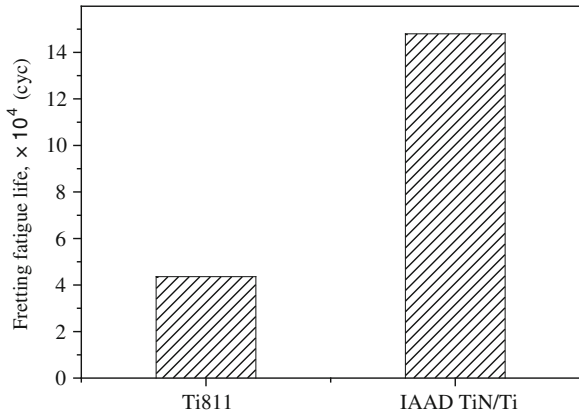
coating, which may be attributed to the high density, higher microhardness, and good ductility of the coating.

Figure 77.7 compares the fretting fatigue lives (FFL) of the Ti-811 alloy (labeled BM) and the IAAD TiN/Ti coating (labeled TiN/Ti) at 350 °C. The FFL of the Ti-811 alloy at increased temperature was improved by a factor of 2.4 by the IAAD TiN/Ti coating. The reasons for this may be summarized as follows: The TiN/Ti coating showed good wear resistance, high ductility, and high bond strength. Moreover, the surface contact regime between the TiN/Ti coating and the fretting pads involved the convex peaks contacting the flat surface, which resulted from the softer Ti particles randomly distributed in the hard TiN/Ti coating. The contact area and fretting area were decreased, so the probability of crack initiation was reduced. The softer Ti particles on the harder TiN coating surface provided a good solid lubricating function and absorbed some fretting movement energy. Therefore, the wear resistance of the Ti-811 alloy was significantly improved by

the TiN/Ti coating. Simultaneously, the pure Ti interlayer and the mixed Ti and N gradient layer formed a good transition layer between the TiN coating and the Ti-811 alloy substrate. The transition layer not only resulted in the hardness of the whole coating gradually changing along the coating thickness, but also improved the bond strength of the coating. At the same time, cracks initiated in the TiN coating surface were arrested by this transition layer. Hence, the fatigue resistance of the TiN coating was improved. The internal stress of the TiN/Ti coating was relaxed and the ductility of the coating was enhanced due to the soft Ti particles interfusing in the coating.

77.4 Conclusions

In this paper, the effects of the TiN/Ti composite coating prepared by an IAAD technique on the FFR of Ti-811 titanium alloy at increased temperature were investigated. This analysis leads to the following conclusions: A TiN/Ti coating could be prepared on a Ti-811 titanium alloy substrate by IAAD technique. The TiN/Ti coating exhibited high hardness, excellent bonding strength, high load-bearing capability, good ductility, and a low coefficient of friction, and so the wear resistance of the Ti-811 titanium alloy was significantly improved by the coating at 350 °C. The FFL of the Ti-811 alloy with the TiN/Ti coating was improved by a factor of 2.4 as compared to the uncoated substrate at 350 °C because of the excellent wear and fatigue resistance and good ductility of the coating.

References

1. James CW, Edgar AS (2003) Progress in structural materials for aerospace systems. Acta Mater 51:5775–5799
2. Ray AK, Das G, Ranganath VR (2004) Failure of connecting pins of a compressor disc in an aero engine. Eng Fail Anal 11:613–617
3. Bhaumik SK, Rangaraju R, Venkataswamy MA (2002) Fatigue fracture of crank shaft of an aircraft engine. Eng Fail Anal 9:255–263
4. Hutson AL, Niinomi M, Nicholas T (2002) Effect of various surface conditions on fretting fatigue behavior of Ti–6Al–4V. Int J Fatigue 24:1223–1234
5. Wei R, Shankar M, Jeffrey H (2004) Evaluation of coatings on Ti–6Al–4V substrate under fretting fatigue. Surf Coat Technol 192:177–188
6. Hyukjae L, Shankar M, Shamachary S (2005) Investigation into effects of re-shot-peening on fretting fatigue behavior of Ti–6Al–4V. Mater Sci Eng A 390:227–232
7. Liu DX, He JW (2005) Comparative study on the fretting fatigue and fretting wear behaviors of titanium alloy subject to various surface modifications. Tribology 25:13–17
8. Sung JH, Kim TH, Kim SS (2001) Fretting damage of TiN coated Zircaloy-4 tube. Wear 250:658–664

Chapter 78
An Organizational Mode with Reputation for O2O E-Commerce

Zhijian Yang

Abstract Group-buying as an O2O (online to off-line) e-commerce mode application has become into a hot spot of e-commerce applications. Compared with the traditional e-commerce mode, its ultra-low price with limited time has attracted many people's attention. However, the way of its profitability is very single and easier to be copied, which results in much weaker sustainable development capability. Meanwhile, the demonstrated organizational mode and the issues of trust will be also key factors that restrict the development of group-buying. Combining with traditional e-commerce mode, this paper mainly explores the popular O2O organizational mode and analyzes its limitations as well as future trends. An improved O2O e-commerce mode with reputation is proposed considering the status of current user's passive participating in O2O e-commerce. A third-party pay platform and credit evaluation platform are introduced to guarantee the success of trade.

Keywords O2O · E-commerce · Organizational mode · Group-buying · Reputation

78.1 Introduction

With the development of Internet technologies, e-commerce has gradually been becoming the part of everyday life of people. O2O is the first mode that comprehensively integrates online virtual economy and off-line entity stores into B2B, B2C, C2C, as well as the corollary of mobile Internet technology development

Z. Yang (✉)
School of Management, Northwestern Polytechnical University, xi'an 710072 Shanxi, China
e-mail: yzhj@nwpu.edu.cn

spread to daily life. The consumption pattern of mobile Internet is gradually becoming mature and be recognized as the development of mobile terminals.

Off-line businesses and enterprises can simply and rapidly release their information on the O2O e-commerce-trading Web sites. Besides, they also can constantly update dynamic information posing a continuing attraction to the consumers. Consumers can filter goods and services online in real time and then go to the store to purchase and for consumption. Supported by the 3G technology, consumers can easily find useful online information by the GPS of mobile terminal to position (location) stores, which saves time and cost for consumers.

Owing to the product of dummy market cannot be touched and the trading is anonymous, the information asymmetry of the e-commerce transactions is increased. Trust reflects the degree of entities' reliability, integrity, and ability in the deal [1]. Traditional e-commerce mode such as B2B, B2C, and C2C are built on foundation of the Internet, which logistics and capital are separated in the trading process. Consumers need to provide personal information to the site while shopping, which makes Internet transactions surfer a greater risk. The new O2O e-commerce mode brings us a huge market capacity and unprecedented opportunities, but we will also face many problems such as false propaganda, fake goods, trading funds security, as well as the dishonest commitment. In the case of lacking rules relating to online security, the trust has played an irreplaceable role in order to ensure that you achieve the desired results [2]. The lose in trust has become a key factor that makes consumers refuse to join in the online trading [3], thus introducing the mechanism of trust into e-commerce can effectively improve the quality of trade [4]. Trust from creation to development or disappear that the development processes are considered to be repeated, and the related studies confirm that the two sides continued to adjust the trust in the course of trading [5, 6]. Because organizational mode is a key factor to affect the efficiency and safety of trading, this paper will mainly discuss the organizational mode of O2O e-commerce.

78.2 The O2O E-Commerce Mode

O2O (online to off-line) e-commerce mode is the fusion of online Internet resources and off-line entity economy, in which consumers can screen the goods and services published online before they go to the entity store to buy and for consumption. Besides, the businessman can attract and detect tourists online, and consumers and businessmen will realize the dynamic interaction process.

The core of O2O mode is that it can draw the online consumer to the entity store. Businessmen provide the discount information or services of off-line shops for online consumers, by way of transferring them to off-line customers. Consumers can gain commodities' information and preferential vouchers, and even make order and payment. Lastly, they go to off-line merchants to enjoy services. Consumers and businessmen can interact with each other through the online

O2O-trading platforms. Meanwhile, the platform can monitor the transactions real time. Thus, not only consumers can explore the ratio of high-quality goods and services, but also the businessman can realize the maximization of the commercial value.

78.3 O2O E-Commerce Organizational Model

The booming development of electronic commerce needs the guarantee of security capital flow, and the online electronic payment of e-commerce has become a key link. Accordingly, the development of electronic commerce is starving for business of financial institutions, technology, and online payment intermediation's support. Therefore, the construction of Internet banking has not only become an inevitable trend, but also the foundation of the smooth development of electronic commerce.

A complete e-commerce activity at least involves four parts: manufacturers, merchants, customer, and financial institutions [7–9]. The intervention of bank can solve the electronic commercial payment bottleneck, which can accelerate the velocity of money, enhance the competition ability of the bank, and increase the deposits and poundage's income of bank. Ultimately, it brings new profit growth point to the banking industry.

The development of the third-party payment provides a strong support for capital, which ensures sellers receive the payment after delivering goods and buyers receive the goods after making payment. Nowadays, the progress of mobile technology promotes the mobile business development, which consumers can do real-time-trading activities with mobile terminal. Meanwhile, the geographic location technology provides mobile business with incomparable advantages.

78.3.1 O2O Organizational Model of Traditional Online Payment

Internet banking is a virtual counter in the Internet, by which the user can enjoy round-the-clock online financial services regardless of time or space restrictions. It provides online payment in addition to the traditional commercial banking business.

As the O2O electronic commerce organization mode shown in Fig. 78.1, the customers can conduct real-time electronic business transactions after opening the online payment function in financial institutions' account. Both buyers and sellers release demand and supply information on the O2O online application platform, thereby they will bargain over the price before concluding the transaction. Thus, buyers directly make payment to the sellers with the bank account through the
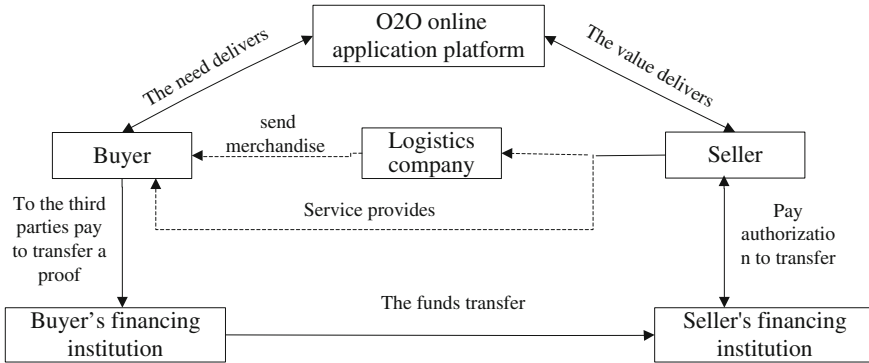
Fig. 78.1 O2O organizational model of traditional online payment

Internet banking. And sellers make shipment of goods to the buyers immediately after receiving the payment. This model can ensure the money of both buyers and sellers to circulate fast and improve its liquidity.

78.3.2 O2O Organizational Model of the Third-Party Payment

The third-party payment model is an Internet-based means of exchange that provides online and off-line payment channels enabling two trading parties' online payment, fund settlement, inquiries, and statistics [10]. It offers necessary support for ensuring a successful business in e-commerce that is independent of banks, Web sites, and merchants. It is mainly used to guarantee the security so as to dissolve the risk of trade between both parties.

The third-party platform has taken most of the online payment market shares of electronic commerce sharing its superiorities such as good compatibility, credit agencies, safety, and convenience. The third-party payment can effectively ensure the safety of fund for both buyers and sellers in O2O e-commerce transactions, and it can reduce the malicious consumption of the buyer and the dishonest transaction of the seller.

O2O organizational model of the third-party payment is shown in Fig. 78.2. Both buyers and sellers release demand and supply information on the O2O online application platform, thereby they will bargain over the price before concluding the transaction. The buyers and the sellers need to register an account on the third-party payment platform. The buyers transfer trading capital to the third-party platform account through financial institutions' account in e-commerce transactions. In the end, the buyers transfer capital to the sellers' account from the third-party platform account after receiving the goods or accepting services.
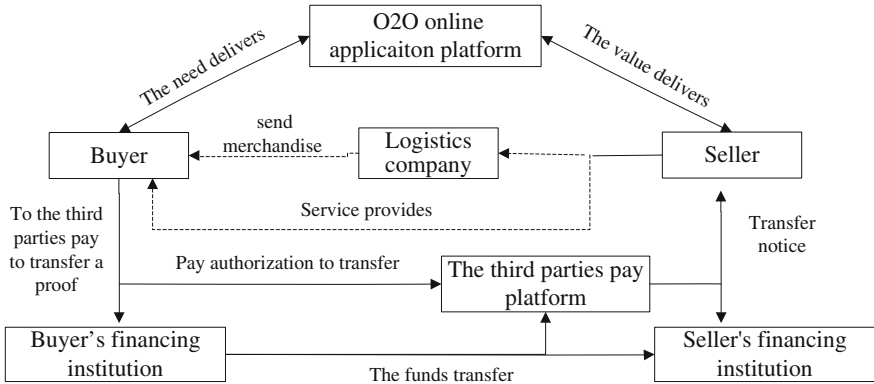
Fig. 78.2 The third-party payment O2O organizational model

78.3.3 O2O Organizational Model of Mobile Payment

Mobile payment model is an alternative payment method that consumers can use a mobile phone, handheld computer, or other mobile terminal to pay for various kinds of services or goods instead of paying with cash or credit cards. Mobile payment emphasizes its mobility and convenience. Its mobility enables users to pay for the goods through mobile Internet by virtue of mobile phone's SIM card at any time or any place. The convenience makes users utilize the advantages of geographic location technology to serve local businessmen and consumers. Besides, it can show goods' information through electronic information channel and entity channel before conducting an online transaction.

As shown in Fig. 78.3, both buyers and sellers release demand and supply information on the O2O online application platform, thereby they will bargain over the price before concluding the transaction. The buyers use cell phone account established in mobile operators as the mobile payment account. Buyers make payment to the sellers directly with mobile payment account. And sellers make shipment of the goods to the buyers immediately after receiving the payment.

78.4 An Improved O2O Organizational Model

78.4.1 O2O E-Commerce's Limitation

At present, both vendors and purchasers are just passive participation in group-buying, which is one of the mainstreams of O2O e-commerce mode. Under the present circumstances, the sellers cannot update goods' information according to the transaction data in real time, and it will restrict them obtaining the biggest
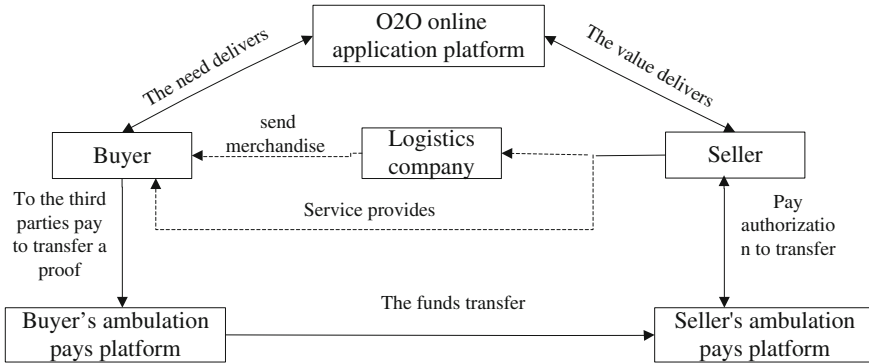
Fig. 78.3 Mobile payment O2O organizational model

value. Meanwhile, consumers can only choose the released information passively. They cannot interact with each other in order to pursuit the maximum effectiveness. Therefore, a completely open O2O platform for sellers and buyers is becoming the innovation power of electronic commerce, which will break through the current O2O e-commerce mode's development bottlenecks.

There are many problems related to group-buying Web sites. First of all, sellers sell fake commodities with extremely low price to attract buyers to take part in the activity. Second, sellers sell the goods with low discount price to consumers after driving up the original price, which is much higher than the market price. Third, sellers set many restrictive clauses in consumption time, consumption amount, consumption frequency, and etc. Fourth, some group-buying Web sites sell more services concerned with the popular entertainment, tourist lodging, domestic service, hairdressing fitness, and etc. than its capacity with low prices that result in failure to realize the commitment. As a new business area, O2O e-commercial mode has a mass of potential user group, which will become the mainstream of e-commerce in the future.

As we all know, the existing safety problem in payment restricts the development of electronic commerce. Internet banking or mobile payment is used as the means of payment. And the third-party payment is used as the guarantee of transactions that ensures the safety of funds. But some unscrupulous dealers may use the relations of cooperation with the financial institutions, mobile operators, and the third-party payment platform to obtain funds, and later they close the O2O online application platforms in which consumers will suffer a lot.

78.4.2 An Improved O2O Organizational Model

An open platform which can integrate Internet and mobile Internet is needed in order that it can promote the commercial value of O2O e-commerce. Business and
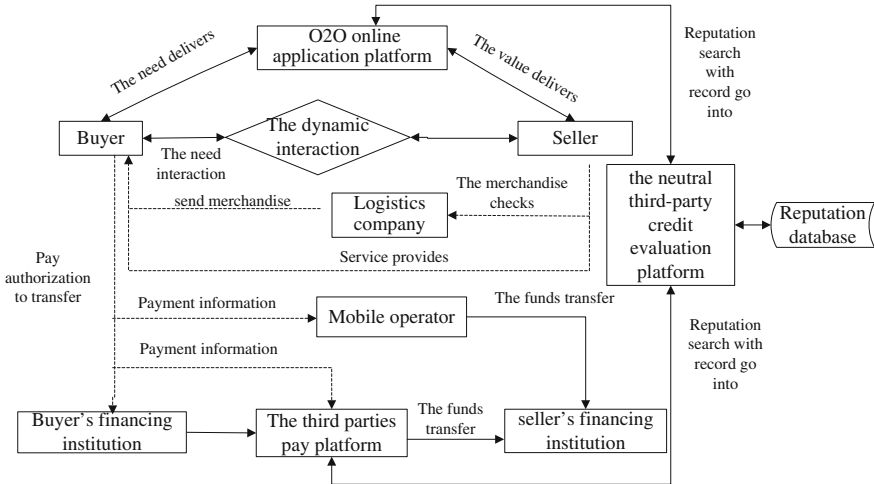
Fig. 78.4 An improved O2O organizational model

enterprise can simply and rapidly deploy online stores through this platform. And it can attract consumers to stores that offer discount vouchers and benefit returns. At the same time, a good credit-trading platform cannot only provide convenient releasing information condition, good user interface, and perfect interactive function, but also a good third-party payment, real qualification examination, an authentic credit evaluation of after-sale service, and other securities. The Fig. 78.4 is an improved O2O organization mode that introduces an active interaction mechanism, and the neutral third-party credit evaluation platform as the reference of O2O e-commerce transactions.

The improved O2O organization mode introduces a reputation database managed by the neutral third-party credit evaluation platform. The reputation database uses both buyers and sellers' identity as the only identification. Furthermore, it contains both parties' credit records of all O2O online application platforms and credit evaluation information of the third-party payment platforms.

78.5 Conclusions

This paper analyzed the traditional e-commerce modes and compared them with the O2O e-commerce. Studying the advantages and disadvantages of the current popular O2O e-commerce organizational mode, this paper introduces a new O2O e-commerce organizational model. Although the new model can enhance the freedom choice of choice and the safety of transaction of both buyers and sellers, the third-party payment credit library as a reputation database which should be provided by the third-part evaluation platform. The credit library transaction

platform is opened to all O2O e-commerce Web sites, so the personal privacy is in a significant threat. Meanwhile, the security of the Internet banking and mobile payment, the habit of consumers using O2O e-commerce, and the method of credit evaluation are still needed further research.

References

1. Gefen D, Straub DW (2004) Consumer trust in B2C e-commerce and the importance of social presence: experiments in e-products and e-services. Omega Int J Manage Sci 6:407–424
2. Jones GR, George JM (1998) The experience and evolution of trust: implications for cooperation and teamwork. Acad Manag Rev 23:531–546
3. Rutter J (2001) From the sociology of trust towards a sociology of 'e-trust'. Int J New Prod Dev Innov Manage 2:371–385
4. Hitoshi Y, Kazunari I, Toshizumi O (2004) Modeling reputation management system on online C2C market. Comput Math Organ Theory 10:165–178
5. Lewicki RJ, McAllister DJ, Bies RJ (1998) Trust and distrust: new relationships and realities. Acad Manag Rev 23:438–458
6. McKnight DH, Choudhury V, Kacmar C (2002) The impact of initial consumer trust on intentions to transact with a web site: a trust building model. J Strateg Inf Syst 11:297–323
7. Matthias M, Bernd B, Ralf H (2006) An approach to online reliability evaluation and prediction of mechanical transmission components. Int J Autom Comput 3:207–214
8. Watson I (1997) Applying case-based reasoning techniques for enterprises system. Morgan Kaufmman Publisher, CA
9. Burkhard HD (2001) Similarity and distance in case-based reasoning. Fundamenta Informaticae 47:201–215
10. Yong XU, Jin DL (2010) The credit risk analysis and prevention of third party payment platform. Sci Technol Manage Res 10:174–176

Retraction Note to: The Uncommanded Autofeather System Research of Turboprop Aircraft

Bai-ping Yang

Erratum to:
Chapter 38 in: J. Wang (ed.), *Proceedings of the First*
Symposium on Aviation Maintenance and Management-
Volume II, **Lecture Notes in Electrical Engineering 297,**
DOI 10.1007/978-3-642-54233-6_38

This article, published in Lecture Notes in Electrical Engineering Volume 297, 2014, pp 339–347, has been retracted at the request of the author and conference organizer, because of error in data processing.

The online version of the original chapter can be found under
DOI 10.1007/978-3-642-54233-6_38

B. Yang (✉)
AVIC Xi'an Aircraft Industry Company LTD, Xi'an 710089, China
e-mail: qinglongdragon@163.com